URS

SEISMIC STUDY OF INDUSTRIAL STEEL STORAGE RACKS

C.K. Chen
Roger E. Scholl
and John A. Blume

June 1980

prepared for
the National Science Foundation
and for the Rack Manufacturers Institute
and Automated Storage and Retrieval Systems
(Sections of the Material Handling Institute)

prepared by
URS/John A. Blume & Associates, Engineers
130 Jessie Street (at New Montgomery)
San Francisco, California

INTENTIONALLY BLANK

50272-101

REPORT DOCUMENTATION PAGE	1. REPORT NO. NSF/RA-800279	2.	3. Recipient's Accession No. PB81 142101

4. Title and Subtitle	5. Report Date
Seismic Study of Industrial Steel Storage Racks	June 1980
	6.
7. Author(s) C. K. Chen, R. E. Scholl, J. A. Blume	8. Performing Organization Rept. No.
9. Performing Organization Name and Address URS/John A. Blume & Associates, Engineers 130 Jessie Street (at New Montgomery) San Francisco, CA 94105	10. Project/Task/Work Unit No. 11. Contract(C) or Grant(G) No. (C) (G) PFR7914360
12. Sponsoring Organization Name and Address Engineering and Applied Science (EAS) National Science Foundation 1800 G Street, N.W. Washington, D.C. 20550	13. Type of Report & Period Covered 14.

15. Supplementary Notes

16. Abstract (Limit: 200 words)

Development of criteria and procedures for the seismic design of industrial steel storage racks is reported. The investigation focused on mathematical models for predicting earthquake response of racks and obtaining experimental data to quantify limit behavior of racks under earthquake conditions. Methodology consisted of subjecting four types of full-scale storage racks to simulated earthquake motions. Full-scale static-cycle tests were performed on two types of racks and antilever and portal tests were conducted on several rack assemblies to obtain information on load deformation characteristics. Shaking table tests were performed to evaluate seismic response effects on different types of merchandise. Table test responses were compared with predicted results using linear and nonlinear mathematical models. Response spectrum and time-history analyses were performed, and simplified static code methods were studied and compared. In general, the racks performed well and predictably during the shaking tests. The ductility and energy dissipation capacity of the racks were much larger in longitudinal than in transverse direction. Responses predicted agreed well with experimental results. Seismic design criteria consistent with the philosophy of the Uniform Building Code were recommended.

17. Document Analysis a. Descriptors

Mathematical models	Design criteria	Dynamic tests
Earthquake resistant structures	Deformation	Static tests
Earthquakes	Simulation	Storage racks

b. Identifiers/Open-Ended Terms
Uniform Building Code

Earthquake Hazards Mitigation

c. COSATI Field/Group

18. Availability Statement	19. Security Class (This Report)	21. No. of Pages
NTIS	20. Security Class (This Page)	22. Price

(See ANSI-Z39.18) See Instructions on Reverse

OPTIONAL FORM 272 (4-77)
(Formerly NTIS-35)
Department of Commerce

ABSTRACT

This project developed criteria and procedures for the seismic design of industrial steel storage racks.

Four types of full-scale storage racks were subjected to simulated earthquake motions using a 20-ft-square shaking table. In addition, full-scale static-cyclic tests were performed on two types of racks, and cantilever and portal tests were conducted on several rack subassemblies to obtain detailed information on load deformation characteristics, particularly for the semi-rigid beam-column joints. Finally, shaking table tests were performed on a full-scale rack to evaluate the seismic response effects of different types of typical merchandise.

The responses measured during the shaking table tests were then compared with results predicted using linear and nonlinear mathematical models. Response spectrum and time-history analyses were performed, and simplified static code methods were also studied and compared.

In general, the racks performed well and predictably during the shaking table tests. The ductility and energy-dissipation capacity of the racks are much larger in longitudinal (moment-resisting frame) direction than in the transverse (braced frame) direction. The responses predicted theoretically were in good agreement with the experimental results. Seismic design criteria consistent with the philosophy of the *Uniform Building Code* are recommended.

CONTENTS

Preceding page blank

CONTENTS

APPENDICES

TABLES

CONTENTS (Continued)

CONTENTS (Continued)

CONTENTS (Continued)

page

FIGURES

CONTENTS (Continued)

page

CONTENTS (Continued)

CONTENTS (Continued)

CONTENTS (Continued)

CONTENTS (Continued)

CONTENTS (Continued)

CONTENTS (Continued)

CONTENTS (Continued)

EXECUTIVE SUMMARY

Objective

The objective of this study was to perform the investigations necessary to develop realistic criteria and procedures for the seismic design of industrial steel storage racks. Specifically, the work was directed toward the development of mathematical models useful for predicting earthquake response of racks and toward obtaining experimental data to quantify limit behavior of racks under earthquake conditions.

Background

The use of industrial steel racks is involved in some part of the production-distribution-sales-consumption cycle of nearly 40% of all goods consumed in the United States. Industrial racks are used in all parts of the U.S., including areas subject to moderate and major seismic ground motions. The criteria for design and construction of industrial racks have been developed by the manufacturer and traditionally have been directed primarily at gravity loading, with little attention given to earthquake loading.

The need for considering seismic lateral force effects was recognized by the Rack Manufacturers Institute (RMI) in the 1972 edition of *Interim Specification for the Design, Testing, and Utilization of Industrial Steel Storage Racks* (the most recent edition of the RMI specification is dated 1979). These criteria specify lateral forces based on a formulation similar to that specified for the seismic design of buildings.

At about the same time, the International Conference of Building Officials (ICBO) included seismic design requirements for storage racks in the 1973 *Uniform Building Code* (*UBC*) based on a formulation similar to that commonly used for seismic design of building components. The approach adopted by ICBO generally imposed much more severe constraints on design than the procedure adopted by RMI. Because of the lack of definitive experimental and engineering evidence to establish precise dynamic response characteristics and lateral force failure mechanisms, it has been impossible to determine the appropriateness of either of the two sets of criteria.

In 1973 and 1974, URS/John A. Blume & Associates, Engineers, conducted initial studies for RMI to determine the earthquake response behavior of typical steel storage racks. These studies included measurements of the dynamic response characteristics of representative rack installations, dynamic analyses of the racks, correlation of the measured and analytical data, and determination of seismic design criteria consistent with the *UBC* philosophy for buildings. On the basis of the initial findings, recommendations for seismic design criteria for industrial steel storage racks were included in the 1976 edition of the *UBC*. However, further studies were needed to obtain experimental data to quantify the limit behavior of racks under earthquake conditions.

Scope

The following principal tasks were performed in connection with this project:

- Static-cyclic tests of rack subassemblies
- Static-cyclic tests of full-scale racks
- Structural performance full-scale shaking table tests
- Merchandise shaking table tests
- Engineering analysis reconciliations

Subassembly tests of four types of racks were conducted as part of this project; in addition, the results of 20 subassembly tests conducted by 3 different manufacturers and by Cornell University are also reported here. To verify the applicability of these subassembly tests, full-scale static-cyclic tests of two different types of standard pallet racks were conducted. Finally, structural performance shaking table tests were conducted to verify actual earthquake performance of full-scale standard pallet racks, drive-in racks, and stacker racks. All full-scale racks tested in this study were anchored to the table (or floor for static-cyclic tests), except that one rack was left unanchored in order to evaluate the difference in seismic performance between the anchored and unanchored conditions.

Postearthquake investigations have revealed that stored merchandise is likely to shift or fall during strong ground motion. Recognizing this, but also recognizing that it would be impractical to establish the effective masses of loose merchandise during full-scale shaking table testing, it was concluded that rigid concrete weights tied to the racks would be used as live loads for the structural performance shaking table testing. To verify the validity of this practice, a separate series of tests was conducted to determine the effects of loose merchandise on rack response to shaking.

Engineering analysis reconciliations included development of mathematical models; comparison of rigorous linear and nonlinear time-history analyses with experimental results; and comparison of results from the response spectrum method and two simplified equivalent static analysis methods, the *UBC* and Applied Technology Council (ATC-3) methods. These analyses, with the test results, were then used to evaluate the applicability of the *UBC* seismic criteria to racks.

Major Findings

Subassembly Tests. Results from the cantilever and portal tests conducted at Stanford University and Cornell University and by several manufacturers were reported in this study. In all, tests of 24 types of rack components from 7 different manufacturers were correlated and compared. The following conclusions can be drawn:

- In most test cases, the moment-rotation (M-θ) relationships are very nonlinear. It is sometimes difficult to define a suitable linear range for elastic design and analysis.
- In general, the M-θ relationships for both test methods (portal and cantilever) are similar in shape and moment capacity. However, the stiffness from the cantilever tests is lower than that from the portal tests. The difference in the values of the joint rotational spring constant (K_θ) estimated for elastic analysis and design is on the order of 2.
- The cantilever test is sufficient for practical engineering purposes. The test is simple and requires only lateral load and displacement measurements, which are easy to carry out. However, the test should be conducted for loading in both the positive and the negative directions.

Merchandise Tests. Both shaking table and pull-release free-vibration tests were conducted to study the seismic response characteristics of the various types of merchandise, both tied to the rack with metal straps and not tied to the rack. Single-degree-of-freedom tests were performed: the rack was anchored to the shaking table, loaded with merchandise, and tested in both the longitudinal and transverse directions. The conclusions that can be drawn from this study, for the specific types of merchandise tested and for horizontal excitation only, are as follows:

- Substantial horizontal diaphragm action can be developed through the combination of stored material and pallets or metal decking, regardless of the type of material or whether it is tied to the rack.
- For all tests, little difference in global and local responses was found between the cases in which merchandise was tied to the rack and those in which merchandise was not tied to the rack. This finding justifies the use of tied live loads for the analytical response predictions.
- In all tests of merchandise that was not tied, all merchandise tested was very stable, and no movement of stored material was observed except for some of the uppermost cartons of paper products. The maximum floor (pallet) accelerations measured in the longitudinal test direction ranged from approximately 0.2g for the cases of canned goods (2,300 lb/beam) to 0.7g for lightweight paper products (500 lb/beam).

Because the merchandise tests did not include vertical acceleration, the project report was augmented in this area by citing merchandise and rack performance during recent earthquakes (presented in Appendix C).

Full-Scale Rack Tests. Four types of typical full-scale storage racks were subjected to simulated earthquake motions using the 20-ft-square shaking table facility at the Richmond field station of the University of California, Berkeley. The types of storage racks tested were: single standard pallet rack, back-to-back pallet rack, drive-in rack, and stacker rack. Three racks were anchored to the table and tested under live loads simulated by concrete blocks (1,000 lb/block) in each of the two principal directions. One rack (the back-to-back pallet rack) was tested without anchors to the table. The standard pallet racks tested were three stories high and two bays wide. The drive-in rack was three stories high, two bays wide, and three bays deep. The stacker rack was five stories high, four bays wide, and two bays deep. The ground motion was simulated by accelerograms recorded during the 1940 El Centro N-S earthquake and the 1966 Parkfield earthquake. For each rack tested, the amplitudes of the table motions were increased progressively from very slight motions causing only elastic response to severe earthquakes causing material yielding and structural damage. The racks tested were designed for use in areas of minor to moderate seismicity.

of full-scale standard pallet racks provided by two different manufacturers were subjected to static-cyclic tests in each of the two principal directions.

The findings from these two testing programs are summarized as follows:

- In general, the racks performed well during the shaking table tests, with the exception of the drive-in and stacker racks in the transverse direction. Considerable buckling was observed in first-story diagonal members of these two rack configurations when the racks were excited at very low levels (1/4 and 1/2 the Parkfield record, respectively).
- The global and local response amplitudes measured from the shaking table tests for the pallet rack that was not anchored to the table are higher than those for the anchored rack under the same input signal.
- The base plates for all racks that were anchored to the table (or the floor for the static-cyclic tests) provide a significant fixity against rotation, which, in turn, reduces the moment at the first-level columns.
- The fundamental periods of vibration range from 2 sec to 3 sec for the standard pallet and drive-in racks in the longitudinal direction and 0.5 sec to 1.0 sec for the standard pallet, drive-in, and stacker racks in the transverse direction.
- The first-mode damping values are much larger in the longitudinal direction (ranging from 3% to 9% of critical) than in the transverse direction (ranging from 0.5% to 3% of critical).
- The contribution to story shear of the p-δ effect is very significant in the moment-resisting frame direction and should be considered in response prediction and design.
- During the shaking table tests, the maximum drifts observed for the standard pallet and the drive-in racks in the longitudinal direction were 0.07 and 0.03 times the story height (H), respectively. This indicates that the racks can tolerate much greater drift than that allowed in the *UBC* method ($0.005H \times 3/K$) or the ATC method ($0.015H$).
- For the racks tested on the shaking table, strong localized deformations were observed at the connections between the open-section diagonal bracing members and the open-section columns. This type of deformation should be considered in making detailed response predictions in the braced-frame rack configuration.

Theoretical Prediction of the Response of Rack Structures. One of the primary objectives of the structural performance shaking table tests was to obtain experimental data on the actual performance of various types of full-scale rack structures in order to test the adequacy and effectiveness of the various analytical procedures and assumed mathematical models.

Frequency analyses of linear mathematical models were carried out to compare calculated periods of vibration and mode shapes with those observed during the low-amplitude shaking table tests and the pull-release free-vibration tests. The best-fit linear model developed for each rack configuration was used as a basis for performing linear and nonlinear time-history analysis, and the calculated periods and mode shapes were used to perform the response spectrum analysis. The calculated fundamental periods of vibration for each structure were used to determine the base shear coefficients for use in the *UBC* and the ATC-3 methods. The conclusions that can be drawn from these studies are as follows:

- In general, the responses predicted theoretically for all racks studied in this report were in good agreement with the experimental results.
- To develop appropriate mathematical models, rack storage levels are assumed to be sufficiently rigid, and two-dimensional models are considered to be adequate for practical purposes. Fictitious restraining floor beams can be added to simulate the actual column base fixity condition. Minimum net section properties and centerline dimensions are used.
- Modeling parameters such as K_θ (semirigid joints), I_f (semifixed column bases), and k (localized deformation at connections between the open-section column and open-section bracing members) should be considered in theoretical prediction of rack response.
- In the longitudinal direction, the lateral forces determined by the *UBC* method (assuming the best site condition, i.e., S = minimum) are roughly equivalent to those using the response spectrum method with intensity levels of slightly more than 1/2 the El Centro or the Parkfield record. However, in the transverse direction, the *UBC* lateral forces are approximately equivalent to 1/4 to 1/2 the El Centro and Parkfield records.
- For the braced-frame systems, the lateral forces determined by the *UBC* method are higher than those by the ATC method. However, for the moment-resisting frame system, the results from the ATC method are

slightly higher than those from the *UBC* method. For this comparison, the base shears for the *UBC* method were multiplied by a factor of 1.6 for the braced-frame system and 1.28 for the moment-resisting frame system, to equate working stress design to ultimate strength design; the base shears from the ATC method were modified by a capacity-reduction factor of 0.9.

Seismic Design Criteria and Procedures. The following conclusions and recommendations can be drawn from this study. Seismic design procedures according to the 1976 *UBC* and 1979 RMI specification are illustrated in Appendices D through H of this report.

- The lateral force provisions recommended in the 1976 *UBC* (Standard No. 27-11) appear generally to provide adequate seismic resistance in racks similar to those studied in this report except that the load factor (modifier) of 1.25 recommended in the *UBC* for all members in braced frames may not be adequate. A larger load factor or some modifications to the rack fabrication are needed to preclude early nonductile damage during strong earthquake shaking.
- The *UBC* formulas for determining the fundamental periods of vibration, such as $T = 0.05\ h_n/\sqrt{D}$ and $T = 0.1N$, are not applicable to rack structures. The Rayleigh method (Equation 12-3 in the *UBC*) or a frequency analysis using an appropriate mathematical model (computer-analysis method) are more desirable.
- The use of more detailed dynamic analysis procedures should not be ruled out, particularly in the design of an unusual rack structure. The response spectrum approach is a simple method of dynamic analysis that takes into account the true dynamic response nature of the racks to a greater extent than does the *UBC* procedure.

Further Studies

The following further studies (in order of importance) are recommended:

- This study shows that the *UBC* method generally provides adequate earthquake resistance except that a larger load factor or some design modifications to braced-frame systems are needed to preclude early nonductile damage during a strong earthquake. If eccentric bracing is proposed as a means of improving the seismic performance of braced frames as described in Appendix I, dynamic analyses and static-cyclic tests similar to those conducted at the University of California, Berkeley, in connection with the development of eccentrically braced frames for buildings are needed to justify the applicability of this system to rack structures. Experiments on a shaking table are also very desirable.

- Although it was deemed necessary for this study to conduct the full-scale rack tests independently in each of the two principal directions, this test method does not realistically represent actual earthquake shaking. Shaking table tests should therefore be conducted to investigate the response characteristics of storage racks at different orientations.
- Although this study recommends the Rayleigh method (Equation 12-3 in the *UBC*) or a frequency analysis using an appropriate mathematical model for determining periods of vibration, it will be beneficial to the rack industry to develop empirical period formulas for static code use and a limit value on the design period, such as are used in the ATC-3 method.
- Although this study recommends seismic design criteria consistent with the philosophy of the *UBC* for rack design, the ATC method could be widely used in the near future. Because of this, it will be beneficial to determine appropriate values for the response modification factor, R.
- Results from the shaking table and static-cyclic tests revealed that the column bases should not be considered either fixed or hinged but rather as partially fixed. Quantitative experimental data are needed to appropriately incorporate this parameter into mathematical models to account for actual column base conditions. In addition, experimental investigations are needed to define the parameter k for braced-frame systems as subassembly tests are needed to define K_θ for semirigid-frame systems.

ACKNOWLEDGMENTS

The work described in this report was supported by the National Science Foundation (NSF) and by the Rack Manufacturers Institute and Automated Storage and Retrieval Systems, two product sections of the Material Handling Institute (MHI); J. B. Scalzi is the NSF program manager, and T.W. Shea is the Executive Director of MHI. These sources of support are gratefully acknowledged.

In addition, invaluable assistance was rendered by many other persons and organizations. R. W. Clough directed the shaking table tests at the University of California, Berkeley, and consulted on interpretation of test data and on the analytical study. R. M. Stephen and D. Steele assisted in conducting the tests. At Stanford University, H. W. Krawinkler directed the subassembly tests and the static-cyclic tests. P. H. Cheng and T. Pekoz made comments and suggestions that proved useful in the course of the study.

In-house consultation was provided by S. A. Freeman, who carefully reviewed the entire manuscript and made many valuable comments and suggestions during the course of the study. P. K. Lum assisted in modifying the computer programs for data reduction and analytical correlation.

The members of the advisory committee provided overall guidance and review on the project. In addition to J. A. Blume, they are: R. W. Clough, E. D. Birnbaum, J. Colloton, L. B. Donkle, H. H. Klein, R. S. McLean, H. Shah, and F. A. Tully.

The manufacturers who provided racks or components for testing, or who contributed subassembly test data, are: Interlake, Inc.; Republic Steel Corporation; Frazier Industrial Co.; Artco Corporation; The Paltier Corporation; and Speedrack, Inc.

N. F. Ullman of the Oakland Warehouse Operation Department of Safeway Stores was helpful in providing merchandise for the merchandise tests.

E. Tajima of Nippon Filing Co., Tokyo, provided photographs of damage from the Miyagi-Ken-oki earthquake for use in Appendix C.

Finally, R. F. Nowacki edited this report and supervised its publication.

1. INTRODUCTION

1.1 Project Objective

The objective of this study was to perform the investigations necessary to develop realistic criteria and procedures for the seismic design of industrial steel storage racks. Specifically, the work was directed toward the development of mathematical models useful for predicting earthquake response of racks and toward obtaining experimental data to quantify limit behavior of racks under earthquake conditions.

1.2 Background

The use of industrial steel racks is involved in some part of the production-distribution-sales-consumption cycle of nearly 40% of all goods consumed in the United States. Industrial racks are used in all parts of the U.S., including areas subject to moderate and major seismic ground motions. The criteria for design and construction of industrial racks have been developed by the manufacturer and traditionally have been directed primarily at gravity loading, with little attention given to earthquake loading.

Currently more than 30 companies in the United States manufacture and market industrial steel storage racks. In general, each of the companies produces racks that are of a distinct design. In addition, several specific types of racks are produced; the most common are: standard pallet racks, drive-in racks, drive-through racks, stacker racks, and cantilever racks. The standard pallet rack is most commonly used, but the stacker rack is becoming increasingly popular because of its automated merchandise-handling features.

The Rack Manufacturers Institute (RMI) and Automated Storage and Retrieval Systems, sister organizations that are affiliates of the Material Handling Institute, have actively pursued development and establishment of specifications for the design, testing, and utilization of industrial steel storage racks. In 1964, RMI first issued a standard, *Minimum Engineering Standards for Industrial Steel Storage Racks*, but seismic design requirements were not included. The need for considering seismic lateral force effects was recognized by RMI in the 1972 edition of *Interim Specification for the Design, Testing, and*

Utilization of Industrial Steel Storage Racks[1] (the most recent edition of the RMI specifications is dated 1979). These criteria specify lateral forces based on a formulation similar to that specified for the seismic design of buildings.

At about the same time, the International Conference of Building Officials (ICBO) included seismic design requirements for storage racks in the 1973 *Uniform Building Code* (*UBC*)[2] based on a formulation similar to that commonly used for seismic design of building components. The approach adopted by ICBO generally imposed much more severe constraints on design than the procedure adopted by RMI. Because of the lack of definitive experimental and engineering evidence to establish precise dynamic response characteristics and lateral force failure mechanisms, it has been impossible to determine the appropriateness of either of the two criteria.

In 1973 and 1974, URS/John A. Blume & Associates, Engineers (URS/Blume), conducted initial studies for RMI to determine the earthquake response behavior of typical steel storage racks. These studies included measurements of the dynamic response characteristics of representative rack installations, dynamic analyses of the racks, correlation of the measured and analytical data, and determination of seismic design criteria consistent with the *UBC* philosophy for buildings. The results of these studies were summarized in three URS/Blume reports: a November 1973 report[3] on the seismic investigation of steel storage racks, a December 1973 supplementary report[4] that provided practical guidelines for the application of the findings of the November report, and a March 1974 report[5] providing design examples. A supplement to the March 1974 report[6] was issued in July 1975.

On the basis of these initial findings, reduced recommendations for seismic design criteria for industrial steel storage racks were included in the 1976 edition of the *UBC*.[7] However, further studies were needed to obtain experimental data to quantify the limit behavior of racks under earthquake conditions.

1.3 Project Scope

This project considered standard pallet racks, drive-in racks, and stacker racks. Despite the variety of racks available, the basic structural framing systems in use are limited. A moderate testing program that would have industry-wide applicability was thus considered feasible. The structural system of many racks installed today consists of braced frames in the transverse direction (perpendicular to the aisle) and moment-resisting space frames in the longitudinal direction (parallel to the aisle). Another important characterization of these racks is that, in the space frame, the beam-to-column connections are semirigid. This aspect requires specific consideration because of the high degree of joint nonlinearity and because of the substantial variations in the beam-to-column connections produced by the various manufacturers.

A convenient means for evaluating joint looseness is conducting static-cyclic subassembly tests of either beam-column configurations or portal configurations. Because of the simplicity of these types of tests, various manufacturers could conduct tests of their particular beam-column connection configurations and thereby vastly extend the applicability of the limited amount of testing that was feasible in this project. Subassembly tests of four types of rack components were conducted as part of this project; in addition, the results of 20 subassembly tests conducted by 3 different manufacturers and by Cornell University are also reported here.

To verify the applicability of these subassembly tests, full-scale static-cyclic tests of two different types of standard pallet racks were conducted. Finally, structural performance shaking table tests were conducted to verify actual earthquake performance of full-scale standard pallet racks, drive-in racks, and stacker racks.

Another important factor in evaluating the seismic performance of racks is column base fixity. Arguments can be made for and against anchoring rack columns at their base. Tests involving both lagged and unlagged (anchored and unanchored) racks were conducted as part of this project because no experiment has heretofore been available to address this matter.

Postearthquake investigations have revealed that stored merchandise is likely to shift or fall during strong ground motion. Recognizing this, but also recognizing that it would be impractical to establish the effective masses of loose merchandise during full-scale shaking table testing, it was concluded that rigid concrete weights tied to the racks would be used as live loads for the structural performance shaking table testing. A separate series of tests was conducted to determine the effects of loose merchandise on rack response to shaking.

Details regarding the specific types of racks tested and the analysis of the response data in connection with these various tests are presented in Chapters 2 through 5.

Chapter 6 gives a general description of various theoretical methods that can be used to perform seismic design/analysis evaluation for structures, including rigorous linear and nonlinear response analysis and simplified equivalent static analysis methods, such as the *UBC* and Applied Technology Council (ATC-3)[8] methods. Chapters 7 through 12 apply these various design/analysis methods to each of the racks tested on the shaking table and compare the results to those obtained experimentally.

Following is a list of the principal tasks that were performed in connection with this project:

- Static-cyclic subassembly tests
- Static-cyclic full-scale tests
- Structural performance full-scale shaking table tests
- Merchandise shaking table tests
- Engineering analysis reconciliations

A commentary on the adequacy of various rigorous and simplified seismic analysis/design procedures is given in Chapter 13, and an overall summary of the study, with conclusions and recommendations, is presented in Chapter 14.

2. SUBASSEMBLY TESTS

2.1 Introduction

To achieve the objective of establishing realistic seismic design criteria for steel storage racks, subassembly tests were needed to provide mathematical modeling guidelines regarding joint looseness and joint capacity for the various types of racks being manufactured and marketed. As part of this study, subassembly tests of four types of rack components were conducted at Stanford University.[9]

Because the Stanford testing was limited to these four types, results of subassembly tests conducted by various RMI member companies as well as test results obtained at Cornell University[10] are also summarized in this report.

In all, tests of 24 types of rack components from 7 different manufacturers were correlated and compared. The test procedures were generally in accordance with those described in References 11 and 12, but, to account for variation in lateral force and to facilitate more general use, the test results required special evaluation, as described in Sections 2.3 and 2.4.

2.2 Types of Rack Components

Table 2.1 shows types of connection and shapes and moments of inertia of beams and columns. The pallet beams of all 24 types of racks were welded to connector angles or plates, which, in turn, permitted connection to the columns through hook-type grips (Types A and C), stud-type grips (Type B), or bolts (Types D, E, and G). In a Type F connection, additional bars were used to join the connectors to the columns. The components of all racks were made of cold-formed steel, except Type D (columns and beams) and Types E-1 and E-2 (beams), which were made of hot-rolled structural steel. It can be seen from Table 2.1 that the shapes of the rack components are common in the storage rack industry and the results can be considered representative of industry practice.

2.3 Cantilever Tests

An inherent part of the typical design is the semirigid beam-to-column connection. For lateral (earthquake) response purposes, this type of connection imposes beam-column joint looseness and raises questions regarding joint capacity. To predict the earthquake response and capacity of such structures analytically, it is essential that information concerning joint looseness and joint capacity be obtained.

Results of the cantilever tests are specifically intended to provide a quantitative measure of the relative rotations between beams and columns. The moment-rotation (M-θ) relationships thus determined can be used as joint rotational springs for analytical modeling purposes. In addition, the results of the cantilever tests are intended to provide information concerning the ultimate capacity of a joint.

Procedures. Twenty rack types from seven different manufacturers underwent cantilever testing. Figure 2.1 shows the test setup. The columns were rigidly connected to fixed supports at both ends to prevent translation and rotation at these points. The load was applied by means of a hydraulic jack, and its magnitude was measured by means of a linear potentiometer or a dial gage. In some tests, two tests each for positive and negative moment application were conducted. The moment was considered positive when causing tension at the bottom fiber of the pallet beam in a realistic rack configuration (as indicated in Figure 2.1). Two rotational gages were used in some of the tests to measure the rotations of the beams (θ_b) close to the connector and the rotation of the column (θ_c) at the column centerline. However, as will be explained next, these rotational measurements were not considered necessary.

Evaluation of the Moment-Rotation Relationship. The applied moment, M, for the test is:

$$M = P(L_b + \frac{d_c}{2}) \tag{2.1}$$

θ can be obtained from the measured value of the tip deflection, δ, and computations of the elastic beam deflections, δ_b, and the column rotation, θ_c, i.e.:

$$\theta = \frac{\delta - \delta_b}{L_b + \frac{d_c}{2}} - \theta_c \tag{2.2}$$

where:

$$\delta_b = \frac{P(L_b + \frac{d_c}{2})^3}{3EI_b} \tag{2.2a}$$

$$\theta_c = \frac{P(L_b + \frac{d_c}{2})L_b}{16EI_c} \tag{2.2b}$$

The dimensions used in these equations are shown in Figure 2.1. I_b and I_c are moments of inertia of beam and column, respectively; E is the modulus of elasticity; and P is the applied load.

Alternatively, θ can be obtained as the difference between the rotation measurements $(\theta_b - \theta_c)$. Tests conducted at Stanford University showed reasonably good agreement (within about 10%) between the experimentally measured rotations and those computed analytically from Equation (2.2). This indicates that the analytical estimate for computing rotations is adequate and that rotation measurements may not be necessary for the cantilever tests. Thus, the cantilever test results presented in this report were all based on beam tip deflection measurements and the use of Equation (2.2).

Results. Table 2.2 shows the member properties, the estimated joint spring constants K_θ for elastic analysis and design, the failure moments, and the modes of failure for the 20 rack types tested, Types A through G. Most of the K_θ values were in the range of 200 to 1,000 kip-in./rad. Types D-5 and D-6, which were made of hot-rolled structural steel, were the exceptions.

In all tests, the strength of the rack assembly was governed by the connection instead of by the beam itself. Deformations in the connectors, tearing of the column perforations, and fracture of the beam-connector welds were commonly observed. The estimated failure moments were based on the final test loading, when severe damage was observed and the tests were terminated. Again, the failure moments of Types D-5 and D-6 were much higher than those for racks made of cold-formed steel. Figures 2.2 through 2.21 show the moment-rotation curves for each of the rack types tested. Figures 2.2, 2.3, 2.12, and 2.20 present the moment-rotation relationships in the two directions of applied load for Types A-1, B-1, C-1, and F-1, respectively. A comparison of these figures indicates a significant difference in strength and stiffness between positive and negative moments. The curves presented in Figures 2.2 to 2.21 show that, except for a few cases, early nonlinear behavior was observed. This nonlinearity made it difficult to define a linear range suitable for elastic analysis and design.

A comparison of the M-θ curves shown in Figures 2.2 and 2.4 for rack types B-1 and B-2, respectively, reveals the influence of the connector plates. For each test case, the columns were identical; however, Type B-1 used the 8-in. connector plate, and Type B-2 used the 6-in. connector. The strength and stiffness properties were significantly different for these two cases. The modes of failure were also different, as indicated in Table 2.2. In the case of Type B-1, the beam-to-connector weld fractured; in the case of Type B-2, the stud was broken, and distortions of the connector and of the column at the perforations were detected.

As might be expected, the strength and stiffness of the rack subassembly increased with an increase of the values of I_c and I_b. This is clearly shown in the test results from the Type B racks shown in Figures 2.22 to 2.25. The values of I_c and I_b are also indicated in these figures. The results show consistently higher strength and stiffness for stiffer rack components, except that the moment strength of Type B-4 was slightly smaller than that of Type B-9.

In contrast to these results are the results shown in Figure 2.26 comparing Type D-5 with Type D-6. The stiffness of the Type D-5 rack, with smaller beam members, was almost twice as large as that of the Type D-6 assembly up to a moment of 20 kip-in. Beyond this limit, the D-6 rack showed much greater stiffness than the D-5 rack.

2.4 Portal Tests

An alternative to the cantilever test is the portal test illustrated in Figure 2.27. Results of portal tests are intended to be used to study the interaction between pallet beams and upright frames in a realistic situation and to obtain information concerning joint rotational springs for analytical modeling purposes. The results are also intended to be compared with those obtained from the cantilever tests.

Procedures. Eight types of racks from five manufacturers underwent portal tests. Figure 2.27 shows the test setup. The rack consisted of two upright frames mounted on hinges created on four half-round bars (or equivalent). The bases of the columns provided restraint against lateral translation but not against rotation. A plate bolted to the two frames was used to distribute the lateral loads equally to the two frames. Deflections due to the lateral loading were measured at the level of the centerline of the beams. The portal test setup shown was tested under simultaneous vertical-service live load and lateral load applications. One test (Type B-1) was carried out under cyclic loading to obtain information on the hysteretic behavior of the load-deflection (moment-rotation) response of beam-to-column connections.

Strain and rotation gages were installed in some cases to measure the moment at the centers of posts and the relative rotation between beams and columns close to the joints, respectively. However, tests conducted at Stanford University showed that the accuracy of the M-θ relationships for individual joints obtained from portal tests depended strongly on precise measurement of beam moment. Such precision is difficult to achieve. The study further indicated that the analytical estimates of average moment and rotation evaluated from the lateral displacement measurements were reliable average values compared with the joint moments and rotations actually measured. Thus, the results from the portal tests presented in this report are based on the average moment-rotation relations determined analytically from the displacement measurements, as described in the next section.

Evaluation of the Moment-Rotation Relationship. The average moment at each of the joints can be expressed as:

$$\bar{M} = \frac{H}{2}h + V\delta \qquad (2.3)$$

where:

δ = the side sway deflection corresponding to a lateral load H applied to one portal frame

V = the axial force in a column due to vertical loads

The average joint rotation, assuming that the moments due to a lateral load are equal at each joint, is given by:

$$\theta = \frac{\delta}{h} - \frac{\bar{M}h}{3EI_c} - \frac{\bar{M}L}{6EI_b} \tag{2.4}$$

where:

I_b = moment of inertia of beam

I_c = moment of inertia of column

E = the modulus of elasticity

L = the length of beam plus d_c

Results. Table 2.3 presents the member properties (I_b and I_c), the estimated K_θ for elastic analysis and design, the failure moments, and the modes of failure for the five rack types tested, Types A, B, C, D, and F. The member sizes used in Types A-1, B-1, C-1, and F-1 were identical for both cantilever and portal tests. Thus, as expected, the modes of failure for each rack type were very similar to their counterparts observed in the cantilever tests. All portal tests were conducted monotonically. On the Type B-1 rack, a cyclic-loading test was also conducted.

Figure 2.28 shows a comparison of average M-θ relationships for Type A-1 tested with different simulated vertical live loads (half and full design live loads). In spite of the large difference in simulated vertical loads between the two cases, the M-θ curves were quite similar. This is because the end moments induced from the vertical loads were very small (flexible beam-column connections) compared to moments due to lateral loads.

The results from all portal tests using monotonic loading are shown in Figures 2.28 and 2.29 and 2.31 through 2.36. The M-θ curves shown in these figures indicate early nonlinear behavior, and, in most cases, the K_θ values for elastic analysis and design were difficult to define.

Figure 2.30 presents the M-θ relationships of the cyclic-loading test performed on Type B-1. Loading histories were applied with symmetric cycles of stepwise increasing displacement amplitude, and three cycles of equal amplitude were conducted in each step. As observed by Krawinkler et al. of Stanford University, during the cyclic loading test, cracking occurred at the welds between the beams and connectors at a displacement amplitude of 1.5 in., which was smaller than the displacement at which cracking occurred in the monotonic test of Type B-1. The cyclic-loading test further indicated that the strength and ductility obtained from monotonic loading tests might not be sufficient to determine the behavior of a rack assembly under seismic excitation.

Figures 2.37 to 2.39 present comparisons of the M-θ curves from the cantilever and portal tests for Types A-1, B-1, and F-1, respectively. It can be seen that the diagrams for both test methods are similar in shape and moment capacity. However, the results from the portal tests show a significantly higher initial stiffness. This indicates that the stiffness depends on the shear-to-moment ratio, which is substantially higher in the portal tests because of the presence of vertical loads. The figures also clearly show the early nonlinear behavior found in both test methods. The difference in initial K_θ value estimated for elastic analysis and design from both test methods was on the order of 2, as shown in Figures 2.37 to 2.39 (also compare Figures 2.2 and 2.28, 2.3 and 2.29, and 2.20 and 2.36).

2.5 The Influence of the Joint Spring Constant on Seismic Analysis and Design

As stated previously, the objective of the subassembly tests was to provide mathematical modeling guidelines regarding joint looseness and joint capacity. This section presents a brief summary of results from a seismic analysis of the standard pallet rack using two different values of K_θ. It is intended to study the influence of K_θ values on the selection of member sizes on the basis of the 1976 *UBC* seismic requirements. The detailed procedures of seismic analysis will be discussed in Chapter 7.

The standard pallet rack (using the Type B-1 components) used in the shaking table tests (see Chapter 4) was used for this analysis. Two values of K_θ were selected for study: 500 kip-in./rad. and 1,000 kip-in./rad. The following assumptions were used: (1) the centerline dimensions were used; (2) the section properties were assumed to be those supplied by the manufacturer; (3) the column base was assumed to be pinned; (4) the base shear was assumed to be $V = CW$ where $C = \frac{1}{15\sqrt{T}}$, and W = total weight; (5) the p-δ effect was considered.

As might be expected, the story displacements were quite sensitive to the joint springs assigned. However, the difference in calculated base shears and member forces was not very significant. In this case study, the 50% decrease in the value of K_θ used resulted in about a 5% to 6% increase in critical member forces.

2.6 Summary and Conclusions

Although the subassembly testing reported here was limited to 24 types from 7 manufacturers, it is expected that much of what has been learned can be applied to other rack assemblies from different manufacturers. That is, the validity of these tests has been demonstrated in this study, and, if moment-rotation flexibility information is needed for other types of rack assemblies, these same simple and economical test procedures can be used. The summary of this report is rather brief; readers are urged to refer to the original reports for more detailed information.

Cantilever Tests:

- In all tests, the strength of the rack assembly was governed by the connection rather than by the beam itself. Deformation in the connectors, tearing of the column perforations, and fracturing of the beam-connector weld were commonly observed.
- In most test cases, the moment-rotation relationships are very nonlinear. It is sometimes difficult to define a suitable linear range for elastic design and analysis.
- The stiffness and strength properties are significantly different for positive and negative moments.
- The stiffness and strength properties differ with the connectors used, increasing with the connector length (Type B-1 versus Type B-2). The modes of failure are also different for both cases.
- The stiffness and strength properties differ for each combination of beam and column; in general, they increase with the moments of inertia of beam and column (Type B-5 versus Type B-6; Type B-7 versus Type B-8; Type B-2 versus Type B-3; Type B-4 versus Type B-5).
- The values of K_θ estimated for elastic analysis and design are in the range of 300 to 1,000 kip-in./rad from various combinations of rack components, with the exception of very high K_θ values for Type D racks made of hot-rolled structural steel.

- Tests at Stanford University show very good agreement (within 10%) between the measured rotations and those computed analytically from Equation (2.2). These results indicate that rotational measurements may not be necessary in the cantilever tests, which greatly simplifies the test procedures.

Portal Tests:

- The results of tests of Type A-1 racks show no significant difference in the stiffness and strength properties when the moment-to-shear ratio is varied (i.e., half and full vertical load cases).
- The modes of failure in the portal tests are similar to those observed in the cantilever tests. The portal test is essential to give an overall picture (e.g., joint capacity versus stiffness). However, to construct a complete M-θ curve up to failure, the applied lateral load has to be increased to as high as 100% of the vertical load, which is not realistic.
- In all portal test cases, high initial stiffness and early nonlinear behavior were observed.
- Tests conducted at Stanford University show that the analytical estimates of average moment and rotation estimated from the lateral displacement measurements compared favorably with the actual measured joint moments and rotations.

Cantilever versus Portal Tests:

- The cantilever test is simple and economical; the portal test is costly and complex for industry to perform.
- The portal test is essential to give an overall picture (e.g., joint capacity versus stiffness). However, to construct a complete M-θ curve up to failure, the applied lateral load has to be increased to as high as 100% of the vertical load, which is not realistic.
- In general, the M-θ relationships for both test methods are rather similar in shape and moment capacity. However, the stiffness from the cantilever test is smaller than that from the portal tests. The difference in K_θ values estimated for elastic analysis and design is on the order of 2.
- The study of the influence of different values of K_θ (500 versus 1,000 kip-in./rad), used in accordance with the 1976 *UBC* seismic design requirements, shows that the member forces are approximately 5% to 6% larger when K_θ = 500 kip-in./rad.

- The cantilever test is sufficient for practical engineering purposes. The test is simple and requires only lateral-load and displacement measurements, which are easy to carry out. However, the test should be conducted for loading in both the positive and the negative directions.
- To predict the seismic responses and capacity of full-scale rack structures analytically, the behavior of beam-to-column connections can be modeled by linear or nonlinear rotational springs obtained experimentally for positive and negative moments.

TABLE 2.1

CONNECTIONS AND SECTION PROPERTIES OF RACK COMPONENTS

Rack Type	Shape		Moment of Inertia (in.^{4})		Connector Length (in.)	Connections	Remarks
	Column	Beam	Column	Beam			
A-1	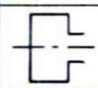	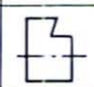	1.037	2.664	7	hook-type grips	cold-formed steel
B-1	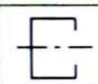	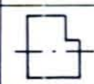	1.144	3.265	8	stud-type grips	"
B-2	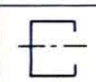	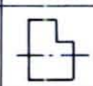	1.144	2.081	6	"	"
B-3	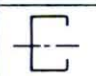	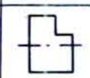	0.857	2.081	6	"	"
B-4	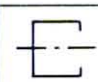	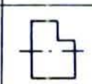	3.316	7.228	6	"	"
B-5	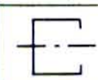	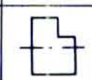	1.316	7.228	6	"	"
B-6	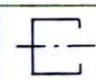	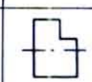	1.316	0.739	6	"	"
B-7	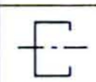	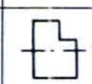	0.611	0.739	6	"	"
B-8	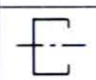	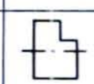	0.611	1.948	6	"	"
B-9	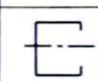	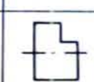	3.316	1.947	6	"	"
C-1	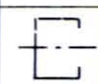		2.206	1.175	5-1/4	hook-type grips	"
C-2	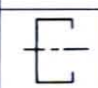	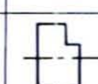	0.691	5.549	6	"	"

TABLE 2.1 (Continued)

Rack Type	Shape		Moment of Inertia ($in.^4$)		Connector Length (in.)	Connections	Remarks
	Column	Beam	Column	Beam			
D-1	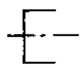	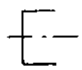	1.660	1.660	7	bolts	hot-rolled steel
D-2	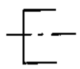	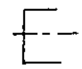	3.850	3.850	7	"	"
D-3	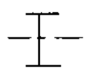	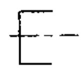	1.380	1.660	6	"	"
D-4	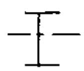	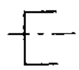	2.520	1.660	6	"	"
D-5	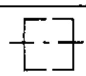	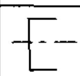	3.320	1.660	7	"	"
D-6	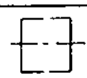	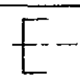	3.320	3.850	7	"	"
E-1	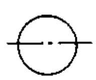	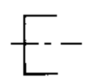	0.916	1.660	6	"	beam: hot-rolled; column: cold-formed
E-2	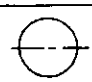	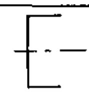	0.916	7.500	6	"	"
E-3	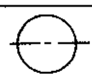	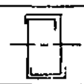	0.916	1.220	6	"	cold-formed steel
E-4	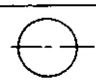	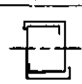	0.916	4.780	6	"	"
F-1	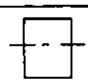	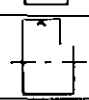	0.671	2.319	6-1/2	hook-type grips	"
G-1	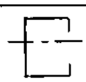	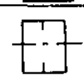	1.855	2.516		bolts	"

TABLE 2.2

SUMMARY OF CANTILEVER TEST RESULTS

Rack Type	Moment of Inertia (in.^{4})		K_θ (kip-in./rad)	M_f (kip-in.)	Mode of Failure
	Column	Beam			
A-1	1.037	2.664	600	36.0-41.0+	The hooks pulled out of the column perforations.
B-1	1.144	3.265	1,000	29.0-33.0+	Fracture of the connector weld.
B-2	1.144	2.081	470	19.2	Distortions of the connector and at the column perforations. The upper stud broke.
B-3	0.857	2.081	350	19.2	Tearing of the column perforations.
B-4	3.316	7.228	1,000	19.7	The upper stud pulled out.
B-5	1.316	7.228	800	19.7	The stud pulled out. Tearing of the column perforations.
B-6	1.316	0.739	450	16.0	"
B-7	0.611	0.739	300	13.3	Tearing of the column perforations.
B-8	0.611	1.948	400	18.0	"
B-9	3.316	1.948	750	21.0	The stud pulled out.
C-1	2.206	1.175	200	5.0-18.0+	Fracture of the connector weld.
C-2	0.691	5.549	750	22.3	The hooks pulled out.
D-5	3.320	1.660	4,500	38.2	The connector deformed and cracked through.
D-6	3.320	3.850	2,500	65.0	The connector deformed.
E-1	0.916	1.660	900	31.6	"
E-2	0.916	7.500	750	24.5	"
E-3	0.916	1.220	750	24.6	"
E-4	0.916	4.780	600	24.9	"
F-1	0.671	2.319	750	18.0-23.0+	Distortions of the connector and at the column perforations.
G-1	1.855	2.516	350	20.4	The bolt pulled through.

K_θ = estimated joint spring for elastic analysis and design

M_f = failure moment, defined as the final test loading when severe damage was observed

TABLE 2.3

SUMMARY OF PORTAL TEST RESULTS

Rack Type	Moment of Inertia ($in.^4$)		K_θ (kip-in./rad)	M_f (kip-in.)	Mode of Failure
	Column	Beam			
A-1	1.037	2.664	1,000	35.0	The connectors deformed.
B-1	1.144	3.265	2,000	30.0 28.0	Fracture of the connector weld.
C-1	2.206	1.175	200	10.0	"
D-1	1.660	1.660	500	57.9	The connectors deformed and cracked.
D-2	3.850	3.850	--	36.7	The connectors deformed.
D-3	1.380	1.660	600	33.0	The connectors deformed and the connector finger pulled out from the slot.
D-4	2.520	1.660	--	32.0	"
F-1	0.671	2.319	1,250	20.0	Distortions of the connector and at the column perforations.

K_θ = estimated joint spring for elastic analysis and design

M_f = failure moment, defined as the final test loading when severe damage was observed

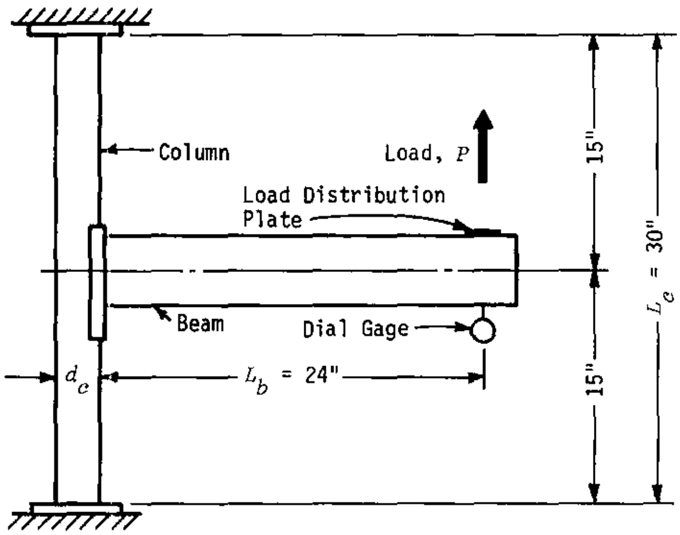

FIGURE 2.1 CANTILEVER TEST SETUP

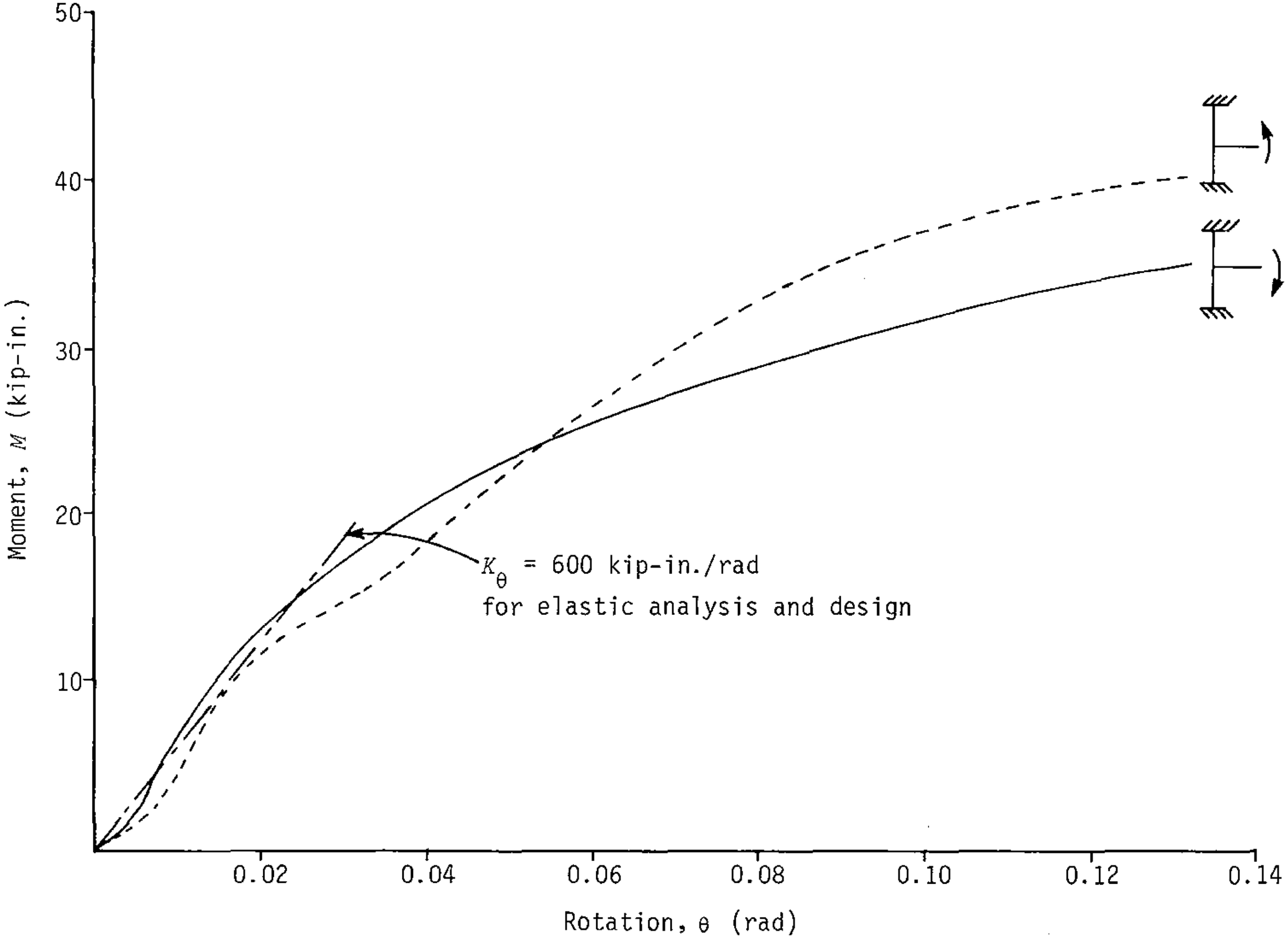

FIGURE 2.2 MOMENT-ROTATION CURVES FOR CANTILEVER TESTS OF RACK TYPE A-1

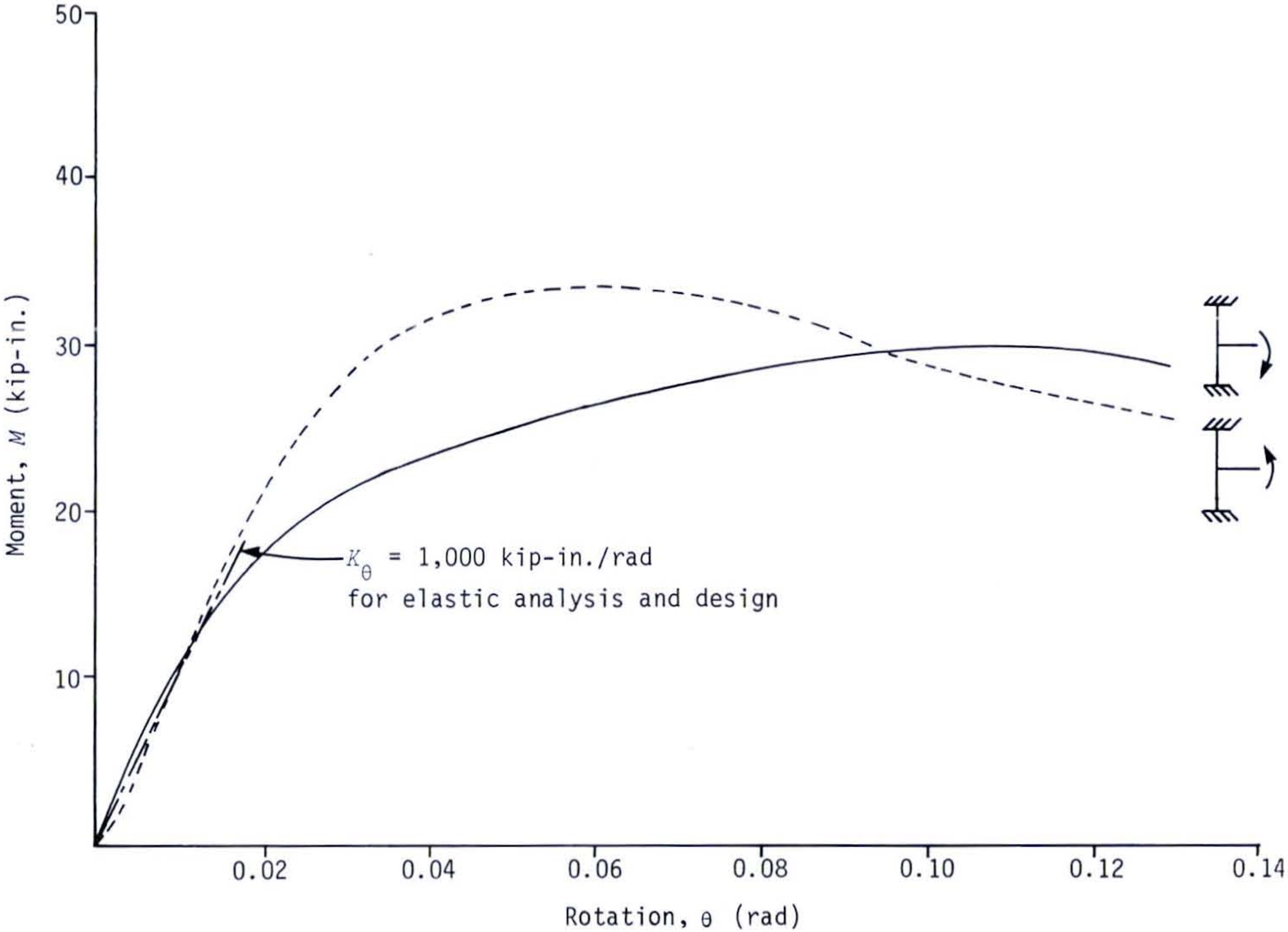

FIGURE 2.3 MOMENT-ROTATION CURVES FOR CANTILEVER TESTS OF RACK TYPE B-1

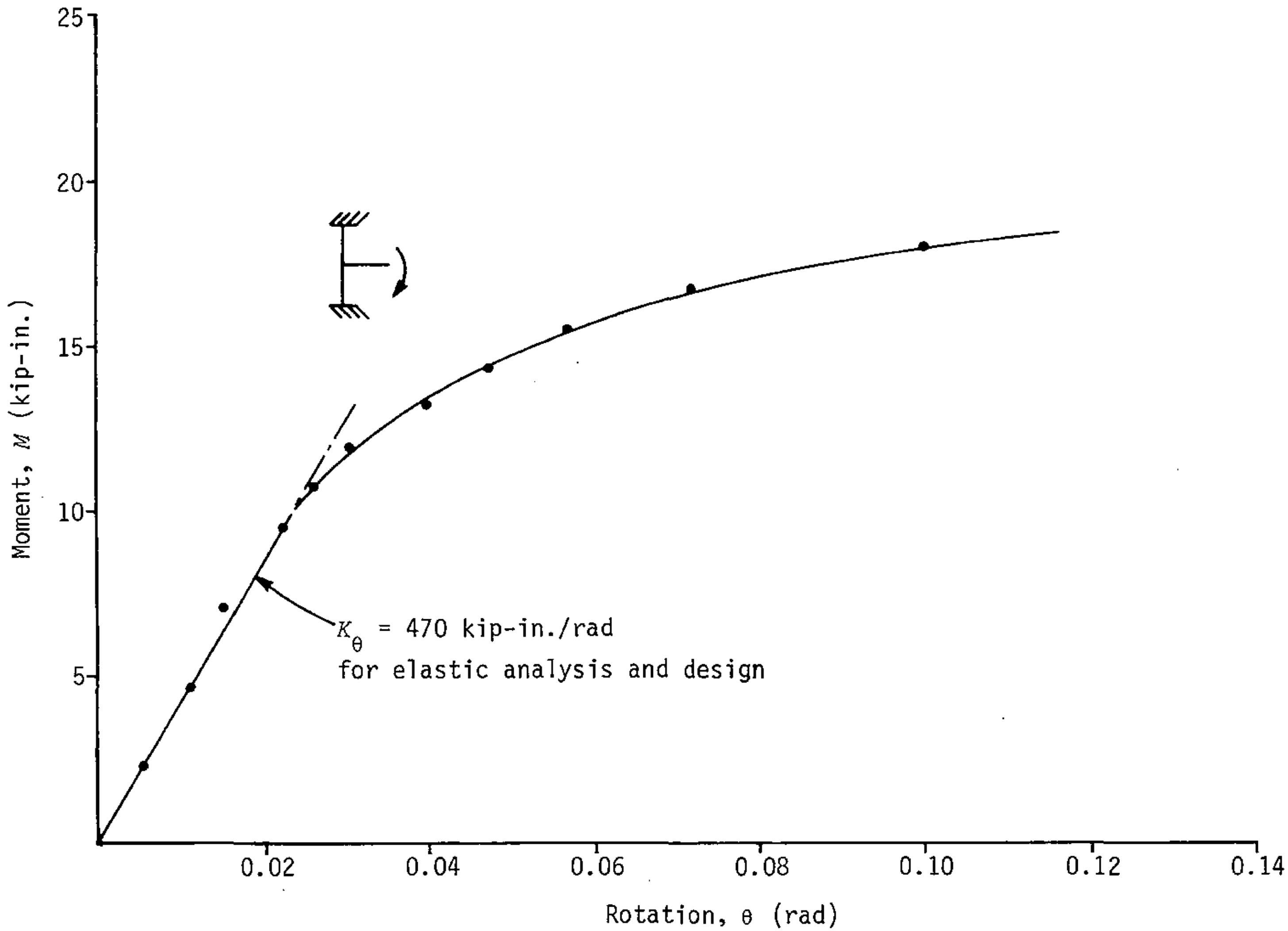

FIGURE 2.4 MOMENT-ROTATION CURVE FOR CANTILEVER TEST OF RACK TYPE B-2

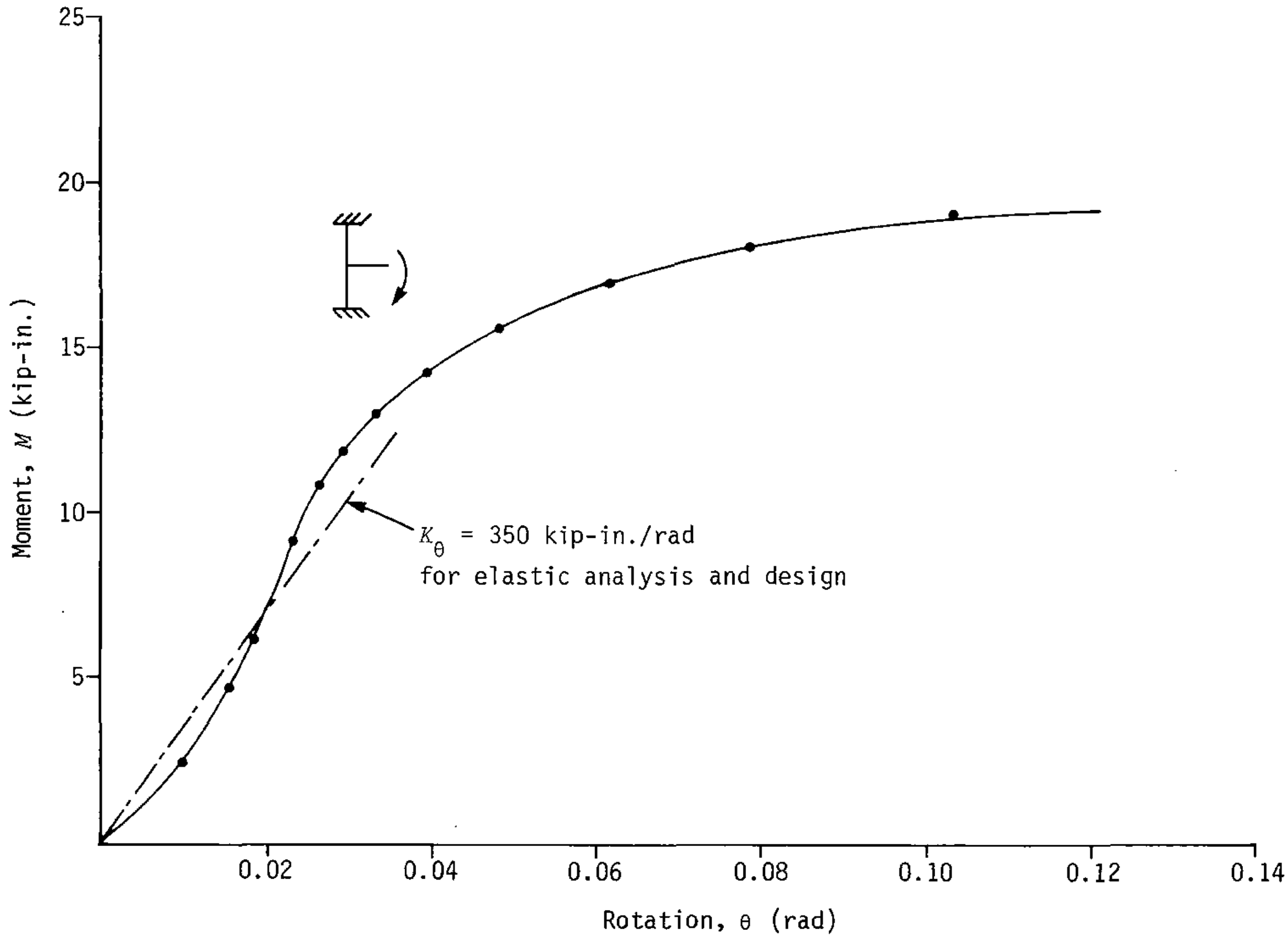

FIGURE 2.5 MOMENT-ROTATION CURVE FOR CANTILEVER TEST OF RACK TYPE B-3

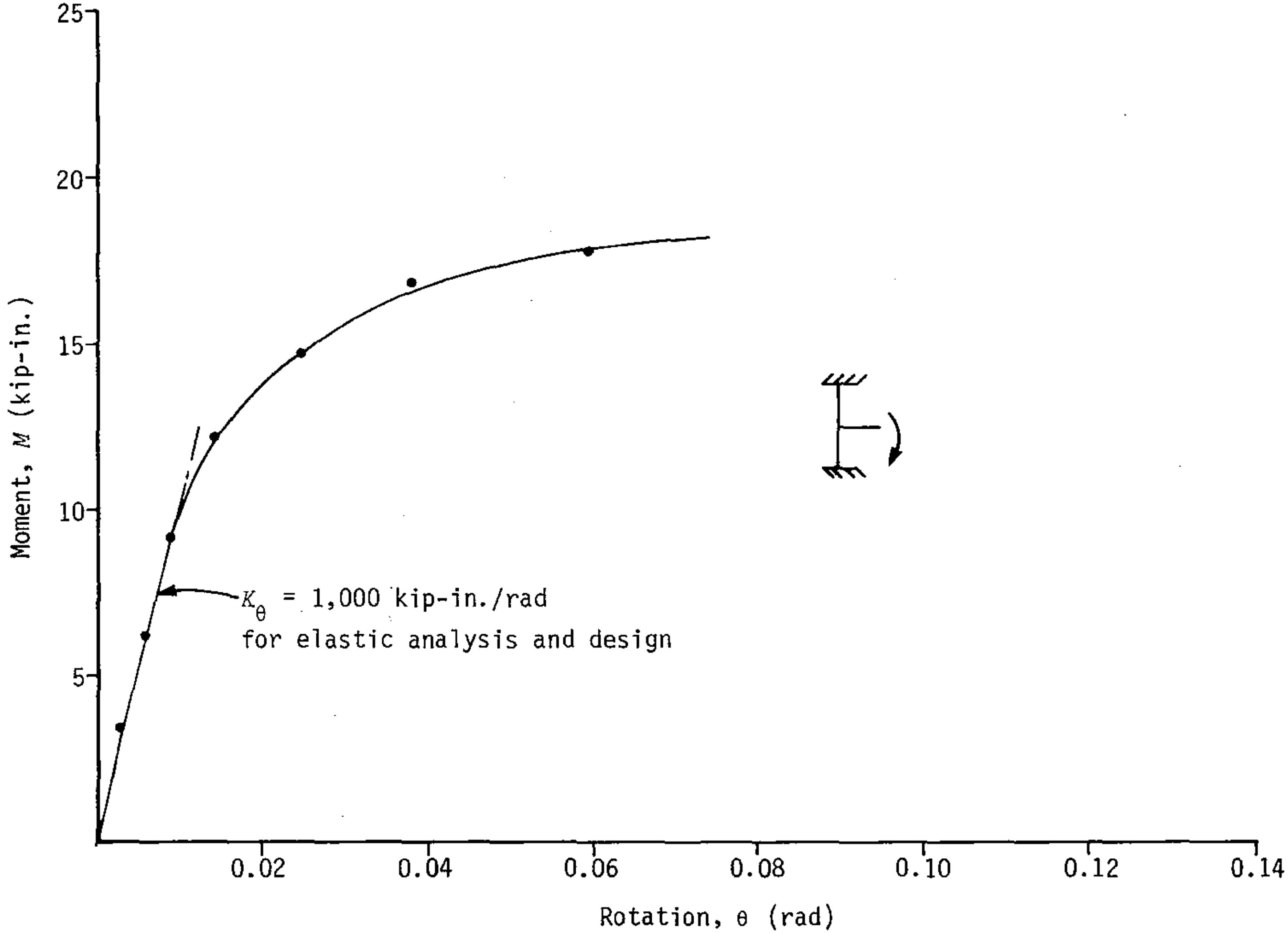

FIGURE 2.6 MOMENT-ROTATION CURVE FOR CANTILEVER TEST OF RACK TYPE B-4

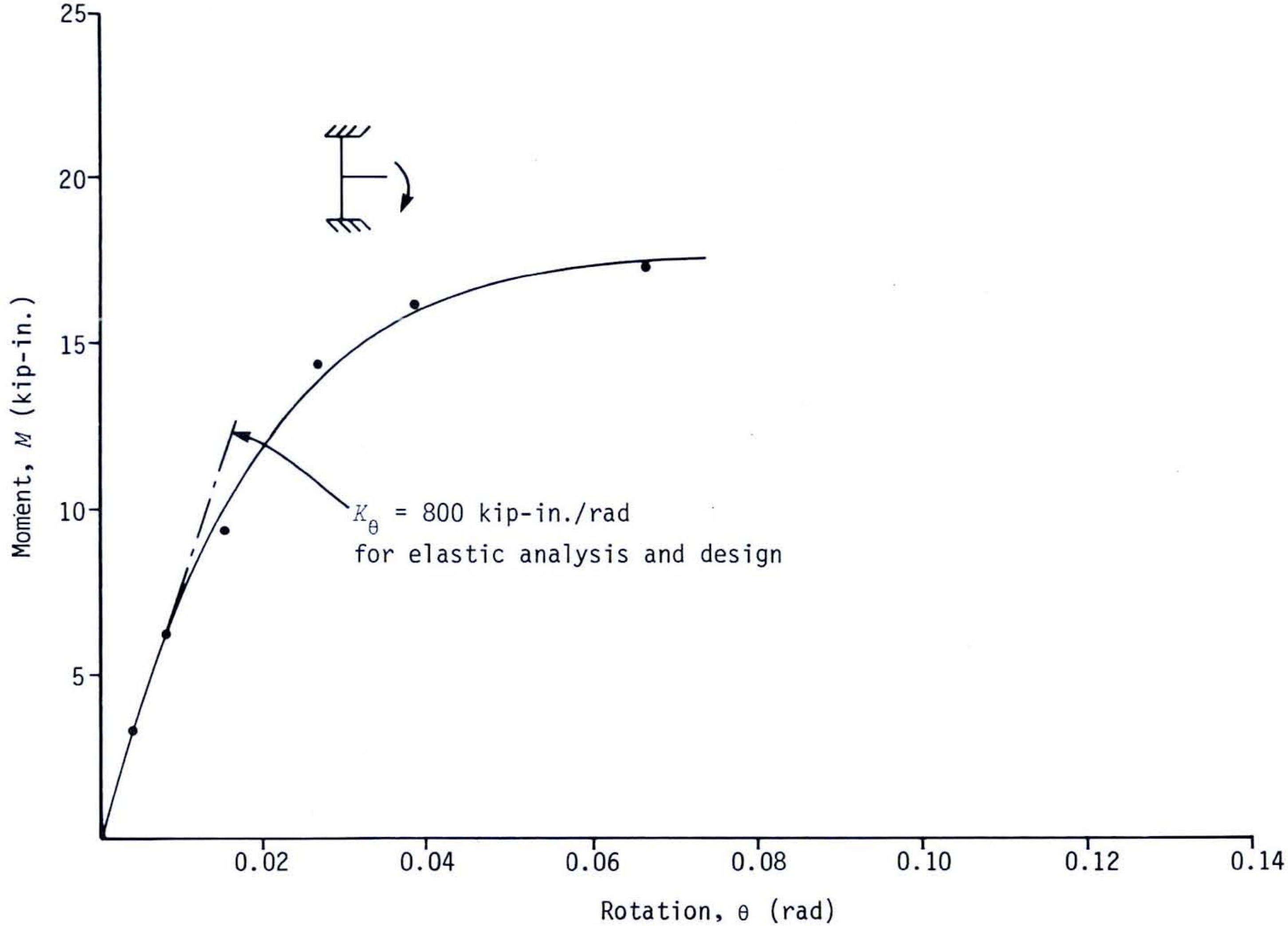

FIGURE 2.7 MOMENT-ROTATION CURVE FOR CANTILEVER TEST OF RACK TYPE B-5

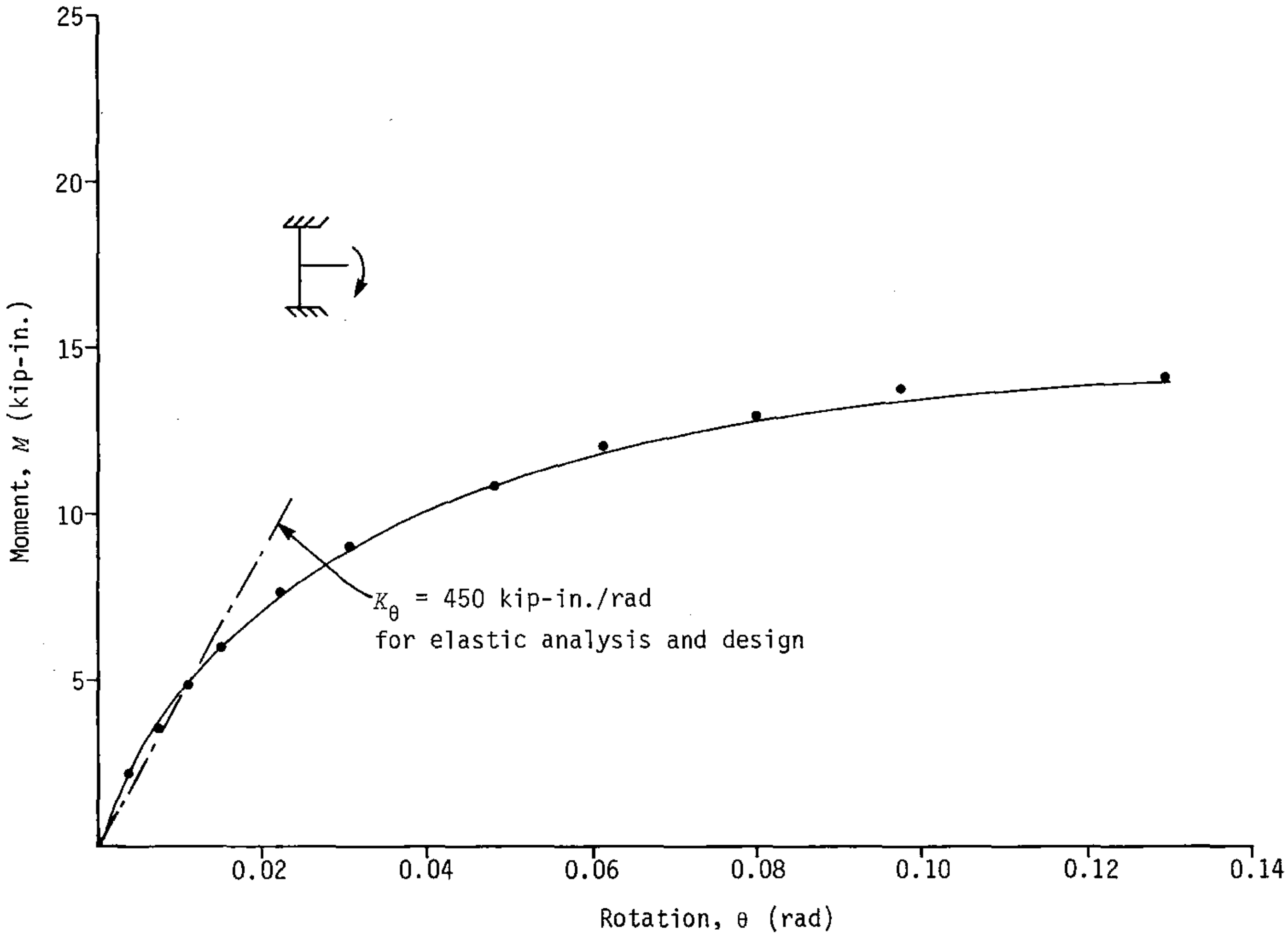

FIGURE 2.8 MOMENT-ROTATION CURVE FOR CANTILEVER TEST OF RACK TYPE B-6

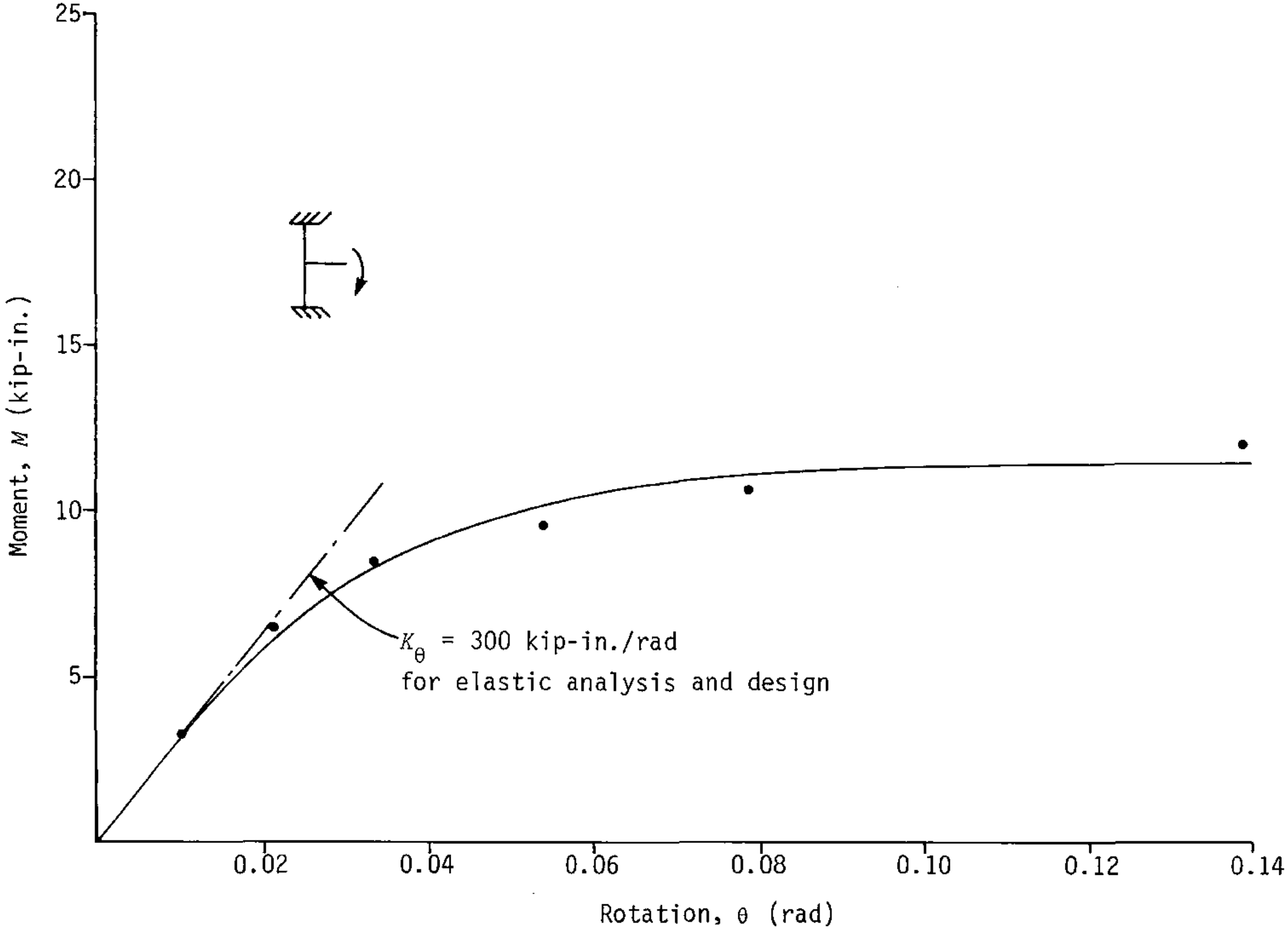

FIGURE 2.9 MOMENT-ROTATION CURVE FOR CANTILEVER TEST OF RACK TYPE B-7

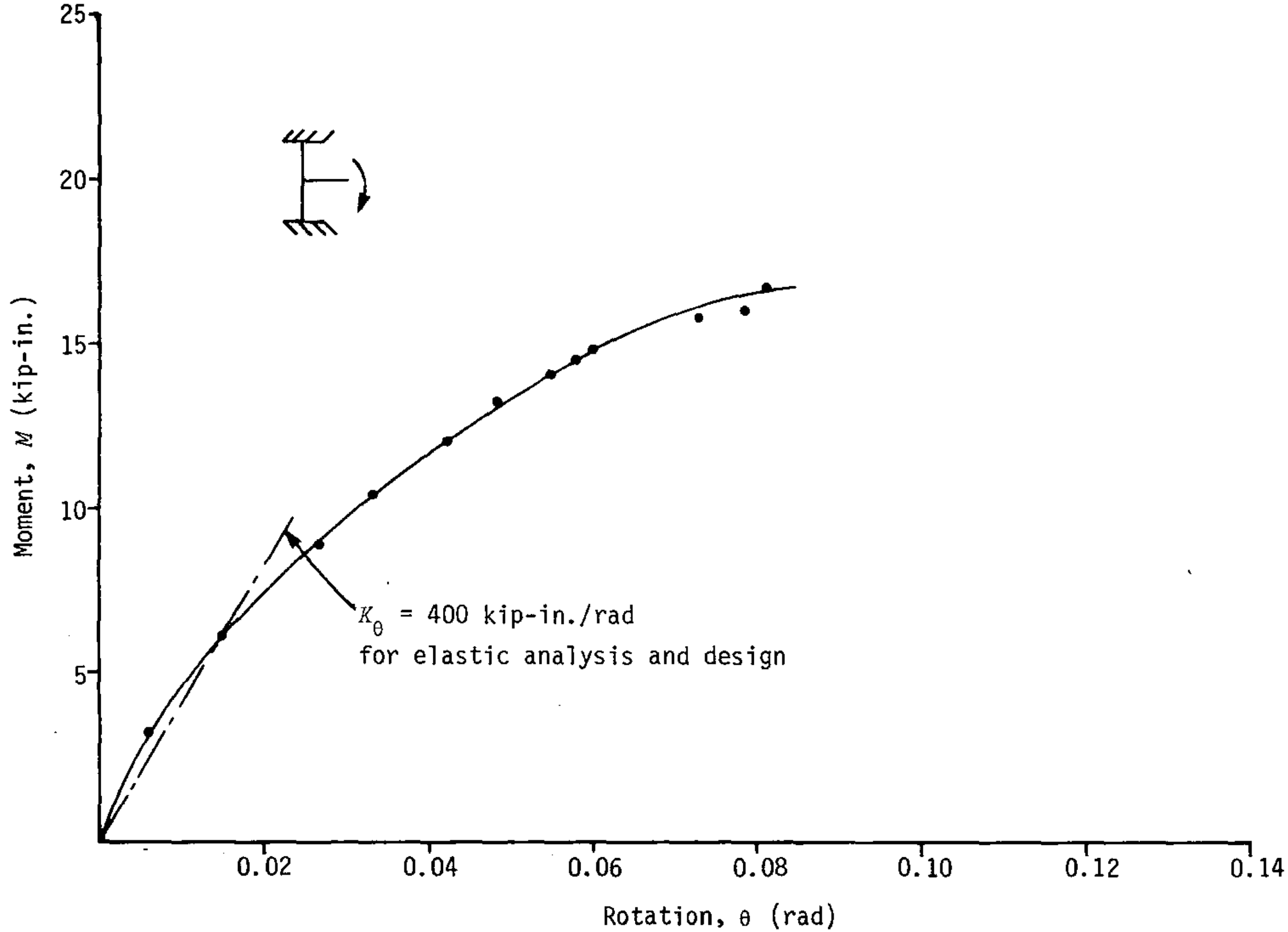

FIGURE 2.10 MOMENT-ROTATION CURVE FOR CANTILEVER TEST OF RACK TYPE B-8

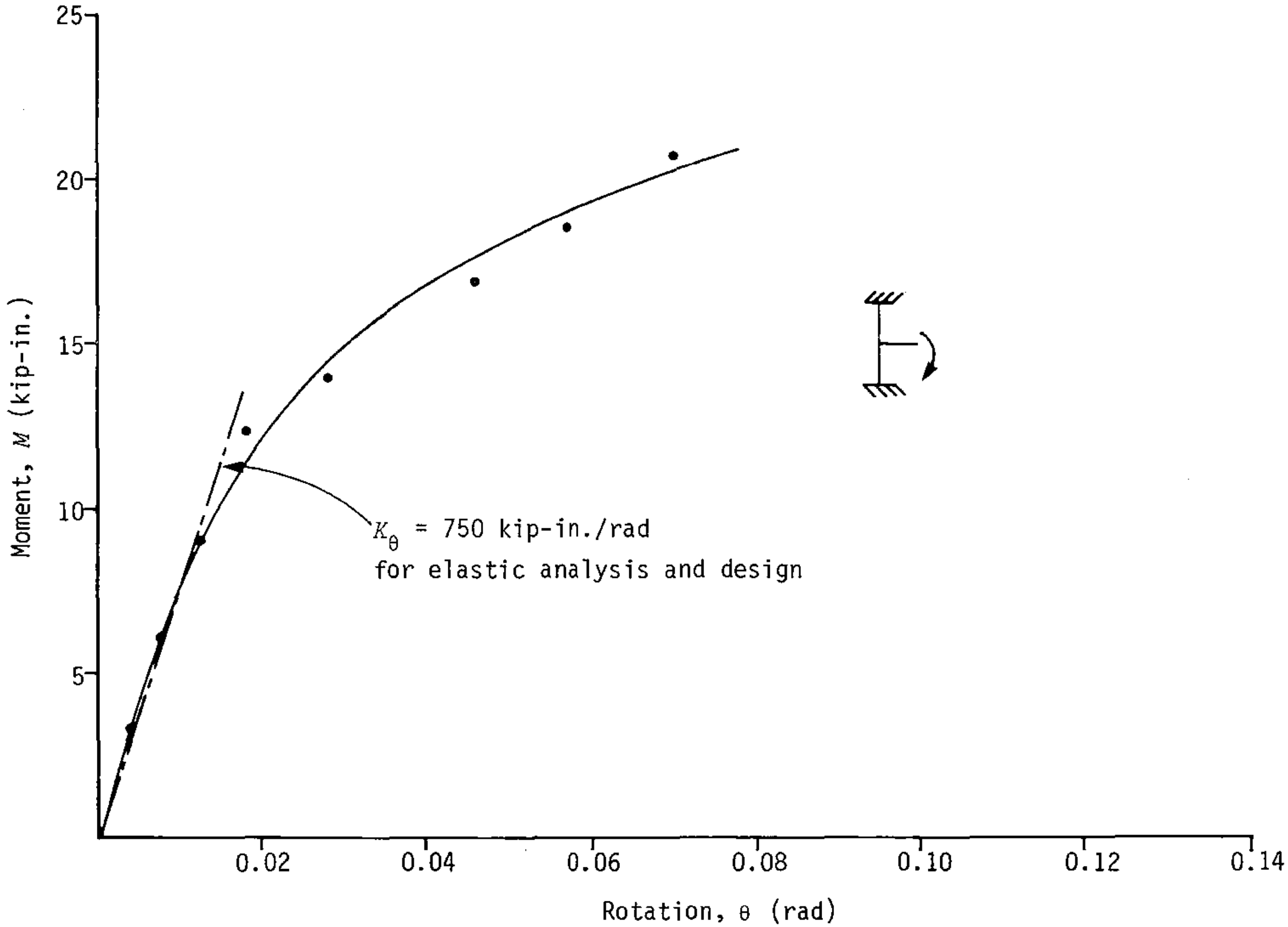

FIGURE 2.11 MOMENT-ROTATION CURVE FOR CANTILEVER TEST OF RACK TYPE B-9

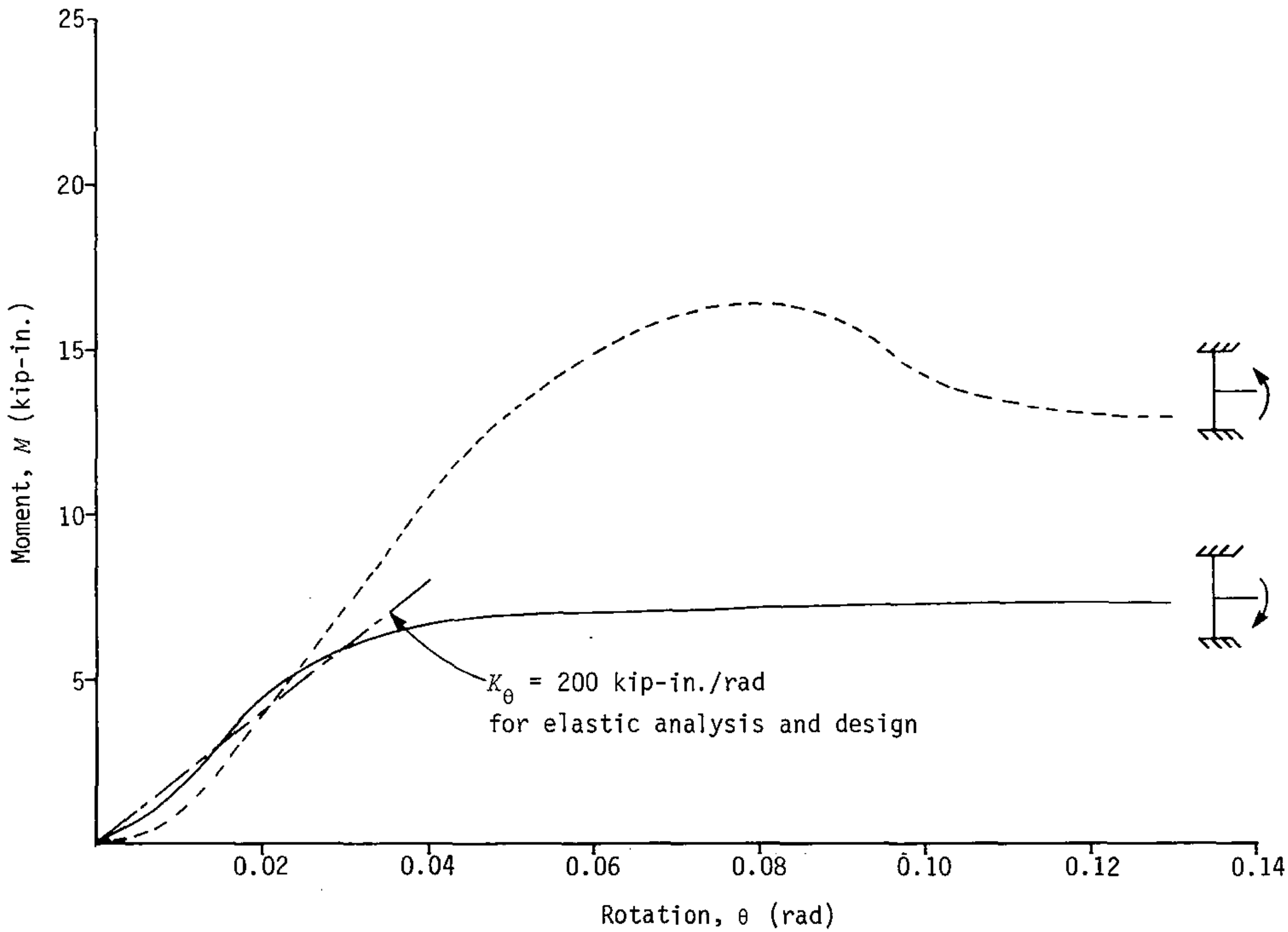

FIGURE 2.12 MOMENT-ROTATION CURVES FOR CANTILEVER TESTS OF RACK TYPE C-1

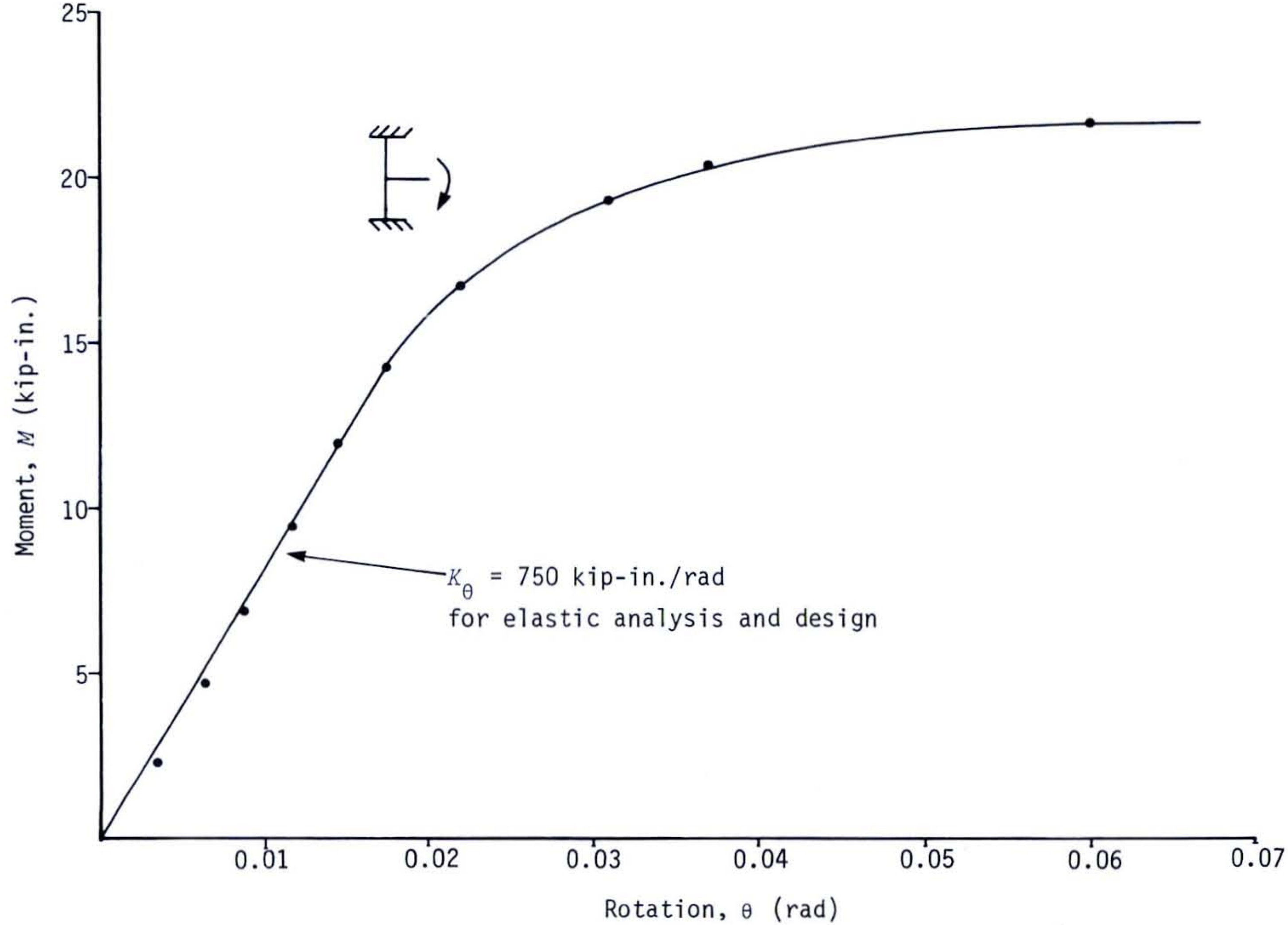

FIGURE 2.13 MOMENT-ROTATION CURVE FOR CANTILEVER TEST OF RACK TYPE C-2

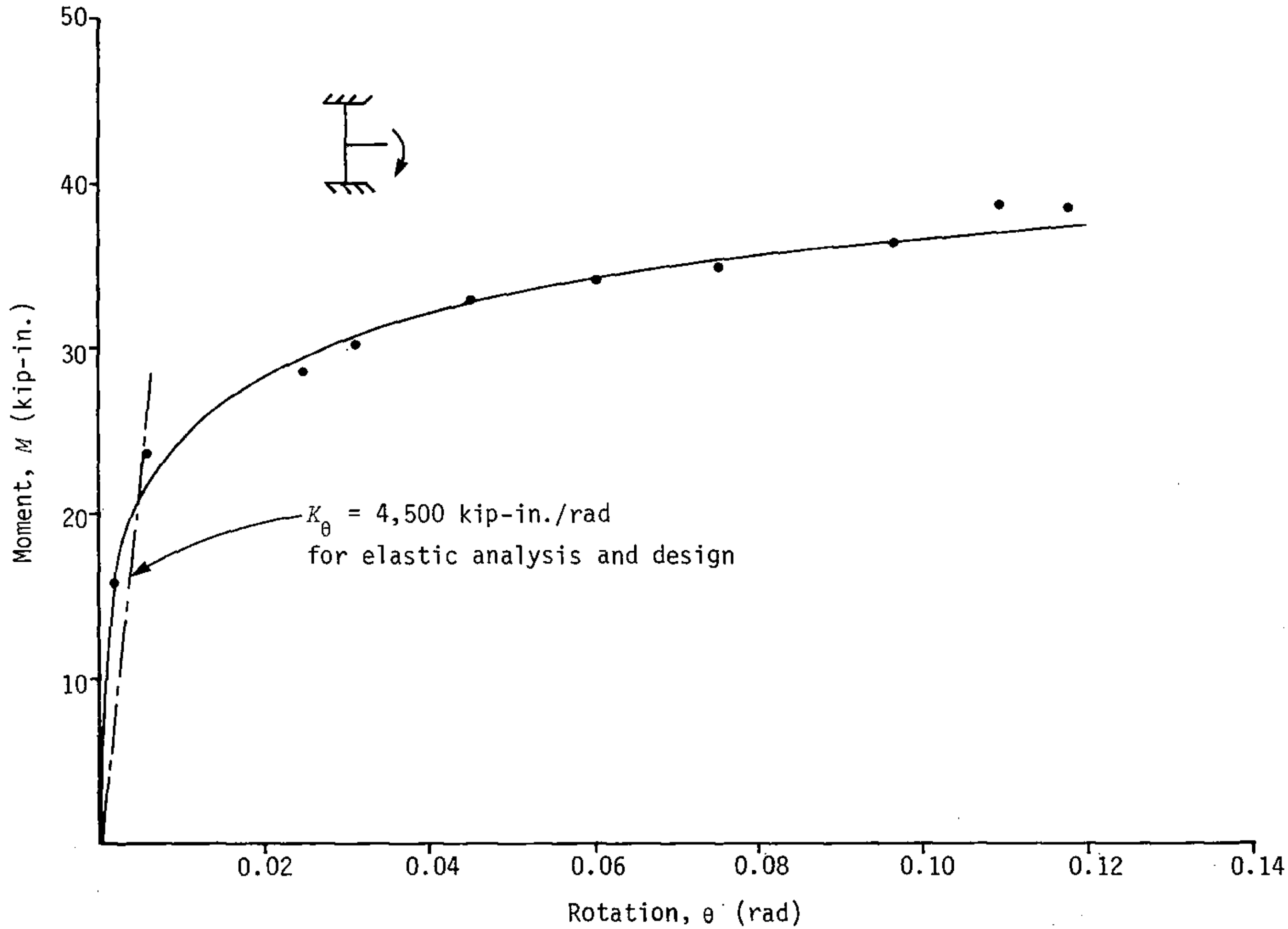

FIGURE 2.14 MOMENT-ROTATION CURVE FOR CANTILEVER TEST OF RACK TYPE D-5

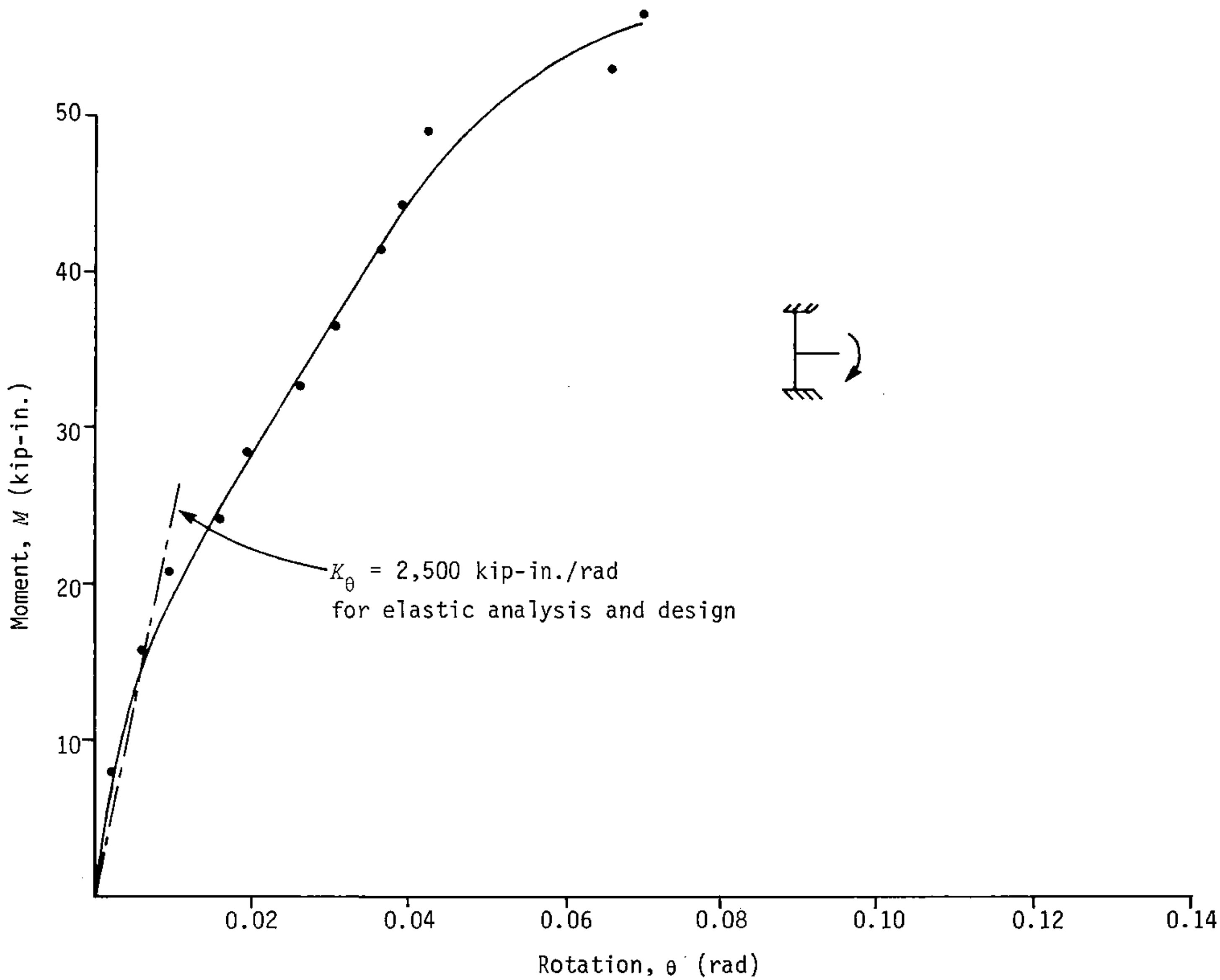

FIGURE 2.15 MOMENT-ROTATION CURVE FOR CANTILEVER TEST OF RACK TYPE D-6

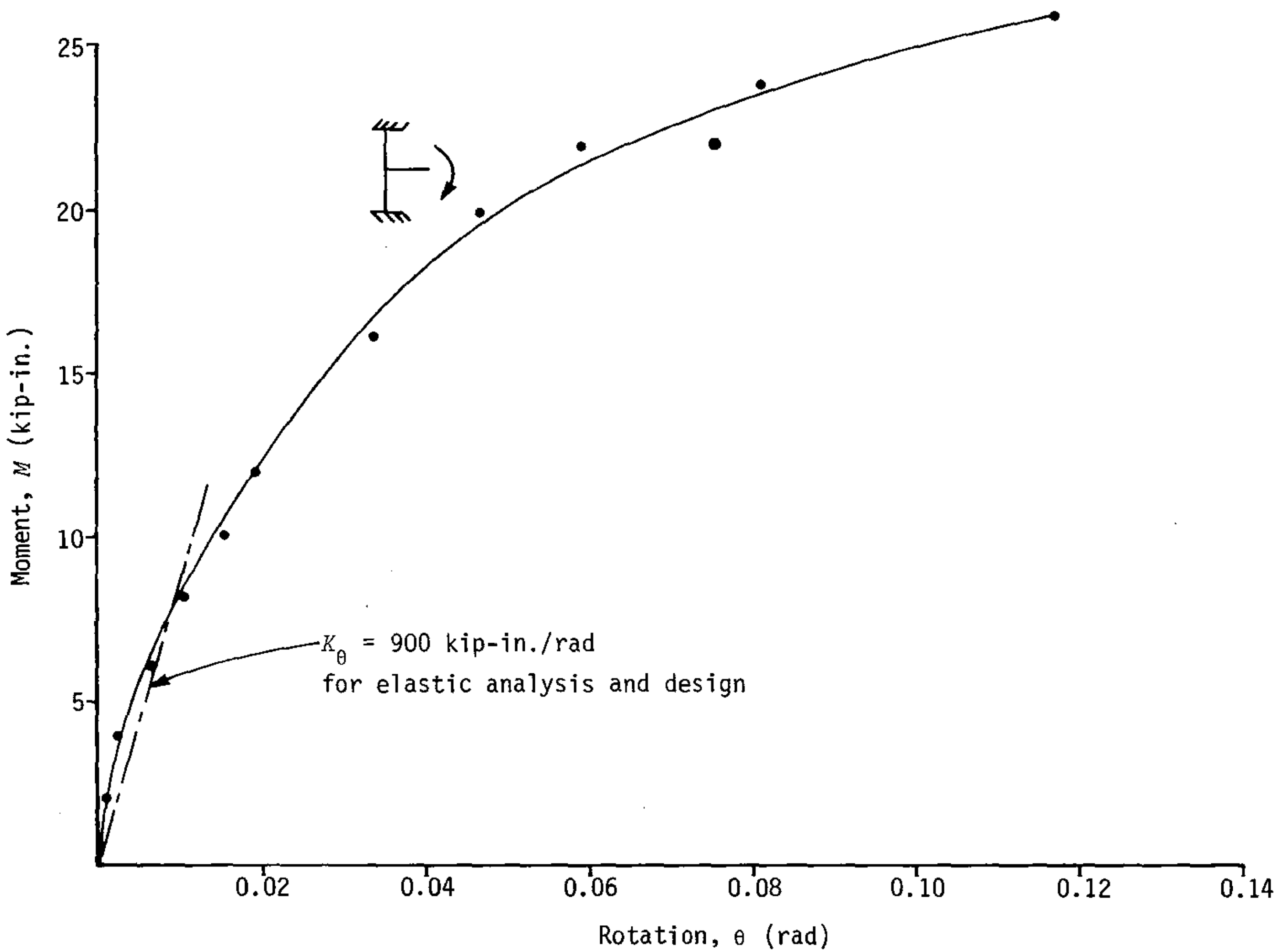

FIGURE 2.16 MOMENT-ROTATION CURVE FOR CANTILEVER TEST OF RACK TYPE E-1

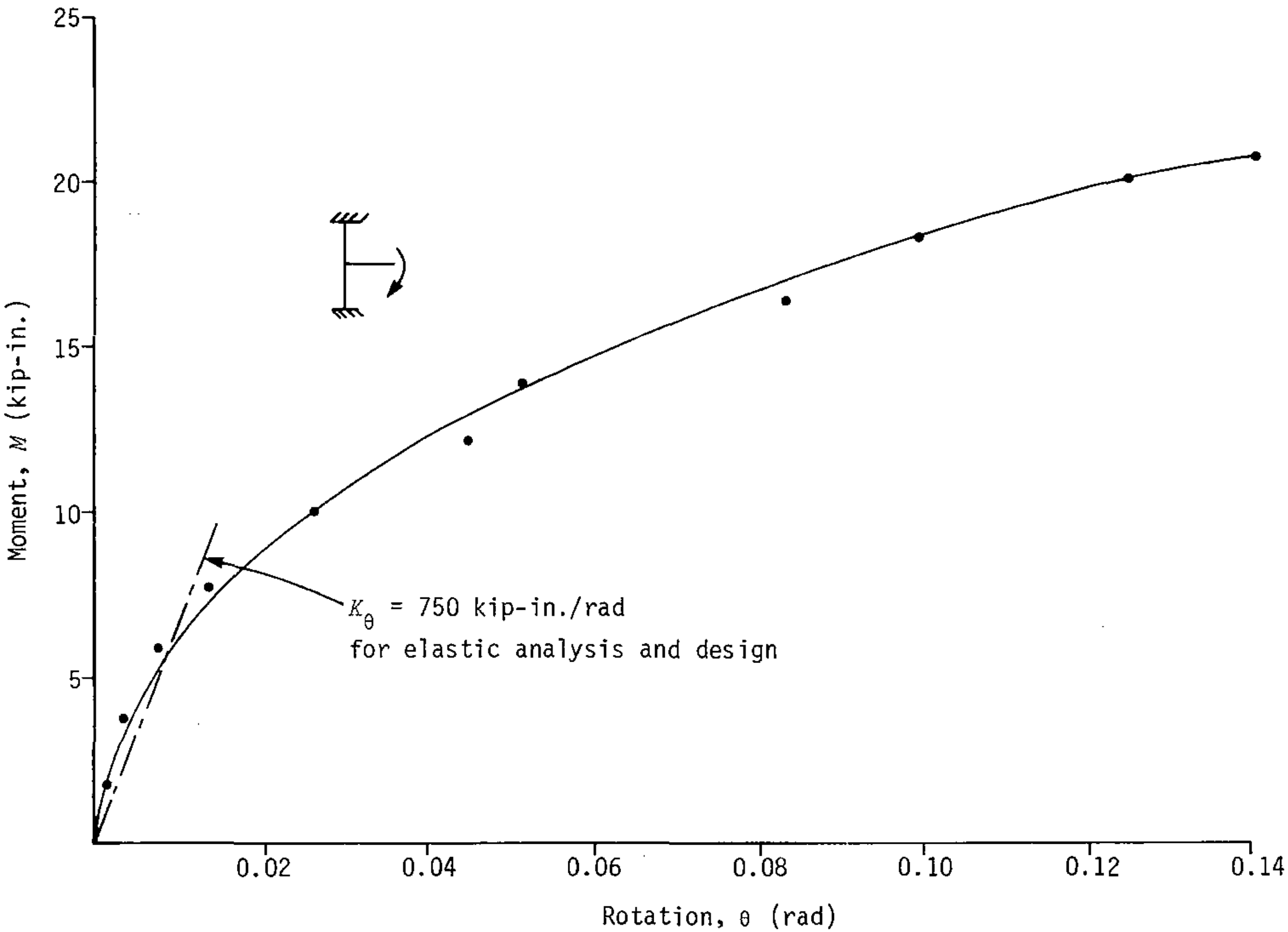

FIGURE 2.17 MOMENT-ROTATION CURVE FOR CANTILEVER TEST OF RACK TYPE E-2

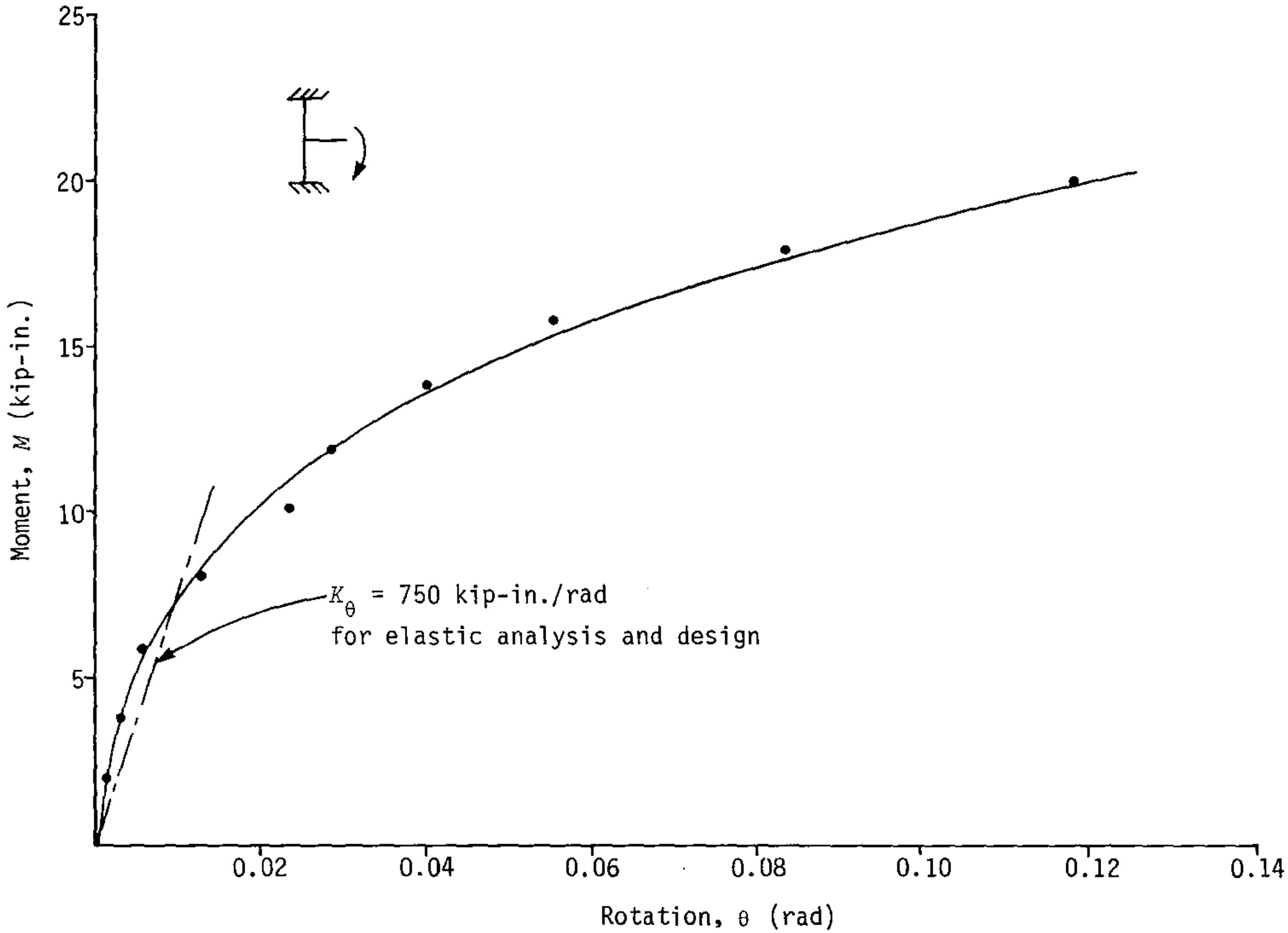

FIGURE 2.18 MOMENT-ROTATION CURVE FOR CANTILEVER TEST OF RACK TYPE E-3

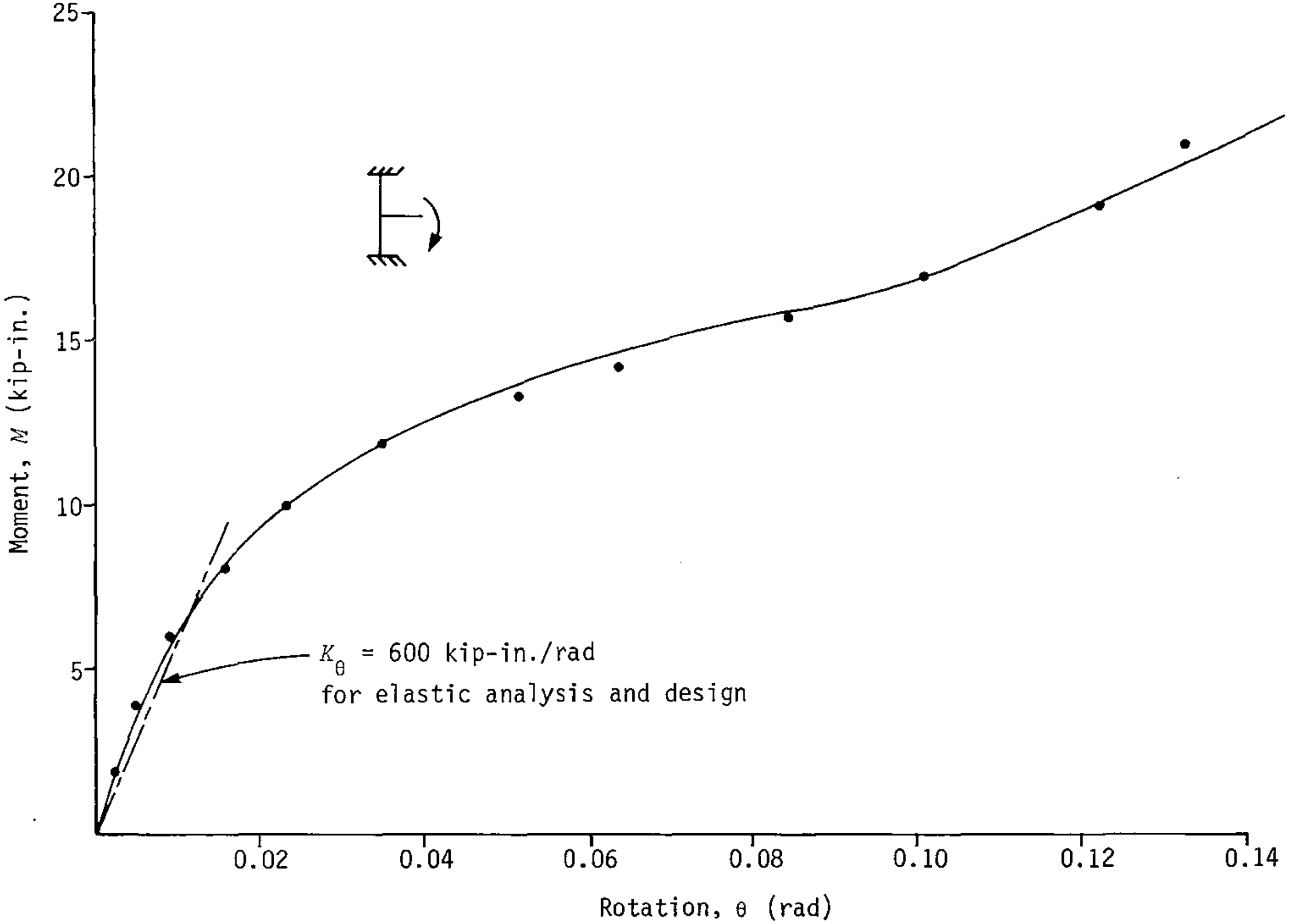

FIGURE 2.19 MOMENT-ROTATION CURVE FOR CANTILEVER TEST OF RACK TYPE E-4

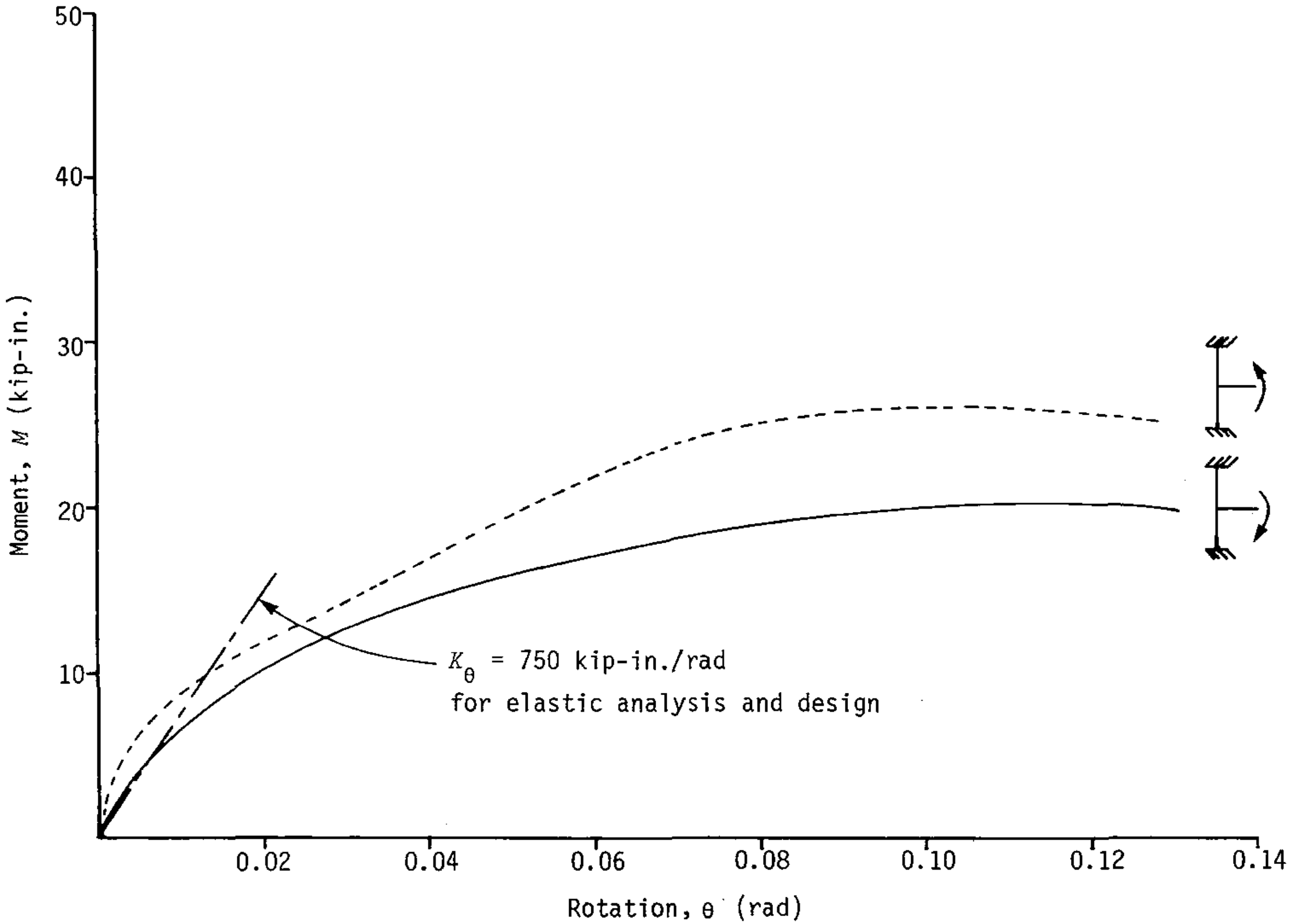

FIGURE 2.20 MOMENT-ROTATION CURVES FOR CANTILEVER TESTS OF RACK TYPE F-1

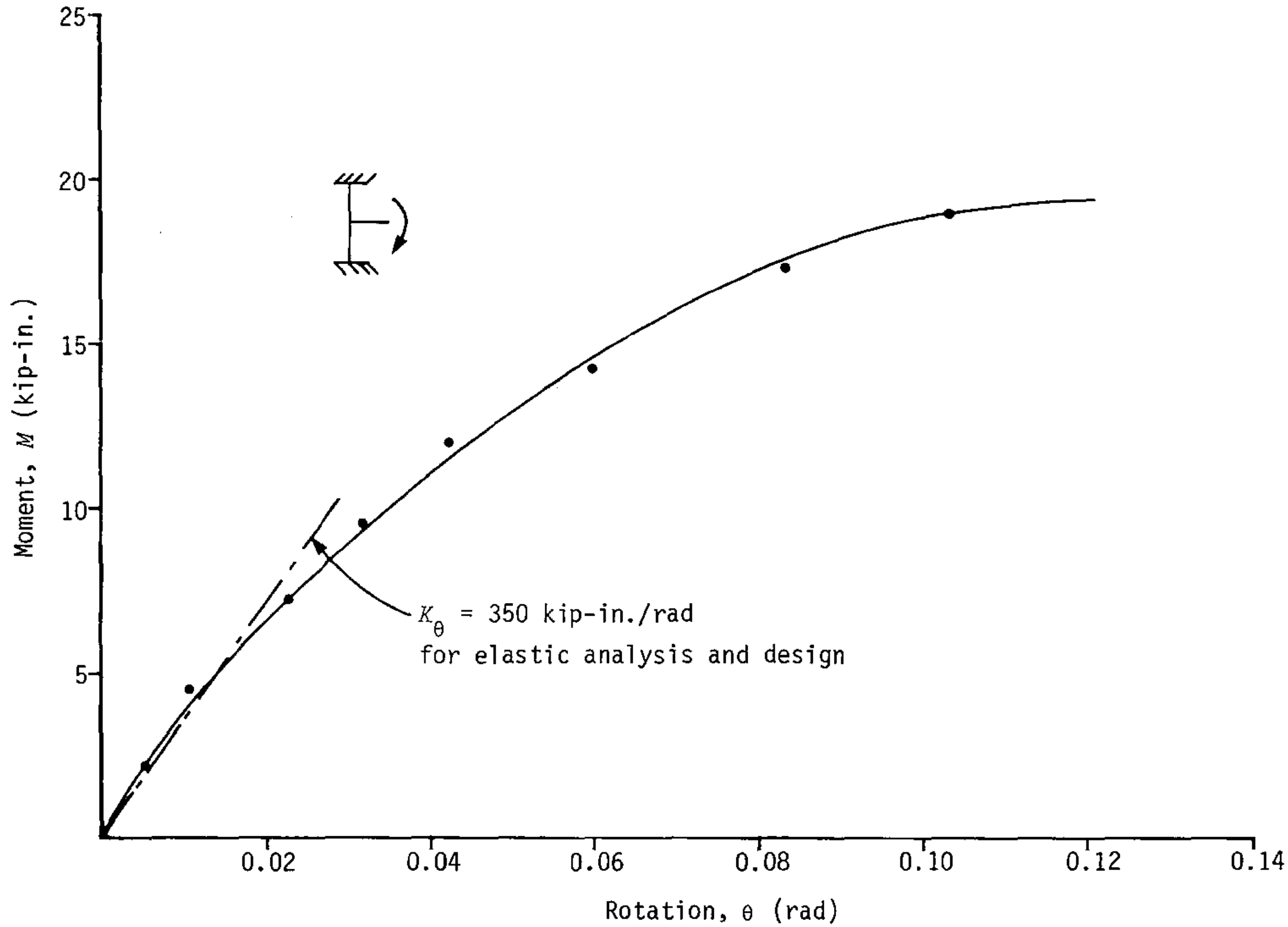

FIGURE 2.21 MOMENT-ROTATION CURVE FOR CANTILEVER TEST OF RACK TYPE G-1

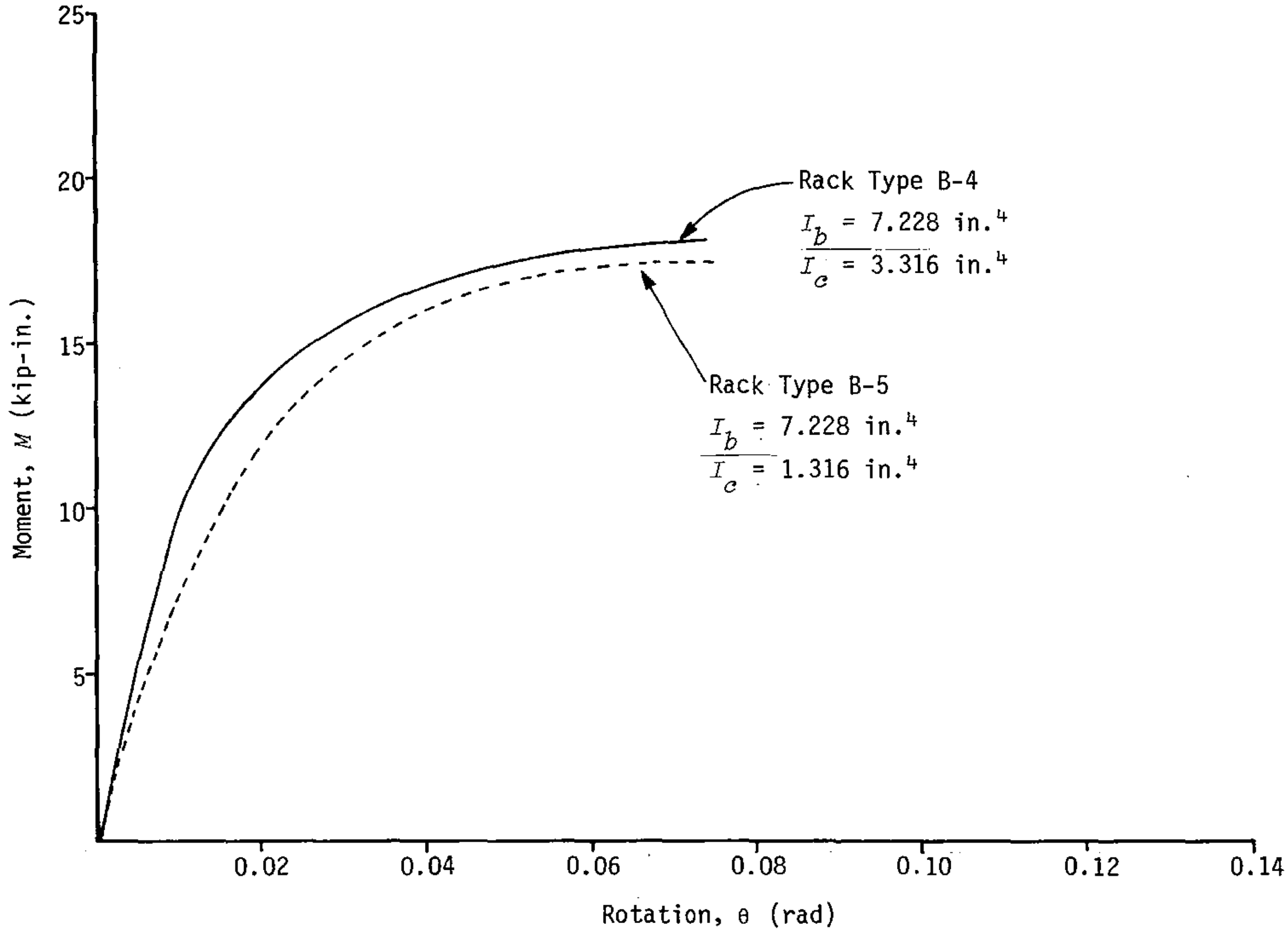

FIGURE 2.22 MOMENT-ROTATION CURVES FOR CANTILEVER TESTS OF RACK TYPES B-4 AND B-5

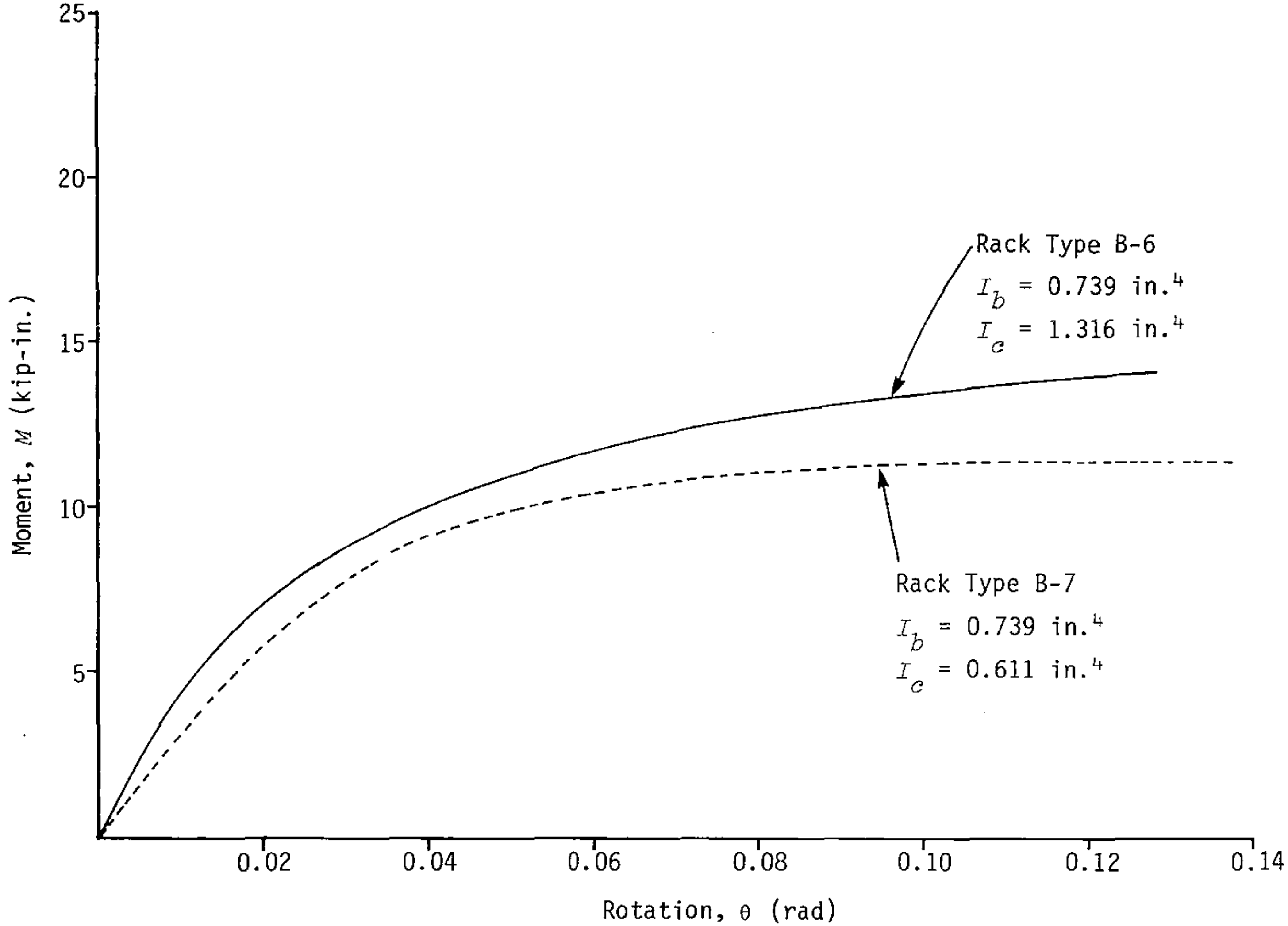

FIGURE 2.23 MOMENT-ROTATION CURVES FOR CANTILEVER TESTS OF RACK TYPES B-6 AND B-7

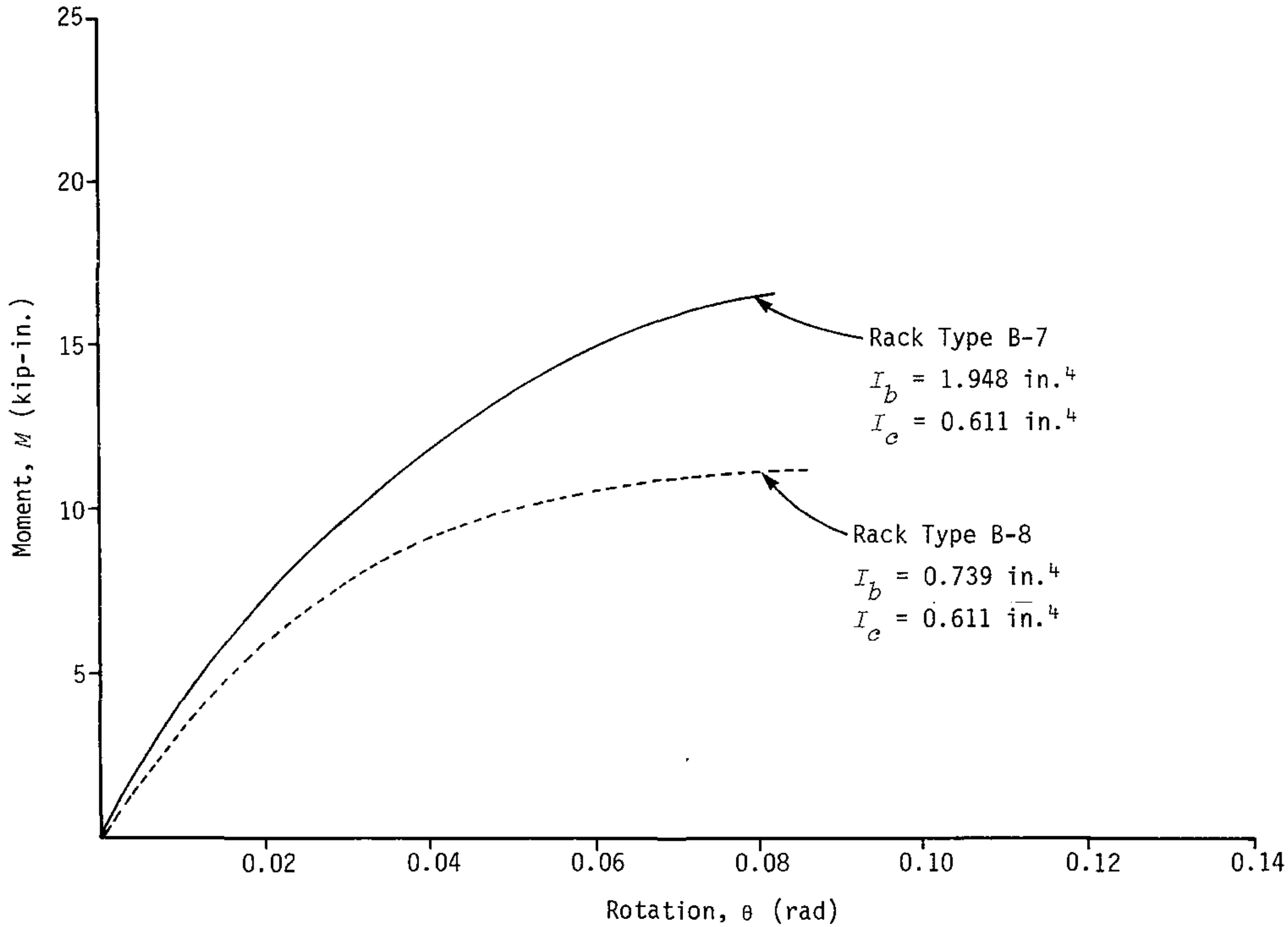

FIGURE 2.24 MOMENT-ROTATION CURVES FOR CANTILEVER TESTS OF RACK TYPES B-7 AND B-8

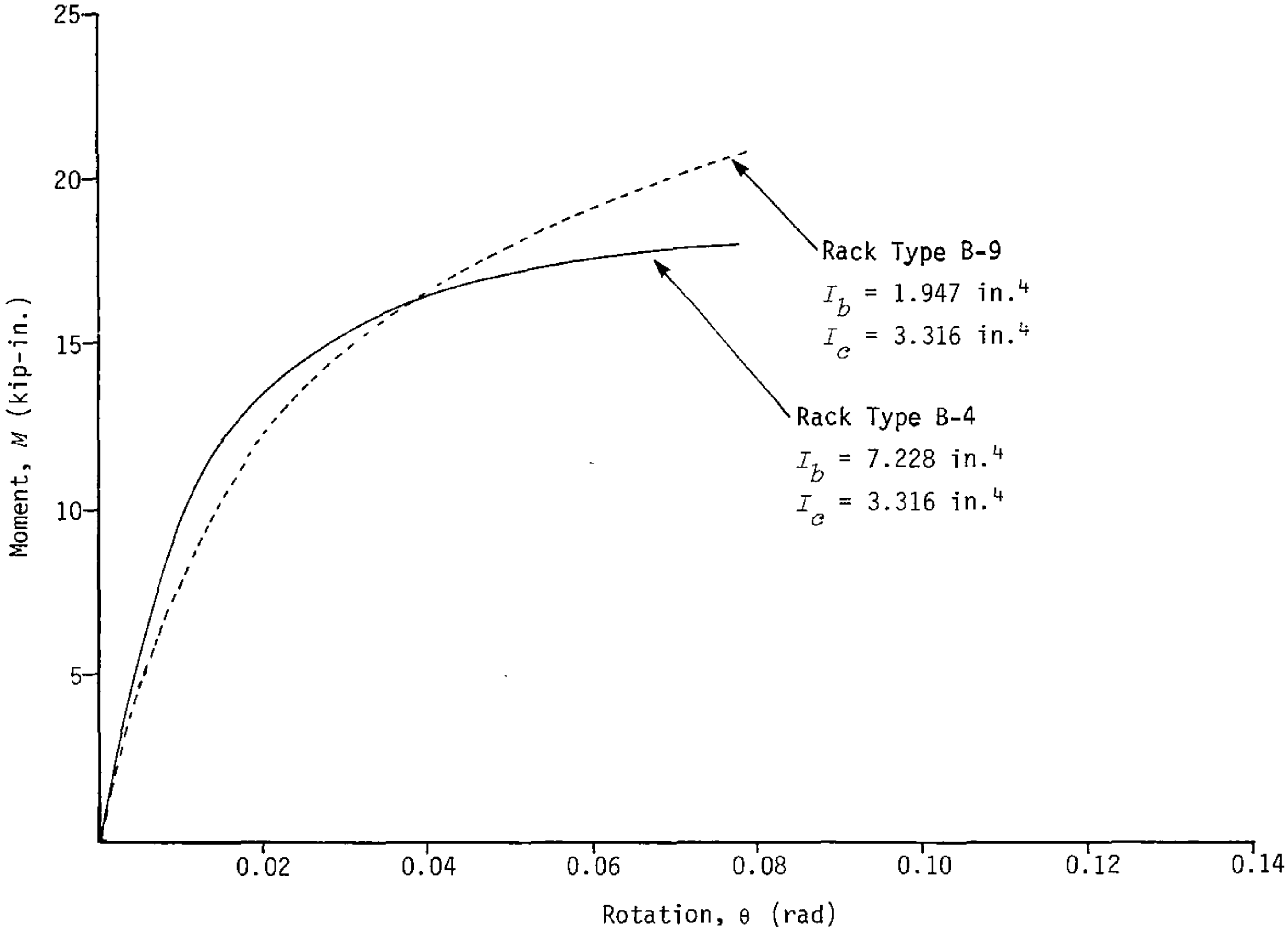

FIGURE 2.25 MOMENT-ROTATION CURVES FOR CANTILEVER TESTS OF RACK TYPES B-4 AND B-9

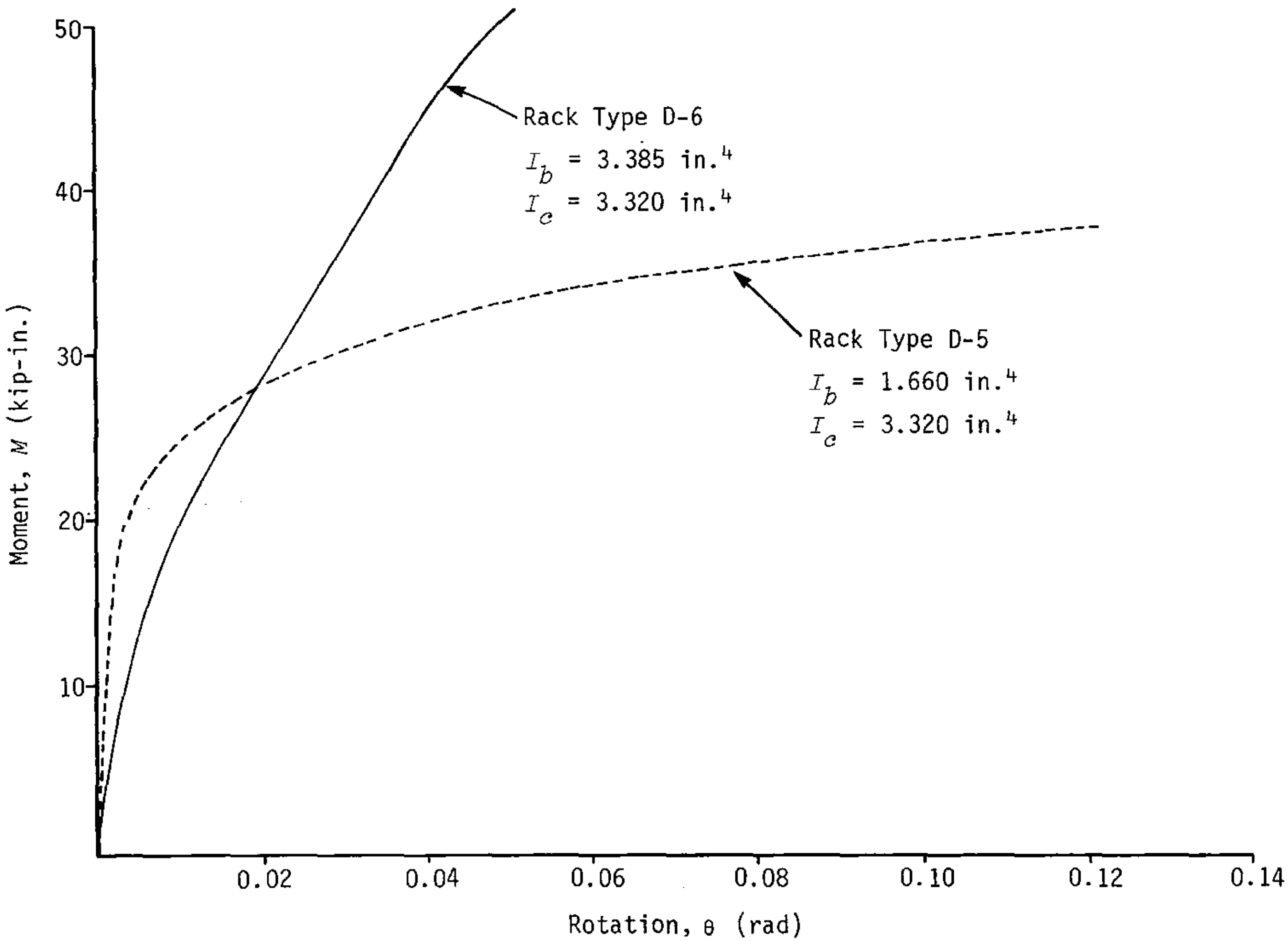

FIGURE 2.26 MOMENT-ROTATION CURVES FOR CANTILEVER TESTS OF RACK TYPES D-5 AND D-6

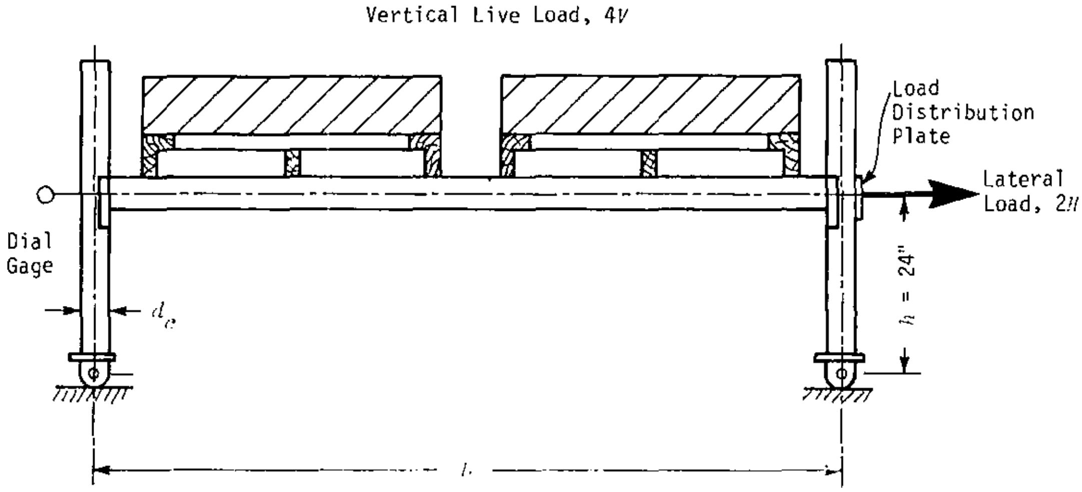

FIGURE 2.27 PORTAL FRAME, TEST SETUP

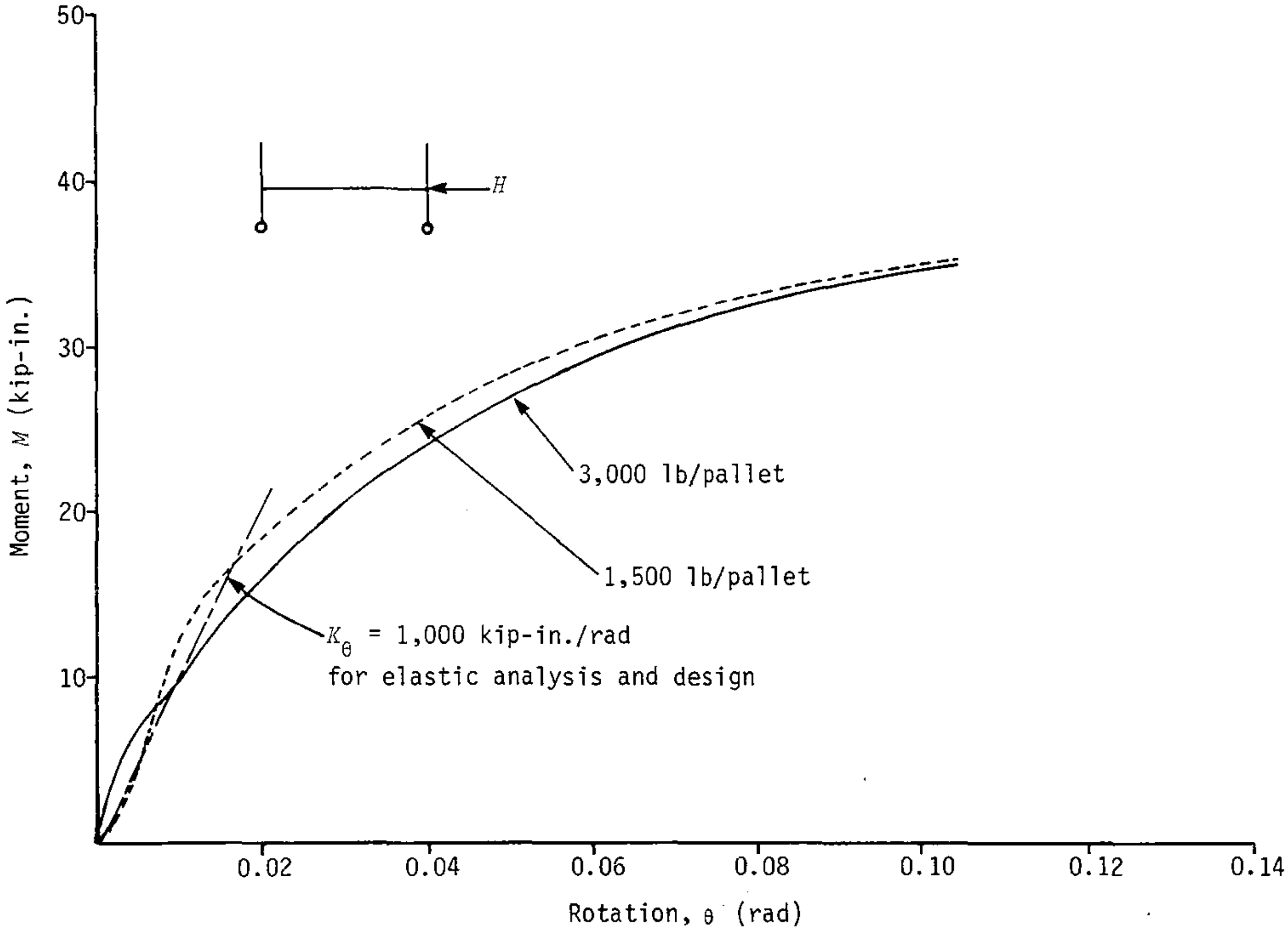

FIGURE 2.28 AVERAGE MOMENT-ROTATION CURVES FOR PORTAL TESTS OF RACK TYPE A-1

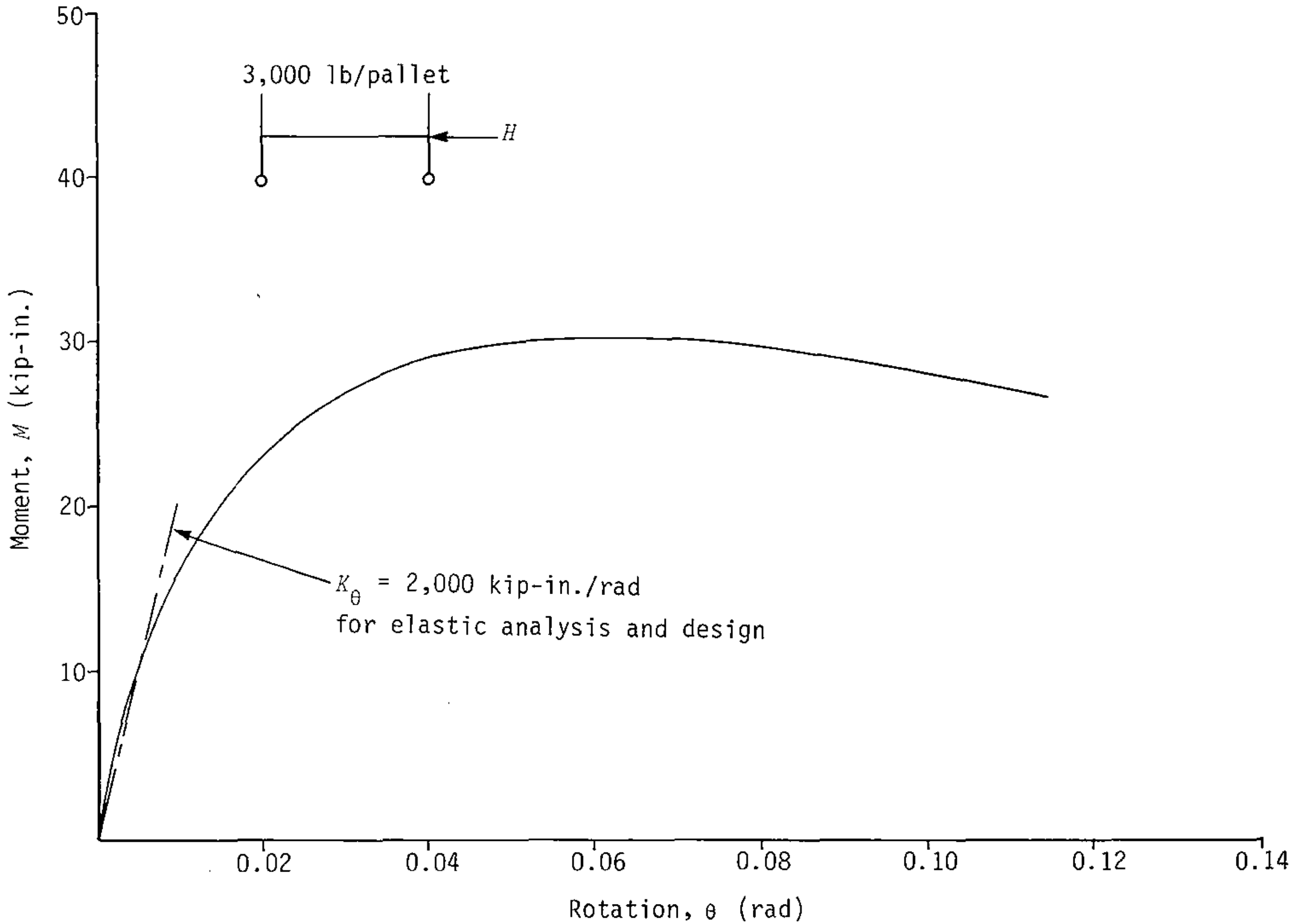

FIGURE 2.29 AVERAGE MOMENT-ROTATION CURVE FOR PORTAL TEST OF RACK TYPE B-1

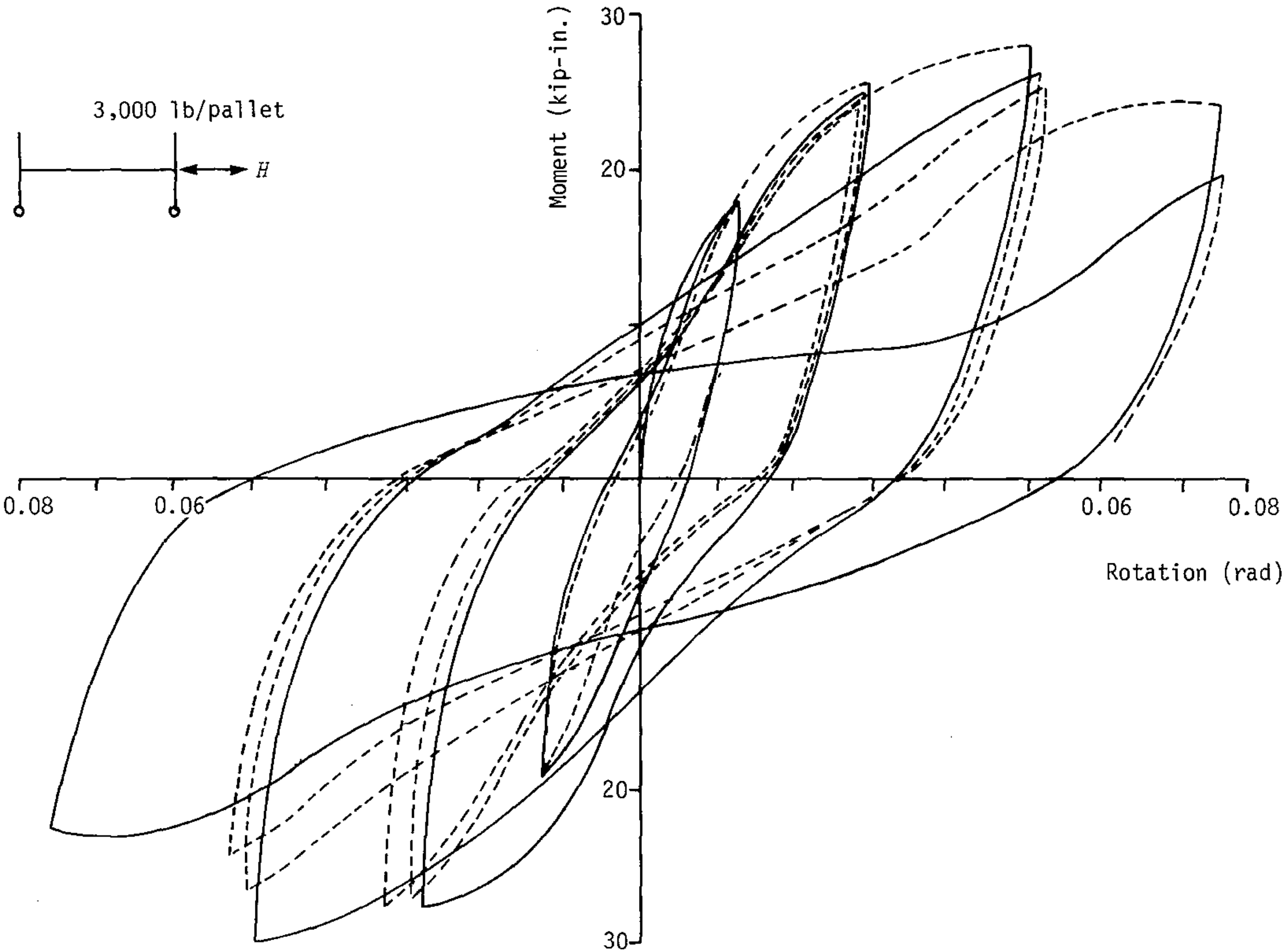

FIGURE 2.30 AVERAGE MOMENT-ROTATION CURVES FOR PORTAL TESTS OF RACK TYPE B-1

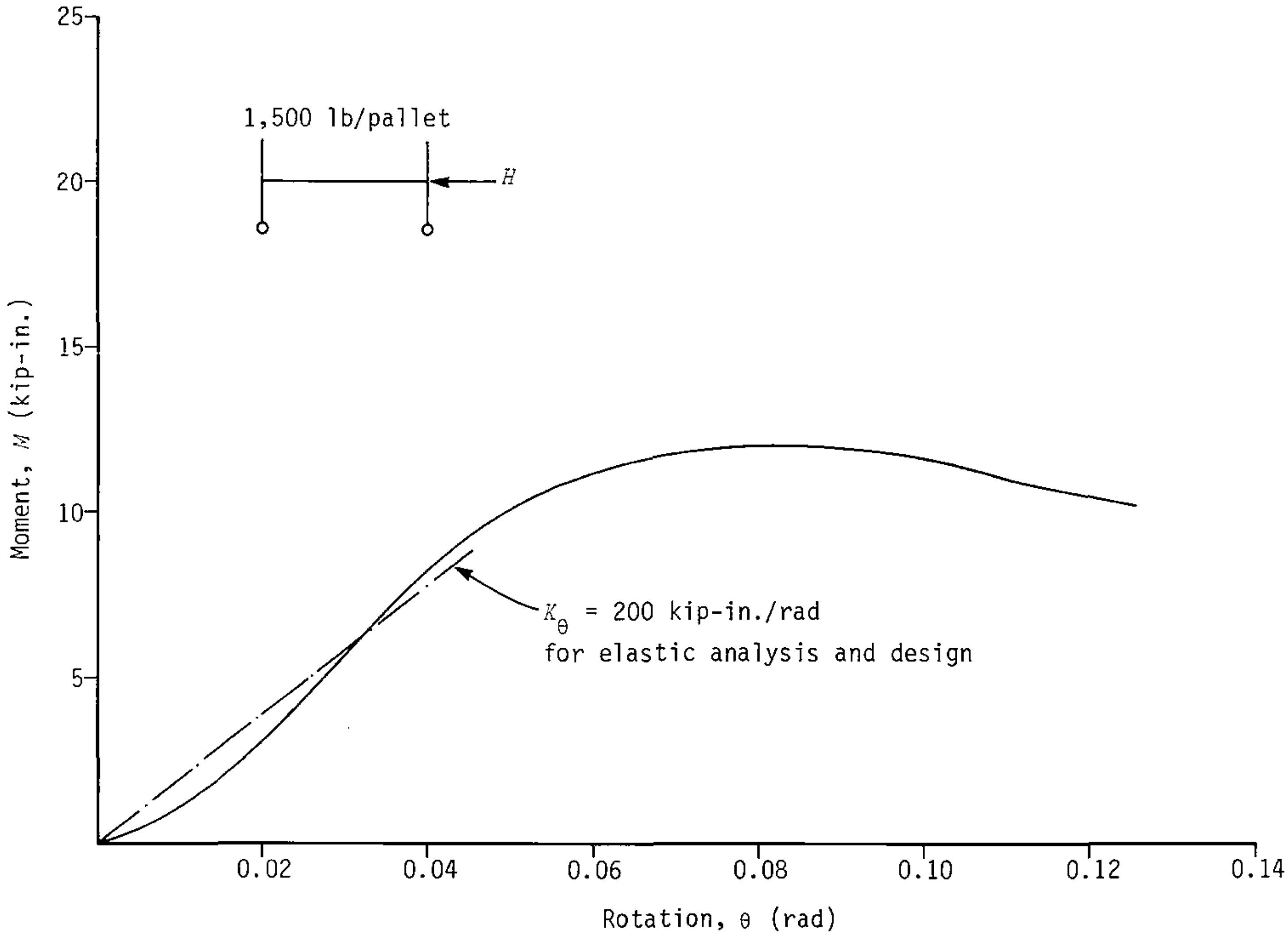

FIGURE 2.31 AVERAGE MOMENT-ROTATION CURVE FOR PORTAL TEST OF RACK TYPE C-1

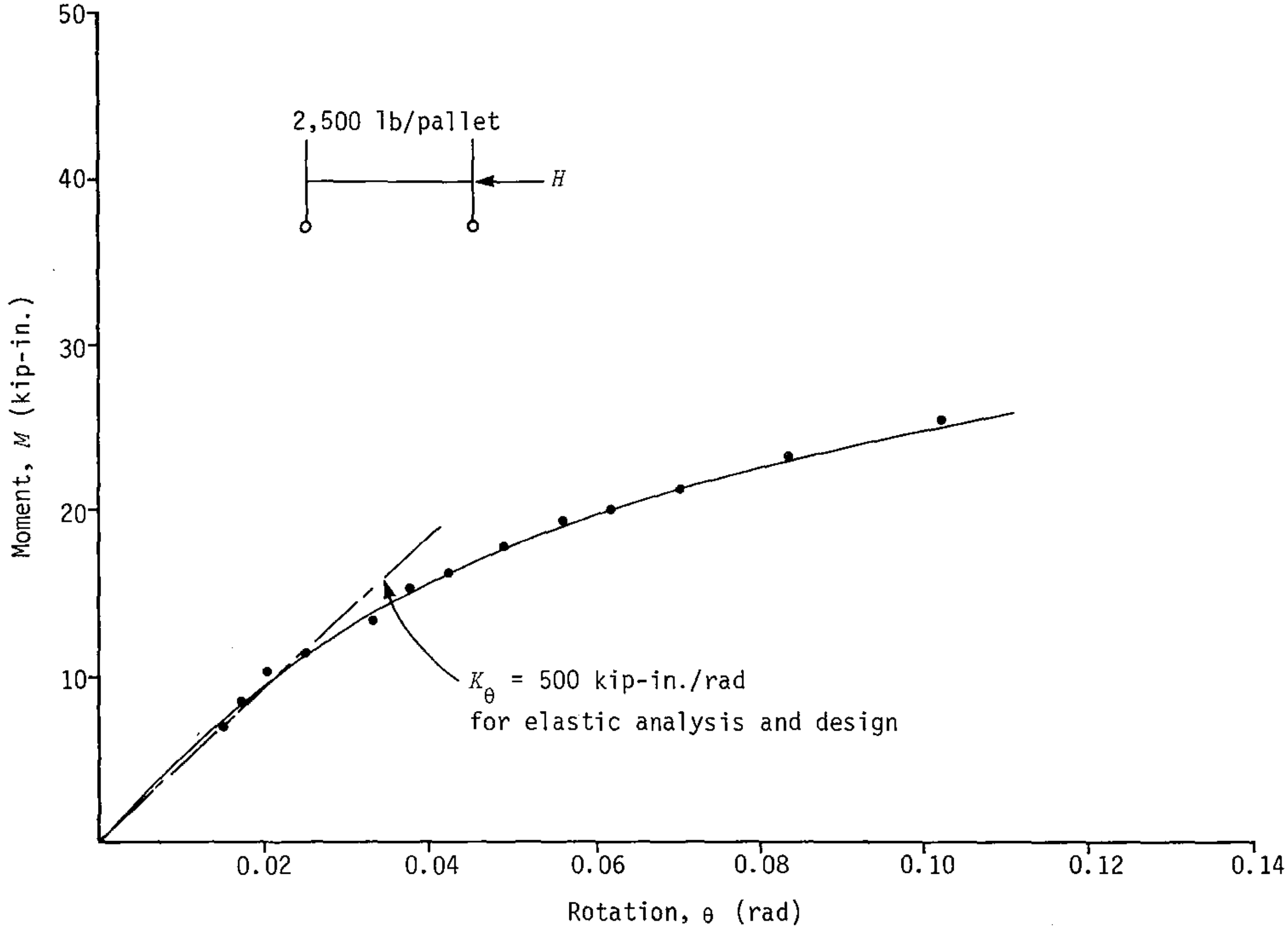

FIGURE 2.32 AVERAGE MOMENT-ROTATION CURVE FOR PORTAL TEST OF RACK TYPE D-1

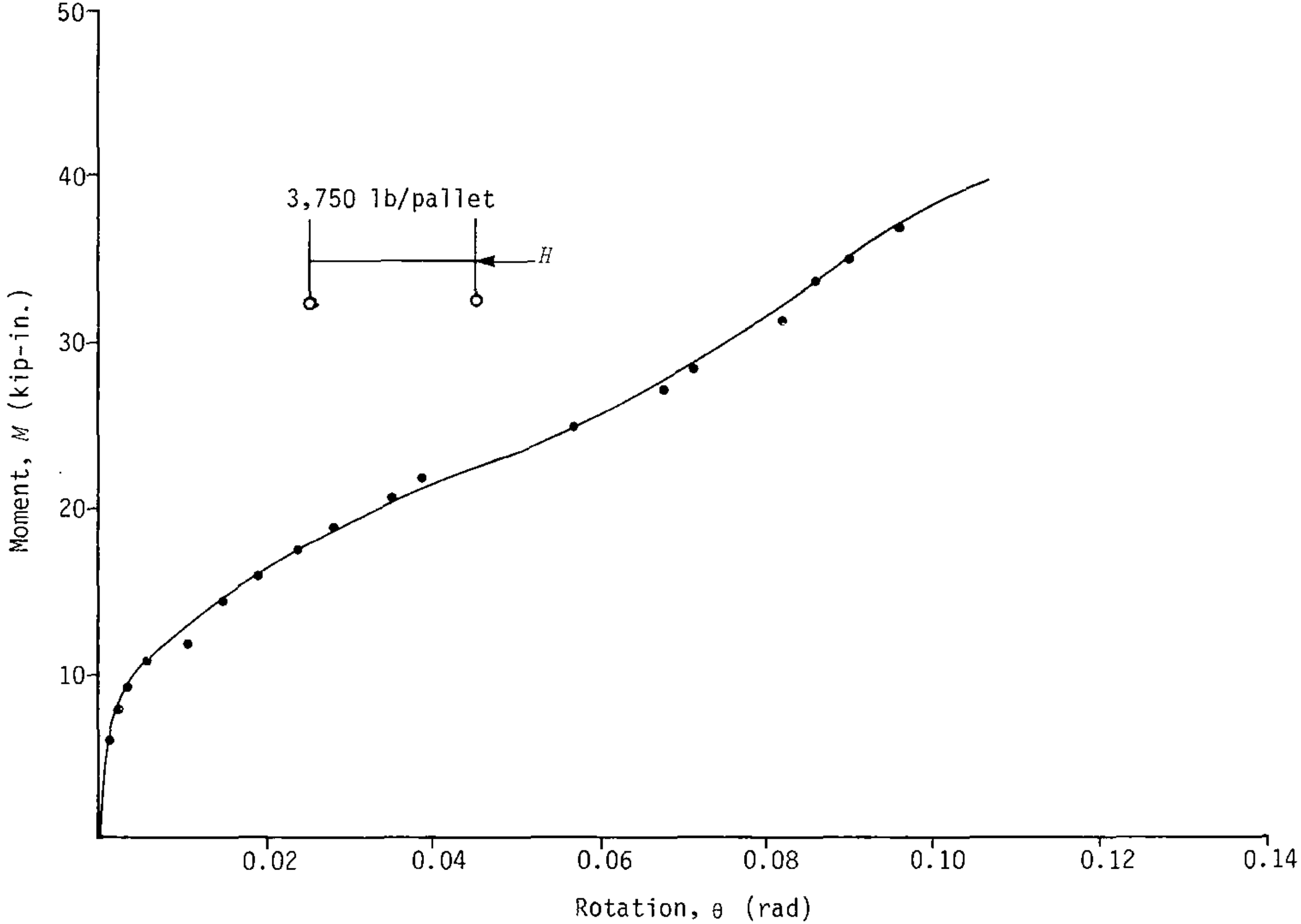

FIGURE 2.33 AVERAGE MOMENT-ROTATION CURVE FOR PORTAL TEST OF RACK TYPE D-2

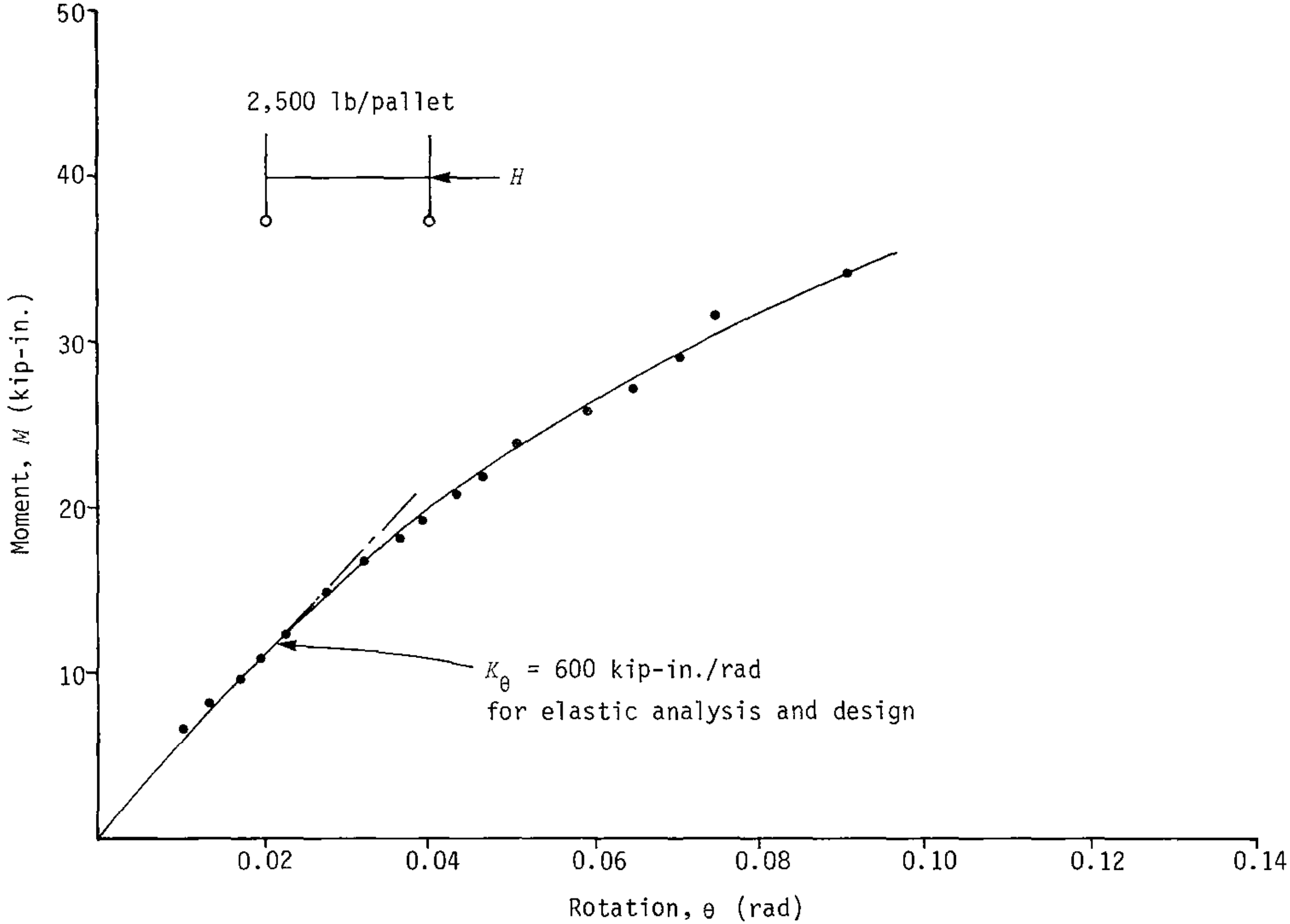

FIGURE 2.34 AVERAGE MOMENT-ROTATION CURVE FOR PORTAL TEST OF RACK TYPE D-3

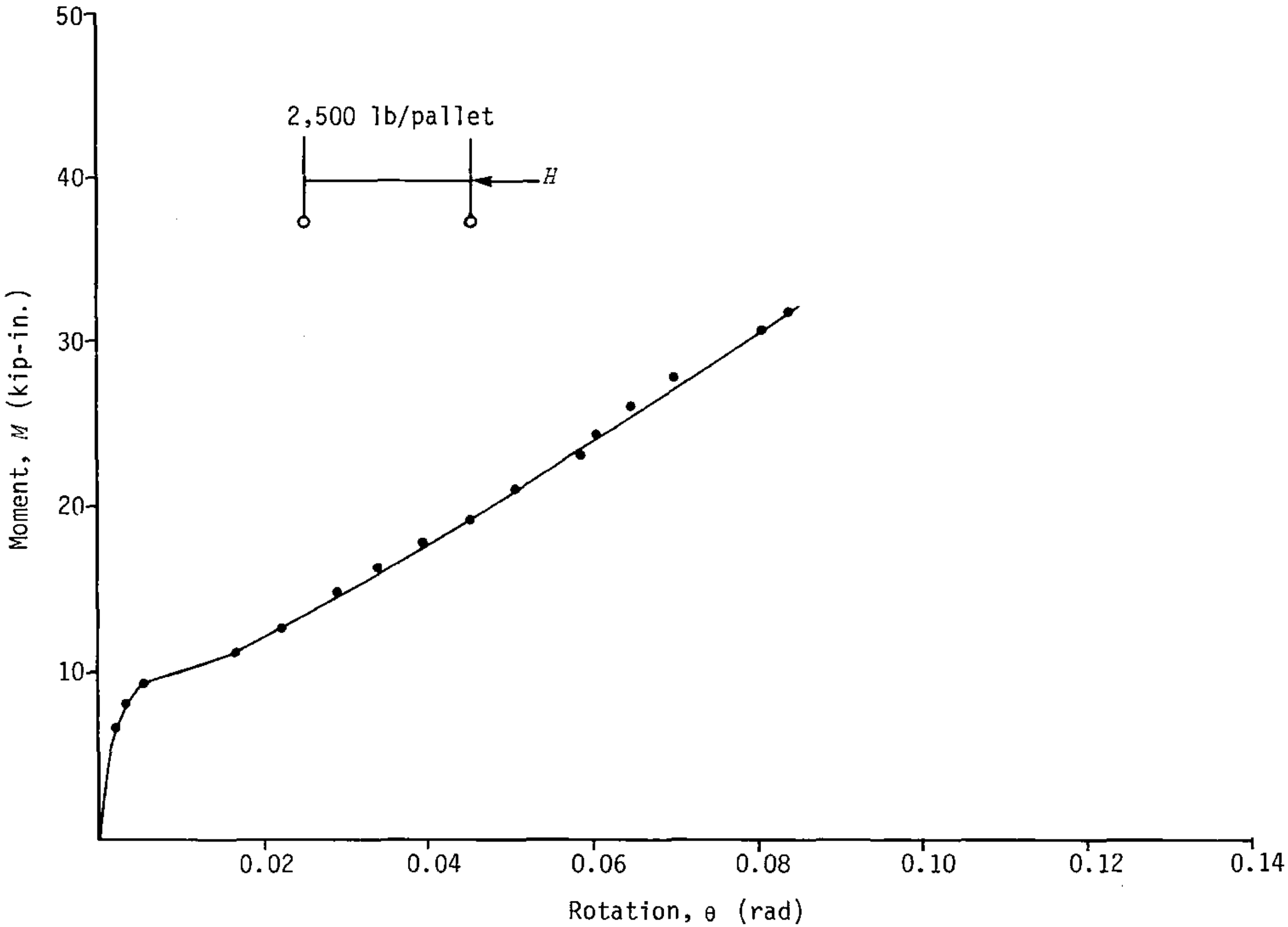

FIGURE 2.35 AVERAGE MOMENT-ROTATION CURVE FOR PORTAL TEST OF RACK TYPE D-4

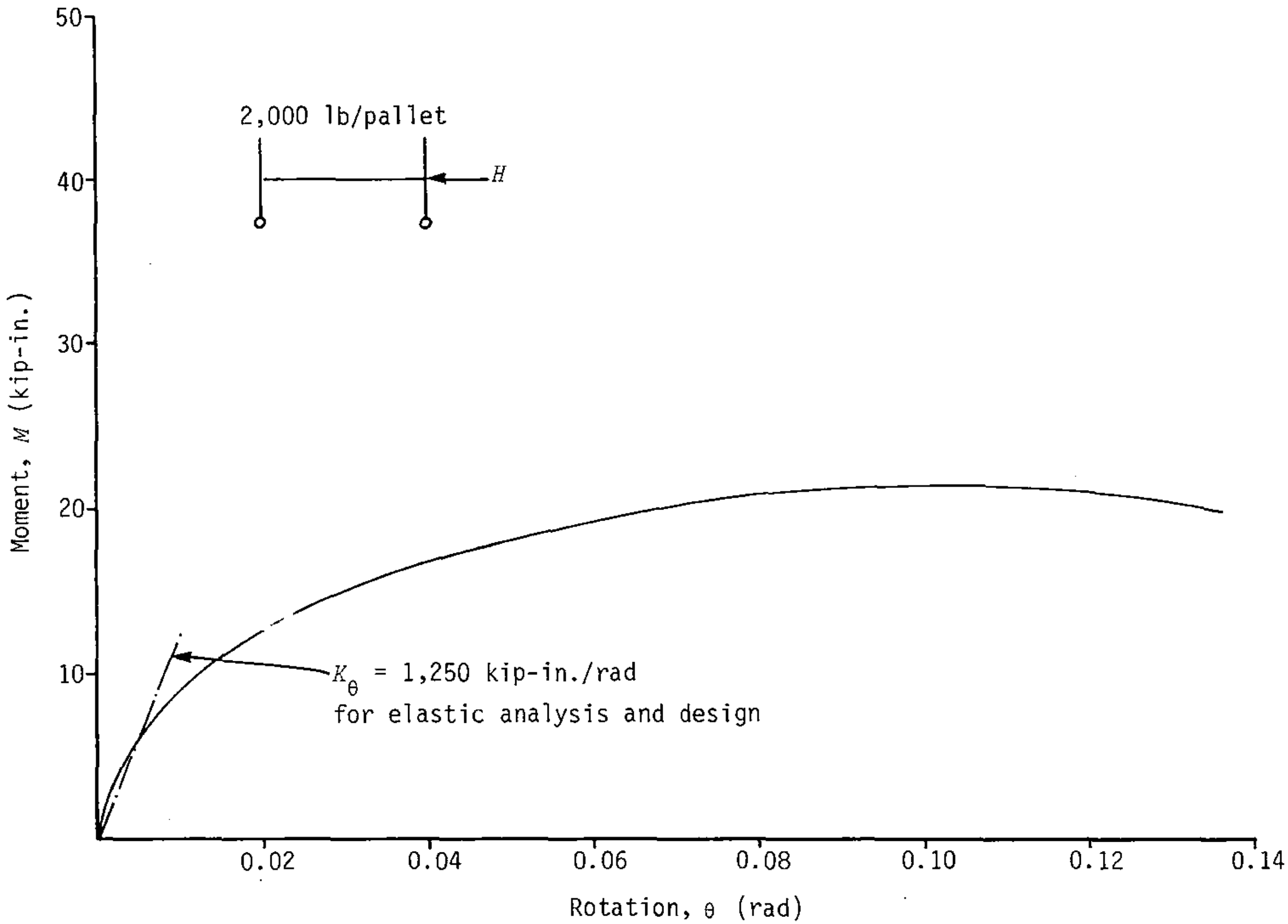

FIGURE 2.36 AVERAGE MOMENT-ROTATION CURVE FOR PORTAL TEST OF RACK TYPE F-1

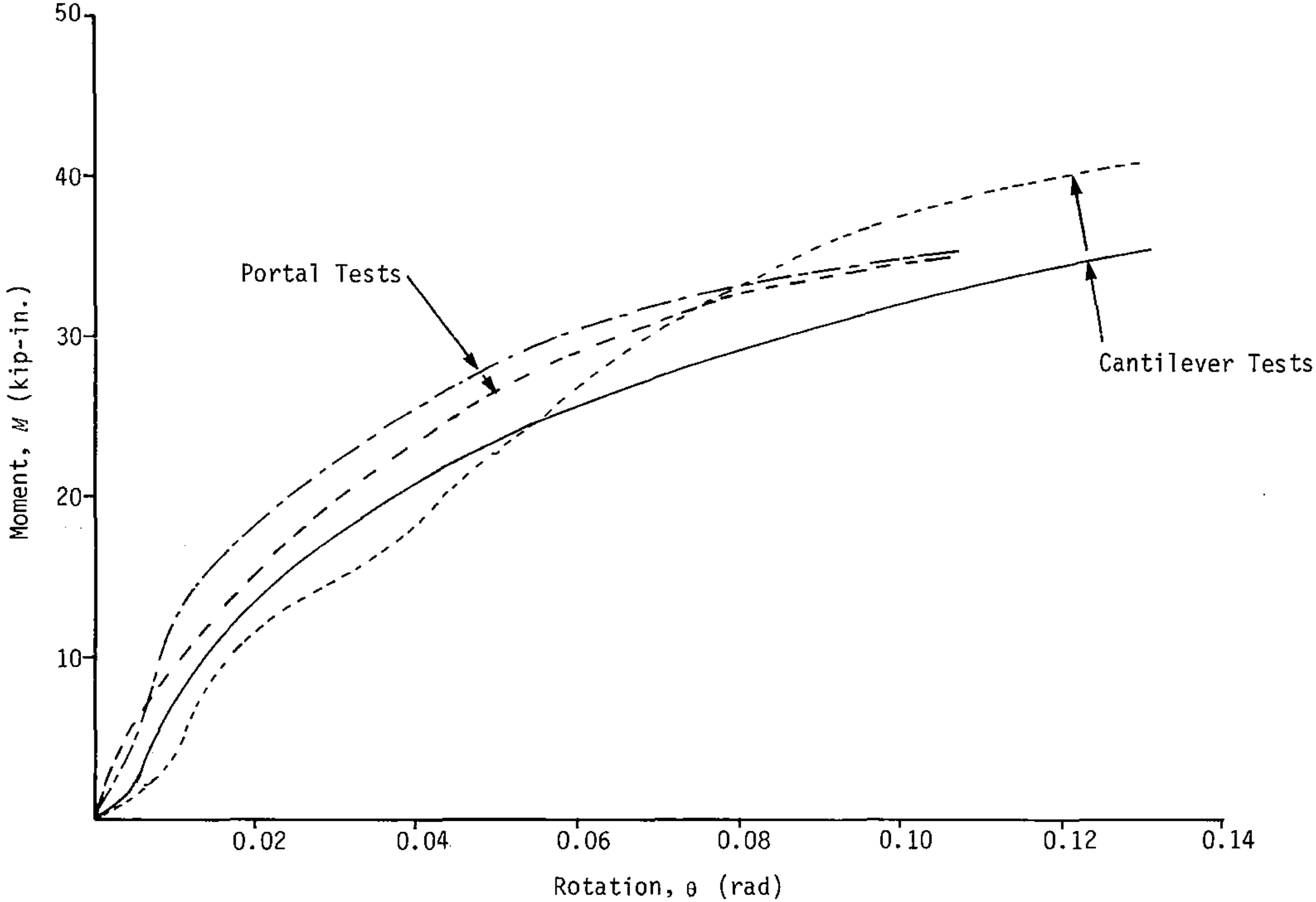

FIGURE 2.37 MOMENT-ROTATION CURVES FOR CANTILEVER AND PORTAL TESTS OF RACK TYPE A-1

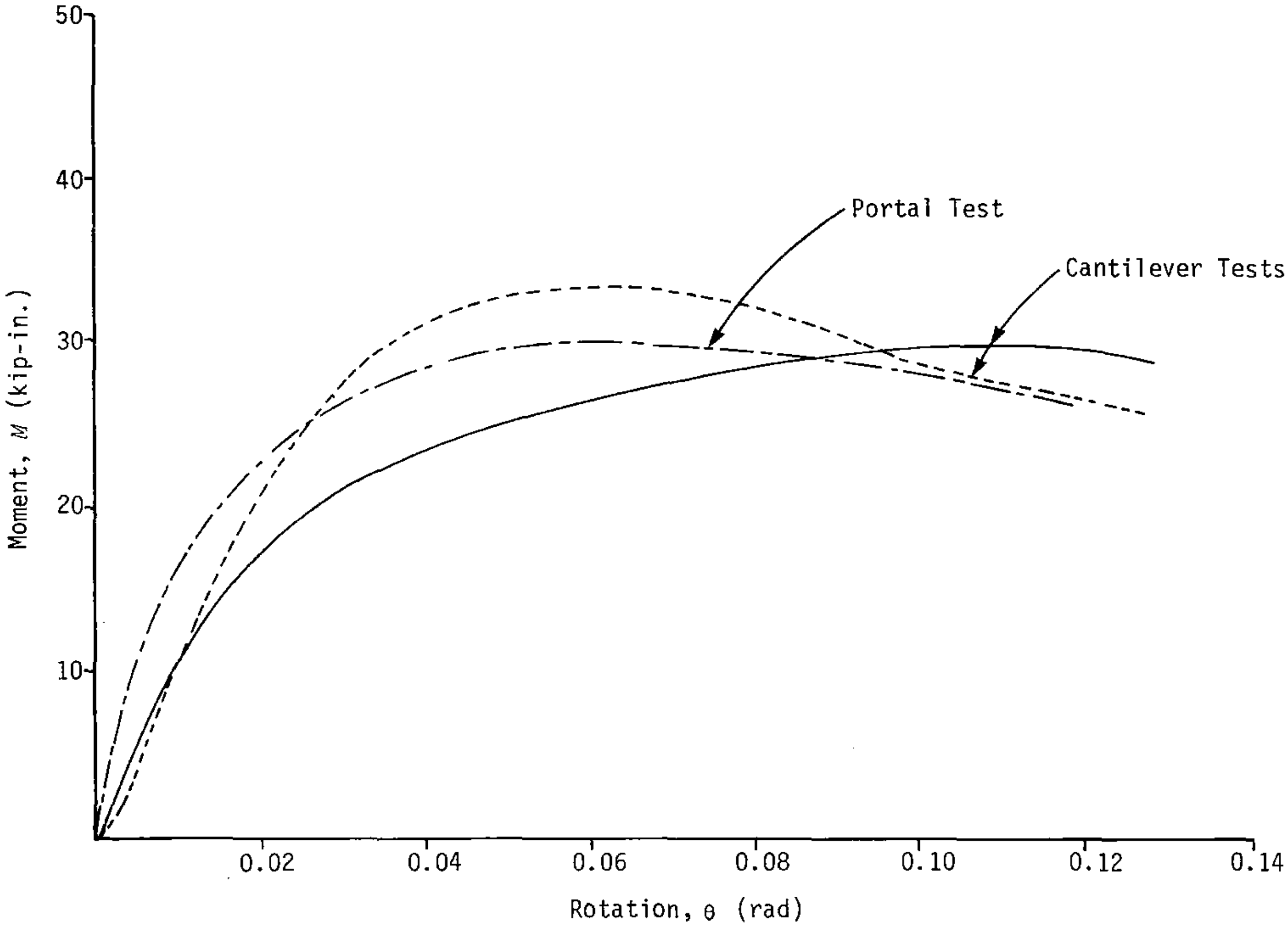

FIGURE 2.38 MOMENT-ROTATION CURVES FOR CANTILEVER AND PORTAL TESTS OF RACK TYPE B-1

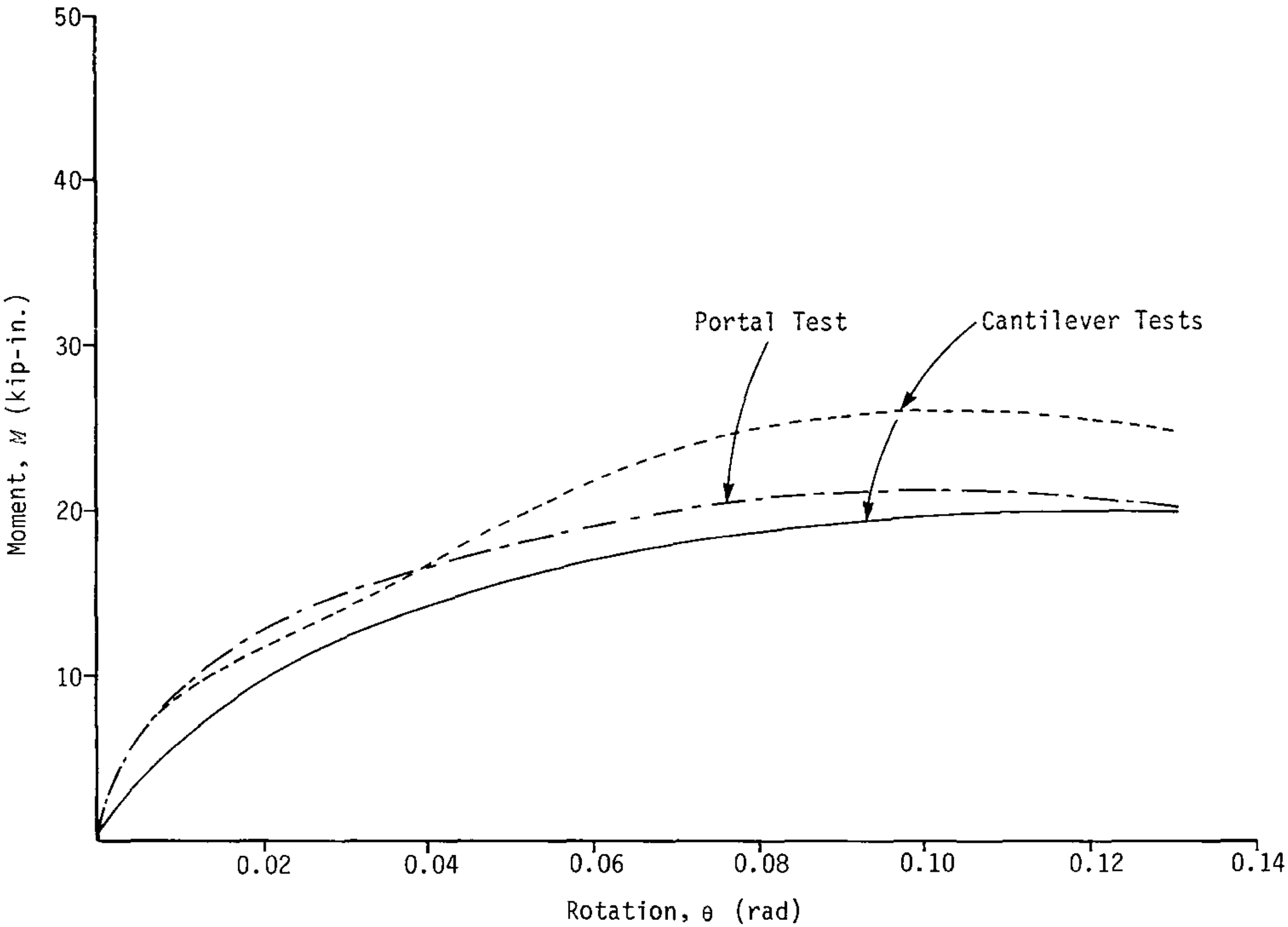

FIGURE 2.39 MOMENT-ROTATION CURVES FOR CANTILEVER AND PORTAL TESTS OF RACK TYPE F-1

INTENTIONALLY BLANK

3. STATIC-CYCLIC TESTS

3.1 Introduction

This chapter summarizes the results from the static-cyclic tests conducted at Stanford University on full-scale three-level standard pallet racks. The complete results were published by Krawinkler, et al.[9] The primary objective of this test program was to study the interaction between pallet beams, columns, and connections under gravity loads and seismic effects simulated by quasi-static cyclic load application at the level of the pallet beams on the third story. Four rack assemblies were tested, two in the longitudinal direction and two in the transverse direction. In the longitudinal direction, the assemblies act as moment-resisting frames with semirigid connections; in the transverse direction, the lateral-load-resisting units are braced frames.

3.2 Test Structures

Table 3.1 summarizes the types of rack tests conducted. The typical rack configuration tested in the longitudinal direction is shown in Figure 3.1. The rack consists of three upright frames, with columns spaced approximately 40 in. apart and connected by horizontal beams spaced 5 ft vertically. The 99-in. horizontal beams are connected to the columns by connector plates, which, in turn, permit two types of connection to the columns: racks using hook-type grips are referred to as Type A; racks using stud-type grips are referred to as Type B. The Type A connector plates are 7 in. long, and the Type B plates are 8 in. long. In the transverse test direction, a rack consisting of only two upright frames was tested in order to assure an equal distribution of lateral load to the frames.

Figure 3.2 shows the shapes of the rack components; Table 3.2 lists their section properties. The Type A and Type B rack components used in the static-cyclic tests correspond to the Type A-1 and B-1 components in the subassembly tests presented in Chapter 2. The configuration and section properties of Rack Type B are the same as those used in the shaking table tests described in Chapter 4 (standard pallet rack).

Preceding page blank

3.3 Longitudinal Tests

Experimental Setup. The experimental setup for the longitudinal tests is shown in Figure 3.3. The base plates welded to the ends of the columns were provided with single holes through which the racks were bolted to the floor. Each rack has two frames, labeled as L1 and L2 in Figure 3.3. These frames are parallel to each other and are essentially identical. Frame L1 was fully instrumented, while frame L2 was only partially instrumented, primarily to verify the degree of symmetry attained in the response.

Strain gages similar to those used in the cantilever and portal tests reported in Chapter 2 were mounted on the beams of the first level to measure the strains in the beams close to the connections. The positions of the strain gages in the beams relative to the adjacent joints, which were the same as in the cantilever tests, permitted a direct measurement of beam moments. Strain gages were also mounted on the center columns and on one of the exterior columns of frame L1 to obtain qualitative measurements of the flexural strains in the columns.

The lateral displacement measurements for frames L1 and L2 were made at all three levels by a combination of LVDTs and linear potentiometers attached to the exterior column faces at the centerline of the beams. Continuous readings were obtained for the lateral load-deflection curves for the third level and first level, and intermittent readings were obtained for the deflection at the second level.

The gravity loads were simulated with 1,000-lb concrete blocks resting on wooden pallets, one pallet per frame, per level, per bay. For test A-R-1, the rack was loaded with 1/2 live load (1,500/lb pallet), while, for test B-R-1, it was loaded with full live load (3,000/lb pallet). The lateral load was applied to the rack assembly at the third level by means of a hydraulic jack connected at one end to a rigid wide-flange section and at the other end to a distribution plate bolted to the two frames at the third level.

Loading Histories. After the application of the vertical loads, all the strain gages, LVDTs, and potentiometer readings were zeroed. The lateral load was applied quasi-statically to permit accurate force and displacement control and recording of visual observations. The racks were subjected to cyclic loading with increasing displacement amplitudes up to 6 in. Three symmetric cycles were carried out at each displacement amplitude. The loading arrangement did not permit cyclic loading beyond a displacement of 6 in., but loading was continued monotonically until either failure was imminent or the displacement limit of the loading arrangement was reached.

The deflection histories at the third level for tests A-R-1 and B-R-1 are presented in Figure 3.4.

Test Results. Both rack assemblies during tests A-R-1 and B-R-1 exhibited only a rather small linear range. At low levels of loading, the beam-to-column connections behaved nonlinearly; at a much later state, nonlinearity was caused by inelastic response in the center columns.

In test A-R-1, no sign of imminent failure was evident at the maximum displacement of 17.3 in., although failure of the center column was expected at at a much smaller displacement amplitude due to the combined action of axial load and bending moment. However, the axial load was too small to affect the capacity of the column significantly. Consequently, flexural plastic hinges developed in the center column above and below the beam-to-column connection, leading to a very ductile response of the rack assembly. Some distress was observed at the exterior beam-to-column connection, which attracted the highest bending moment in the pallet beams.

In test B-R-1, buckling of the center columns was imminent at a lateral displacement of 9.0 in., at which point the test was terminated. In this assembly, the axial load on the center columns was too high to permit the development of flexural plastic hinges and consequent redistribution of moments. All beam-to-column connections exhibited little distress and would have been capable of resisting higher moments.

The maximum interstory drifts in tests A-R-1 and B-R-1 were found to be approximately $0.12H$ and $0.07H$, respectively (H = story height). This result clearly shows that the racks can tolerate much greater drift limits than are specified by the *UBC* ($0.005H \times 3/K$) and ATC-3 ($0.015H$).

The maximum amplification ratios of story shear due to the p-δ effect were estimated to be approximately 1.8 and 2.2 for tests A-R-1 and B-R-1, respectively. Thus, the p-δ effect will greatly affect the response of the racks in the longitudinal direction.

It was observed from the column strain-gage measurements that the moment at the center column base was always a significant portion of the column moment at the first-floor level near the top. Thus, the column bases provide a significant restraint against rotation, which, in turn, reduces the column moments at the first-floor level.

3.4 Transverse Tests

Experimental Setup. A plan view of the experimental setup for the transverse tests is shown in 3.5a. Only single-bay assemblies were tested to assure an equal distribution of lateral load to the two upright frames. Gravity loads between the upright frames were simulated with four 1,000-lb concrete blocks per level, which corresponds to 2/3 live load. Because it was intended to test the behavior of interior bays with zero moments in the columns in the longitudinal direction, 1,000-lb concrete blocks were suspended from cantilever beams as shown in Figure 3.5b, to equilibrate the beam moments at the joints. In this manner, the loading condition of interior bays with 2/3 live-load was simulated. Knee braces were added to prevent displacement in the more flexible longitudinal direction. The lateral load was applied by a hydraulic jack attached to the middle of a distribution beam at the third level so that the load would be distributed equally between the two frames.

The instrumentation consisted of LVDTs and linear potentiometers to measure the horizontal deflection at the three levels of the two frames, designated T1 and T2. Strain gages were attached to the columns below the first level and also to the braces that join the columns below the first level. Strain gages were applied in pairs to obtain average readings of axial strains in columns and braces.

Loading Histories. The lateral load was again applied quasi-statically. Load control was used for most of the test to control the loading history except at amplitudes causing severe strength and stiffness degradation where displacement control was applied. The racks were subjected to cyclic loadings with increasing amplitude of load or displacement. Again, three cycles were carried out at each amplitude. The history of lateral deflection at the third level for tests A-R-2 and B-R-2 is shown in Figure 3.6.

Test Results. Both rack assemblies exhibited nonlinear response characteristics at relatively low lateral loads. Because the diagonal braces were connected eccentrically to the columns, significant weak axis bending in the columns occurred. This bending, in combination with high axial forces, accounted for some of the inelastic behavior; however, most of the inelastic action must be attributed to other sources, which differ for the two rack types.

In test A-R-2, the nonlinear behavior was caused primarily by local bending of the 1/4-in.-thick base plates at the column-to-floor connections. Because of the large height-to-width ratio of the upright frames, the uplift forces developed in one of the columns caused a brittle fracturing at the weld connecting the column to the base plate before the buckling loads in columns or braces were attained. The magnitude of the uplift force at which weld fracture occurred was approximately 7,000 lb.

In test B-R-2, no welds fractured at the base plates; however, early nonlinear behavior was observed at the connections between the open-section bracing elements and the open-section columns. Localized plastic bending in the lips of the columns was evident at low loads, followed at higher loads by local buckling of the open-section bracing elements. Distinct local buckling was also visible between perforations in the columns. The strong local buckling in the bracing elements and the plastic bending in the lips of the columns limited the strength of the upright frames and were the cause of significant stiffness deterioration.

The measured deflected shapes of the rack assemblies clearly illustrate the difference in the behavior of the rack assemblies in tests A-R-2 and B-R-2. In test A-R-2, the rack responded primarily in a flexural cantilever mode (the rate of deflection increased with height); in test B-R-2, the rack responded in a shear-type mode (the largest relative deflection was in the first story) once inelastic deformations at the brace-to-column connections dominated the response.

TABLE 3.1

SUMMARY OF STATIC-CYCLIC RACK TESTS

Test Direction	Rack Type	Designation	Configuration	Vertical Load Per Pallet (lb)
Longitudinal	A	A-R-1	3 stories high 2 bays wide 1 bay deep	1,500
	B	B-R-1		3,000
Transverse	A	A-R-2	3 stories high 1 bay wide 1 bay deep	2,000
	B	B-R-2		2,000

TABLE 3.2

SECTION PROPERTIES OF RACK ELEMENTS

Type	Element	A (in.^{2})	I_x (in.^{4})	I_y (in.^{4})	S_x (in.^{3})	S_y (in.^{3})	r_x (in.)	r_y (in.)	F_y (kip/in.^{2})
A	Beam	1.010	2.664	1.104	1.109	0.746	1.624	1.045	50
	Column	0.672	1.037	0.318	0.691	0.277	1.228	0.688	50
	Brace	0.370							30
B	Beam	1.288	3.265	1.195	1.496	0.760	1.630	0.986	45
	Column	0.688	1.144	0.879	0.756	0.586	1.288	1.130	45
	Brace	0.318	0.125	0.075	0.131	0.100	0.628	0.4087	45

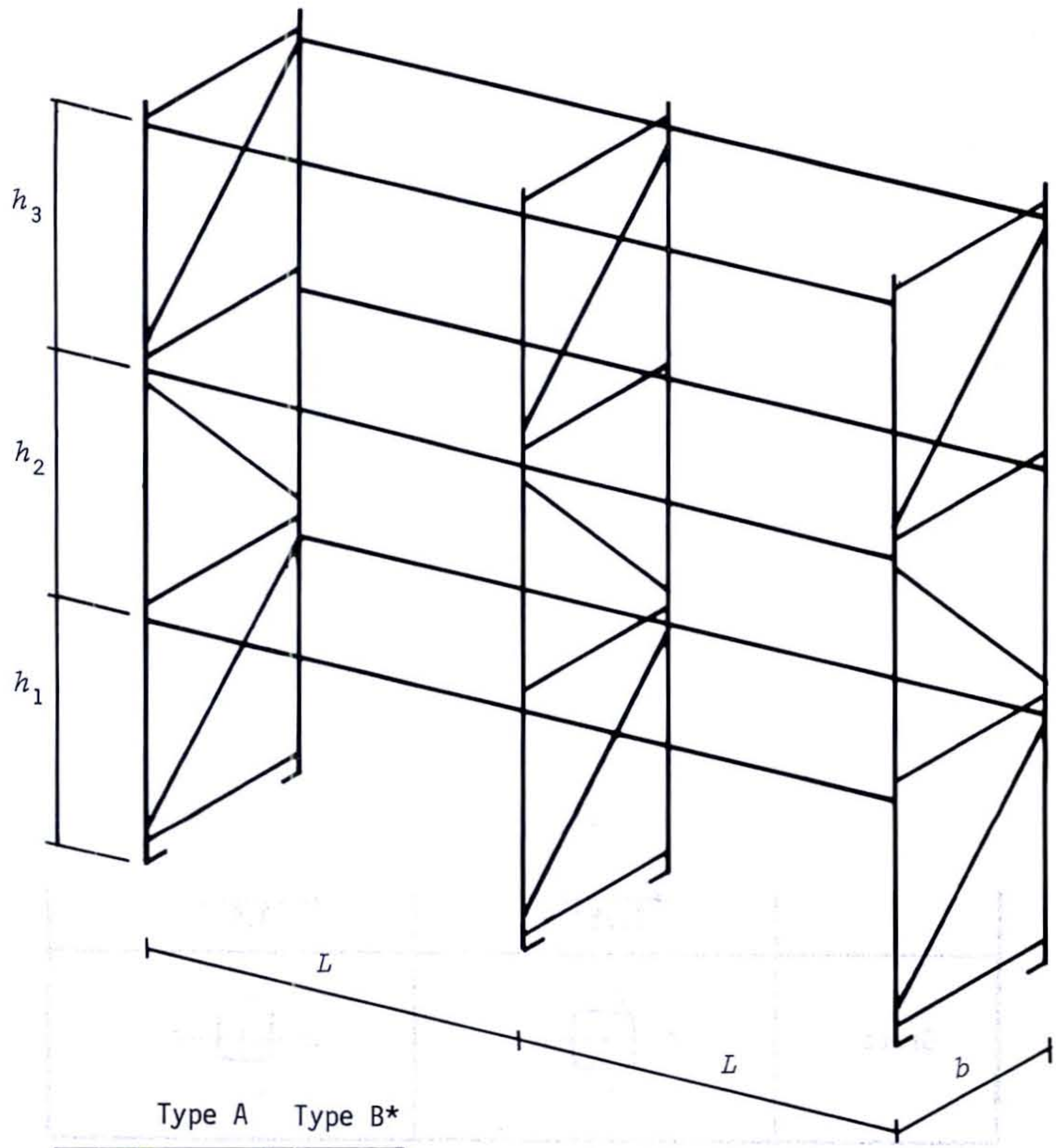

	Type A	Type B*
L	99 in.	99 in.
b	40 in.	39 in.
h_1	58 in.	58 in.
h_2	58 in.	58 in.
h_3	58 in.	58 in.

*Horizontal braces were provided only at the top level and the base of the Type B rack assembly.

FIGURE 3.1 RACK CONFIGURATION

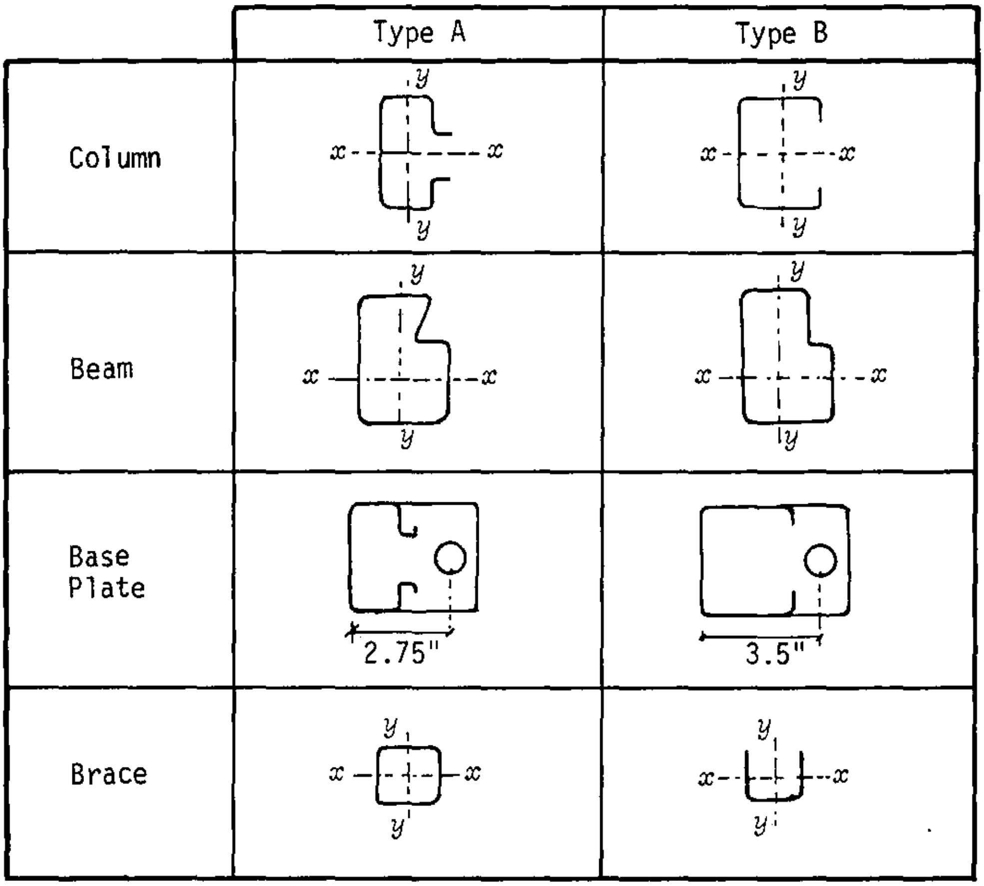

FIGURE 3.2 SHAPES OF RACK ELEMENTS

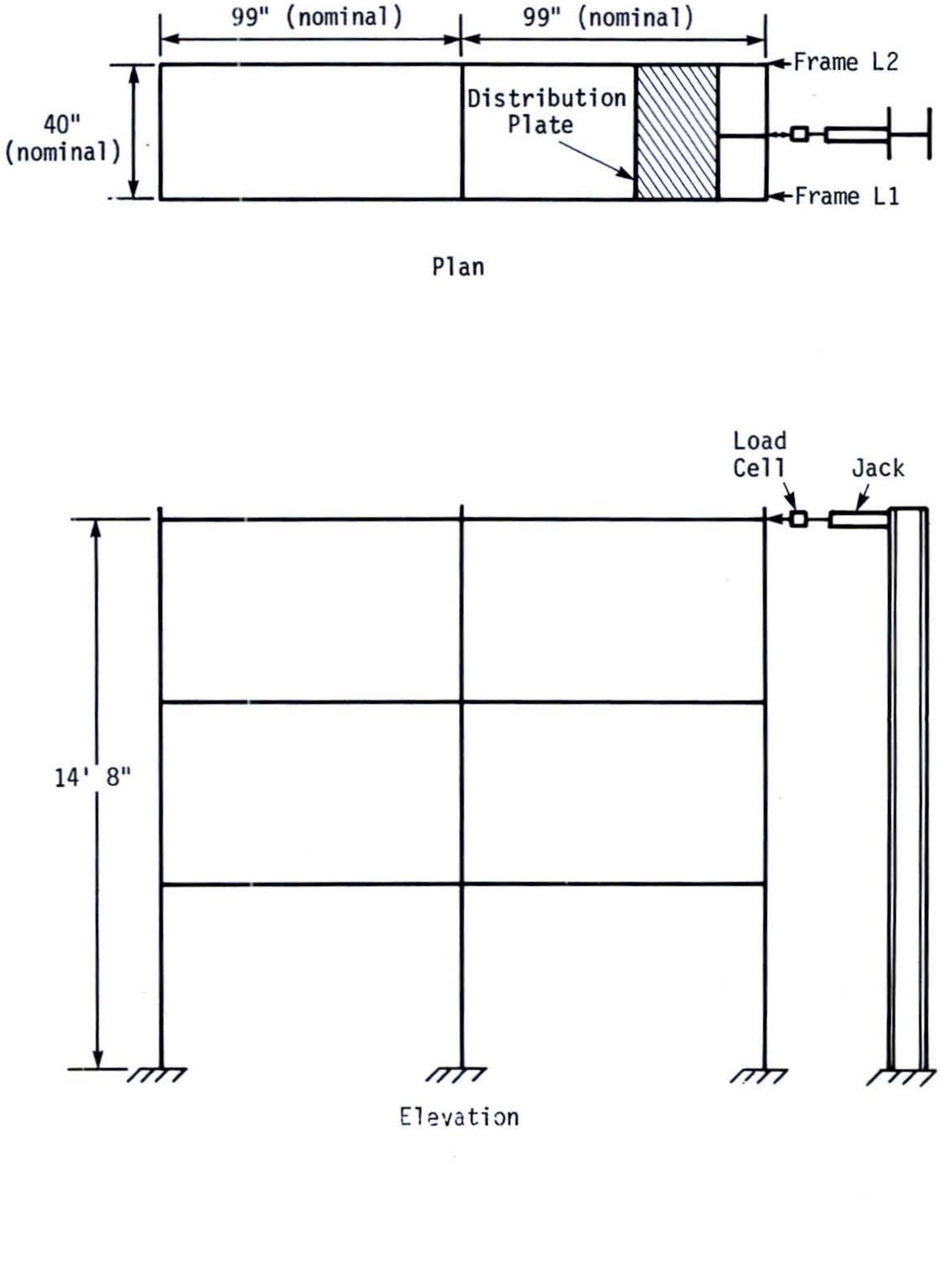

FIGURE 3.3 EXPERIMENTAL SETUP, LONGITUDINAL TESTS

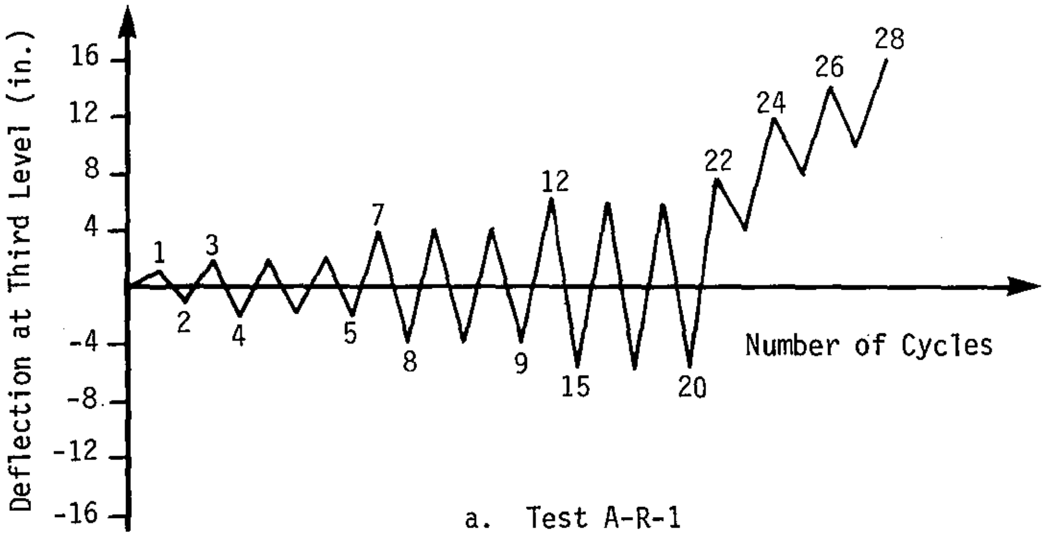

a. Test A-R-1

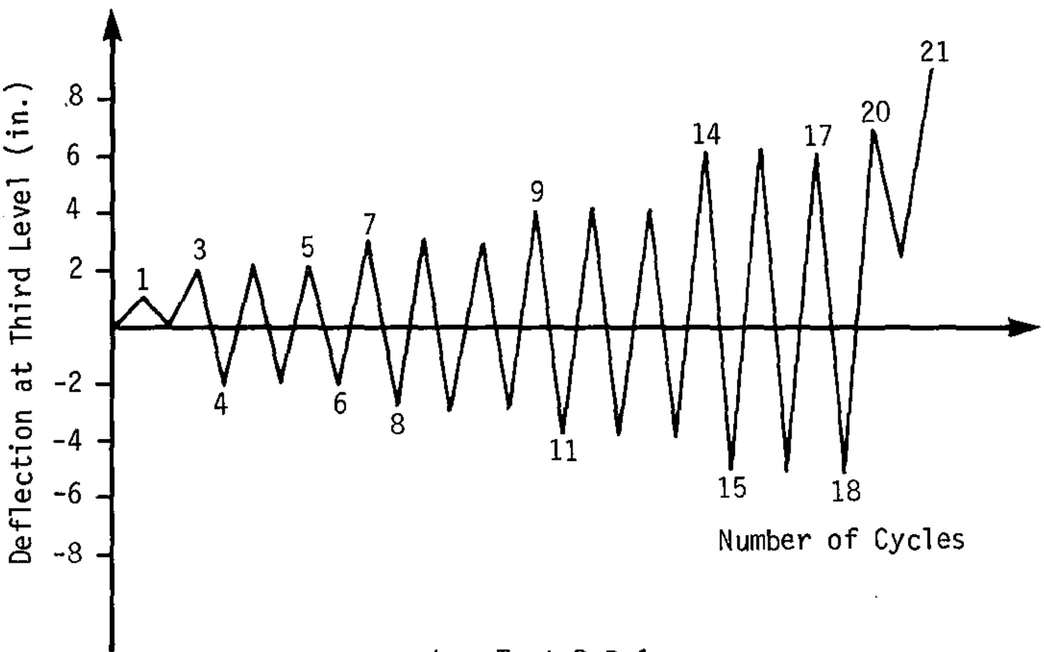

b. Test B-R-1

FIGURE 3.4 DEFLECTION HISTORY AT THIRD LEVEL

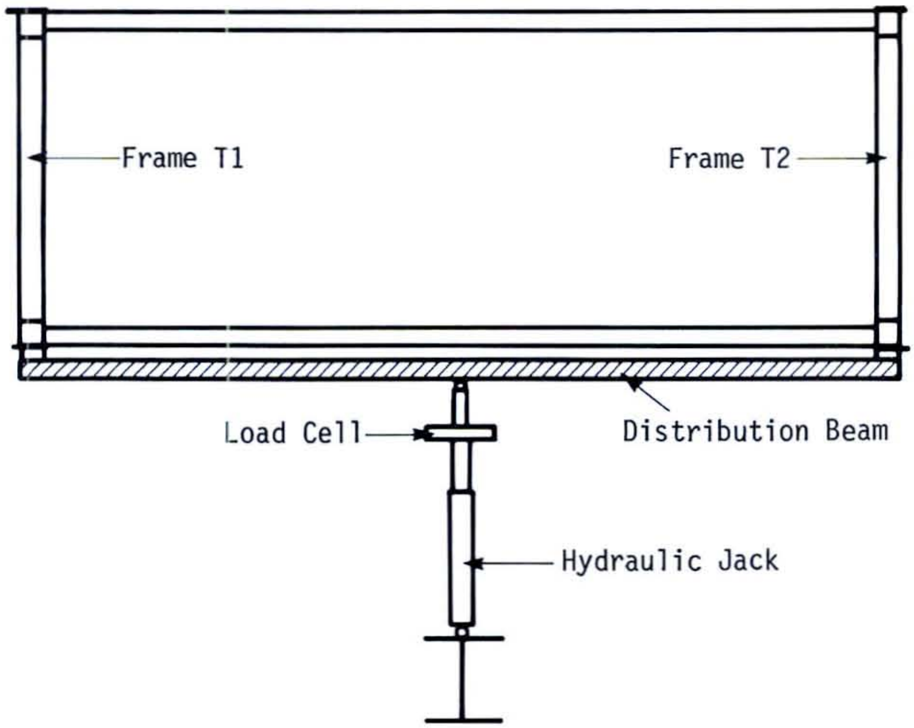

a. Experimental Setup

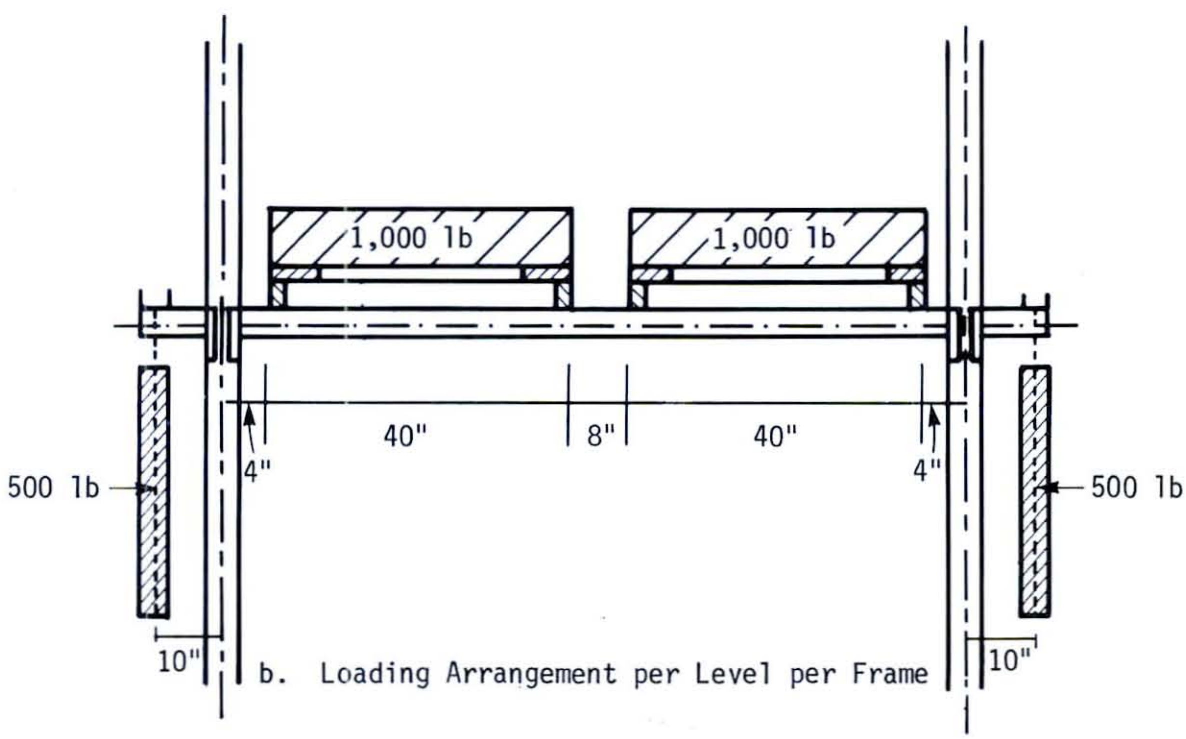

b. Loading Arrangement per Level per Frame

FIGURE 3.5 EXPERIMENTAL SETUP AND LOADING ARRANGEMENT, TRANSVERSE TESTS

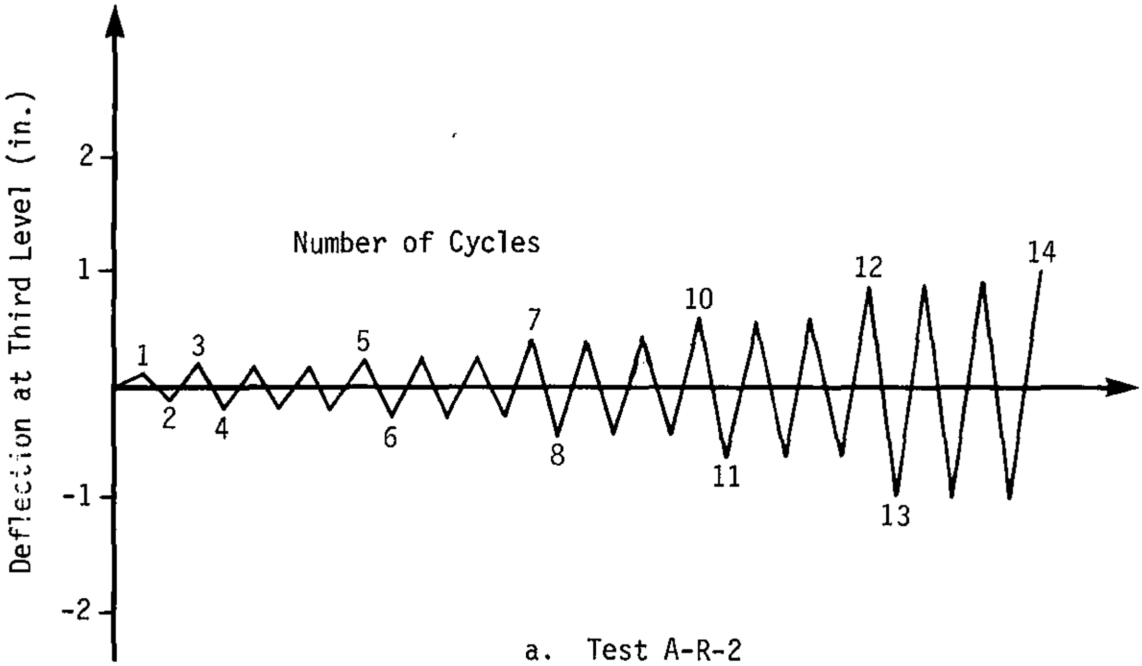

a. Test A-R-2

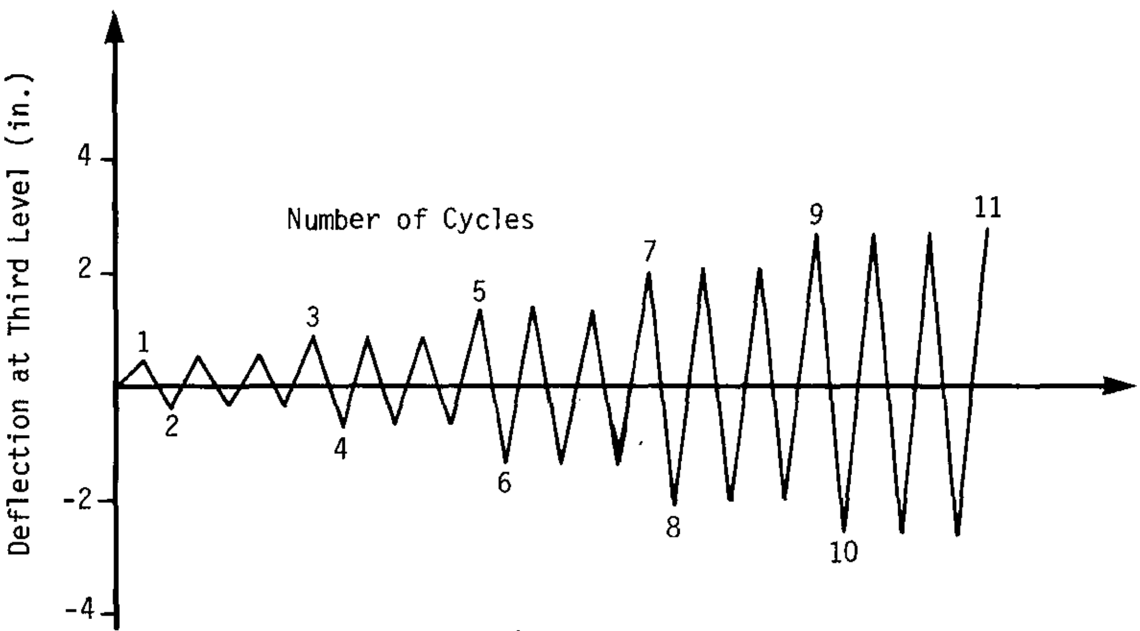

b. Test B-R-2

FIGURE 3.6 DEFLECTION HISTORY AT THIRD LEVEL

4. STRUCTURAL PERFORMANCE SHAKING TABLE TESTS

4.1 Description of Test Structures

Four types of typical full-scale storage racks were subjected to simulated earthquake motions using the 20-ft-square shaking table facility at the Richmond field station of the University of California, Berkeley. The types of storage racks tested were: standard pallet rack, back-to-back pallet rack, drive-in rack, and stacker rack. Three racks were anchored to the table and tested under live loads simulated by concrete blocks (1,000 lb/block) in each of the two principal directions. One rack (the back-to-back pallet rack) was tested without anchors to the table. The rack configurations selected for investigation are summarized in Table 4.1. Basic section properties as supplied by the manufacturers for beams, columns, braces, and other elements are listed in Table 4.2.

The racks to be tested were supplied by various manufacturers. The selection of these racks was based on the manufacturers' brochures (or standard loading tables) in accordance with industry practice. The test structures were not modified or reinforced for this study. The maximum simulated storage weights were 3,000 lb/pallet for the standard pallet and drive-in racks and 2,000 lb/pallet for the stacker rack.

Brief descriptions of different types of storage racks investigated in this study are presented next.

Standard Pallet Rack. The standard pallet rack is probably the most common type of rack used for industrial storage. Figure 4.1 shows photographs of standard pallet rack assembly on the shaking table. The standard pallet rack modular assembly consists of prefabricated uprights in the rack transverse direction and horizontal beams spanning between successive uprights in the longitudinal direction.

The uprights have two posts 43 in. apart (outside dimensions) that are connected by horizontal members spaced 5 ft vertically. The uprights are braced in their plane with single-diagonal bracing between the vertical post and horizontal member panel points. Upright posts have bearing plates at the bottom that have a single hole for installation of a floor anchor. Connections of upright frame members are button welded. The beam end connections (shelf connectors) are of the clip-in type, and the upright posts are slotted along their full height to allow variations in beam vertical spacings.

Figure 4.2 shows the rack configuration and detailed connections.

Back-to-Back Pallet Rack. Figure 4.3 shows the back-to-back pallet rack assembly. This rack assembly is essentially the same as the standard pallet rack except that rigid row spacers are provided to tie two identical pallet racks together. This assembly was not anchored to the shaking table. The rigid row spacers are shown later in Figure 4.9.

Drive-In Rack. In the drive-in storage rack, storage pallets are supported by rail members spanning between support arms that cantilever from the columns rather than by beams spanning the bay width as in the standard pallet rack. The drive-in rack is accessible from one side, but forklifts cannot pass all the way through it. The drive-in storage rack tested is shown in Figure 4.4.

Upright frame (and anchor frame) assemblies are similar in construction to those described for the standard pallet racks. The frames are connected by a continuous rail that supports the pallets. In the longitudinal direction, the upright frames are connected at the top by continuous tie members (overhead tie beams). For the anchor frames, ties (anchor beams) are provided at each story level. Horizontal-load-carrying systems for the drive-in rack typically consist of bracing in the transverse direction and frame action in the longitudinal direction of the racks.

Figure 4.5 shows the configuration and dimensions of the drive-in rack assembly. The connection details are illustrated in Figure 4.6.

Stacker Racks. Stacker racks are part of an industrial storage system that generally uses floor-running stacker cranes for storage and retrieval of goods in large distribution centers. Stacker cranes are usually remote-controlled and can operate in narrow aisles so that material storage density can be maximized. With computerized controls, stacker racks can provide an efficient, inventory-controlled material-handling system. A recent survey of the rack industry, published as "Don't Make Racks an Afterthought"[13] in *Handling & Shipping*, shows an increase in the use of stacker racks from 6% of the total rack market in 1971 to 20% in 1975, with a prediction of 35% in 1981.

Stacker rack frame assemblies resemble the drive-in rack configuration previously described but are usually more complex structures because they are larger. Horizontal-load-carrying systems generally consist of bracing in the transverse direction and frame action combined with supplemental bracing in the longitudinal direction.

Figure 4.7 shows the stacker rack assembly on the shaking table. The dimensions and connection details are illustrated in Figures 4.8 and 4.9, respectively.

4.2 The Test Facility

The Shaking Table. The U.C. Berkeley earthquake simulator facility, shown in Figure 4.10, is described in detail by Rea and Penzien.[14] The facility consists of a 20 ft by 20 ft posttensioned concrete slab shaking table that can move simultaneously in one horizontal direction and in the vertical direction, its associated electrohydraulic drive, its electronic control, and its data-acquisition and -processing system.

Figure 4.11 indicates the limiting ranges of the dynamic performance of the shaking table. The maximum displacement and velocity that can be achieved by the shaking table in the horizontal motion are 5 in. and 25 in./sec, respectively. When loaded with its upper limit of 100 kips, the shaking table can move in the horizontal direction a maximum of 0.67g and, simultaneously, about 0.5g in the vertical direction. The shaking table was designed to have a natural frequency greater than 20 Hz so that it would behave essentially as a rigid body in the typical operating frequency range of 0-10 Hz.

Data-Acquisition System. Associated with the shaking table is a data-acquisition and -processing system that is based on a NOVA 1200 minicomputer in conjunction with a moving-head magnetic disc unit. The system is capable of data acquisition up to 128 transducer channels at a usual rate of around 50 samples/sec/channel. The data can convert to digital form through a 9-track Wang digital magnetic tape recorder for data reduction on the CDC computer system. A Versate printer/plotter was also used to perform preliminary data processing.

4.3 Instrumentation

The instrumentation served to define the table and individual story accelerations and displacements and the local member deformations during each test. Story accelerations and displacements were measured by accelerometers and potentiometers, respectively. Electrical resistance strain gages and displacement transducers (DCDTs) were installed at critically stressed locations in members to measure local deformation quantities at any time during each test. Table 4.3 summarizes all transducer channels used for global and local response measurements.

Kistler Model 305T nonpendulous, force balance servo accelerometers, with a Kistler model 515T servo amplifier attached were installed to measure accelerations of both the test structure and the shaking table. The accelerometers have a range of ±50g at a sensitivity of 100 mV/g. Accelerations can be measured to an accuracy of up to 0.0001g at the highest gain set for the amplifier.

To measure the absolute horizontal displacements, Series 1800-30A Houston Scientific potentiometers were adopted. This transducer has a travel range of ±15 in. Figure 4.12(b) shows the potentiometer attached to an independent reference frame, located outside the shaking table. Light nylon radio dial cables were utilized to connect the clip pins of the potentiometers to their targets on the structure.

Sanborn model 7 DCDT-500 displacement transducers with a stroke of ±1/2 in. were used in opposing pairs to measure average end rotations (or curvatures) of members. The transducers were mounted in aluminum frames set at a distance of 3 in. between two target frames. Figure 4.13 illustrates typical setups of these DCDT gages to measure the average rotation at the top and bottom ends of the first-level column.

Electrical resistance strain gages manufactured by Micro-Measurements, model EA-06-250 BG 120, were used in the tests.

4.4 Input Table Motions

The input signals from actual strong-motion accelerograms chosen for this study were the 1940 El Centro north-south and the 1966 Parkfield records. The El Centro signal was used for most of the tests. The Parkfield signal, having significantly different frequency content from the El Centro record, was chosen to determine how the structures would behave and how well the mathematical models would work when an input signal other than the El Centro earthquake motion was used. The acceleration time histories, the displacement records, and the response spectra of the different test intensities are shown in Figures 4.14 through 4.19. The El Centro earthquake motions are designated EC, and the Parkfield earthquake inputs are assigned PF. The number preceding these designations is the fraction of the maximum intensity recorded. The designations 1/4 EC and 1/2 EC, respectively, represent tests performed using the El Centro signal with the maximum intensities about 1/4 and 1/2 that of the actual El Centro record. No time scaling of the input signal was performed because the testing was not intended to be a model test of any prototype structure.

4.5 Test Procedures and Test Runs

Test Procedures. For the entire test program, except for the types of table motions used, the same test procedures were used in conducting the tests.

For each test day, all transducer channels were calibrated by means of the voltage change at a known deflection of a gage. After satisfactory calibration factors for all channels have been obtained, the final calibration was transferred to magnetic tape for permanent storage. However, before a test, this information was called into the disc to prepare for data acquisition.

The table motion was calibrated to obtain the functional relationship between the peak responses of the table and the control span setting. By means of this relationship, the desired table intensity in each test could be prescribed by selecting an appropriate span setting value for the signal to be used.

During each test run, transducer calibrations, zero readings, and test readings for the entire time history were collected for each channel and stored by the computer on a magnetic disc. These temporary data were transferred to magnetic tape for permanent storage if the test run was determined to be satisfactory. In addition, a log record was maintained during each test to describe all of the test conditions to which the structure was subjected.

Each dynamic test was begun by taking zero readings of all transducers a few minutes before the test. During the actual test, the data-acquisition system was turned on a few seconds before the table motion was initiated. After the significant part of the earthquake record had been used to excite the structure, the table was stopped, but the data-acquisition system continued to operate for about 10 to 20 sec longer so that the final free vibration could be recorded. The test results were then examined by using the minicomputer of the data-acquisition system, which printed out the maximum and minimum values for each data channel and their corresponding times. If the results were satisfactory, the test data were then transferred to magnetic tape for storage and data reduction.

Free vibrations were applied to some of the test structures to obtain their small-amplitude dynamic properties. The test structures were mounted on the shaking table, and the vibration was generated by imposing a static horizontal deflection on the structure and then releasing this force suddenly. The recorded acceleration signal for each top story level was then filtered through a band-pass filter, with the bandwidth selected to cover the expected frequencies. The data were then displayed on visicorder paper for frequency and damping evaluation.

Dynamic Test Runs. Tables 4.4 through 4.11 present all dynamic test runs conducted for the structural performance shaking table test program. In these tables, the test identification (Test I.D.) consist of the date and the test number for that date. In addition, live load cases, table motions, signals, and remarks on tests are included in the tables. For convenience, these tests are divided into three phases:

Phase I - Standard Pallet Rack Tests

		Total Test Runs	Selected Runs for Analysis
I-1:	Longitudinal Test	11	8
I-2:	Transverse Test	11	5
I-3:	Longitudinal Test (Back-To-Back)	7	5
I-4:	Transverse Test (Back-To-Back)	8	-
		37	18

Phase II - Drive-In Rack Tests

		Total Test Runs	Selected Runs for Analysis
II-1:	Longitudinal Test	9	7
II-2:	Transverse Test	4	3
		13	10

Phase III - Stacker Rack Tests

		Total Test Runs	Selected Runs for Analysis
III-1:	Longitudinal Test	10	8
III-2:	Transverse Test	8	6
		18	14

From the above summary it can be seen that 68 dynamic test runs were conducted and 42 runs were selected for detailed data evaluation. Results of these selected test runs will be presented briefly in Sections 4.8-4.14.

4.6 Data Reduction

Raw Data. For each test run, the table control signals, the table motions, and the global and local responses of the structure were sampled at a rate of approximately 50 points/sec and recorded in digital form on a magnetic disc. This information was then transferred to a 9-track magnetic tape, where it was treated as a single record stored on a logic file. Since the 9-track tapes were not compatible with the 7-track tape system of the CDC 6600/7600 computers at the University of California Lawrence Berkeley Laboratory Computing Center, a compatible program was written to convert the original data tapes to the 7-track tapes for data reduction.

All data were expressed as five-digit floating numbers in units of g for acceleration, inches for displacement, mils per inch for strain, and kips for the table actuator force.

The total records for the El Centro and Parkfield signals are about 43 sec and 24 sec, respectively. These records include the final free-vibration data after the table was stopped and a few seconds of initial zero values before the table was started.

Reduction Processes. The data are generally presented in the form of time-history plots of the response parameters, with some response spectrum and Fourier amplitude curves. The computer program SMIS[15] was used extensively, with some modifications for Fourier spectrum calculation and response spectrum plotting. A brief description of the table and response parameters and their processing sequences follows.

The table motions are essential information for analytical predictions of the structure responses. The basic table motions are presented in the form of time-history plots of acceleration and displacement. The table velocities were not recorded directly, but they could be calculated by integration of accelerations.

Another significant way of describing the table motions is by means of response spectra. The response spectra are essential for dynamic analysis using the response spectrum method. Thus, the absolute accelerations, relative velocities, and relative displacements were computed and plotted on log-log graphs, considering damping ratios of 1%, 3%, 5%, and 8% of critical.

The global response of the complete structural system can be obtained by accelerometer and potentiometer measurements made at each story level. The absolute story accelerations were measured directly from the accelerometers and required no reduction process.

Fourier spectra were computed from the story acceleration time histories using the fast Fourier transform algorithm, using 1,024 (or 2,048) discrete values to make a time record of about 20.17 sec (or 40.34 sec) duration. Sufficient trailing zeroes were added to the time histories to achieve this duration, if needed. These transforms were then smoothed by a running average technique, replacing the central point with the weighted average of five consecutive points. From these spectra, the natural frequencies of the structure can be identified.

The story displacements relative to the table were obtained by subtracting the table displacements from the absolute story displacements. The inter-story drifts were determined in a similar manner. The story shear was obtained by summing the story inertia forces (story mass times story acceleration) from the top to the story level in question. Likewise, the story overturning moments were found by summing the moments of the story inertia forces about the level under consideration.

The numerous strain gages installed at the various structure members made it possible to evaluate internal deformations of the members at any time during each test. Unfortunately, no calibration tests were performed to establish the relationships of flexural strains versus moments (or axial strains versus axial forces). Therefore, in this report, member strains (mil/in.) were used instead of member forces.

The DCDT gages (Figure 4.13) were used to measure the average end rotations of critical column members. The average end rotation θ can be expressed as

$$\theta = \frac{|\Delta_1| + |\Delta_2|}{h}$$

where Δ_1 and Δ_2 are the extensions of contractions of two parallel chords and h is the gage length (see Table 4.3 for the gage lengths corresponding to various test runs). If the calibration data between moment and rotation are available, the average moment M can be determined as

$$M = \frac{EI}{L} \cdot \theta$$

where:

E = modulus of elasticity

I = moment of inertia of the column section about the axis in question

L = distance between two aluminum frames (3 in.)

The above relationship assumes that the relative rotations between two sections are small and that plane sections remain plane after deformation.

4.7 Test Results - Introduction

The results obtained from the selected test runs are organized into separate sections for each rack tested. Each presents the instrumentation plan, a brief discussion of global and local responses, and a summary of the seismic behavior observed for each rack assembly.

Tests are identified by rack type, test direction, live load, and intensity and signal used. Abbreviations for these are as follows:

Rack Type:	SP	Standard pallet rack
	DI	Drive-in rack
	ST	Stacker rack
Test Direction:	L	Longitudinal
	T	Transverse
Live Load:	1	Full live load
	2/3	2/3 live load
	1/2	1/2 live load
Intensity/Signal:	1/4 EC	1/4 the actual El Centro signal
	1/4 PF	1/4 the actual Parkfield signal
	etc.	

The method of applying live load for the shaking table tests was to make up concrete blocks that were bolted to the wooden pallets, which, in turn, were bolted to the racks (or banded with metal straps for the drive-in and stacker racks). While this method is not realistic in industry practice, it was deemed essential for obtaining experimental data on the performance of the racks and testing the adequacy and effectiveness of the various analytical procedures and assumed mathematical models. It would be impossible to model the rack structures with unknown effective mass mounted on the racks. However, this unrealistic method of applying live load is justified by the merchandise shaking table test results (Chapter 5).

4.8 Test Results - Standard Pallet Rack, Longitudinal

Eleven test runs were conducted in this series. Eight test runs were selected for detailed data evaluation. A summary of selected extreme quantities and dynamic response properties for these runs is presented in Table 4.12. Instrumentation channels used for data analysis are shown in Figure 4.20. Four test runs were selected for presentation here. One test was conducted with 2/3 live load (i.e., 2,000 lb/pallet), and the others were conducted with full live load (i.e., 3,000 lb/pallet).

Global Responses. Figures 4.21a through 4.21d show the absolute story accelerations for the four test runs. The responses are seen to contain not only the first mode but also the higher modes of vibration. The vibration periods of the three modes, as experimentally determined by a fast Fourier transform analysis of the third-level acceleration, are shown in Table 4.12. The story displacements, relative to the table, shown in Figures 4.22a through 4.22d indicate in general the predominant first-mode vibration with varying amplitude. For the SP-L-1-1/2 EC test case, only 10 sec of response are included in this presentation because of the failure of the data-acquisition system at about 12 sec.

Figures 4.23a through 4.23d illustrate the time-history plots of the base shears and overturning moments determined by inertia forces for the four test runs. These results, along with the interstory drift plots (first floor relative to table), can be used to determine the contribution of the p-δ effect to the column moment. The equivalent total story shear can be approximately expressed as

$$V_T = V_I + V_P$$

where:

V_I = story shear determined by inertia forces

$V_P = \frac{\Sigma W.\delta}{H}$

= lateral force induced due to the p-δ effect

ΣW = the summation of all weights supported above

δ = interstory drift

H = story height

From the above expression, the ratio V_T/V_I (the amplification of story shear due to the p-δ effect) can be determined as shown in Table 4.13. This clearly shows that the contribution of story shear due to the p-δ effect is significant and should be considered in response prediction and design.

Local Responses. The time-history plots of the column end rotations measured with the DCDT gages are shown in Figures 4.24a through 4.24d. It can be seen that the rotations (or bending moments if the calibration curve of rotations versus known moments is available) at both ends of the center first-level column are almost in the same order of magnitude. Thus, the base plates provide a significant fixity against rotation, which, in turn, reduces the moment at the first-level columns. The calculated rotations at the initiation of yield are about 2.14×10^{-3} rad and 1.73×10^{-3} rad for the 2/3 and full live loads, respectively. The detailed procedures for evaluating the yield rotations (described in Appendix A) were based on Section 3.6.1 of the 1968 edition of *Specifications for the Design of Cold-Formed Steel Structural Members*,[16] published by the American Iron and Steel Institute (here called AISI 3.6.1), assuming that the members would not be subject to torsional-flexural buckling. The results clearly indicate that, during the SP-L-1-1/2 EC and SP-L-1-1/2 PF tests, the column end rotations exceeded the yield value of $\phi_y = 1.73 \times 10^{-3}$ rad. The estimated rotational ductility ratios for all test runs selected for study are also shown in Table 4.12.

Summary. The selected results presented above show no evidence of structural damage. However, for test run SP-L-1-1.33 EC, the input table motions were increased to produce a maximum horizontal acceleration of about 1.33 times the actual El Centro signal with the addition of vertical excitation. This test run caused some minor distress at the top end of the center first-level column. The maximum interstory drift was approximately 4 in. (or $0.069H$), and the rotational ductility ratio was estimated to be about 2.6 (see Table 4.12).

The natural periods of vibration and damping values observed are summarized in Table 4.12 and plotted in Figure 4.25. The periods were determined from (1) a fast Fourier transform analysis of the third-floor acceleration records during the shaking table excitation, and (2) a free-decay measurement after the table was stopped. For comparison, the results from the pull-release tests are also shown in Figure 4.25. The variation of dynamic properties with respect to the input signals, intensities, and the test sequence is clearly shown in the figure. Because of the looseness of semirigid connections, the damping values are relatively high, as would be expected. The damping values, which ranged from 3% to 9% of critical, were based on the free-decay data after the table was stopped and on the free-vibration measurements from the pull-release tests.

The contribution to story shear of the p-δ effect is very significant. Table 4.13 presents this secondary effect based on the data shown in Table 4.12. The amplification ratios of V_T/V_I are estimated to be in the range of 1.3 to 1.6. It is evident that the p-δ effect will greatly affect the response of the racks and should be considered in response prediction and design.

The results from the rotation measurements presented for each individual test run clearly demonstrate that the column base did provide a considerable restraint against rotation, which, in turn, reduced the column moments at the first-story level.

4.9 Test Results - Standard Pallet Rack, Transverse

Eleven tests were carried out for this test series (see the summary in Table 4.5). Five test runs were selected for detailed data analysis. Table 4.14 summarizes the results of some extreme quantities and dynamic response properties from these selected test runs. The instrumentation channels used for data reduction are illustrated in Figure 4.26. Three test runs were selected for discussion here. One test run was simulated with 2/3 live load (i.e., 2,000 lb/pallet), and the other two runs were loaded with the full live load (i.e., 3,000 lb/pallet).

Global Responses. Figures 4.27a and 4.27b display, for two test cases, the time-history plots of the story displacements (relative to the table) measured at the third-story level of three upright frames, from which it can be seen that the global response of the three frames was nearly identical. Some minor difference in magnitude might be visible; this was probably caused by unavoidable minor unsymmetry in stiffness and mass distribution. However, during the SP-T-1-1/2 EC test, a significant unsymmetrical response was observed (Figure 4.27c) because the story overturning moment greatly exceeded the limiting value required to initiate uplift at the exterior frame column. This condition caused the weld fracture at the northwest column base.

Figures 4.28a through 4.28c and 4.29a through 4.29c illustrate for the three test runs the absolute story accelerations and the relative story displacements measured at the center frame. The response is seen to be dominated by the first mode, with the second mode visible in the first-level acceleration records. The periods of vibration were determined by fast Fourier transform analysis of the third-level acceleration records and are indicated in Table 4.14.

Figures 4.30a through 4.30c present the base shears and overturning moments for the three test cases, on the assumption that the horizontal floor diaphragm was perfectly rigid and that the total mass was equally distributed to each upright frame. Figure 4.30c shows that the overturning moment did greatly exceed the estimated limiting value of 183 kip-in. required to initiate uplift at the exterior frame columns, which, in turn, caused the weld fracture at the northwest column base.

Local Responses. The axial strains of the two bottom diagonal members for the three test runs, shown in Figures 4.31a through 4.31c, indicate nearly symmetric response. However, it can be seen that the center diagonal brace attracted slightly more story shear than the exterior member. All strains measured during this test series were within the strain yield limit of ε_y = 0.49 mil/in. in accordance with AISI 3.6.1.

The column axial strains and end rotations near the base for the three test cases are shown in Figures 4.32a through 4.32c. The column axial strain plots, comparing the north and south center columns, demonstrate the expected antisymmetric response behavior. It can be observed from the column rotation measurements that the column bases provide a significant fixity against rotation. During the SP-T-1-1/2 EC test, the rotation at the south center column near the base exceeded the estimated yield value of $\phi_y = 0.51 \times 10^{-3}$ rad.

Summary. The weakest spots of this rack assembly during the shaking table tests were at the weld connecting the column to the base plate. As shown in Table 4.5, the welds began to fracture at a very low level of excitation (1/4 PF) when the rack was loaded with 2/3 live load. A weld fracture at the connection between the open-section diagonal element and the column is shown in Figure 4.33. It may be concluded that the connections of the column to the brace and to the base plates with only a few button welds are not sufficient to develop the full capacities of the members. This undesirable design practice can be easily improved by fully welding around these connections. Noticeable distress of all columns near the base plate except one at the northeast column was observed (Figure 4.33) when the structure was loaded with the full live load under the 1/2 EC input table motion. The estimated maximum rotational ductility ratio of the column near the base plate was approximately 1.9, as determined by procedures described in Appendix A. As the input signal increased to 5/8 EC combined with an appropriately scaled vertical motion, the undamaged northeast column also suffered damage near the base.

The measured fundamental period of vibration and damping values of the standard pallet rack tested in the transverse direction are plotted in Figure 4.34. As expected, the damping or energy-absorbing capacities were smaller (ranging from 0.5% to 1.6% of critical) than those observed in the longitudinal direction. Strong amplitude dependance on the periods of vibration, as observed in the longitudinal test, was not evident in the transverse test case.

For this test series, the column end rotation measurements by DCDT gages show that the column base plate did contribute considerable fixity against rotation. This indicates that the upright posts near the base plate are the most critical spots, subject not only to axial loads but also to bending moments. The interaction between axial load and bending moment can be treated by means of the M-P interaction equation illustrated in Appendix A.

Because of the braced-frame system in the transverse test direction, the estimated p-δ effect was not significant and need not be considered in rack design.

Before the vibration tests, a mathematical model was developed to predict the natural periods of vibration of the rack assembly in the transverse direction. The mathematical model assumed: (1) beam-column elements for the upright posts; (2) truss elements for the diagonal braces; (3) center-to-center dimensions; (4) pinned bases; and (5) equal distribution of the total mass to each upright frame. From these assumptions, the fundamental periods were calculated to be 0.41 sec and 0.50 sec for the 2/3 and full live load cases, respectively. These predicted periods were substantially lower than the observed periods from the pull-release tests (0.66 sec and 0.84 sec for 2/3 and full load cases, respectively). The difference between prediction and measurement was attributable to the strong localized deformations at the connections between the open-section diagonal bracing elements and the open-section columns. Static cyclic tests on the full-scale rack conducted at Stanford University[9] showed early nonlinear behavior and strong local deformation at these connections. This localized deformation affects response predictions significantly.

4.10 Test Results - Comparison of Anchored and Unanchored Standard Pallet Racks

A record of the shaking table tests in the longitudinal direction of the back-to-back pallet rack, which was not anchored to the table, was presented in Table 4.7. Eight tests were carried out for this series, and five test runs were selected for detailed data analysis. Table 4.15 summarizes the results of selected extreme quantities for this test series along with the results from the standard pallet rack anchored to the table. The instrumentation channels used for data reduction are shown in Figure 4.35. Only two individual test runs were selected for presentation in this report.

Global Responses. For all tests conducted on the back-to-back pallet rack, the time-history plots of the third-level relative displacements measured at different frames showed symmetrical response and no torsional vibration. Figure 4.36 shows a typical example using the input signal of 5/8 EC. This observation can provide a good basis for comparing the seismic behavior of anchored versus unanchored (lagged versus unlagged) test cases.

A comparison of interstory drifts for both anchored and unanchored pallet racks, shown in Figure 4.37, clearly indicates that the interstory drifts of the unanchored rack were greater than those of the anchored rack under the same input signal. Figure 4.38, comparing the base shears for both cases, indicates that the anchored rack displayed lower story forces than the unanchored rack.

Table 4.16 shows a comparison of the base shears for anchored and unanchored conditions. The base shears determined by inertia forces are consistently larger for the unanchored rack, and the shears that result from the p-δ effect also favor the anchored rack.

Local Responses. The local response measurements from the DCDT gages mounted at both ends of the first-level center columns for both test cases clearly favor the anchored case (Figures 4.39 and 4.40). The rotational ductility ratios at the top end of the center first-level columns listed in Table 4.15 indicate consistently larger ductility ratios for the unanchored rack subjected to the same input motion.

Collapse of the Structure. The structure collapsed during the high-amplitude excitation using simultaneously the maximum horizontal and vertical accelerations of 0.44g and 0.2g, respectively. Figure 4.41 shows the horizontal table acceleration and displacement used for this test run.

Figure 4.42 shows that the collapse occurred at about 7 sec. The maximum third-level relative displacements (Figure 4.42) and the maximum interstory drifts (Figure 4.43) were approximately 12 in. and 6 in., respectively. The amplification of the story shear due to the p-δ effect seems to be responsible for the collapse of the rack assembly. This was verified by the film taken during the test, which clearly shows that the collapse was initiated by the large side sway at the top of the first-story level, which was followed by kicking of the bottom ends of the first-level columns. The absence of lagging at the base of the columns undoubtedly contributed to the collapse. Figure 4.44 shows the totally collapsed rack structure.

4.11 Test Results - Drive-In Rack, Longitudinal

As shown in Table 4.8, nine tests were conducted for this test series, of which seven were selected for detailed data evaluation. Table 4.17 summarizes some of the extreme values and dynamic properties from these seven tests. Instrumentation channels used for data analysis are shown in Figure 4.45. Only three test runs simulated with the full live load (i.e., 3,000 lb/pallet) were selected for presentation in the following.

Global Responses. For all tests conducted in this test series, no torsional response was observed for this unsymmetrical frame system. Figure 4.46 shows a typical example comparing the third-story displacements relative to the table of three frames parallel to each other. It can be seen from this comparison that the displacements from these three frames were identical, although the frame system in the test direction was unsymmetrical. However, the calculations presented in Appendix B show that the torsional response contributed only about 3% to 6% of the total response and was not visible from the displacement time-history plots.

Figures 4.47 and 4.48 display, for the DI-L-1-1/4 EC test, the story acceleration records showing primarily the first and second modes, with a strong second mode visible in all acceleration records. Comparison of these story acceleration records measured at the two exterior frames also indicates the close resemblance between the story levels. These observations were typical of all test runs conducted in this test series.

Figures 4.49a through 4.49c show, for the three test runs, the relative story displacements at various story levels. Figures 4.50a through 4.50c display time-history plots of the base shears and overturning moments for three different tests. The inertia forces were obtained from the product of total mass per floor and the average values of the corresponding acceleration time histories measured at two exterior upright and anchor frames. The influence of the p-δ effect on the story shear was found to be very significant. Table 4.18 summarizes the results of all test data analyzed.

Local Responses. Figures 4.51a through 4.51c present for the three test runs the local response measurements of the column end rotations by the DCDT gages. A comparison of the measured column end rotations at the top and near the base of the first-floor critical column again indicates that the column base plate provides a significant restraint against rotation. The time-history plots of column end rotation, as shown in these figures, clearly show that the rotations did not exceed the yield values ($\phi_y = 9.6 \times 10^{-3}$ rad and

12.1 x 10^{-3} rad for the anchor and upright frames, respectively). The procedures used to obtain these yield values are similar to those shown in Appendix A for the standard pallet rack.

Summary. The input signal used in the last test run for this test configuration was scaled to produce a maximum horizontal acceleration about 5/8 that of the actual El Centro record with the addition of an appropriately scaled vertical acceleration (DI-L-1-5/8 EC). No structural damage was observed. However, the amplification of story shear due to the p-δ effect was found to be very significant. Because of the experience of the total collapse of the pallet rack and for safety, it was decided to stop the test. No test conducted in this series showed evidence of material yielding.

The measured dynamic response properties of the drive-in rack assembly tested in the longitudinal direction are shown in Table 4.17. It is evident that the structure was very flexible. The fundamental periods of vibration ranged from 2.5 sec to 3.3 sec when the rack was loaded with the full live load (3,000 lb/pallet). The damping values observed from the shaking table free-decay data were 4% to 9% of critical, which is very similar to those found for the standard pallet rack tested in the longitudinal direction.

The drive-in rack assembly in the longitudinal direction consists of two upright and two anchor frames, as shown in Figure 4.45. Although the structural system and stiffness for these two types of frames are quite different, no torsion was detected from the displacement time-history plots. A calculation was performed to distribute the total horizontal shear carried by each of the parallel frames due to the eccentric horizontal load (the centers of rigidity and mass do not coincide). The results, presented in Appendix B, indicate that the torsional effect is insignificant (approximately 3% to 6% of the total). This negligible torsional effect enables one to model this structure two-dimensionally. This will greatly simplify the analysis procedure.

The influence of the p-δ effect on the story shear is very significant. The amplification ratios for each test run as presented in Table 4.18 are in the range of 1.3 to 1.6. It is apparent from the results shown in the table that the p-δ effect will greatly affect the response of this rack assembly in the longitudinal direction.

Local response measurements of the column rotations at the top and the bottom ends of the first-story level have shown that the column base plate did provide considerable restraint against rotation, as was observed in the standard pallet rack test cases.

4.12 Test Results - Drive-In Rack, Transverse

Four tests simulated with the 2/3 live load (2,000 lb/pallet) were conducted for this test configuration (see Table 4.9). Three test runs were subjected to detailed data analysis. Table 4.19 summarizes some of the extreme values and dynamic response properties for this test series. Instrumentation channels used for data reduction are shown in Figure 4.52. Two tests were selected for presentation in the following.

Global Responses. For all tests conducted in this test series, the displacement time-history plots measured at the three parallel frames were nearly identical. Some minor difference in magnitude was evident and was probably caused by unavoidable minor unsymmetry in mass distribution and stiffness. Figure 4.53 shows, for the DI-T-2/3-1/4 EC test, a typical example comparing the third-level displacements measured at the three frames. The story displacements for the two test runs, shown in Figures 4.54a and 4.54b, indicate the predominant first-mode contribution. Considerable permanent set in the displacement response was evident in the case of the run with the input signal of 1/4 the Parkfield record as shown in Figure 4.54b. Figures 4.55a and 4.55b display, for the two test cases, the story accelerations, which again indicate that the response is dominated by the first mode. The fundamental periods of vibration for these test runs were 0.58 sec and 0.59 sec, respectively, as determined from the fast Fourier analysis of the third-level acceleration records. The estimated base story forces showing in Figures 4.56a and 4.56b for the two test runs assume the rigid horizontal floor diaphragm and equally distributed mass to each frame.

Local Responses. The local response measurements on the bottom diagonal braces in Figures 4.57a and 4.57b demonstrate that the bottom diagonal members in the upright frame did exceed the theoretical yield strain limit (ε_y = 0.31 mil/in.) but that the diagonal members in the anchor frame did not exceed the yield strain value (ε_y = 0.42 mil/in.). Considerable buckling and permanent set were observed in the case of the test run with the input signal of 1/4 the Parkfield record. The values of ε_y were determined from AISI 3.6.1.

<u>Summary</u>. As described above, considerable buckling of the bottom diagonal braces in the upright frames was observed when the table was shaken by the input signal of 1/4 PF. Nevertheless, the test was continued for this damaged structure. The last test run was conducted with a maximum acceleration about 1/2 that of the actual El Centro record (DI-T-2/3-1/2 EC). The fundamental period of vibration increased substantially from 0.59 sec to 0.67 sec for this last test run. The buckling of the bottom diagonal members in the upright frames became more severe (Figure 4.58). In addition, two tack welds broke at the connections between the open-section columns and the open-section braces in the anchor frame. This behavior clearly shows that the diagonal braces in the upright frames were underdesigned (the slenderness ratio l/r is 177 compared with 155 for the anchor frame).

The fundamental periods of vibration observed before the structural damage were around 0.56 sec to 0.59 sec. As might be expected in the braced-frame system, the damping values observed are relatively small (around 2% of critical), and therefore very similar to those found in the standard pallet transverse test case. The p-δ effect in this test configuration is insignificant. The amplification ratio was estimated to be about 1.05.

4.13 Test Results - Stacker Rack, Longitudinal

Ten tests were carried out for this test configuration (see Table 4.10). Eight tests were selected for detailed data analysis. Table 4.20 summarizes selected extreme values and dynamic properties from the eight test runs.

Instrumentation channels used for the data analysis are shown in Figure 4.59. The results of the three test runs loaded with the full live load (i.e., 2,000 lb/pallet) are presented next.

Global Responses. The displacement records for all tests conducted on this rack configuration show that the response was symmetric; no torsion was observed. This is shown in the displacements measured at the sixth level of three parallel frames (Frames A, C, and D) for the test run with the input signal of 1/4 the El Centro record (Figure 4.60). The displacements are seen to be identical both in phase and in magnitude. The time-history plots shown in Figure 4.61 also indicate close similarity of the acceleration records measured for Frames A and C.

The story displacements shown in Figures 4.62a and 4.62b indicate considerable difference in response, although both cases were conducted under the same earthquake signal but at different intensity levels (1/4 EC versus 1/2 EC). Figure 4.62c shows the story displacements that occurred when the structure was subjected to the input signal of 1/2 the Parkfield record. Significant difference in response was observed from these three test runs. However, the response was generally in the first-mode vibration. Figures 4.63a through 4.63c display the story accelerations for the three test cases with considerable second-mode contribution visible in the records. The base shears and overturning moments shown in Figures 4.64a through 4.64c for the three test runs were determined from the story inertia forces at each level, i.e., the product of the average measured story accelerations and the total story mass.

Local Responses. Figures 4.65a through 4.65c show, for the three test runs, the local response measurements on the two bottom diagonal tie rods. Because the recorded strain values represent only dynamic strains (or forces), the diagonal axial strains in compression were clipped off at a level representing the magnitude of the pretension strain (force). However, this was not shown in the case of the test run with the input signal of 1/2 the Parkfield record (Figure 4.65c). During this test, there was no pretension strain because the joints connecting the rods and the rod supports had loosened as a result of previous high-amplitude excitation.

Comparison of the column axial strains (not shown) generally indicates antisymmetric responses of Columns A-4 versus A-2, B-4 versus B-2, and D-4 versus D-2 (i.e., the overturning moment could be determined if the strain-force functional relationships were available). As might be expected, because of the specific location of the diagonal braces, the axial strains at the exterior columns (A-1 and A-5) were relatively small compared with the column axial strains at Frames 2 and 4.

Summary. The last two test runs for the rack configuration shown in Table 4.20 were performed using nearly the same input table motions. (This was done by mistake; the original intention was to add the appropriately scaled vertical acceleration to the last test run.) However, the results provided some interesting seismic behavior. As noted in footnotes c and d of Table 4.20, Test 221178.5 was conducted when the diagonal rods were loose, whereas the last test run (221178.6) was carried out when the rods were tied with some pretension force. Comparison of the selected extreme values shown in the table indicates that the test case with the loose diagonal rods was more favorable than the test case with the tied rods. In addition, buckling of columns between the bottom diagonal rods (columns B-4, B-2, C-4, and C-2 between the second and third levels) was observed (Figure 4.66).

As shown in Table 4.20, the periods varied considerably for each test (from 0.94 sec to 1.4 sec for the full live load, as determined by a fast Fourier transform analysis of the sixth-level acceleration records), caused in part by the looseness of the diagonal rods but also by the degradation in stiffness. The damping values evaluated from the shaking table free-decay data were in the range of 4% to 6%.

Because the displacement records show that the response was symmetric and no torsion was observed, two-dimensional nonlinear mathematical modeling is possible.

Since the rack stability is dependent on the diagonal bracing, the p-δ effect is insignificant, as might be expected. The maximum amplification of the story shear due to the p-δ effect was found to be approximately 1.08. For industry design practice, the p-δ effect need not be considered in the design analysis.

4.14 Test Results - Stacker Rack, Transverse

Eight tests were conducted in this test series (see Table 4.11), and six test runs were selected for detailed data analysis. Table 4.21 presents the results of selected extreme quantities and dynamic response properties. Instrumentation channels used for the data analysis are shown in Figure 4.67. A brief discussion of the test results from three of the test runs conducted with the full live load (i.e., 2,000 lb/pallet) is presented in the following.

Global Responses. Figures 4.68 and 4.69 show for the ST-T-1-1/4 EC test the displacement and acceleration time-history plots observed at the sixth level of three parallel upright frames (Frames A, C, and E). Comparison of these plots indicates that the responses were similar in phase but not in magnitude. This unsymmetric nature of response in magnitude was probably caused by unavoidable minor unsymmetry in stiffness and mass distribution. It was also probably due to the rigidity added to the interior floor diaphragms by the horizontal cross-braces at the sixth and third floors between Frames B and D. The above observation was typical for all test runs conducted in this test series.

Figures 4.70 and 4.71 display, for the three test runs, the displacements and accelerations observed for three floors of Frame C. The figures indicate primarily first-mode vibration. During the most severe shaking table excitation (with the input signal of 1/2 the Parkfield record), the maximum sixth-level displacement and acceleration were about 3.0 in. and 1.0g, resepctively.

Local Responses. The local response measurements of the brace axial strains (north and south bottom floors), shown in Figures 4.72 and 4.73 for the three test runs, clearly indicate that the interior frames attracted more shear forces than the exterior frames. During test ST-T-1-1/2 PF, all interior bottom diagonal members exceeded the theoretical yield strain limit of ε_y = 0.32 mil/in. and buckled considerably; permanent set was also evident (see Figures 4.72c and 4.73c). The value of ε_y was determined from AISI 3.6.1.

Summary. For this test series, structural damage was evident in the test run with the input signal of 1/2 the Parkfield record (ST-T-1-1/2 PF). All interior bottom diagonal braces buckled considerably. In addition, some minor distress was observed for all interior columns near the base plates (Figure 4.74). For this test assembly, weld fracture at the base plates did not take place, although, in some test runs, the column axial forces due to overturning moment exceeded the limiting value required to initiate uplift in the exterior frame columns. This indicates that the application of a continuous weld at the connection of column and base plate is very effective. (The columns used in the stacker rack and the standard pallet rack tests were identical. The latter case used few button welds around the base plates and suffered weld fracture at very low-amplitude shaking levels; the former case used a continuous weld around the base plates and suffered no weld fracture).

The fundamental periods of vibration and the damping values for each test run are shown in Table 4.21. For the full live load test case, the periods changed from 0.65 sec to 0.68 sec before structural damage took place. The period increased substantially during the last test run when the structure suffered considerable damage. The damping values based on the shaking table free-decay data are relatively higher than those for the standard pallet assembly in the transverse direction.

The rack assembly used for this test series consists of ten identical upright frames, which, in turn, form five double upright frames parallel to the direction of table motion. Examination of the local response measurements of the column axial strains near the base plates and the bottom diagonal strains has shown antisymmetric response in phase; each upright frame responded independently. This observation is significant for the mathematical modeling of the stacker rack assembly in the transverse direction.

As expected, the p-δ effect is insignificant for the braced-frame system used in this test series. The local deformation at the connection between the open-section column and the open-section brace is significant, as in the case of the standard pallet and the drive-in rack tested in the transverse direction.

TABLE 4.1

TYPES OF RACK ASSEMBLY

Rack Type	Configuration	Column Base	Simulated Storage Weight	
			Per Pallet	Total
Standard Pallet	2 bays wide 1 bay deep 3 stories high	Anchored	2/3 Live Load: 2,000 lb Full Live Load: 3,000 lb	24,000 lb and 36,000 lb
Back-to-Back Pallet	2 bays wide 2 bays deep 3 stories high	Unanchored	Full Live Load: 3,000 lb	72,000 lb
Drive-In	2 bays wide 3 bays deep 3 stories high	Anchored	2/3 Live Load: 2,000 lb Full Live Load: 3,000 lb	36,000 lb and 54,000 lb
Stacker	4 bays wide 2 bays deep 5 stories high	Anchored	1/2 Live Load: 1,000 lb Full Live Load: 2,000 lb	40,000 lb and 80,000 lb

TABLE 4.2

SECTION PROPERTIES OF RACK ELEMENTS

Rack	Member	Shape	F_y ksi	A in.^{2}	I_x in.^{4}	I_y in.^{4}	S_x in.^{3}	S_y in.^{3}	r_x in.^{2}	r_y in.^{2}
Standard Pallet Rack	Column	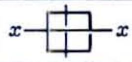	45	0.688	1.144	0.879	0.756	0.586	1.288	1.130
	Beam	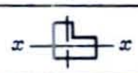	45	1.288	3.265	1.195	1.496	0.760	1.630	0.986
	Brace	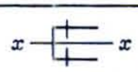	45	0.318	0.125	0.075	0.131	0.100	0.628	0.409
Drive-In Rack	Column (Anchor)	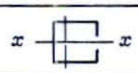	36	0.753	2.206	0.942	1.103	0.543	1.711	1.118
	Column (Upright)	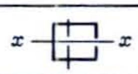	36	1.317	3.777	1.565	1.889	0.900	1.694	1.090
	Beam (Anchor)	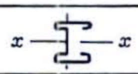	36	1.094	1.175	0.722	0.940	0.501	1.024	0.803
	Beam (Tie)	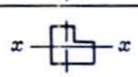	36	0.456	0.332	0.285	0.270	0.253	0.853	0.790
	Brace	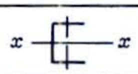	36	0.326	0.257	0.049	0.225	0.074	0.920	0.390
	Pallet Rail	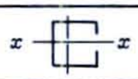	36	0.678	1.180	0.817	0.768	0.510	1.318	1.097
	Spacer	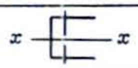	36	0.260	--	--	--	--	--	--
Stacker Rack	Column	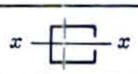	45	0.688	1.144	0.879	0.756	0.586	1.288	1.130
	Beam (Tie)	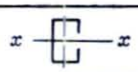	45	0.542	0.668	0.240	--	--	--	--
	Brace	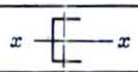	45	0.318	0.125	0.075	0.131	0.100	0.628	0.409
	Pallet Rail	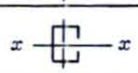	45	0.434	0.545	0.198	0.363	0.195	1.121	0.676
	Rod Support	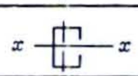	45	1.035	1.530	1.367	--	--	--	--
	Diagonal Rod	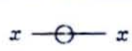	36	0.785	0.049	0.049	0.098	0.098	0.250	0.250

TABLE 4.3

SUMMARY OF TRANSDUCERS INSTALLED FOR GLOBAL AND LOCAL RESPONSE MEASUREMENTS

Rack Type	Test Direction	Transducer Channels				
		Accelerometer	Potentiometer	DCDT*	Strain Gage	Total
Standard Pallet	Longitudinal	9	6	6 (5.38)	8	29
	Transverse	9	9	6 (5.38)	7	31
Back-to-Back Pallet	Longitudinal	9	12	6 (5.38)	7	34
	Transverse	9	12	6 (5.38)	7	34
Drive-In	Longitudinal	9	14	8 (6.75)	6	37
	Transverse	9	9	8 (6.75)	6	32
Stacker	Longitudinal	8	12	8 (5.50)	12	40
	Transverse	8	12	8 (5.50)	10	38

*Gage lengths between two parallel chords are shown in inches in parentheses.

TABLE 4.4

RECORD OF SHAKING TABLE TESTS - PHASE I-1

Test No.	Test I.D.	Live Load	Table Motion			Remarks
			Signal	Maximum Horizontal	Maximum Vertical	
1	120178.1	2/3	El Centro	0.04g	no	Instrument check run.
2	120178.2	2/3	El Centro	0.07g	no	
3	120178.3	2/3	Parkfield	0.10g	no	Modified version of Parkfield signal.
4	120178.4	2/3	Parkfield	0.22g	no	" " "
5	120178.5	2/3	El Centro	0.17g	no	
6	170178.1	full	Parkfield	0.07g	no	
7	170178.2	full	El Centro	0.16g	no	One button weld at NW column base broke.
8	170178.3	full	Parkfield	0.14g	no	
9	170178.4	full	El Centro	0.20g	0.11g	
10	170178.5	full	El Centro	0.30g	0.16g	
11	170178.6	full	El Centro	0.43g	0.21g	Minor local damage (buckling) at top of both center bottom-story columns, near the connector plates.

NOTE

Rack Type: standard pallet rack, anchored

Rack Configuration: 2-bay wide x 1-bay deep x 3-story high, longitudinal

Date of Testing: January 12, 1978; January 17, 1978

TABLE 4.5

RECORD OF SHAKING TABLE TESTS - PHASE I-2

Test No.	Test I.D.	Live Load	Table Motion			Remarks
			Signal	Maximum Horizontal	Maximum Vertical	
1	240178.1	2/3	El Centro	0.07g	no	
2	240178.2	2/3	Parkfield	0.08g	no	Two button welds at NW column base broke.
3	240178.3	2/3	El Centro	0.16g	no	Two more welds at NW column base broke. Column and base at NW were free of contact.
4	240178.4	2/3	Parkfield	0.15g	no	No additional failure of welds at base was observed.
5	260178.1	full	El Centro	0.08g	no	Broken welds were repaired for this test run.
6	260178.2	full	Parkfield	0.08g	no	
7	260178.3	full	El Centro	0.16g	no	Welds at NW column base broke. Noticeable buckling of column at base on all except NE column.
8	260178.4	full	El Centro	0.20g	0.12g	NW column base was rewelded for this test. Buckling of column in NE column base.
9	260178.5	full	Parkfield	0.15g	no	
10	260178.6	full	El Centro	0.08g	no	Bolts to the table were removed. Column bases moved very slightly, 1/4 in.±.
11	260178.7	full	El Centro	0.21g	0.13g	Base moved 3/4 in. maximum. Welds at one column base and two diagonals broke.

NOTE

Rack Type: standard pallet rack, anchored

Rack Configuration: 2-bay wide x 1-bay deep x 3-story high, transverse

Date of Testing: January 24, 1978; January 26, 1978

TABLE 4.6

RECORD OF SHAKING TABLE TESTS - PHASE I-3

Test No.	Test I.D.	Live Load	Table Motion			Remarks
			Signal	Maximum Horizontal	Maximum Vertical	
1	020278.1	full	El Centro	0.07g	no	
2	020278.2	full	Parkfield	0.07g	no	
3	060278.1	full	El Centro	0.03g	no	Instrument check run.
4	060278.2	full	El Centro	0.16g	no	
5	060278.3	full	Parkfield	0.16g	no	One interior column base in the E-frame twisted.
6	060278.4	full	El Centro	0.20g	0.10g	One button weld broke. One column at base twisted severely. One diagonal buckled. (All in E-frame.)
7	060278.5	full	El Centro	0.30g	0.19g	Similar damage but more severe than test 6. Additionally, major buckling occurred in one column of E-frame.

NOTE

Rack Type: standard pallet rack, unanchored

Rack Configuration: 2-bay wide x 2-bay deep x 3-story high, transverse

Date of Testing: February 2, 1978; February 6, 1978

TABLE 4.7

RECORD OF SHAKING TABLE TESTS - PHASE I-4

Test No.	Test I.D.	Live Load	Table Motion: Signal	Maximum Horizontal	Maximum Vertical	Remarks
1	140278.1	full	El Centro	0.04g	no	Instrument check run.
2	140278.2	full	El Centro	0.08g	no	
3	140278.3	full	Parkfield	0.08g	no	
4	140278.4	full	El Centro	0.15g	no	Movie taken.
5	140278.5	full	Parkfield	0.16g	no	Movie taken.
6	140278.6	full	El Centro	0.20g	0.11g	Movie taken. Column at NW corner moved 1 in.±
7	140278.7	full	El Centro	0.31g	0.17g	Movie taken. Column at NW corner moved 1/4 in. more. Two DTDC gages worked loose.
8	140278.8	full	El Centro	0.44g	0.20g	Movie taken. Total collapse of structure.

NOTE

Rack Type: standard pallet rack, unanchored

Rack Configuration: 2-bay wide x 2-bay deep x 3-story high, longitudinal

Date of Testing: February 14, 1978

TABLE 4.8

RECORD OF SHAKING TABLE TESTS - PHASE II-1

Test No.	Test I.D.	Live Load	Table Motion: Signal	Table Motion: Maximum Horizontal	Table Motion: Maximum Vertical	Remarks
1	090678.1	2/3	El Centro	0.08g	no	All DCDT gages were not connected to the recording system
2	090678.2	2/3	Parkfield	0.08g	no	" " " " " "
3	090678.3	2/3	El Centro	0.16g	no	" " " " " "
4	090678.4	2/3	Parkfield	0.15g	no	" " " " " "
5	130678.1	full	El Centro	0.08g	no	
6	130678.2	full	Parkfield	0.08g	no	
7	130678.3	full	El Centro	0.16g	no	
8	130678.4	full	Parkfield	0.15g	no	
9	130678.5	full	El Centro	0.21g	0.11g	

NOTE

Rack Type: drive-in rack, anchored

Rack Configuration: 2-bay wide x 3-bay deep x 3-story high, longitudinal

Date of Testing: June 9, 1978; June 13, 1978

TABLE 4.9

RECORD OF SHAKING TABLE TESTS - PHASE II-2

Test No.	Test I.D.	Live Load	Table Motion			Remarks
			Signal	Maximum Horizontal	Maximum Vertical	
1	200678.1	2/3	El Centro	0.08g	no	Instrument check run
2	200678.2	2/3	El Centro	0.07g	no	
3	200678.3	2/3	Parkfield	0.08g	no	Bottom diagonal brace at center upright frame buckled considerably.
4	200678.4	2/3	El Centro	0.16g	no	All bottom diagonal braces of upright frames buckled. Two button welds at anchor frames broke.

NOTE

Rack Type: drive-in rack, anchored

Rack Configuration: 2-bay wide x 3-bay deep x 3-story high, transverse

Date of Testing: June 20, 1978

TABLE 4.10

RECORD OF SHAKING TABLE TESTS - PHASE III-1

Test No.	Test I.D.	Live Load	Table Motion			Remarks
			Signal	Maximum Horizontal	Maximum Vertical	
1	171178.1	1/2	El Centro	0.09g	no	All diagonal rods were loose during the test
2	171178.2	1/2	Parkfield	0.08g	no	" " " " " "
3	171178.3	1/2	El Centro	0.17g	no	" " " " " "
4	171178.4	1/2	Parkfield	0.15g	no	" " " " " "
5	221178.1	full	El Centro	0.08g	no	All rods were tied before this test
6	221178.2	full	Parkfield	0.07g	no	
7	221178.3	full	El Centro	0.16g	no	
8	221178.4	full	Parkfield	0.16g	no	
9	221178.5	full	El Centro	0.24g	no	All rods became loose and were retied for the next test
10	221178.6	full	El Centro	0.24g	no	Buckling of columns between the bottom and middle rod supports

NOTE

Rack Type: stacker rack, anchored

Rack Configuration: 4-bay wide x 2-bay deep x 5-story high, longitudinal

Date of Testing: November 17, 1978; November 22, 1978

TABLE 4.11

RECORD OF SHAKING TABLE TESTS - PHASE III-2

Test No.	Test I.D.	Live Load	Table Motion			Remarks
			Signal	Maximum Horizontal	Maximum Vertical	
1	051078.1	1/2	El Centro	0.07g	no	DCDT gages (3-4, 5-6) were not connected to the recording system.
2	051078.2	1/2	Parkfield	0.07g	no	" "
3	051078.3	1/2	El Centro	0.15g	no	" "
4	051078.4	1/2	Parkfield	0.15g	no	" "
5	111078.1	full	El Centro	0.08g	no	Movie taken
6	111078.2	full	Parkfield	0.08g	no	Movie taken
7	111078.3	full	El Centro	0.16g	no	Movie taken
8	111078.4	full	Parkfield	0.16g	no	Movie taken. All interior bottom diagonal braces buckled. All interior bottom columns buckled near base plates.

NOTE

Rack Type: stacker rack, anchored

Rack Configuration: 4-bay wide x 2-bay deep x 5-story high, transverse

Date of Testing: October 5, 1978; October 11, 1978

TABLE 4.12

SUMMARY OF SELECTED EXTREME QUANTITIES AND DYNAMIC PROPERTIES - STANDARD PALLET RACK, LONGITUDINAL DIRECTION

Test ID	Live Load	Table Signal	Maximum Table Acceleration (g)		Maximum Table Displacement (in.)	Maximum Third-Level Relative Displacement (in.)	Maximum Interstory Drift (in.)	Maximum Base Shear/Frame		Maximum Base Overturning Moment/Frame (kip-in.)	Maximum Ductility Ratio[b]	Period (sec)[c]			Damping[c] (% Critical)
			Hori-zontal	Ver-tical				lb	%[a]			Mode 1	Mode 2	Mode 3	
120178.2 (SP-L-2/3-1/4 EC)	2/3	EC	0.071	--	0.58	1.1	0.57 (0.001H)	434	3.4	62	0.3	1.66 (1.50)	0.43	0.22	(2.9)
120178.5 (SP-L-2/3-1/2 EC)	2/3	EC	0.166	--	1.33	2.7	1.20 (0.021H)	840	6.6	100	0.7	1.80 (1.66)	0.47	0.22	(4.8)
170178.1 (SP-L-1-1/4 PF)	Full	PF	0.073	--	0.74	2.0	0.93 (0.016H)	800	4.3	90	0.7	2.06 (2.00)	0.53	0.26	(3.6)
170178.2 (SP-L-1-1/2 EC)	Full	EC	0.162	--	1.33	4.4	2.0 (0.034H)	1,200	6.4	145	1.4	2.22 (2.07)	0.53	0.26	(5.5)
170178.3 (SP-L-1-1/2 PF)	Full	PF	0.141	--	1.60	4.3	2.3 (0.040H)	1,150	6.1	125	1.8	2.30 (2.25)	0.57	0.26	(5.5)
170178.4 (SP-L-1-5/8 EC)	Full	EC	0.202	0.110	1.56	4.9	2.4 (0.041H)	1,510	8.1	160	2.2	2.75 (2.35)	0.57	0.27	(9.0)
170178.5 (SP-L-1-7/8 EC)	Full	EC	0.304	0.163	2.27	6.8	3.2 (0.055H)	1,640	8.7	165	2.4	2.86 (2.70)	0.57	0.27	(6.9)
170178.6 (SP-L-1-1/3 EC)	Full	EC	0.431	0.211	3.05	7.3	4.0 (0.069H)	3,600	19.2	252	2.6	2.85 (2.80)	0.57	0.27	(7.6)

a. Percentage of total tributary weight (ΣW = 12,750 lb for 2/3 live load and 18,750 lb for full live load).

b. Ductility ratio = ϕ_{max}/ϕ_y, where ϕ_{max} is the maximum measured rotation at the top end of the center bottom column, and ϕ_y is the calculated rotation at the initiation of yield.

c. The results shown in parentheses were obtained from the shaking table decay data.

TABLE 4.13

INFLUENCE OF p-δ EFFECT ON STORY SHEAR - STANDARD PALLET RACK, LONGITUDINAL DIRECTION

Signal	Live Load	δ (in.)	V_I (lb)	$V_P = \frac{\Sigma W \cdot \delta}{H}$ (lb)	$V_T = V_I + V_P$ (lb)	$\frac{V_T}{V_I}$
1/4 EC	2/3	0.57	434	121	555	1.28
1/2 EC	"	1.20	840	255	1,095	1.30
1/4 PF	Full	0.93	800	290	1,090	1.36
1/2 EC	"	2.00	1,200	625	1,825	1.52
1/2 PF	"	2.30	1,150	719	1,869	1.63
5/8 EC	"	2.40	1,510	750	2,260	1.50
7/8 EC	"	3.20	1,640	1,000	2,640	1.61
1-1/3 EC	"	4.00	3,600	1,250	4,850	1.35

KEY

δ = Maximum interstory drift

V_I = Maximum base shear by inertia forces

V_P = Base shear due to p-δ effect

H = Story height (60")

V_T/V_I = Amplification ratio

ΣW = 12,750 lb for 2/3 live load
18,750 lb for full live load

TABLE 4.14

SUMMARY OF SELECTED EXTREME QUANTITIES AND DYNAMIC PROPERTIES - STANDARD PALLET RACK, TRANSVERSE DIRECTION

Test ID	Live Load	Table Signal	Maximum Table Acceleration (g)		Maximum Table Displacement (in.)	Maximum Third-Level Relative Displacement[a] (in.)	Maximum Interstory Drift (in.)	Maximum Base Shear/Frame		Maximum Base Overturning Moment/Frame (kip-in.)	Maximum Ductility Ratio[c]	Period (sec)[d]			Damping[d] (% Critical)
			Hori-zontal	Ver-tical				lb	%[b]			Mode 1	Mode 2	Mode 3	
240178.1 (SP-T-2/3-1/4 EC)	2/3	EC	0.073	--	0.61	0.9(W) 1.0(C) 0.9(E)	0.40 $(0.007H)$	1,120	13.1	150	0.3	0.71 (0.68)	0.24	--	(1.0)
260178.1 (SP-T-1-1/4 EC)	Full	EC	0.077	--	0.62	1.3(W) 1.4(C) 1.3(E)	0.59 $(0.010H)$	1,650	13.2	200	0.8	0.87 (0.85)	0.28	--	(1.1)
260178.2 (SP-T-1-1/4 PF)	Full	PF	0.077	--	0.80	1.0(W) 1.1(C) 1.0(E)	0.46 $(0.008H)$	1,200	9.6	160	0.6	0.89 (0.85)	0.30	--	(1.2)
260178.3 (SP-T-1-1/2 EC)	Full	EC	0.158	--	1.29	2.8(W) 2.3(C) 1.8(E)	1.05 $(0.018H)$	2,550	20.4	280	1.9	0.92 (0.90)	0.30	--	(1.0)
260178.4 (SP-T-1-5/8 EC)	Full	EC	0.200	0.120	1.57	2.5(W) 2.5(C) 2.0(E)	1.10 $(0.019H)$	2,780	22.2	310	2.1	0.95 (0.92)	0.30	--	(1.6)

a. W = west frame, C = center frame, E = east frame.

b. Percentage of total tributary weight (ΣW = 8,500 lb for 2/3 live load and 12,500 lb for full live load).

c. Ductility ratio = ϕ_{max}/ϕ_y, where ϕ_{max} is the maximum measured rotation near the base of the center bottom column, and ϕ_y is the calculated rotation at the initiation of yield.

d. The results shown in parentheses were obtained from the shaking table decay data.

TABLE 4.15

SELECTED EXTREME QUANTITIES AND DYNAMIC PROPERTIES - ANCHORED AND UNANCHORED STANDARD PALLET RACKS, LONGITUDINAL DIRECTION[a]

Test ID	Column Base	Table Signal	Maximum Table Acceleration (g)		Maximum Table Displacement (in.)	Maximum Third-Level Relative Displacement (in.)	Maximum Interstory Drift (in.)	Maximum Base Shear (%)	Maximum Base Overturning Moment/Frame (kip-in.)	Maximum Ductility Ratio[b]	Period (sec)		
			Hori-zontal	Ver-tical							Mode 1	Mode 2	Mode 3
170178.2	anchored	EC	0.162	--	1.33	4.4	2.0 (0.033H)	6.4	145	1.4	2.22	0.53	0.26
140278.4	unanchored	EC	0.153	--	1.28	4.6	2.2 (0.038H)	6.7	165	2.1	2.50	0.53	0.27
170178.3	anchored	PF	0.141	--	1.60	4.3	2.3 (0.040H)	6.1	125	1.8	2.30	0.53	0.26
140278.5	unanchored	PF	0.156	--	1.73	4.6	2.4 (0.041H)	6.7	150	2.4	2.50	0.57	0.27
170178.4	anchored	EC	0.202	0.110	1.56	4.9	2.4 (0.041H)	8.1	160	2.2	2.86	0.57	0.27
140278.6	unanchored	EC	0.200	0.110	1.56	5.7	3.3 (0.057H)	12.0	200	3.3	2.86	0.57	0.27
170178.5	anchored	EC	0.304	0.163	2.27	6.8	3.2 (0.055H)	8.7	165	2.4	2.86	0.57	0.27
140278.7	unanchored	EC	0.312	0.165	2.33	8.5	3.7 (0.064H)	23.0	370	3.8	2.86	0.60	0.27
170178.6	anchored	EC	0.431	0.211	3.05	7.3	4.0 (0.069H)	19.2	252	2.6	2.85	0.57	0.27
140278.8	unanchored	EC	0.440	0.200	3.07	12.0	6.0 (0.103H)		Complete collapse of structure				

a. For full live load case only.

b. See Table 4.12.

TABLE 4.16

BASE STORY SHEARS - ANCHORED AND UNANCHORED STANDARD PALLET RACKS, LONGITUDINAL DIRECTION

Signal	Live Load	δ (in.)	V_I (lb)	$V_P = \frac{\Sigma W \cdot \delta}{H}$ (lb)	$V_T = V_I + V_P$ (lb)	$\frac{V_T}{V_I}$
1/2 EC	Full	2.00 (2.20)	1,200 (1,256)	625 (688)	1,825 (1,944)	1.52 (1.55)
1/2 PF	"	2.30 (2.40)	1,150 (1,263)	719 (750)	1,869 (2,013)	1.63 (1.60)
5/8 EC	"	2.40 (3.30)	1,510 (2,237)	750 1,031	2,260 (3,268)	1.50 1.46
7/8 EC	"	3.20 (3.70)	1,640 (4,336)	1,000 (1,156)	2,640 (5,492)	1.61 (1.27)
1-1/3 EC	"	4.00 (6.00)	3,600 (*)	1,250 (1,875)	4,850 (*)	1.35 (*)

* Not obtainable

NOTE

The results of the unanchored rack are shown in parentheses.

KEY

δ = Maximum interstory drift

V_I = Maximum base shear by inertia forces

V_P = Base shear due to p-δ effect

H = Story height (60")

V_T/V_I = Amplification ratio

ΣW = 18,750 lb/frame for full live load

TABLE 4.17

SUMMARY OF SELECTED EXTREME QUANTITIES AND DYNAMIC PROPERTIES - DRIVE-IN RACK, LONGITUDINAL DIRECTION

Test ID	Live Load	Table Signal	Maximum Table Acceleration (g)		Maximum Table Displacement (in.)	Maximum Third-Level Relative Displacement (in.)	Maximum Interstory Drift (in.)	Maximum Base Shear/Frame		Maximum Base Overturning Moment/Frame (kip-in.)	Maximum[b] Ductility Ratio	Period (sec)[c]			Damping[c] (% Critical)
			Hori-zontal	Ver-tical				lb	%[a]			Mode 1	Mode 2	Mode 3	
090678.1 (DI-L-2/3-1/4 EC)	2/3	EC	0.076	--	0.64	2.5	1.04 (0.0149H)	1,810	4.6	--	--	2.6 (2.1)	0.47	--	(5.0)
090678.3 (DI-L-2/3-1/2 EC)	2/3	EC	0.157	--	1.28	5.3	2.30 (0.0329H)	2,990	7.6	--	--	3.1 (2.8)	0.50	--	(9.0)
130678.1 (DI-L-1-1/4 EC)	Full	EC	0.080	--	0.64	3.0	1.16 (0.0166H)	1,950	3.4	400	0.24	2.9 (2.5)	0.53	--	(5.0)
130678.2 (DI-L-1-1/4 PF)	Full	PF	0.077	--	0.79	1.6	0.57 (0.0081H)	1,550	2.7	230	0.33	2.9 (2.4)	0.51	--	(4.0)
130678.3 (DI-L-1-1/2 EC)	Full	EC	0.163	--	1.27	4.0	1.65 (0.0235H)	2,500	4.4	440	0.60	3.2 (2.8)	0.57	--	(8.0)
130678.4 (DI-L-1-1/2 PF)	Full	PF	0.151	--	1.68	3.1	1.26 (0.0180H)	2,600	4.5	720	0.81	3.0 (2.5)	0.56	--	(4.0)
130678.5 (DI-L-1-5/8 EC)	Full	EC	0.211	0.110	1.56	5.2	2.10 (0.0300H)	3,000	5.2	780	0.63	3.3 (2.8)	0.58	--	(7.0)

a. Percentage of total weight (ΣW = 39,450 lb for 2/3 live load and 57,450 lb for full live load).

b. Ductility ratio = ϕ_{max}/ϕ_y, where ϕ_{max} is the maximum measured rotation at the top end of the first-floor center columns, and ϕ_y is the calculated rotation at the initiation of yield.

c. The results shown in parentheses were obtained from the shaking table decay data.

TABLE 4.18

INFLUENCE OF P-δ EFFECT ON STORY SHEAR -
DRIVE-IN RACK, LONGITUDINAL DIRECTION

Signal	Live Load	δ (in.)	V_I (lb)	$V_P = \frac{\Sigma W \cdot \delta}{H}$ (lb)	$V_T = V_I + V_P$ (lb)	$\frac{V_T}{V_I}$
1/4 EC	2/3	1.04	1,815	586	2,401	1.33
1/2 EC	"	2.30	2,990	1,296	4,294	1.43
1/4 EC	Full	1.16	1,950	952	2,902	1.48
1/4 PF	"	0.57	1,550	468	2,018	1.30
1/2 EC	"	1.65	2,500	1,354	3,854	1.54
1/2 PF	"	1.26	2,600	1,034	3,634	1.40
5/8 EC	"	2.10	3,000	1,724	5,724	1.57

δ = Maximum interstory drift

V_I = Maximum base shear by inertia forces

V_P = Base shear due to p-δ effect

H = Story height (70")

V_T/V_I = Amplification ratio

ΣW = 39,450 lb for 2/3 live load
57,450 lb for full live load

TABLE 4.19

SUMMARY OF SELECTED EXTREME QUANTITIES AND DYNAMIC PROPERTIES - DRIVE-IN RACK, TRANSVERSE DIRECTION

Test ID	Live Load	Table Signal	Maximum Table Acceleration (g)		Maximum Table Displacement (in.)	Maximum Third-Level Relative Displacement (in.)[a]	Maximum Interstory Drift (in.)	Maximum Base Shear/Frame		Maximum Base Overturning Moment/Frame (kip-in.)	Maximum Ductility Ratio	Period (sec)			Damping[d] (% Critical)
			Hori-zontal	Ver-tical				lb	%[b]			Mode 1	Mode 2	Mode 3	
200678.2 (DI-T-2/3-1/4 EC)	2/3	EC	0.073	--	0.63	0.98 (W) 0.95 (C) 0.83 (E)	0.36 (0.0051*H*)	2,250	17.0	335	1.3	0.58 (0.56)	--	--	(1.5)
200678.3 (DI-T-2/3-1/4 PF)	2/3	PF	0.069	--	0.80	1.07 (W) 1.05 (C) 0.98 (E)	0.60 (0.0085*H*)	2,600	20.0	325	6.5	0.59 (0.56)	--	--	(1.5)
200678.4 (DI-T-2/3-1/2 EC)	2/3	EC	0.160	--	1.28	1.50 (C)	1.00 (0.0142*H*)	2,700	21.0	450	--	0.67 (0.66)	--	--	(2.0)

a. W = west frame, C = center frame, E = east frame.

b. Percentage of total tributary weight (ΣW = 13,140 lb/frame).

c. Ductility ratio = $\varepsilon_{max}/\varepsilon_y$, where ε_{max} is the maximum measured strain at the first-floor diagonal, and ε_y is the calculated strain at the initiation of yield.

d. The results shown in parentheses were obtained from the shaking table decay data.

TABLE 4.20

SUMMARY OF SELECTED EXTREME QUANTITIES AND DYNAMIC PROPERTIES - STACKER RACK, LONGITUDINAL DIRECTION

Test ID	Live Load	Table Signal	Maximum Table Acceleration (g)		Maximum Table Displacement (in.)	Maximum Fifth-Level Relative Displacement (in.)	Maximum Interstory Drift (in.)	Maximum Base Shear/Frame		Maximum Base Overturning Moment/Frame (kip-in.)	Maximum Ductility Ratio	Period (sec)[b]			Damping[b] (% Critical)
			Hori-zontal	Ver-tical				lb	%[a]			Mode 1	Mode 2	Mode 3	
171178.1 (ST-L-1/2-1/4 EC)	1/2	EC	0.091	--	0.75	1.25	0.35 (0.005*H*)	5,470	11.4	810		0.96 (1.10)	--	--	(3.8)
171178.3 (ST-L-1/2-1/2 EC)	1/2	EC	0.165	--	1.41	2.68	0.92 (0.013*H*)	10,080	21.0	1,550		0.90 1.25 (1.68)	0.20	--	(6.2)
221178.1 (ST-L-1-1/4 EC)	Full	EC	0.083	--	0.72	1.29	0.62 (0.009*H*)	7,480	8.5	1,200		0.94 1.06 (0.95)	--	--	(6.3)
221178.2 (ST-L-1-1/4 PF)	Full	PF	0.074	--	0.83	1.35	0.46 (0.006*H*)	7,440	8.8	1,280		1.08 (0.88)	--	--	(4.7)
221178.3 (ST-L-1-1/2 EC)	Full	EC	0.160	--	1.36	2.55	0.80 (0.011*H*)	12,320	14.0	2,030		1.23 (1.22)	--	--	(6.2)
221178.4 (ST-L-1-1/2 PF)	Full	PF	0.159	--	1.74	3.20	1.10 (0.015*H*)	13,900	15.8	1,830		1.40 (1.67)	--	--	(4.6)
221178.5[c] (ST-L-1-5/8 EC)	Full	EC	0.243	--	2.01	2.94	0.88 (0.012*H*)	14,080	16.0	1,880		1.45 (1.90)	--	--	--
221178.6[d] (ST-L-1-5/8 EC)	Full	EC	0.238	--	2.01	3.60	1.05 (0.015*H*)	17,950	20.4	2,790		1.41 (1.55)	--	--	(5.0)

a. Percentage of total weight (ΣW = 48,000 lb for 1/2 live load and 88,000 lb for full live load).

b. The results shown in parentheses were obtained from the shaking table decay data.

c. Diagonal rods were loose for this testing.

d. Diagonal rods were tied before this testing. Buckling of columns between the bottom and middle rod supports was observed.

TABLE 4.21

SUMMARY OF SELECTED EXTREME QUANTITIES AND DYNAMIC PROPERTIES - STACKER RACK, TRANSVERSE DIRECTION

Test ID	Live Load	Table Signal	Maximum Table Acceleration (g)		Maximum Table Displacement (in.)	Maximum Sixth-Level Relative Displacement (in.)[a]	Maximum Interstory Drift (in.)	Maximum Base Shear/Frame		Maximum Base Overturning Moment/Frame (kip-in.)	Maximum Ductility Ratio[c]	Period (sec)			Damping[d] (% Critical)
			Hori-zontal	Ver-tical				lb	%[b]			Mode 1	Mode 2	Mode 3	
051078.1 (ST-T-1/2-1/4 EC)	1/2	EC	0.066	--	0.59	0.27 (W) 0.39 (C) 0.39 (E)	0.10 (0.0014H)	960	10.0	--	0.33	0.43 (0.41)	--	--	(4.0)
051078.4 (ST-T-1/2-1/2 PF)	1/2	PF	0.140	--	1.67	1.26 (W) 1.71 (C) 1.57 (E)	0.43 (0.0060H)	4,320	45.0	--	1.10	0.47	--	--	--
111078.1 (ST-T-1-1/4 EC)	Full	EC	0.082	--	0.74	0.74 (W) 0.89 (C) 0.84 (E)	0.18 (0.0025H)	2,110	12.0	330	0.72	0.65 (0.56)	--	--	(4.0)
111078.2 (ST-T-1-1/4 PF)	Full	PF	0.077	--	0.84	1.06 (W) 1.35 (C) 1.19 (E)	0.32 (0.0044H)	2,816	16.0	--	1.04	0.67	--	--	--
111078.3 (ST-T-1-1/2 EC)	Full	EC	0.162	--	1.40	1.35 (W) 1.65 (C) 1.35 (E)	0.40 (0.0056H)	3,520	20.0	460	1.25	0.68 (0.56)	--	--	(5.0)
111078.4 (ST-T-1-1/2 PF)	Full	PF	0.157	--	1.70	2.34 (W) 3.00 (C) 2.55 (E)	0.70 (0.0097H)	6,300	35.0	1,170	1.58	0.78	--	--	--

a. W = west exterior frame, C = center frame, E = east exterior frame.

b. Percentage of tributary weight (ΣW = 9,600 lb for 1/2 live load and 17,600 lb for full live load).

c. Ductility ratio = $\epsilon_{max}/\epsilon_y$, where ϵ_{max} is the maximum measured strain at the bottom diagonals and ϵ_y is the calculated strain at the initiation of yield.

d. The results shown in parentheses were obtained from the shaking table decay data.

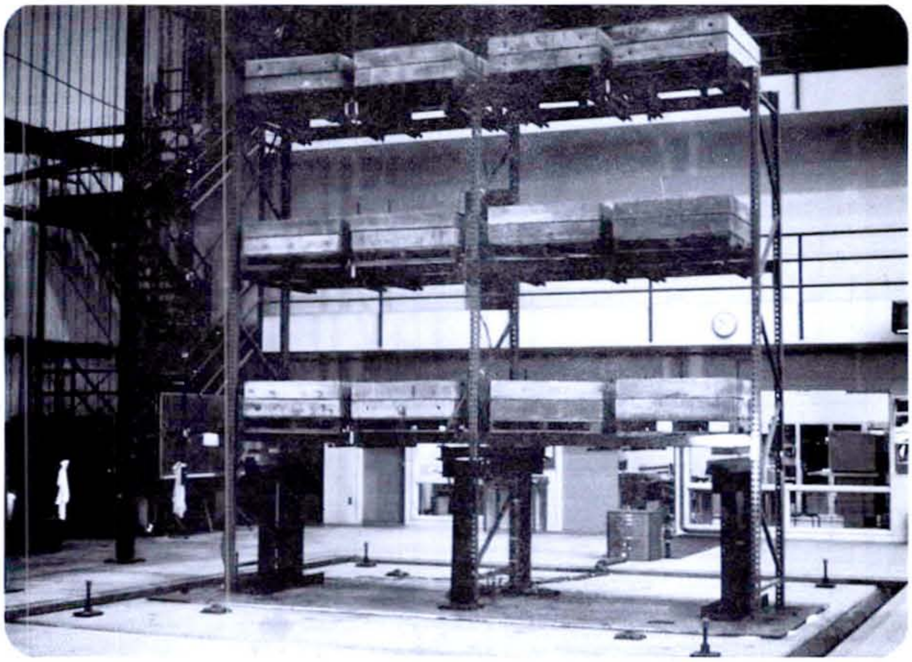

(a) Longitudinal Test

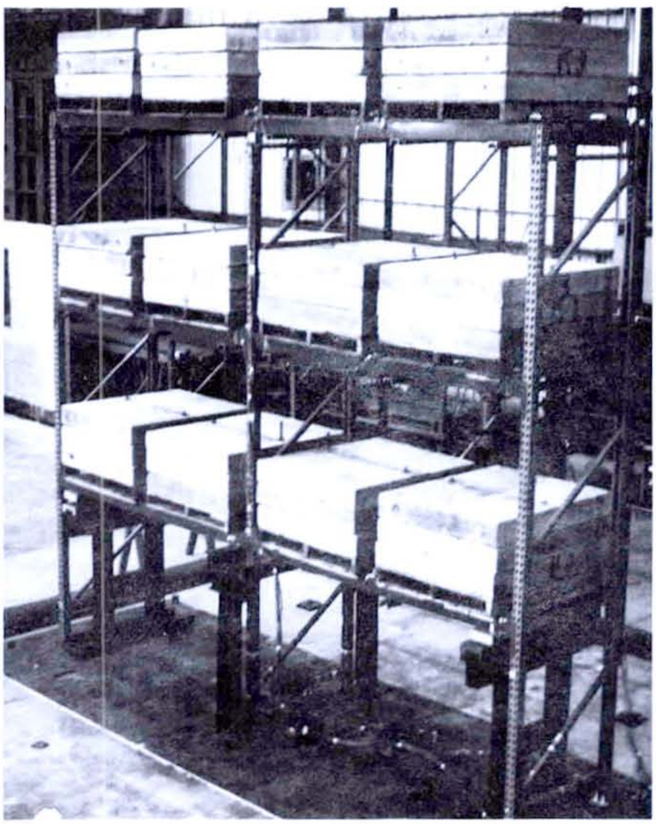

(b) Transverse Test

FIGURE 4.1 STANDARD PALLET RACK ASSEMBLY

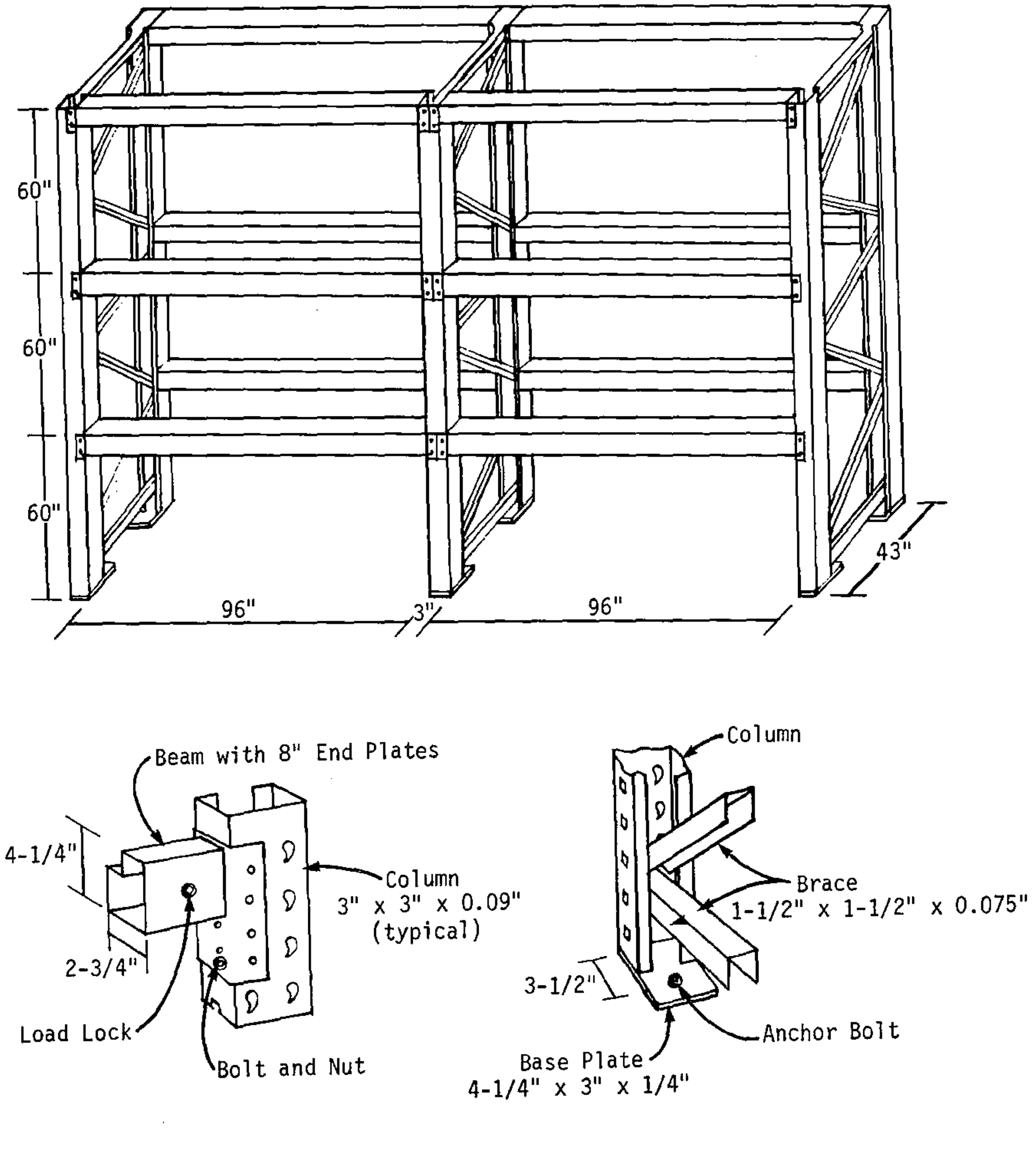

FIGURE 4.2 CONFIGURATION AND CONNECTION DETAILS FOR STANDARD PALLET RACK ASSEMBLY

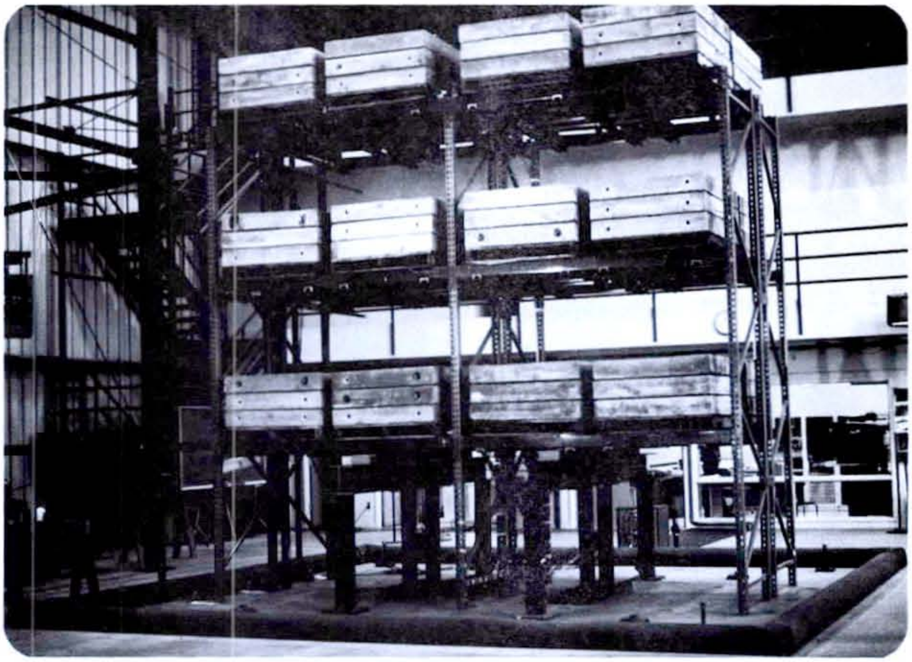

(a) Longitudinal Test

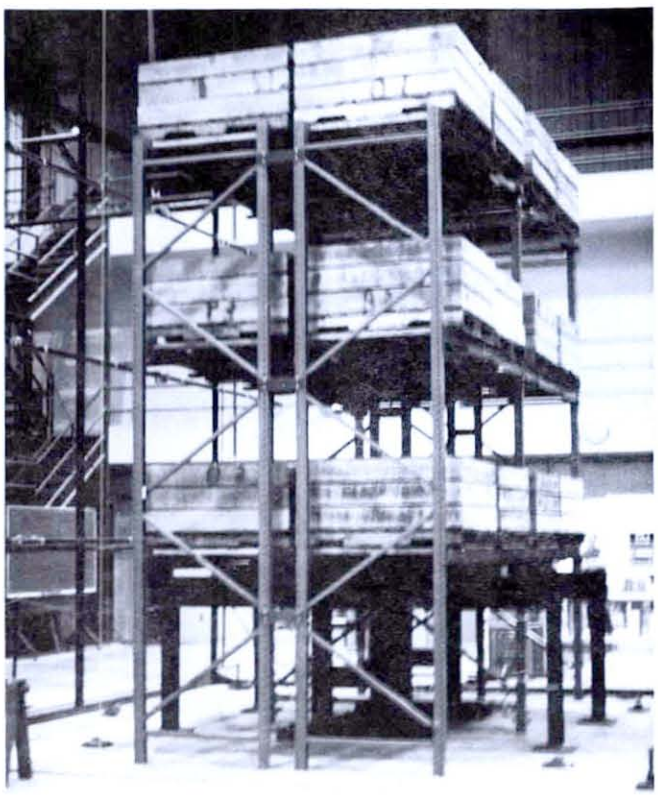

(b) Transverse Test

FIGURE 4.3 BACK-TO-BACK PALLET RACK ASSEMBLY

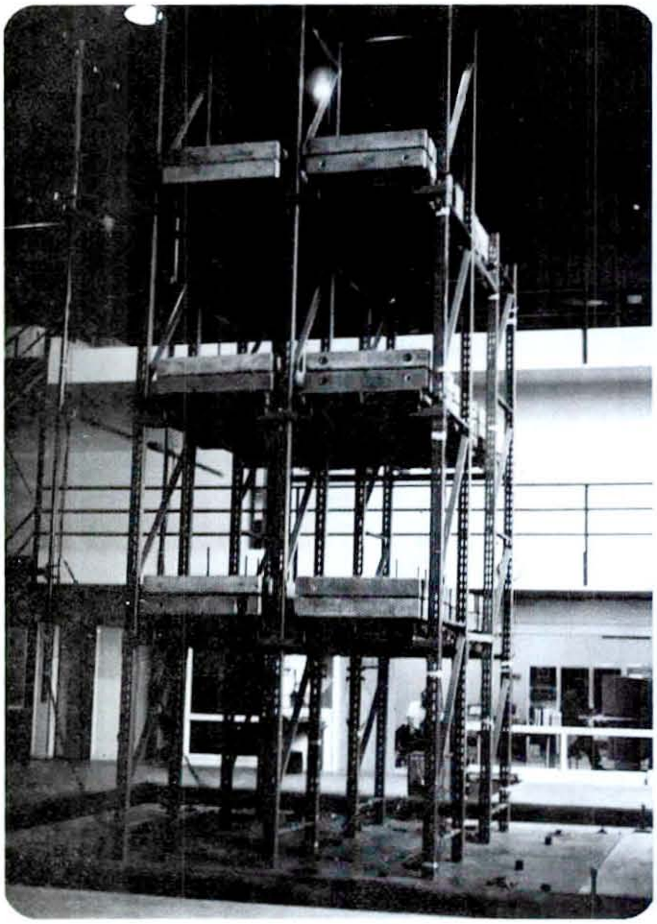

(a) Longitudinal Test

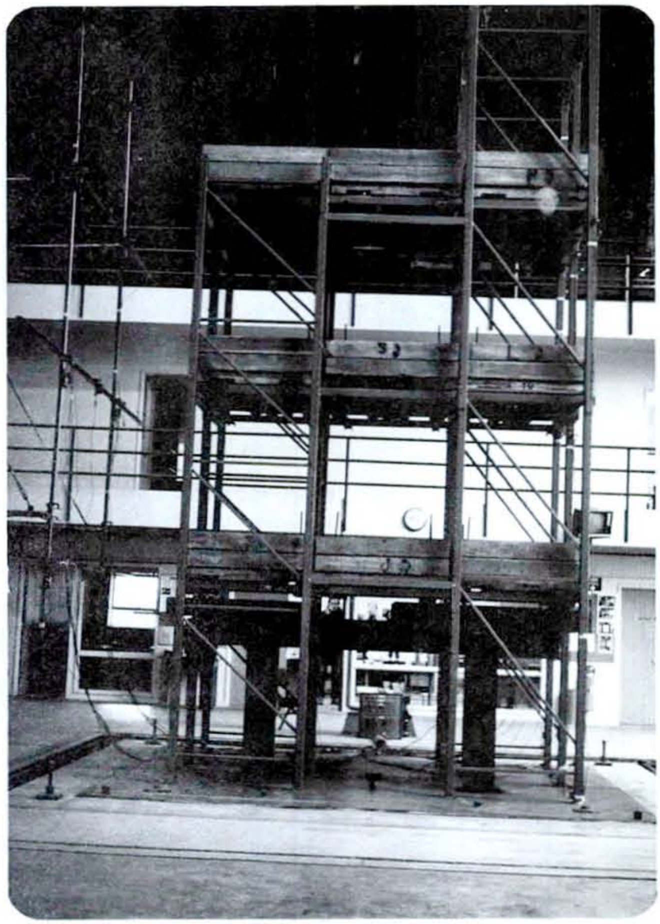

(b) Transverse Test

FIGURE 4.4 DRIVE-IN RACK ASSEMBLY

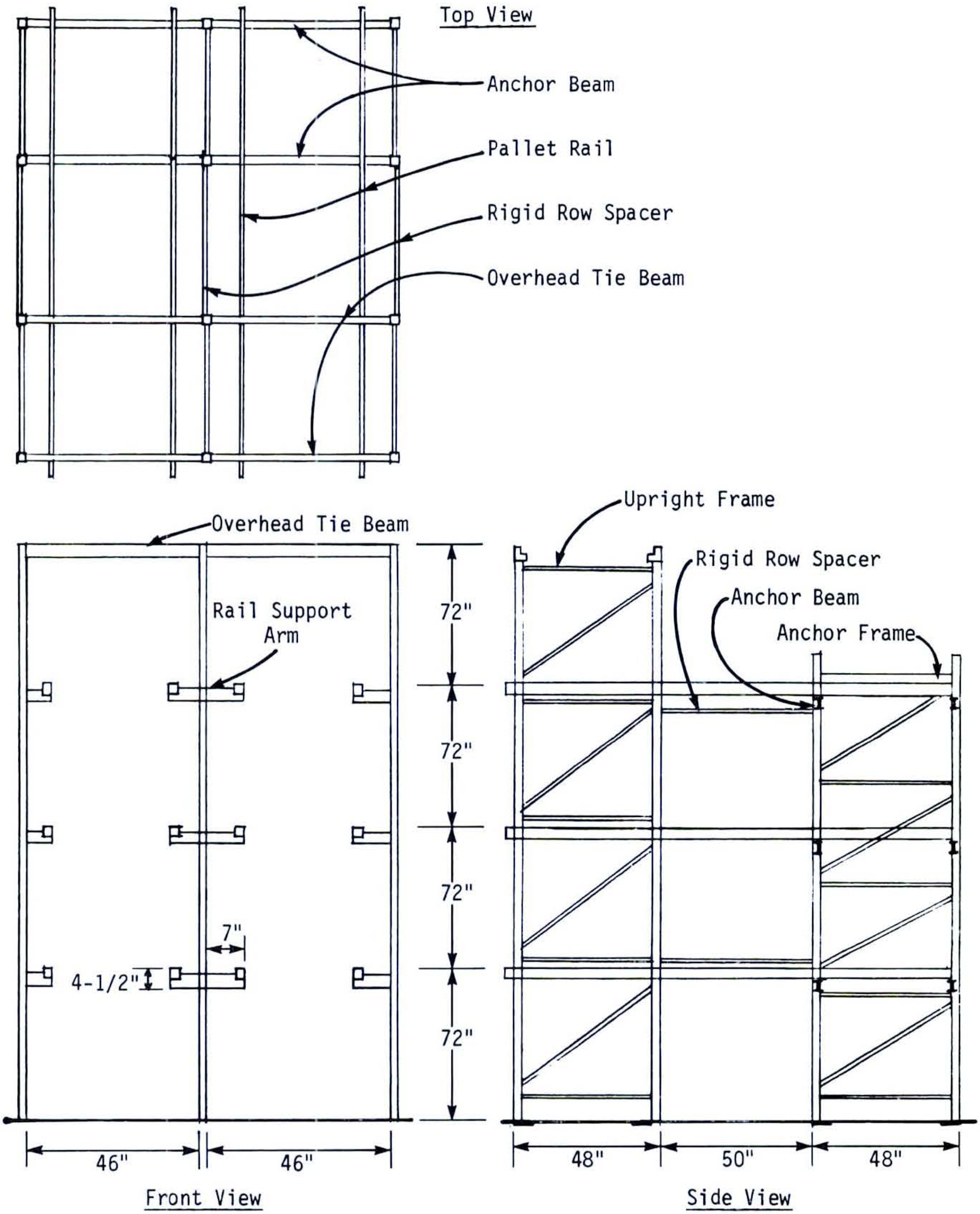

FIGURE 4.5 CONFIGURATION FOR DRIVE-IN RACK ASSEMBLY

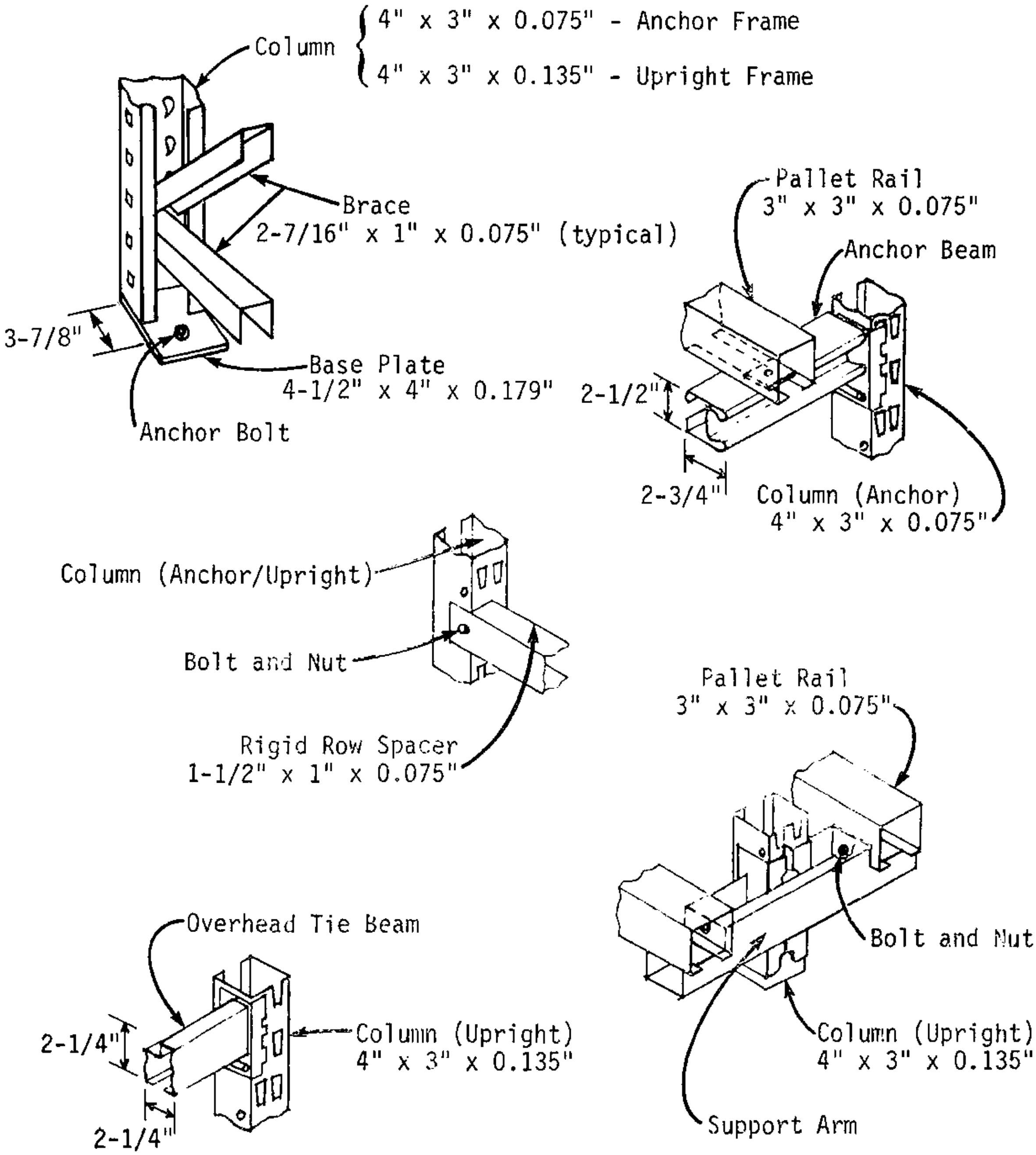

FIGURE 4.6 DETAILED CONNECTIONS FOR DRIVE-IN RACK ASSEMBLY

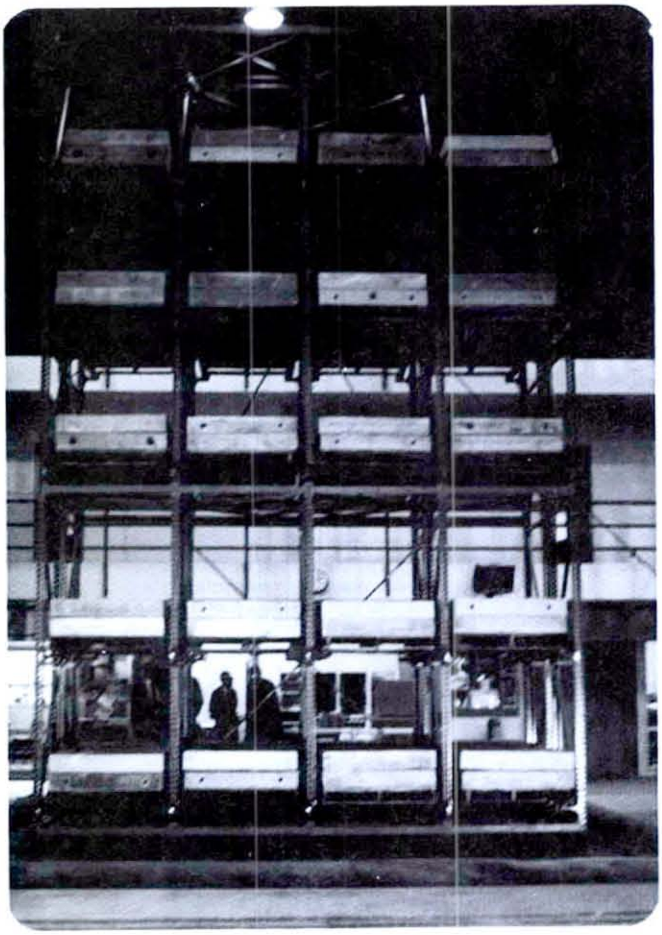

(a) Longitudinal Test

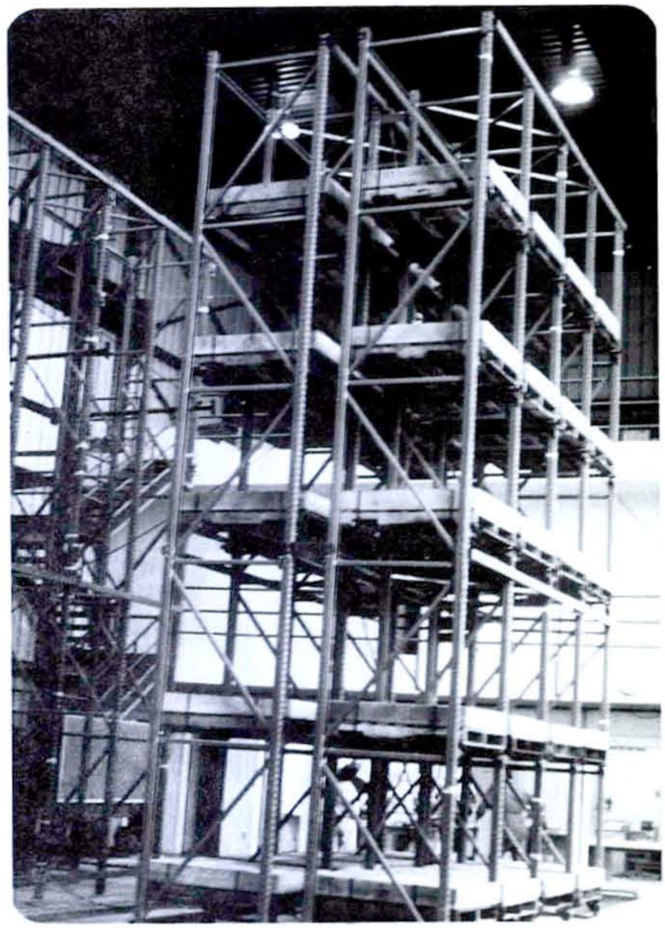

(b) Transverse Test

FIGURE 4.7 STACKER RACK ASSEMBLY

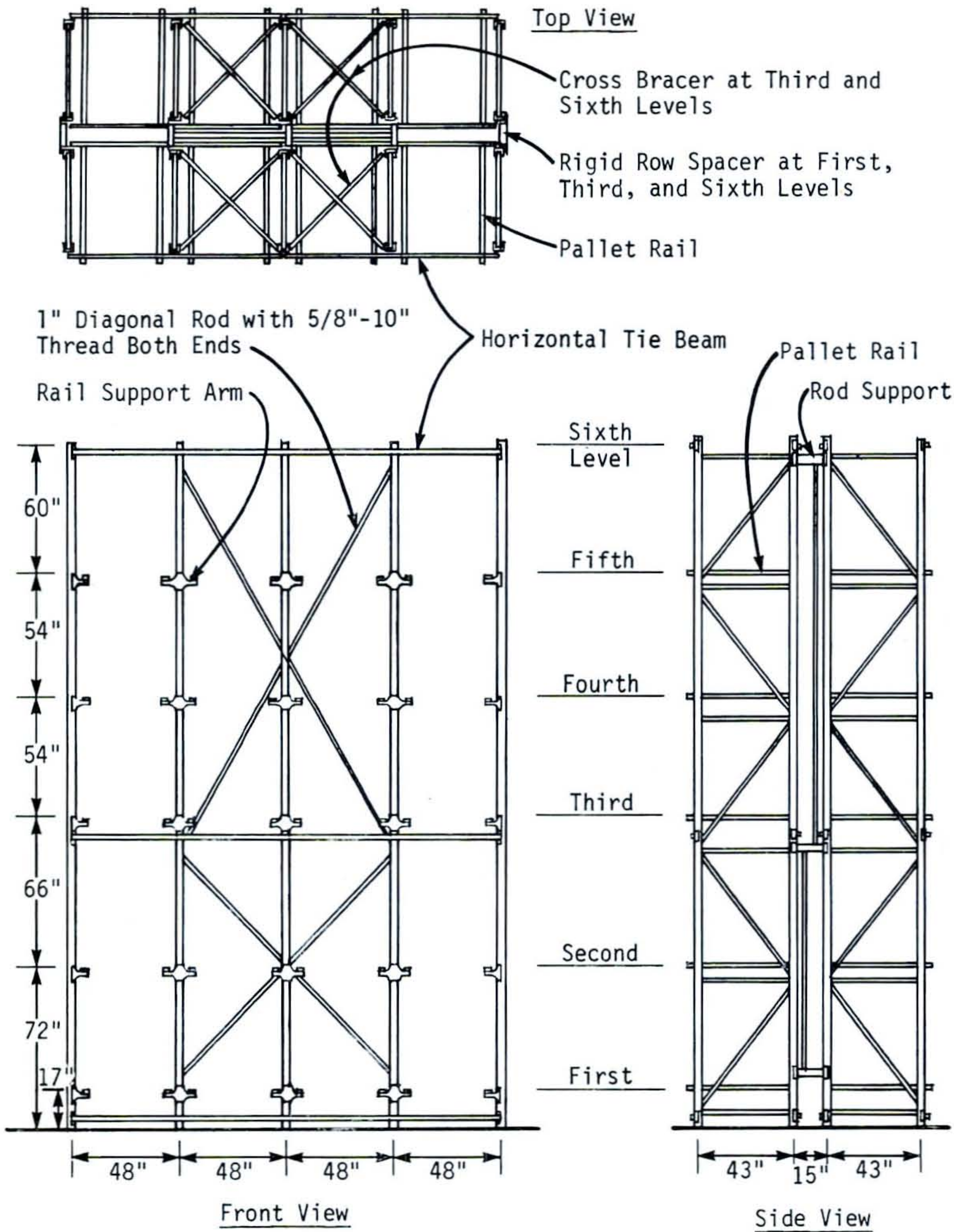

FIGURE 4.8 CONFIGURATION FOR STACKER RACK ASSEMBLY

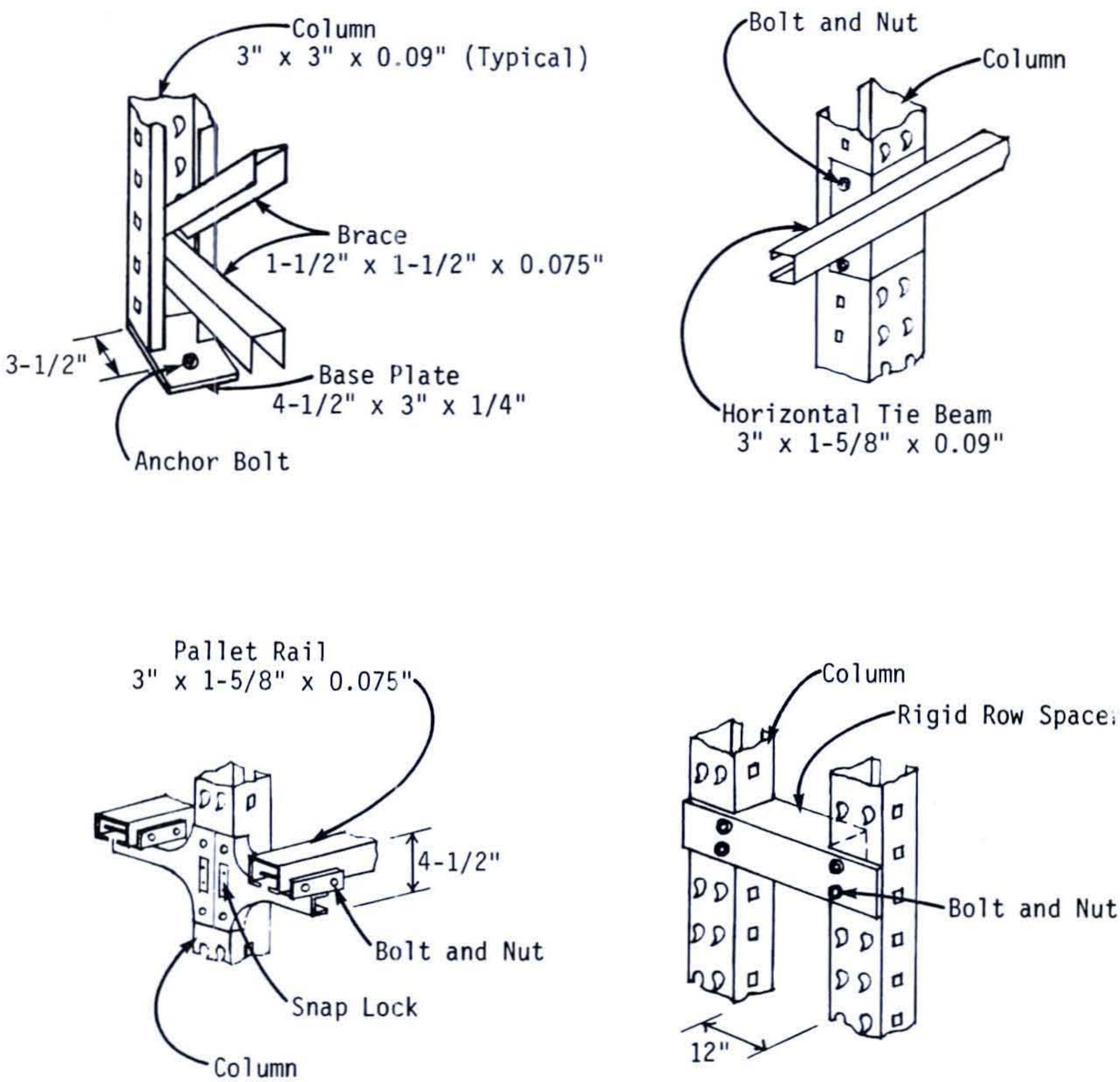

FIGURE 4.9 DETAILED CONNECTIONS FOR STACKER RACK ASSEMBLY

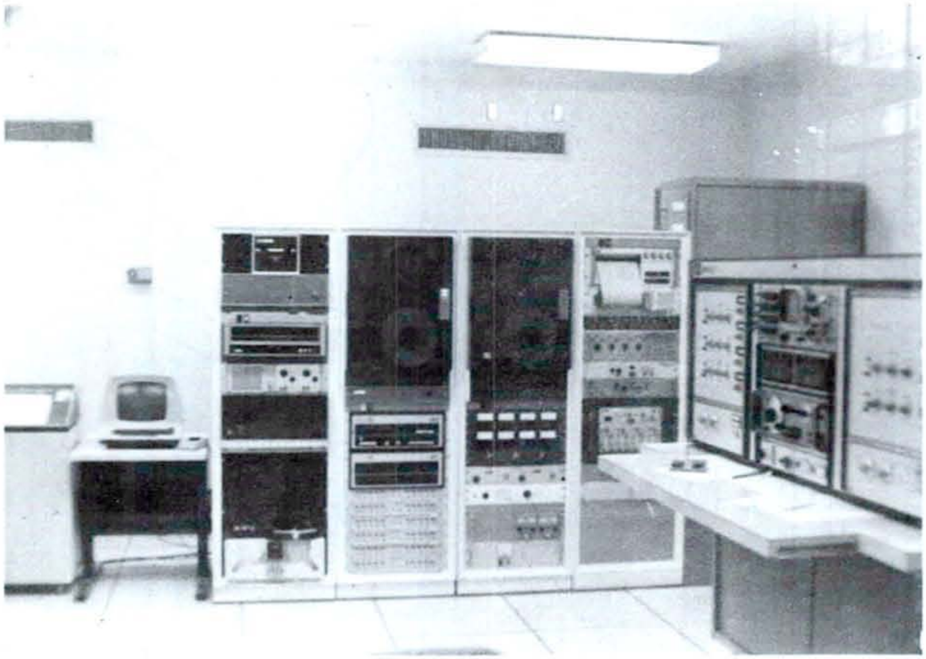

(a) Control Room

(b) Shaking Table

FIGURE 4.10 EARTHQUAKE SIMULATOR

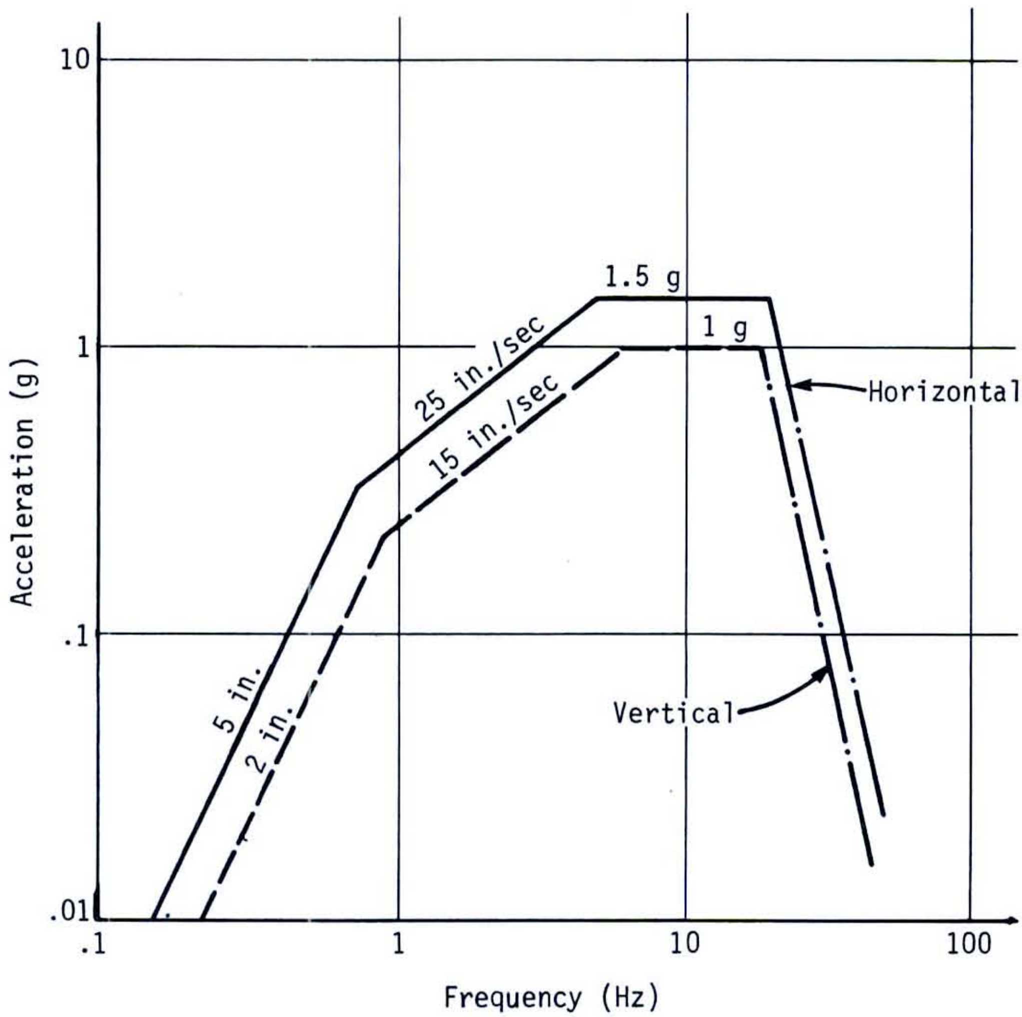

FIGURE 4.11 SHAKING TABLE MOTION LIMITS

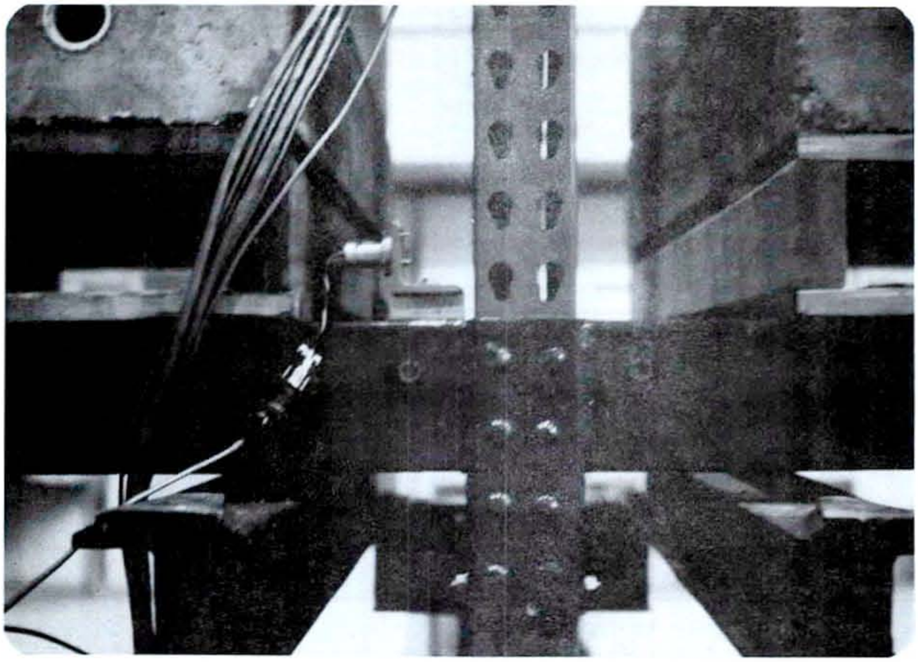

(a) Accelerometer

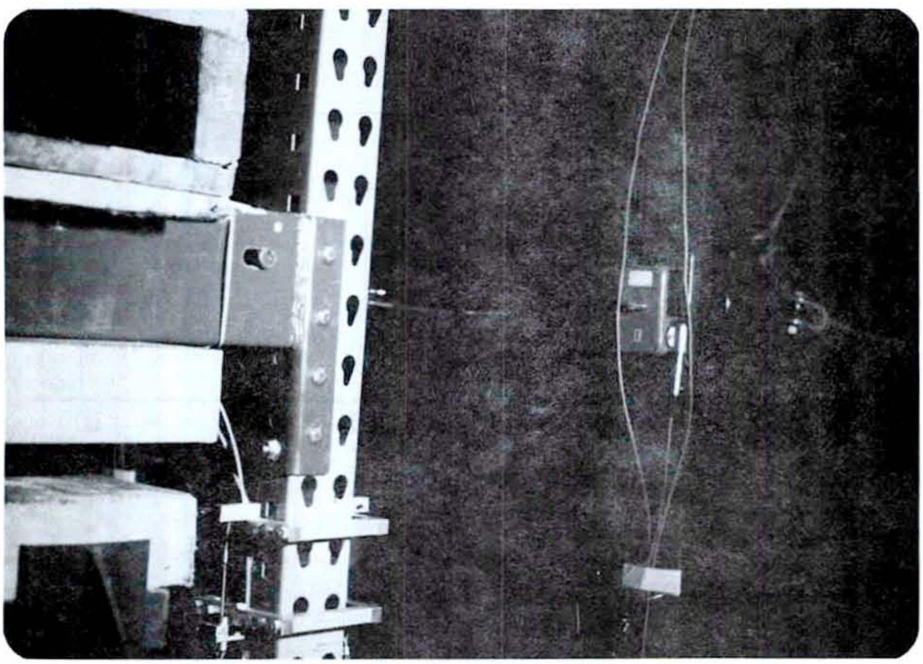

(b) Potentiometer and DCDT Gages

FIGURE 4.12 TYPES OF TRANSDUCERS

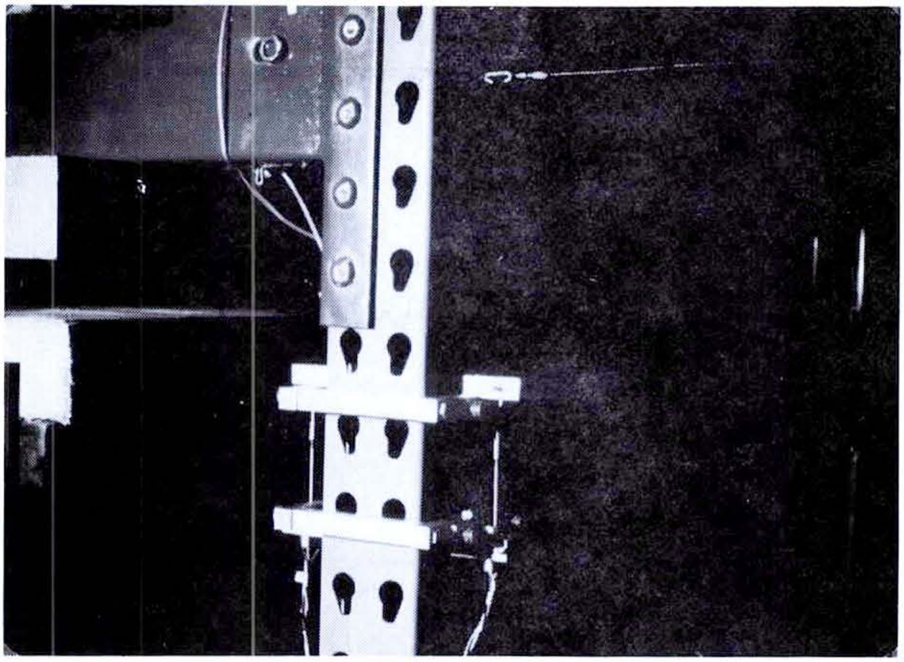

(a) DCDT Gages Mounted Near the Top End of First-Level Column

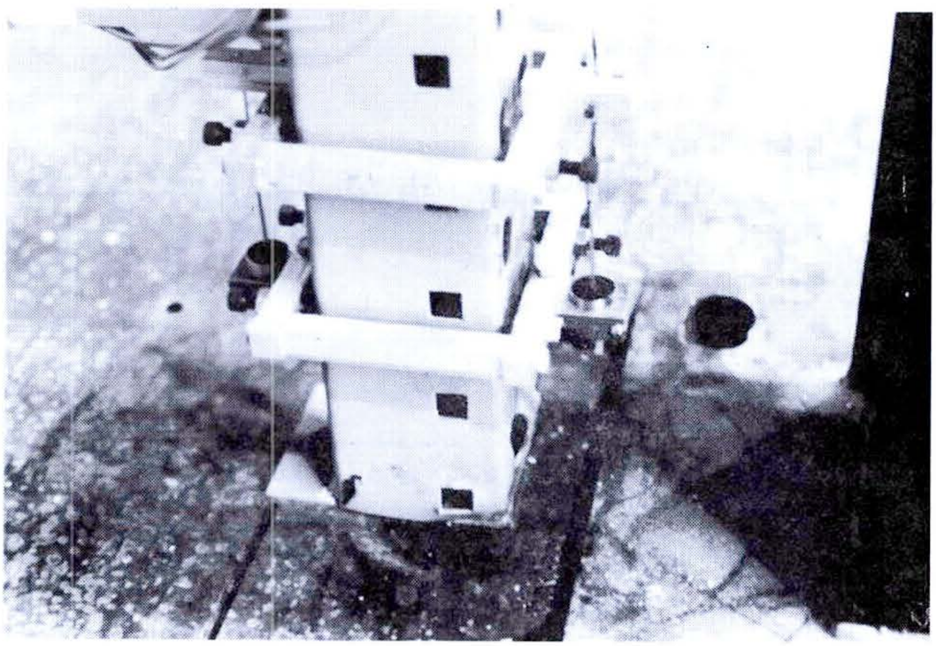

(b) DCDT Gages Mounted Near the Base Plate

FIGURE 4.13 COLUMN END ROTATION MEASUREMENTS

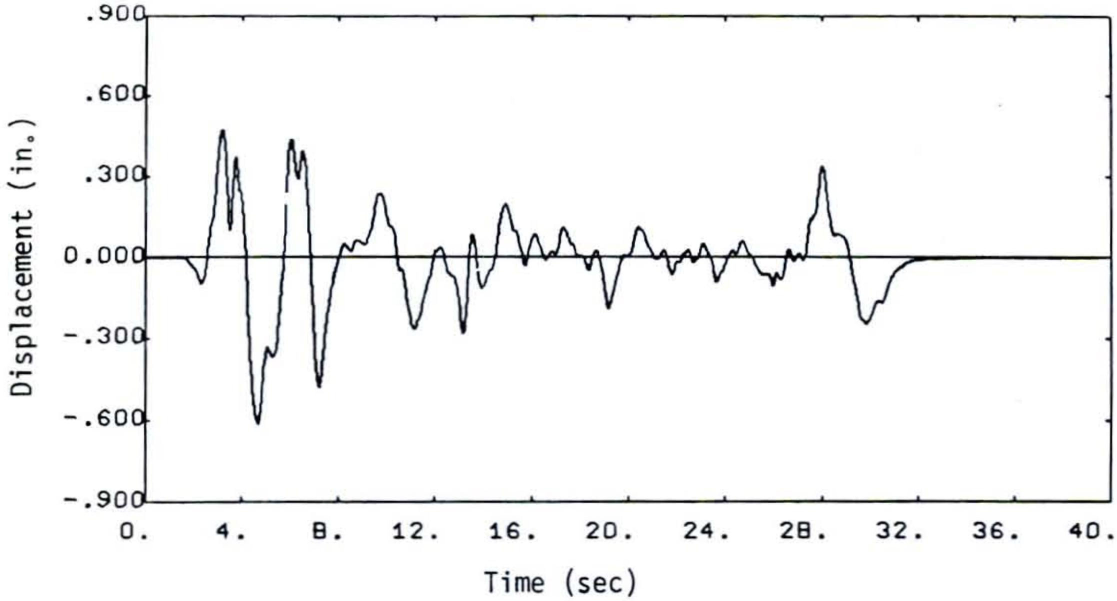

Table Displacement

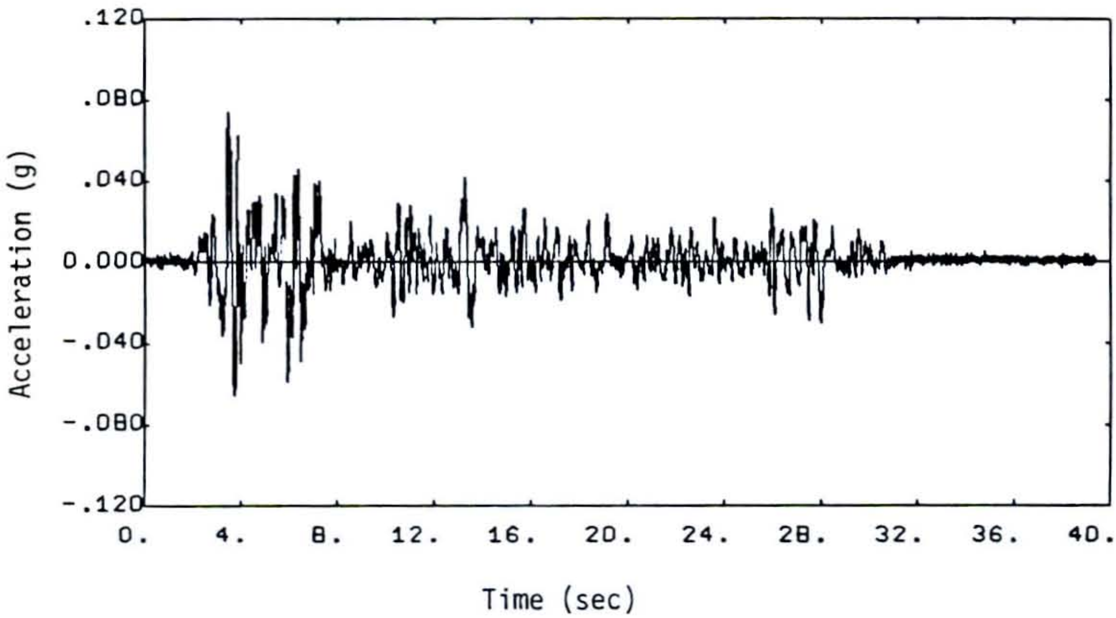

Table Acceleration

FIGURE 4.14 TABLE MOTIONS - 1/4 EC

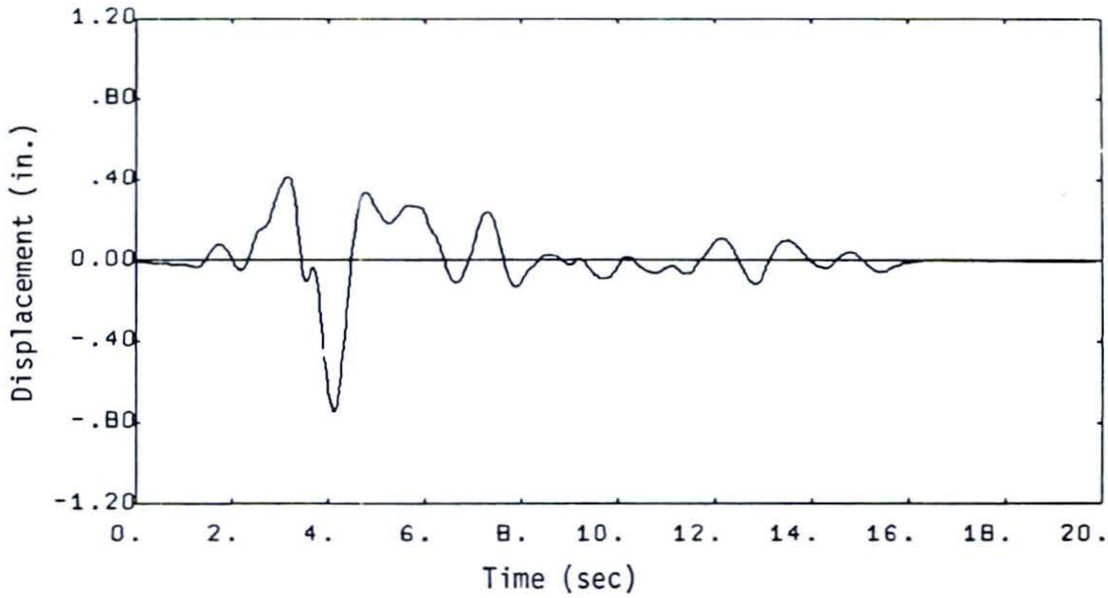

Table Displacement

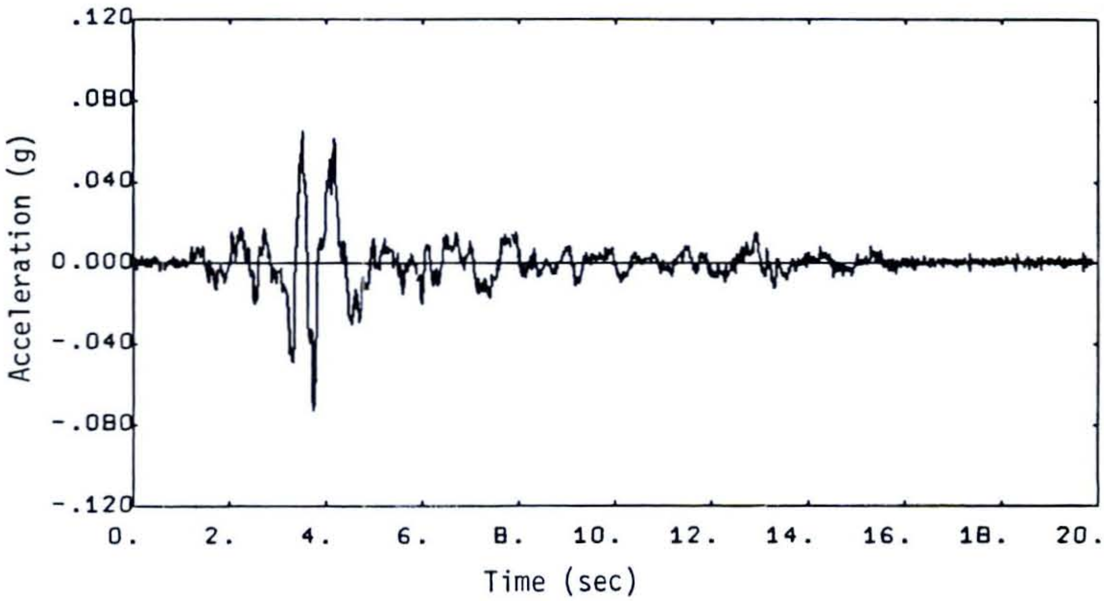

Table Acceleration

FIGURE 4.15 TABLE MOTIONS - 1/4 PF

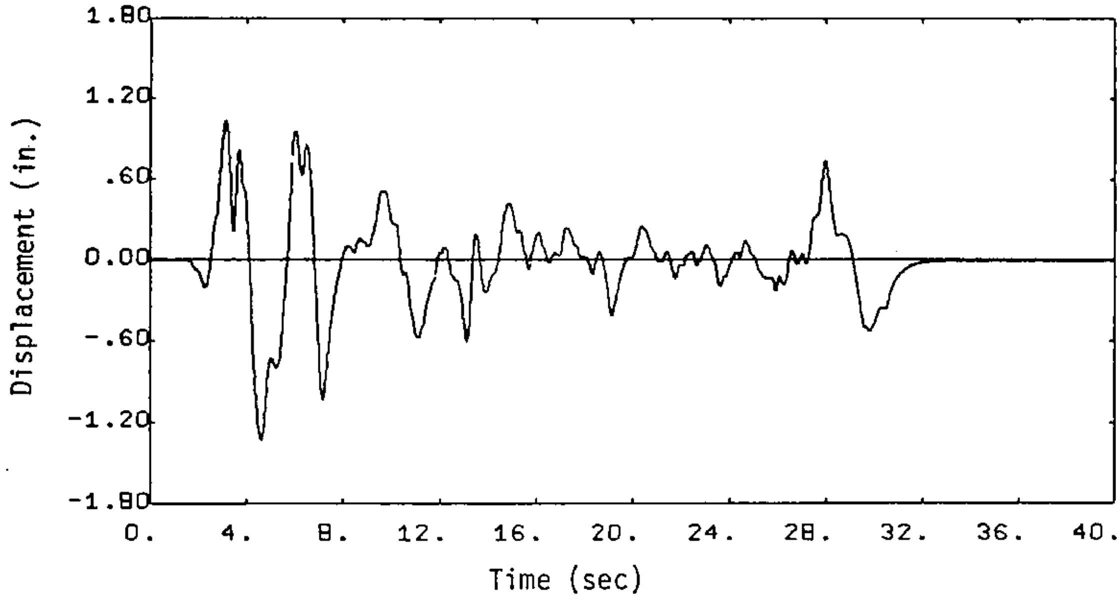

Table Displacement

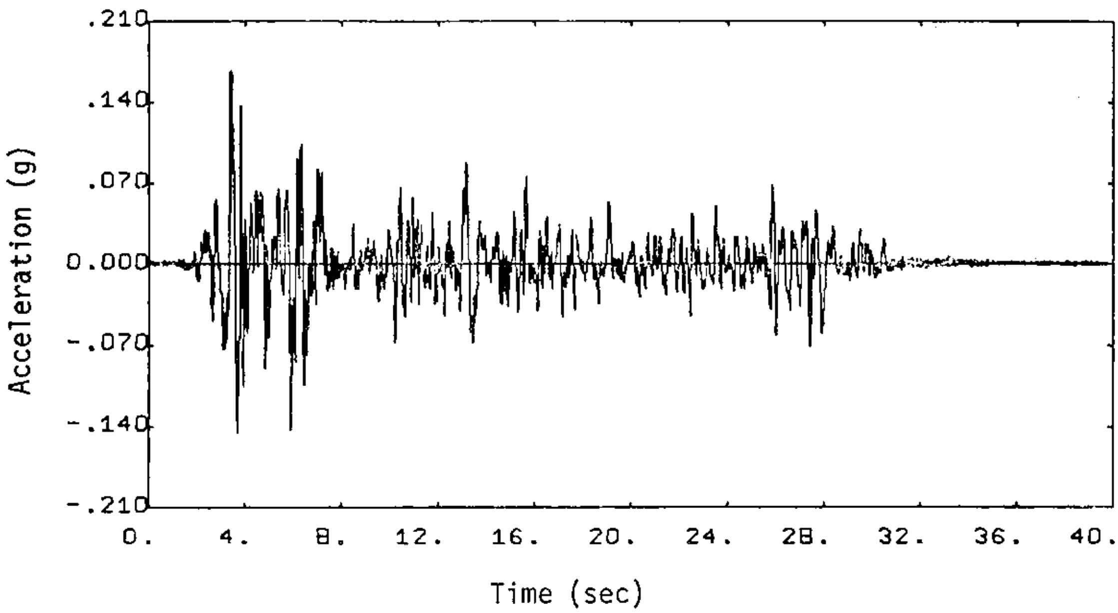

Table Acceleration

FIGURE 4.16 TABLE MOTIONS - 1/2 EC

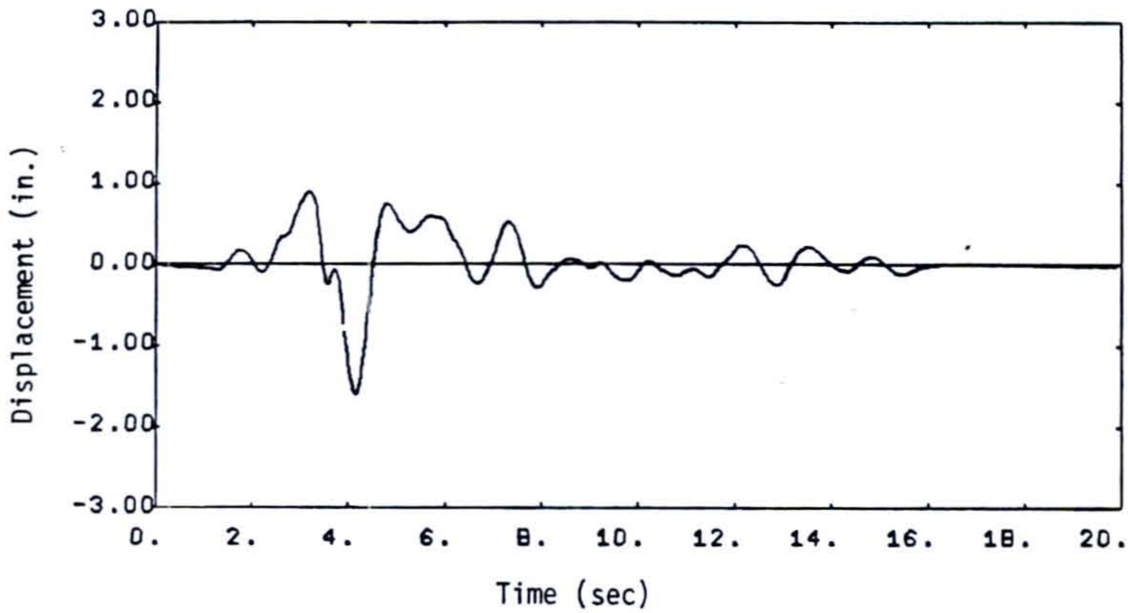

Table Displacement

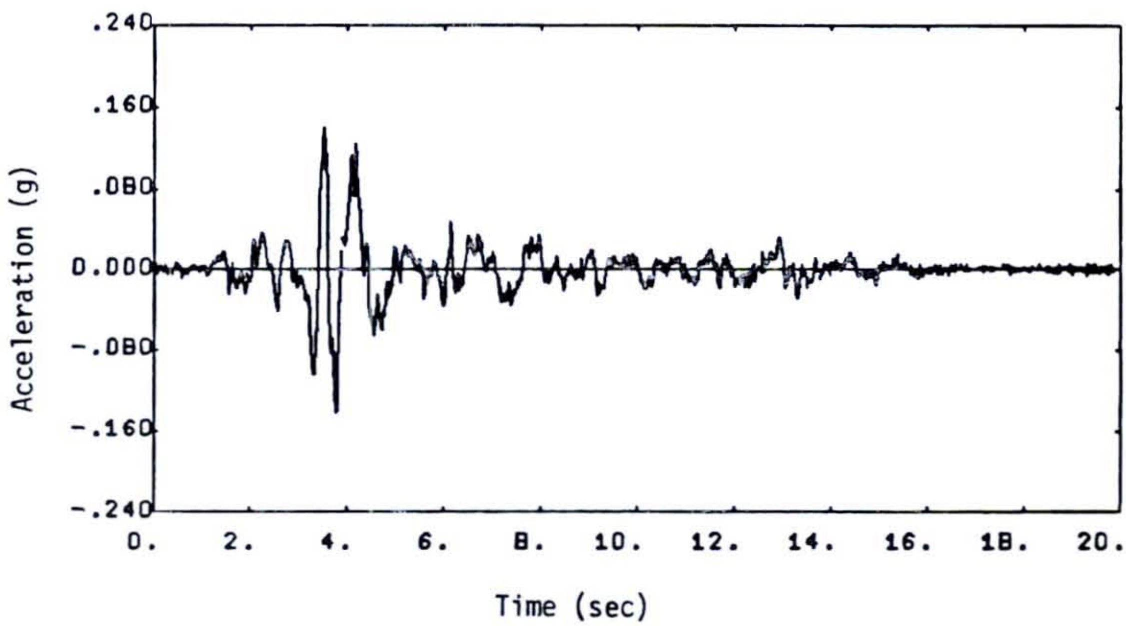

Table Acceleration

FIGURE 4.17 TABLE MOTIONS - 1/2 PF

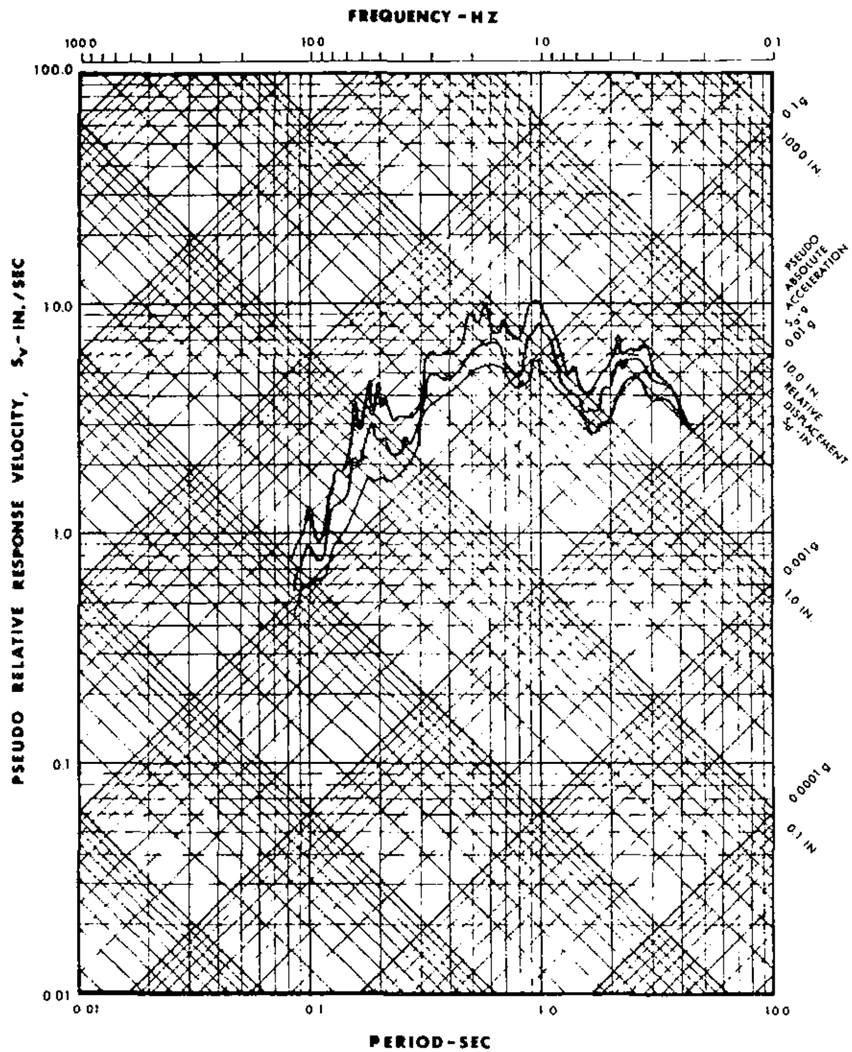

(a) 1/4 EC

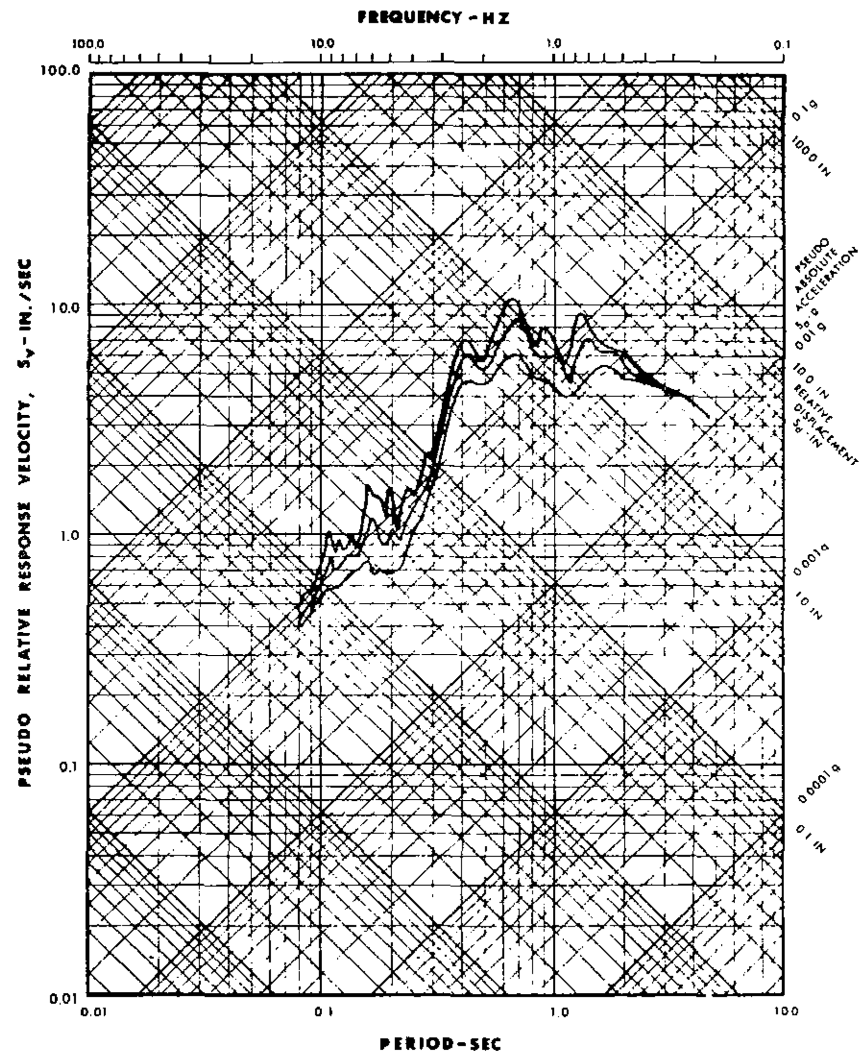

(b) 1/4 PF

FIGURE 4.18 RESPONSE SPECTRA FOR 1/4 EC and 1/4 PF; DAMPING RATIOS = 0.01, 0.03, and 0.08

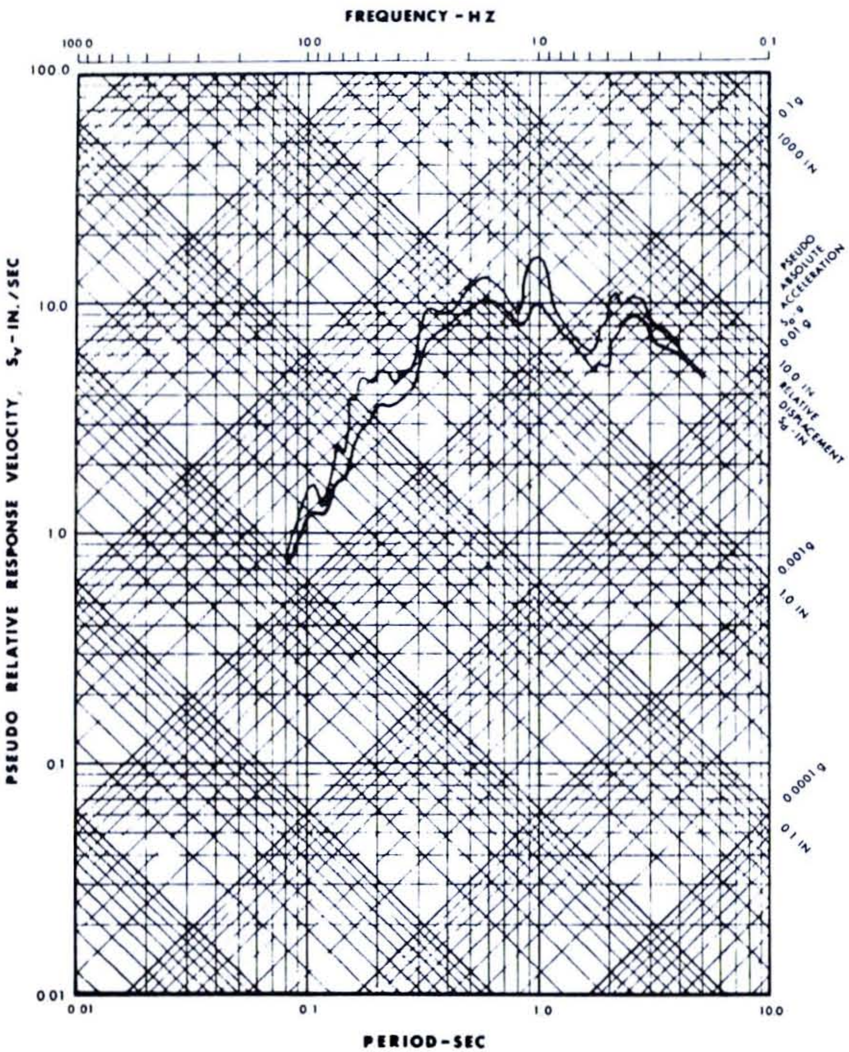

(a) 1/2 EC

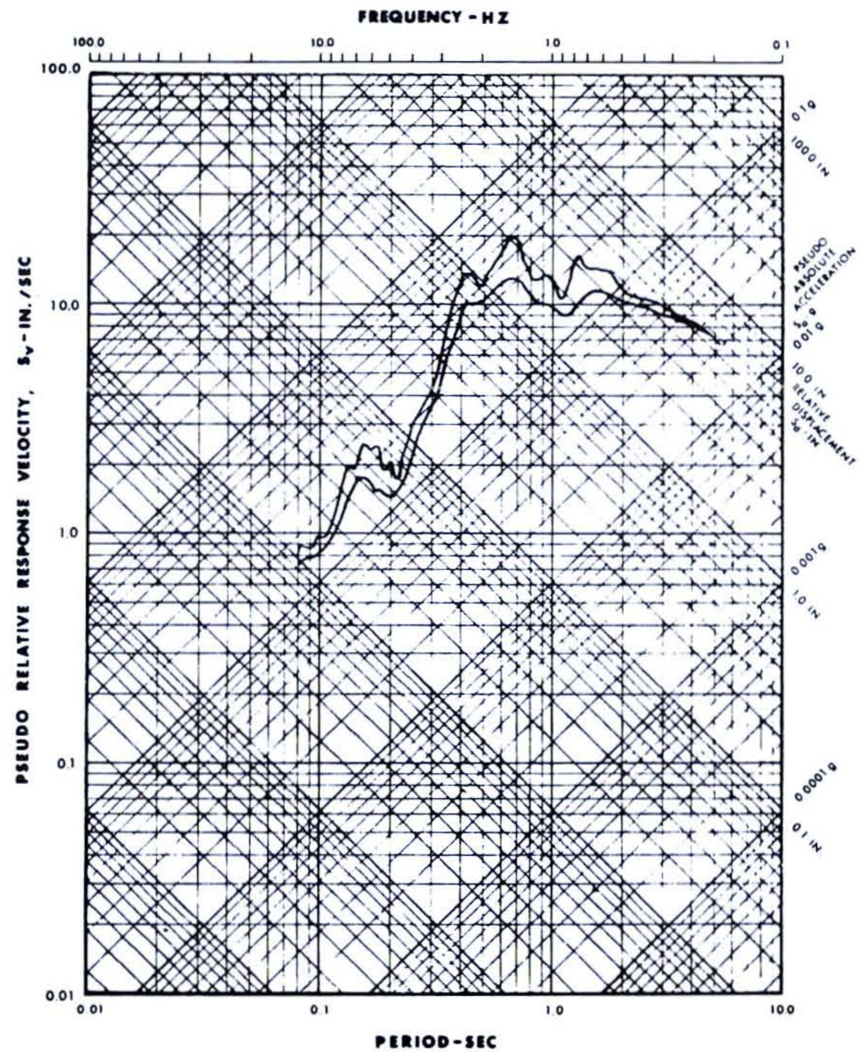

(b) 1/2 PF

FIGURE 4.19 RESPONSE SPECTRA FOR 1/2 EC and 1/2 PF; DAMPING RATIOS = 0.03, 0.08

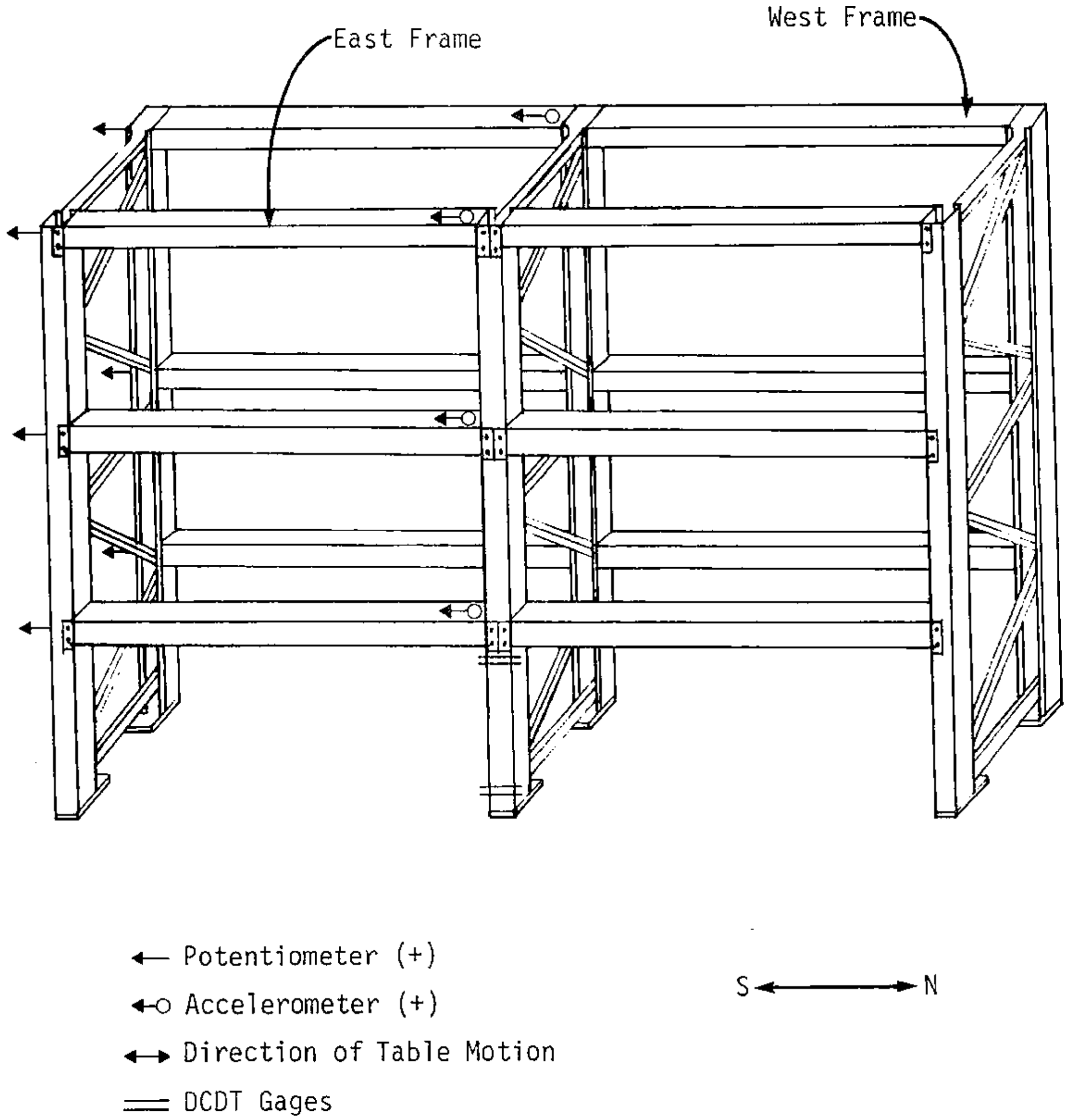

FIGURE 4.20 INSTRUMENTATION CHANNELS USED FOR DATA ANALYSIS: STANDARD PALLET RACK, LONGITUDINAL DIRECTION

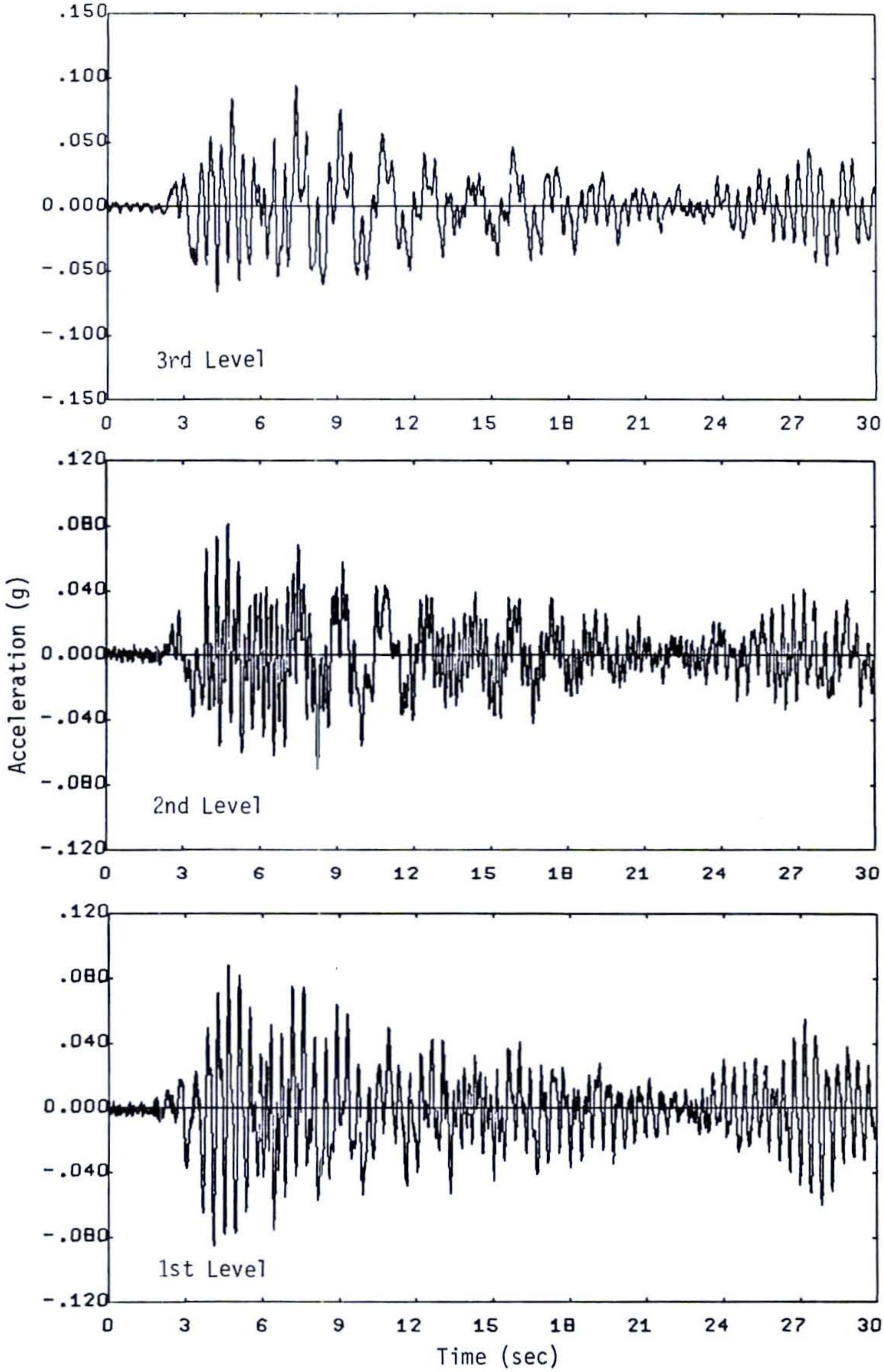

FIGURE 4.21a STORY ACCELERATIONS - TEST 120178.2 (SP-L-2/3-1/4 EC)

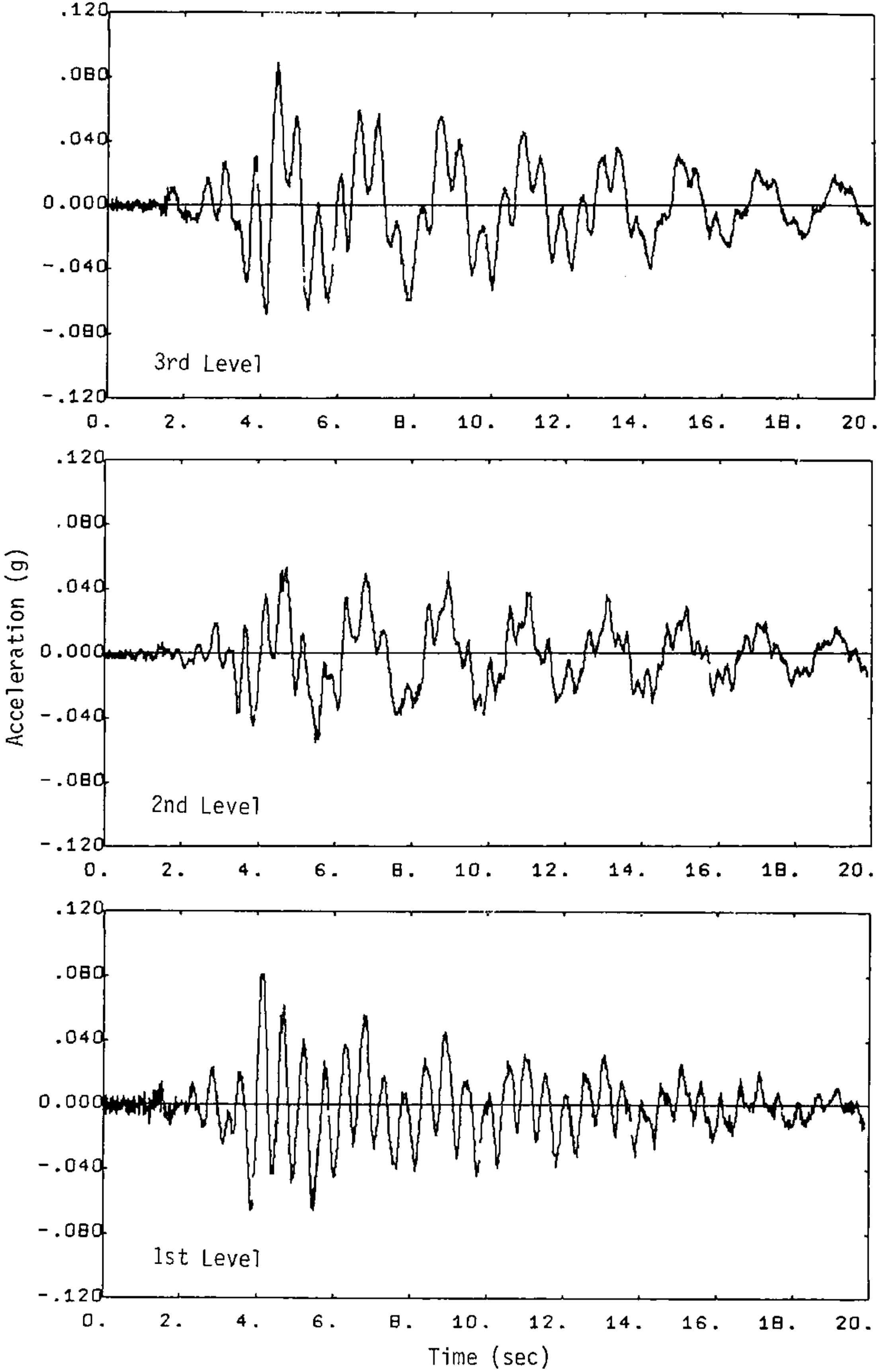

FIGURE 4.21b STORY ACCELERATIONS - TEST 170178.1 (SP-L-1-1/4 PF)

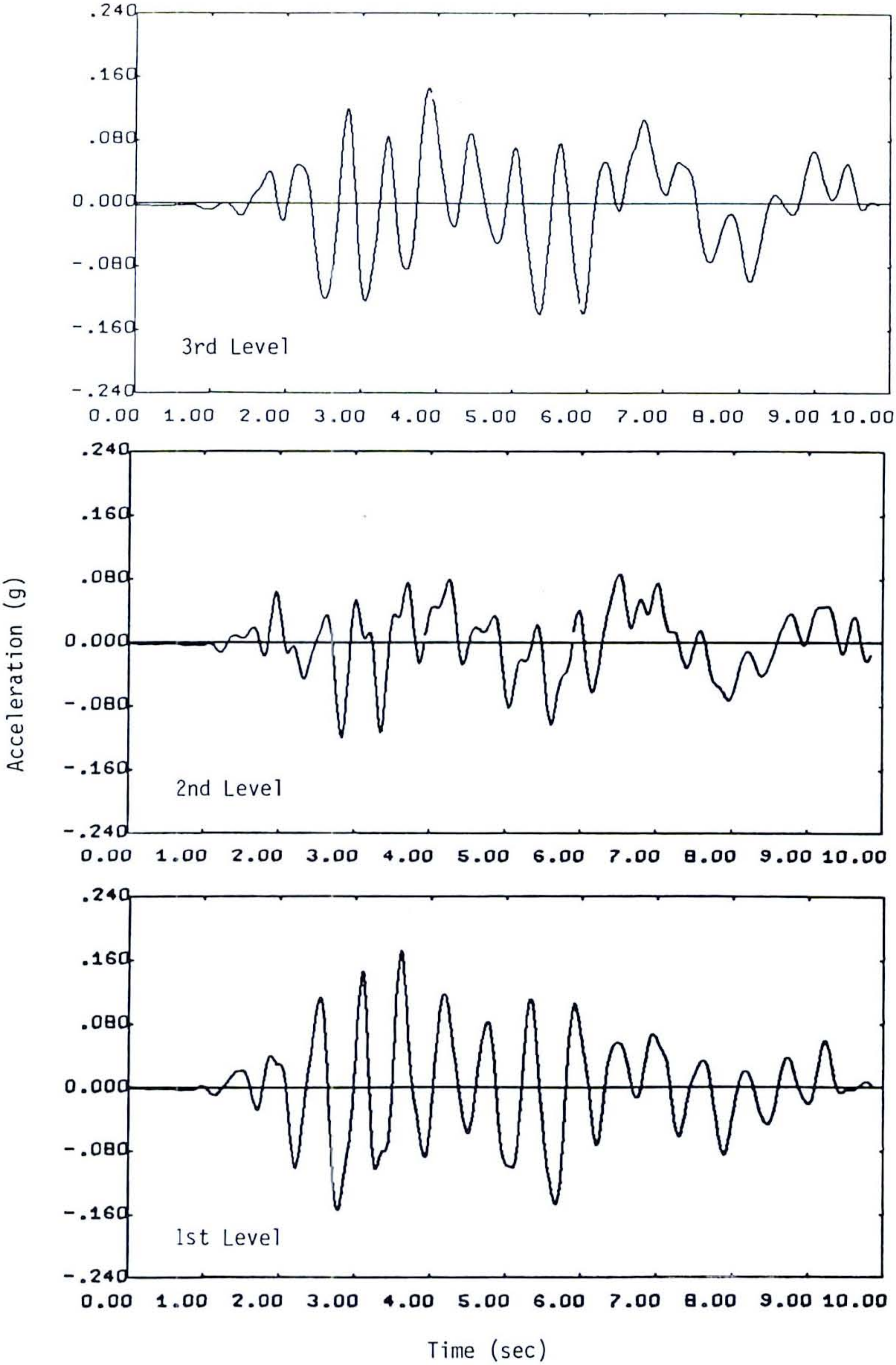

FIGURE 4.21c STORY ACCELERATIONS - TEST 170178.2 (SP-L-1-1/2 EC)

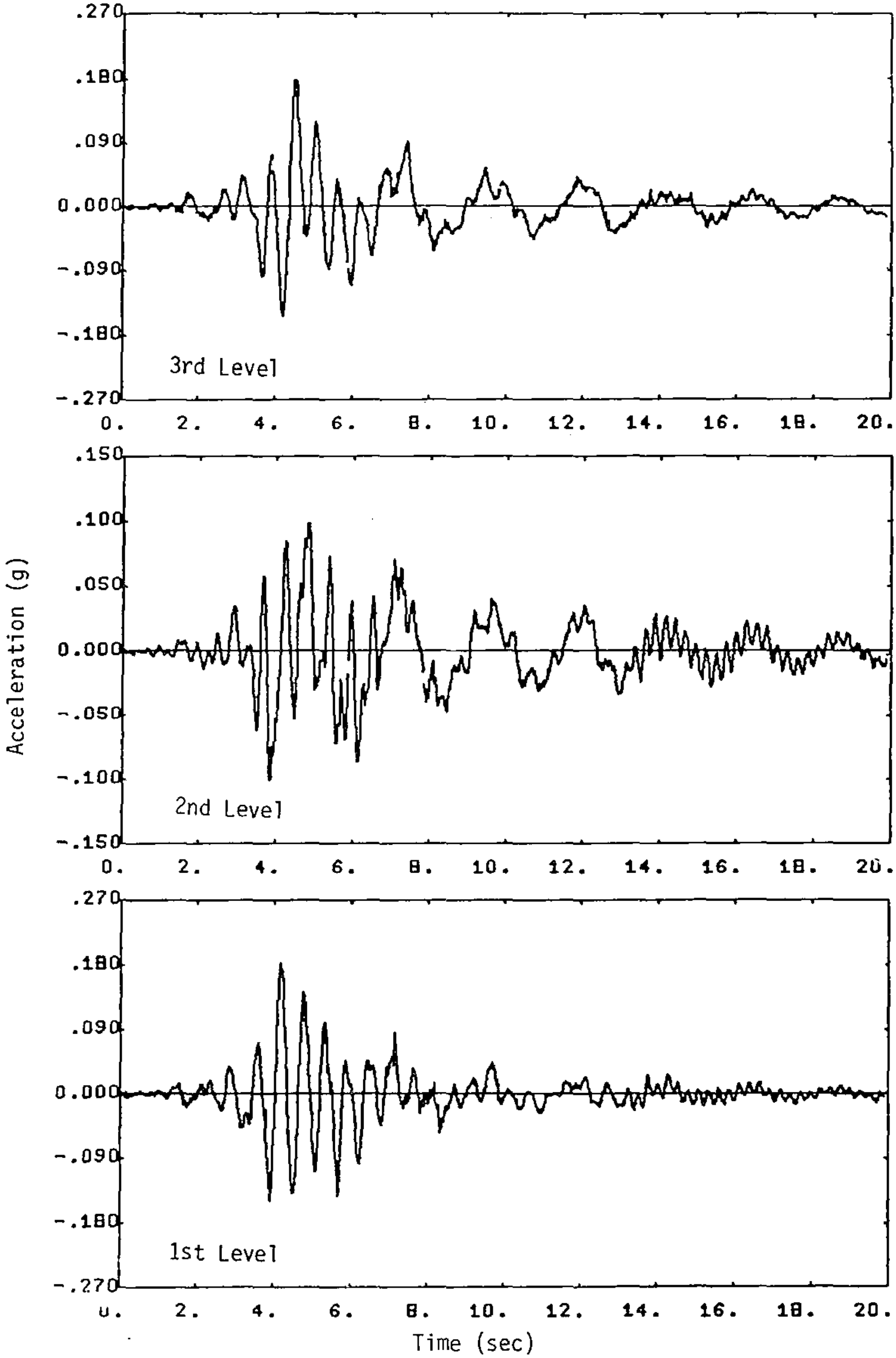

FIGURE 4.21d STORY ACCELERATIONS - TEST 170178.3 (SP-L-1-1/2 PF)

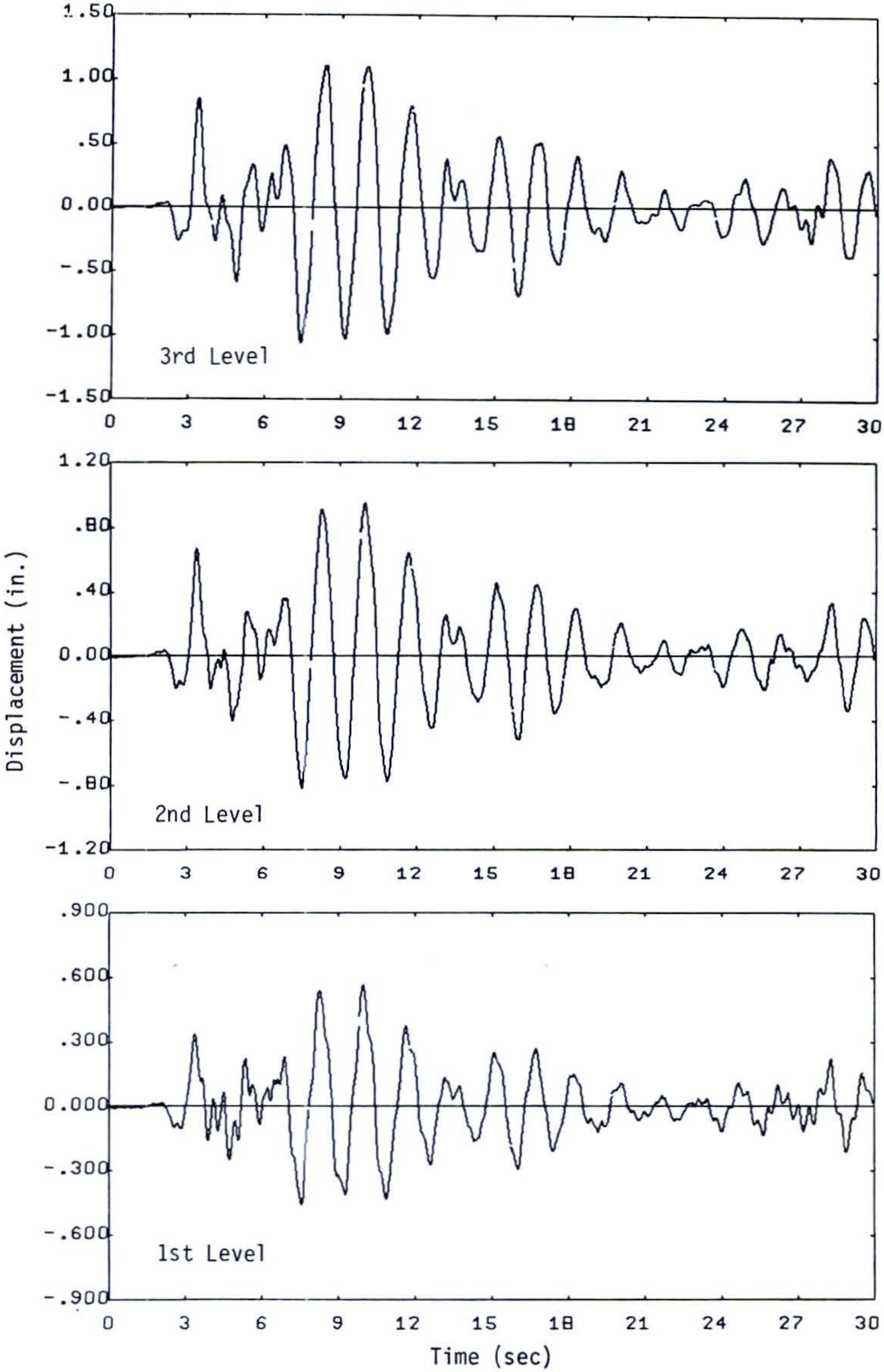

FIGURE 4.22a STORY DISPLACEMENTS RELATIVE TO THE TABLE - TEST 120178.2 (SP-L-2/3-1/4 EC)

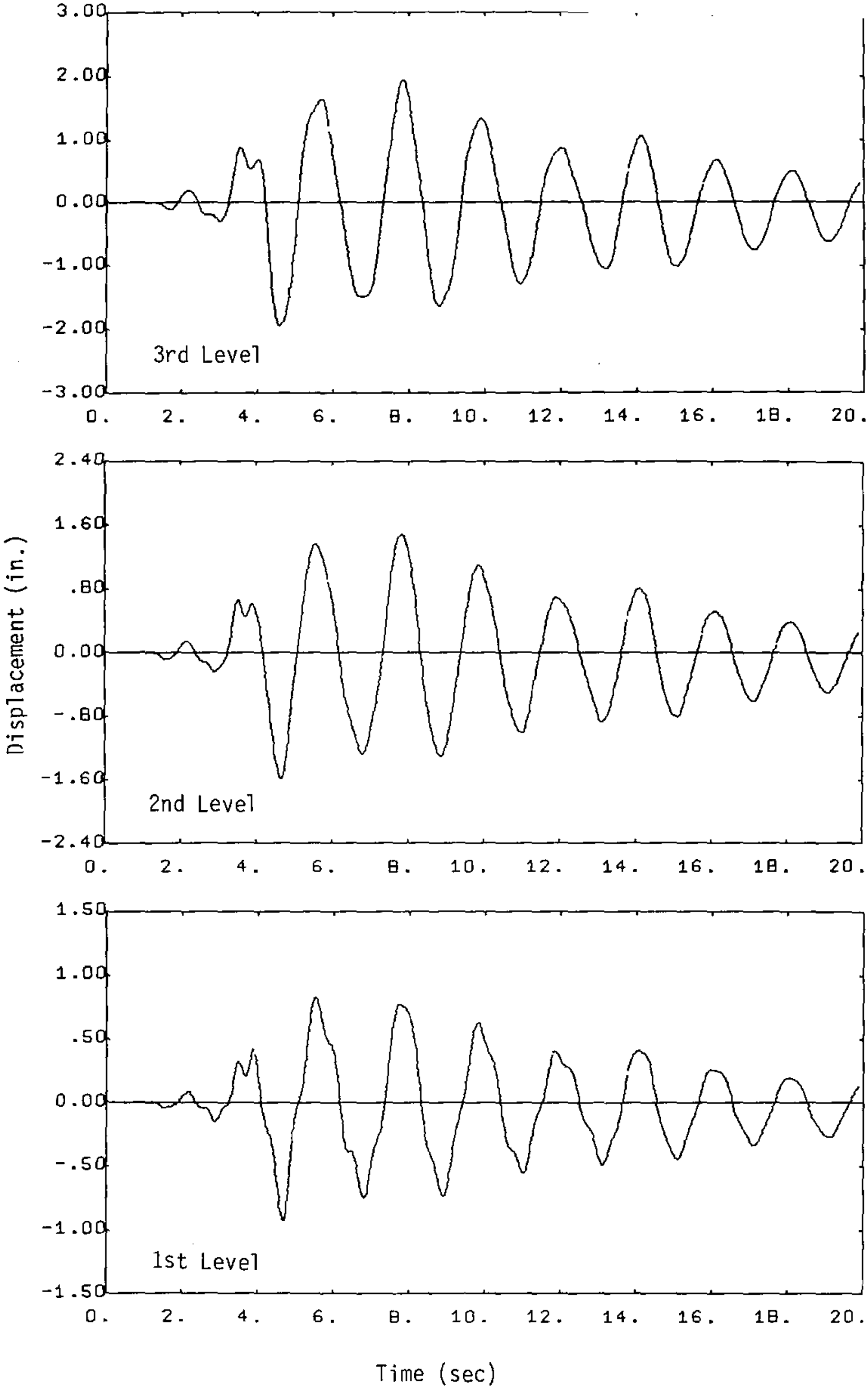

FIGURE 4.22b STORY DISPLACEMENTS RELATIVE TO THE TABLE - TEST 170178.1 (SP-L-1-1/4 PF)

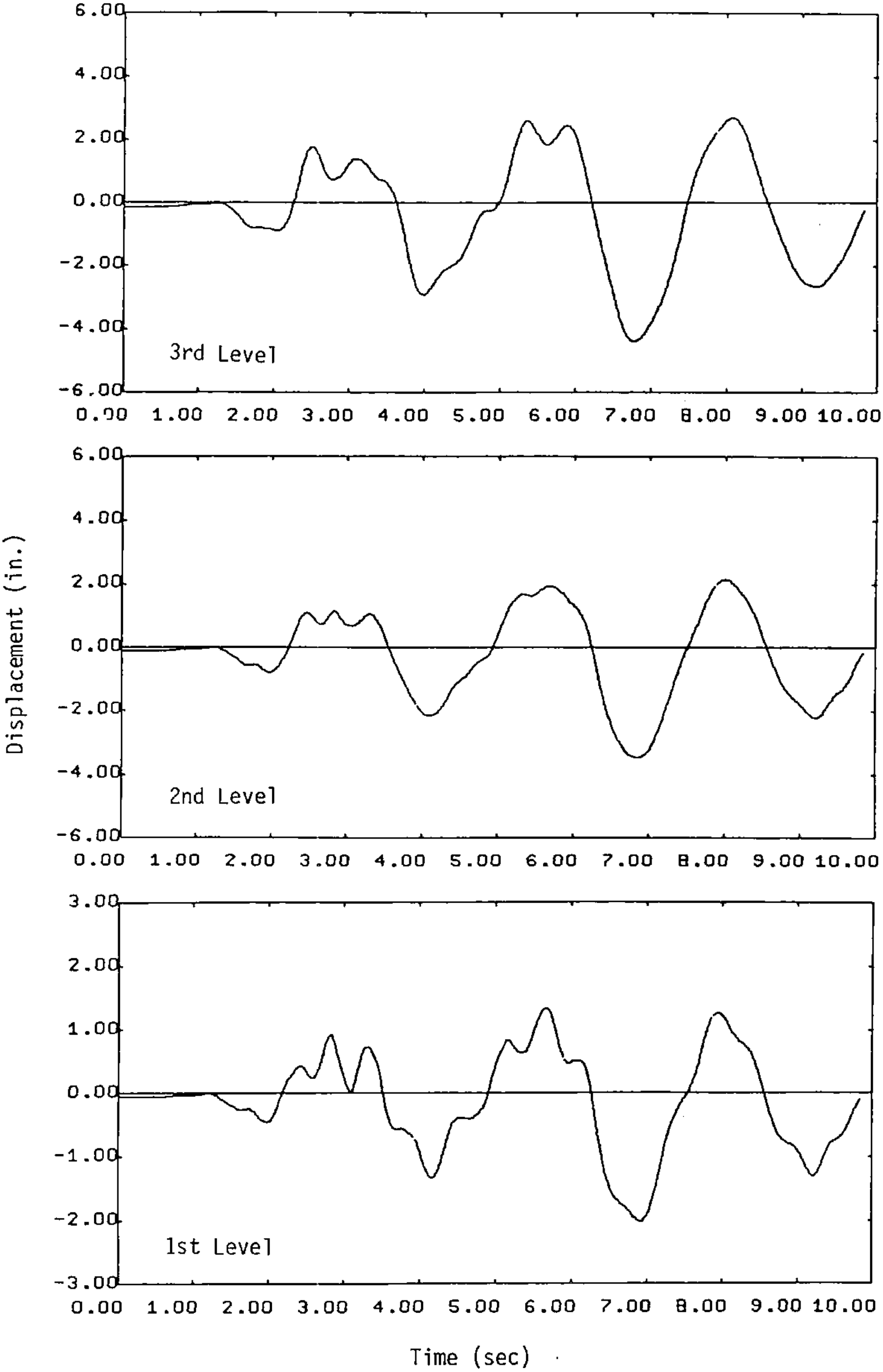

FIGURE 4.22c STORY DISPLACEMENTS RELATIVE TO THE TABLE - TEST 170178.2 (SP-L-1-1/2 EC)

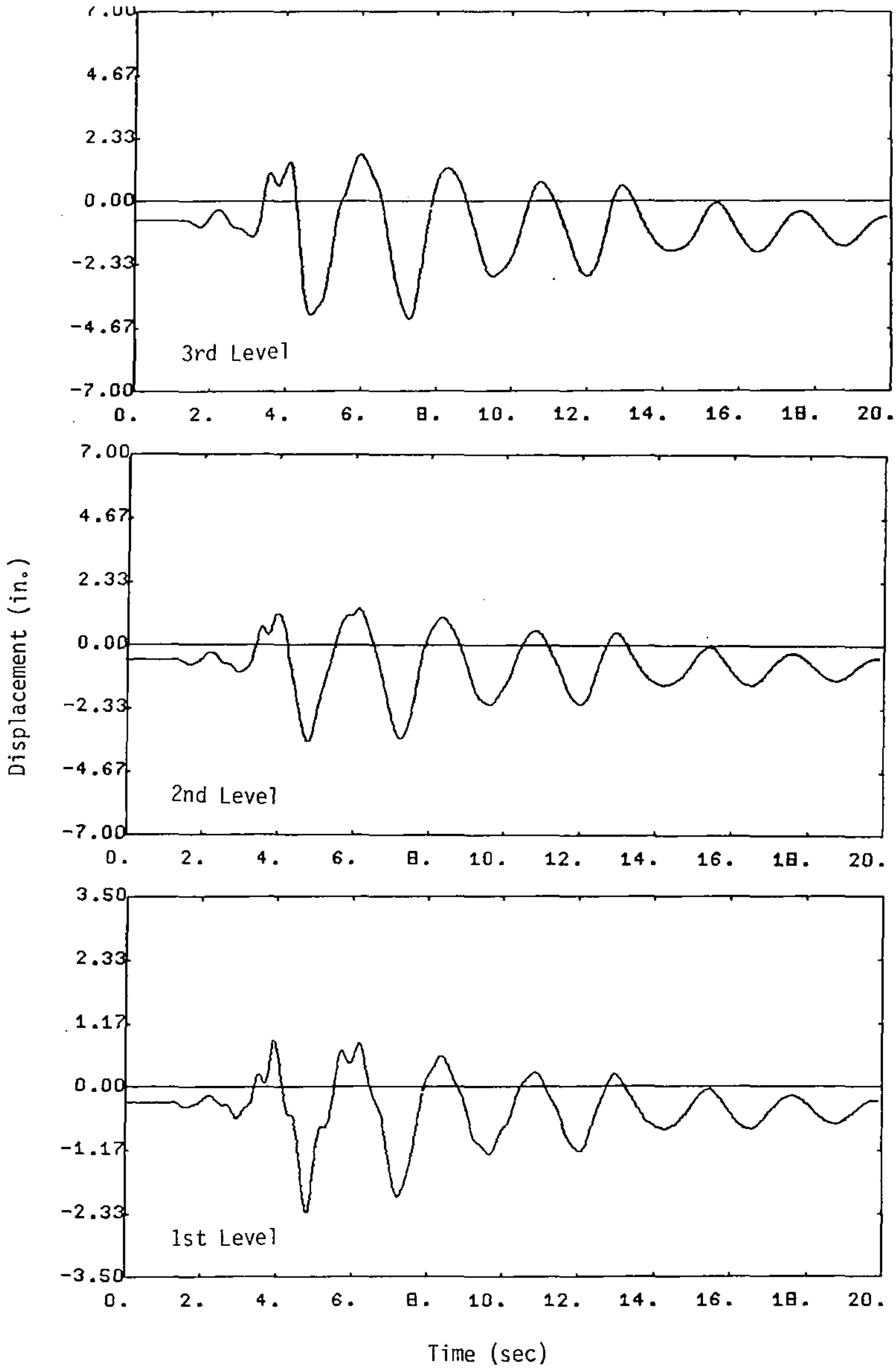

FIGURE 4.22d STORY DISPLACEMENTS RELATIVE TO THE TABLE - TEST 170178.3 (SP-L-1-1/2 PF)

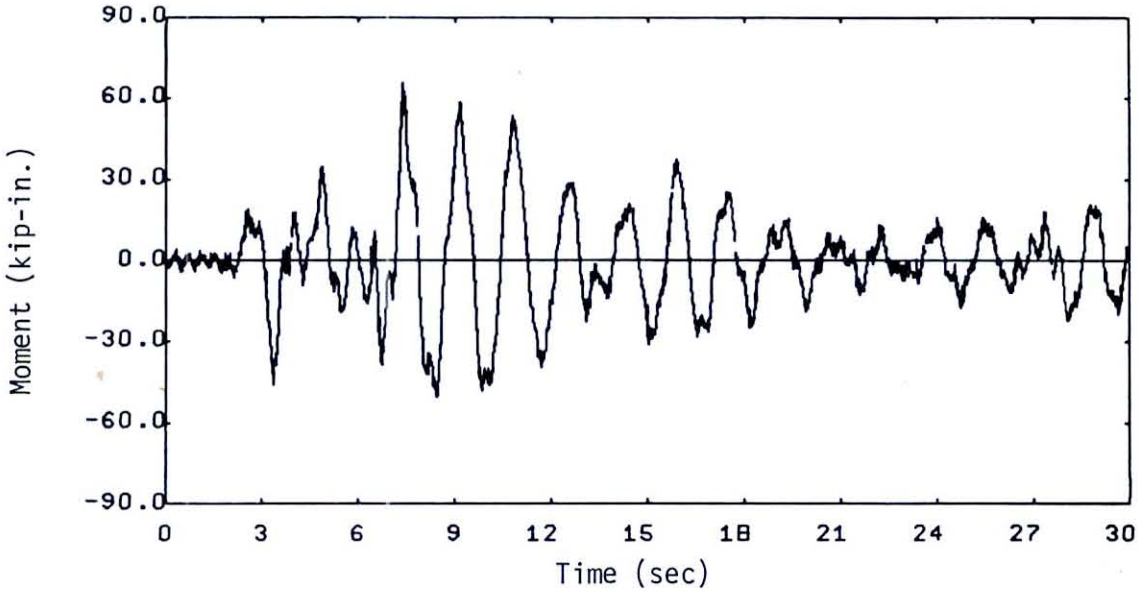

Base Overturning Moment

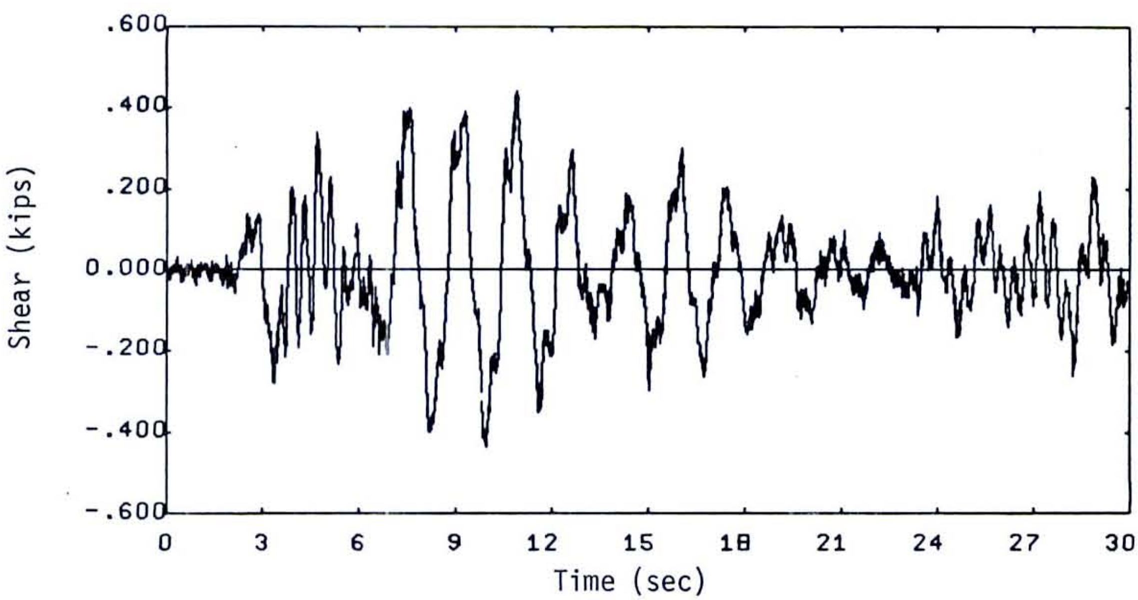

Base Shear

FIGURE 4.23a BASE SHEAR AND OVERTURNING MOMENT - TEST 120178.2
(SP-L-2/3-1/4 EC)

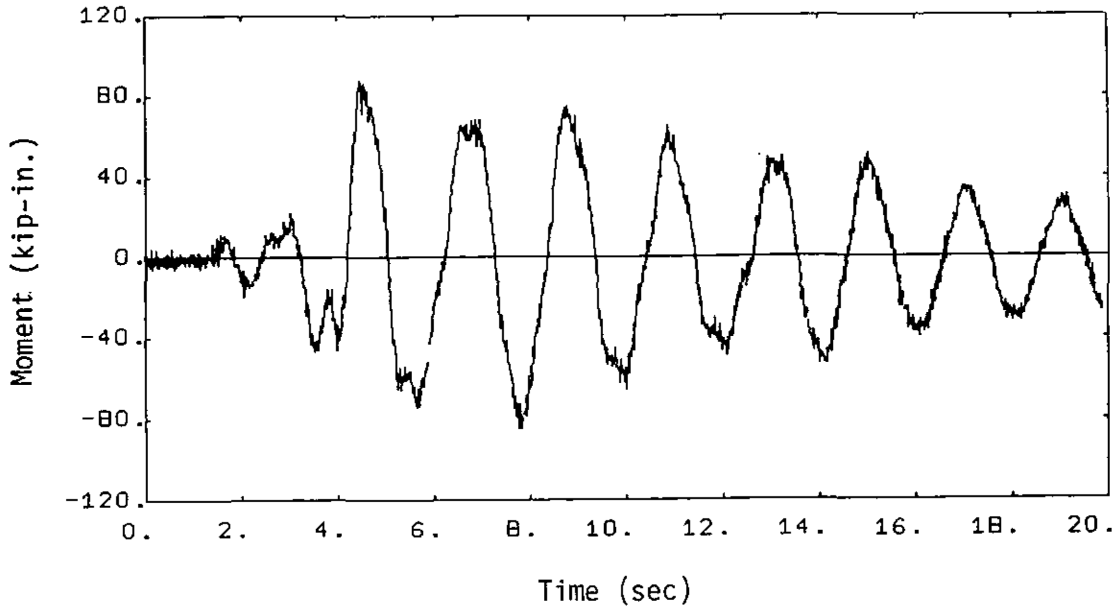

Base Overturning Moment

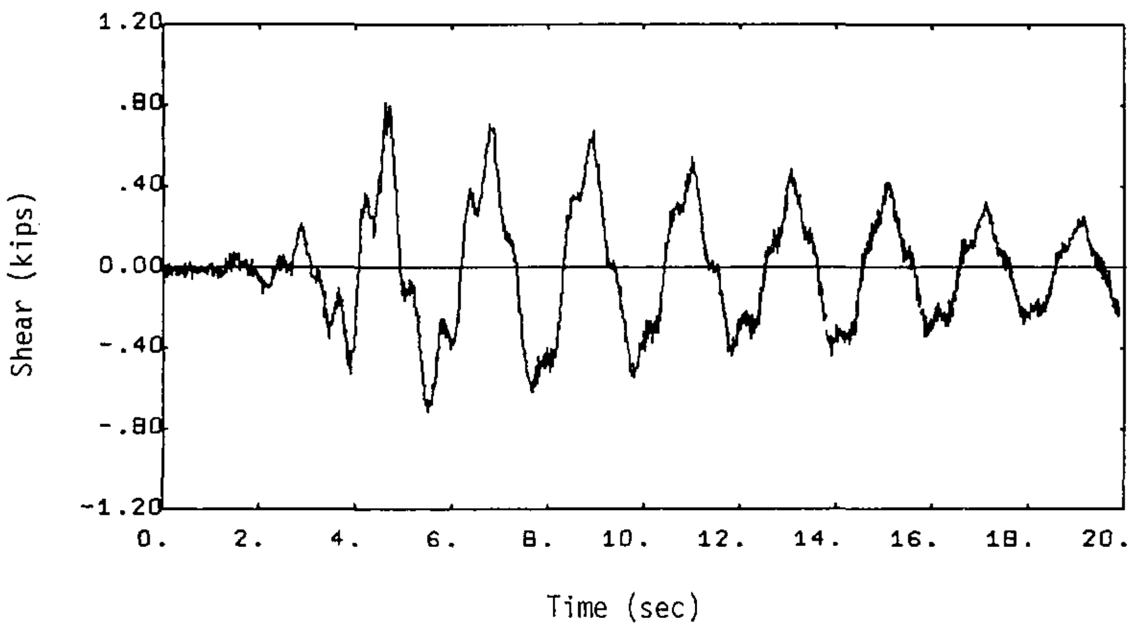

Base Shear

FIGURE 4.23b BASE SHEAR AND OVERTURNING MOMENT - TEST 170178.1 (SP-L-1-1/4 PF)

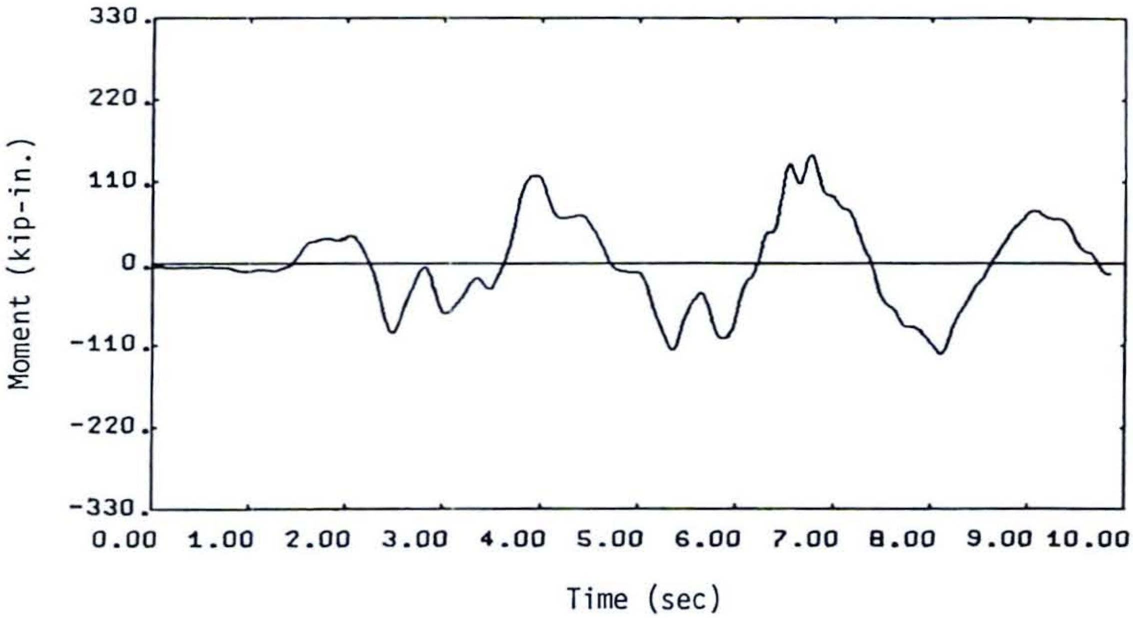

Base Overturning Moment

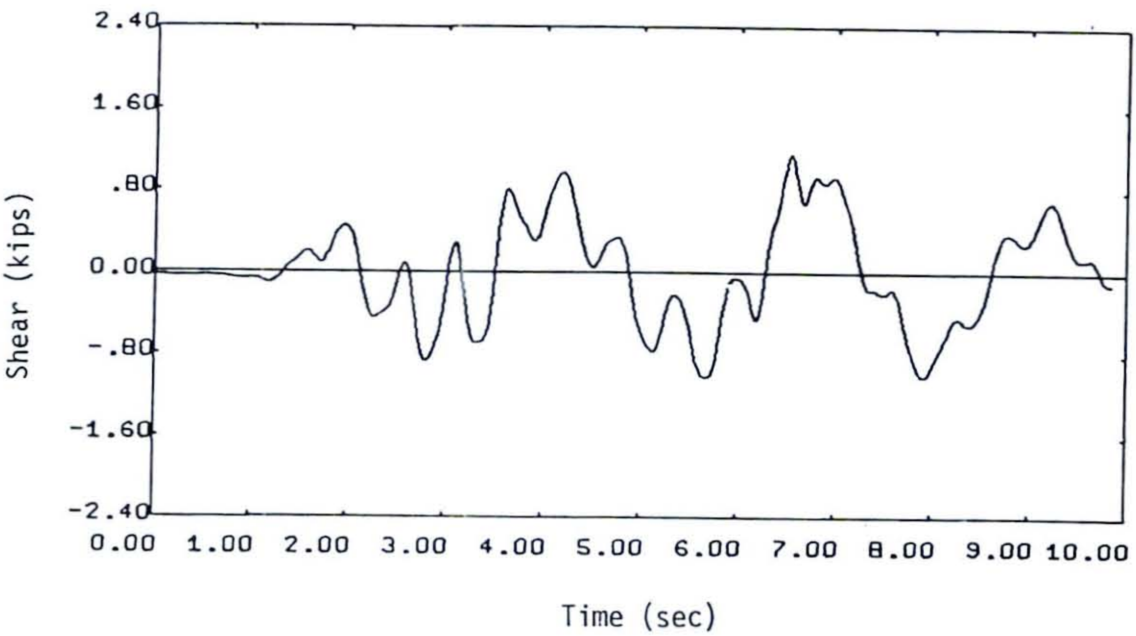

Base Shear

FIGURE 4.23c BASE SHEAR AND OVERTURNING MOMENT - TEST 170178.2 (SP-L-1-1/2 EC)

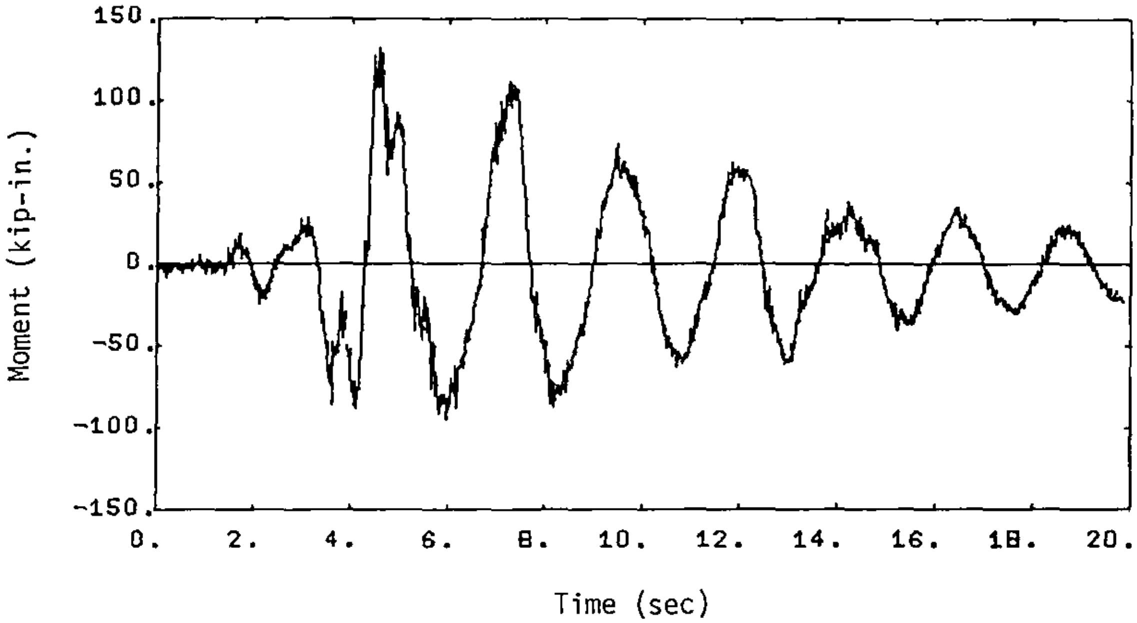

Base Overturning Moment

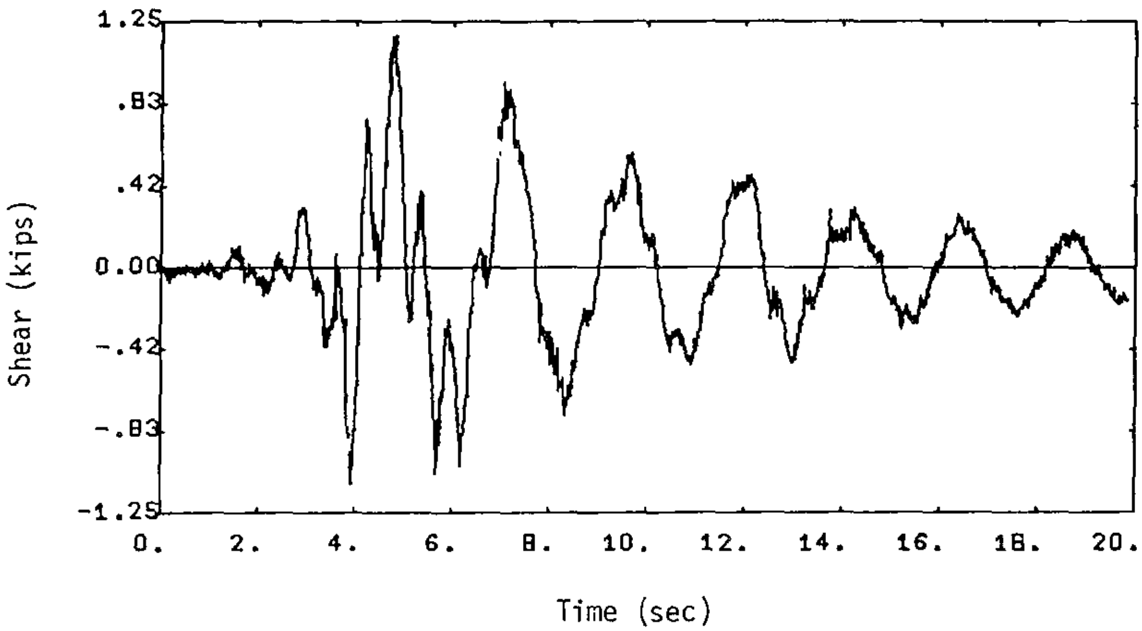

Base Shear

FIGURE 4.23d BASE SHEAR AND OVERTURNING MOMENT - TEST 170178.3 (SP-L-1-1/2 PF)

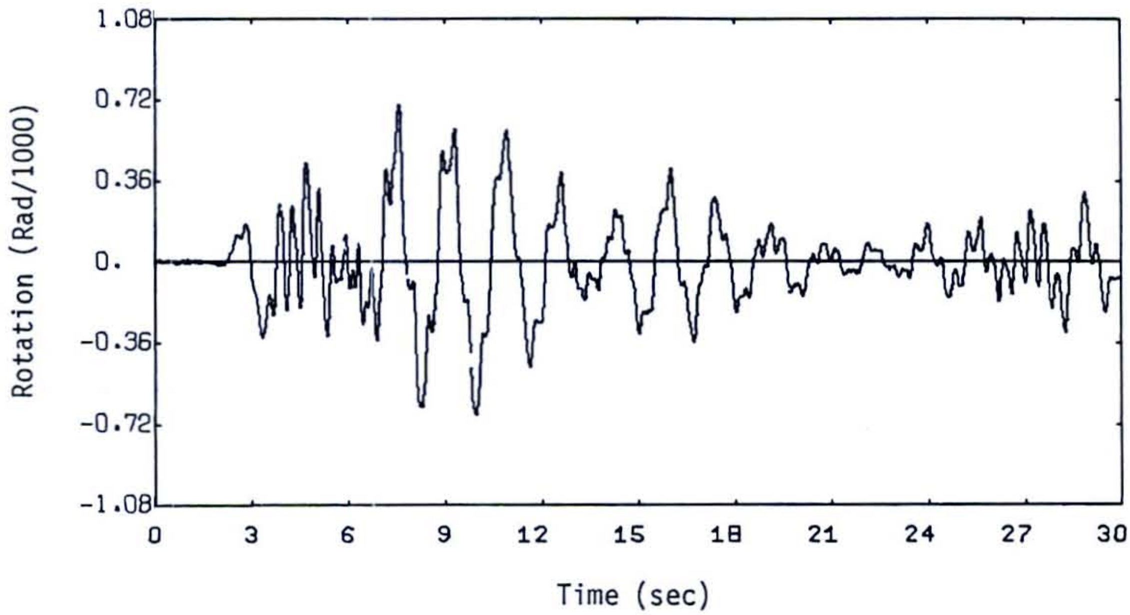

Center Bottom Column - Top End

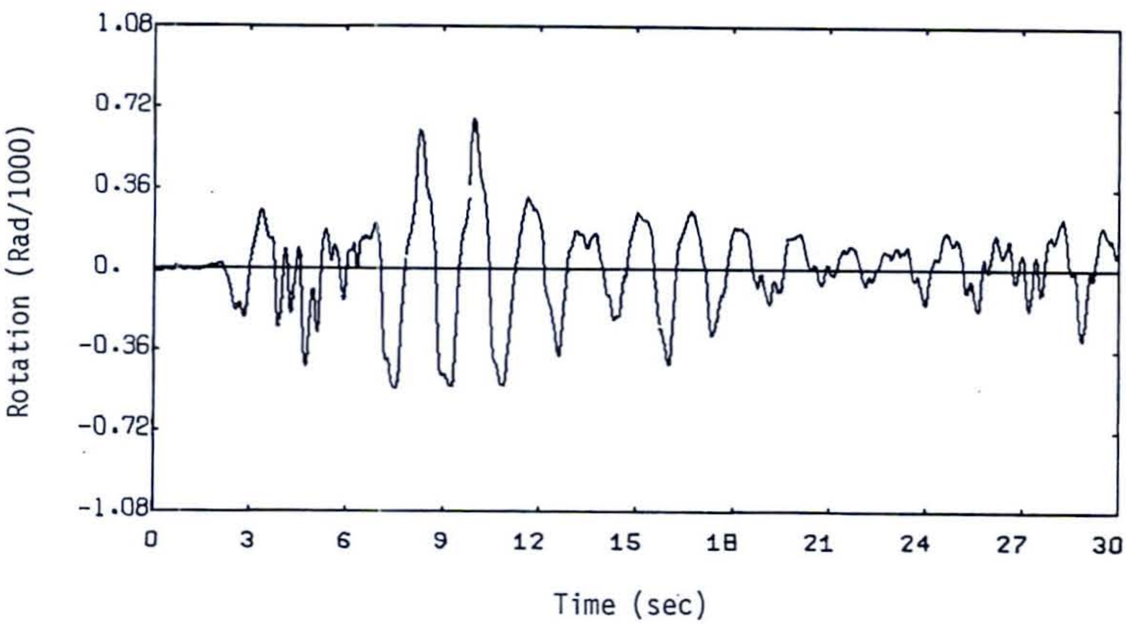

Center Bottom Column - Bottom End

FIGURE 4.24a COLUMN END ROTATIONS - TEST 120178.2 (SP-L-2/3-1/4 EC)

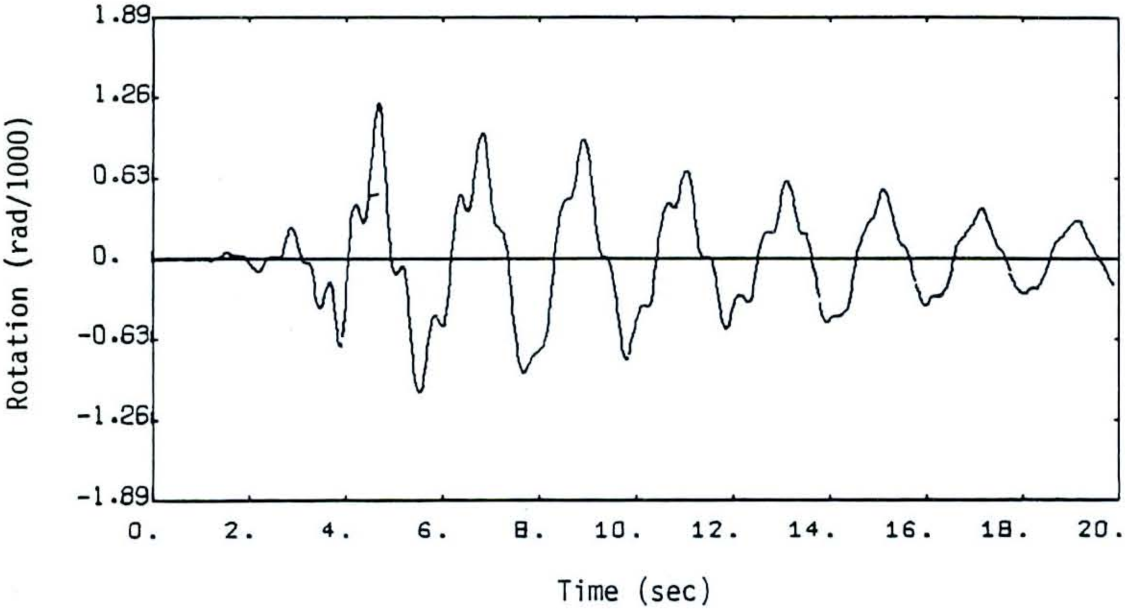

Center Bottom Column - Top End

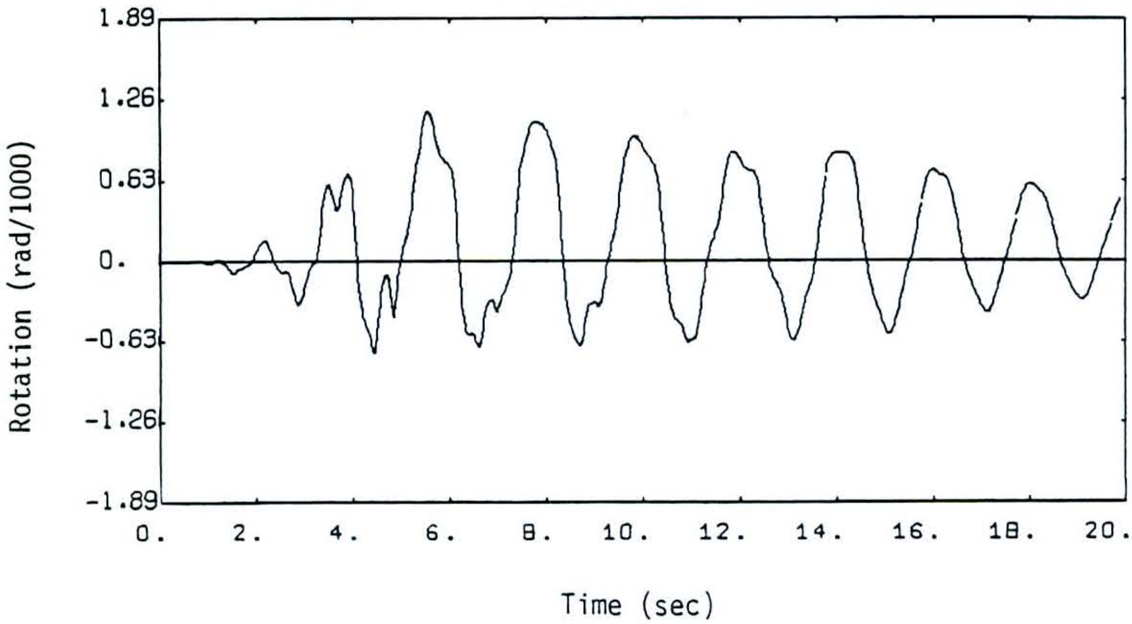

Center Bottom Column - Bottom End

FIGURE 4.24b COLUMN END ROTATIONS - TEST 170178.1 (SP-L-1-1/4 PF)

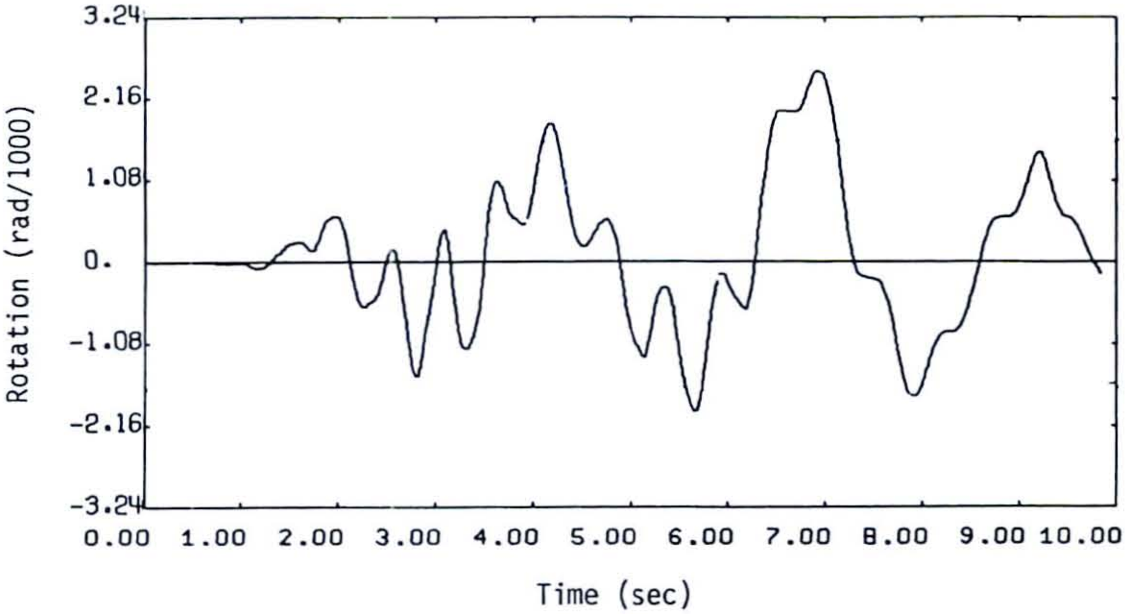

Center Bottom Column - Top End

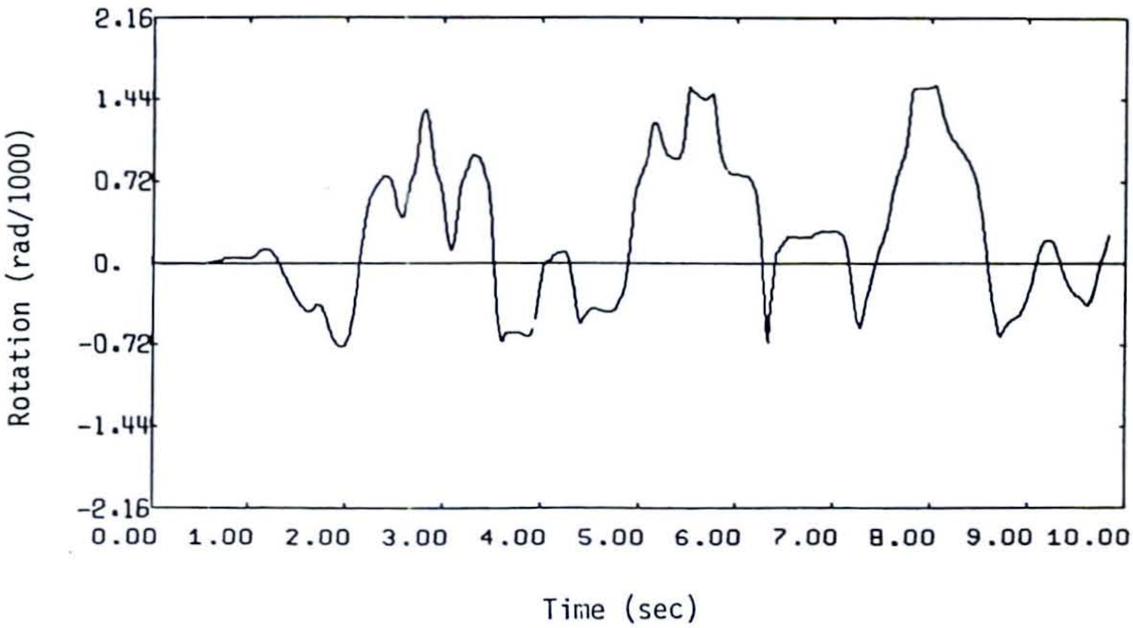

Center Bottom Column - Bottom End

FIGURE 4.24c COLUMN END ROTATIONS - TEST 170178.2 (SP-L-1-1/2 EC)

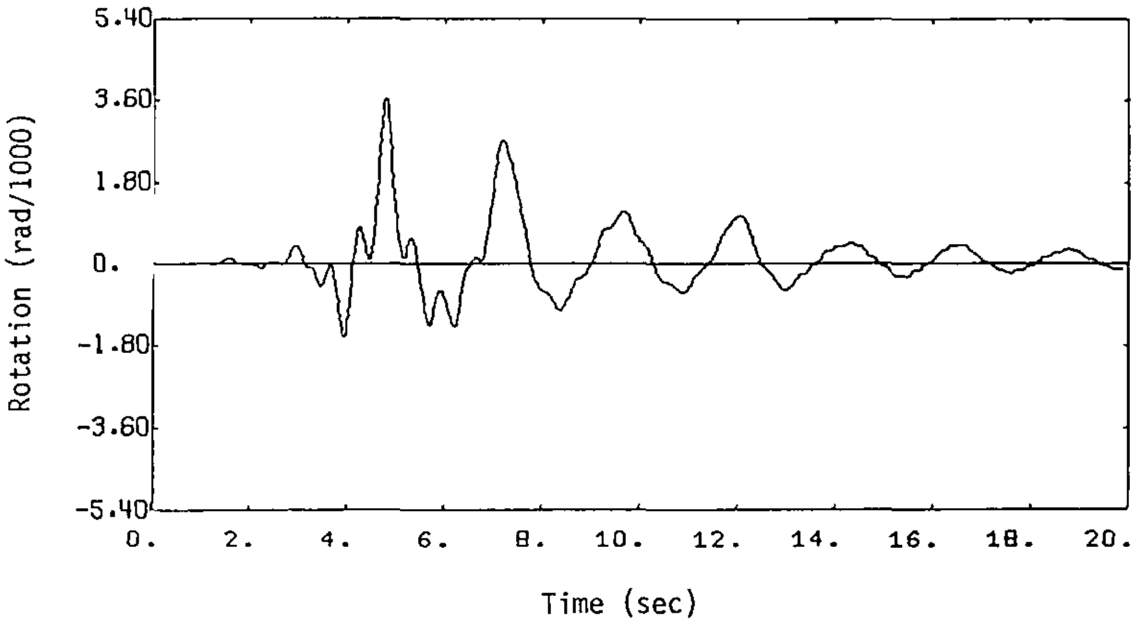

Center Bottom Column - Top End

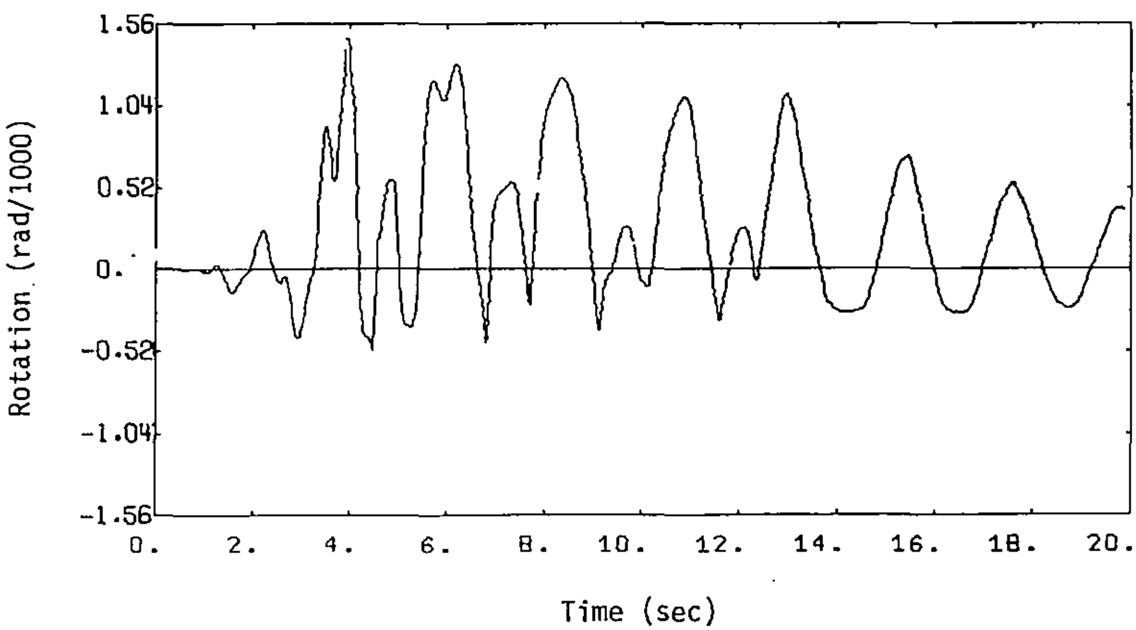

Center Bottom Column - Bottom End

FIGURE 4.24d COLUMN END ROTATIONS - TEST 170178.3 (SP-L-1-1/2 PF)

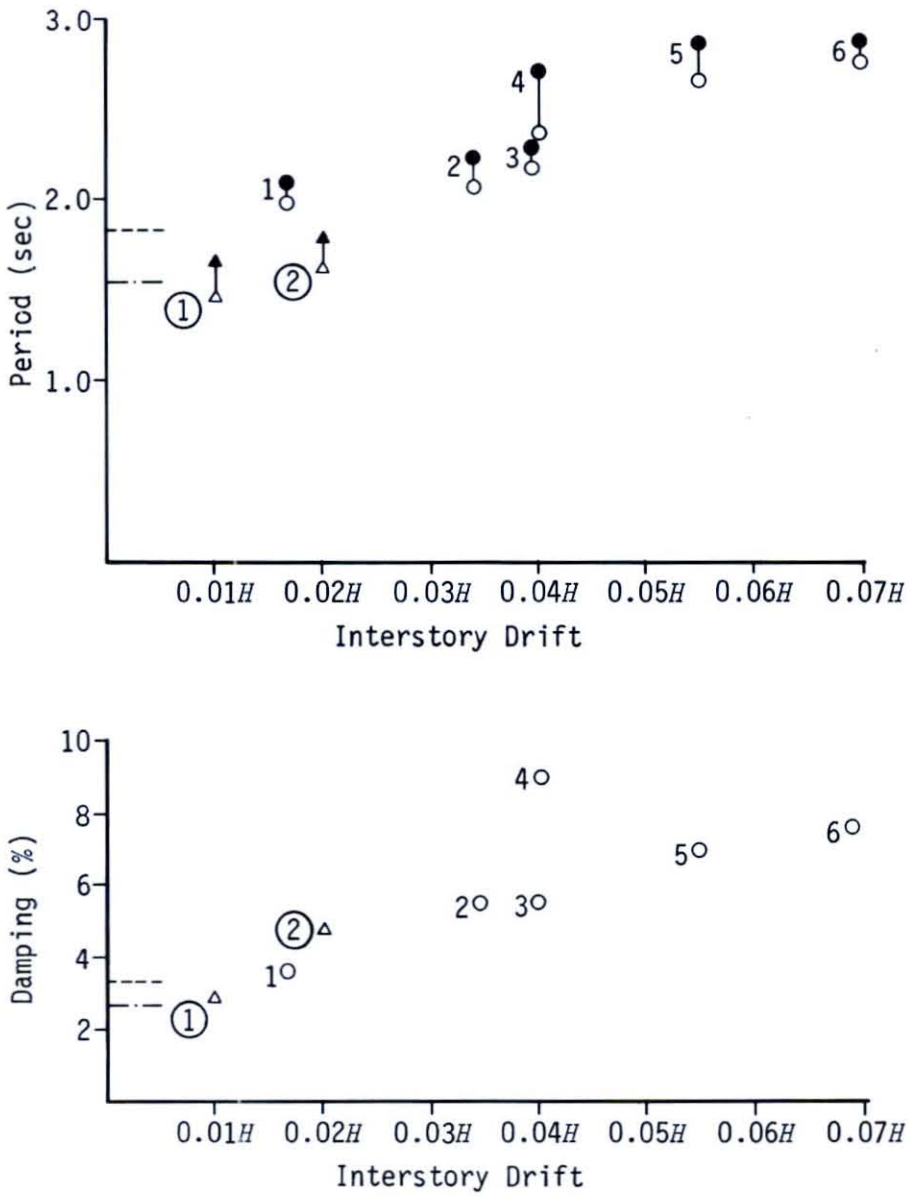

KEY

Test Sequence

1 - 1/4 PF ① - 1/4 EC
2 - 1/2 EC
3 - 1/2 PF ② - 1/2 EC
4 - 5/8 EC
5 - 7/8 EC
6 - 1-1/3 EC

● Shaking table data, full live load
▲ Shaking table data, 2/3 live load
○ Free decay data, full live load
△ Free decay data, 2/3 live load
---- Pull test data, full live load
—·— Pull test data, 2/3 live load
H Height of first story

FIGURE 4.25 DYNAMIC PROPERTIES VERSUS INTERSTORY DRIFTS: STANDARD PALLET RACK, LONGITUDINAL DIRECTION

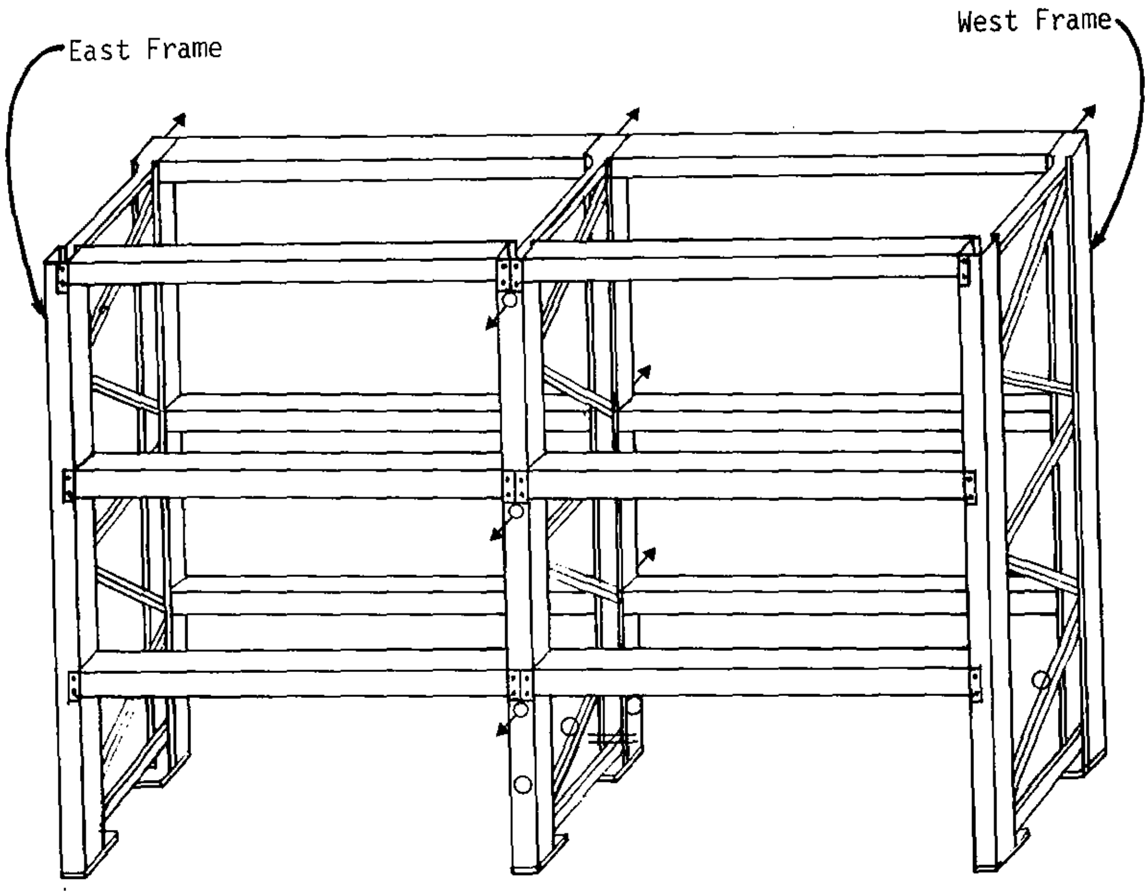

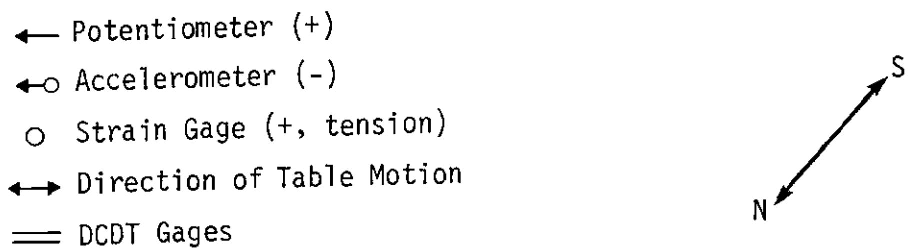

FIGURE 4.26 INSTRUMENTATION CHANNELS USED FOR DATA ANALYSIS: STANDARD PALLET RACK, TRANSVERSE DIRECTION

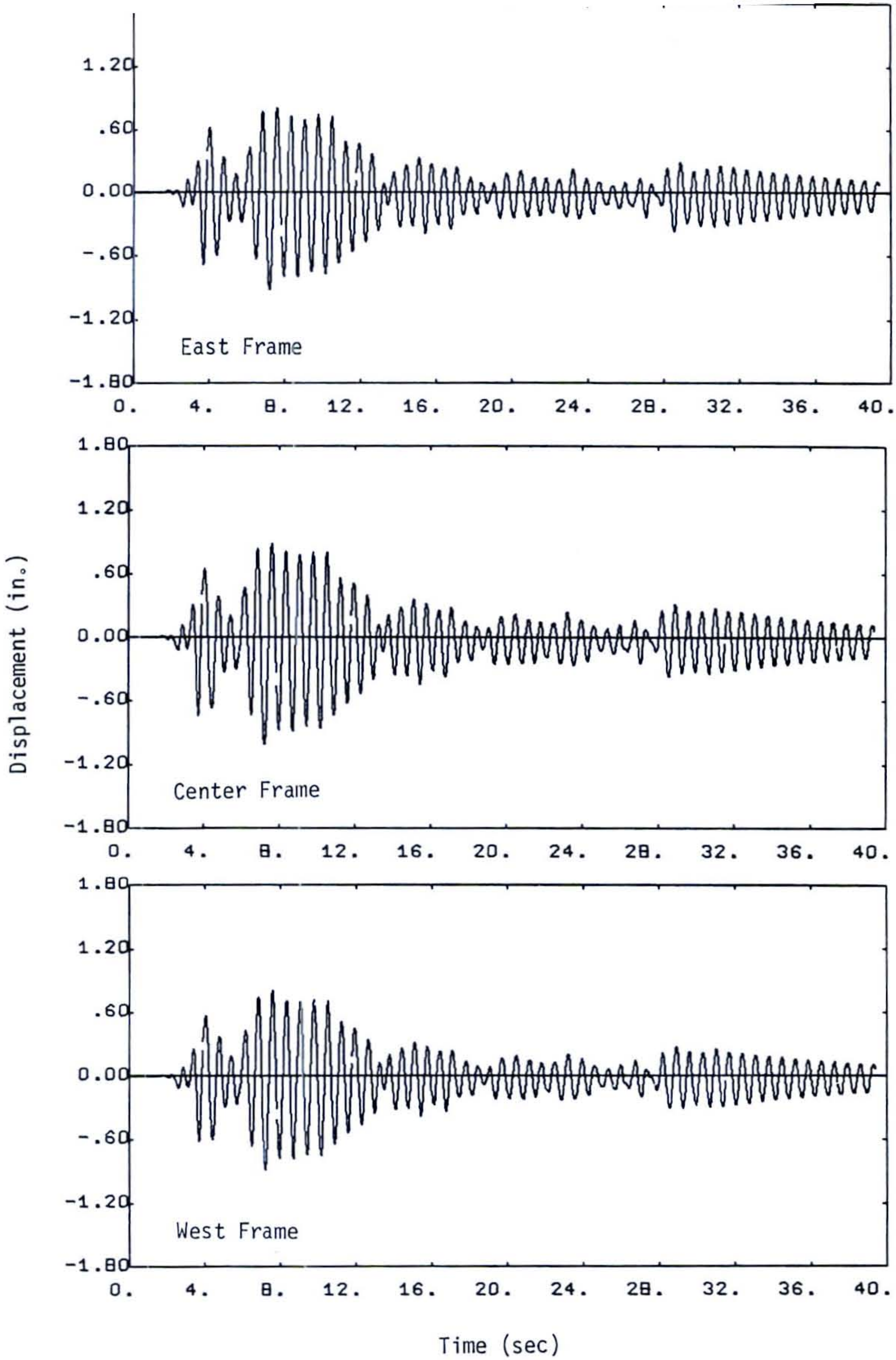

FIGURE 4.27a 3RD LEVEL DISPLACEMENTS RELATIVE TO THE TABLE - TEST 240178.1 (SP-T-2/3-1/4 EC)

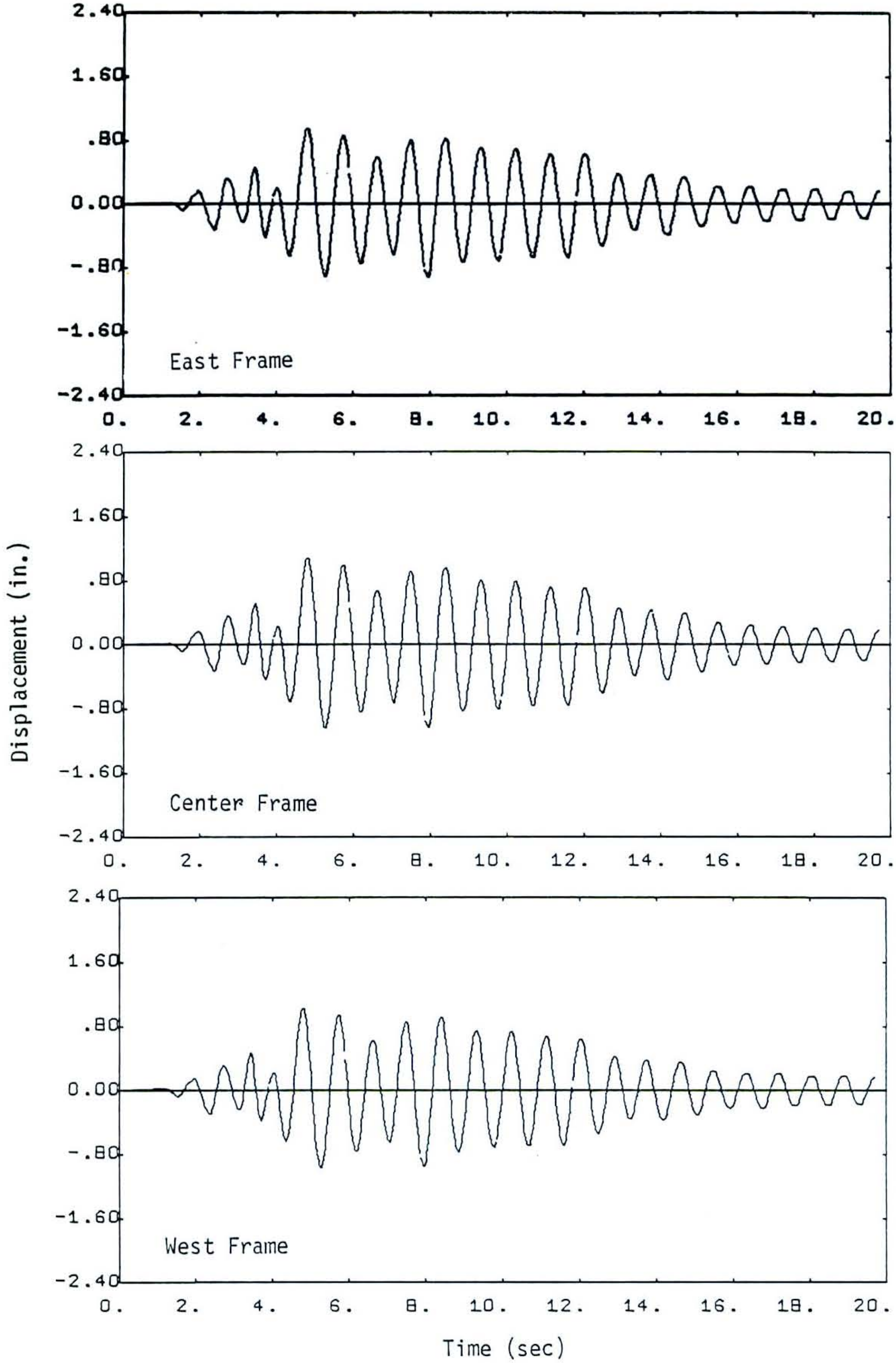

FIGURE 4.27b 3RD LEVEL DISPLACEMENTS RELATIVE TO THE TABLE - TEST 260178.2 (SP-T-1-1/4 PF)

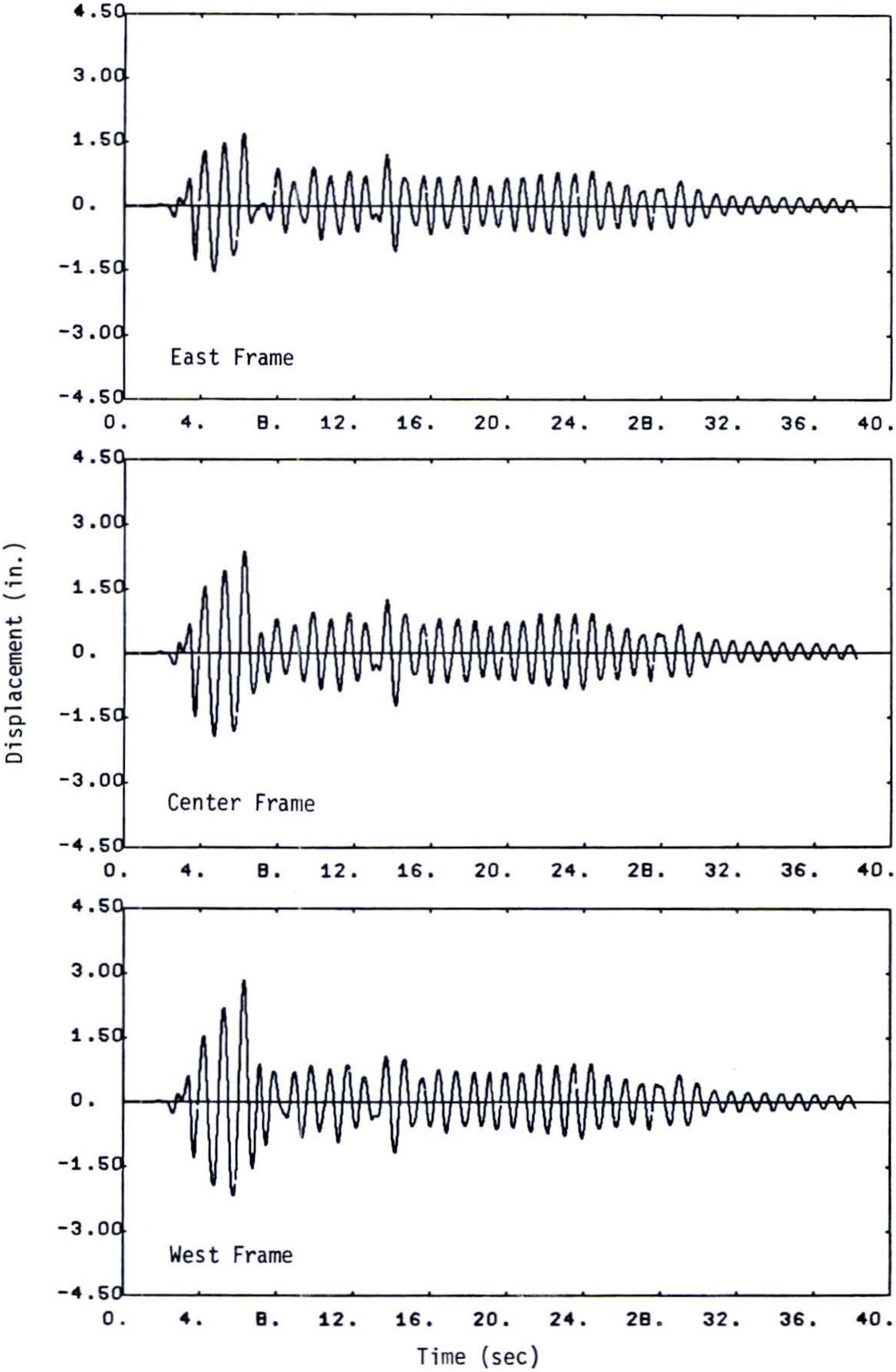

FIGURE 4.27c 3RD LEVEL DISPLACEMENTS RELATIVE TO THE TABLE - TEST 260178.3 (SP-T-1-1/2 EC)

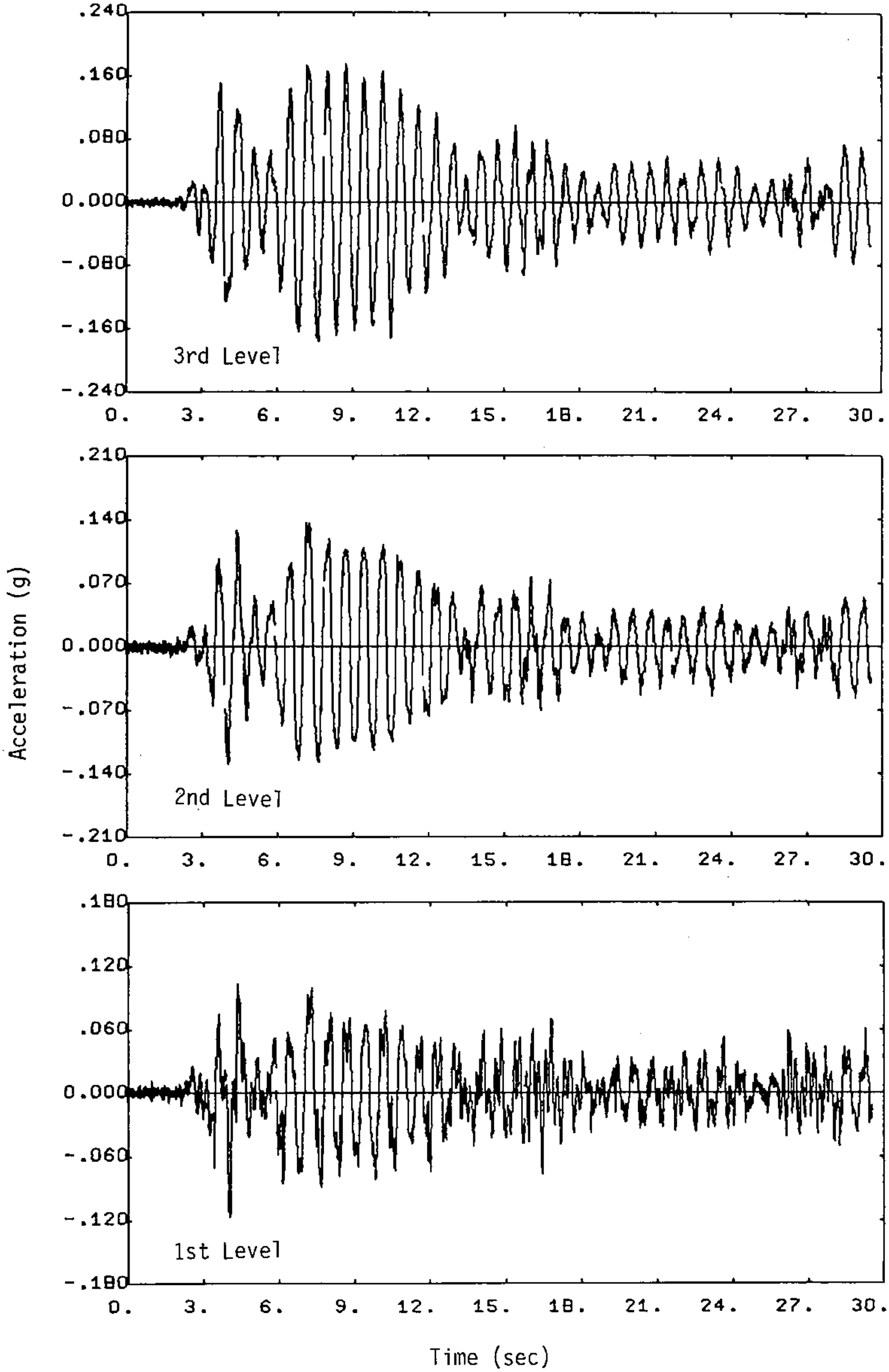

FIGURE 4.28a STORY ACCELERATIONS (CENTER FRAME) - TEST 240178.1 (SP-T-2/3-1/4 EC)

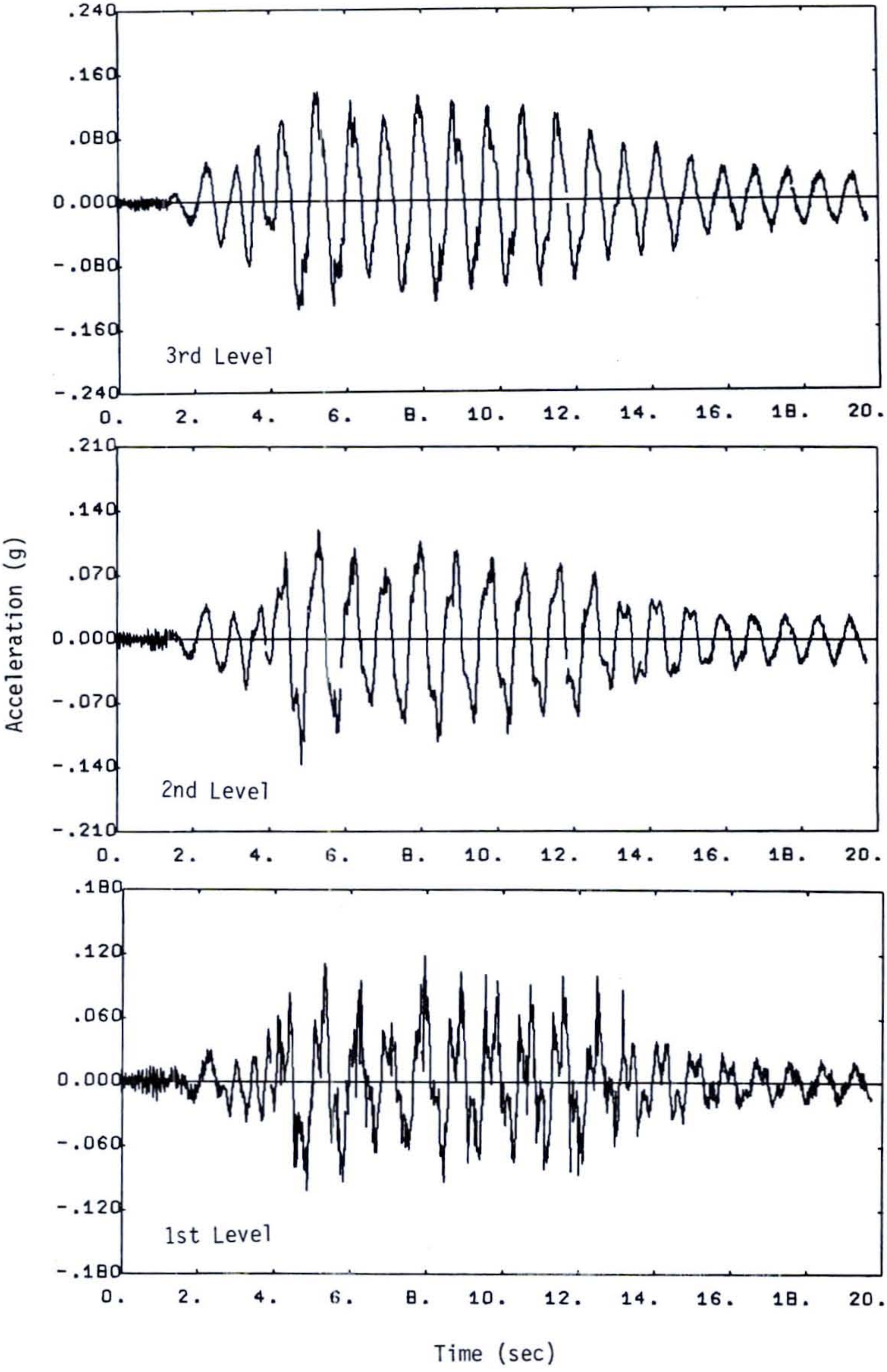

FIGURE 4.28b STORY ACCELERATIONS (CENTER FRAME) - TEST 260178.2 (SP-T-1-1/4 PF)

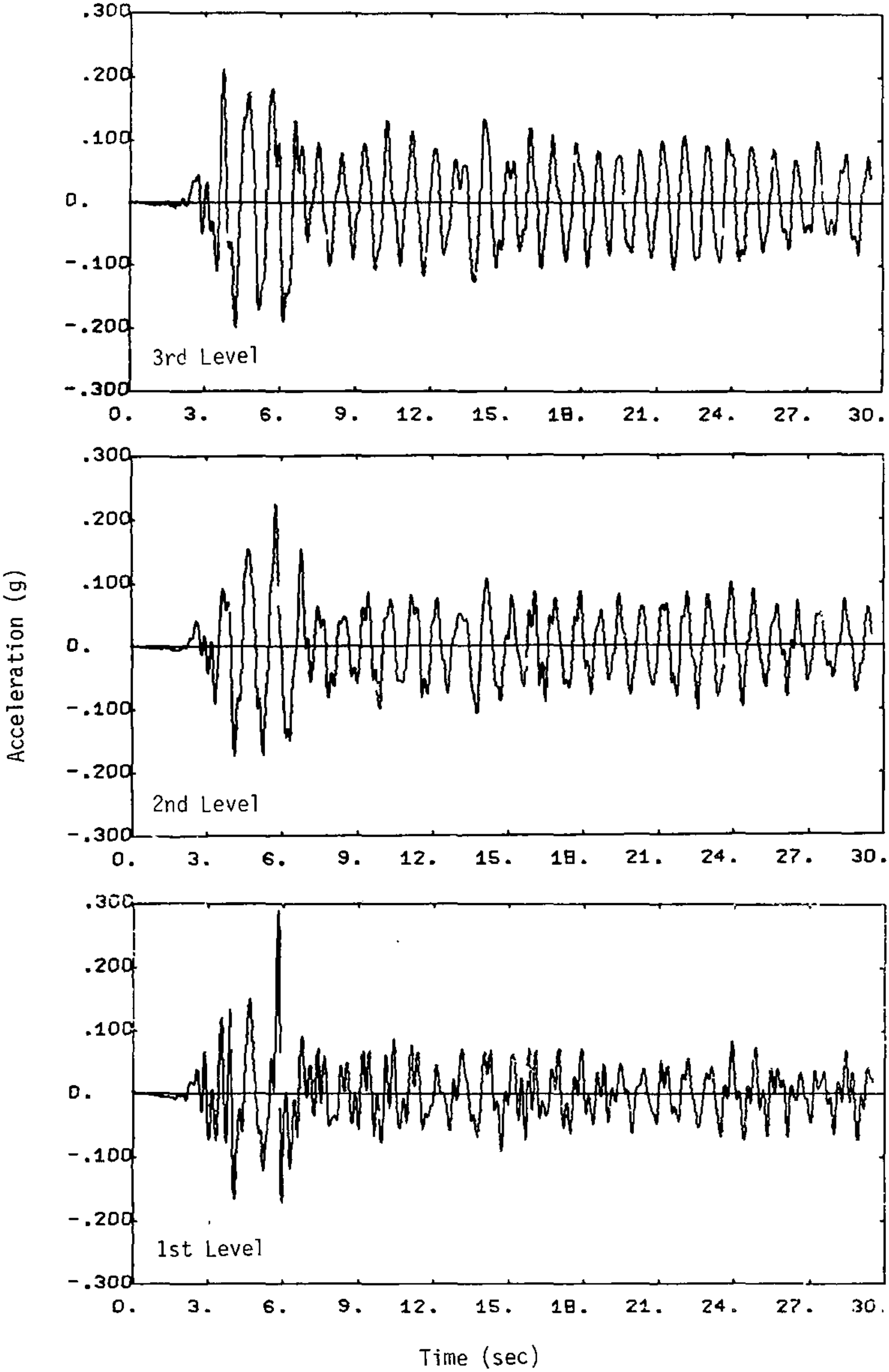

FIGURE 4.28c STORY ACCELERATIONS (CENTER FRAME) - TEST 260178.3 (SP-T-1-1/2 EC)

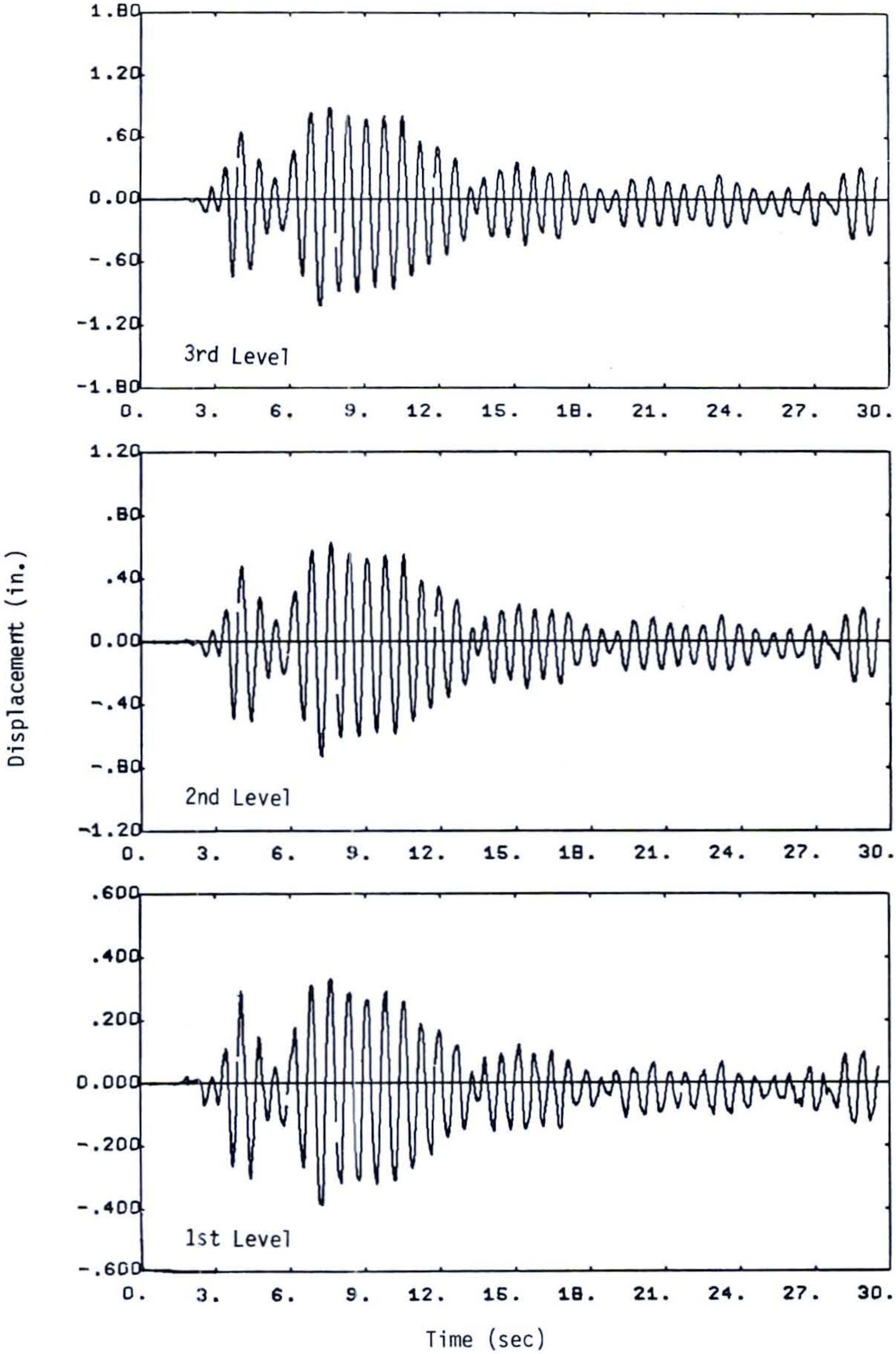

FIGURE 4.29a STORY DISPLACEMENTS RELATIVE TO THE TABLE (CENTER FRAME) - TEST 240178.1 (SP-T-2/3-1/4 EC)

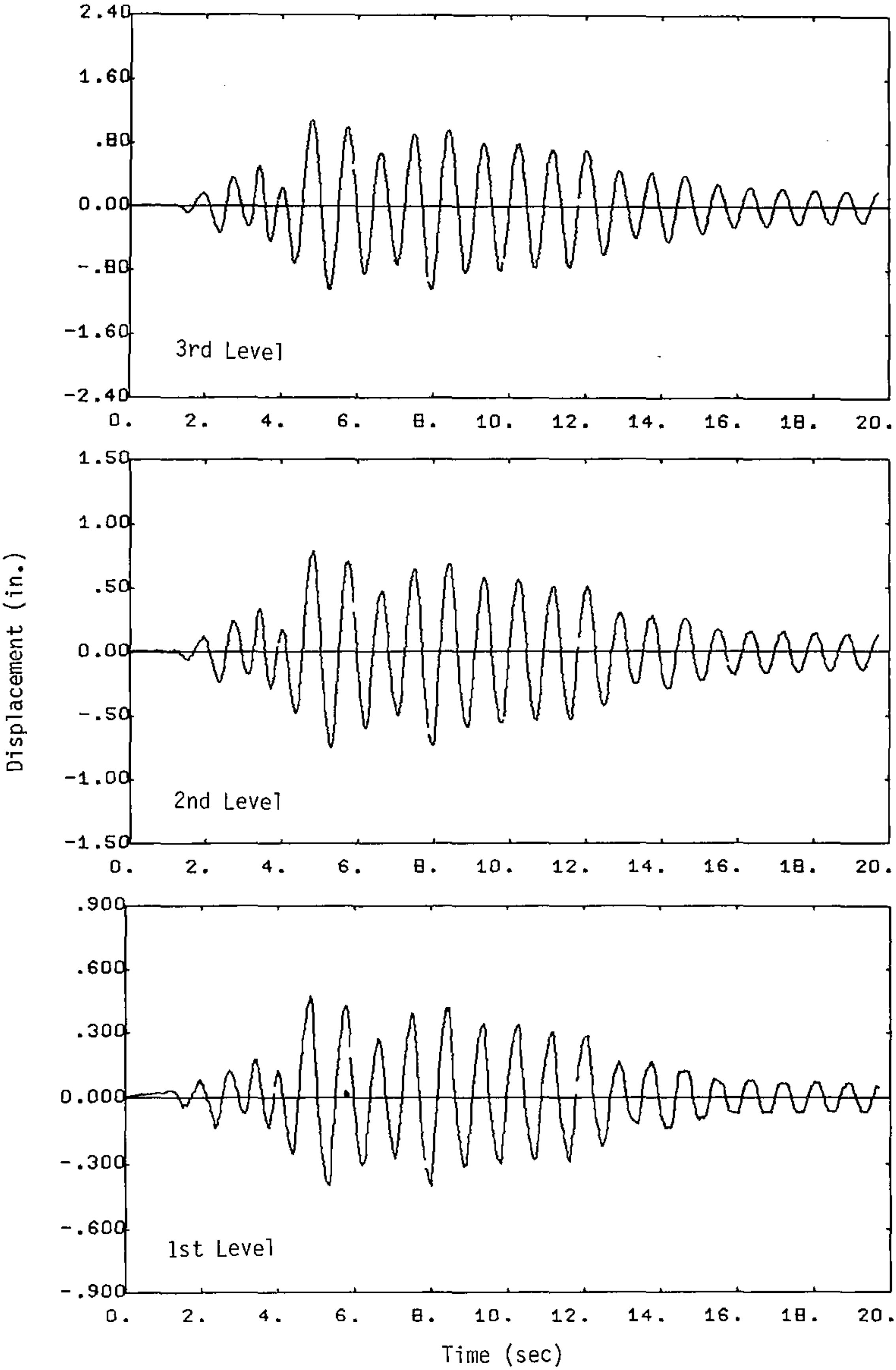

FIGURE 4.29b STORY DISPLACEMENTS RELATIVE TO THE TABLE (CENTER FRAME) - TEST 260178.2 (SP-T-1-1/4 PF)

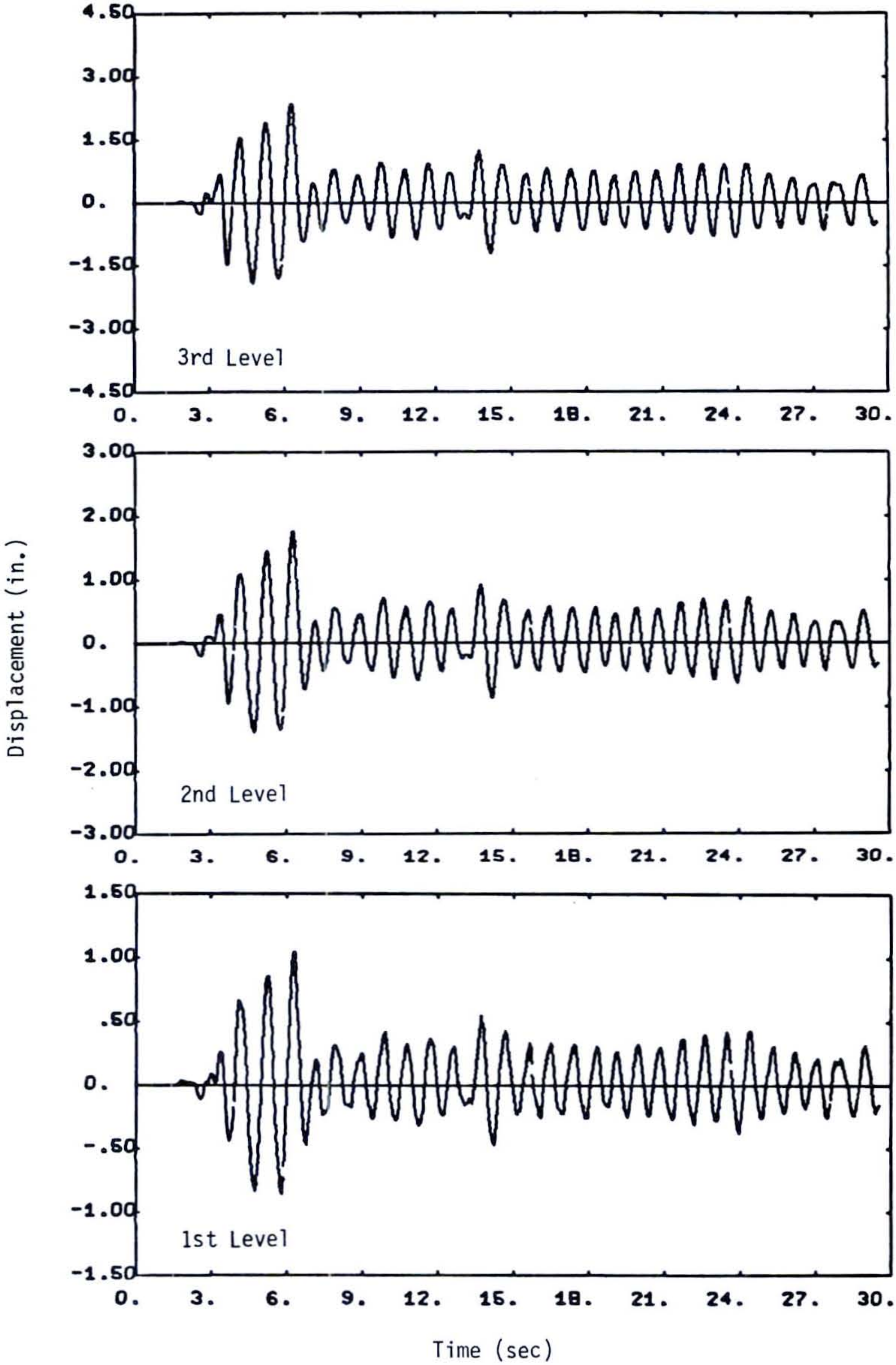

FIGURE 4.29c STORY DISPLACEMENTS RELATIVE TO THE TABLE (CENTER FRAME) - TEST 260178.3 (SP-T-1-1/2 EC)

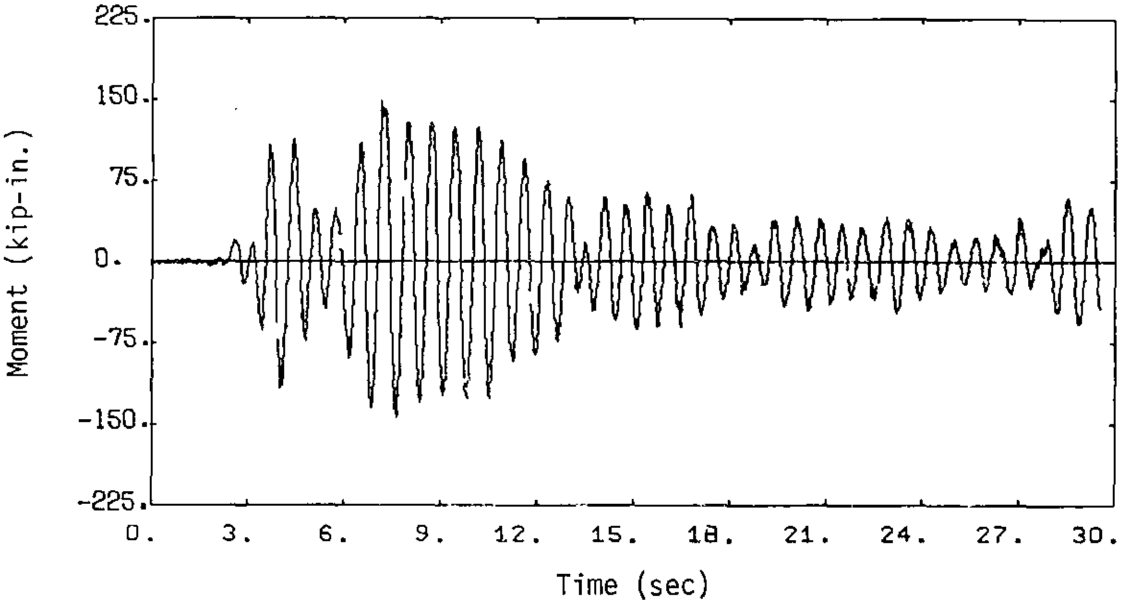

Base Overturning Moment

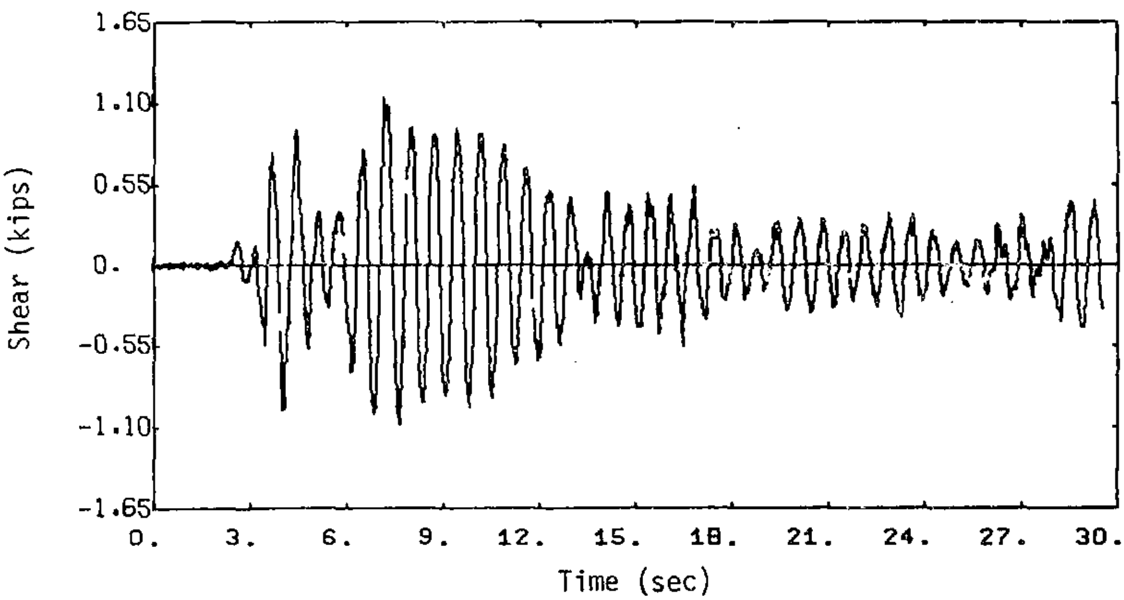

Base Shear

FIGURE 4.30a BASE SHEAR AND OVERTURNING MOMENT (CENTER FRAME) - TEST 240178.1 (SP-T-2/3-1/4 EC)

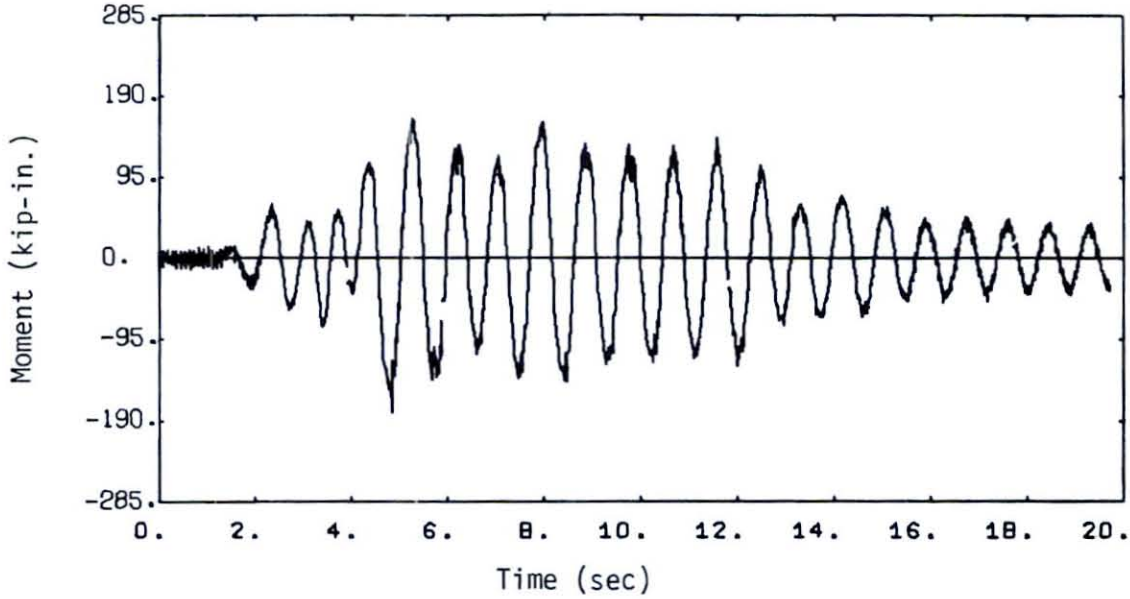

Base Overturning Moment

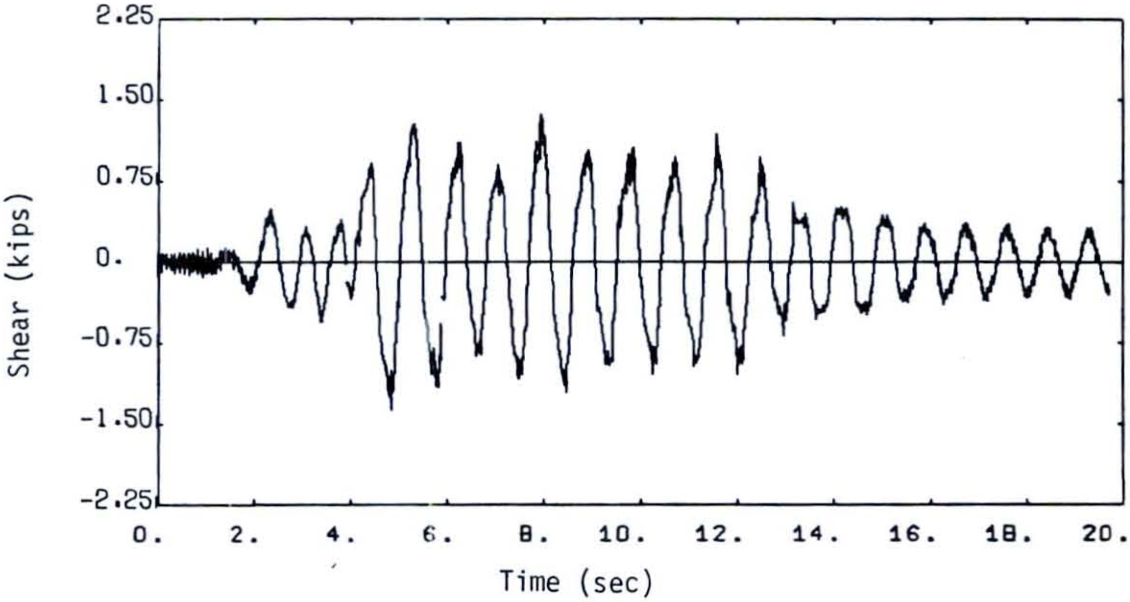

Base Shear

FIGURE 4.30b BASE SHEAR AND OVERTURNING MOMENT (CENTER FRAME) - TEST 260178.2 (SP-T-1-1/4 PF)

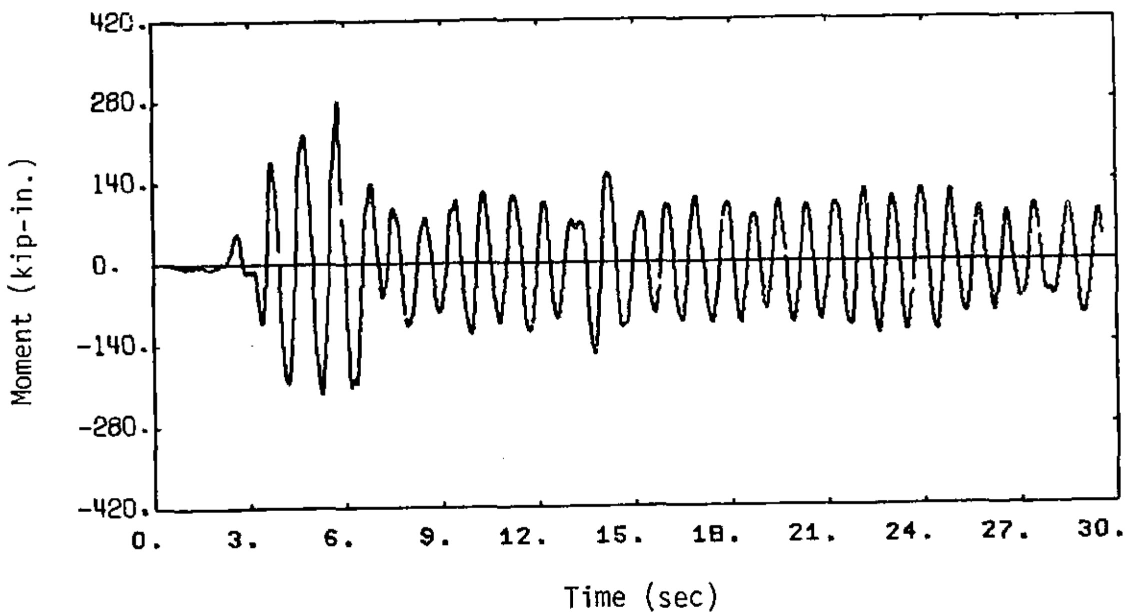

Base Overturning Moment

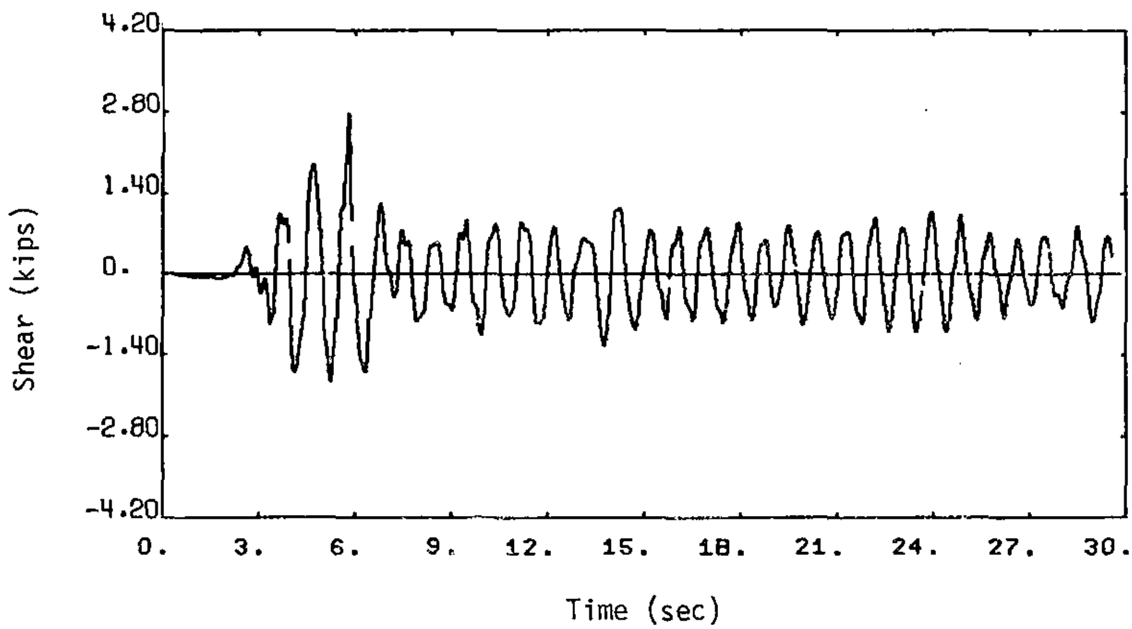

Base Shear

FIGURE 4.30c BASE SHEAR AND OVERTURNING MOMENT (CENTER FRAME) - TEST 260178.3 (SP-T-1-1/2 EC)

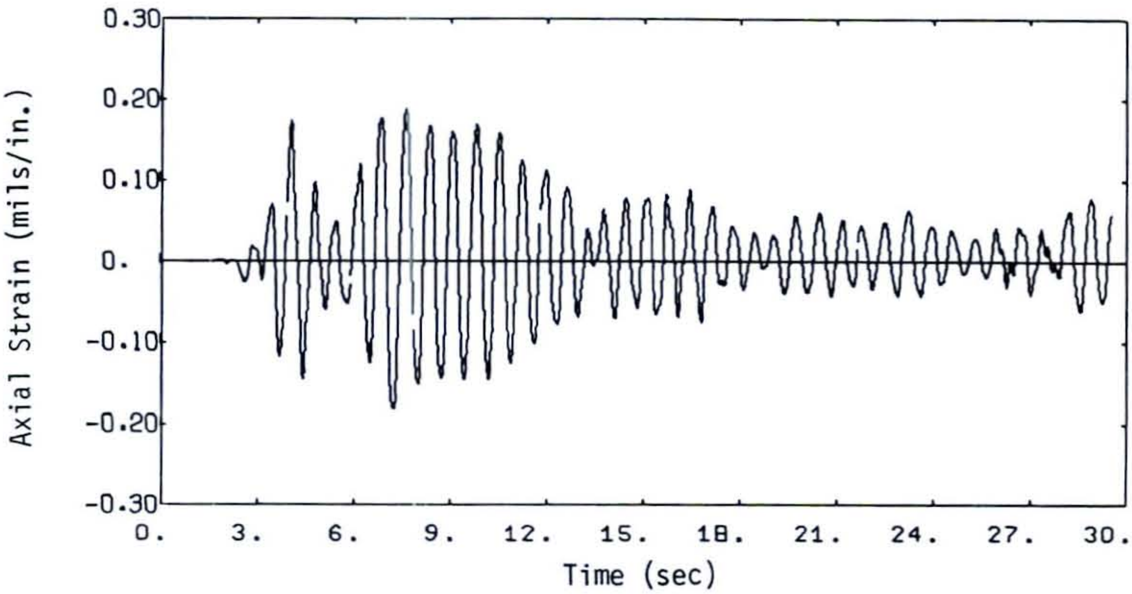

Center Bottom Diagonal

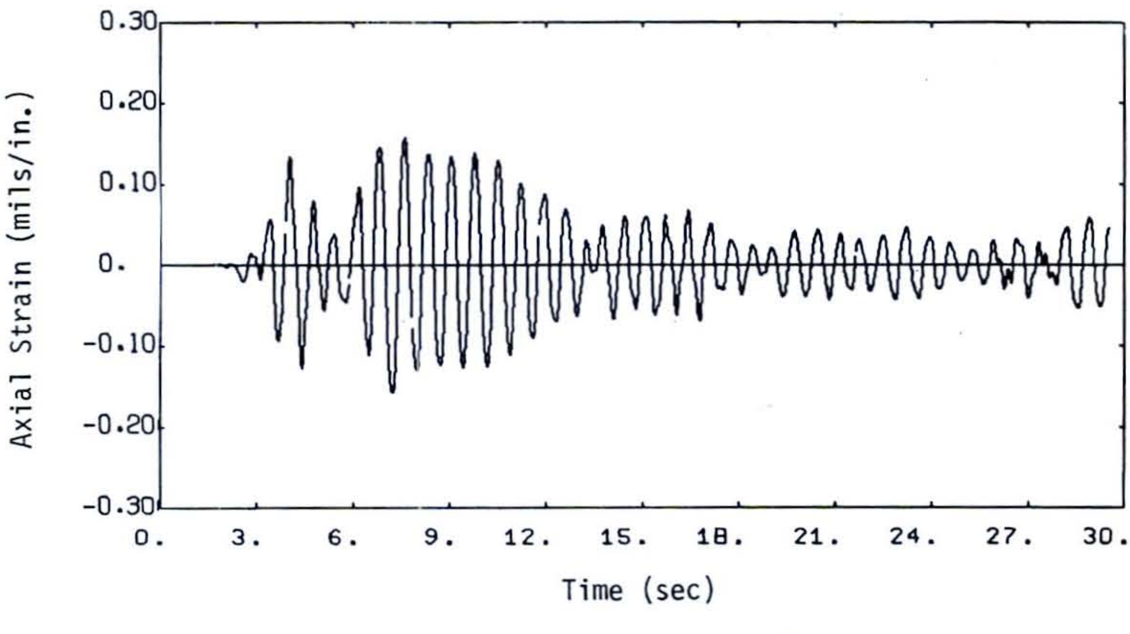

West Bottom Diagonal

FIGURE 4.31a BRACE AXIAL STRAINS - TEST 240178.1 (SP-T-2/3-1/4 EC)

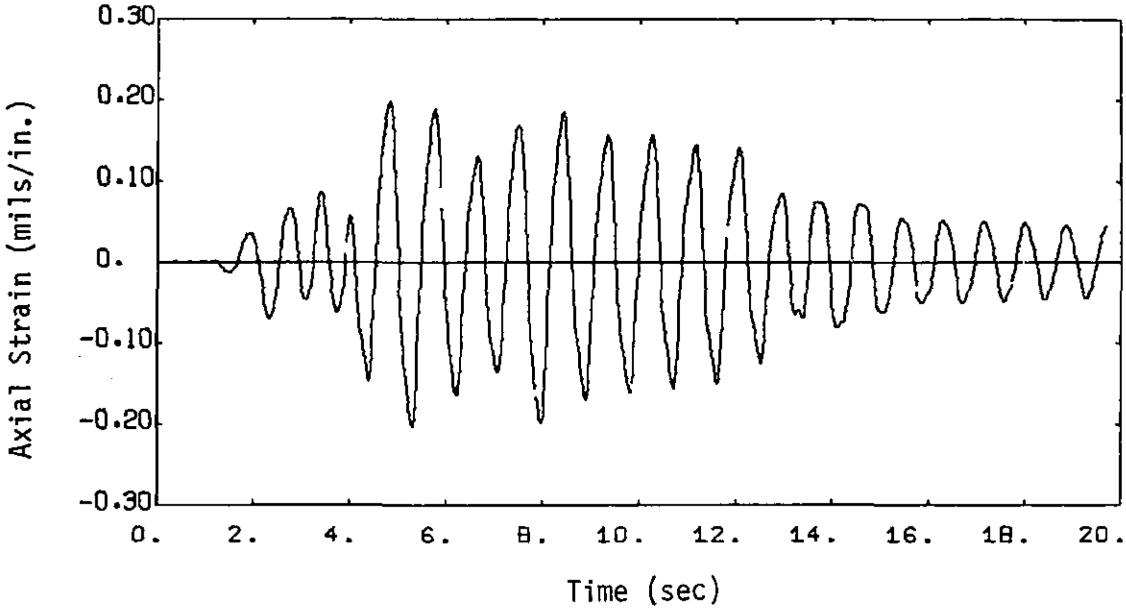

Center Bottom Diagonal

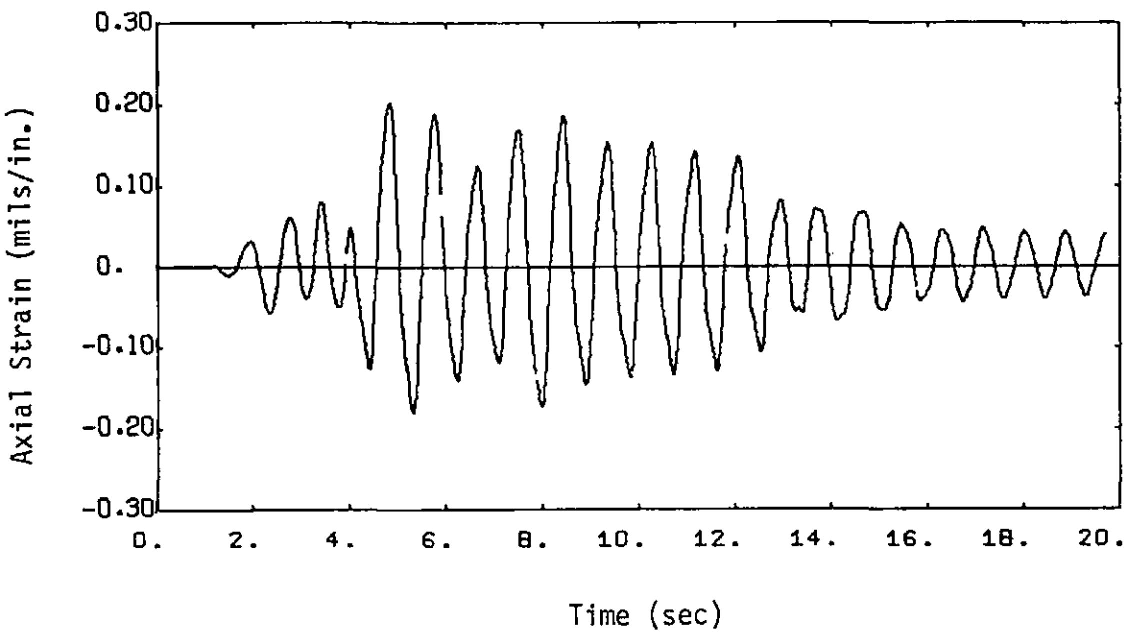

West Bottom Diagonal

FIGURE 4.31b BRACE AXIAL STRAINS - TEST 260178.2 (SP-T-1-1/4 PF)

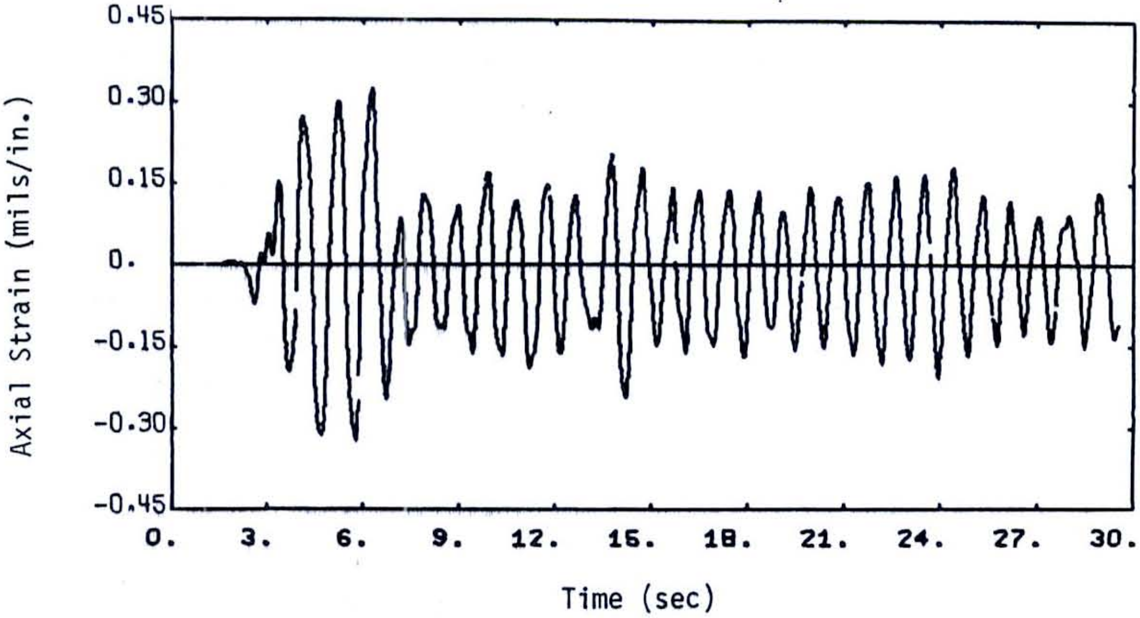

Center Bottom Diagonal

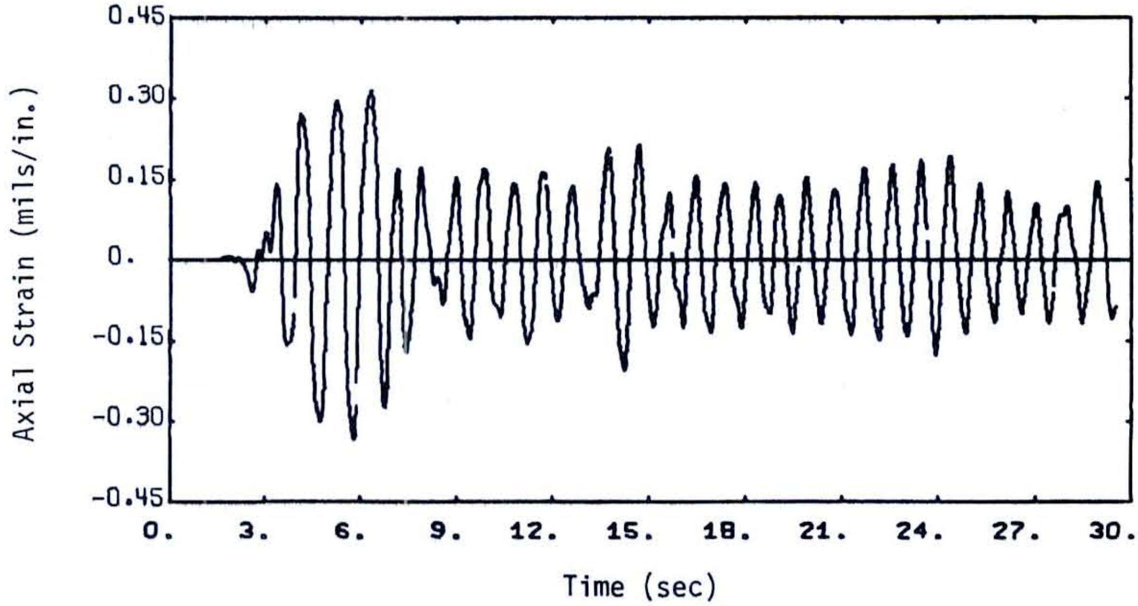

West Bottom Diagonal

FIGURE 4.31c BRACE AXIAL STRAINS - TEST 260178.3 (SP-T-1-1/2 EC)

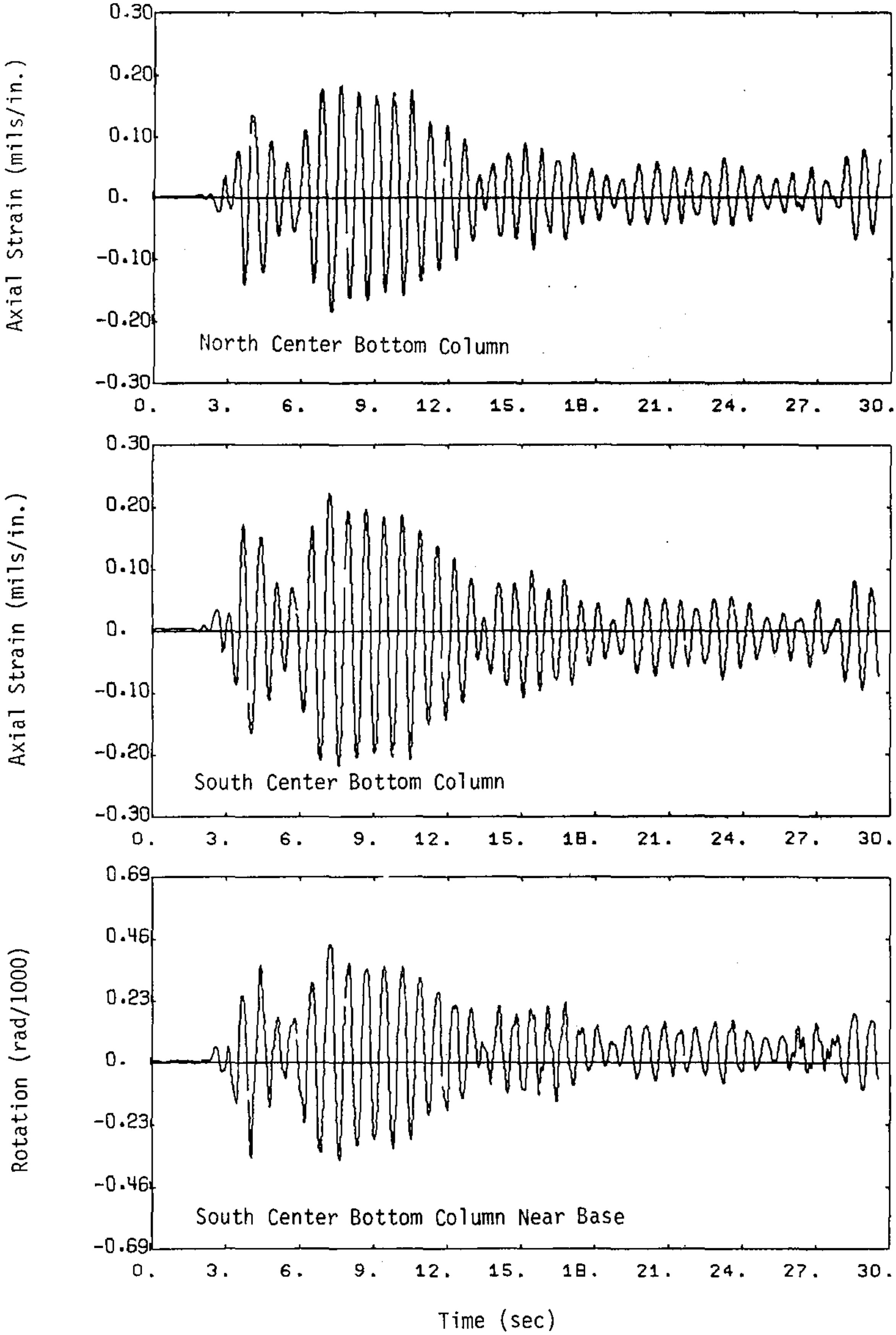

FIGURE 4.32a COLUMN AXIAL STRAINS AND END ROTATIONS - TEST 240178.1
(SP-T-2/3-1/4 EC)

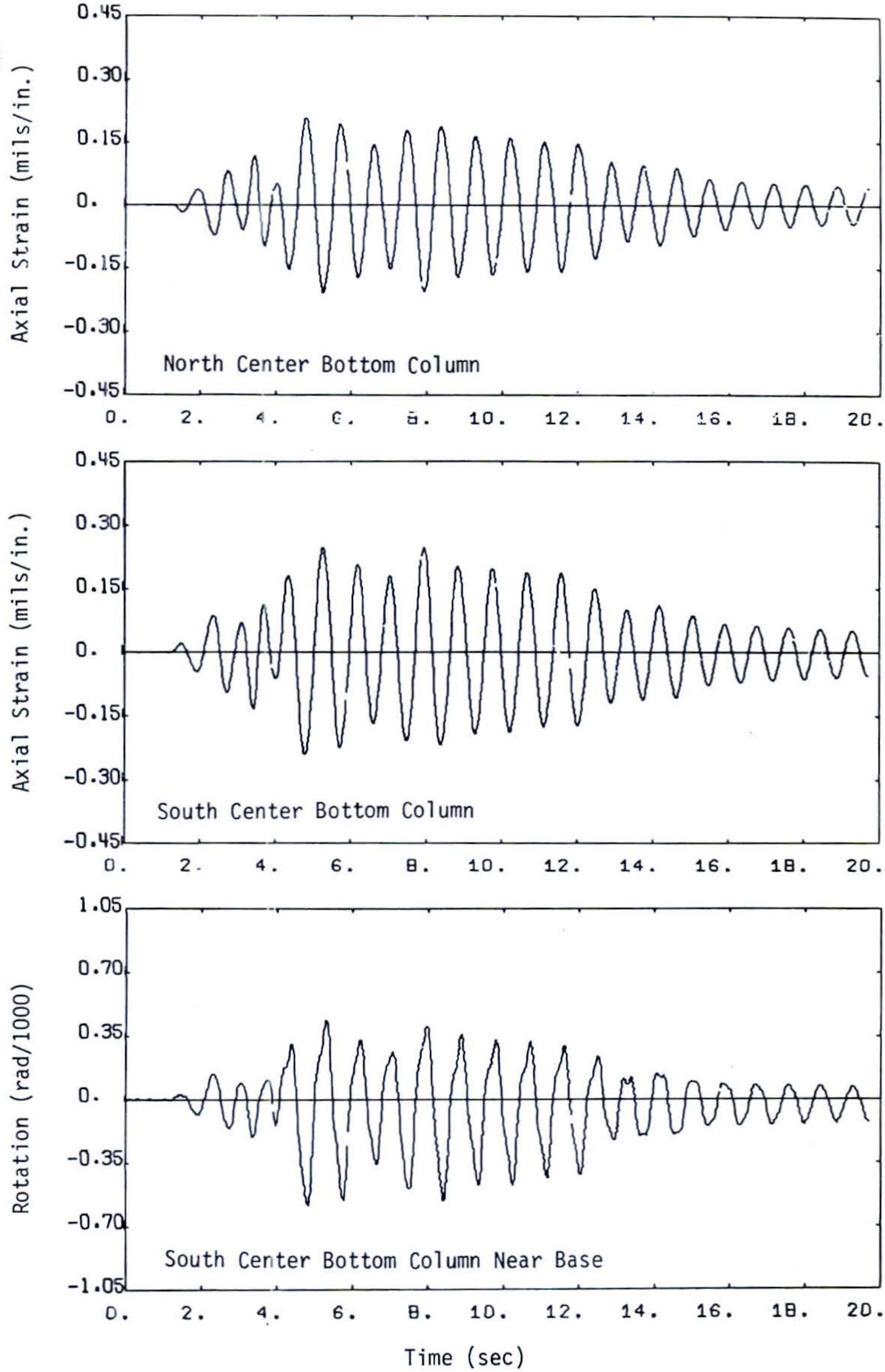

FIGURE 4.32b COLUMN AXIAL STRAINS AND END ROTATIONS - TEST 260178.2 (SP-T-1-1/4 PF)

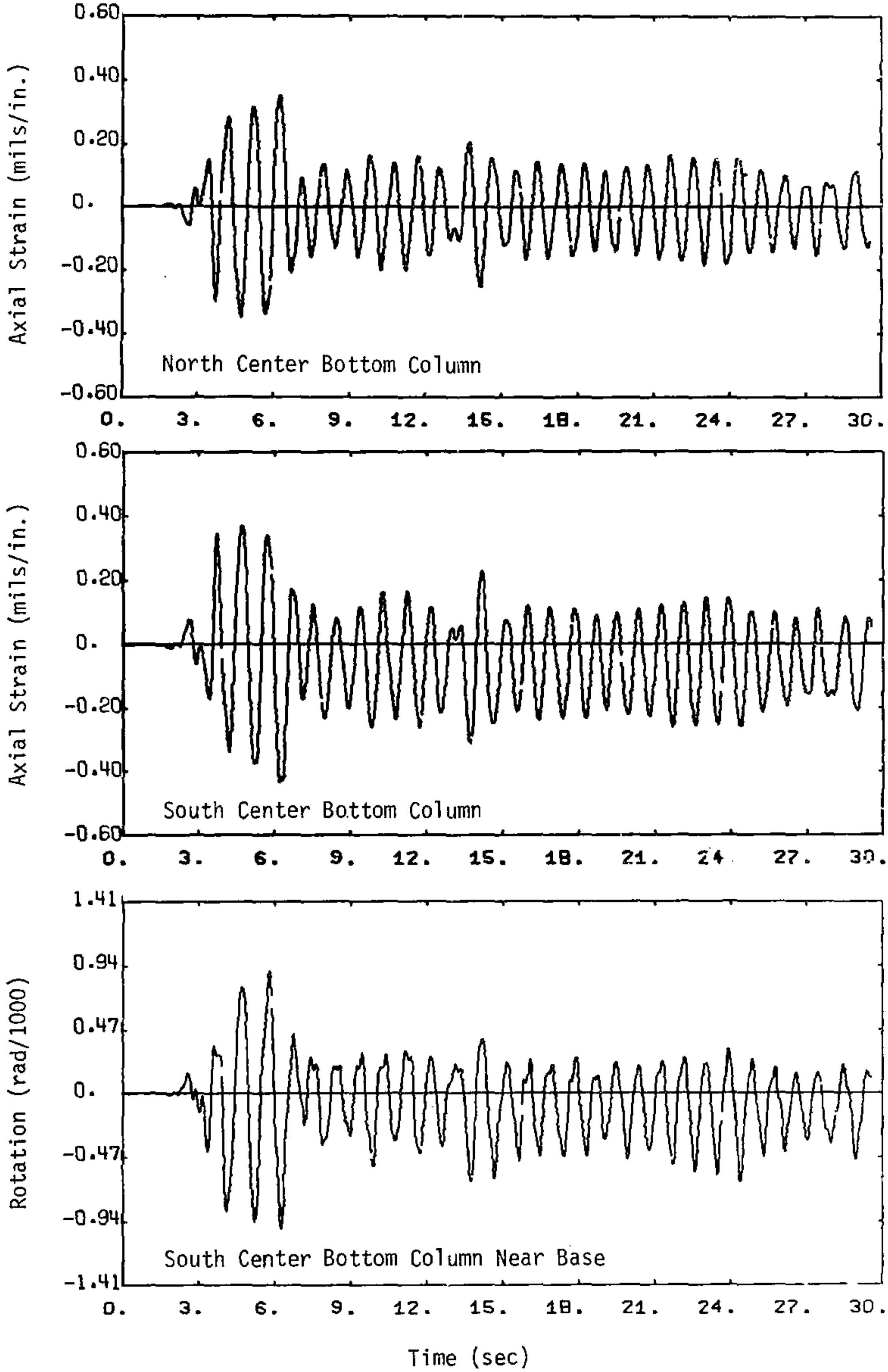

FIGURE 4.32c COLUMN AXIAL STRAINS AND END ROTATIONS - TEST 260178.3 (SP-T-1-1/2 EC)

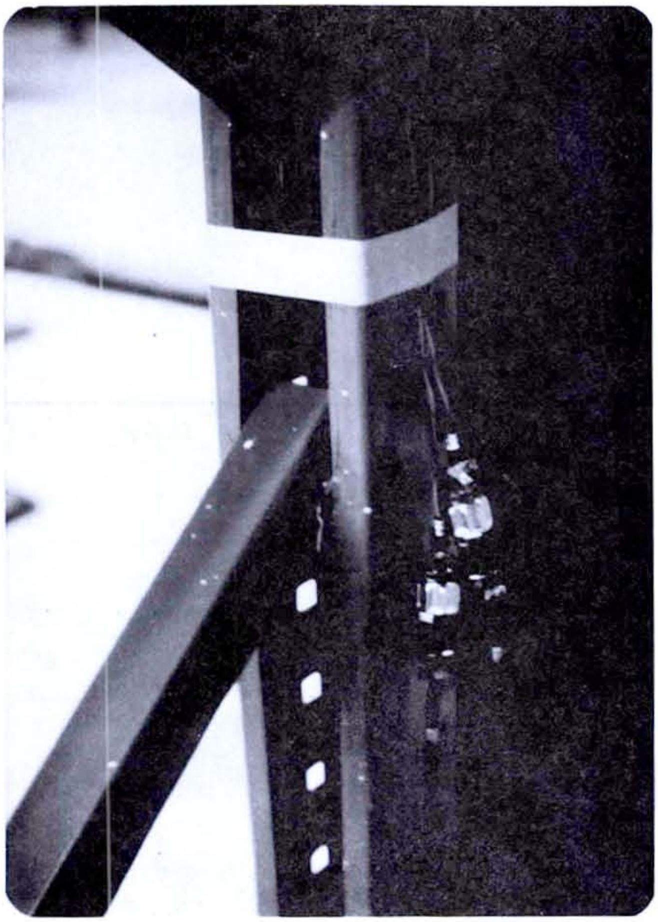

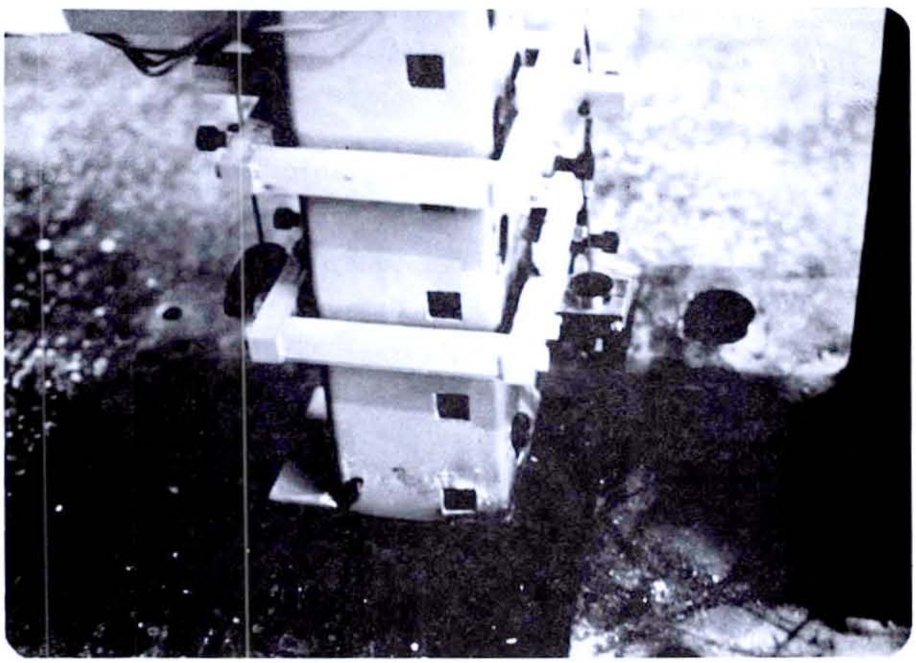

FIGURE 4.33 STRUCTURAL DAMAGE - STANDARD PALLET RACK, TRANSVERSE DIRECTION

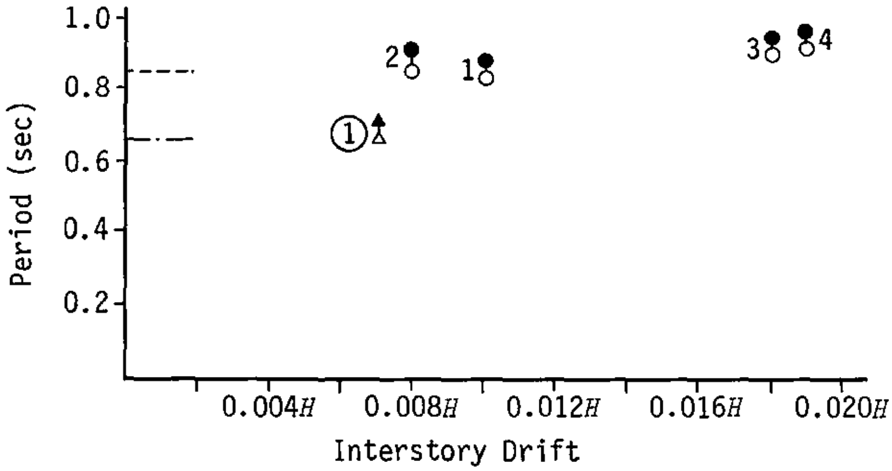

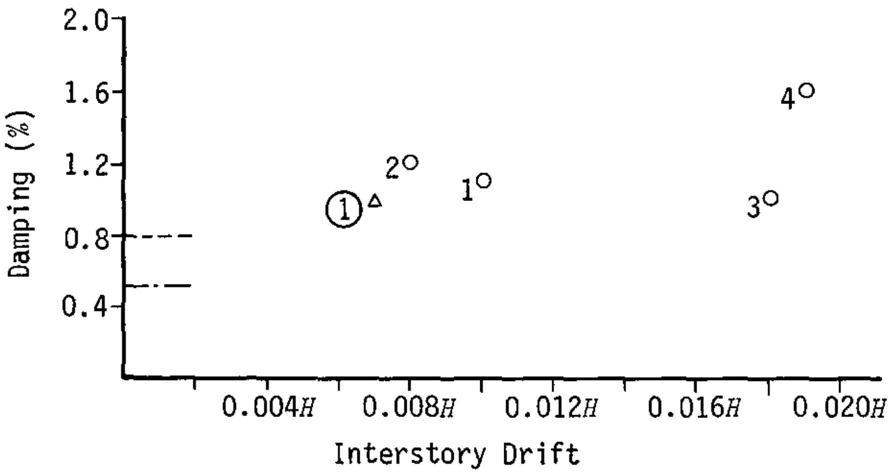

KEY

Test Sequence

1 - 1/4 EC   (1) - 1/4 EC
2 - 1/4 PF
3 - 1/2 EC
4 - 5/8 EC

- ● Shaking table data, full live load
- ▲ Shaking table data, 2/3 live load
- ○ Free decay data, full live load
- △ Free decay data, 2/3 live load
- ---- Pull test data, full live load
- —·— Pull test data, 2/3 live load
- *H* Height of first story

FIGURE 4.34 DYNAMIC PROPERTIES VERSUS INTERSTORY DRIFTS: STANDARD PALLET RACK, TRANSVERSE DIRECTION

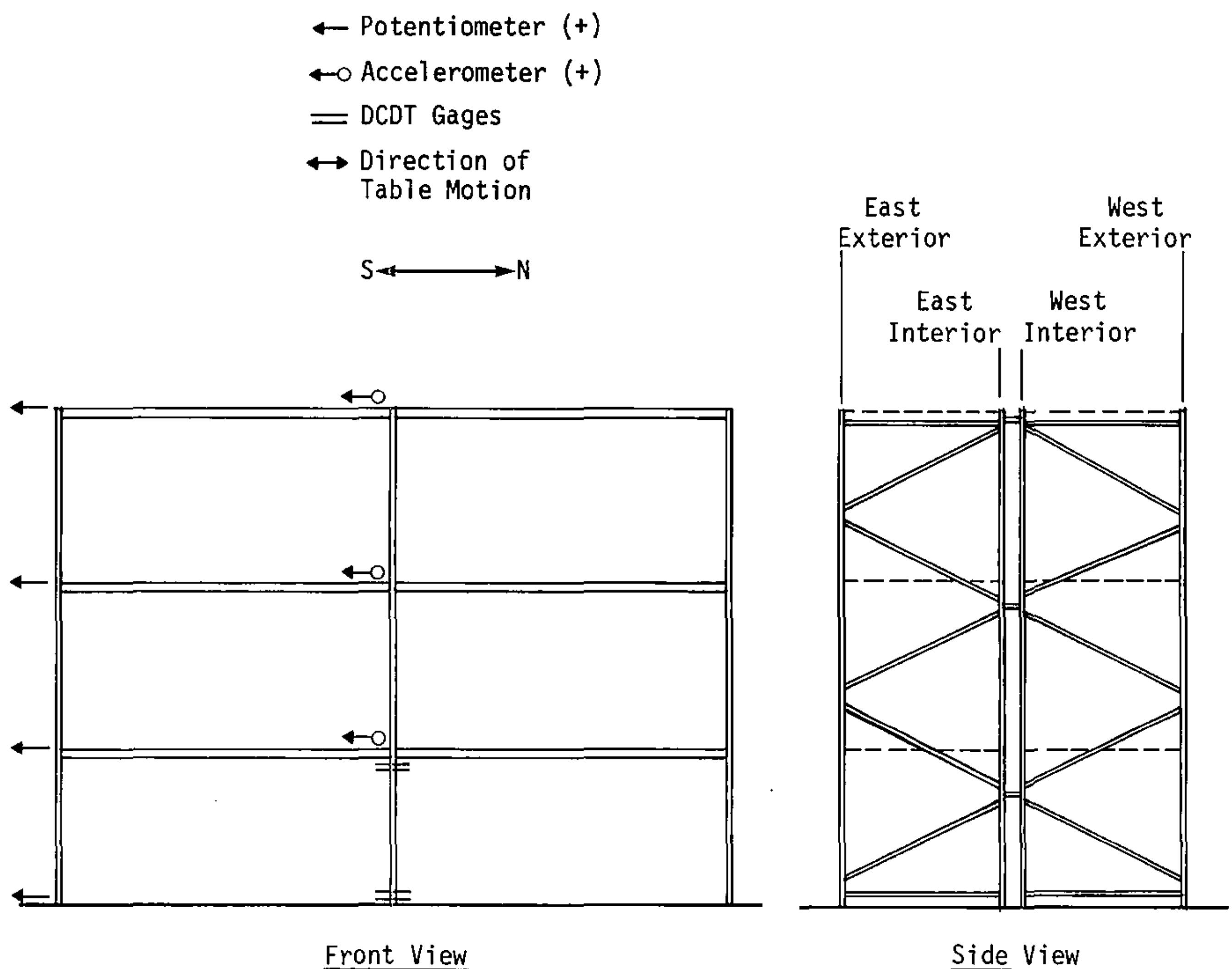

FIGURE 4.35 INSTRUMENTATION CHANNELS USED FOR DATA ANALYSIS: BACK-TO-BACK PALLET RACK, LONGITUDINAL DIRECTION

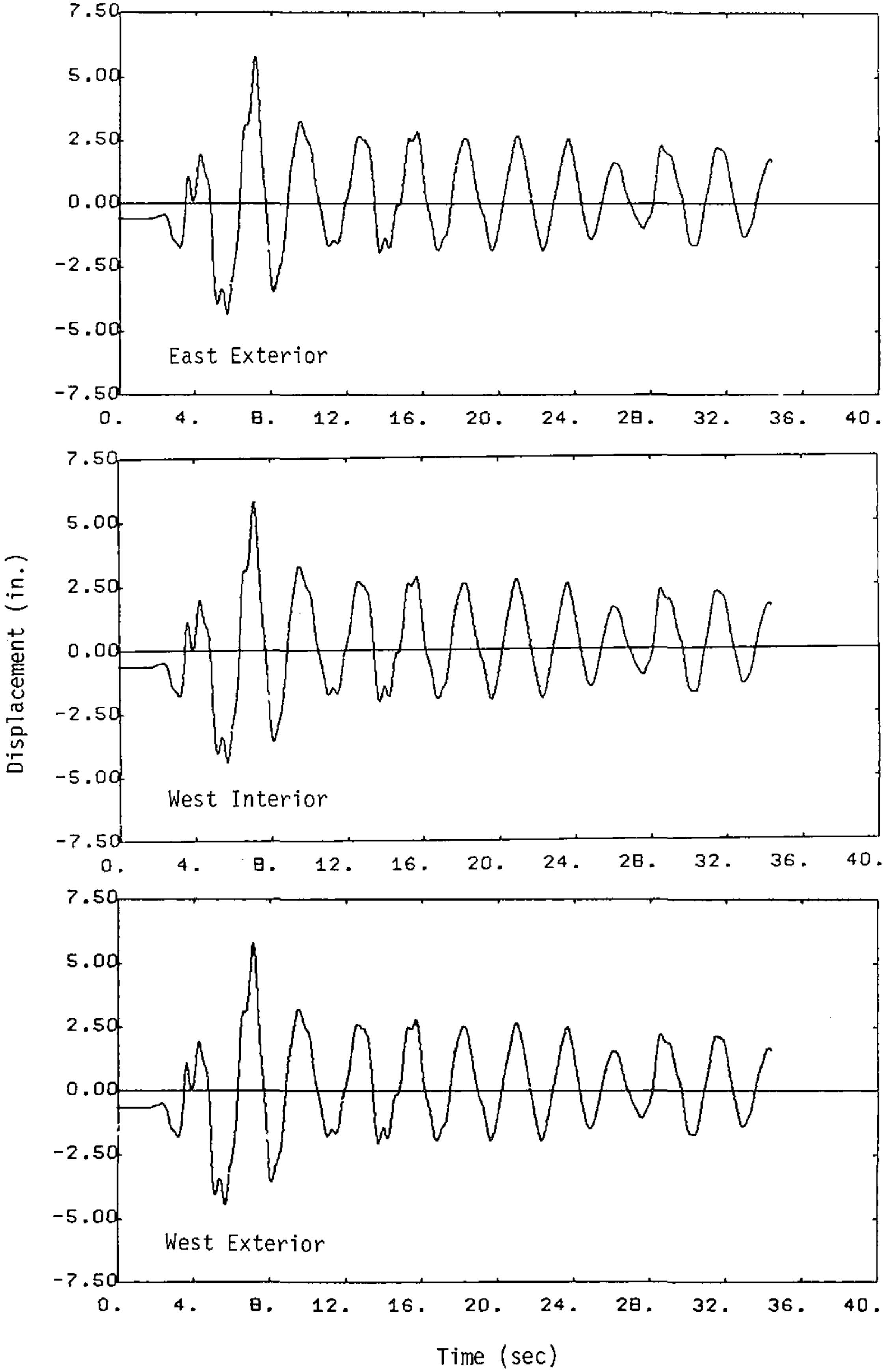

FIGURE 4.36 3RD LEVEL DISPLACEMENTS RELATIVE TO THE TABLE - TEST 140278.6

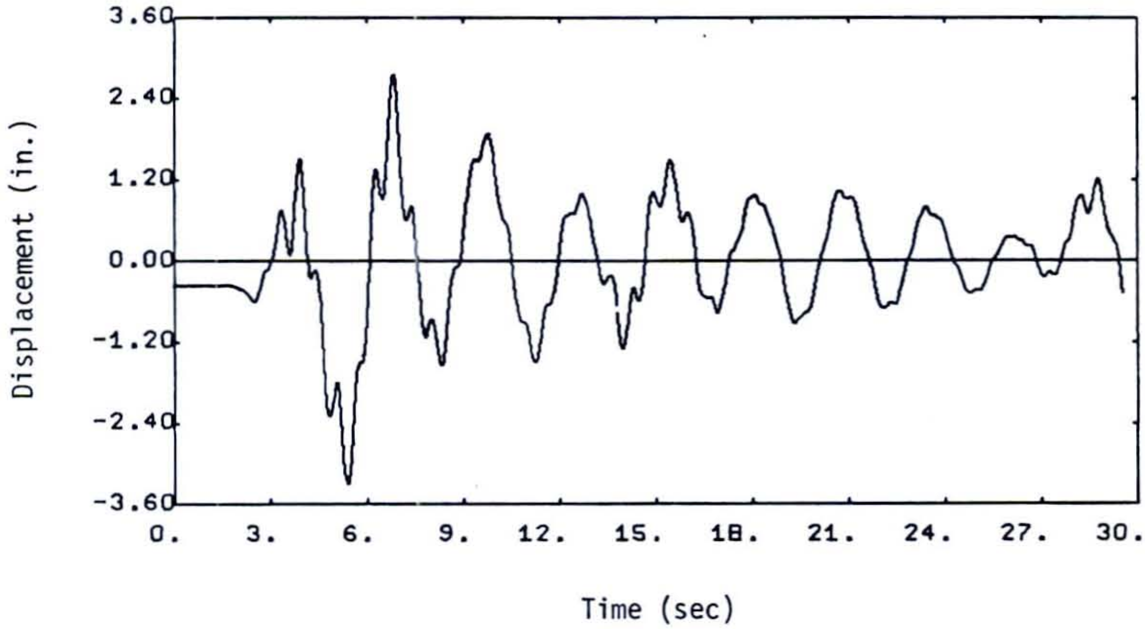

Back-to-Back Pallet Rack (Unanchored)

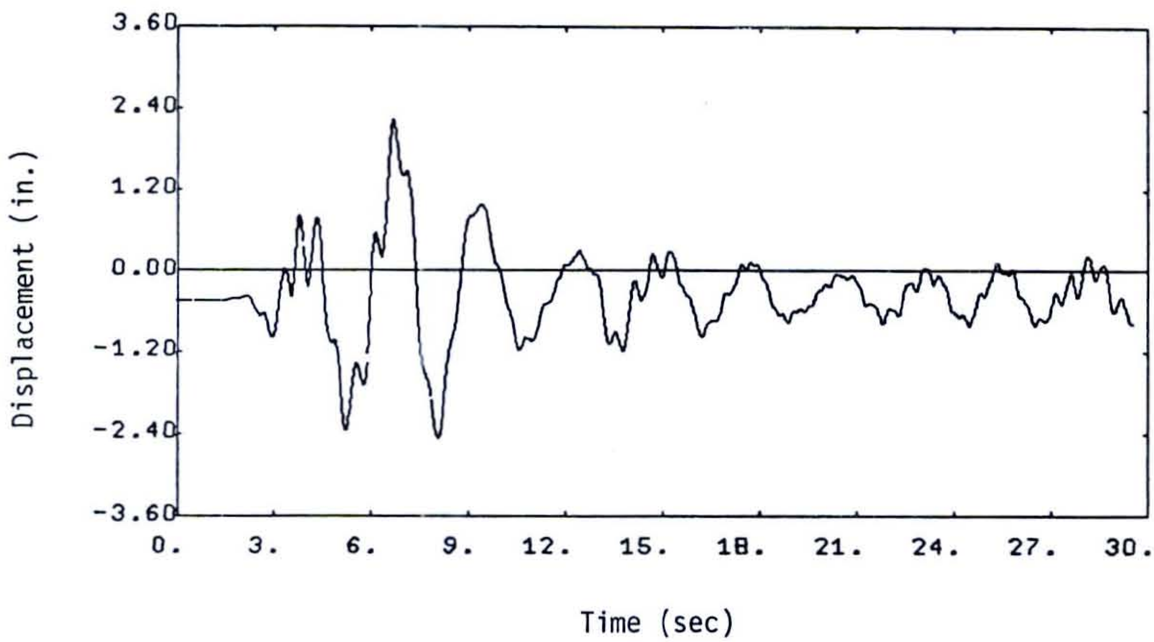

Single Pallet Rack (Anchored)

FIGURE 4.37 INTERSTORY DRIFTS (BOTTOM STORY) - TEST 140278.6 AND TEST 170178.4

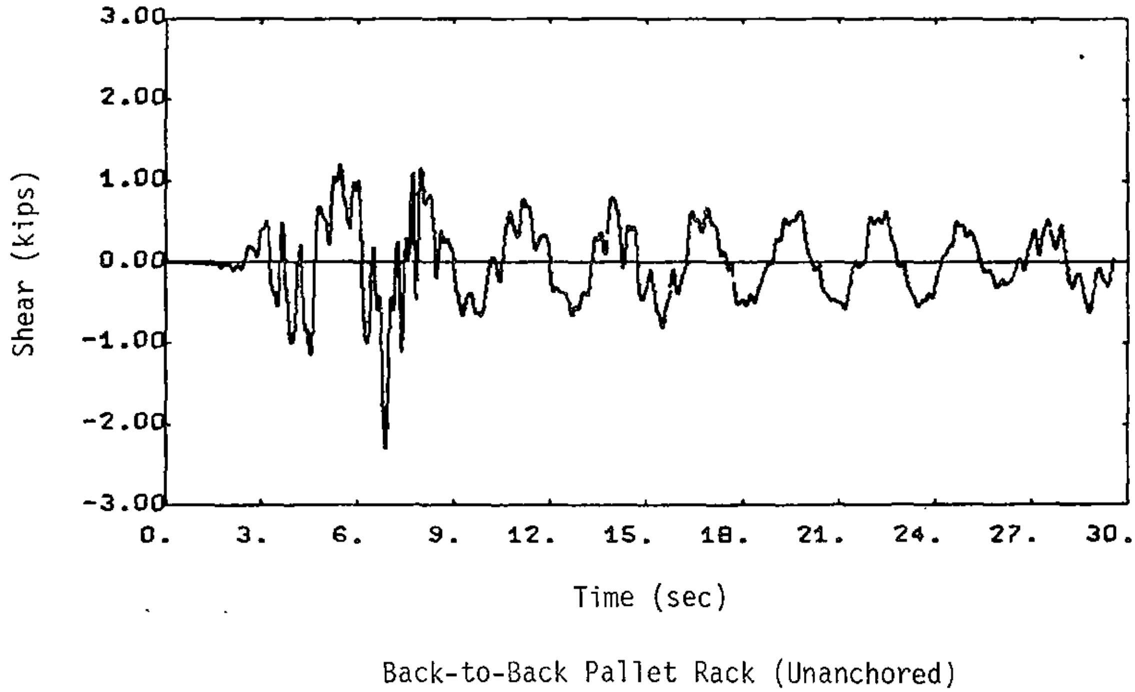

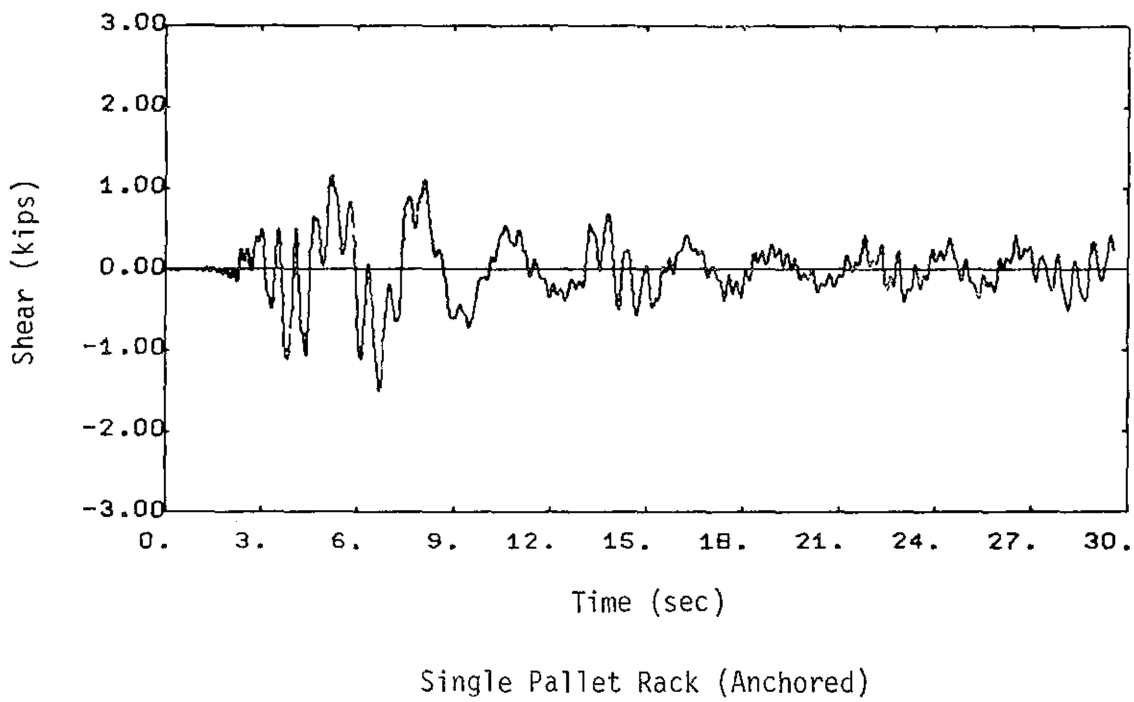

FIGURE 4.38 BASE STORY SHEARS (PER FRAME) - TEST 140278.6 AND TEST 170178.4

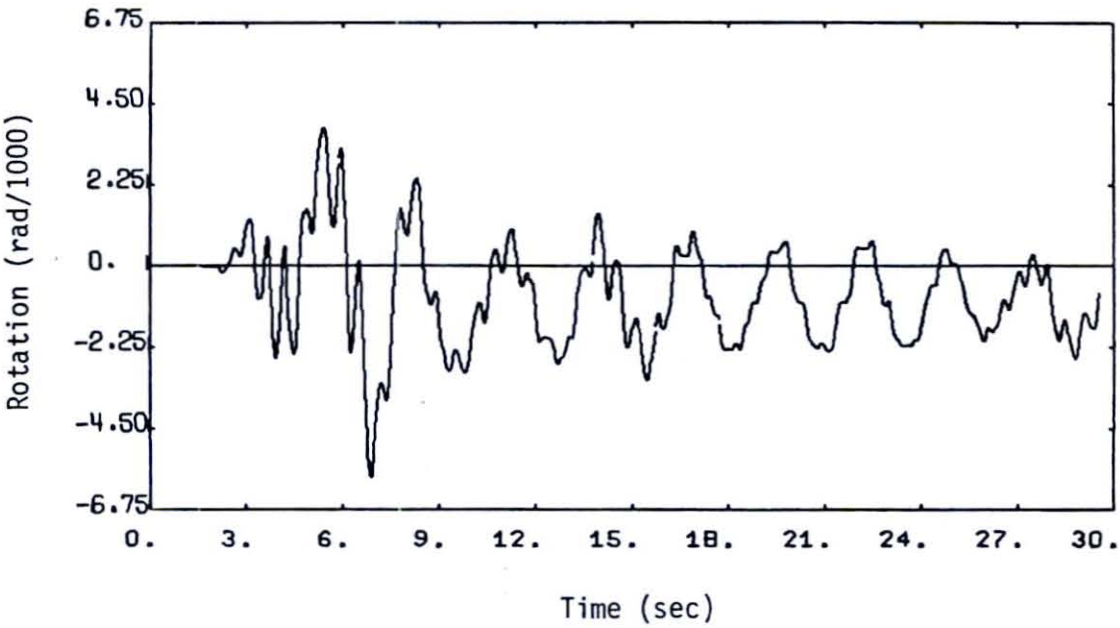

Back-to-Back Pallet Rack (Unanchored)

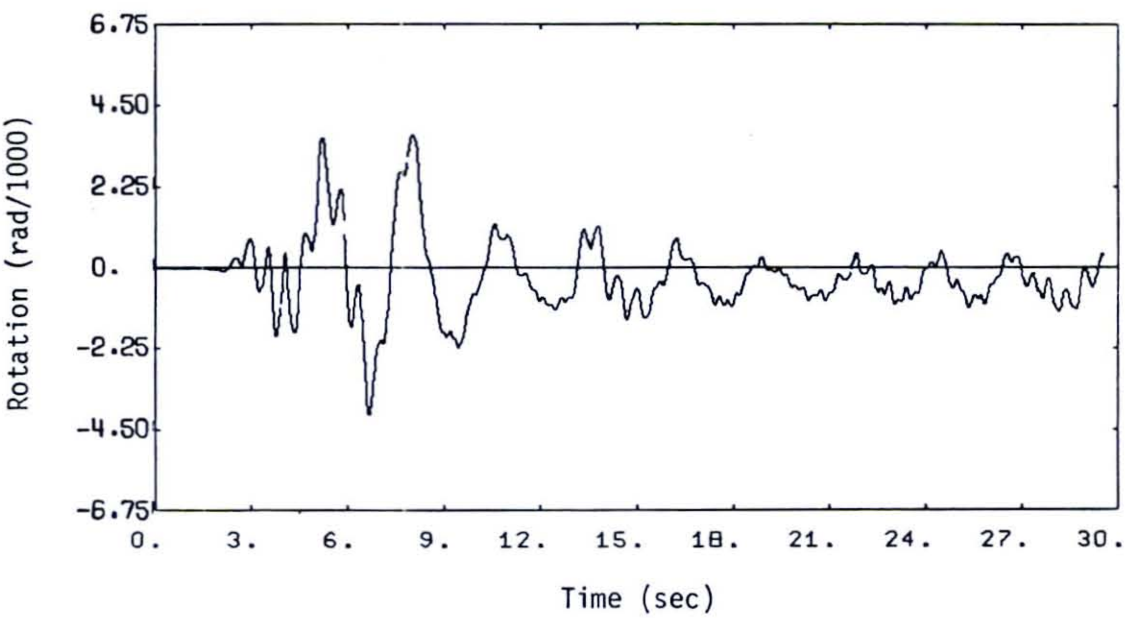

Single Pallet Rack (Anchored)

FIGURE 4.39 COLUMN END ROTATIONS (1ST LEVEL CENTER COLUMN NEAR TOP END) - TEST 140278.6 AND TEST 170178.4

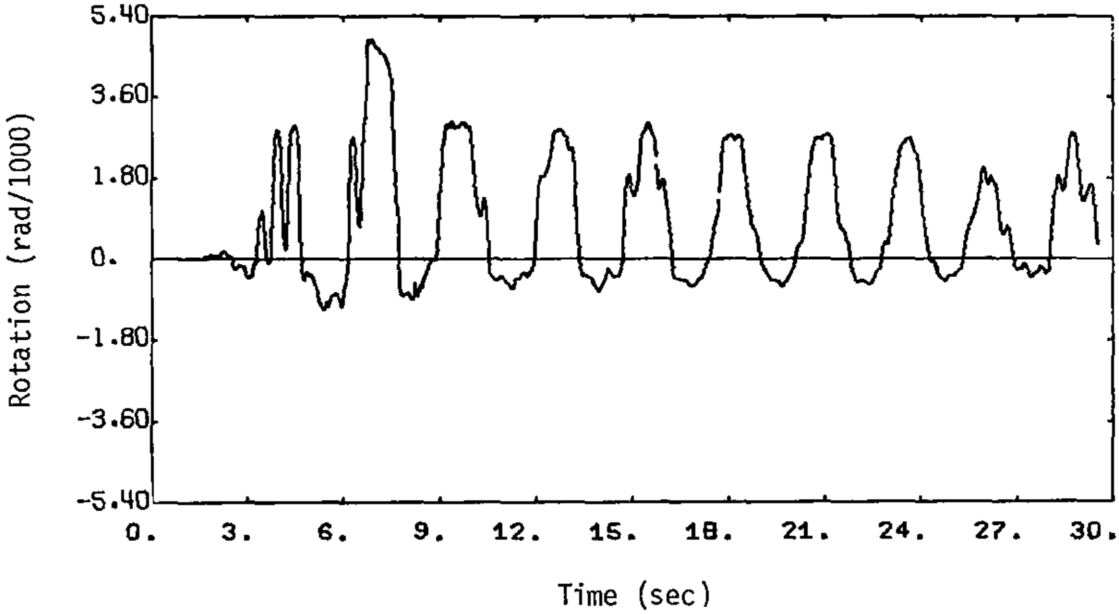

Back-to-Back Pallet Rack (Unanchored)

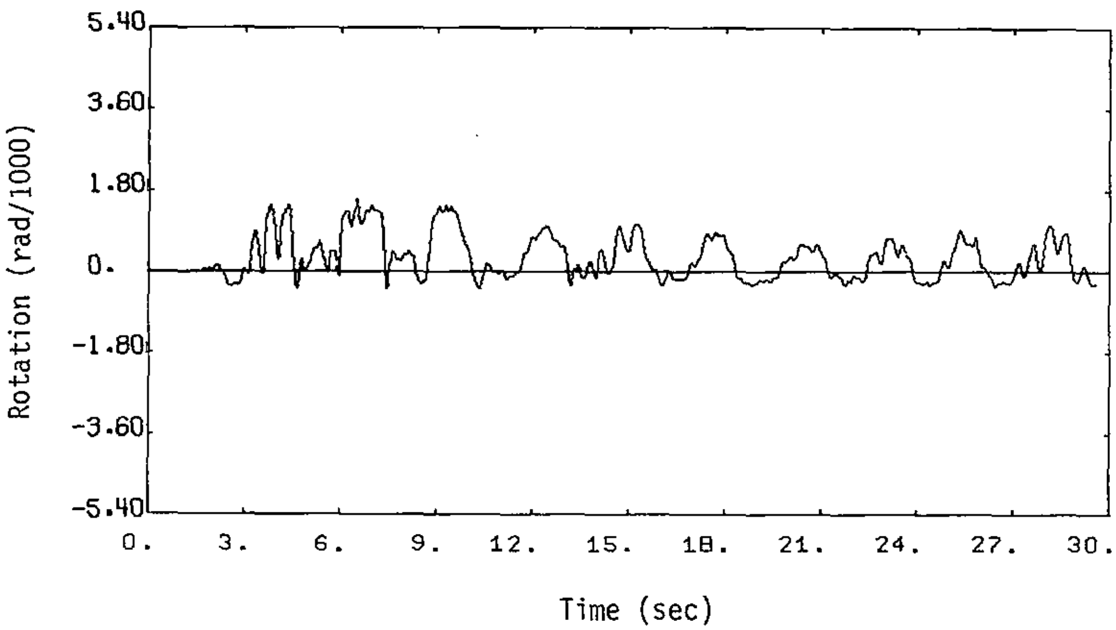

Single Pallet Rack (Anchored)

FIGURE 4.40 COLUMN END ROTATIONS (1ST LEVEL CENTER COLUMN NEAR BASE) - TEST 140278.6 AND TEST 170178.4

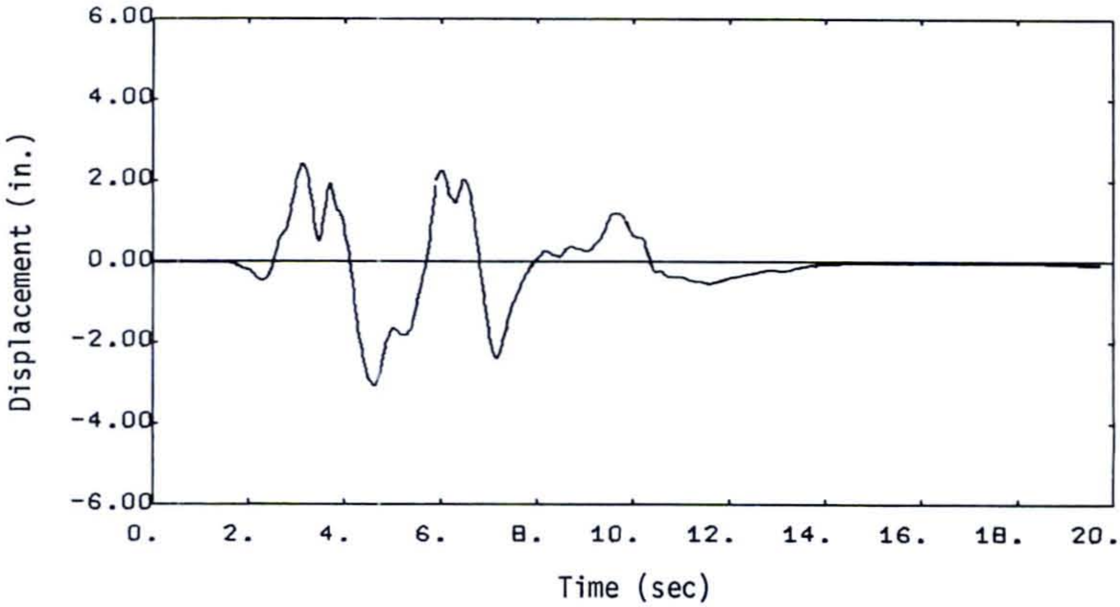

Table Displacement

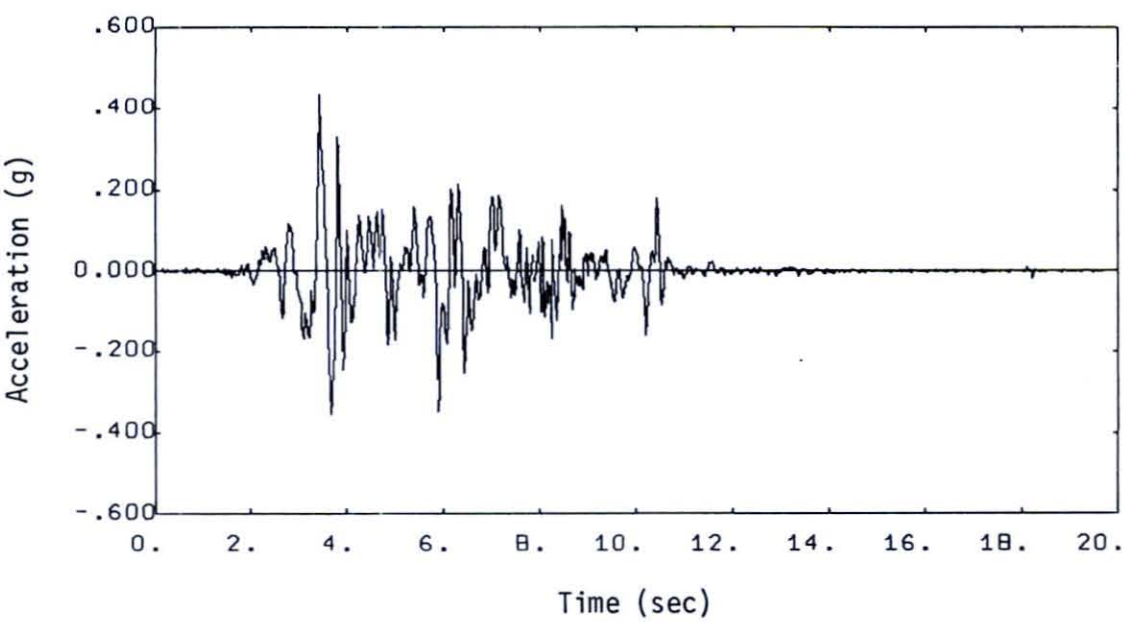

Table Acceleration

FIGURE 4.41 TABLE MOTIONS (HORIZONTAL) - TEST 140278.8

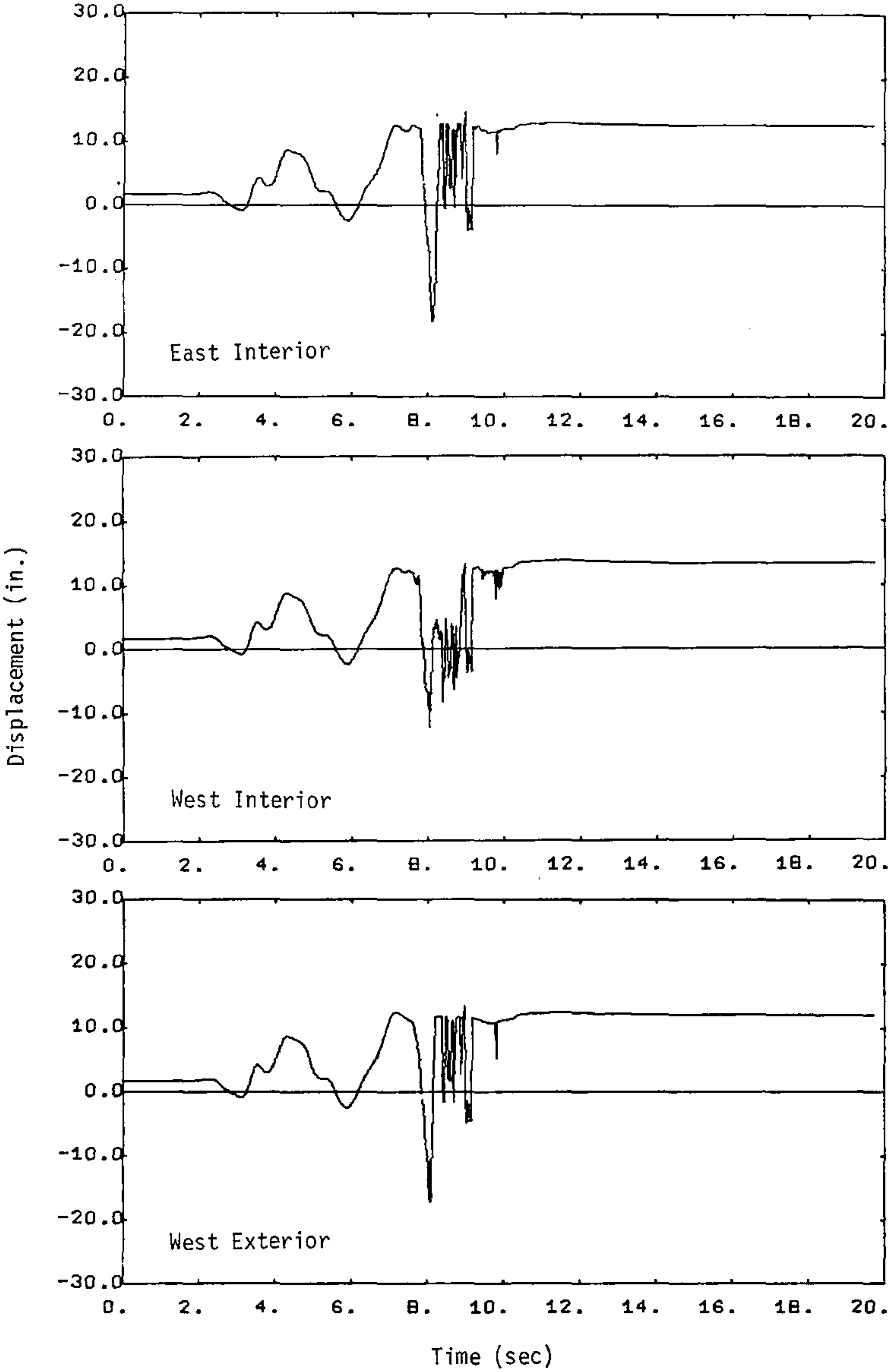

FIGURE 4.42 3RD LEVEL RELATIVE DISPLACEMENTS - TEST 140278.8

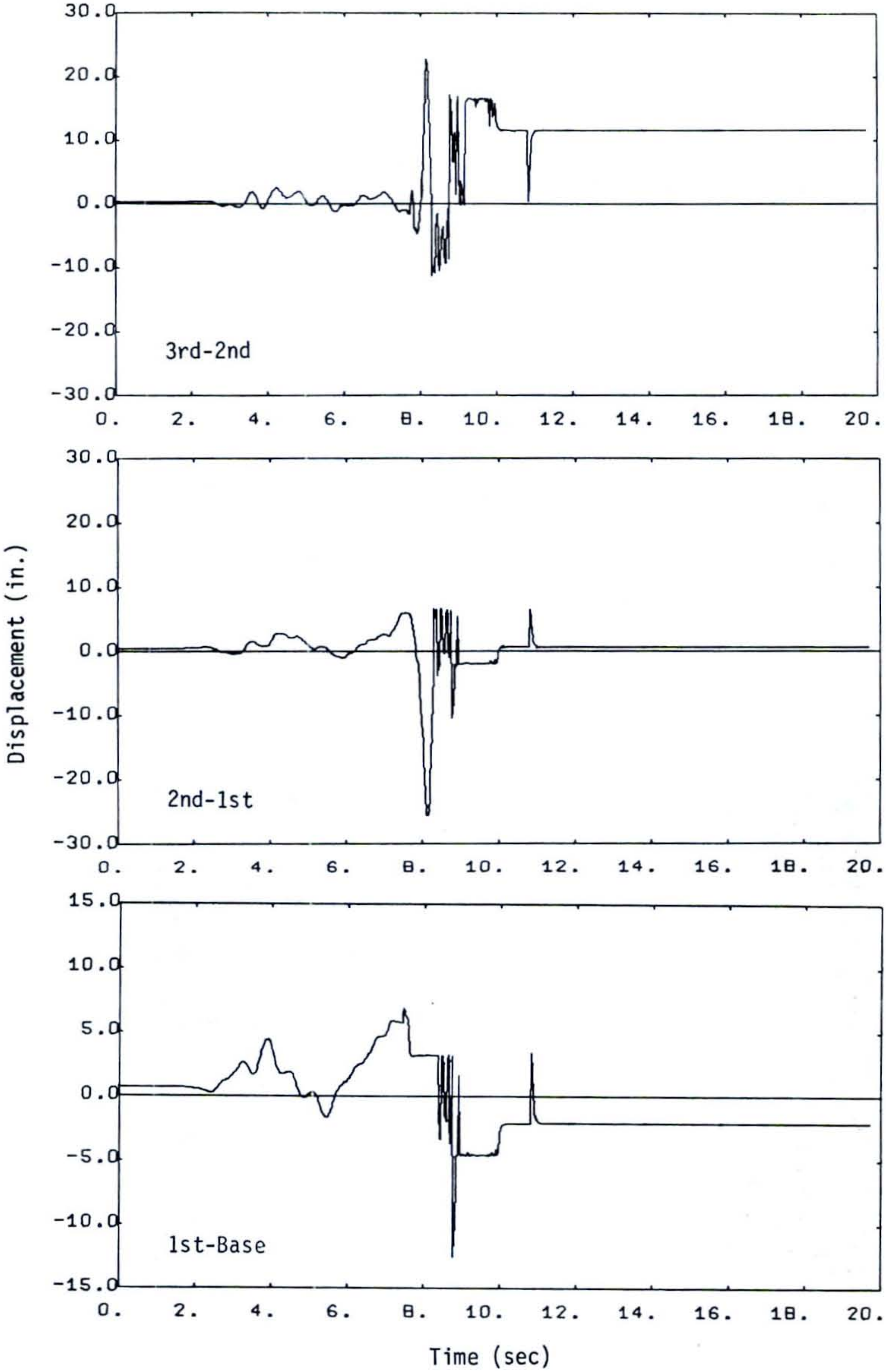

FIGURE 4.43 INTERSTORY DRIFTS - TEST 140278.8

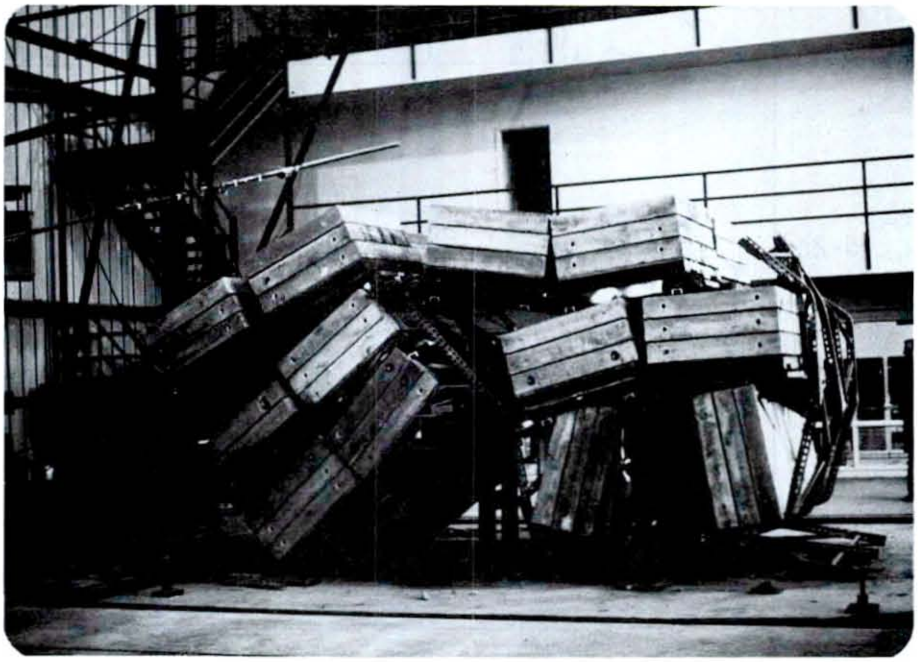

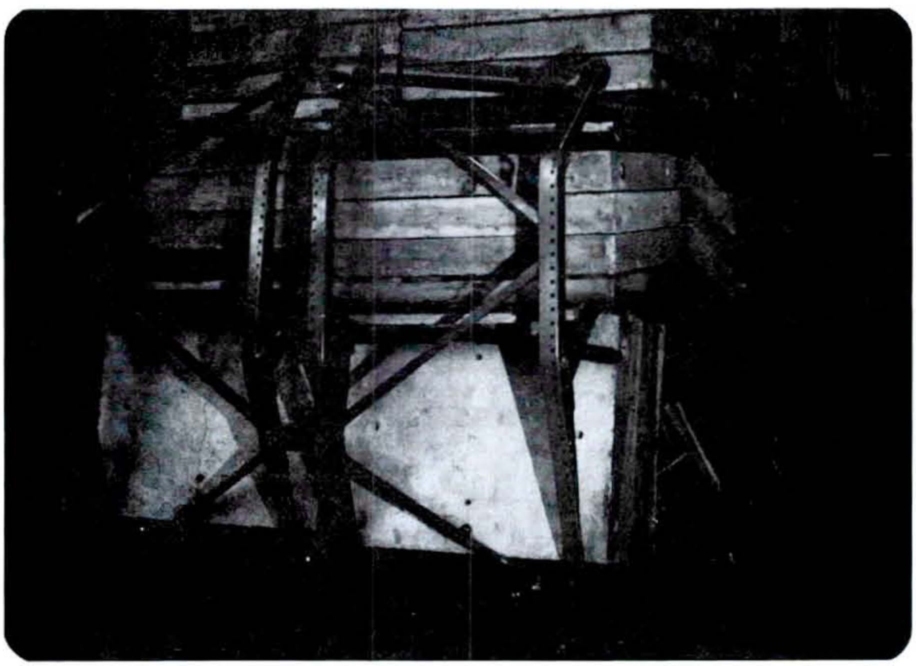

FIGURE 4.44 COMPLETE COLLAPSE OF STRUCTURE - UNANCHORED STANDARD PALLET RACK, LONGITUDINAL DIRECTION

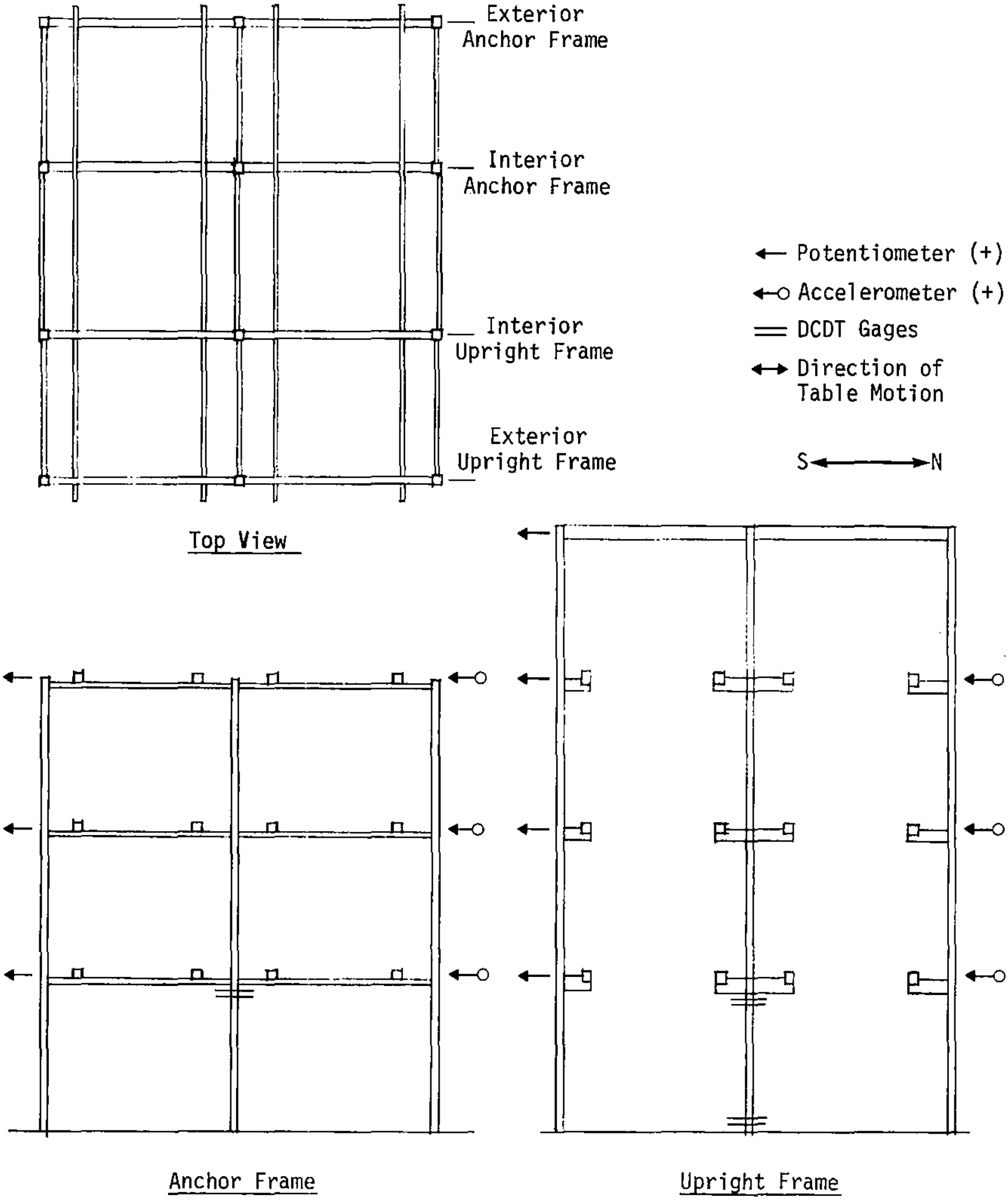

FIGURE 4.45 INSTRUMENTATION CHANNELS USED FOR DATA ANALYSIS:
DRIVE-IN RACK, LONGITUDINAL DIRECTION

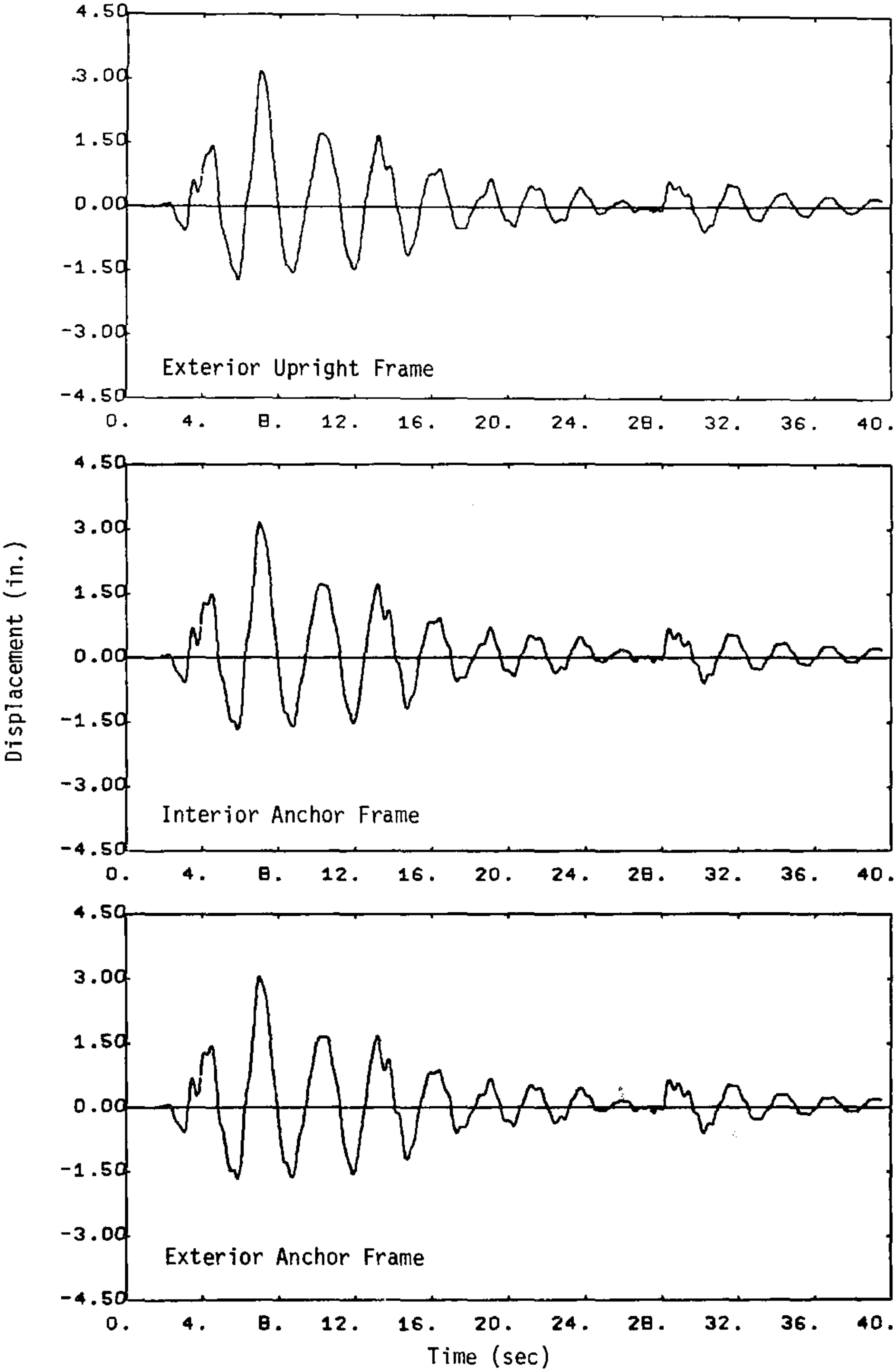

FIGURE 4.46 3RD LEVEL DISPLACEMENTS RELATIVE TO THE TABLE - TEST 130678.1 (DI-L-1-1/4 EC)

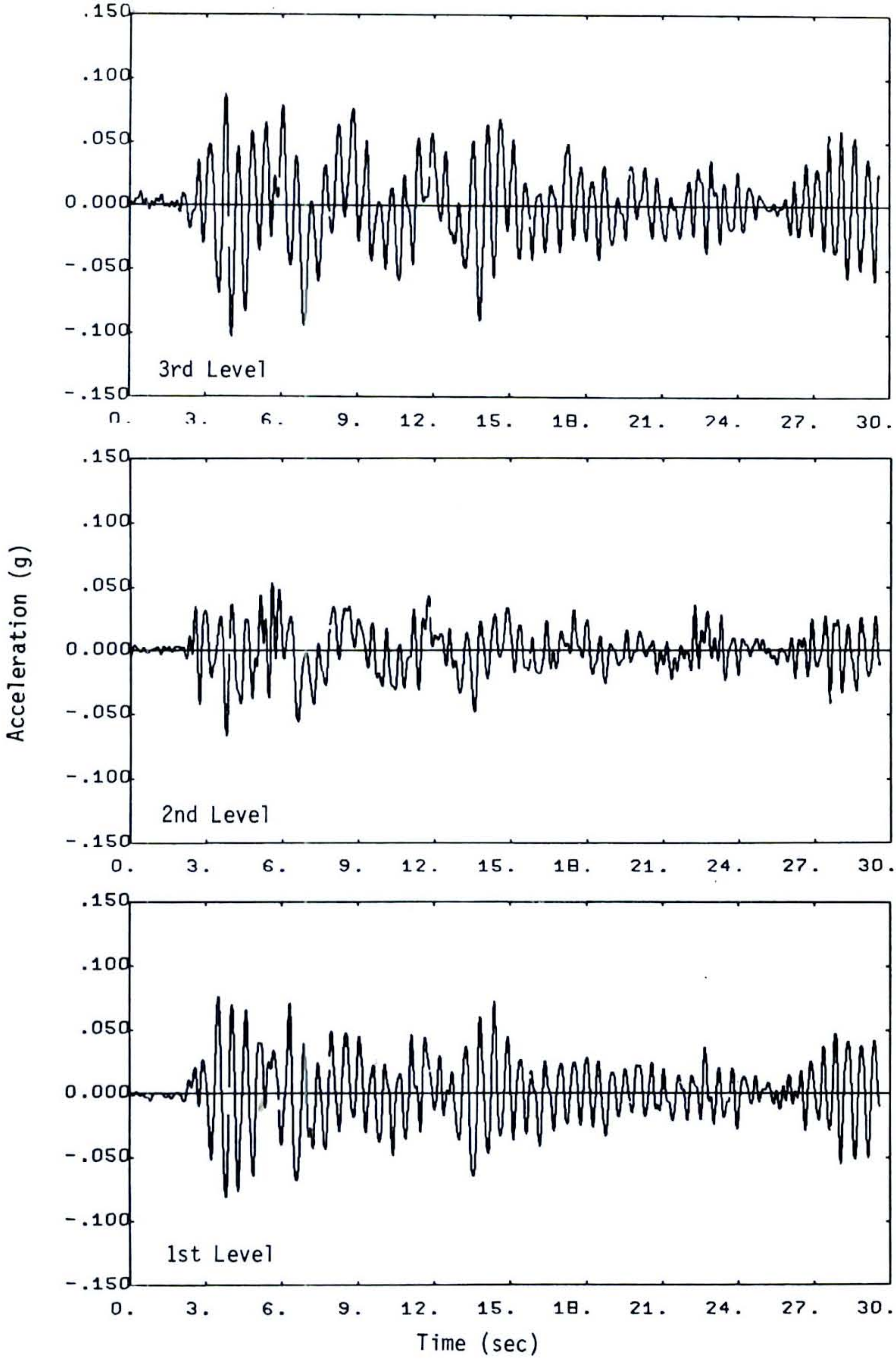

FIGURE 4.47 STORY ACCELERATIONS (EXTERIOR ANCHOR FRAME) - TEST 130678.1 (DI-L-1-1/4 EC)

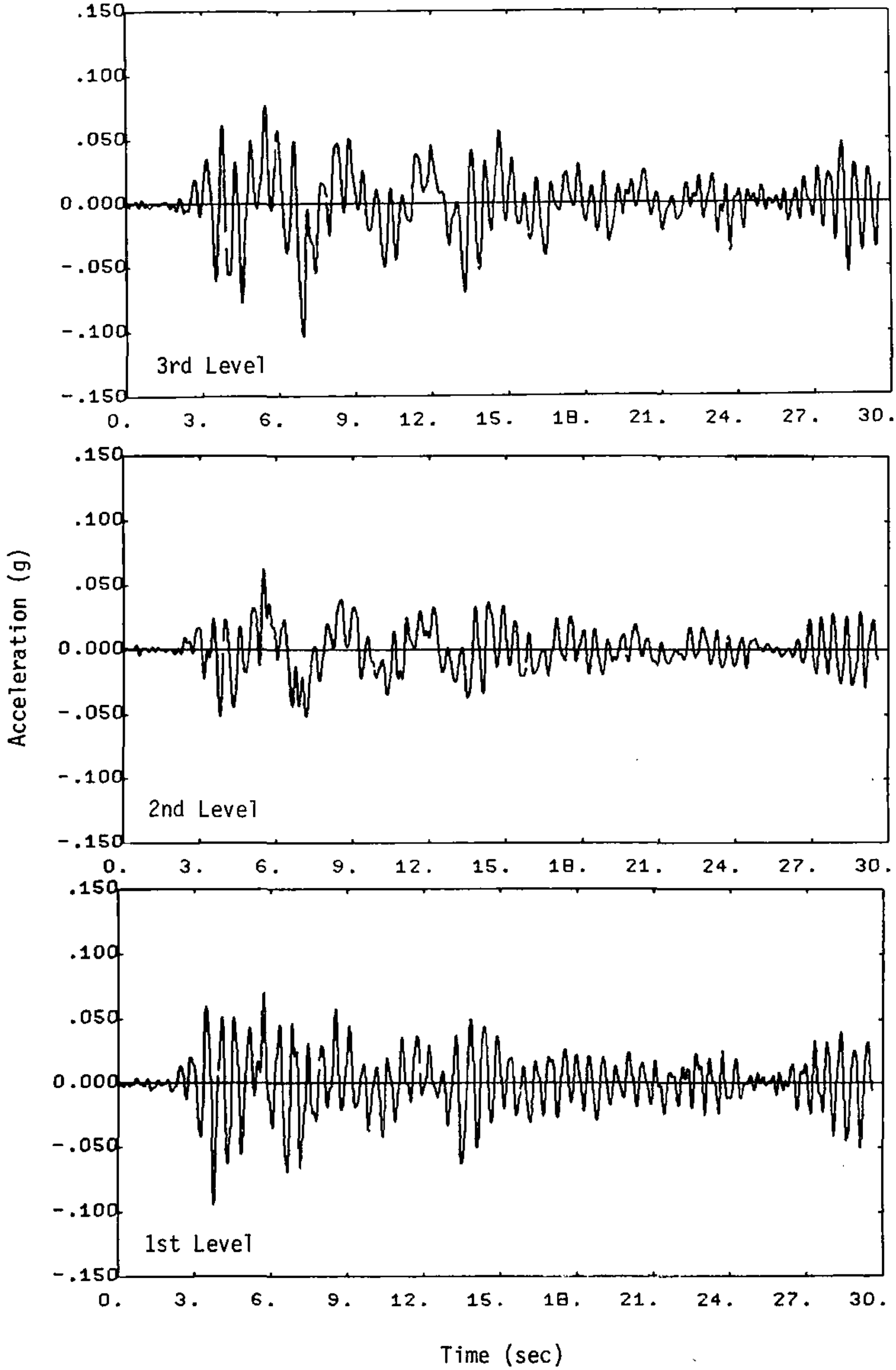

FIGURE 4.48 STORY ACCELERATIONS (EXTERIOR UPRIGHT FRAME) - TEST 130678.1 (DI-L-1-1/4 EC)

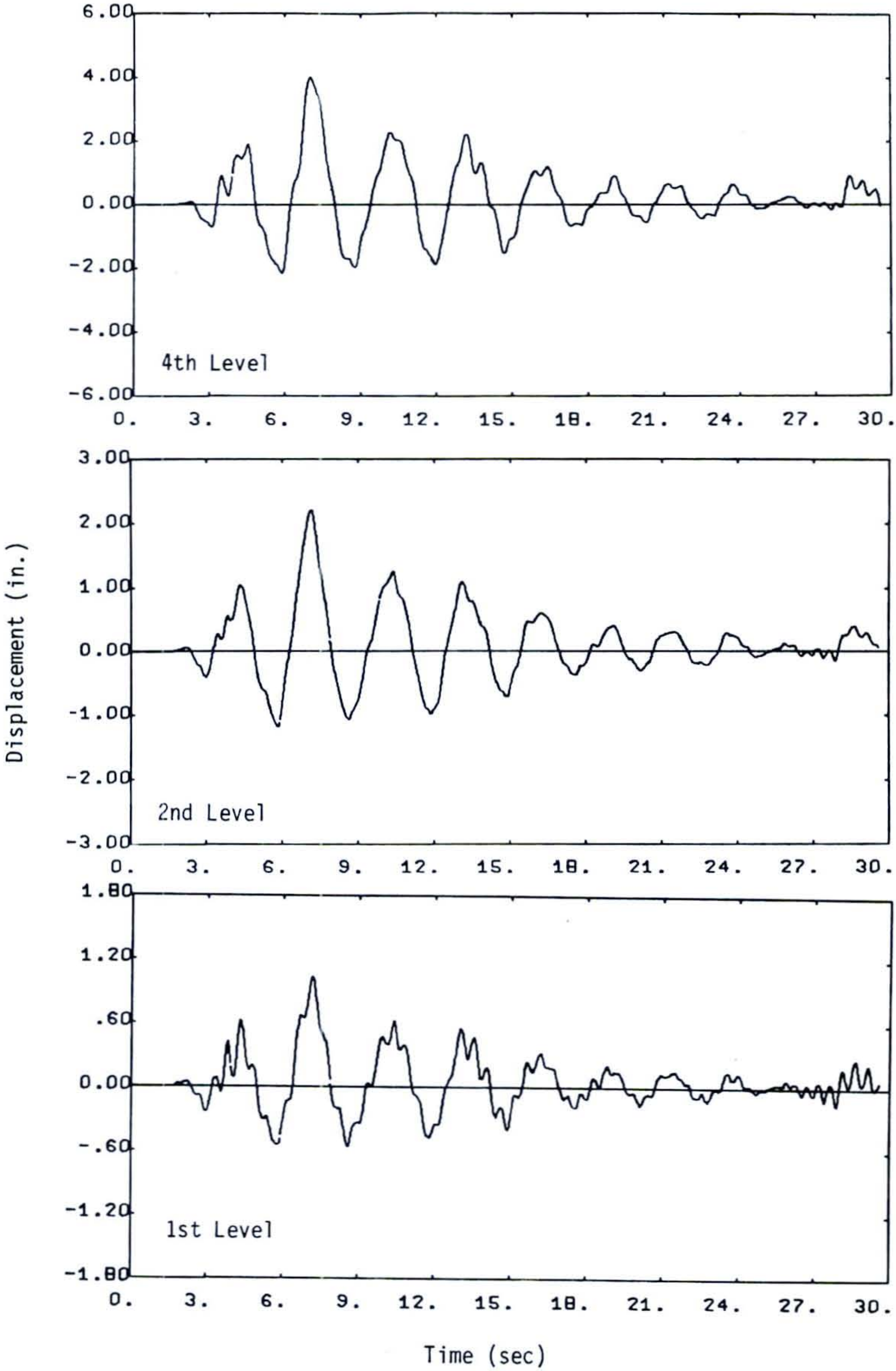

FIGURE 4.49a STORY DISPLACEMENTS RELATIVE TO THE TABLE - TEST 130678.1 (DI-L-1-1/4 EC)

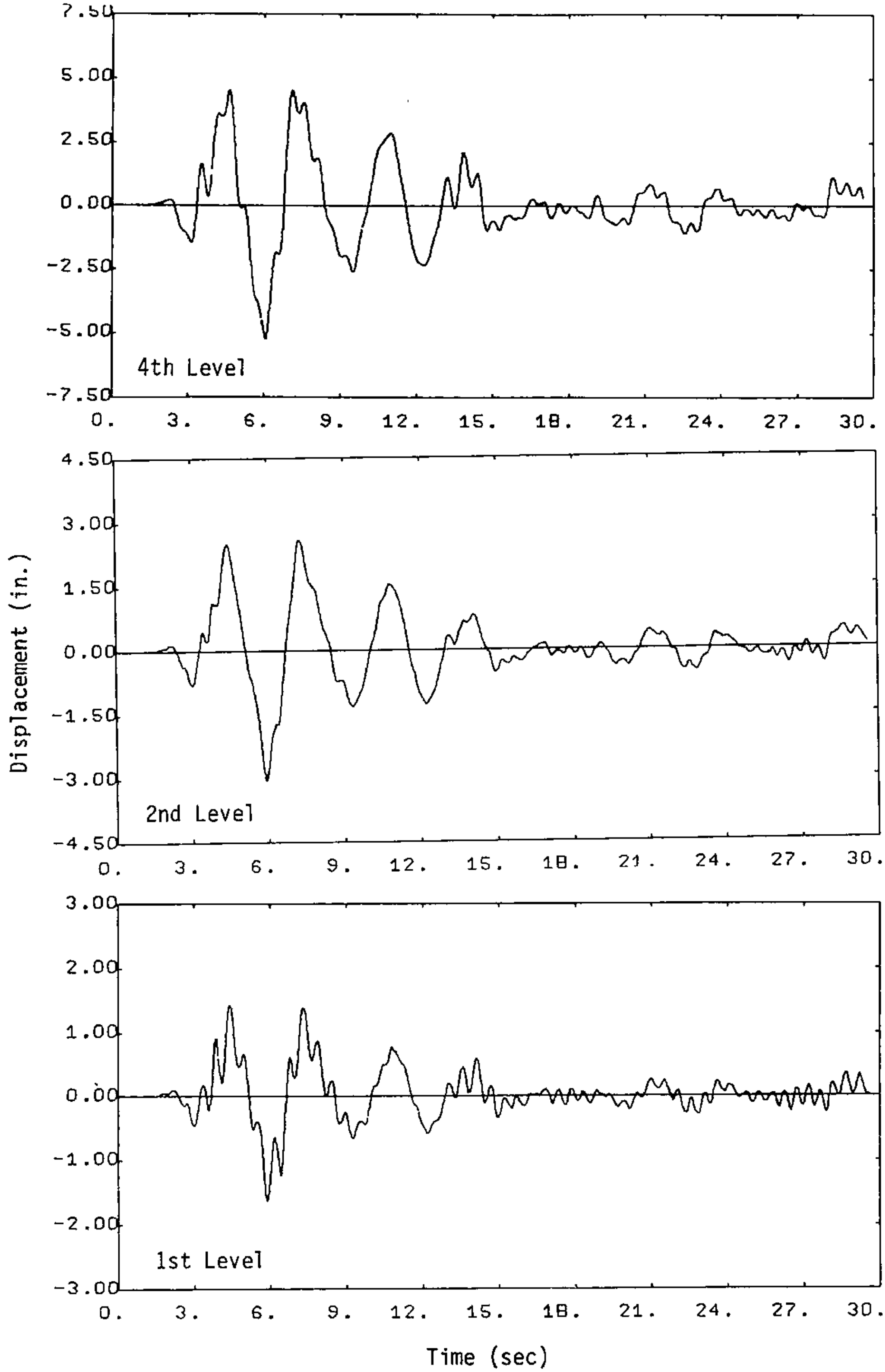

FIGURE 4.49b STORY DISPLACEMENTS RELATIVE TO THE TABLE - TEST 130678.3 (DI-L-1-1/2 EC)

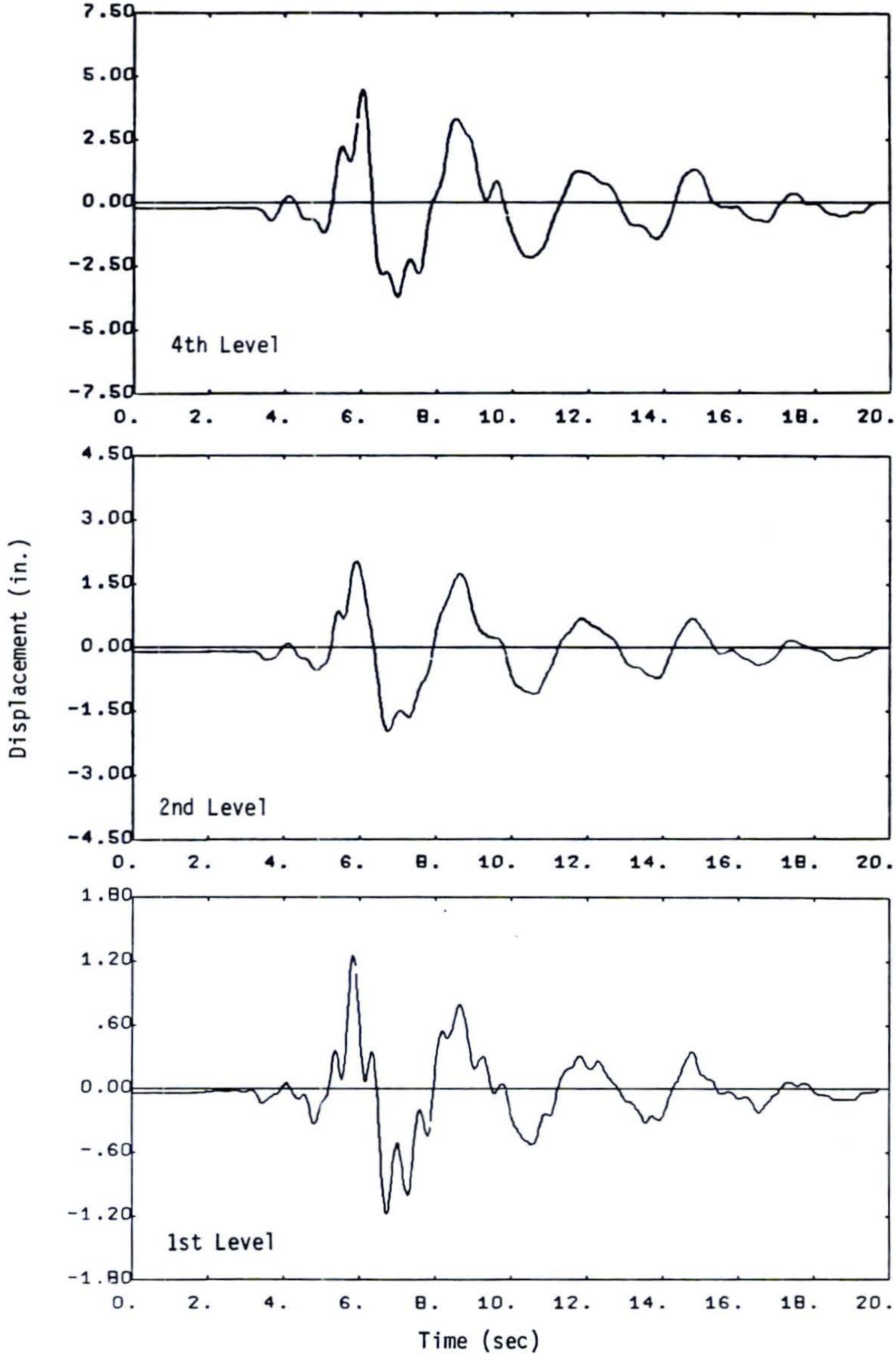

FIGURE 4.49c STORY DISPLACEMENTS RELATIVE TO THE TABLE - TEST 130678.4 (DI-L-1-1/2 PF)

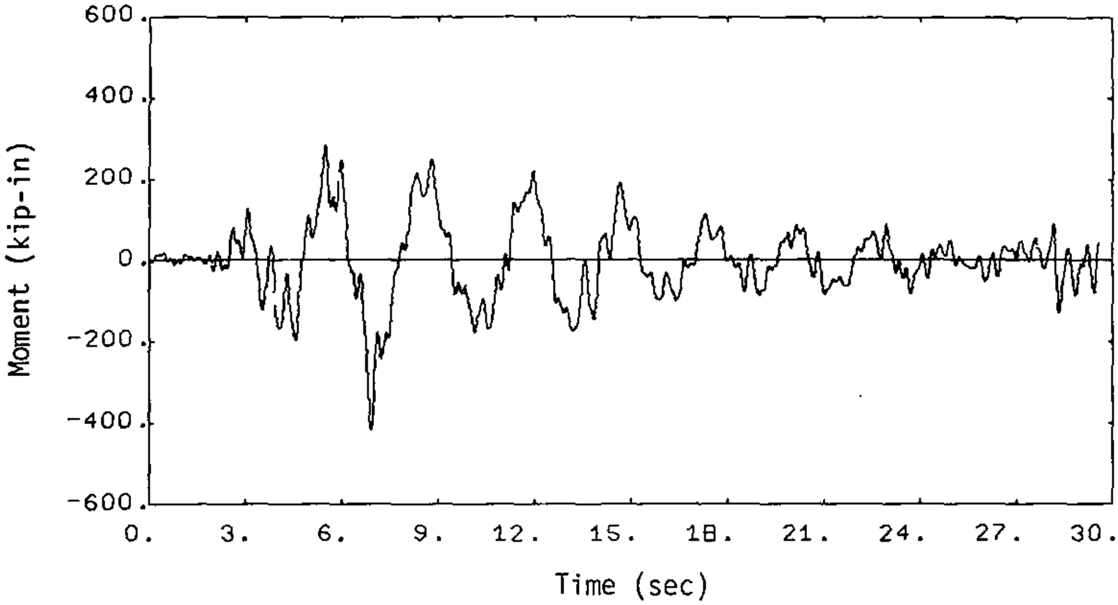

Base Overturning Moment

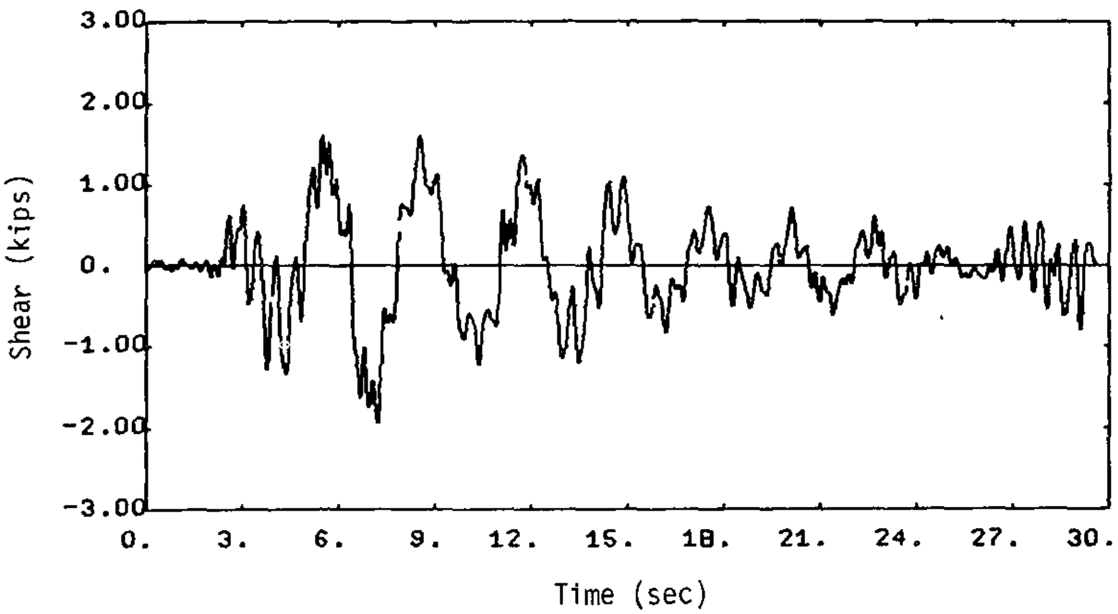

Base Shear

FIGURE 4.50a BASE SHEAR AND OVERTURNING MOMENT - TEST 130678.1 (DI-L-1-1/4 EC)

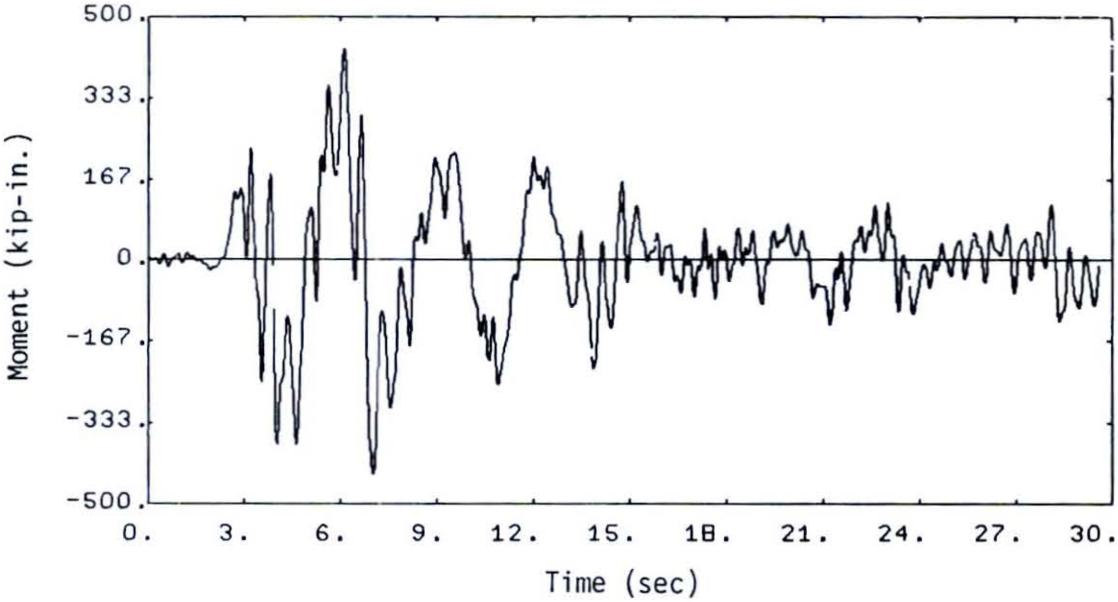

Base Overturning Moment

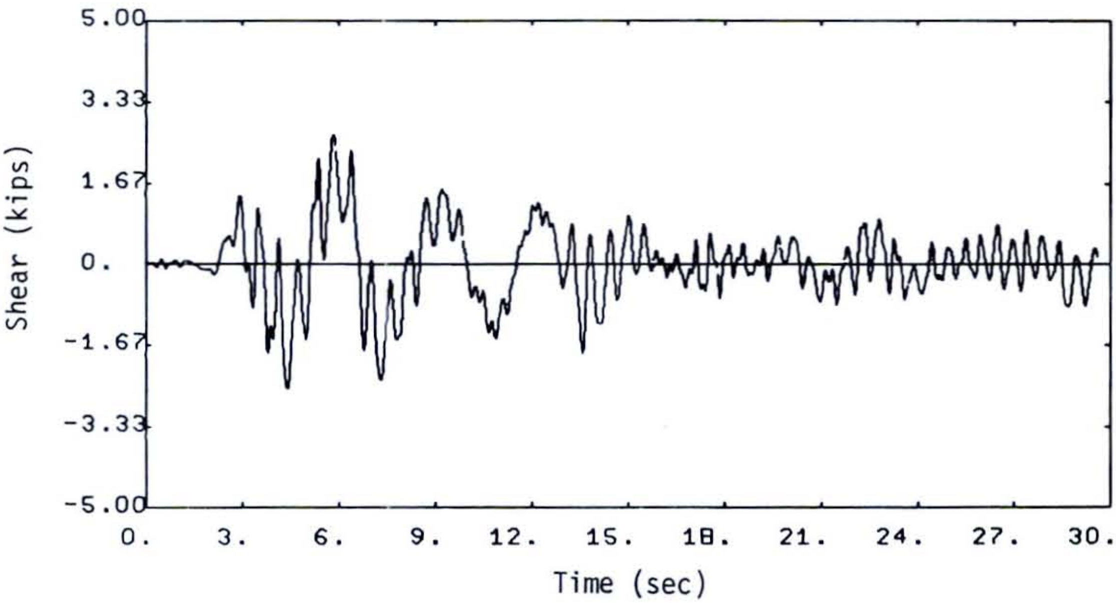

Base Shear

FIGURE 4.50b BASE SHEAR AND OVERTURNING MOMENT - TEST 130678.3 (DI-L-1-1/2 EC)

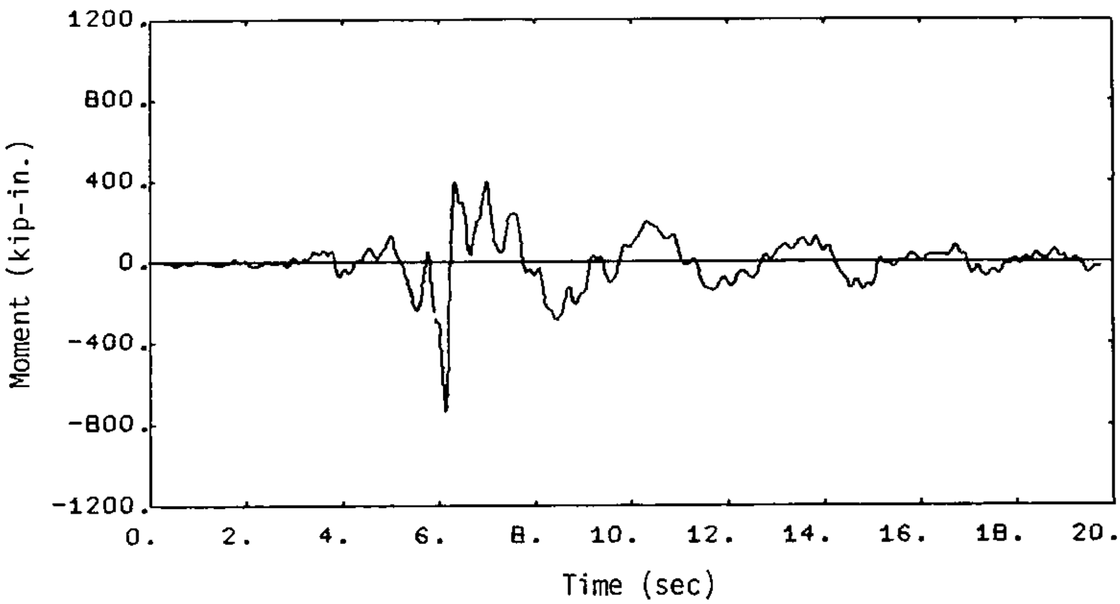

Base Overturning Moment

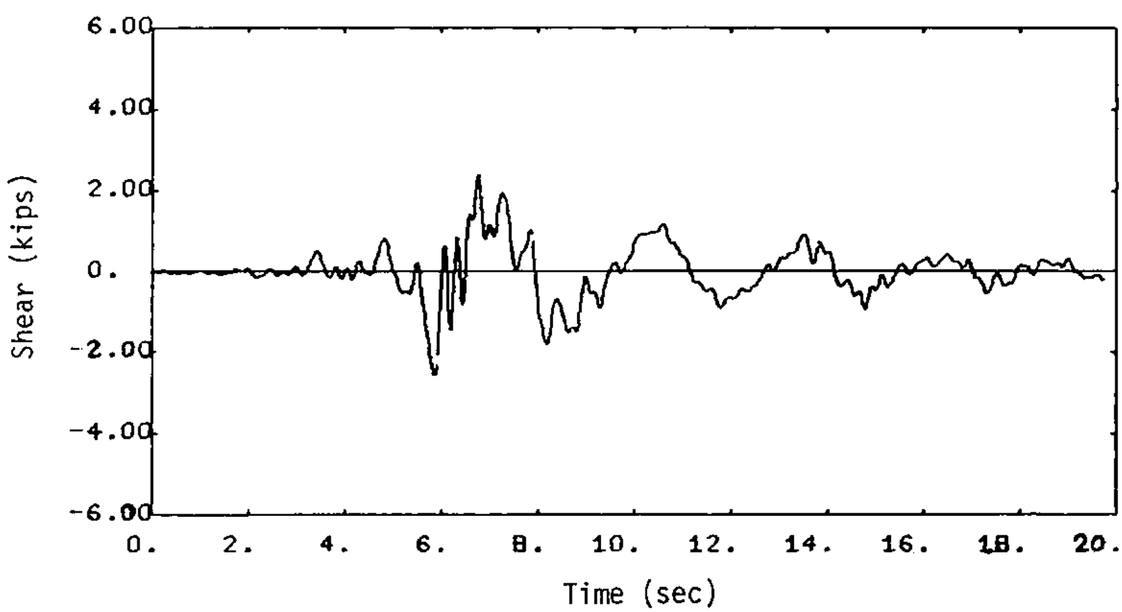

Base Shear

FIGURE 4.50c BASE SHEAR AND OVERTURNING MOMENT - TEST 130678.4 (DI-L-1-1/2 PF)

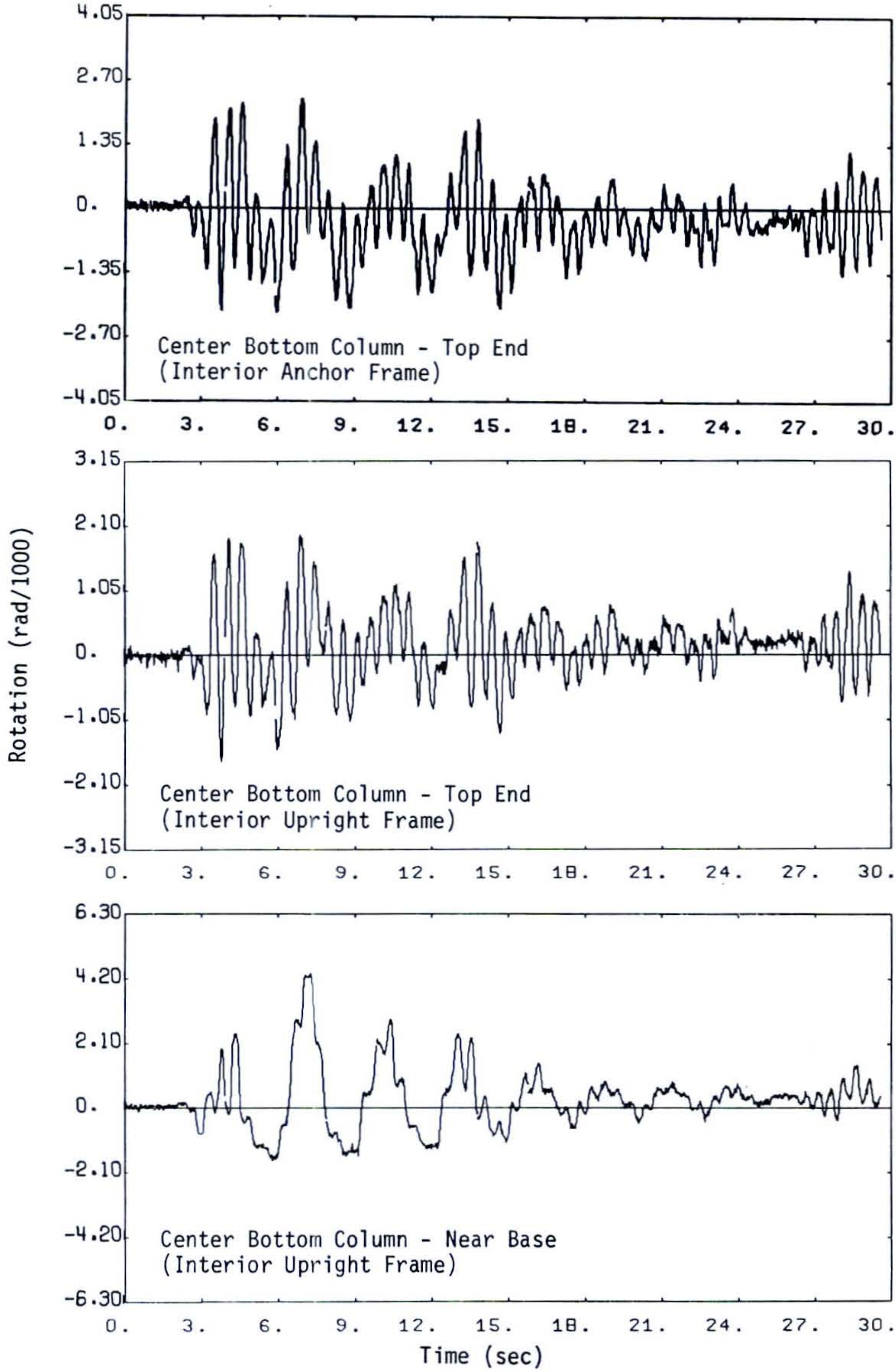

FIGURE 4.51a COLUMN END ROTATIONS - TEST 130678.1 (DI-L-1-1/4 EC)

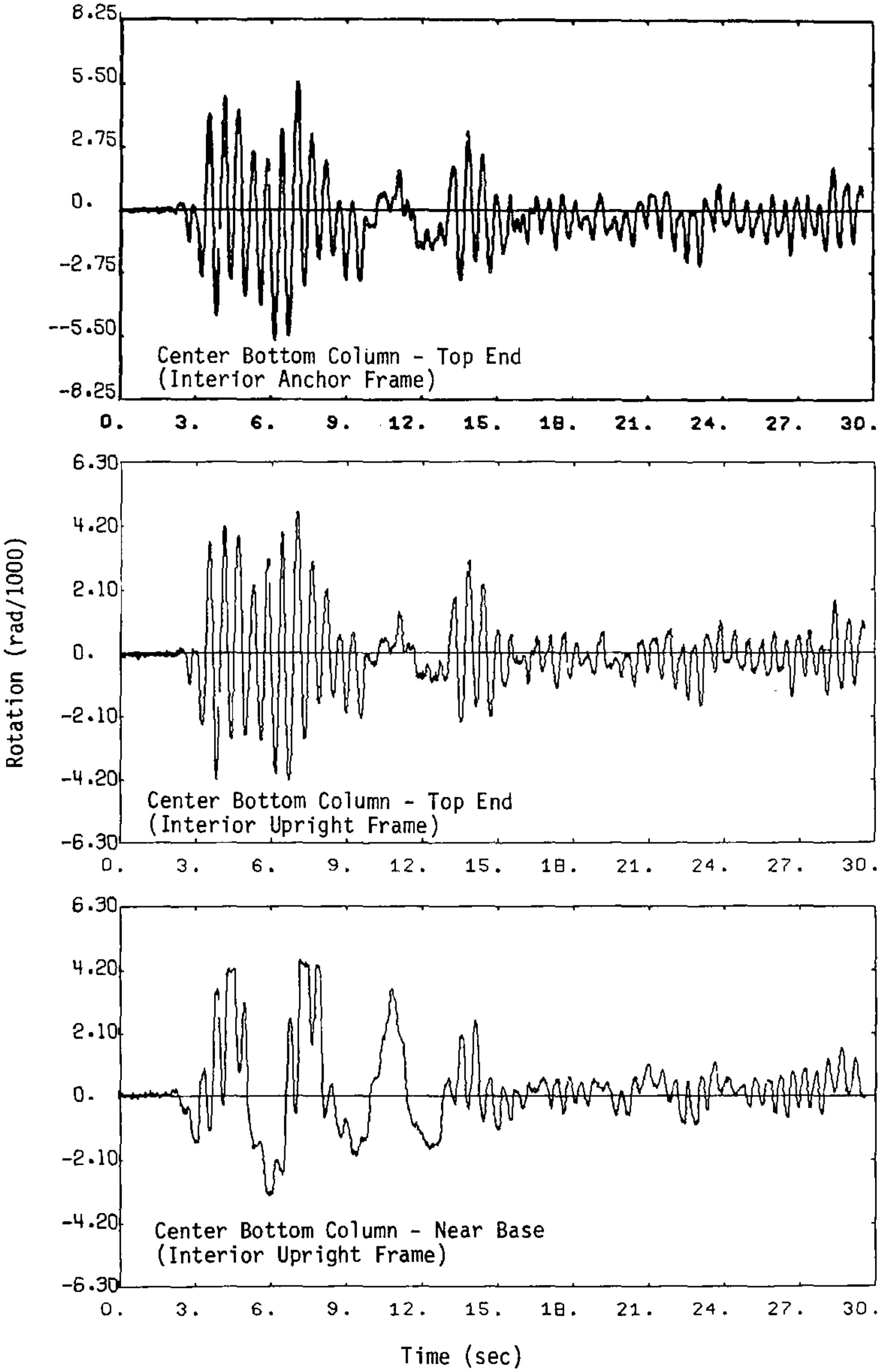

FIGURE 4.51b COLUMN END ROTATIONS - TEST 130678.3 (DI-L-1-1/2 EC)

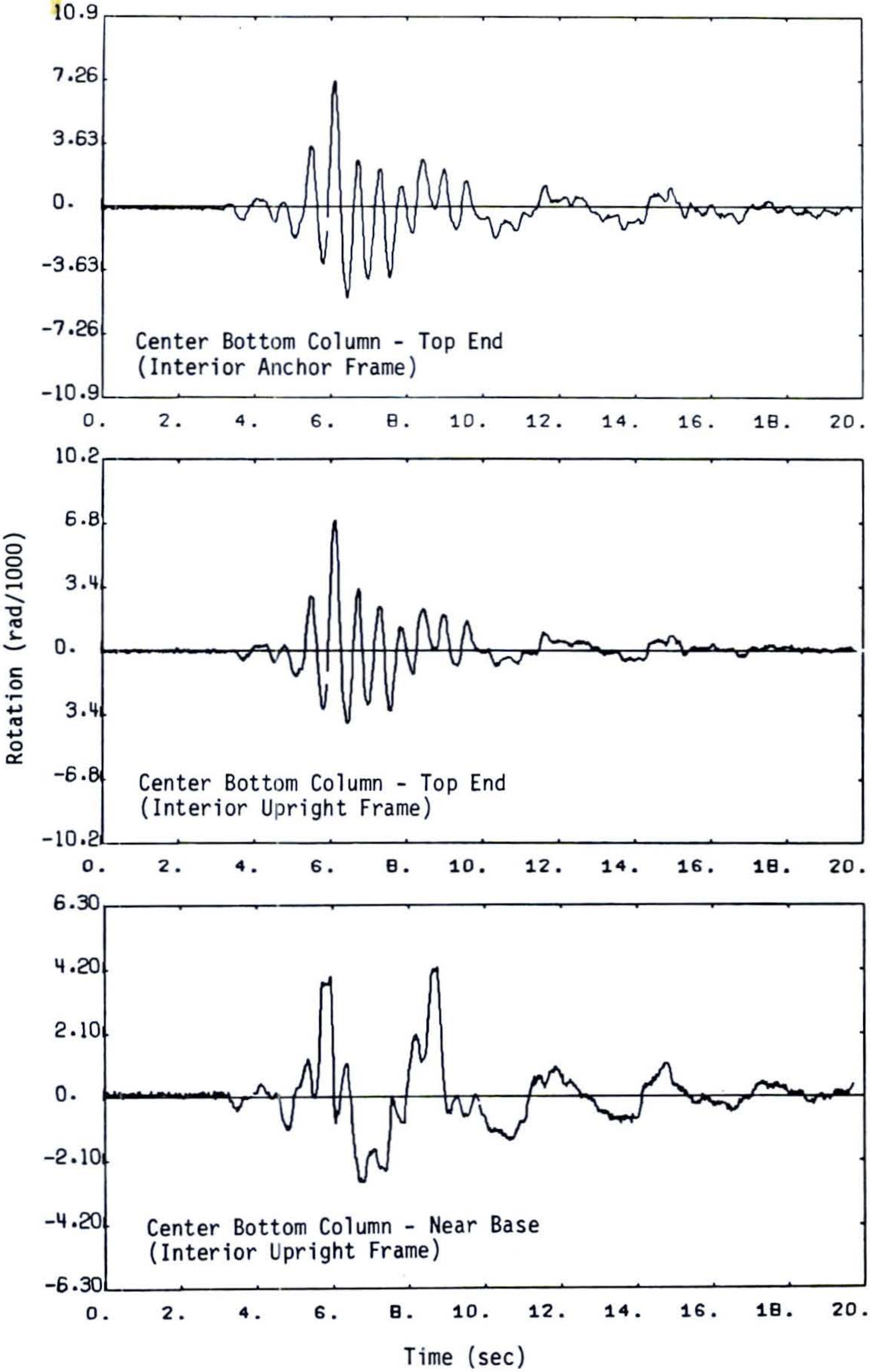

FIGURE 4.51c COLUMN END ROTATIONS - TEST 130678.4 (DI-L-1-1/2 PF)

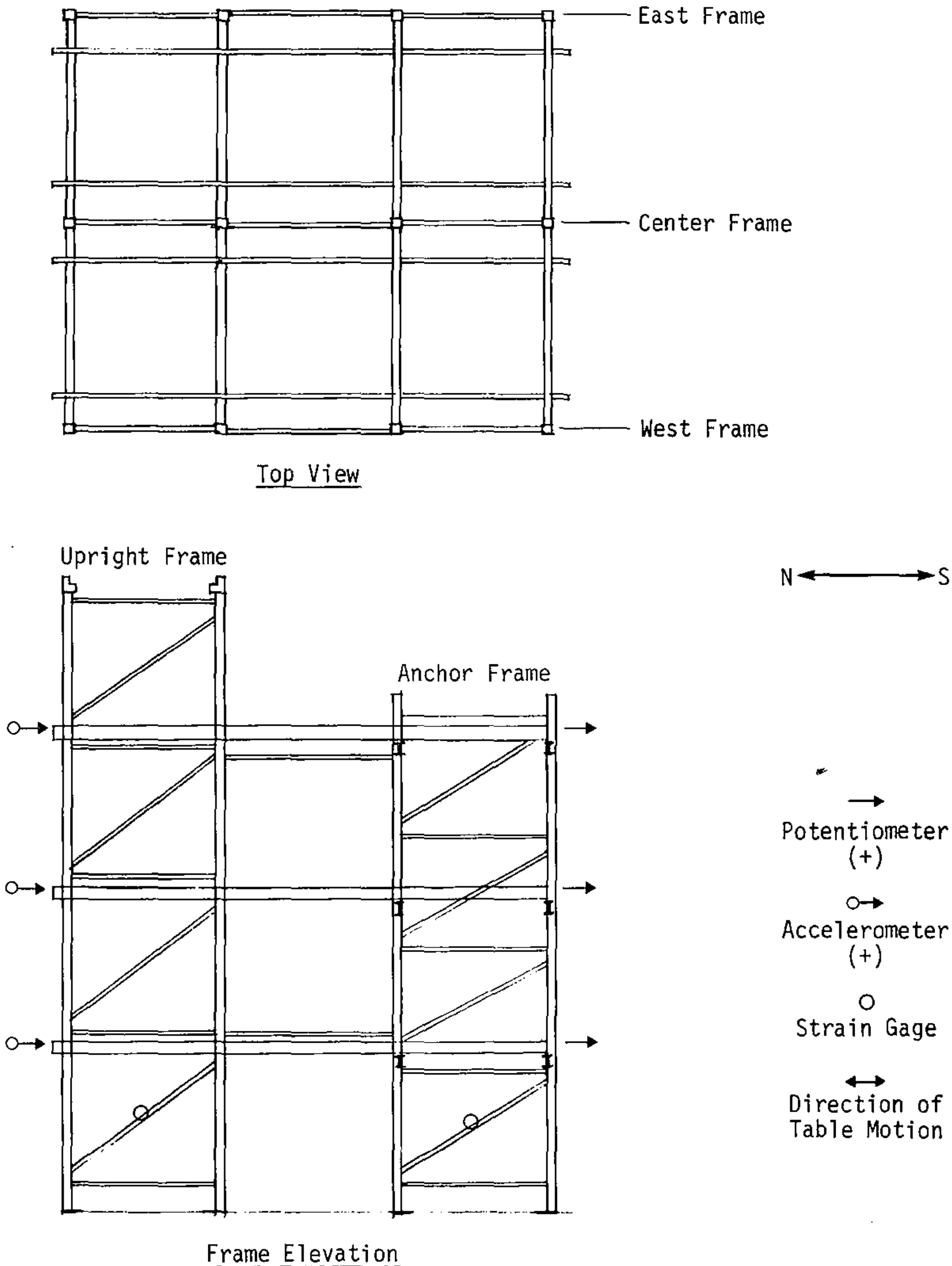

FIGURE 4.52 INSTRUMENTATION CHANNELS USED FOR DATA ANALYSIS: DRIVE-IN RACK, TRANSVERSE DIRECTION

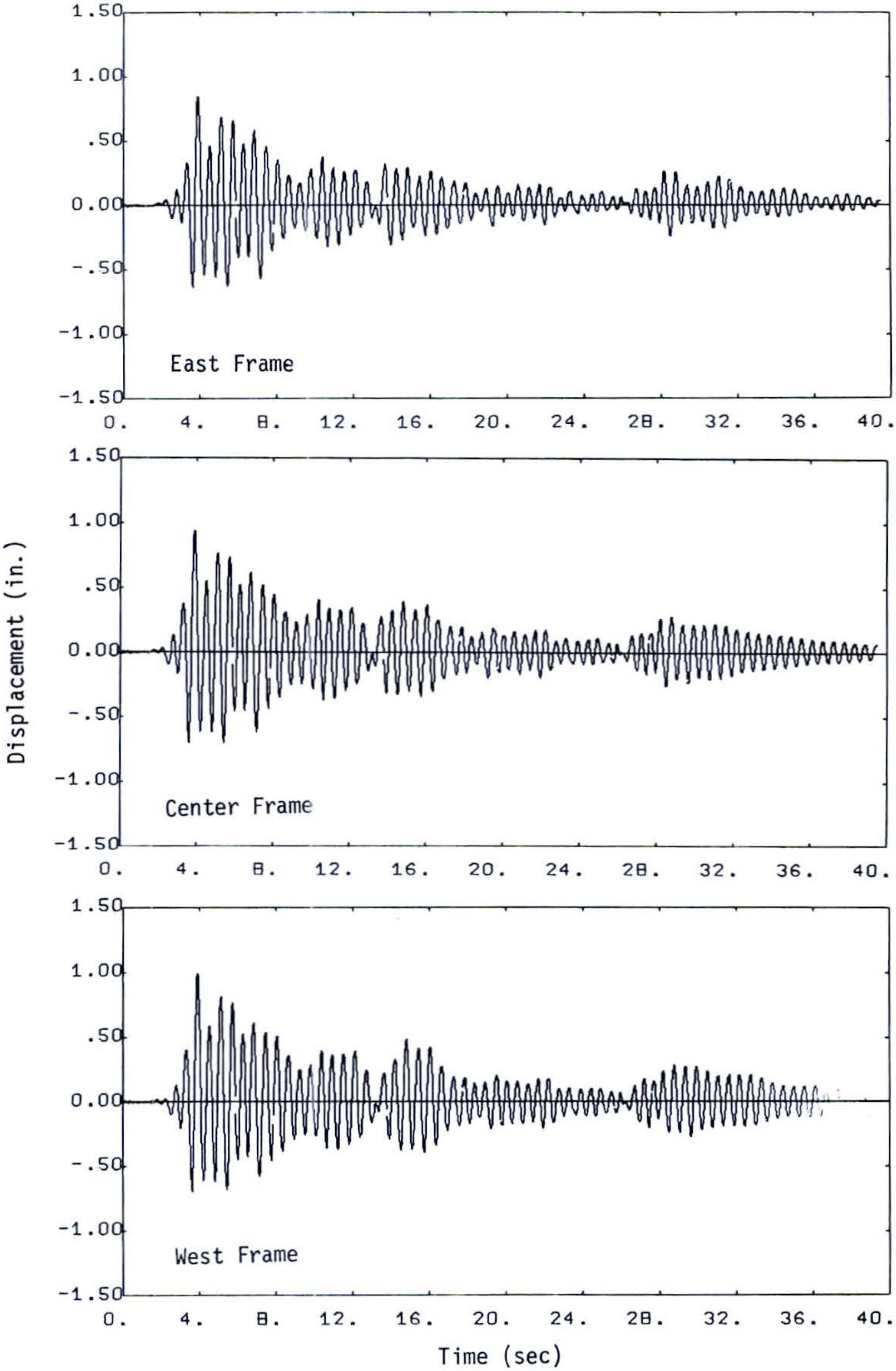

FIGURE 4.53 3RD LEVEL DISPLACEMENTS RELATIVE TO THE TABLE - TEST 200678.2 (DI-T-2/3-1/4 EC)

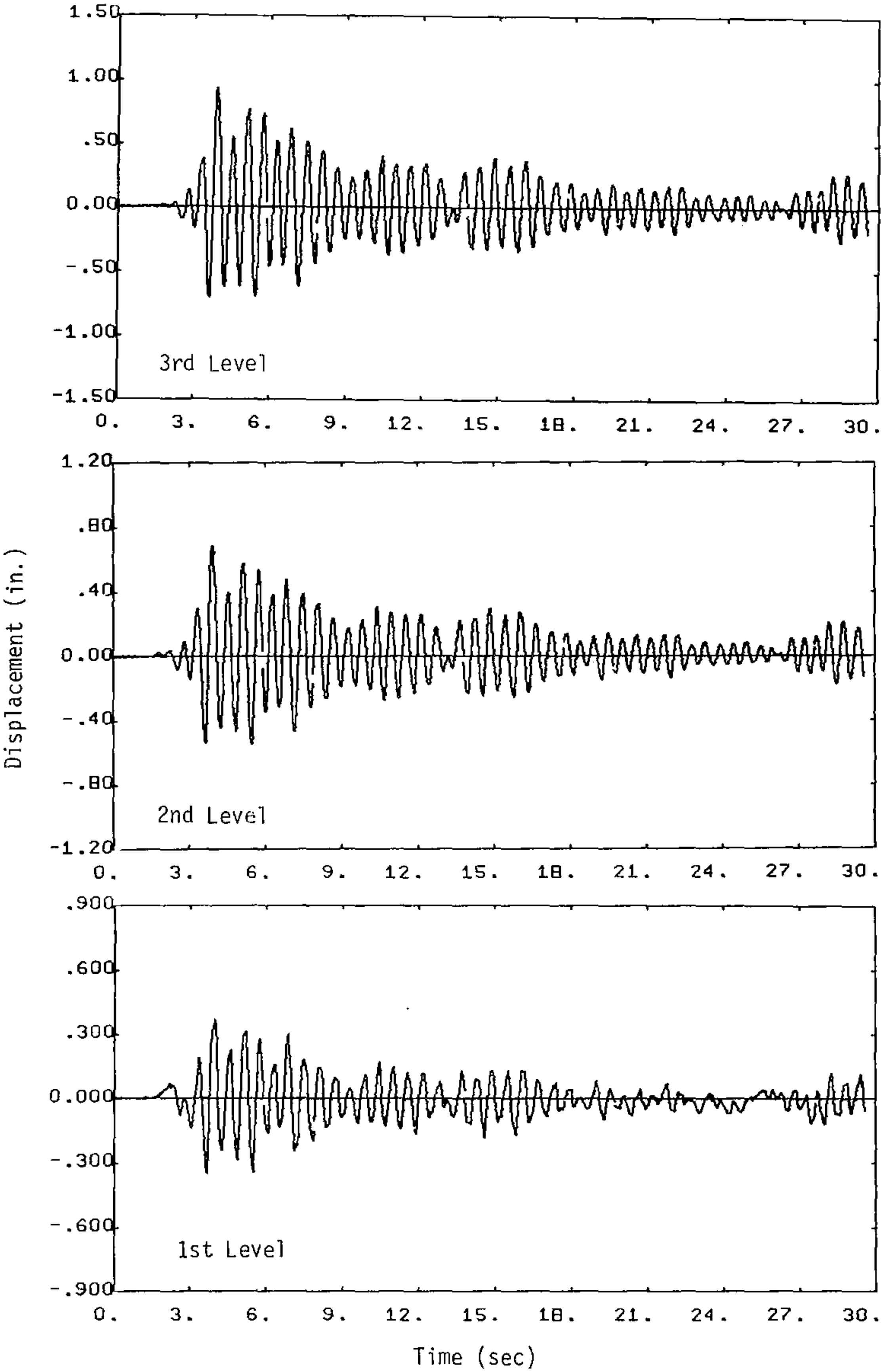

FIGURE 4.54a STORY DISPLACEMENTS RELATIVE TO THE TABLE (CENTER FRAME) - TEST 200678.2 (DI-T-2/3-1/4 EC)

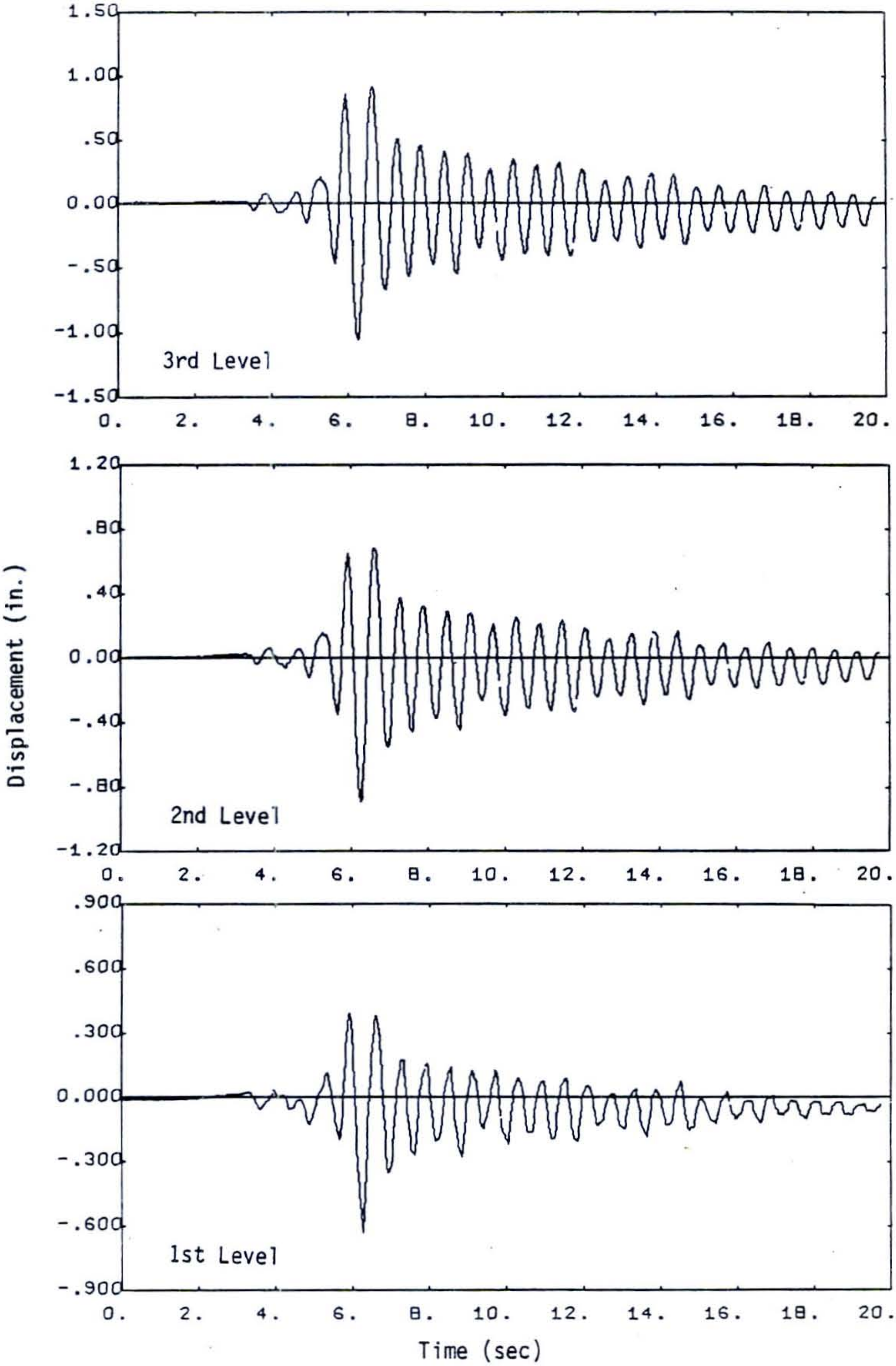

FIGURE 4.54b STORY DISPLACEMENTS RELATIVE TO THE TABLE (CENTER FRAME) - TEST 200678.3 (DI-T-2/3-1/4 PF)

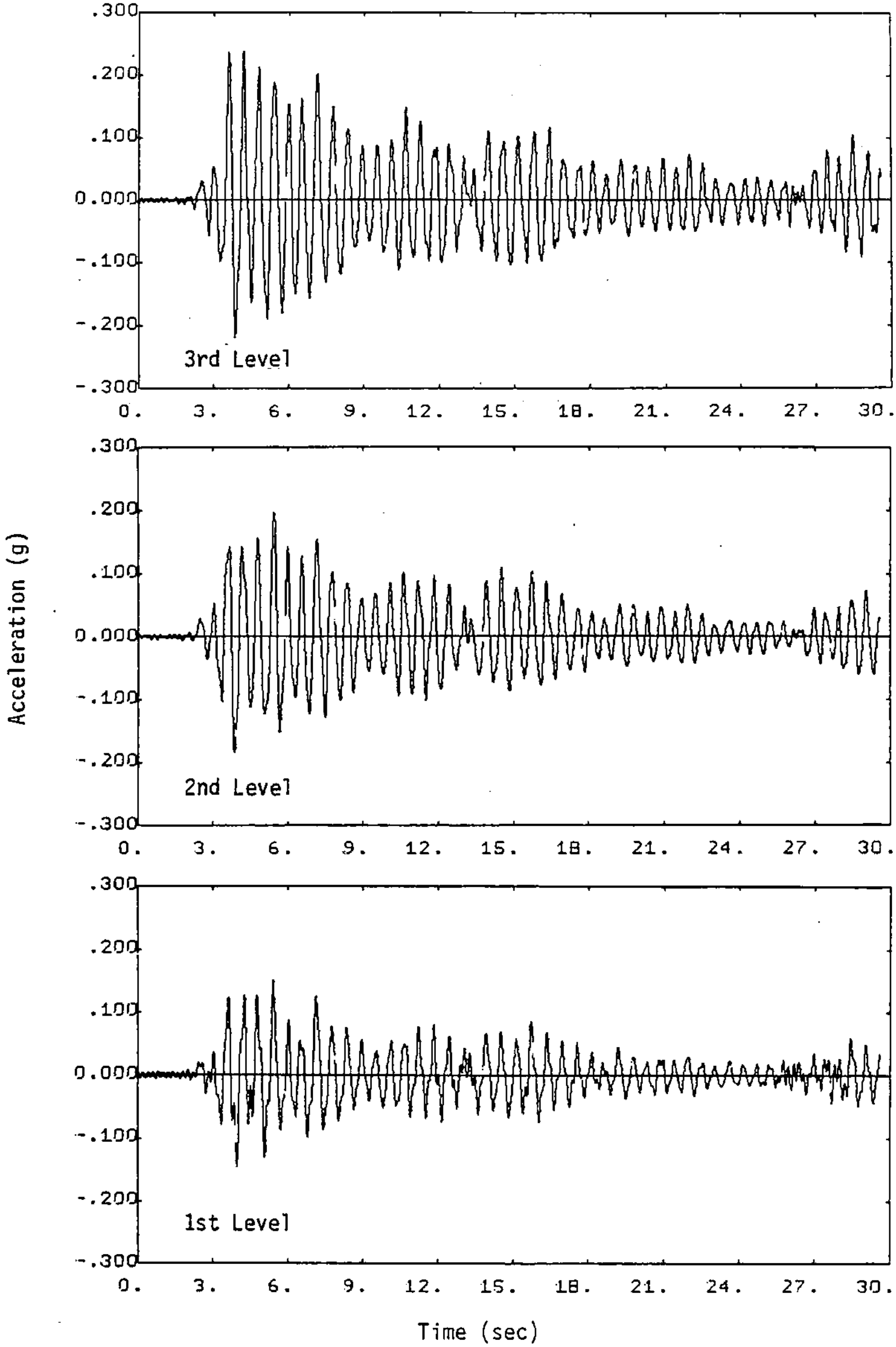

FIGURE 4.55a STORY ACCELERATIONS (CENTER FRAME) - TEST 200678.2 (DI-T-2/3-1/4 EC)

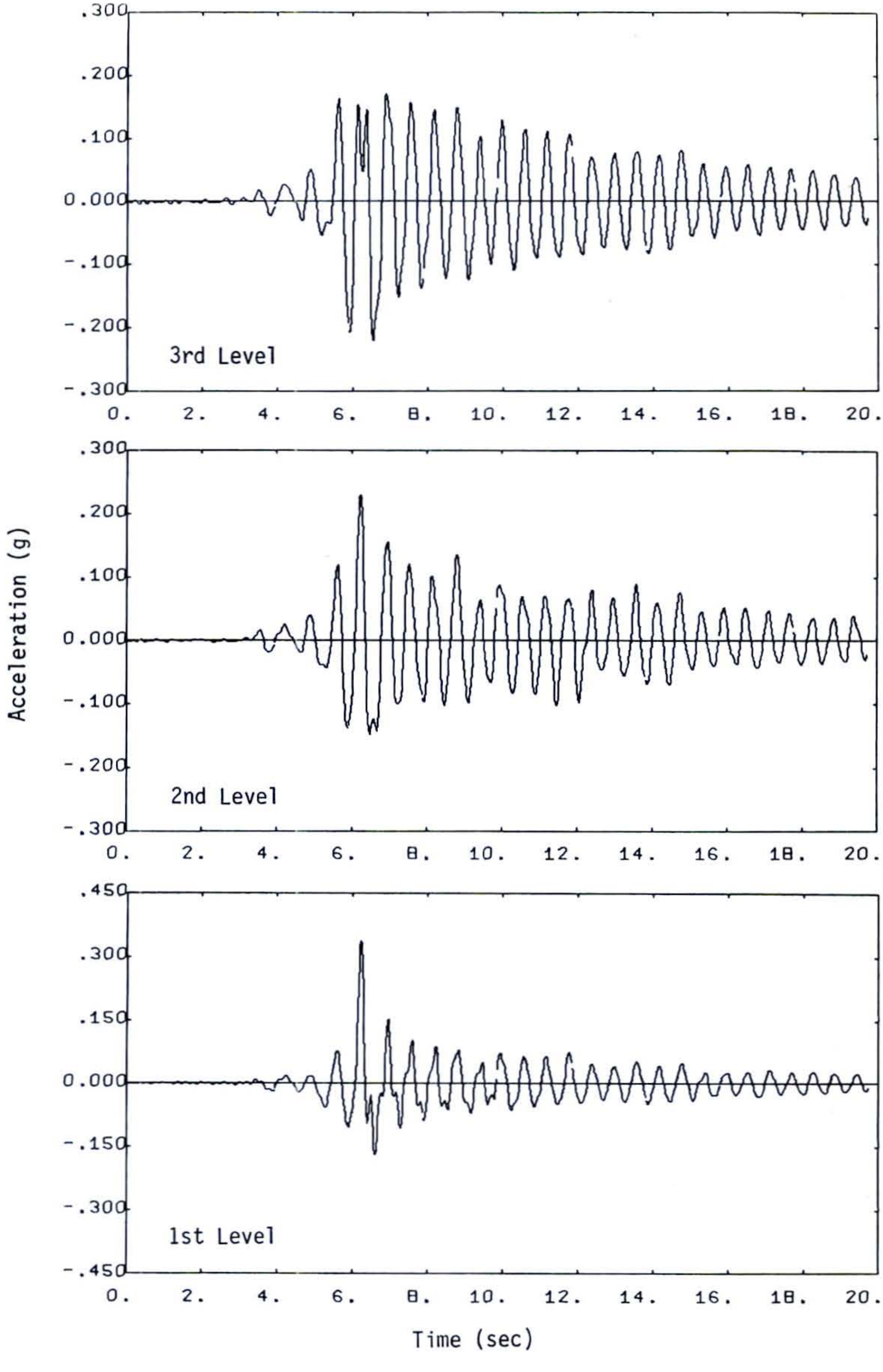

FIGURE 4.55b STORY ACCELERATIONS (CENTER FRAME) - TEST 200678.3 (DI-T-2/3-1/4 PF)

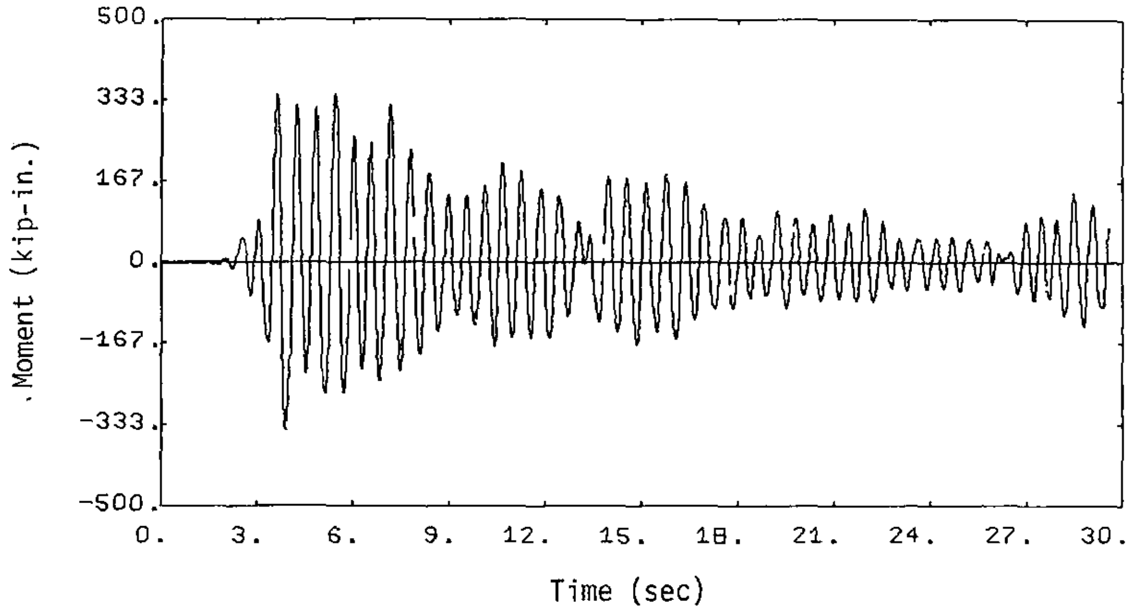

Base Overturning Moment

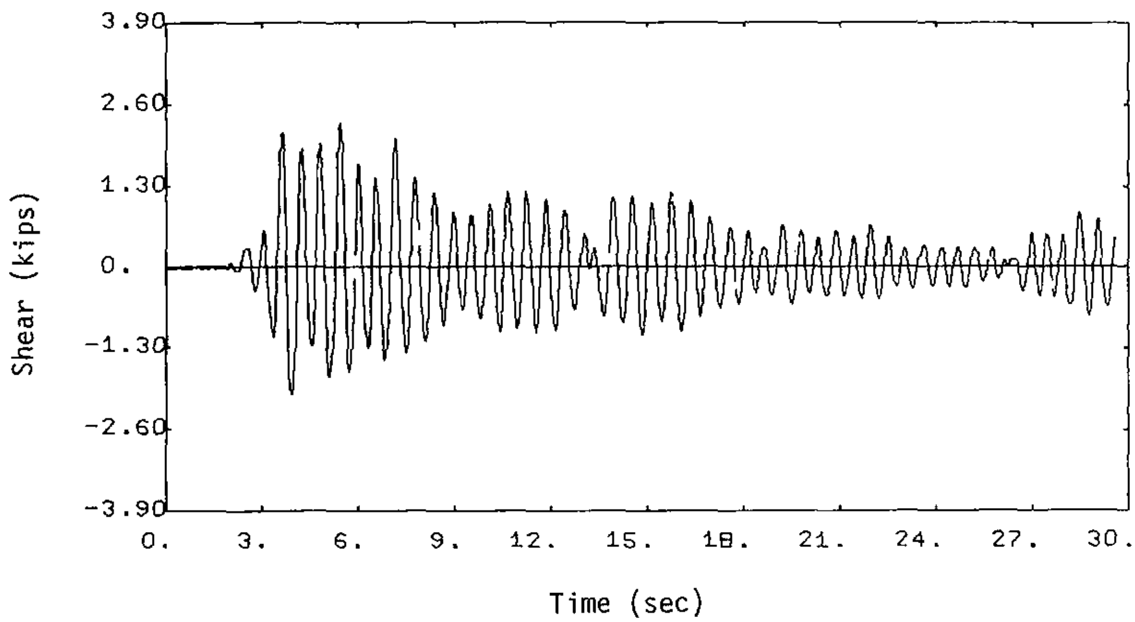

Base Shear

FIGURE 4.56a BASE SHEAR AND OVERTURNING MOMENT (CENTER FRAME) - TEST 200678.2 (DI-T-2/3-1/4 EC)

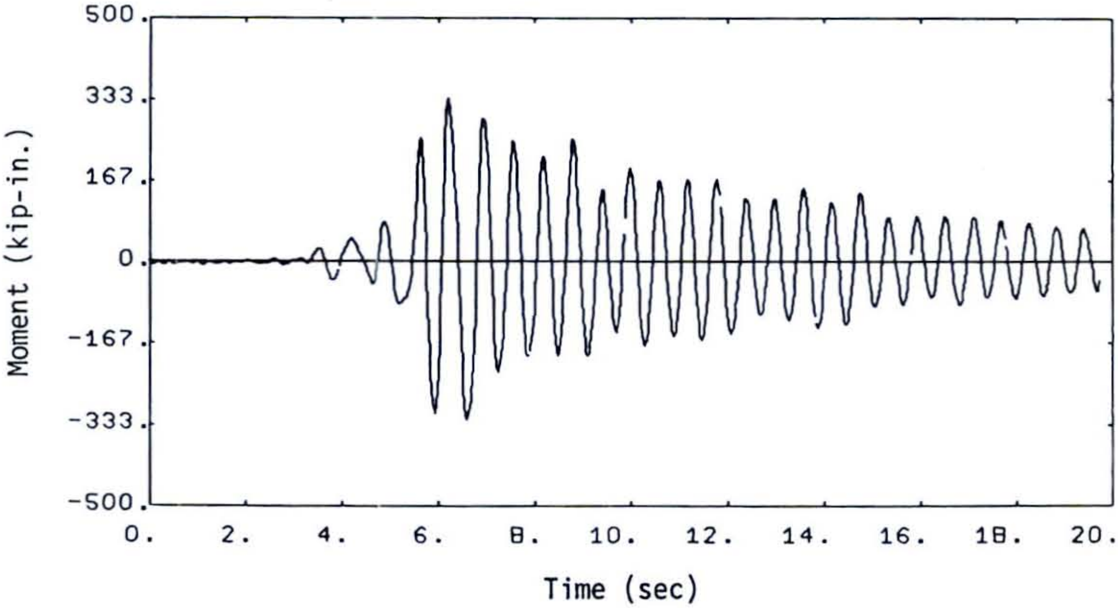

Base Overturning Moment

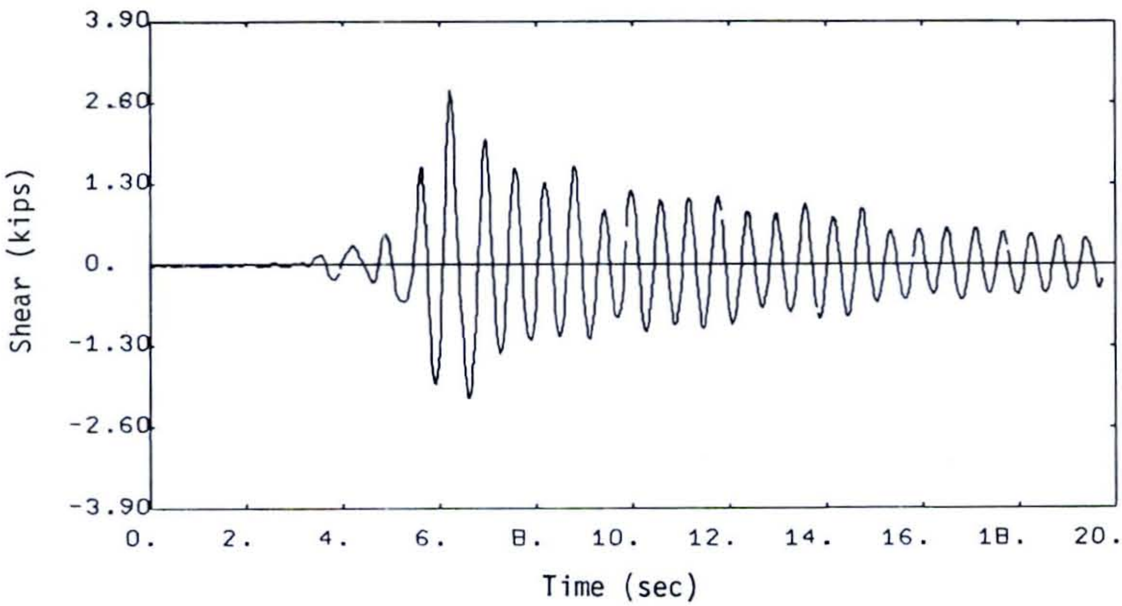

Base Shear

FIGURE 4.56b BASE SHEAR AND OVERTURNING MOMENT (CENTER FRAME) - TEST 200678.3 (DI-T-2/3-1/4 PF)

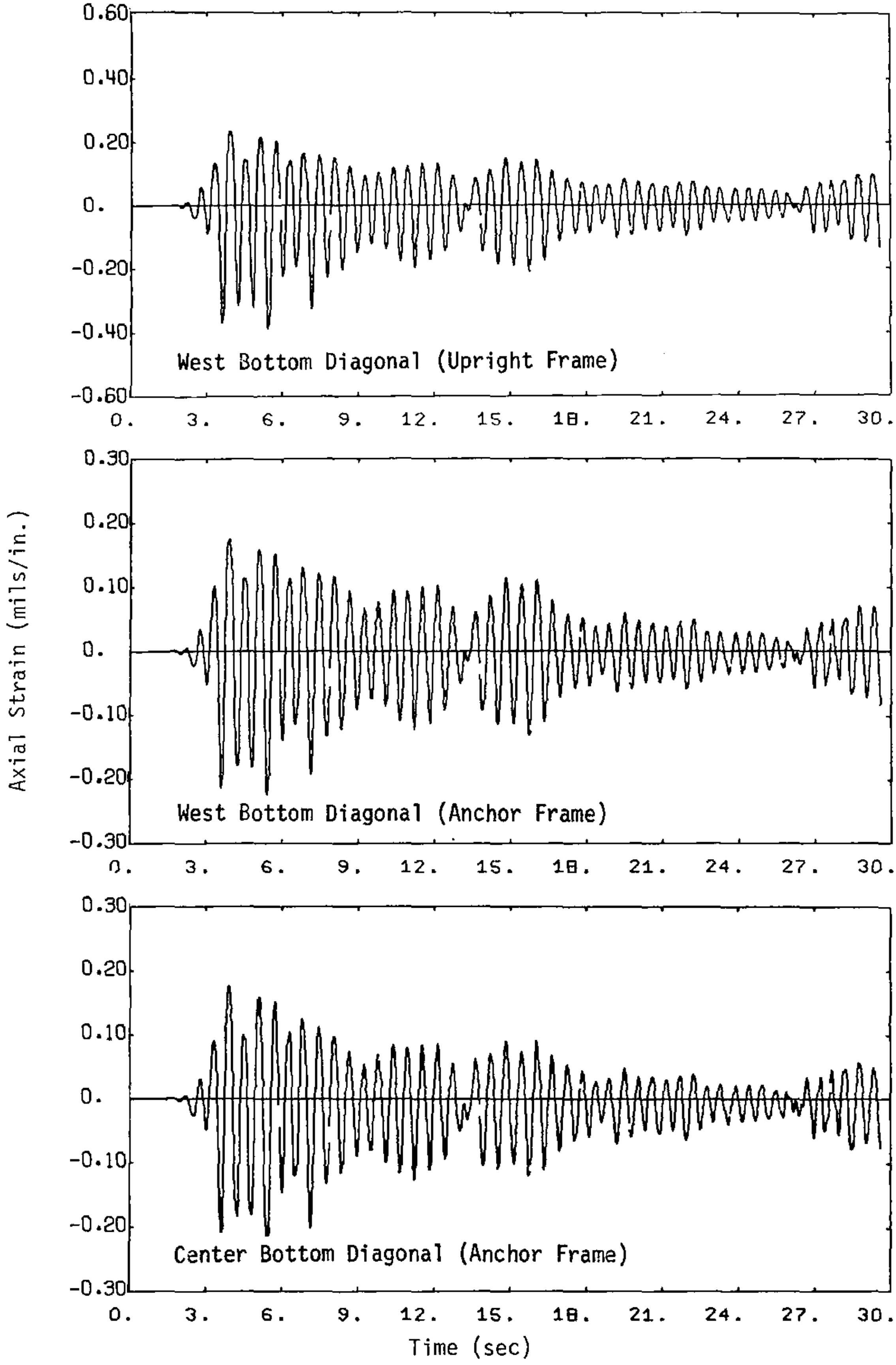

FIGURE 4.57a BRACE AXIAL STRAINS - TEST 200678.2 (DI-T-2/3-1/4 EC)

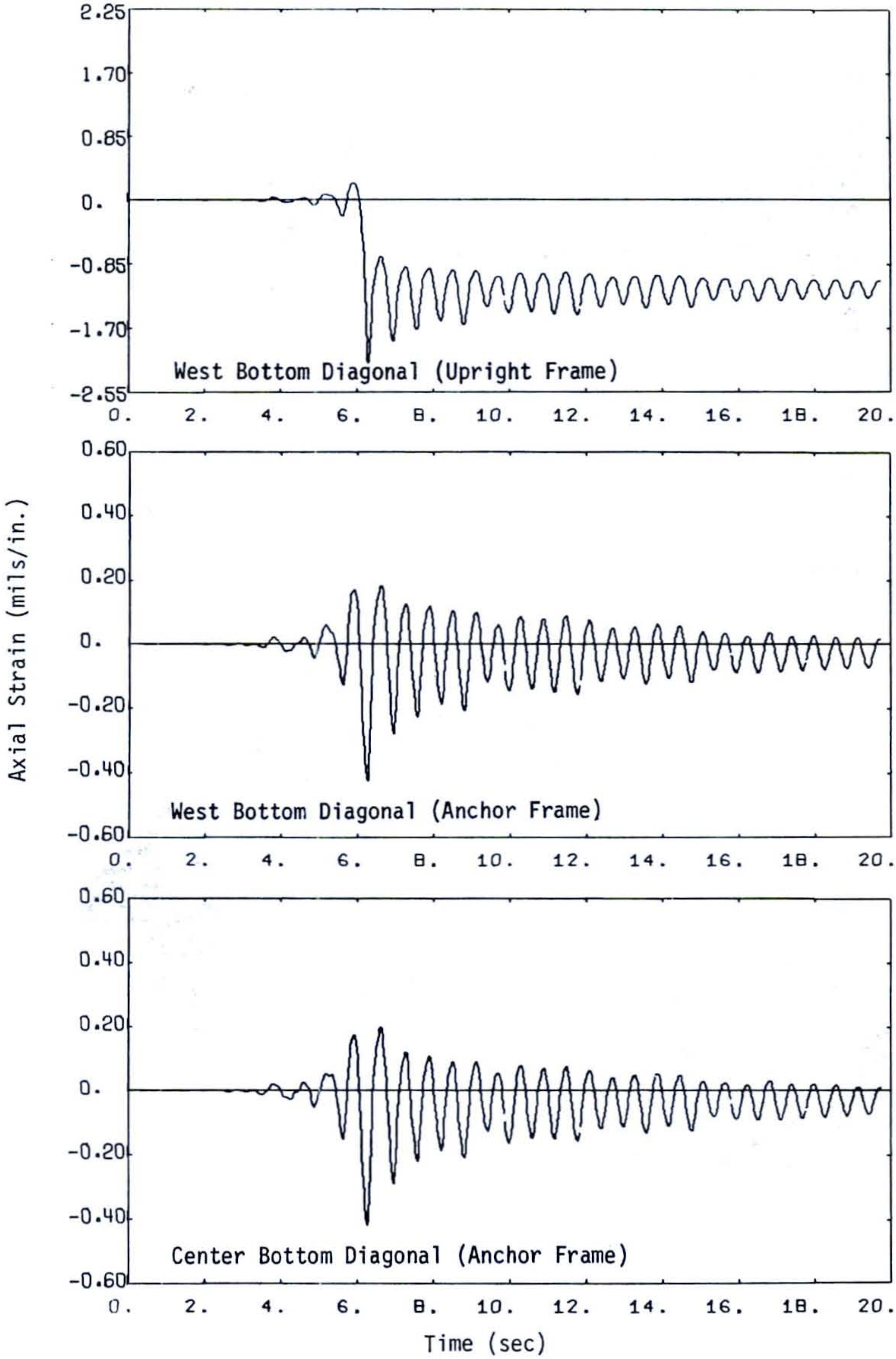

FIGURE 4.57b BRACE AXIAL STRAINS - TEST 200678.3 (DI-T-2/3-1/4 PF)

FIGURE 4.58 STRUCTURAL DAMAGE: DRIVE-IN RACK, TRANSVERSE DIRECTION

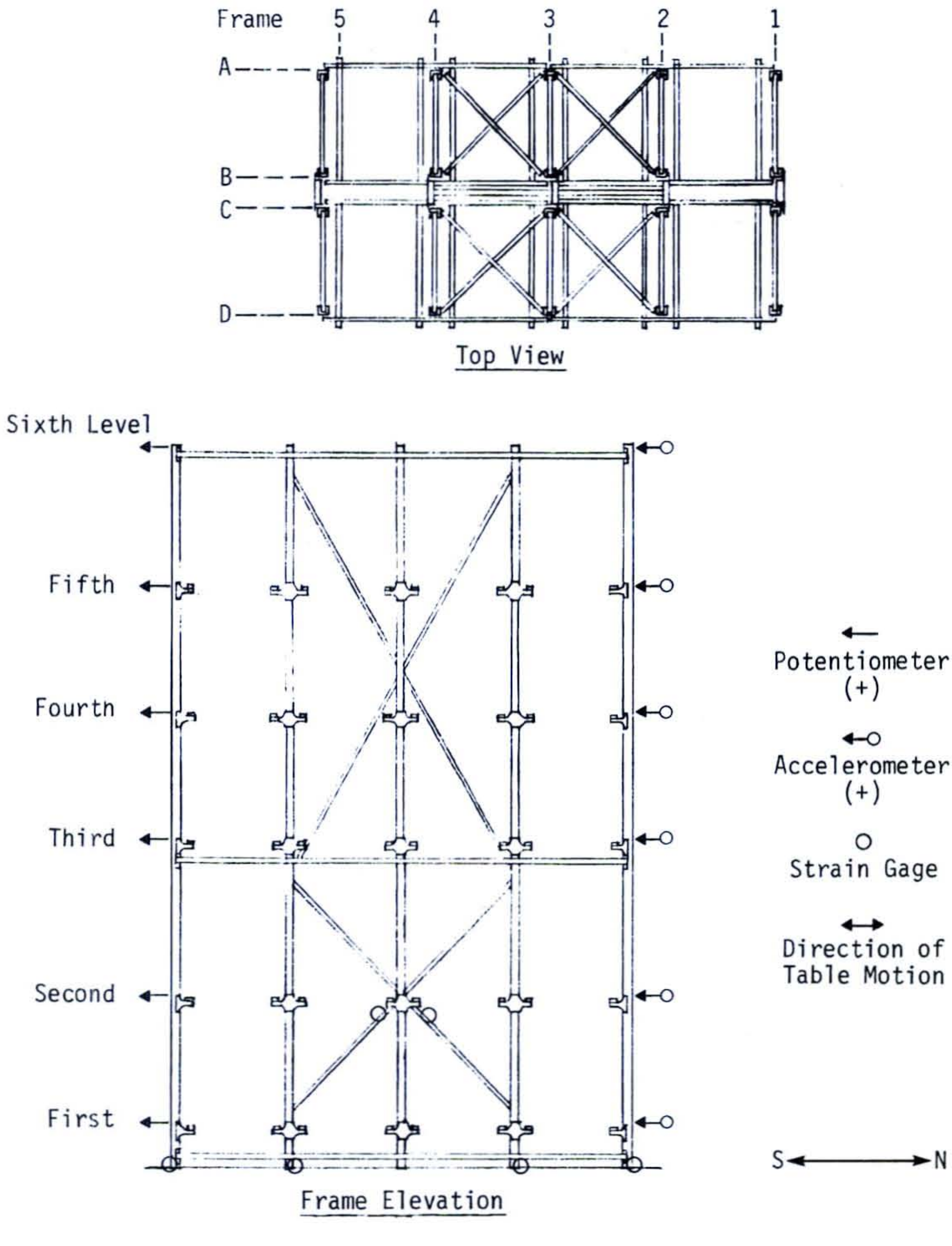

FIGURE 4.59 INSTRUMENTATION CHANNELS USED FOR DATA ANALYSIS: STACKER RACK, LONGITUDINAL DIRECTION

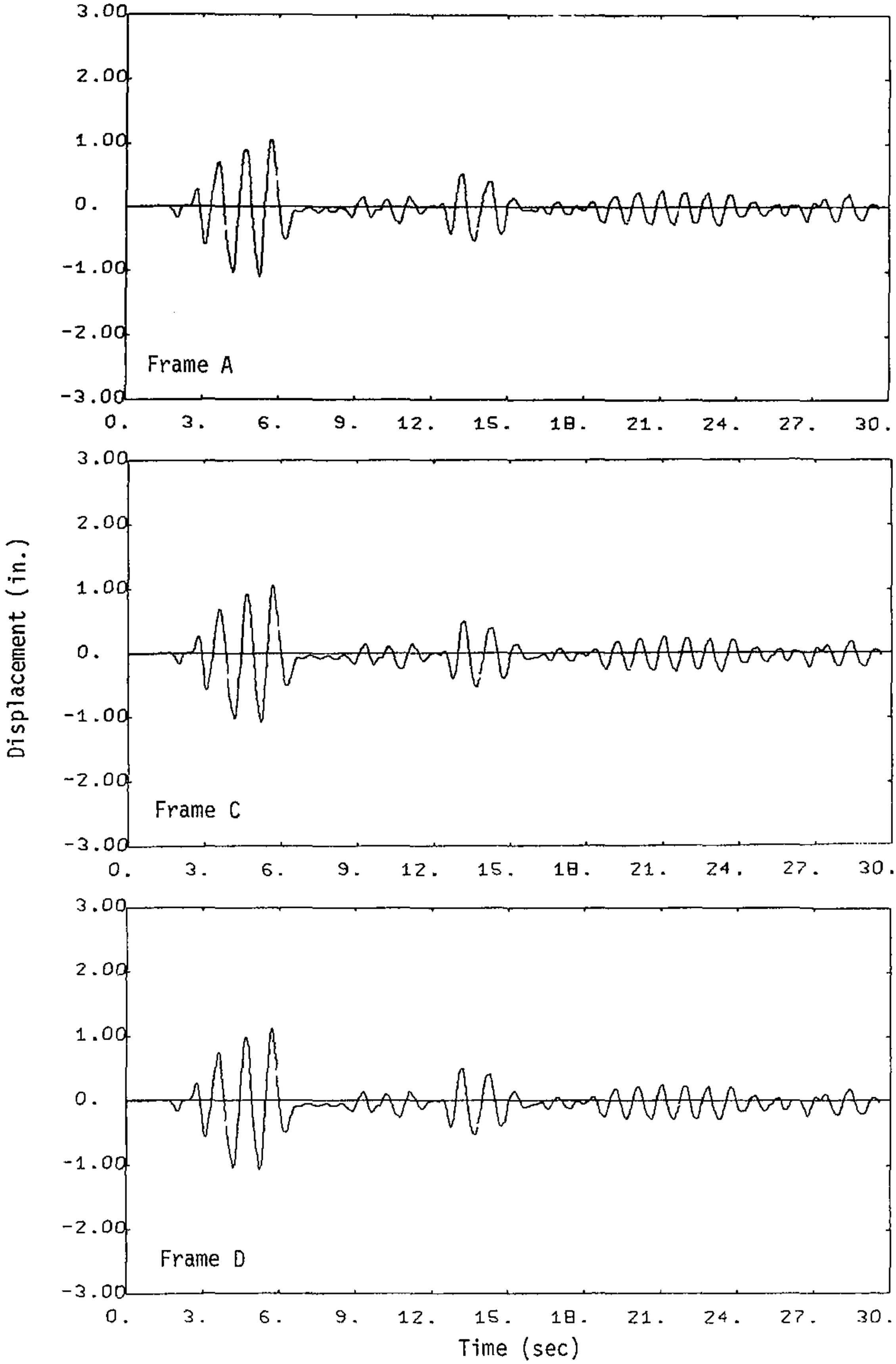

FIGURE 4.60 6TH LEVEL DISPLACEMENTS RELATIVE TO THE TABLE - TEST 221178.1 (ST-L-1-1/4 EC)

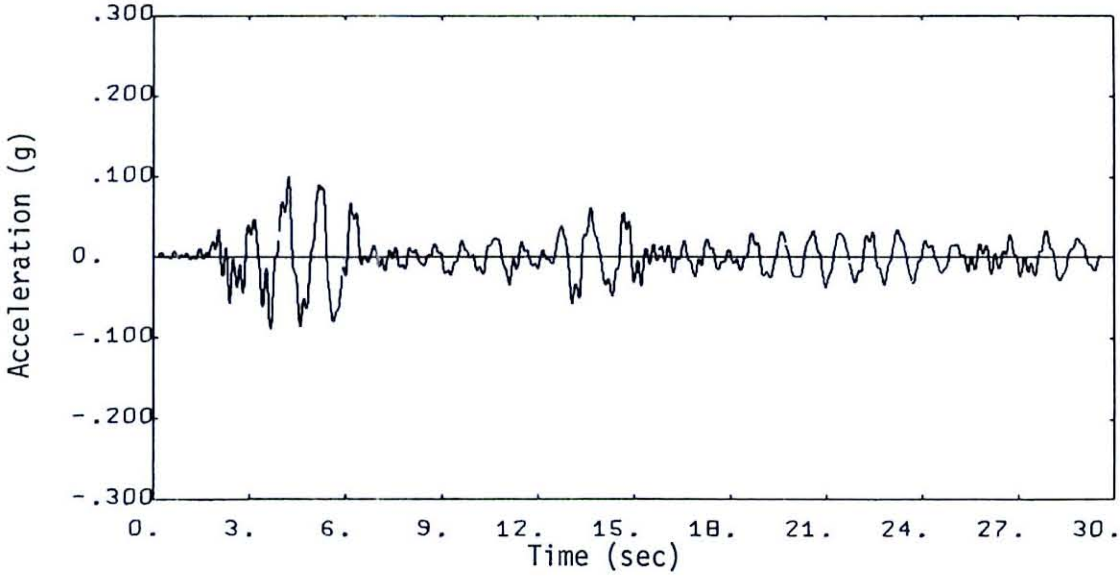

Frame A

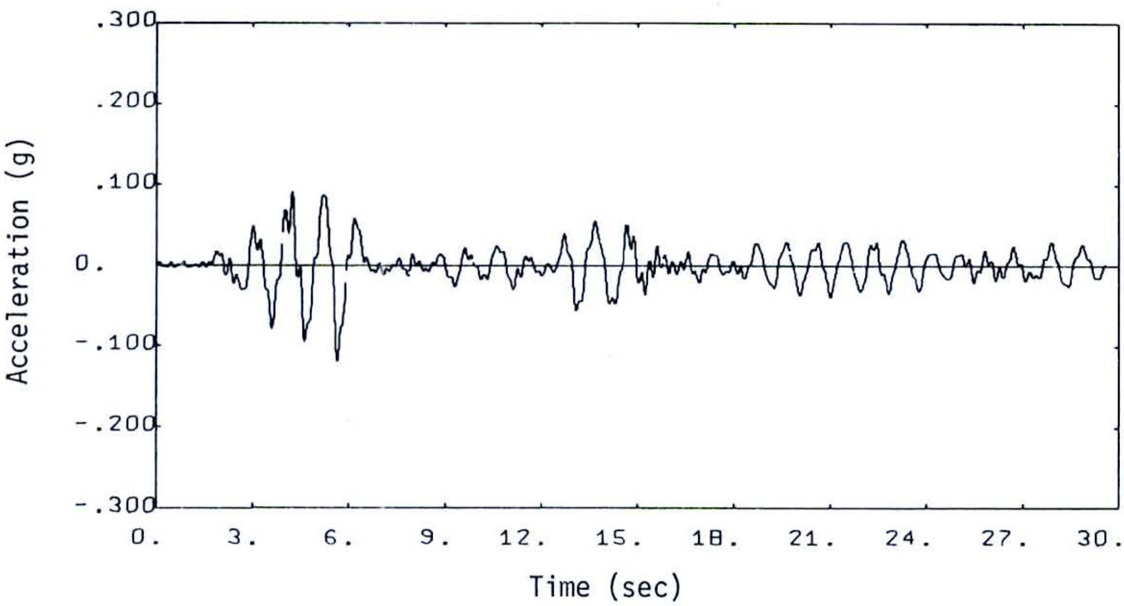

Frame C

FIGURE 4.61 6TH LEVEL ACCELERATIONS - TEST 221178.1 (ST-L-1-1/4 EC)

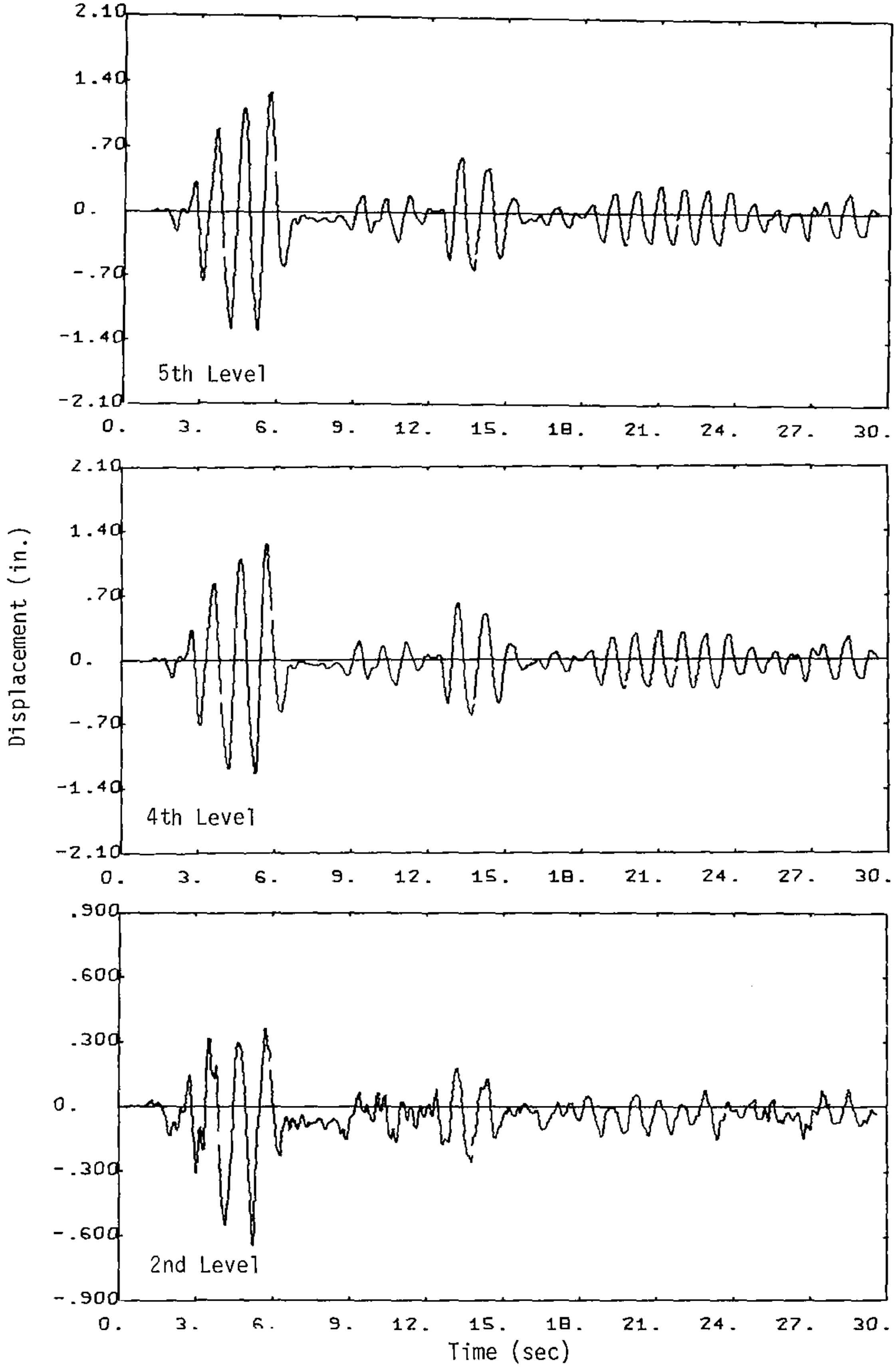

FIGURE 4.62a STORY DISPLACEMENTS RELATIVE TO THE TABLE (FRAME C) - TEST 221178.1 (ST-L-1-1/4 EC)

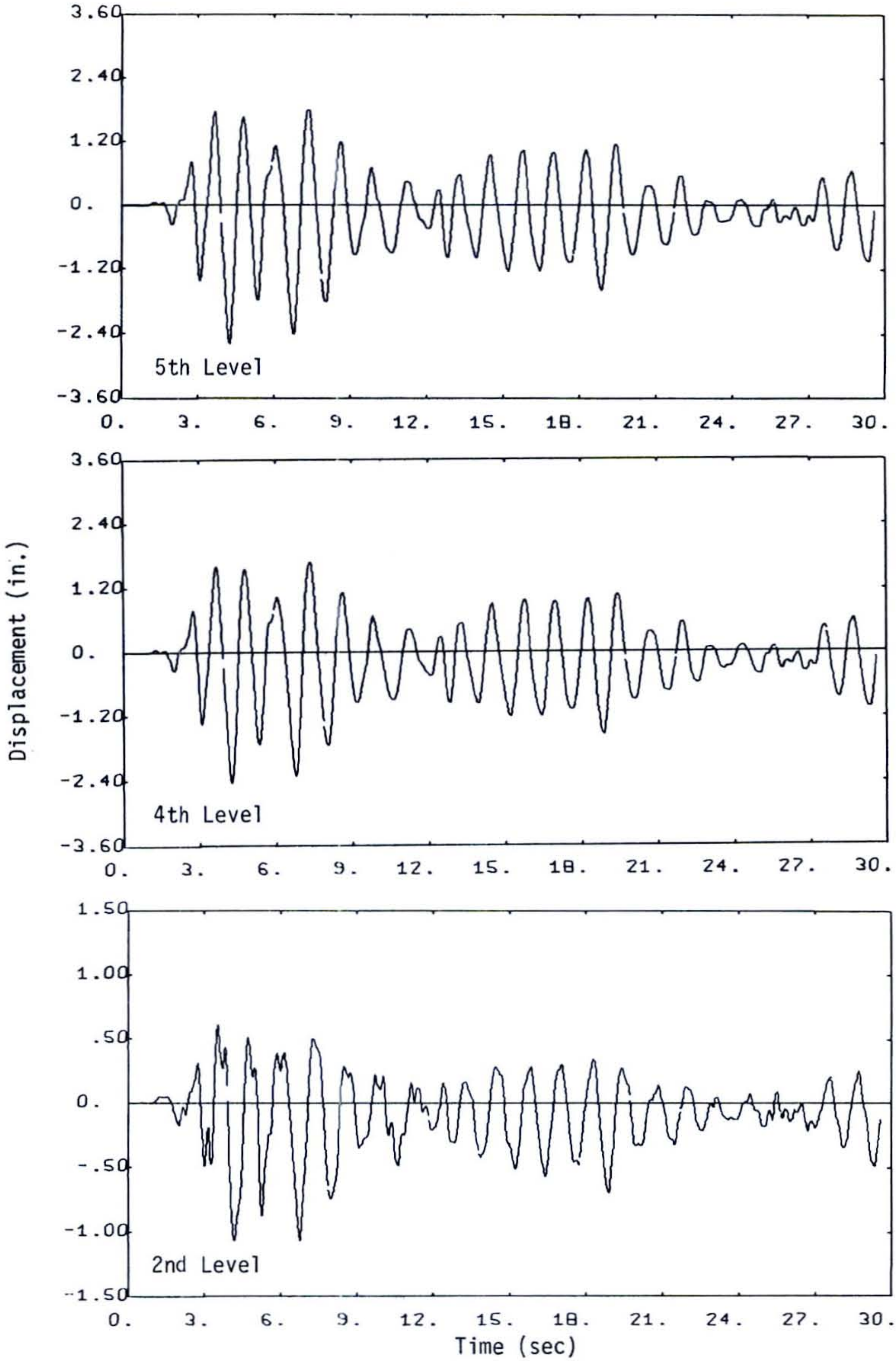

FIGURE 4.62b STORY DISPLACEMENTS RELATIVE TO THE TABLE (FRAME C) - TEST 221178.3 (ST-L-1-1/2 EC)

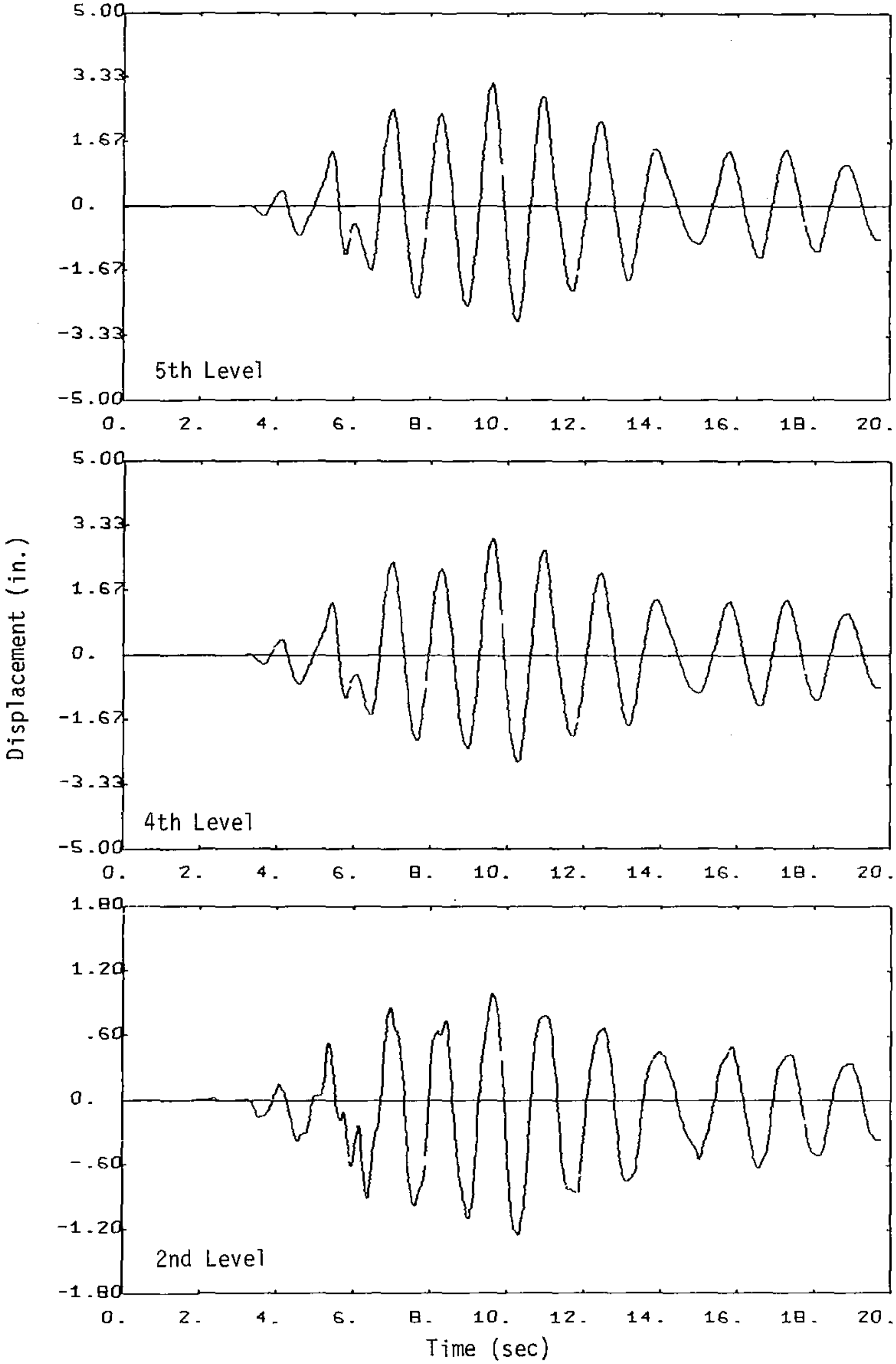

FIGURE 4.62c STORY DISPLACEMENTS RELATIVE TO THE TABLE (FRAME C) - TEST 221178.4 (ST-L-1-1/2 PF)

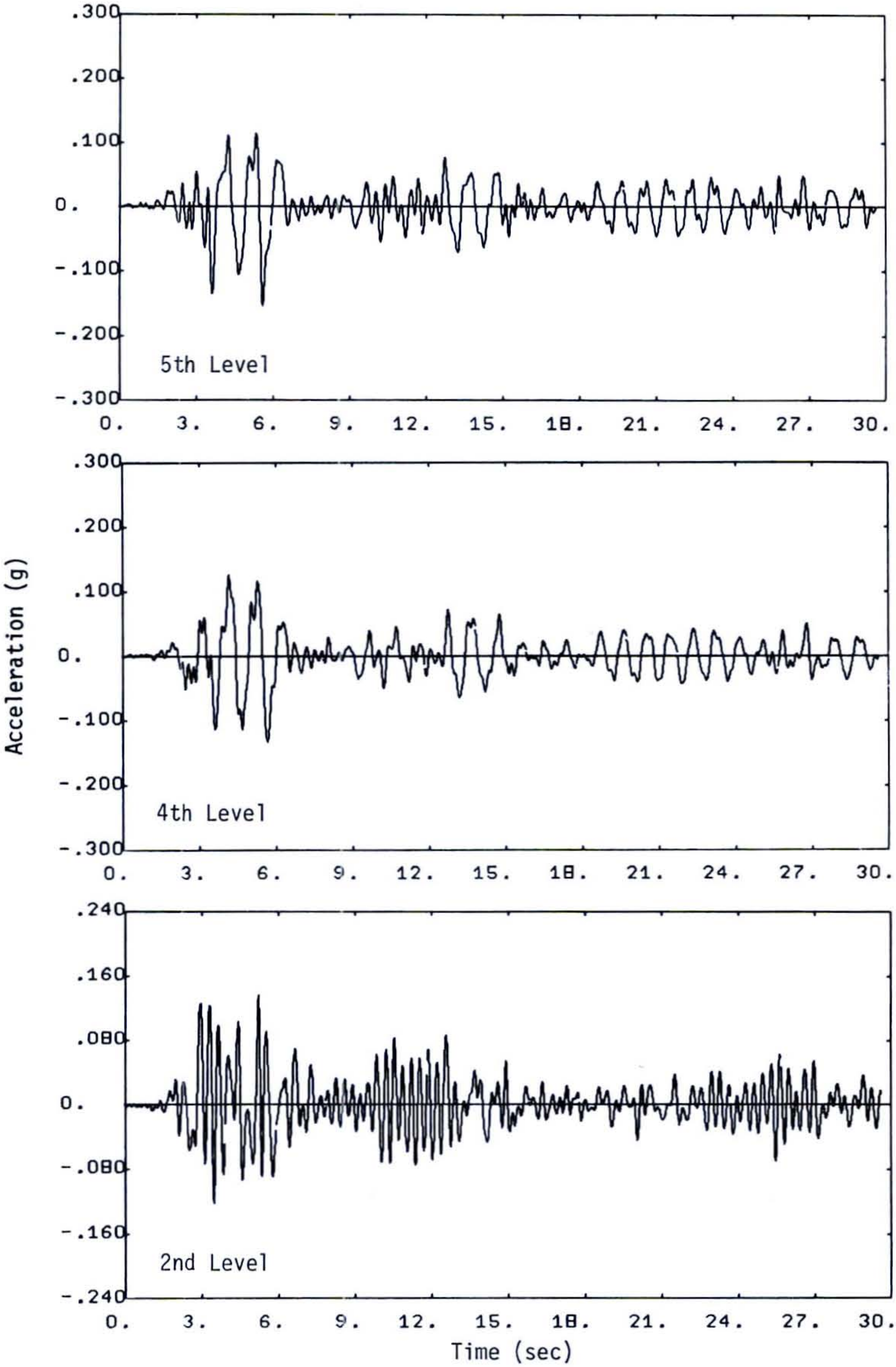

FIGURE 4.63a STORY ACCELERATIONS (FRAME C) - TEST 221178.1 (ST-L-1-1/4 EC)

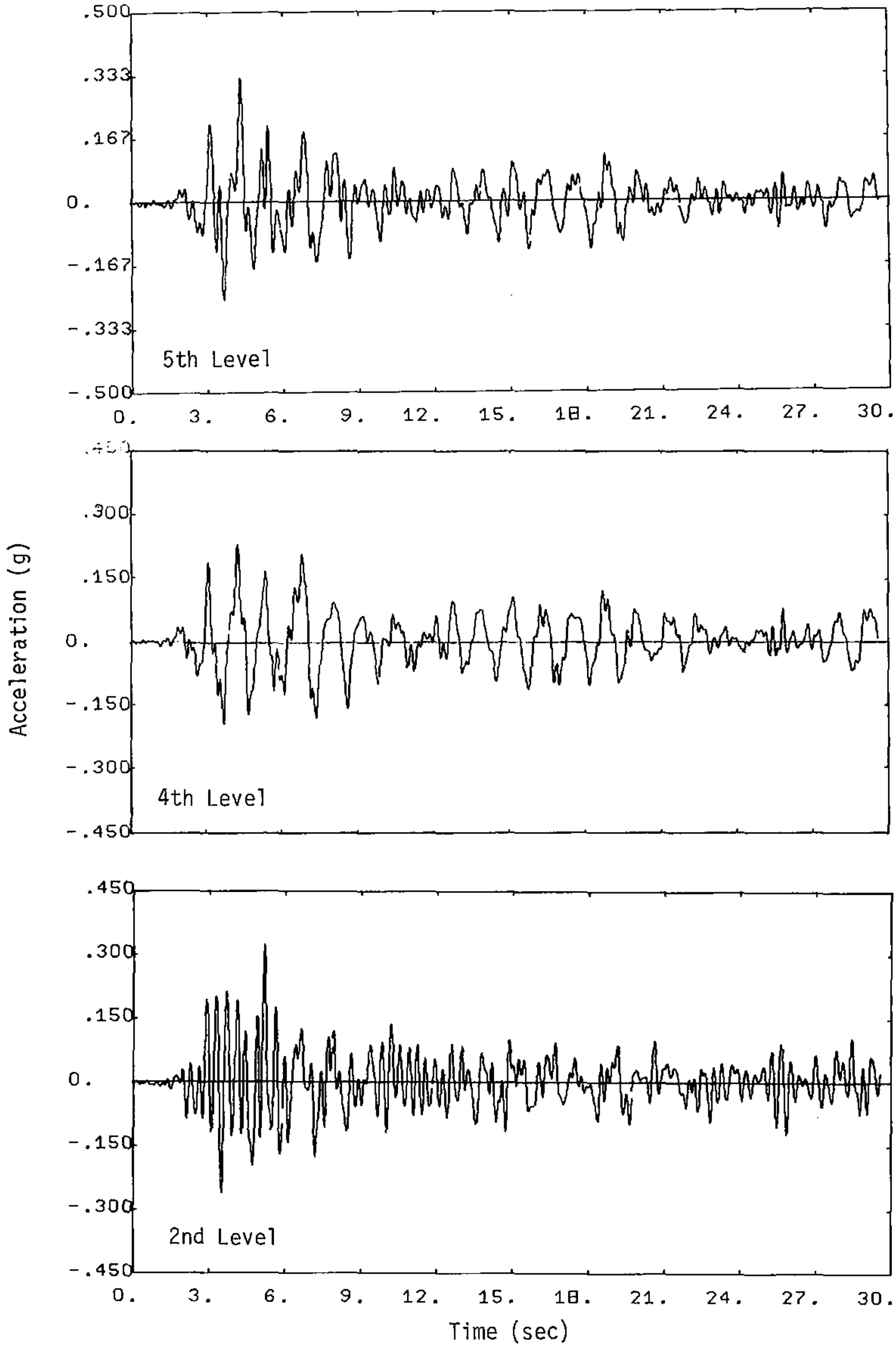

FIGURE 4.63b STORY ACCELERATIONS (FRAME C) - TEST 221178.3 (ST-L-1-1/2 EC)

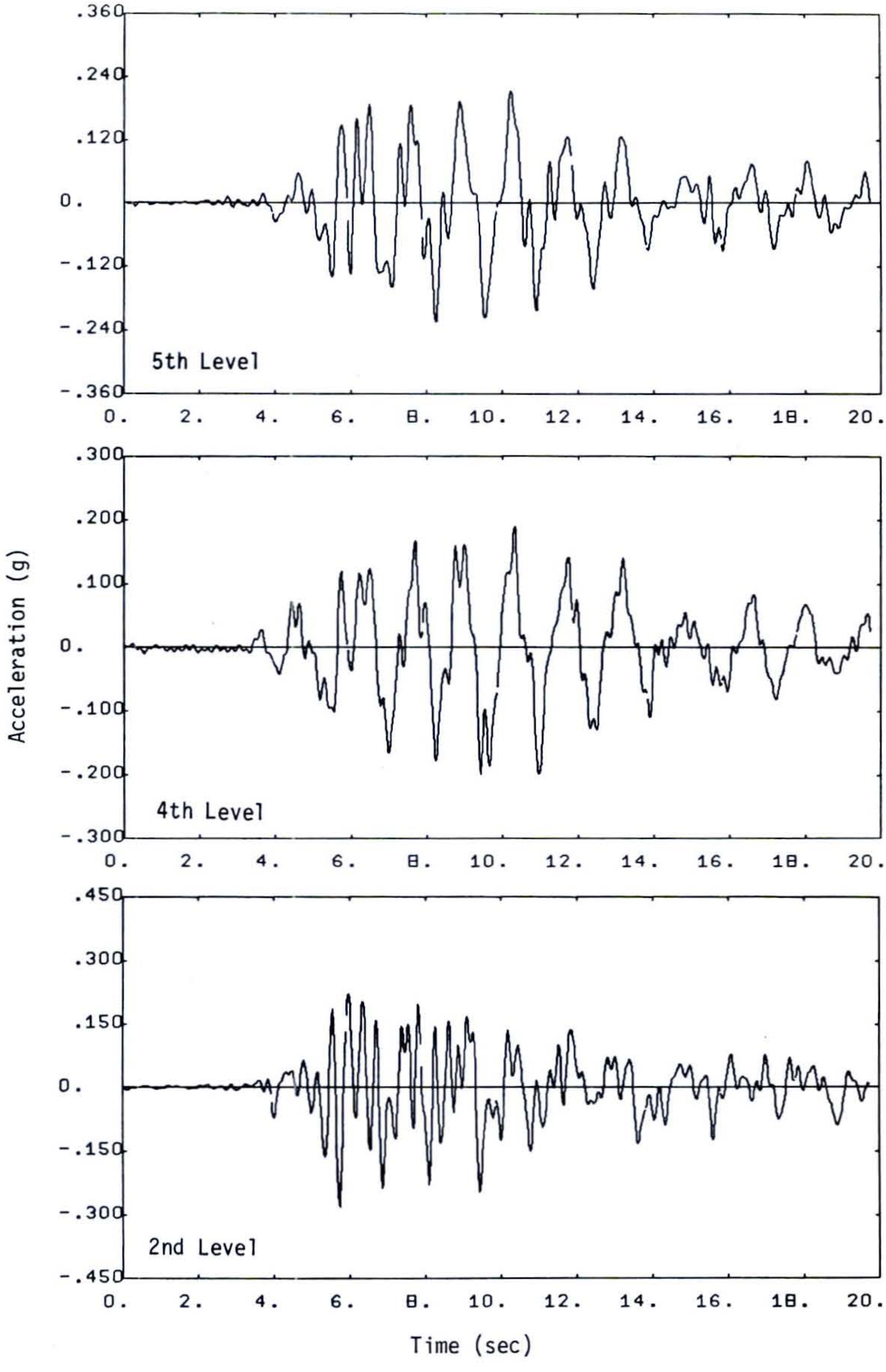

FIGURE 4.63c STORY ACCELERATIONS (FRAME C) - TEST 221178.4
(ST-L-1-1/2 PF)

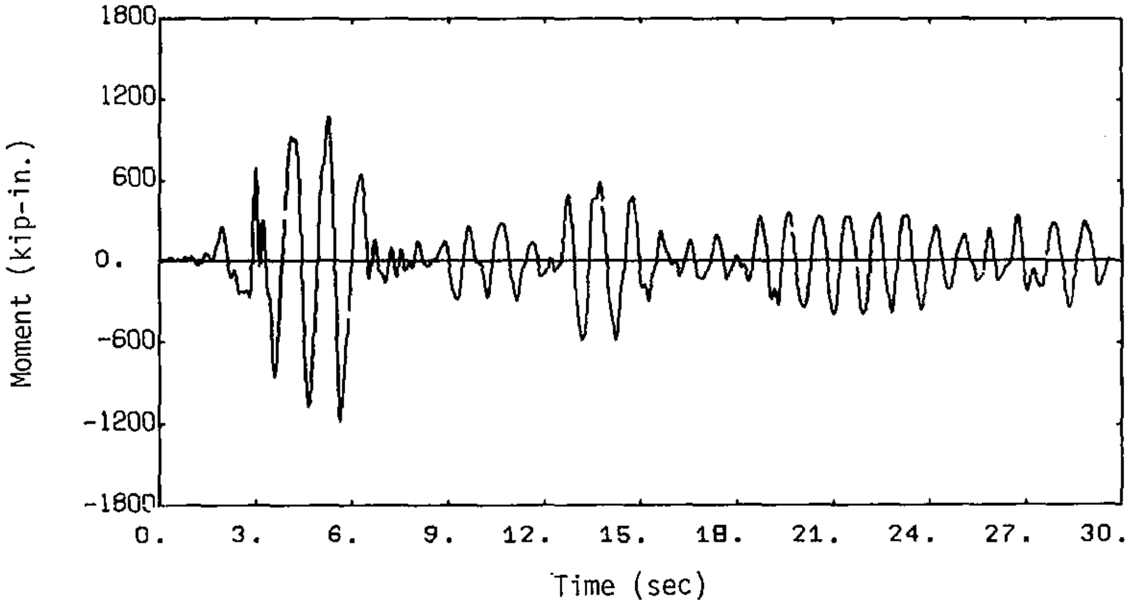

Base Overturning Moment

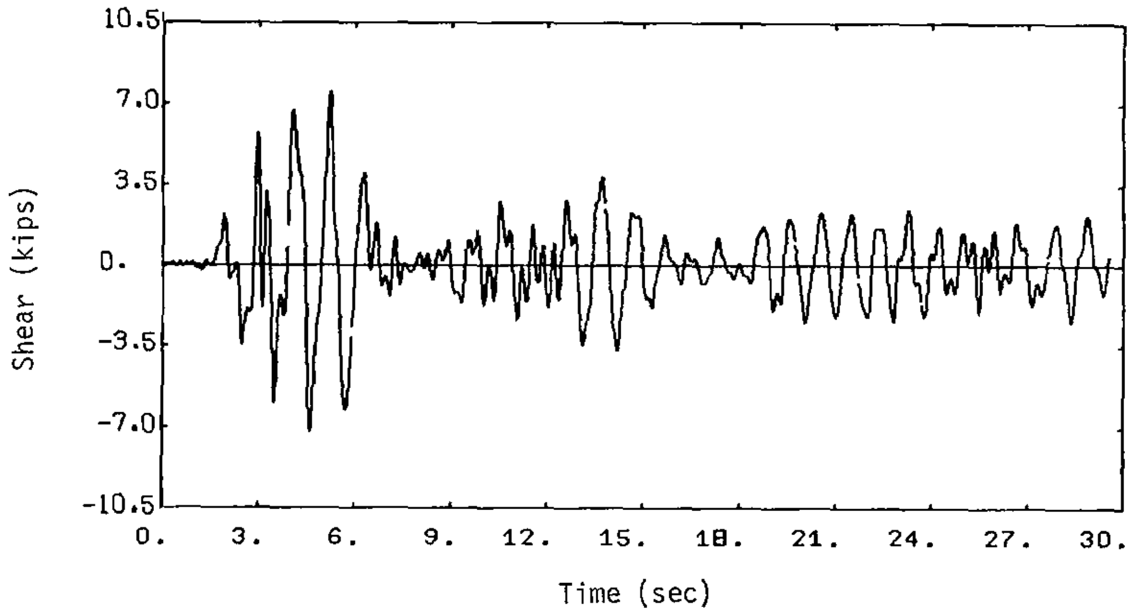

Base Shear

FIGURE 4.64a BASE SHEAR AND OVERTURNING MOMENT - TEST 221178.1 (ST-L-1-1/4 EC)

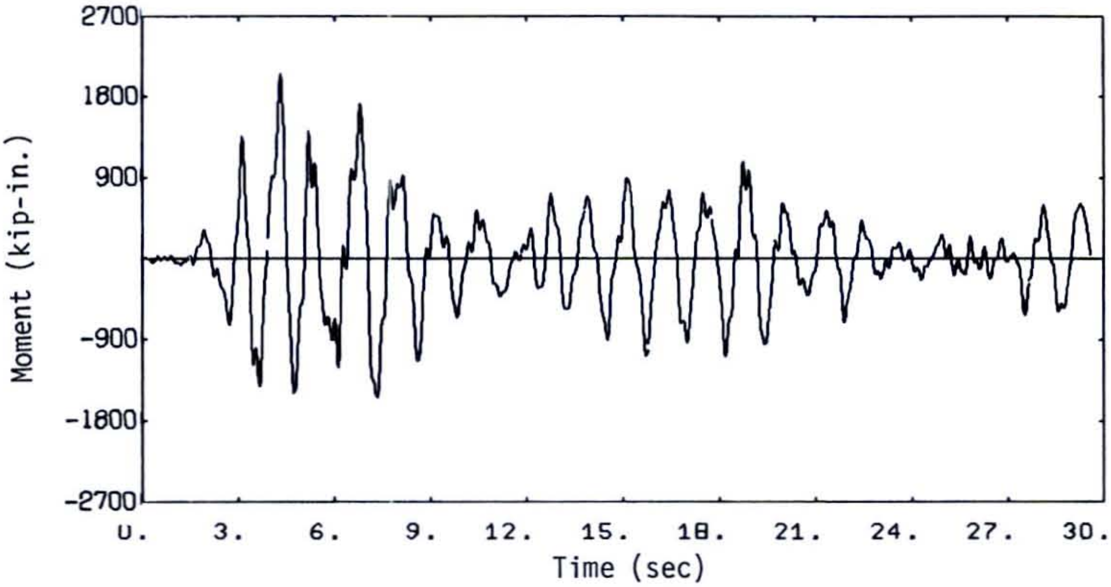

Base Overturning Moment

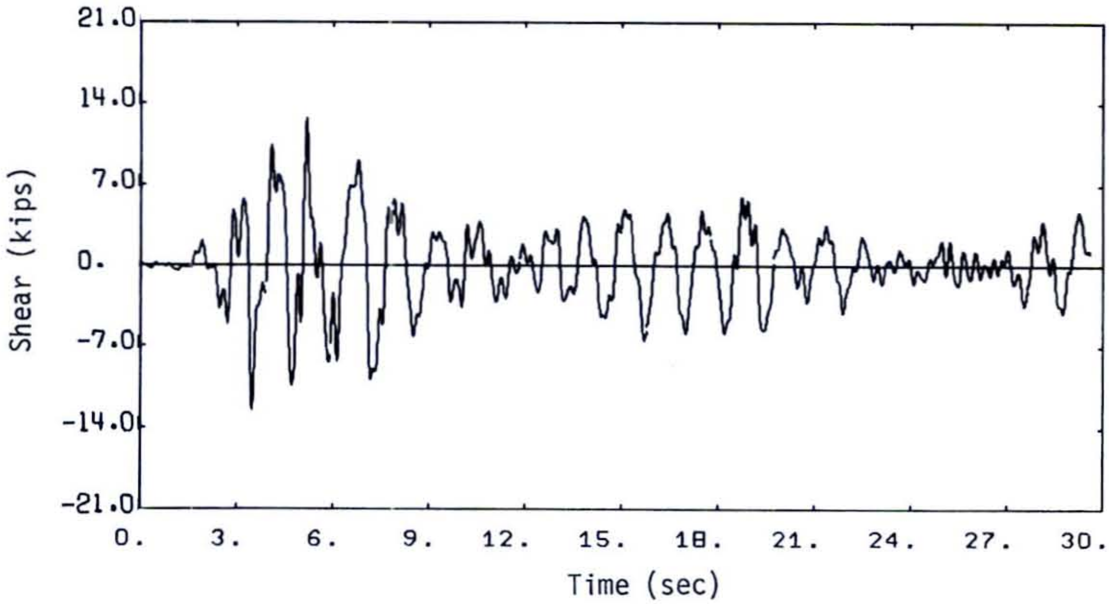

Base Shear

FIGURE 4.64b BASE SHEAR AND OVERTURNING MOMENT - TEST 221178.3 (ST-L-1-1/2 EC)

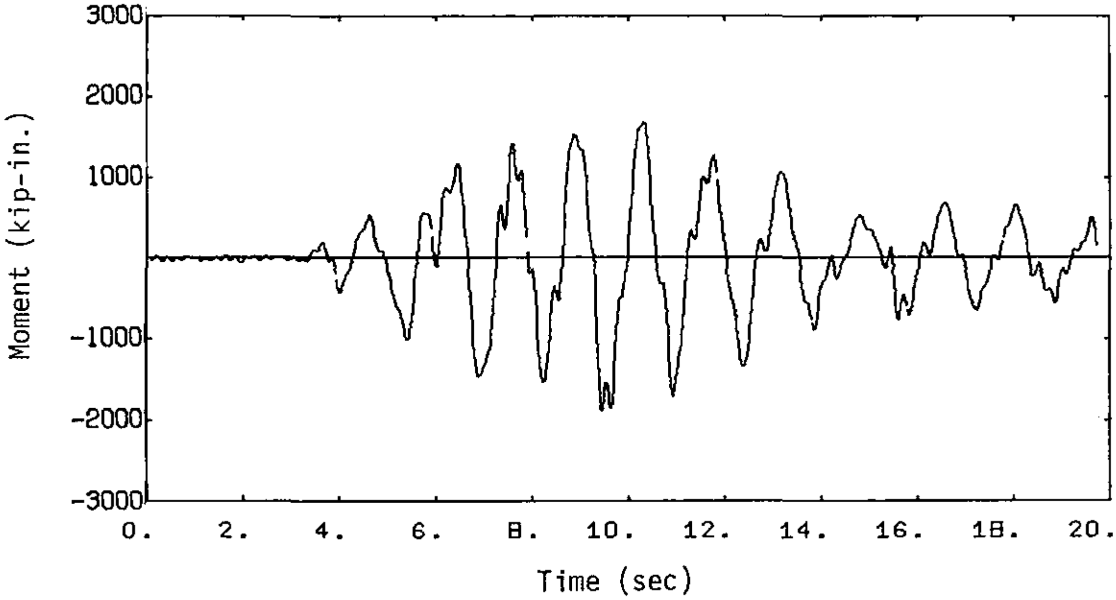

Base Overturning Moment

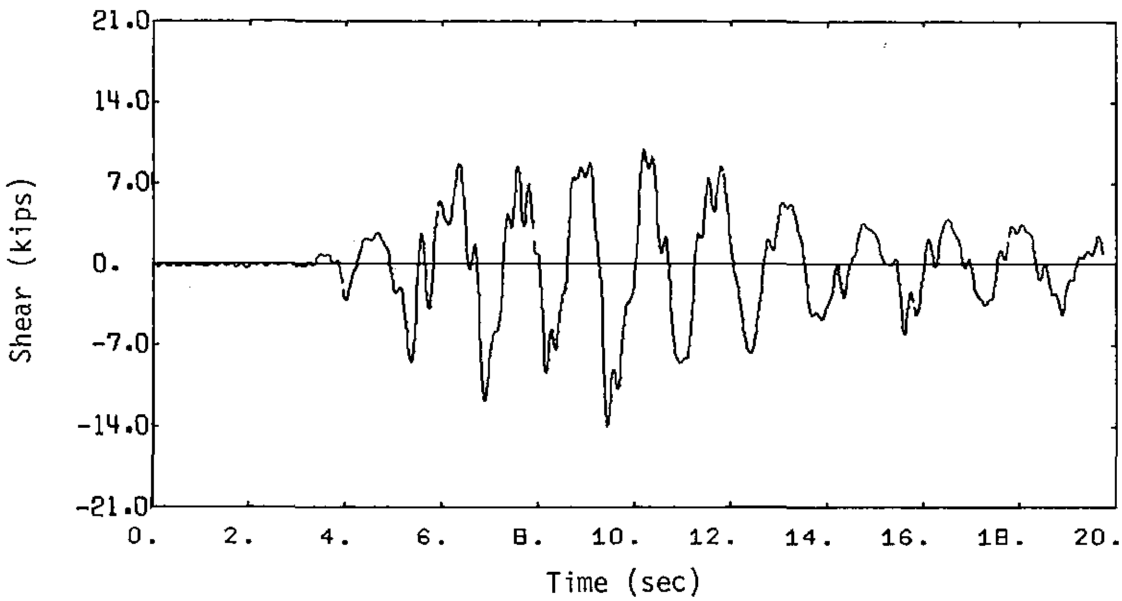

Base Shear

FIGURE 4.64c BASE SHEAR AND OVERTURNING MOMENT - TEST 221178.4 (ST-L-1-1/2 PF)

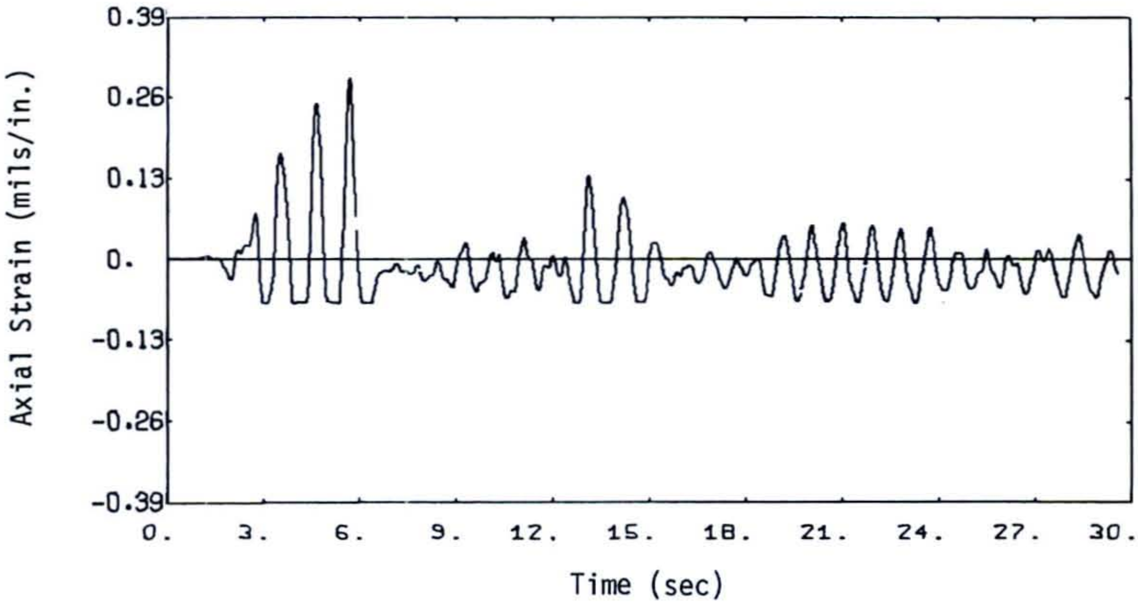

Diagonal Rod 1

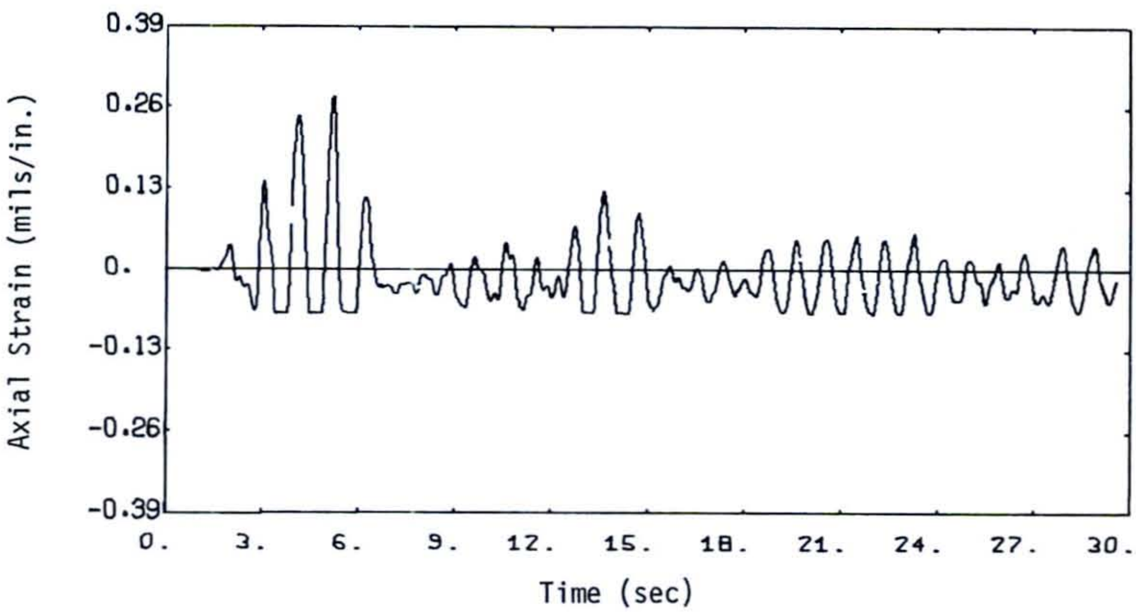

Diagonal Rod 2

FIGURE 4.65a BRACE AXIAL STRAINS - TEST 221178.1 (ST-L-1-1/4 EC)

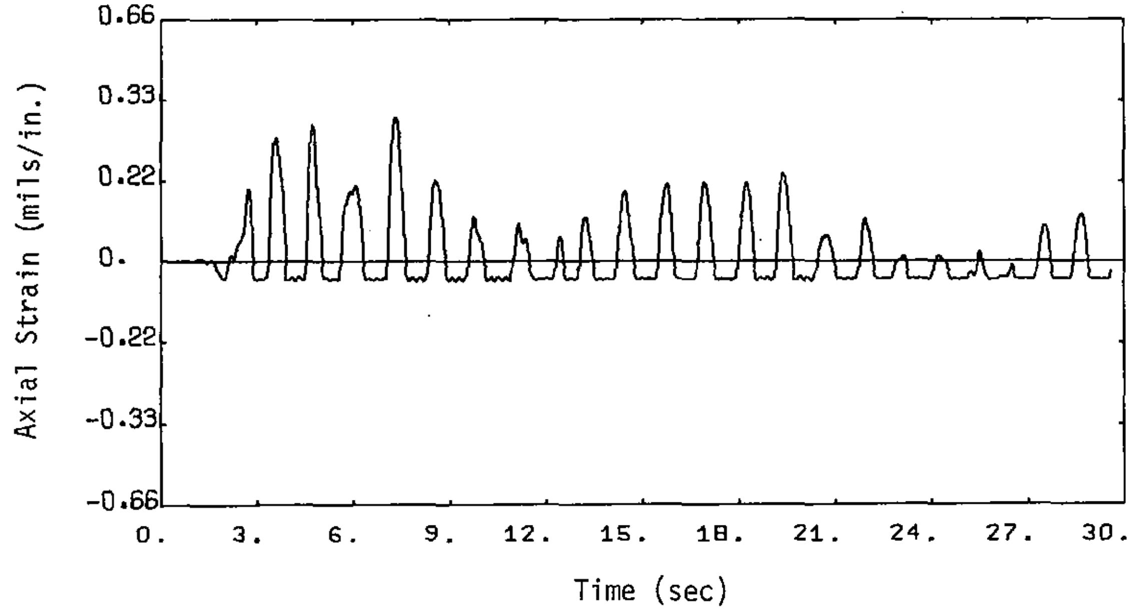

Diagonal Rod 1

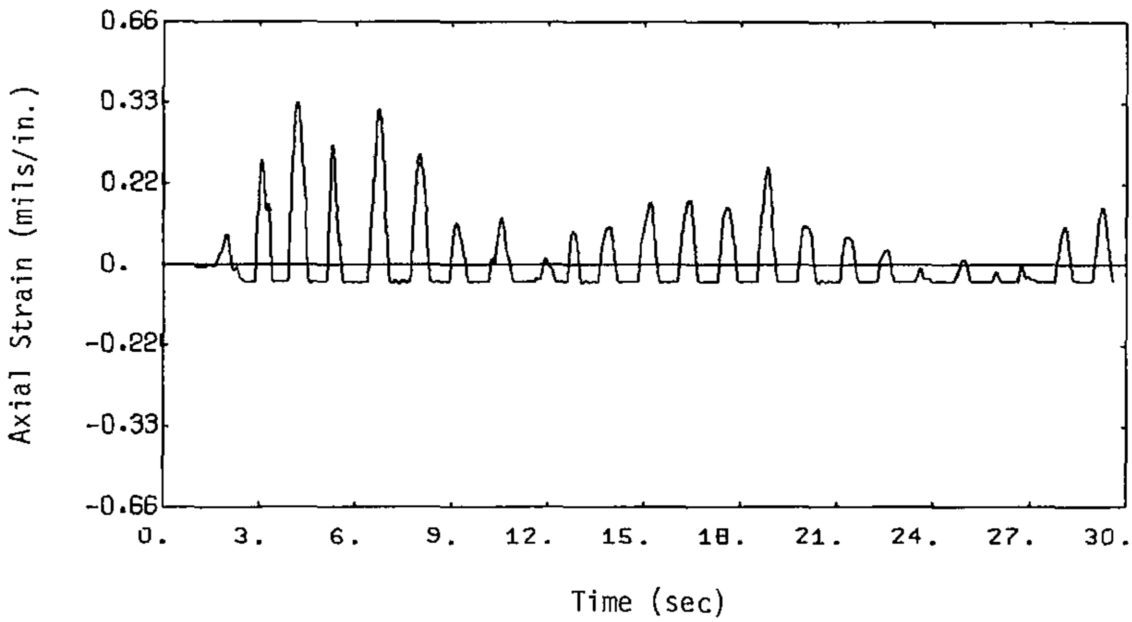

Diagonal Rod 2

FIGURE 4.65b BRACE AXIAL STRAINS - TEST 221178.3 (ST-L-1-1/2 EC)

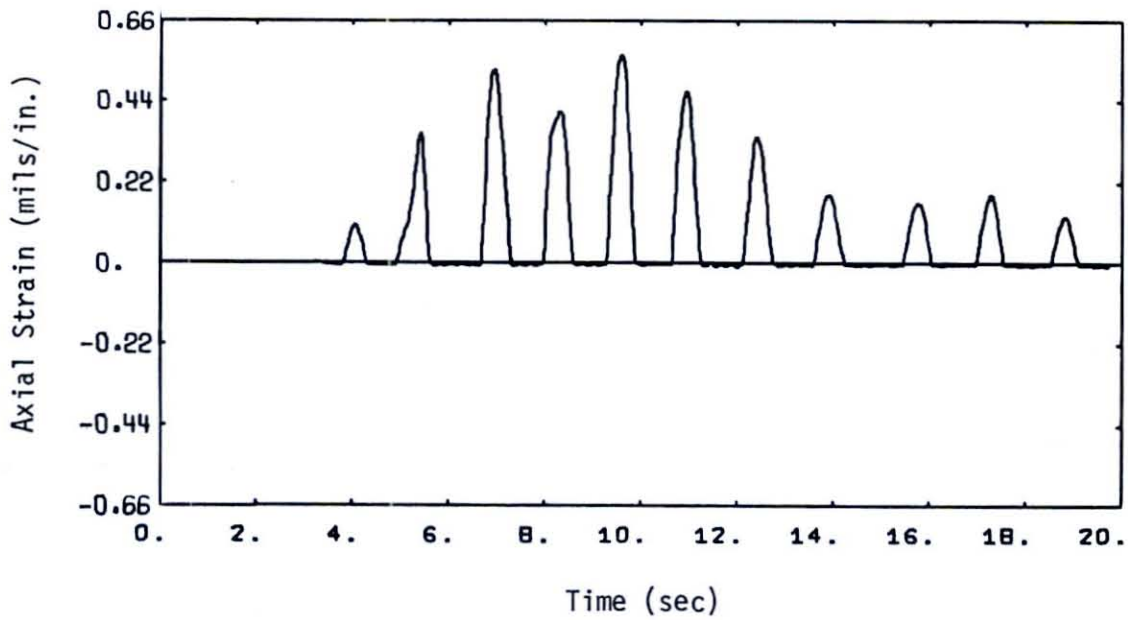

Diagonal Rod 1

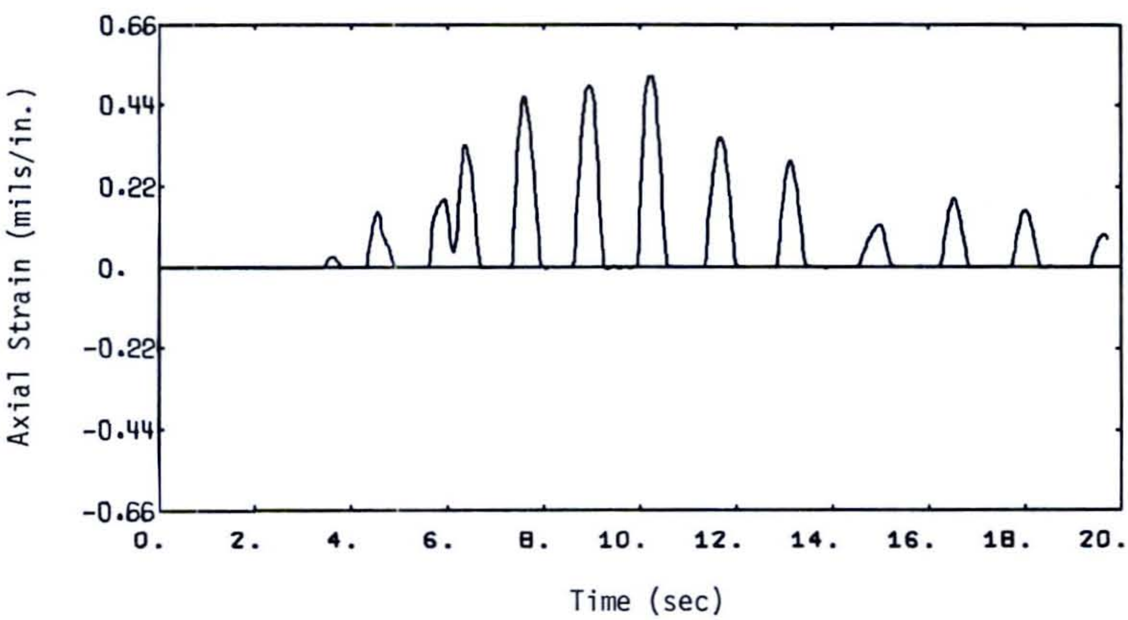

Diagonal Rod 2

FIGURE 4.65c BRACE AXIAL STRAINS - TEST 221178.4 (ST-L-1-1/2 PF)

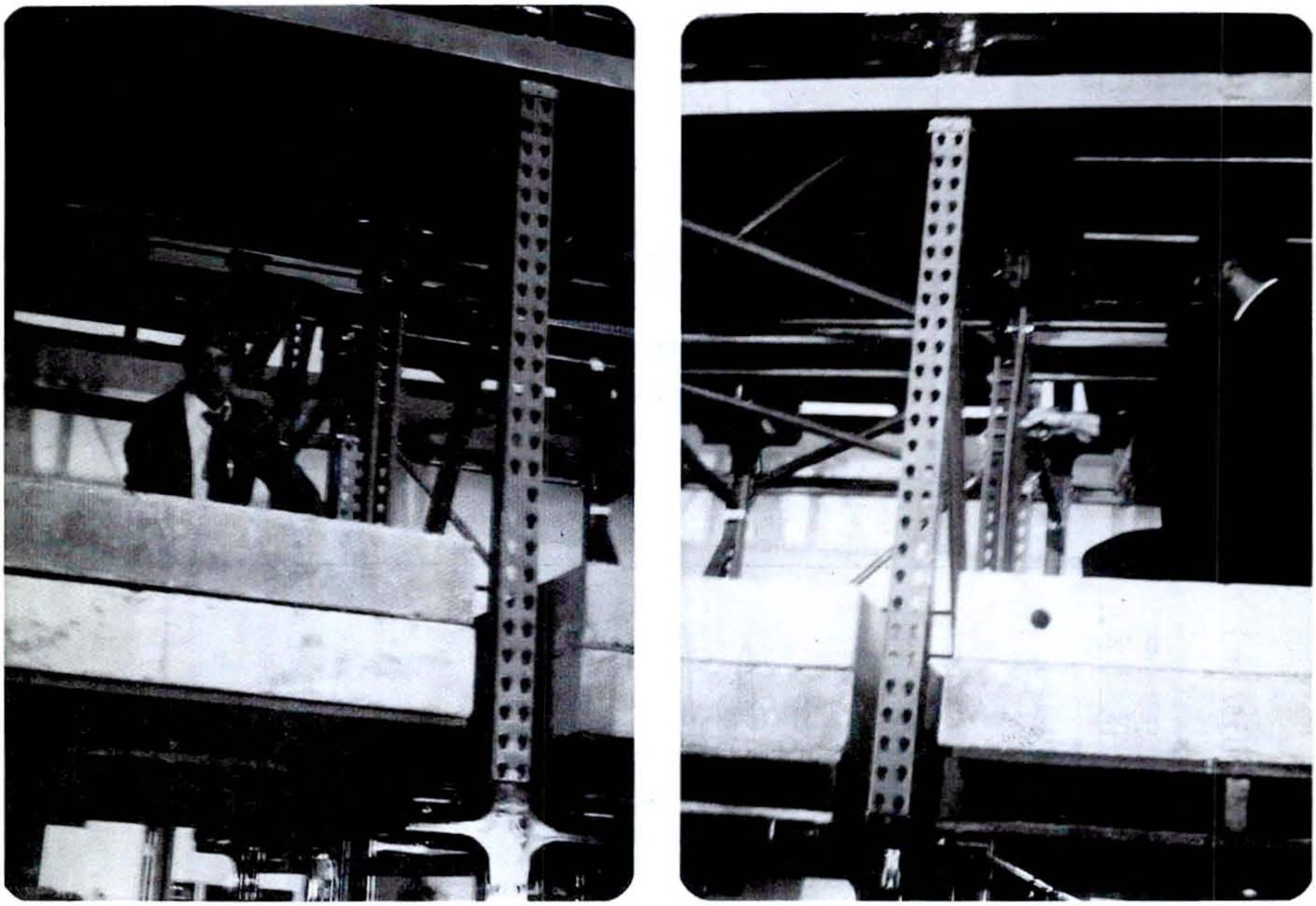

FIGURE 4.66 STRUCTURAL DAMAGE: STACKER RACK, LONGITUDINAL DIRECTION

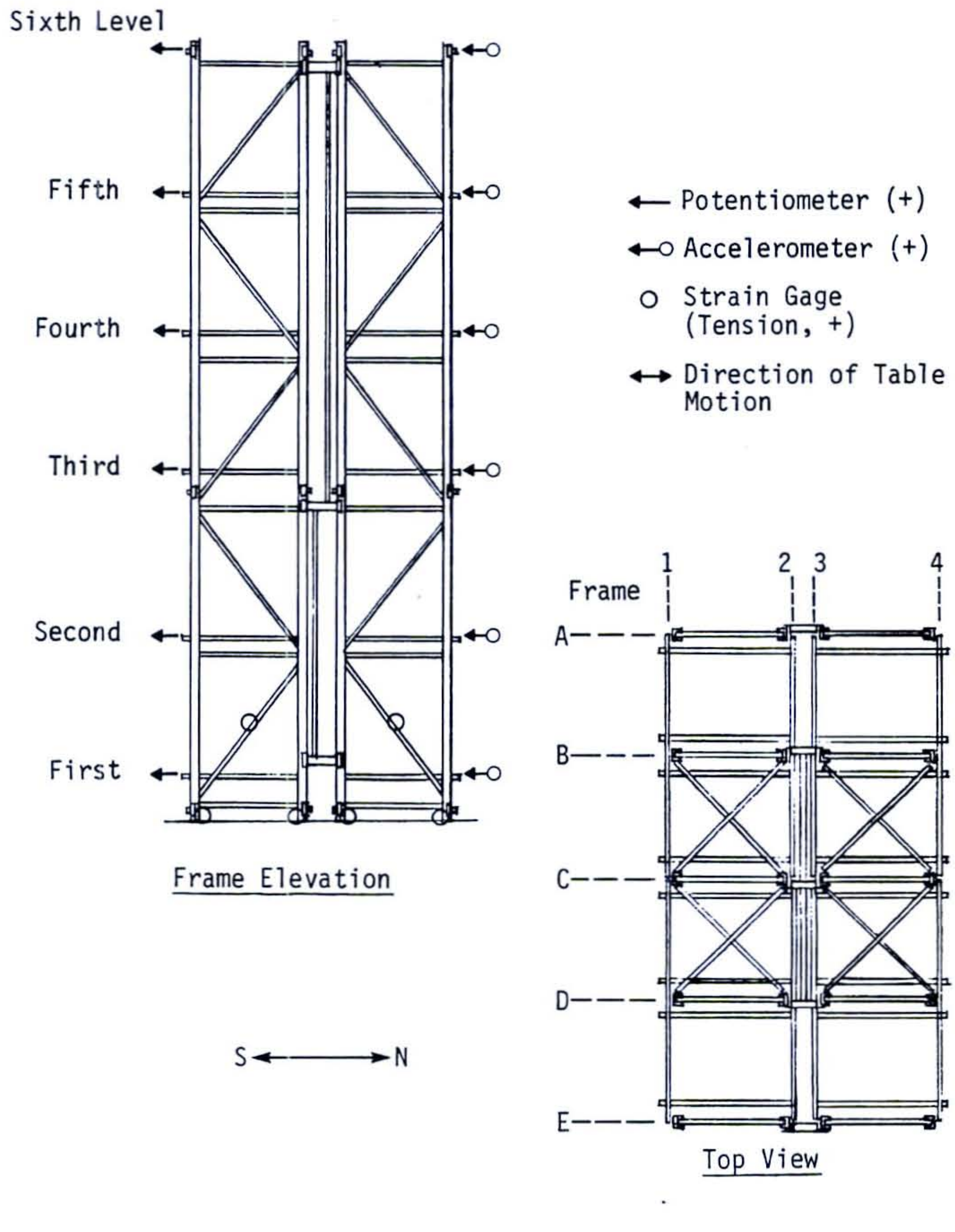

FIGURE 4.67 INSTRUMENTATION CHANNELS USED FOR DATA ANALYSIS: STACKER RACK, TRANSVERSE DIRECTION

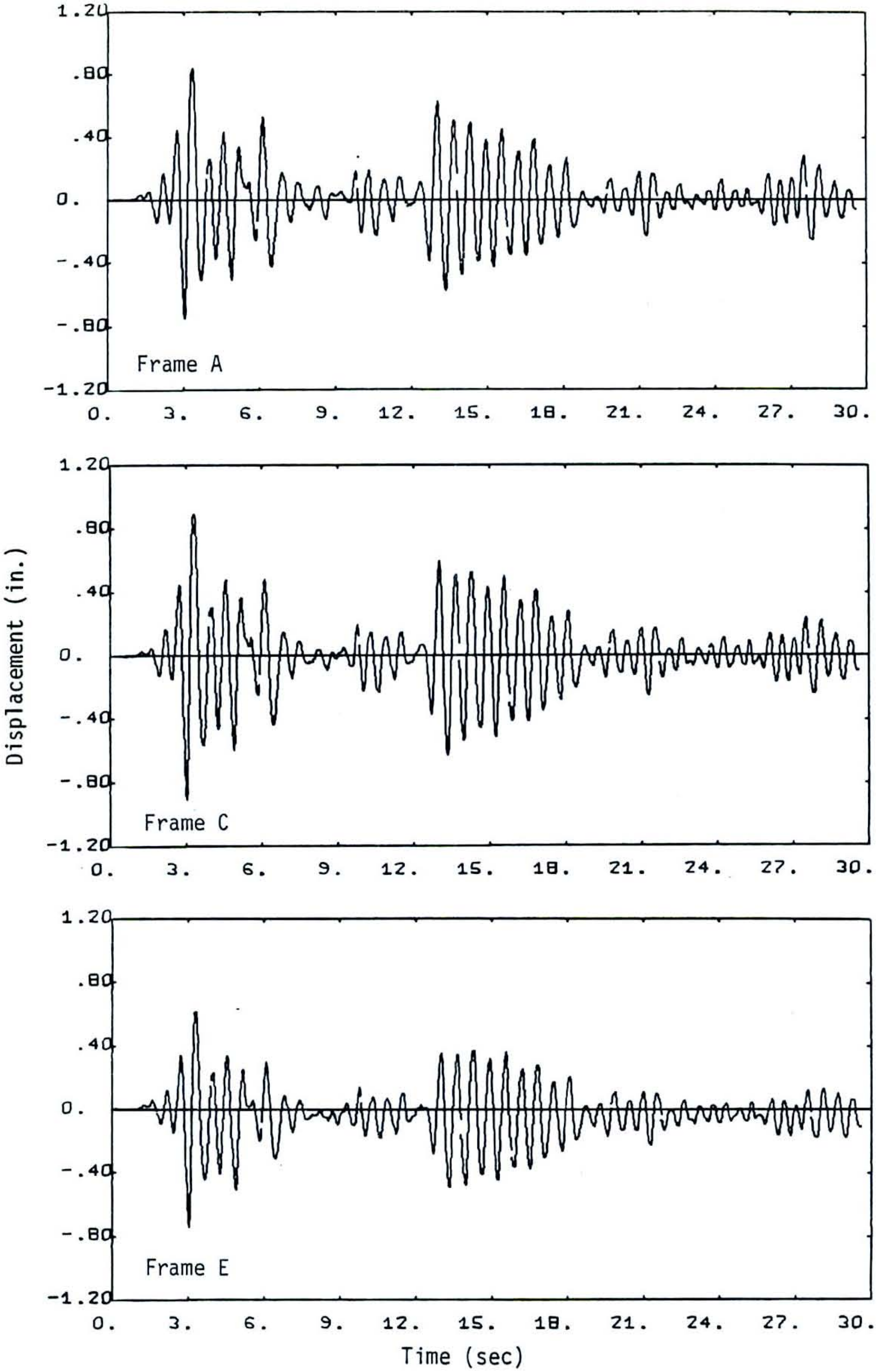

FIGURE 4.68 6TH LEVEL DISPLACEMENTS RELATIVE TO THE TABLE - TEST 111078.1 (ST-T-1-1/4 EC)

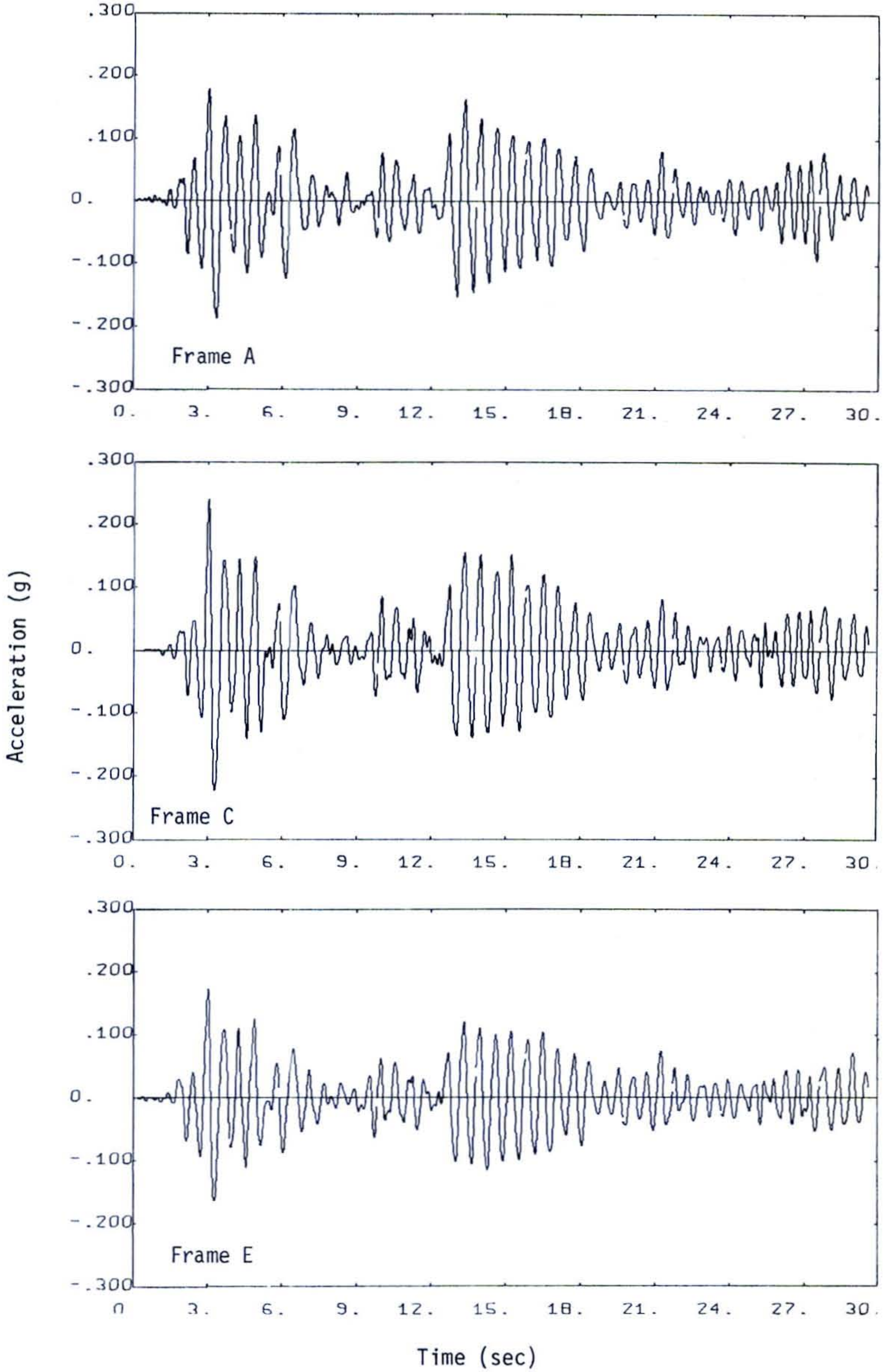

FIGURE 4.69 6TH LEVEL ACCELERATIONS - TEST 111078.1 (ST-T-1-1/4 EC)

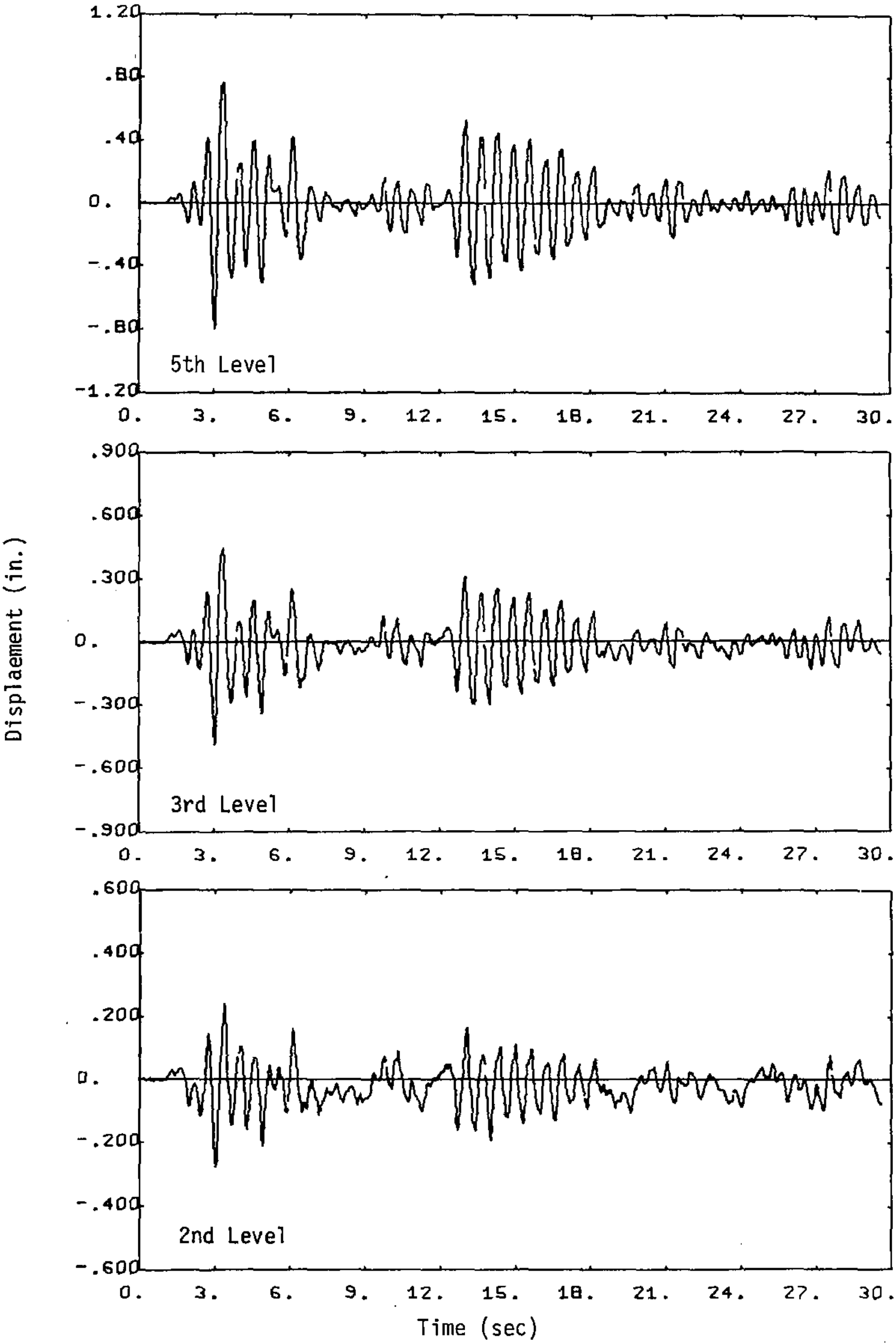

FIGURE 4.70a STORY DISPLACEMENTS RELATIVE TO THE TABLE (FRAME C) - TEST 111078.1 (ST-T-1-1/4 EC)

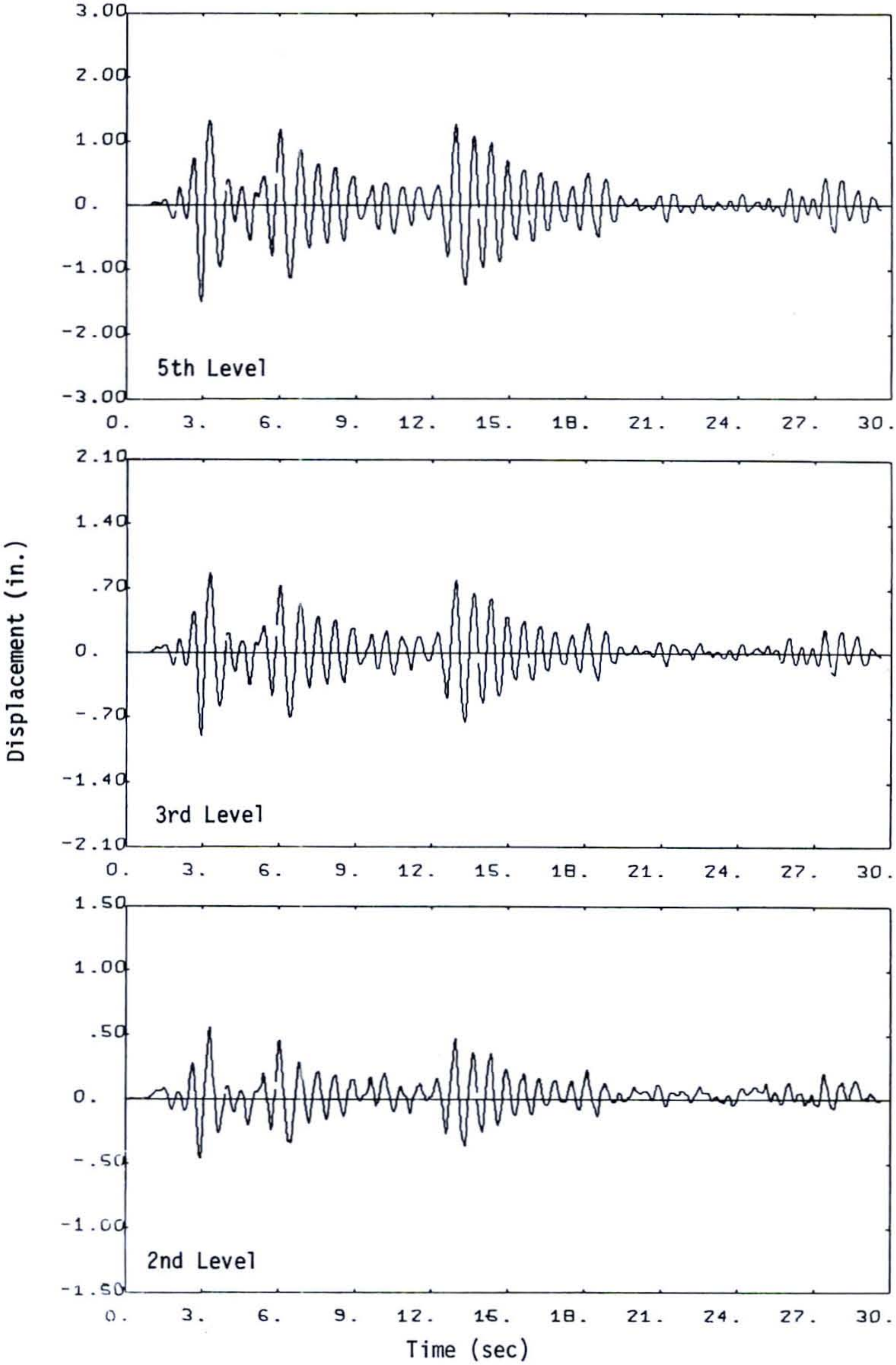

FIGURE 4.70b STORY DISPLACEMENTS RELATIVE TO THE TABLE (FRAME C) - TEST 111078.3 (ST-T-1-1/2 EC)

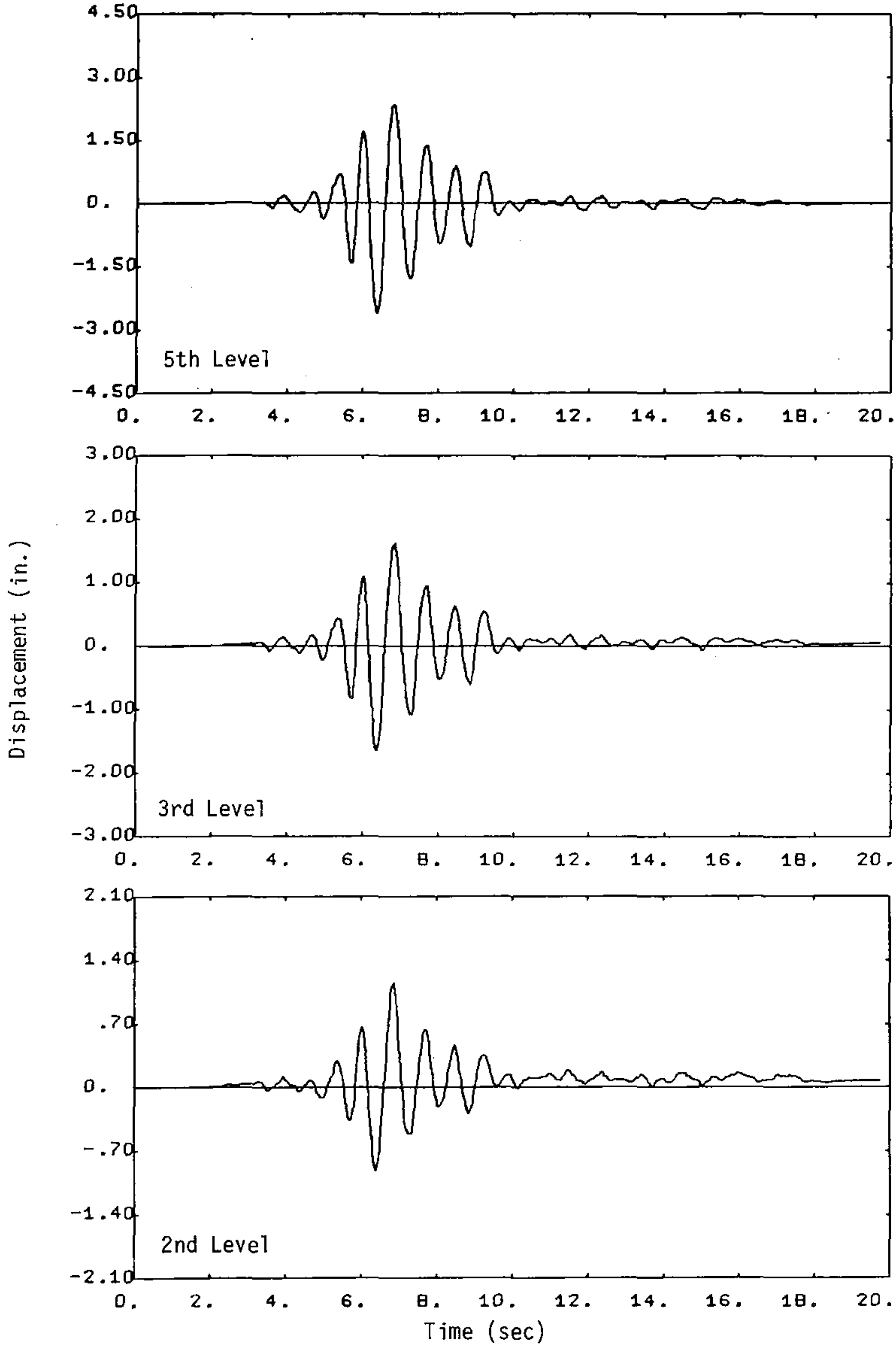

FIGURE 4.70c STORY DISPLACEMENTS RELATIVE TO THE TABLE (FRAME C) - TEST 111078.4 (ST-T-1-1/2 PF)

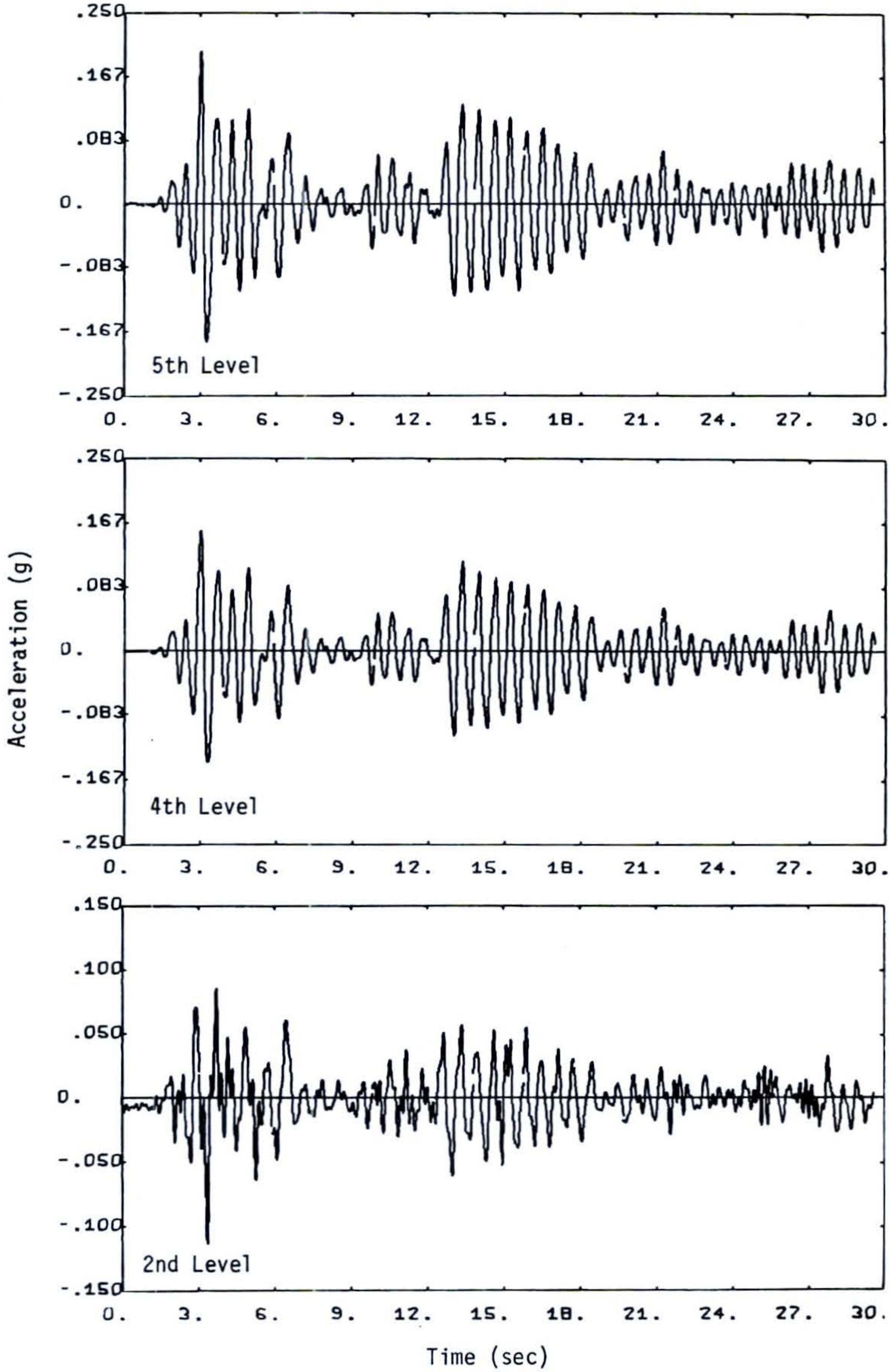

FIGURE 4.71a STORY ACCELERATIONS (FRAME C) - TEST 111078.1 (ST-T-1-1/4 EC)

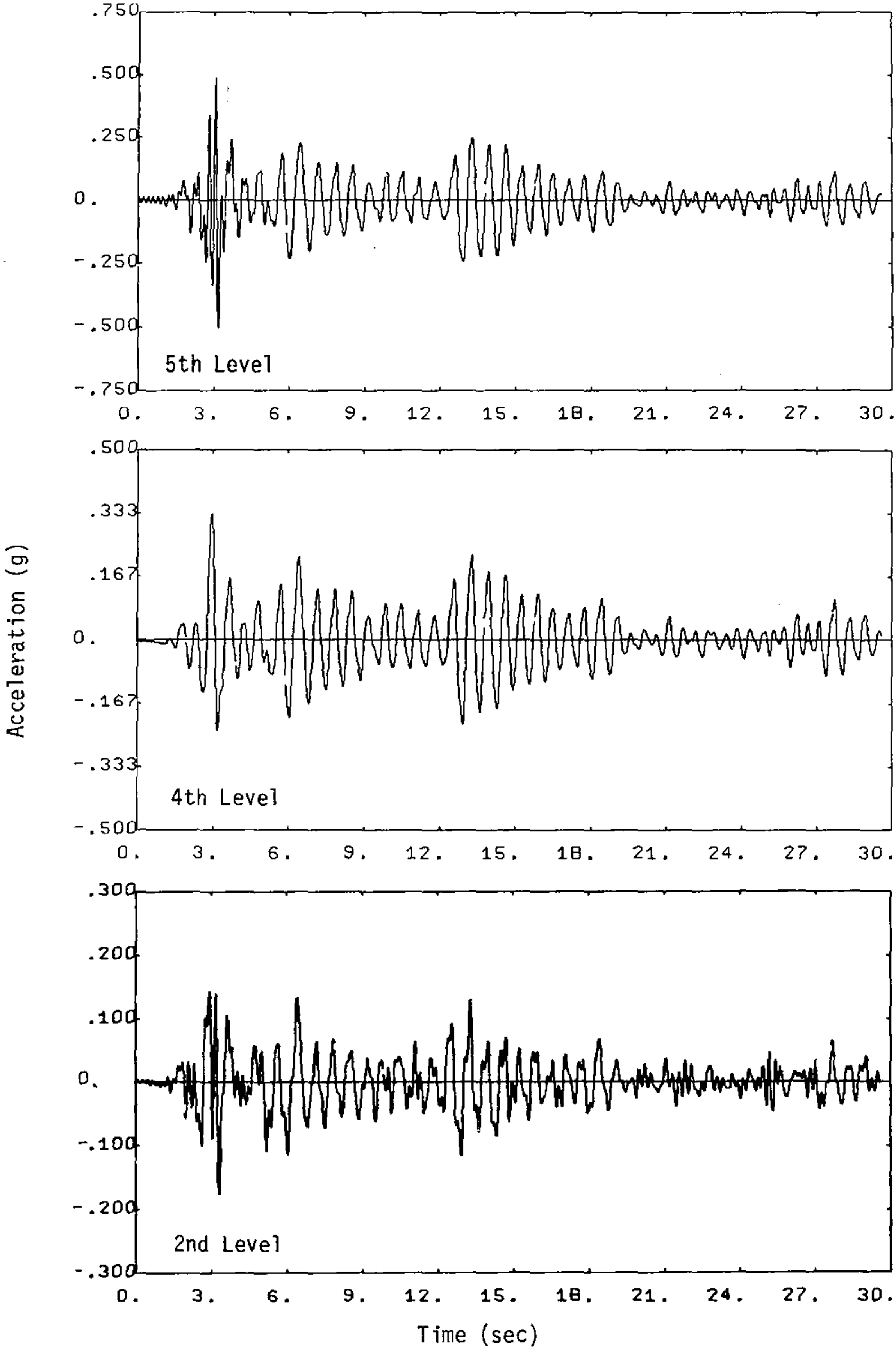

FIGURE 4.71b STORY ACCELERATIONS (FRAME C) - TEST 111078.3
(ST-T-1-1/2 EC)

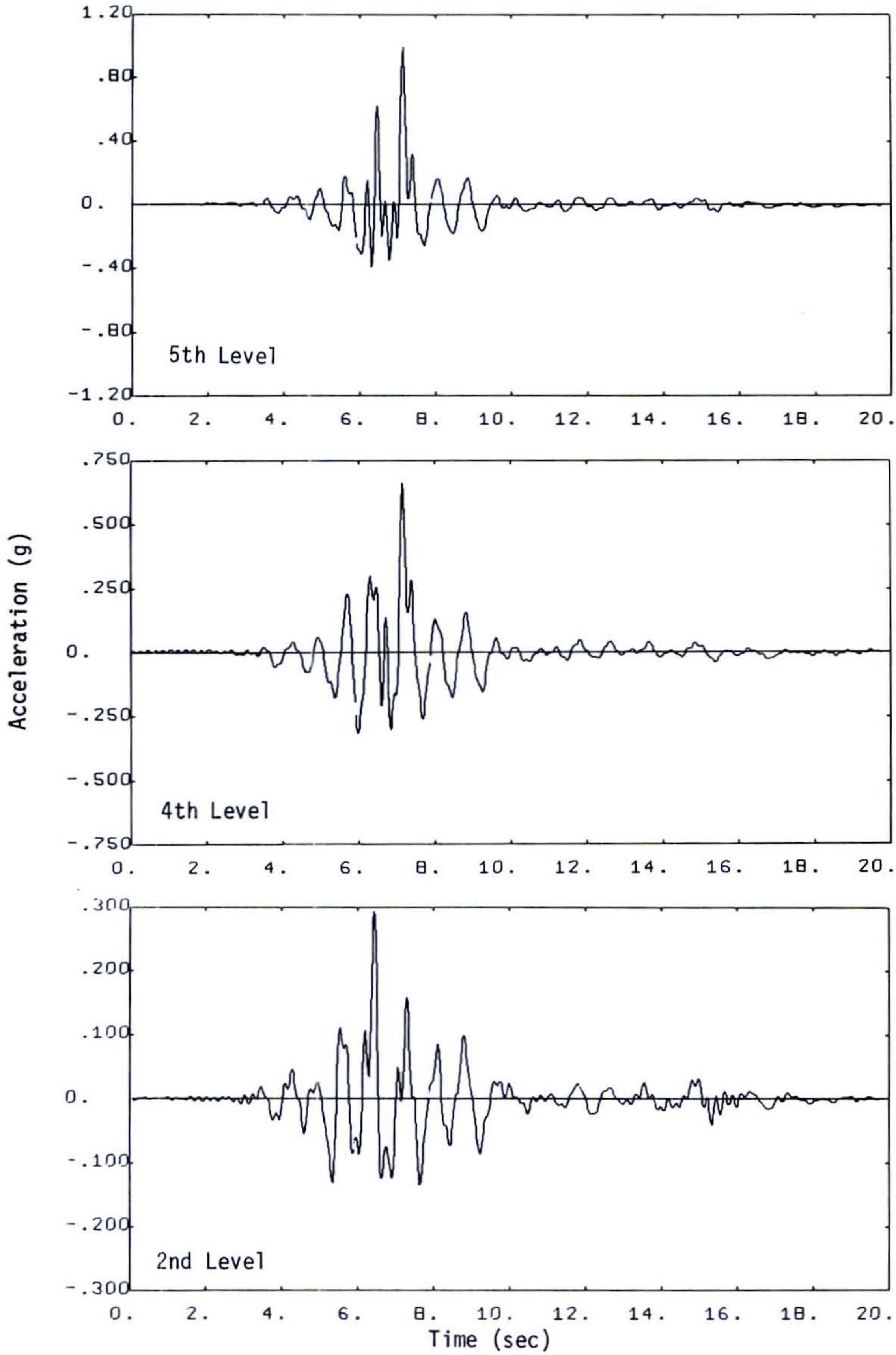

FIGURE 4.71c STORY ACCELERATIONS (FRAME C) - TEST 111078.4 (ST-T-1-1/2 PF)

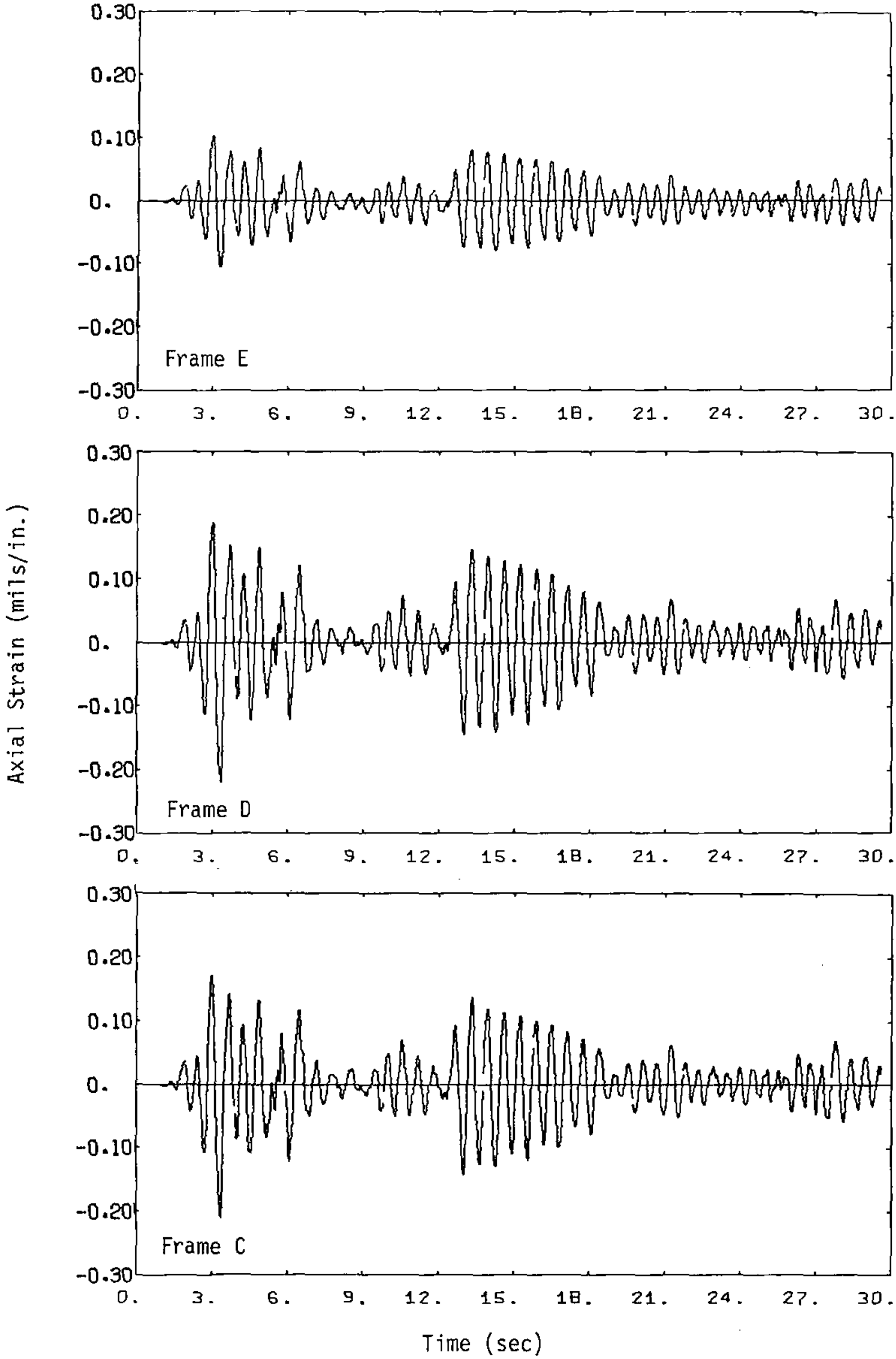

FIGURE 4.72a BRACE AXIAL STRAINS (BOTTOM SOUTH MEMBERS) - TEST 111078.1
(ST-T-1-1/4 EC)

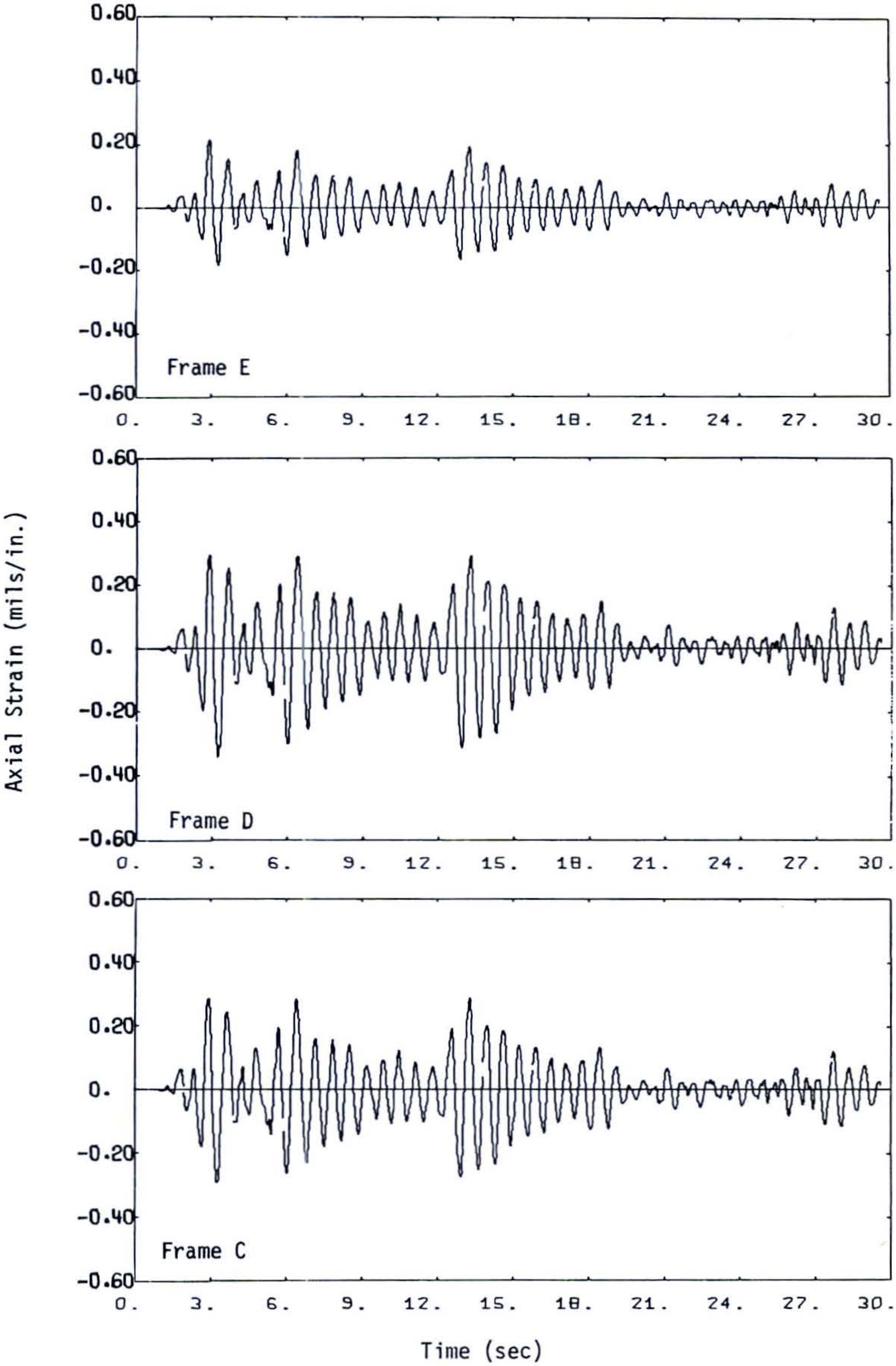

FIGURE 4.72b BRACE AXIAL STRAINS (BOTTOM SOUTH MEMBERS) - TEST 111078.3 (ST-T-1-1/2 EC)

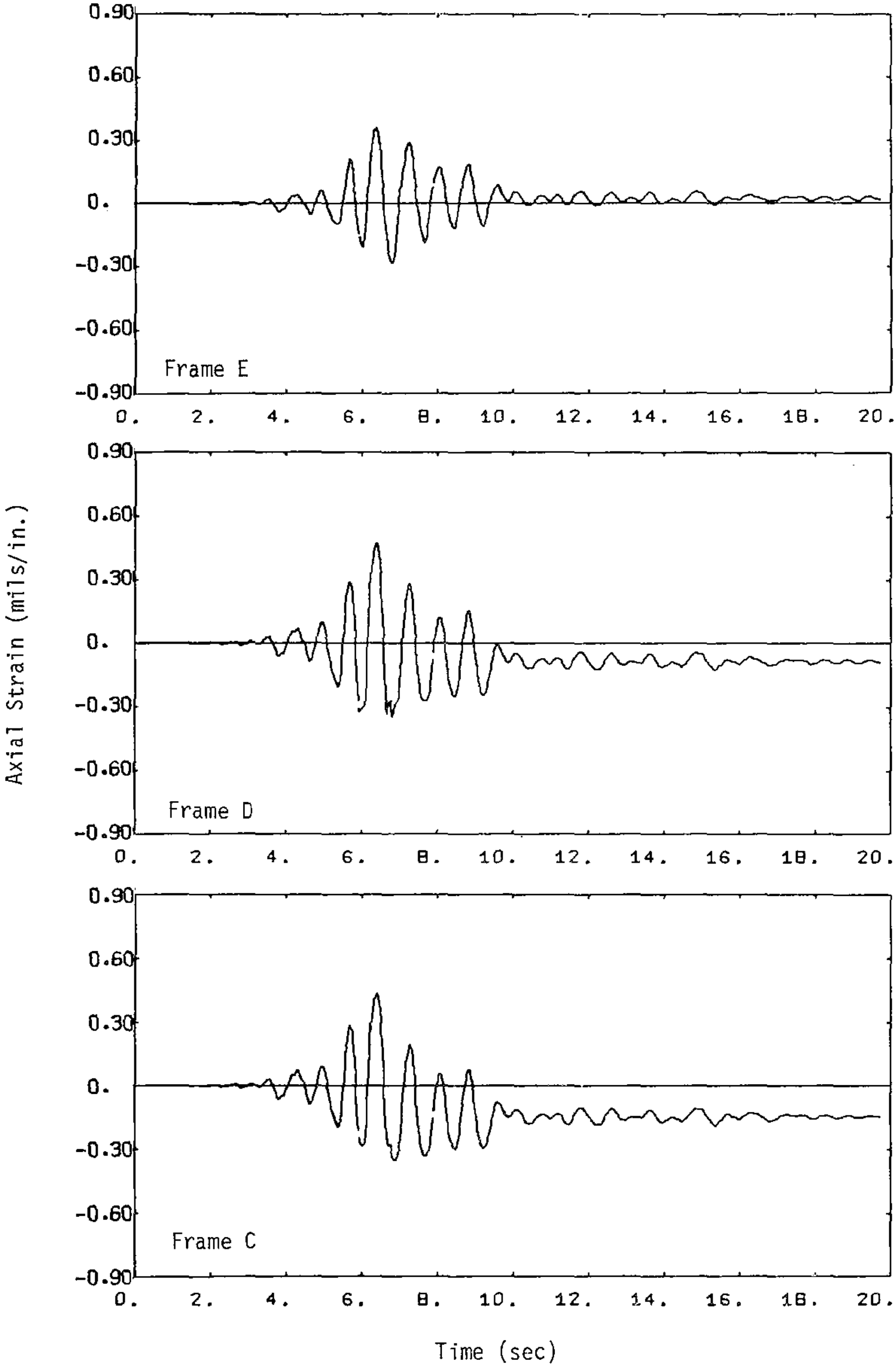

FIGURE 4.72c BRACE AXIAL STRAINS (BOTTOM SOUTH MEMBERS) - TEST 111078.4 (ST-T-1-1/2 PF)

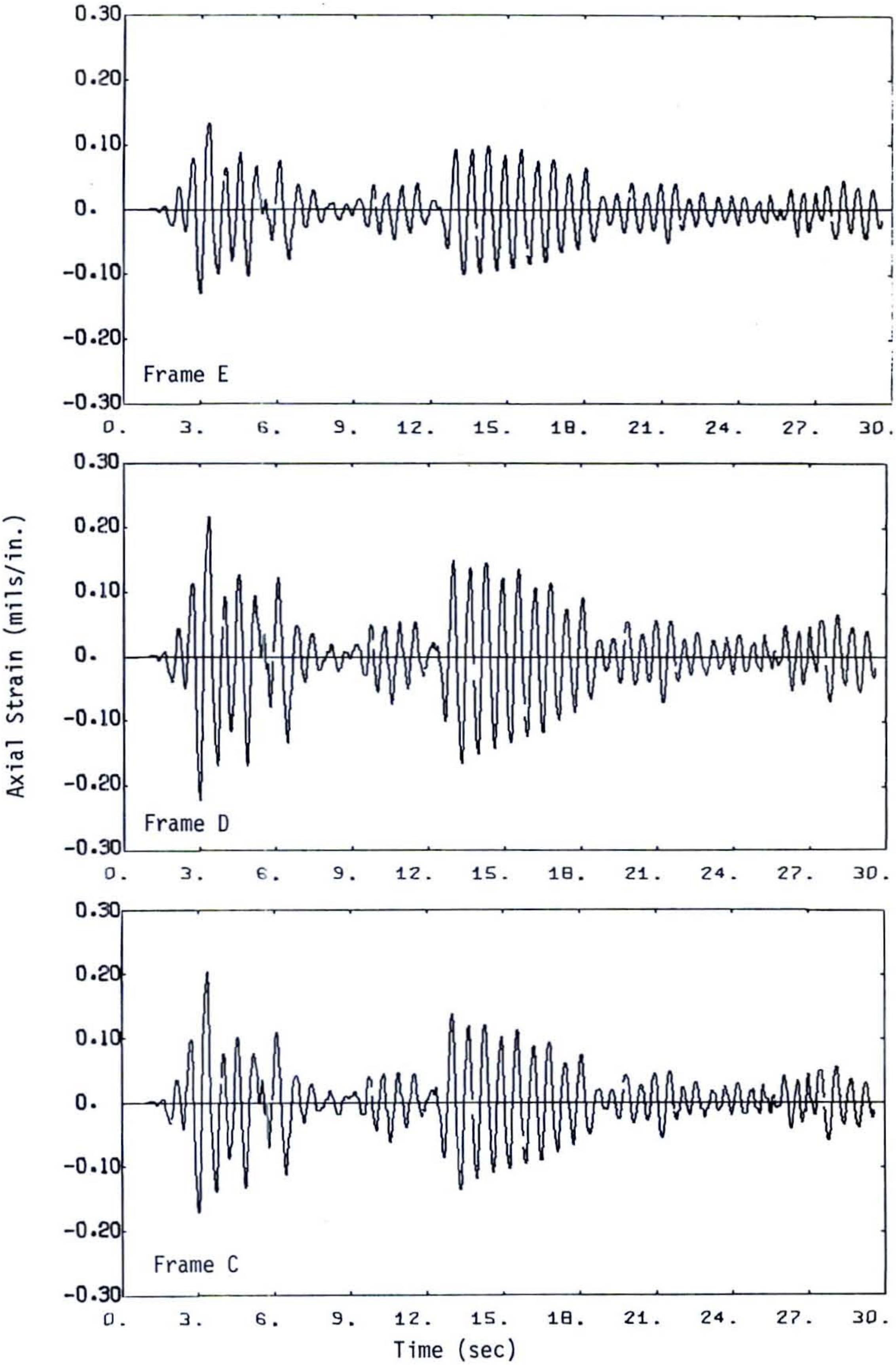

FIGURE 4.73a BRACE AXIAL STRAINS (BOTTOM NORTH MEMBERS) - TEST 111078.1 (ST-T-1-1/4 EC)

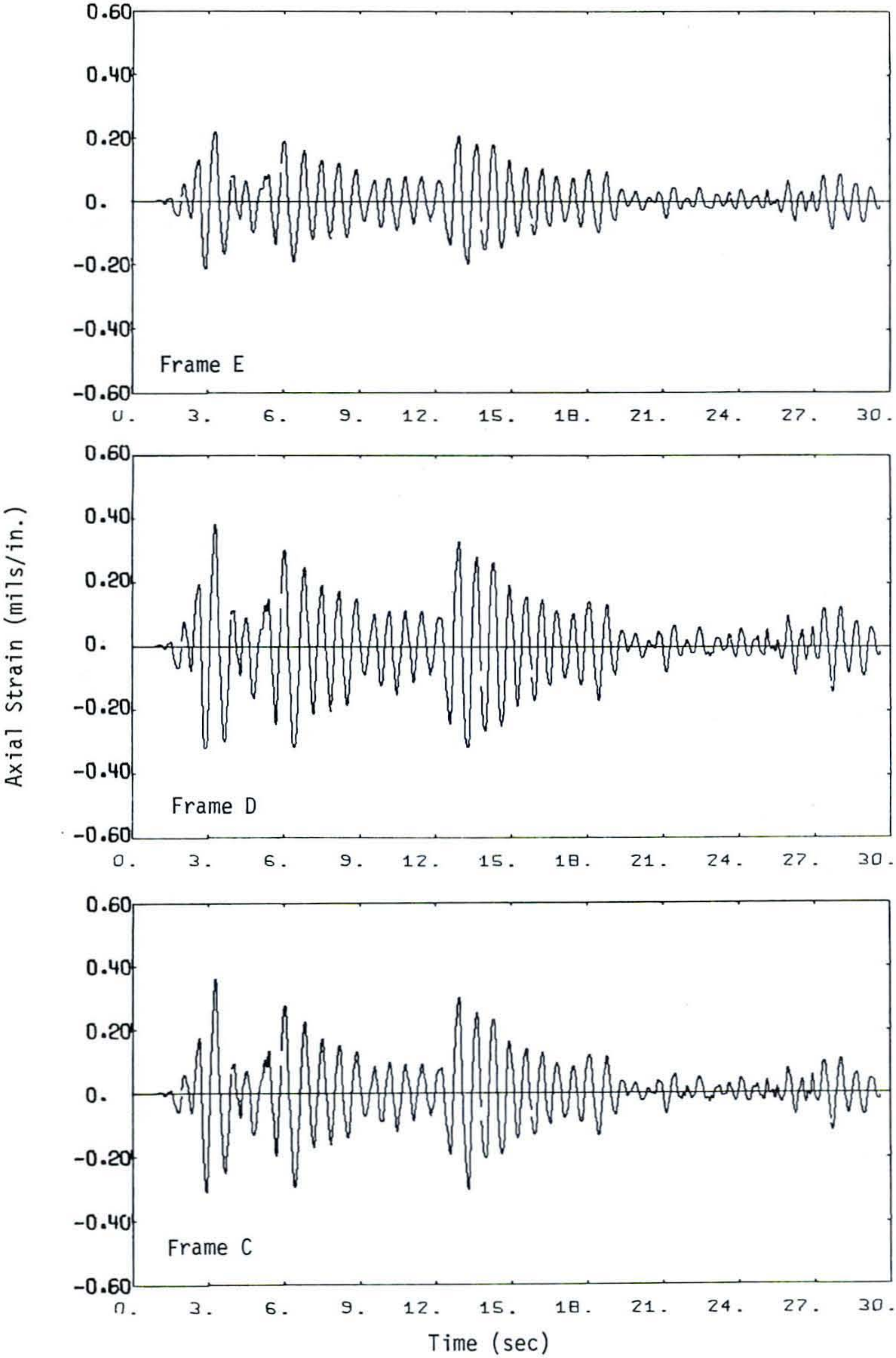

FIGURE 4.73b BRACE AXIAL STRAINS (BOTTOM NORTH MEMBERS) - TEST 111078.3 (ST-T-1-1/2 EC)

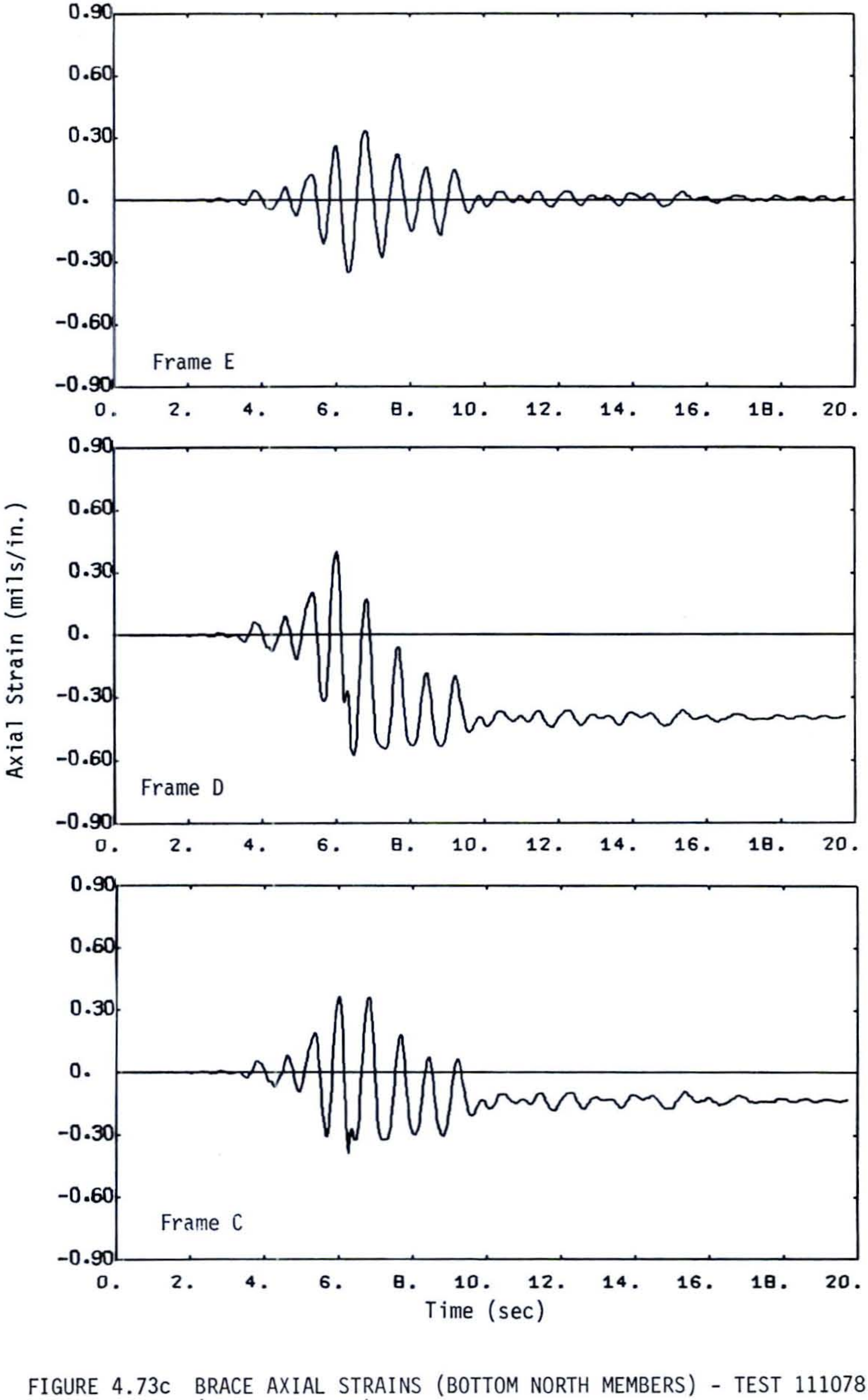

FIGURE 4.73c BRACE AXIAL STRAINS (BOTTOM NORTH MEMBERS) - TEST 111078.4 (ST-T-1-1/2 PF)

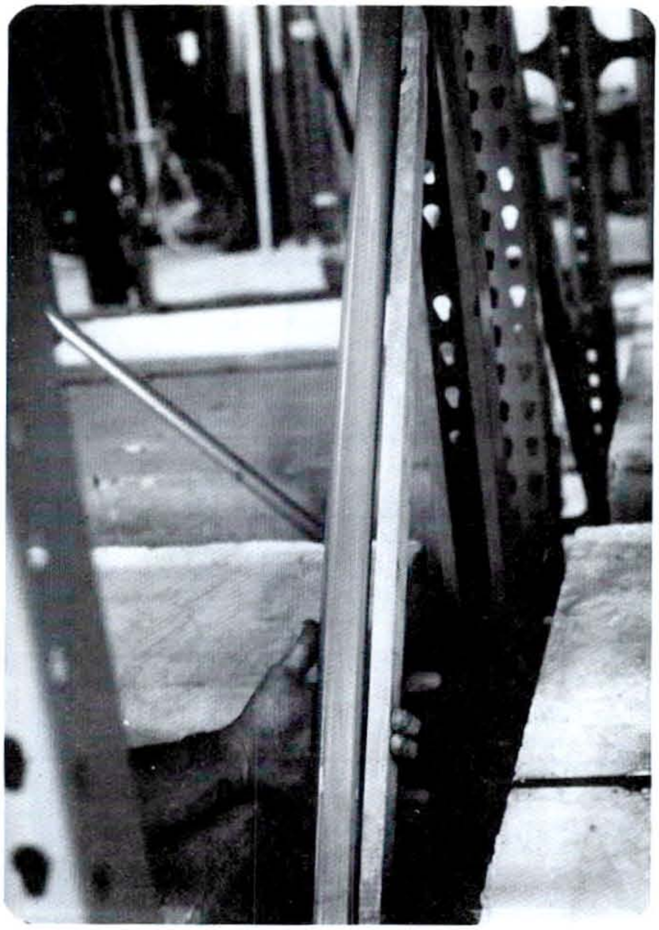

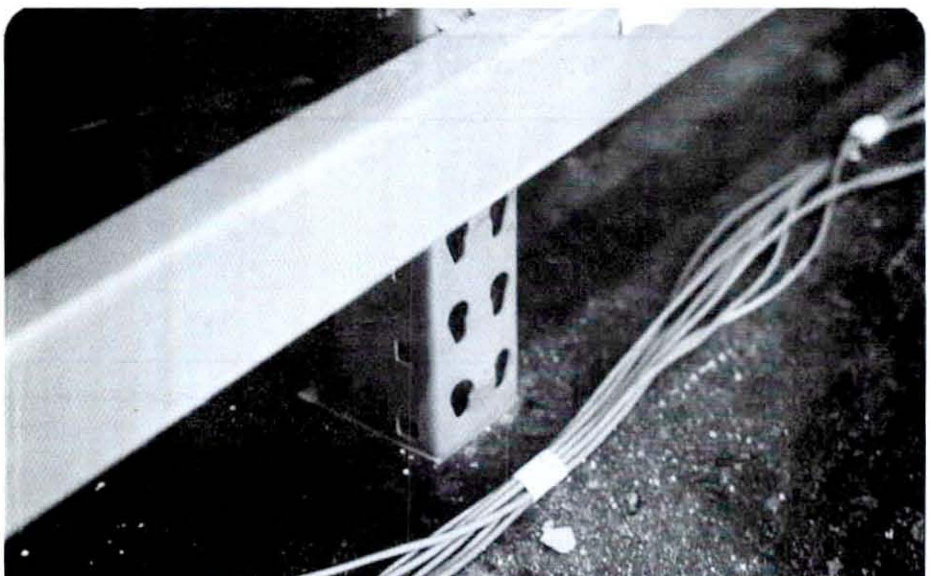

FIGURE 4.74 STRUCTURAL DAMAGE: STACKER RACK, TRANSVERSE DIRECTION

5. MERCHANDISE TESTS

5.1 Introduction

In the structural performance shaking table tests described in Chapter 4, the method of applying live load was to make up concrete blocks that were bolted to the wooden pallets, which, in turn, were bolted to the racks (or banded with metal straps for the drive-in and stacker racks). Although this method is not realistic in industry practice, it was deemed necessary for obtaining experimental data on the performance of the racks and for testing the adequacy and effectiveness of the various analytical procedures and assumed mathematical models. It would be impossible to model the rack structures with unknown effective masses mounted on them. In the experimental study reported in this part of the report, the primary objective was to determine any differences in response characteristics between two test cases: (1) the case in which the merchandise was tied with metal straps to the rack, and (2) the case in which the merchandise was not fastened to the rack. These cases are referred to in this report as Case 1 and Case 2.

Single-degree-of-freedom shaking table tests using various types of merchandise were performed: the rack was anchored to the table, loaded with merchandise, and tested in both the longitudinal and the transverse directions. For each test case, tests were run using horizontal motions of at least two intensity levels. Pull-release tests were conducted prior to the shaking table tests to determine damping values and periods of vibration from free-vibration decay data.

5.2 Types of Merchandise and Test Structure

Table 5.1 lists the eight types of merchandise, designated Types A through H, used in the tests and gives their estimated weights. Figures 5.1 through 5.6 are photographs of the test structure loaded with the eight types of merchandise and mounted on the shaking table. Figure 5.5 also illustrates the setup for the pull-release tests in the transverse direction.

The rack configuration used was a standard pallet rack one bay wide, one bay deep, and two stories high. The rack consisted of two upright frames, with columns spaced 43 in. apart (outside dimension), connected by horizontal beam members spaced 5 ft vertically. The upright frames were braced in their plane with single diagonal braces between panel points of the vertical and horizontal members. The 96-in. horizontal beams were connected to the columns by 6-in. end plates and studs. The columns were anchored to the table by means of bearing plates at their bases.

The section properties supplied by the manufacturer are as follows:

	A (in.^{2})	I_x (in.^{4})	I_y (in.^{4})	γ_x (in.^{2})	γ_y (in.^{2})
Column (net)	0.380	0.522	0.178	1.170	0.684
Beam	1.079	2.590	--	1.549	--
Brace	0.280	--	--	--	--

5.3 Instrumentation and Test Procedures

The same types of transducers used in the structural performance shaking table tests were used to measure global and local responses in the merchandise tests. Figure 5.7 shows the instrumentation channels used for data collection in the two test directions. The El Centro input signal was used extensively for testing. However, for merchandise Type A in the longitudinal direction, the Parkfield signal was also used. The table acceleration time histories, the table displacement records, and the response spectra for different intensity levels can be seen in Figures 4.14 through 4.19. Before the dynamic tests, pull tests were performed for both test cases. The acceleration records were then filtered through a band-pass filter with the bandwidth selected to cover the expected frequencies. The data were displayed on visicorder paper for damping and frequency evaluation. Except for the table motions or intensity levels used, the merchandise tests were conducted in the same way as the structural performance tests. All shaking table data were transferred to magnetic tape for computer analysis.

5.4 Test Results

Tables 5.2 and 5.3 present all dynamic tests conducted for the merchandise testing program. In these tables, the test identifications (Test I.D.) consist of the date and the test number on that date. The tables also list the test cases (tied or not tied), table motions, signals, and remarks on the tests. As the tables indicate, neither merchandise nor wood pallets moved during the testing, except that some of the uppermost paper products and canned goods moved slightly during the longitudinal tests. For each test condition, at least two acceleration levels were used; however, the test run with the higher acceleration level was selected for detailed data evaluation. Time histories of global and local responses were plotted for all tests.

In the following sections, tests are identified using the following notation:

Merchandise Type:	A through H
Test Case:	1 - merchandise tied to the rack 2 - merchandise not tied to the rack
Test Direction:	L - longitudinal T - transverse
Intensity/Signal:	1/2 EC - 1/2 the El Centro signal 5/16 PF - 5/16 the Parkfield signal etc.

Longitudinal Tests. For all tests conducted in the longitudinal direction, the displacement time histories measured at the east and west frames were found to be identical, which demonstrates that the response was symmetric; no torsional vibration was observed. The results of each merchandise type selected for this report are presented in the following order:

1. Story displacements (relative to the table)
2. Story accelerations (average of the two frames)
3. Column flexural strains at the top end of the north-west bottom column

Table 5.4 summarizes selected extreme quantities from the shaking table tests along with the dynamic properties from the pull tests.

Type A merchandise consisted of concrete blocks. Figures 5.8a through 5.8c show the global and local responses for Case 1 and Case 2 (tied and not tied) when the test structure was subjected to motion approximately 5/8 that of the actual El Centro record. It can be seen from these figures that the responses for the two test cases are quite different. The maximum response quantities for Case 2 are slightly smaller than those for Case 1. The damping values determined from the pull tests were approximately 3.1% for Case 1 and 4.1% for Case 2, which verifies that the maximum response values are smaller for merchandise that is not tied to the rack than for tied merchandise.

Figures 5.9a through 5.9c display, for the Type A tests using the Parkfield input signal, displacements, accelerations, and column flexural strains for Case 1 and Case 2. These figures clearly show that the responses are almost identical in phase and magnitude during the early stages of significant vibration (up to about 10 sec). The extreme values are seen to be slightly smaller for Case 2.

Type B merchandise consisted of cases of canned goods. Figures 5.10a through 5.10c present the results. The first few significant cycles of vibration for both Case 1 and Case 2 are nearly identical in phase and magnitude; however, in the middle part of the response (from 15 sec to 20 sec), the period of vibration for Case 2 changes and becomes longer than in the early stage. After approximately 20 sec, the responses are again similar. The damping values estimated from the pull tests were very similar for both test cases (3% versus 3.5%).

Type C merchandise consisted of bags of dried pet food on wood pallets placed on the rack. Figures 5.11a through 5.11c present the results. The results of Cases 1 and 2 resemble each other closely in phase and magnitude except during the period from 10 sec to 12 sec. The damping values determined from the pull tests are also very similar (5.7% versus 6.1%).

For the test series using Type D merchandise, cartons of paper products (paper towels and disposable diapers) on wood pallets were placed on the rack. Figures 5.12a through 5.12c show the displacements, accelerations, and column flexural strains for Cases 1 and 2. The responses are seen to be identical in phase; however, as found in the previous merchandise types, the measured extreme quantities for Case 2 were slightly smaller than those for Case 1.

For the Type E phase of testing, drums filled with water, placed on cradles resting on the horizontal beams, were used as storage material. The responses measured for two test cases, as shown in Figures 5.13a through 5.13c, are in good agreement in phase. The periods, as determined from a fast Fourier analysis of the acceleration records, are identical (0.9 sec).

For the Type F test series, the paper products used as storage material were placed directly on metal decking running the full length of the rack. As shown in Figures 5.14a through 5.14c, the time-history responses measured for Cases 1 and 2 were identical in phase and magnitude after 10 sec of vibration. There are some differences in the responses during the early stage of excitation, but these differences are not significant. The damping values for the two test cases are approximately 5.0% and 6.7%, respectively. Because of the higher damping observed for Case 2, the maximum response quantities were found to be slightly less than those for Case 1.

Type G merchandise consisted of bags of dried pet food loaded on the metal decking. Figures 5.15a through 5.15c show the results of test runs for Cases 1 and 2. Good agreement both in phase and magnitude was observed between the two test cases.

Transverse Tests. For all tests conducted in the transverse direction, the time-history plots of the story displacements measured at the first level of two upright frames are nearly identical. Minor differences in magnitude were probably caused by unavoidable asymmetry in mass distribution and frame stiffness. Table 5.5 summarizes some selected extreme quantities from the shaking table tests. Figures 5.16 through 5.21 show the measured time-history responses for the two test cases for all types of merchandise tested. These figures give the results of each merchandise type selected for presentation in the following sequence:

1. Story displacements (relative to the table) for the east frame
2. Story accelerations (average of the east and west frames)
3. Axial strains (east bottom diagonal brace)

It can be seen from Figures 5.16 to 5.21 that, for each merchandise type, responses for Case 1 closely resemble those for Case 2. Some minor difference in magnitude can be seen in these figures; however, the maximum response values for both test cases were almost the same for every merchandise type tested (see also Table 5.5 for comparison). The findings are consistent with those observed in the longitudinal test runs. Furthermore, a greater degree of similarity between the responses for the two test cases was found in the transverse tests than in the longitudinal tests.

The damping values could be observed from the pull test data displayed on the visicorder paper; however, the plotted amplitudes were too small to permit an accurate determination of the damping capacity.

Applicability of the Test Results to Multistory Rack Structures. Because the results presented thus far are based on single-degree-of-freedom tests, questions might arise as to their applicability to multistory rack structures. Figure 5.22 plots maximum story acceleration against storage weight for both the merchandise tests and the structural performance tests. This relationship was chosen because the story force (mass times acceleration) is the governing factor in the stability of merchandise during seismic excitation.

It can be seen from these data that the single-degree-of-freedom tests are very effective in exciting the structure, particularly in the longitudinal direction. The measured periods of vibration from various types of merchandise ranged from approximately 0.6 sec to 1.2 sec, which coincides with the response spectrum peaks from Figures 4.18 and 4.19. The maximum story accelerations from the merchandise tests are slightly higher than those of the multistory standard pallet rack tests.

The merchandise tests in the transverse direction were not as effective as those in the longitudinal direction. Nevertheless, it can be concluded that the findings from the single-degree-of-freedom tests are applicable to those multistory standard pallet racks used in the testing reported in Chapter 4.

Merchandise Instability Due to Vertical Excitation. Vertical input motion was not applied during any of the merchandise shaking table tests. The reasons are:

- The primary objective of this merchandise testing program was to justify the use of tied live loads for analytical response prediction (mainly for horizontal excitation).
- During earthquake excitation, vertical motion is usually out of phase with horizontal motion.
- Vertical signals usually contain higher frequencies, and, in most cases, the dynamic amplification factor would be approximately 1.0. Assuming that the peak vertical acceleration is 2/3 the peak horizontal acceleration, under the full El Centro or Parkfield earthquake, the frictional force that resists movement of merchandise would be reduced approximately 20%. This reduction would probably not significantly affect the overall stability of the merchandise.

However, in retrospect, it would have been desirable to observe the behavior of merchandise with vertical motion applied simultaneously with the horizontal signal. It was the consensus of the advisory committee for this study that published data on actual merchandise and rack performance during recent strong earthquakes be collected and included in this chapter. This information is presented in Appendix C.

5.5 Summary and Conclusions

The objective of the experimental study reported in this chapter was to determine the seismic response characteristics of the various types of merchandise, both tied to the rack with metal straps and not tied to the rack. The storage weights tested ranged from approximately 500 to 2,300 lb/beam. The merchandise was placed either on wood pallets or on metal decking, both commonly used in the rack industry.

In addition to shaking table tests using actual earthquake signals as input, pull tests were conducted to determine the dynamic response properties at small amplitudes of excitation. The conclusions that can be drawn from this study, for the specific types of merchandise tested and for horizontal excitation only, are as follows:

- Substantial horizontal diaphragm action can be developed through the combination of stored material and pallets or metal decking, regardless of the type of material or whether it is tied to the rack.
- For all tests, little difference in global and local responses was found between the cases in which merchandise was tied to the rack and those in which merchandise was not tied to the rack. This finding justifies the use of tied live loads for the analytical response predictions.
- The damping values determined from the pull tests for merchandise that was not tied are slightly higher than those for tied merchandise. However, the pull tests show no difference in periods of vibration between the two test cases.
- In all tests of merchandise that was not tied, all merchandise tested was very stable, and no movement of stored material was observed except for some of the uppermost cartons of paper products. The maximum floor (pallet) accelerations measured in the longitudinal test direction ranged from approximately 0.2g for the cases of canned goods (2,300 lb/beam) to 0.7g for lightweight paper products (500 lb/beam).
- The single-degree-of-freedom tests employed in this experimental study are very effective in exciting the test structure. The results and findings are applicable to the multistory racks used in the structural performance shaking table tests.

TABLE 5.1

TYPES OF MERCHANDISE

Type	Description	Weight (lb)	Test Direction
A	wood pallets with concrete blocks	2,160	Longitudinal Transverse
B	wood pallets with cases of canned goods	4,620	Longitudinal Transverse
C	wood pallets with bags of material	2,620	Longitudinal Transverse
D	wood pallets with paper products	830	Longitudinal Transverse
E	drums of liquid	1,300	Longitudinal Transverse
F	metal decking with paper products	730	Longitudinal
G	metal decking with cases of canned goods	4,520	Longitudinal
H	metal decking with bags of material	2,520	Transverse

TABLE 5.2

RECORD OF MERCHANDISE SHAKING TABLE TESTS - LONGITUDINAL

Type	Test I.D.	Test Case[a]	Table Motion		Remarks
			Signal	Maximum Acceleration (g)	
A	220678.1	1	EC	0.10	Neither the wood pallets nor the concrete blocks moved when not tied.
	220678.2	1	EC	0.20	
	220678.3	1	PF	0.10	
	220678.4	2	EC	0.10	
	220678.5	2	EC	0.20	
	220678.6	2	PF	0.10	
B	230678.1	1	EC	0.08	Neither the wood pallets nor the merchandise moved when not tied.
	230678.2	1	EC	0.16	
	230678.3	2	EC	0.08	
	230678.4	2	EC	0.16	
C	230678.7	1	EC	0.08	Neither the wood pallets nor the merchandise moved when not tied.
	230678.8	1	EC	0.16	
	230678.9	2	EC	0.08	
	230678.10	2	EC	0.16	
D	230678.11	1	EC	0.08	The top paper boxes moved slightly during test run 230678.14.
	230678.12	1	EC	0.16	
	230678.13	2	EC	0.08	
	230678.14	2	EC	0.16	
E	260678.1	1	EC	0.08	The drum supports moved approximately 1" during the tests.
	260678.2	1	EC	0.20	
	260678.3	2	EC	0.08	
	260678.4	2	EC	0.16	
	260678.5	2	EC	0.20	
F	260678.6	1	EC	0.08	The top paper boxes moved slightly when not tied.
	260678.7	1	EC	0.16	
	260678.8	1	EC	0.25	
	260678.9	2	EC	0.16	
	260678.10	2	EC	0.25	
G	260678.11	1	EC	0.08	The upper canned goods moved slightly when not tied.
	260678.12	1	EC	0.16	
	260678.13	2	EC	0.16	
	260678.14	2	EC	0.24	
	260678.15	2	EC	0.30	

a 1 = merchandise tied to the rack
2 = merchandise not tied to the rack

TABLE 5.3

RECORD OF MERCHANDISE SHAKING TABLE TESTS - TRANSVERSE

Type	Test I.D.	Test Case[a]	Table Motion		Remarks
			Signal	Maximum Acceleration (g)	
A	270678.1 270678.2 270678.3 270678.4 270678.5	1 1 2 2 2	EC EC EC EC PF	0.08 0.16 0.08 0.16 0.16	Neither the wood pallets nor the concrete blocks or merchandise moved when not tied.
B	290678.2 290678.3 290678.4 290678.5	1 1 2 2	EC EC EC EC	0.08 0.16 0.08 0.16	Neither the wood pallets nor the concrete blocks or merchandise moved when not tied.
C	290678.11 290678.12 290678.13 290678.14	1 1 2 2	EC EC EC EC	0.08 0.16 0.08 0.16	Neither the wood pallets nor the concrete blocks or merchandise moved when not tied.
D	290678.17 290678.18 290678.19 290678.20	1 1 2 2	EC EC EC EC	0.08 0.26 0.08 0.26	Neither the wood pallets nor the concrete blocks or merchandise moved when not tied.
E	300678.3 300678.4 300678.5 300678.6	1 1 2 2	EC EC EC EC	0.16 0.33 0.16 0.33	Neither the wood pallets nor the concrete blocks or merchandise moved when not tied.
H	300678.9 300678.10 300678.11 300678.12	1 1 2 2	EC EC EC EC	0.16 0.33 0.16 0.33	Neither the wood pallets nor the concrete blocks or merchandise moved when not tied.

a 1 = merchandise tied to the rack
  2 = merchandise not tied to the rack

TABLE 5.4

SUMMARY OF MERCHANDISE TEST RESULTS - LONGITUDINAL

Type	Test Case[a]	Shaking Table Tests								Pull Tests		
		Test I.D.	Signal	Maximum Table Acceleration (g)	Maximum Table Displacement (in.)	Maximum Story Acceleration (g)	Maximum Relative Story Displacement (in.)	Maximum Strain[b] (mil/in.)	Period (sec)[c]	Period (sec)	Damping (%)	Applied Force (lb)
A	1	220678.2 (A-1-L-5/8 EC)	EC	0.20	1.59	0.44	1.5	0.36	0.67		3.1	400
	2	220678.5 (A-2-L-5/8 EC)	EC	0.20	1.59	0.39	1.5	0.34	0.69		4.1	400
A	1	220678.3 (A-1-L-5/16 PF)	PF	0.10	0.98	0.36	1.3	0.30	0.69		3.1	400
	2	220678.6 (A-2-L-5/16 PF)	PF	0.10	0.99	0.30	1.2	0.27	0.72		4.1	400
B	1	230678.2 (B-1-L-1/2 EC)	EC	0.16	1.28	0.23	2.0	0.42	0.99	0.84	3.2	400
	2	230678.4 (B-2-L-1/2 EC)	EC	0.16	1.27	0.23	2.2	0.47	0.99 1.09	0.82	3.5	400
C	1	230678.8 (C-1-L-1/2 EC)	EC	0.16	1.28	0.25	1.5	0.26	0.89	0.89	5.7	400
	2	230678.10 (C-2-L-1/2 EC)	EC	0.16	1.28	0.25	1.4	0.23	0.89 0.96	0.90	6.1	400
D	1	230678.12 (D-1-L-1/2 EC)	EC	0.16	1.28	0.48	1.0	0.19	0.58 0.62	0.61	4.2	400
	2	230678.14 (D-2-L-1/2 EC)	EC	0.16	1.28	0.46	0.9	0.17	0.58 0.64	0.63	4.4	400
E	1	260678.2 (E-1-L-5/8 EC)	EC	0.20	1.60	0.39	1.2	0.21	0.90	0.88	5.1	400
	2	260678.5 (E-2-L-5/8 EC)	EC	0.20	1.60	0.30	1.2	0.21	0.90	0.88	4.5	400
F	1	260678.8 (F-1-L-3/4 EC)	EC	0.25	1.90	0.70	1.4	0.60	0.57 0.85	0.61	5.0	400
	2	260678.10 (F-2-L-3/4 EC)	EC	0.25	1.90	0.66	1.3	0.55	0.67 0.85	0.62	6.2	400
G	1	260678.12 (G-1-L-1/2 EC)	EC	0.16	1.28	0.21	2.2	0.44	0.98 1.23	1.16	8.9	400
	2	260678.13 (G-2-L-1/2 EC)	EC	0.16	1.28	0.18	1.8	0.36	0.98 1.23	1.18	8.8	400

a. 1 = merchandise tied to the rack
   2 = merchandise not tied to the rack

b. The results shown are based on the strain gage measurements at the top end of the northeast bottom column.

c. Two peaks were shown in some of the Fourier amplitude curves.

TABLE 5.5

SUMMARY OF MERCHANDISE TEST RESULTS - TRANSVERSE

Type	Test Case[a]	Shaking Table Tests								Pull Tests		
		Test I.D.	Signal	Maximum Table Acceleration (g)	Maximum Table Displacement (in.)	Maximum Story Acceleration (g)	Maximum Relative Story Displacement (in.)	Maximum Strain[c] (mil/in.)	Period (sec)	Period (sec)	Damping (%)	Applied Force (lb)
A	1	270678.2 (A-1-T-1/2 EC)	EC	0.16	1.28	0.22	0.19	0.10	0.28	0.26	0.8	400
	2	270678.4 (A-2-T-1/2 EC)	EC	0.16	1.28	0.28	0.18	0.10	0.28	0.27	1.0	400
B	1	290678.3 (B-1-T-1/2 EC)	EC	0.16	1.28	0.17	0.34	0.16	0.47	0.36	e	600
	2	290678.5 (B-2-T-1/2 EC)	EC	0.16	1.28	0.16	0.34	0.16	0.47	0.39	e	600
C	1	290678.12 (C-1-T-1/2 EC)	EC	0.16	1.28	0.18	0.22	0.09	d	0.32	e	600
	2	290678.14 (C-2-T-1/2 EC)	EC	0.16	1.28	0.16	0.21	0.09	d	0.32	e	600
D	1	290678.18 (D-1-T-3/4 EC)	EC	0.26	1.92	0.29	0.14	0.05	d	0.18	e	600
	2	290678.20 (D-2-T-3/4 EC)	EC	0.25	1.91	0.29	0.14	0.05	d	0.19	e	600
E	1	300678.4 (E-2-T-EC)	EC	0.33	2.40	b	0.18	0.09	d	0.20	e	600
	2	300678.6 (E-2-T-EC)	EC	0.33	2.40	b	0.16	0.08	d	0.20	e	600
H	1	300678.10 (H-1-T-EC)	EC	0.33	2.39	0.37	0.23	0.12	d	0.28	e	600
	2	300678.12 (H-2-T-EC)	EC	0.33	2.39	0.38	0.20	0.11	d	0.29	e	600

a. 1 = merchandise tied to the rack
2 = merchandise not tied to the rack

b. A sharp peak was observed in the time-history plots (see Figure 5.20b).

c. The results shown are based on the strain gage measurements on the east frame bottom diagonal brace.

d. Many peaks were shown in the Fourier amplitude curves.

e. See text.

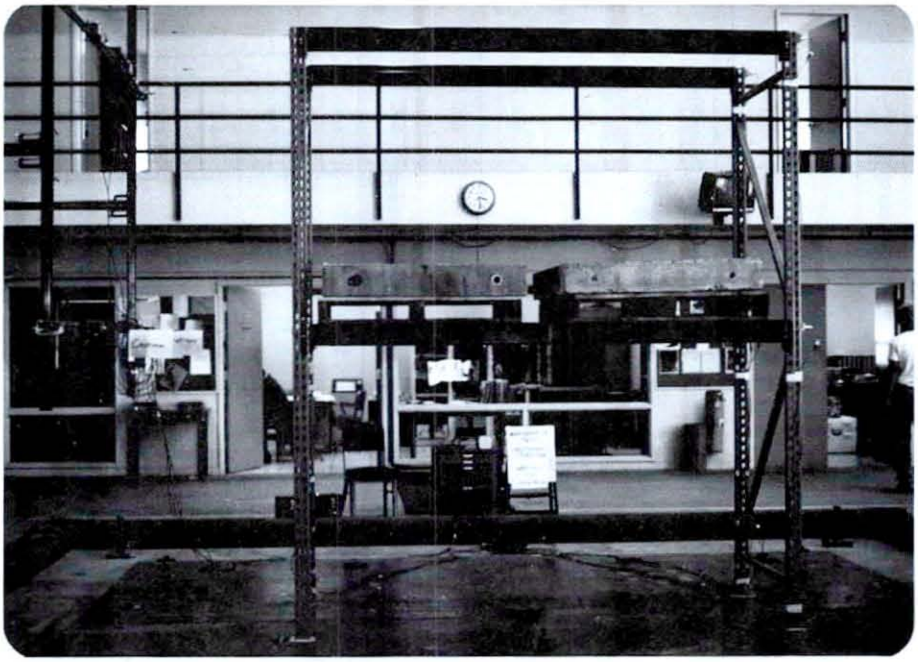

Type A - Not Tied

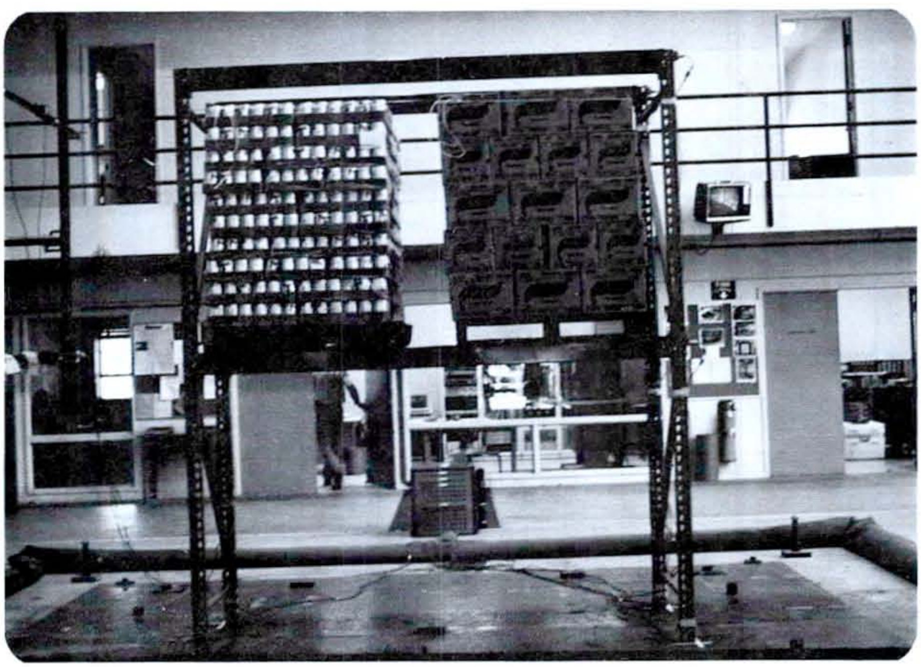

Type B - Not Tied

FIGURE 5.1 MERCHANDISE TYPES A AND B - LONGITUDINAL

Type C - Not Tied

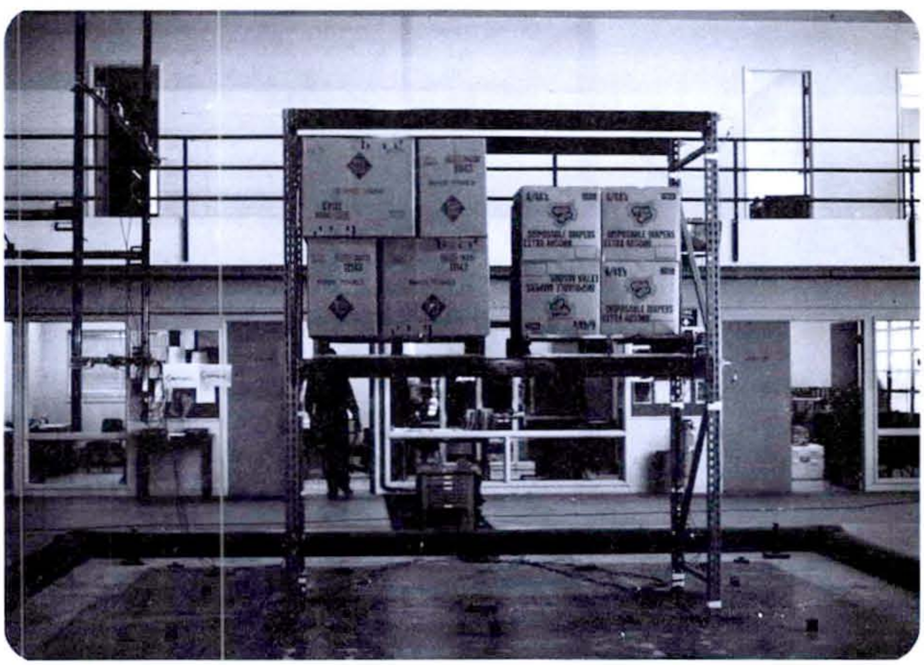

Type D - Not Tied

FIGURE 5.2 MERCHANDISE TYPES C AND D - LONGITUDINAL

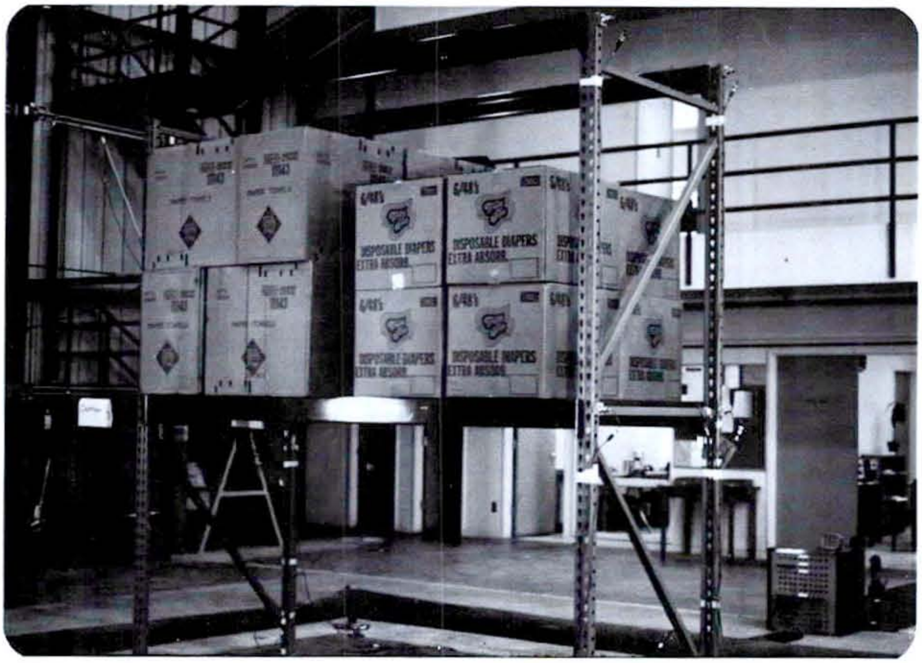

Not Tied

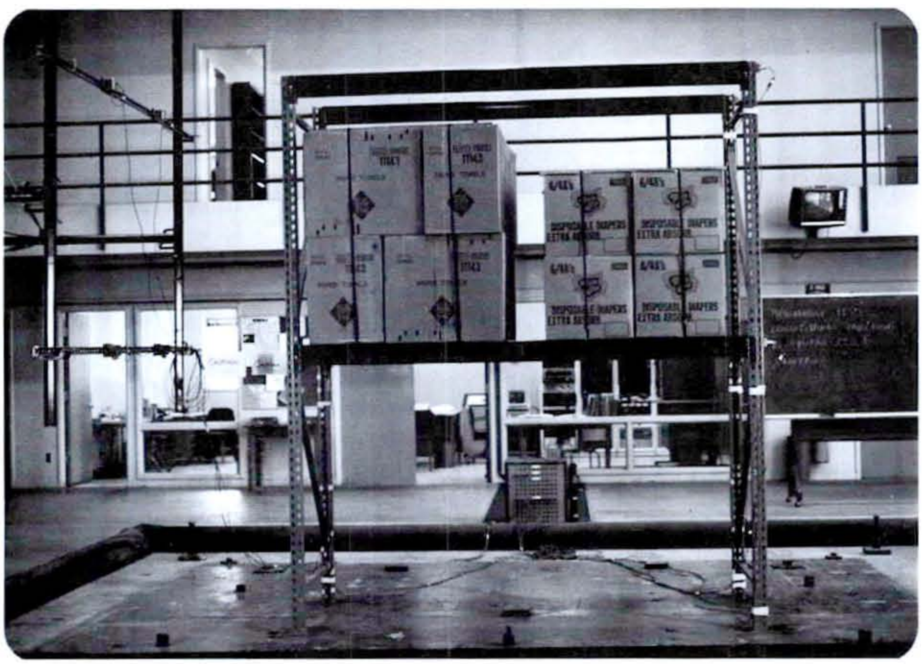

Tied

FIGURE 5.3 MERCHANDISE TYPE F - LONGITUDINAL

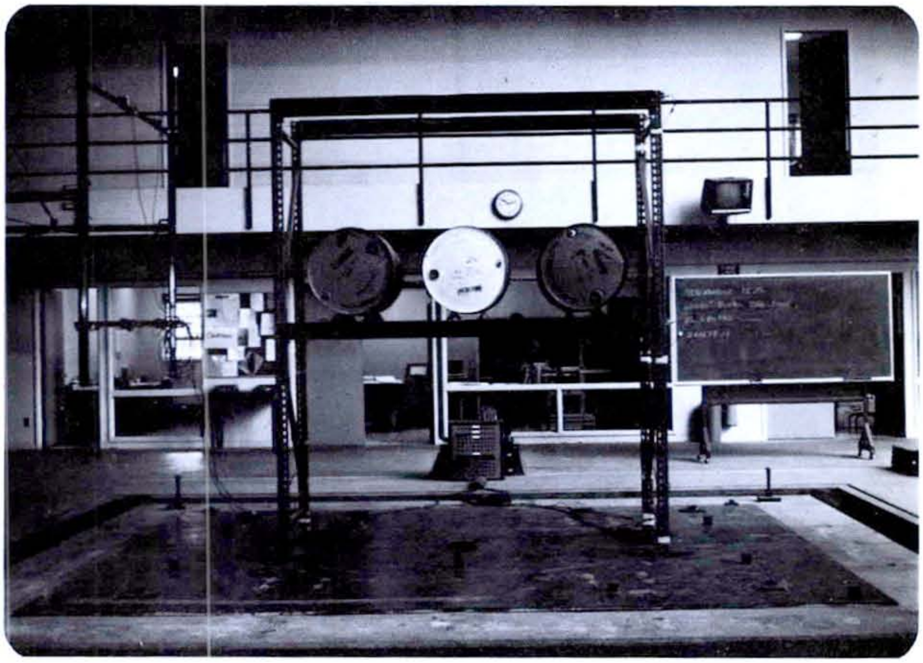

Type E - Not Tied

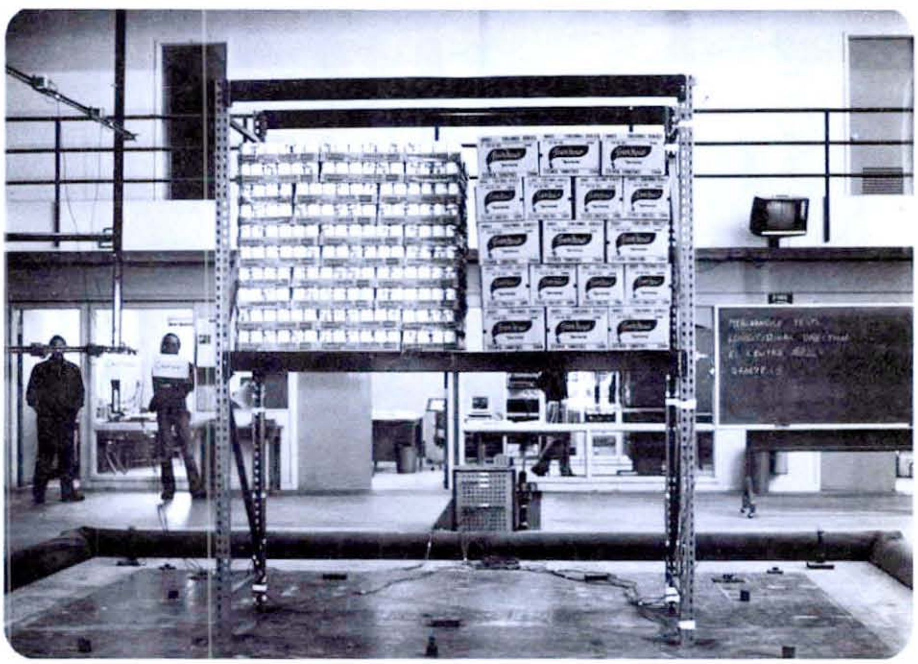

Type G - Not Tied

FIGURE 5.4 MERCHANDISE TYPES E AND G - LONGITUDINAL

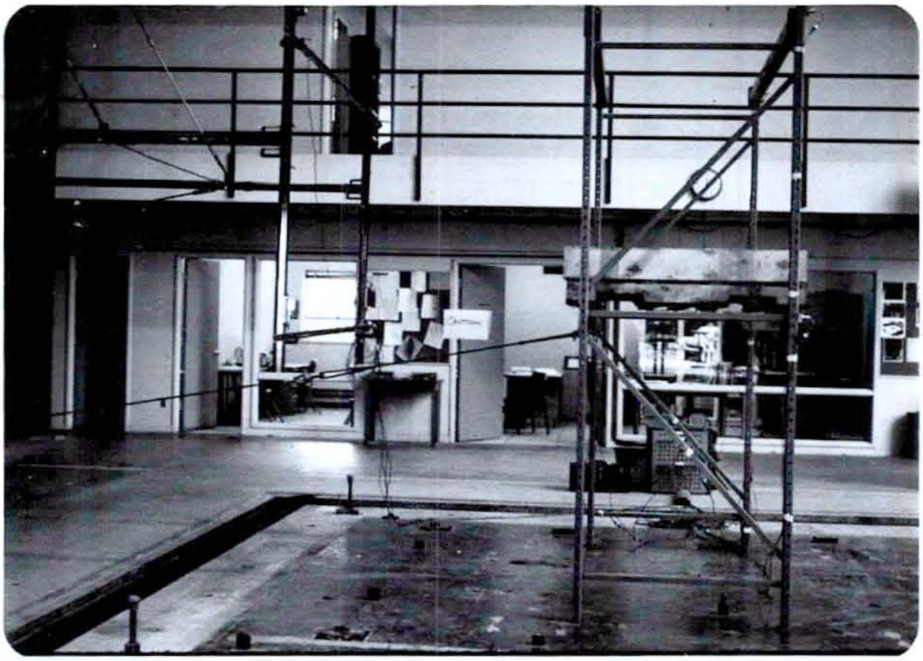

Not Tied

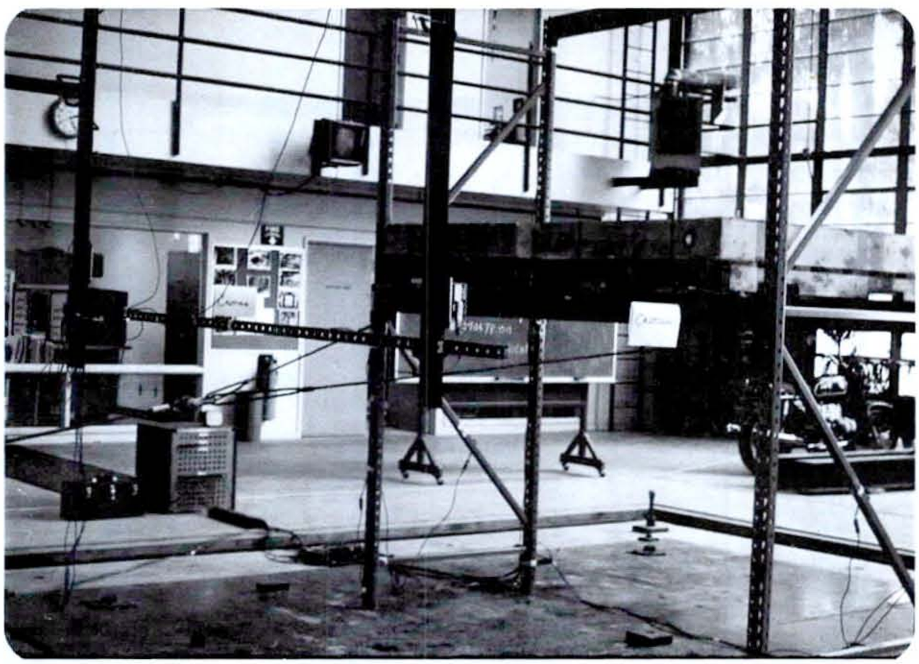

Tied

FIGURE 5.5 MERCHANDISE TYPE A - TRANSVERSE

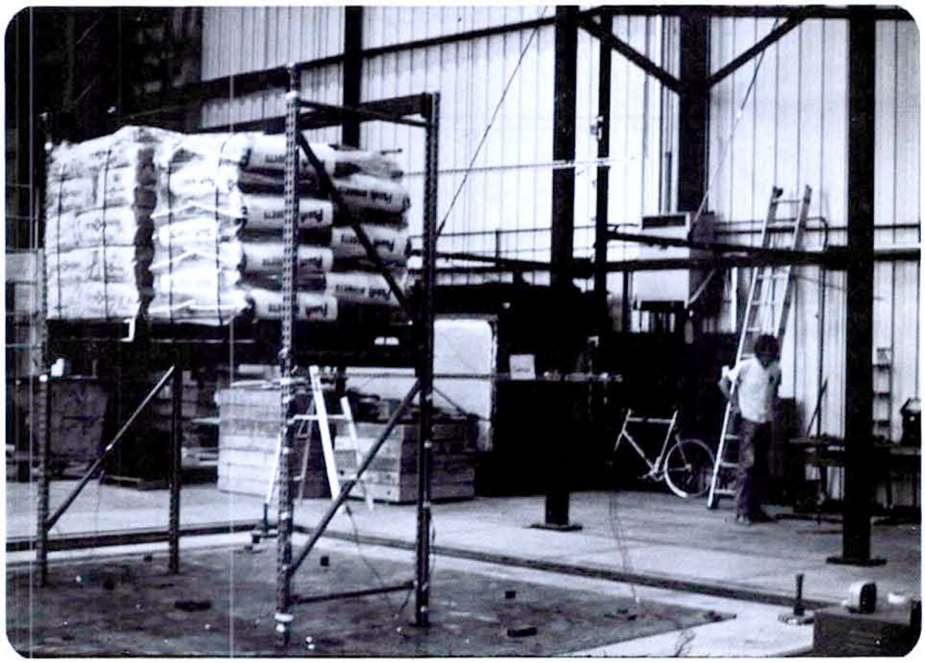

Type C - Tied

Type H - Not Tied

FIGURE 5.6 MERCHANDISE TYPES C AND H - TRANSVERSE

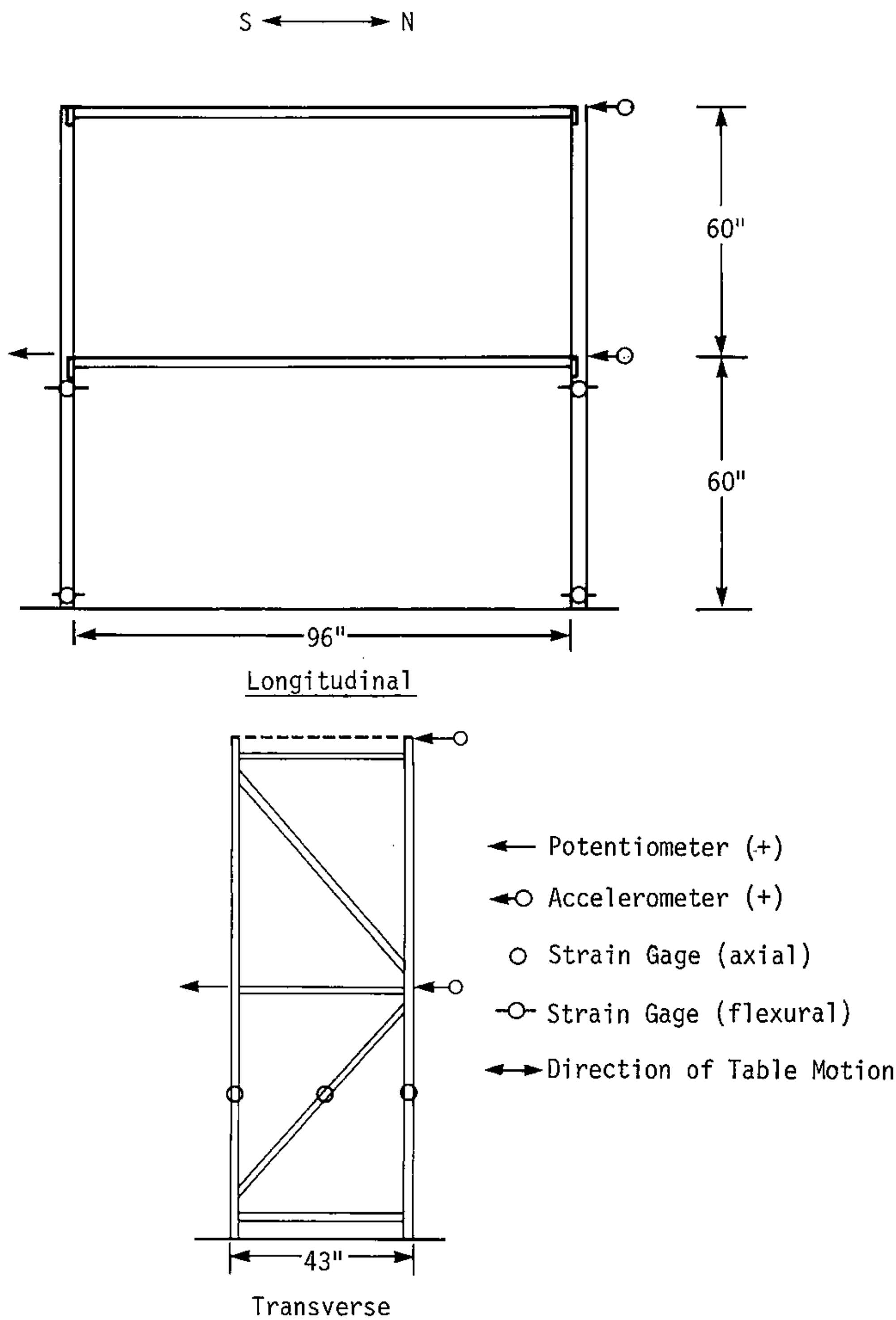

FIGURE 5.7 INSTRUMENTATION CHANNELS USED FOR DATA ANALYSIS IN THE MERCHANDISE TESTS

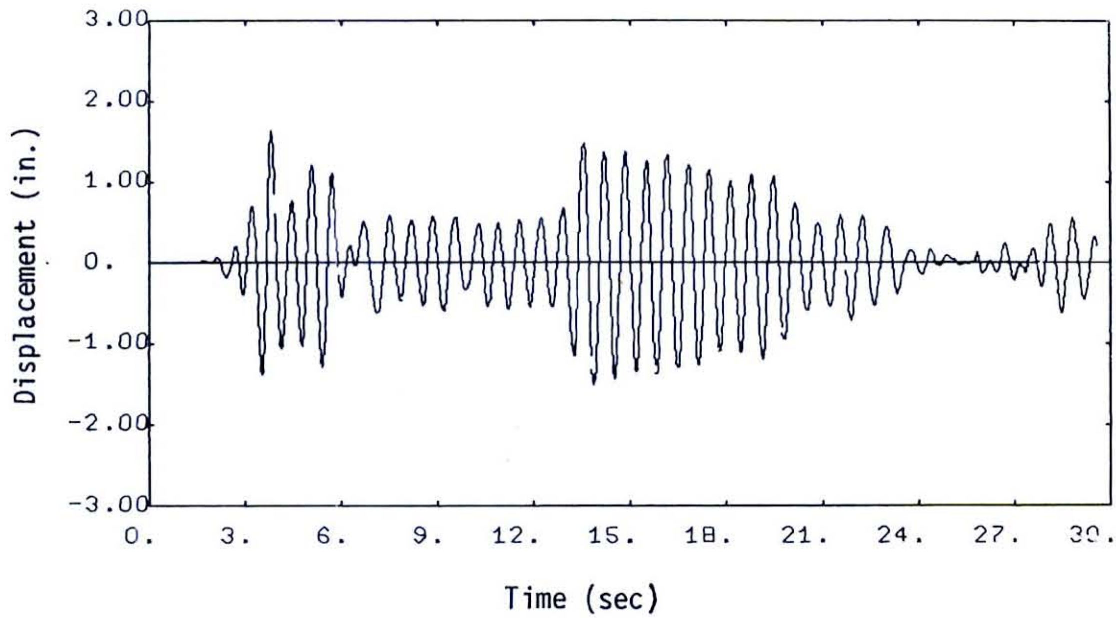

Test A-1-L-5/8 EC

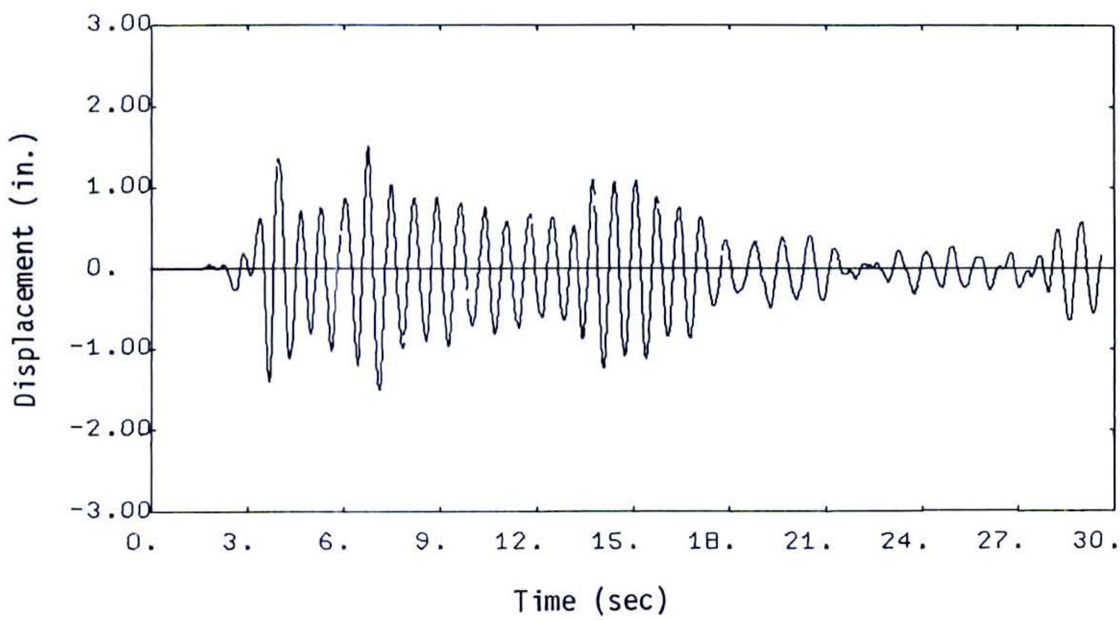

Test A-2-L-5/8 EC

FIGURE 5.8a RELATIVE STORY DISPLACEMENTS - LONGITUDINAL TEST, TYPE A

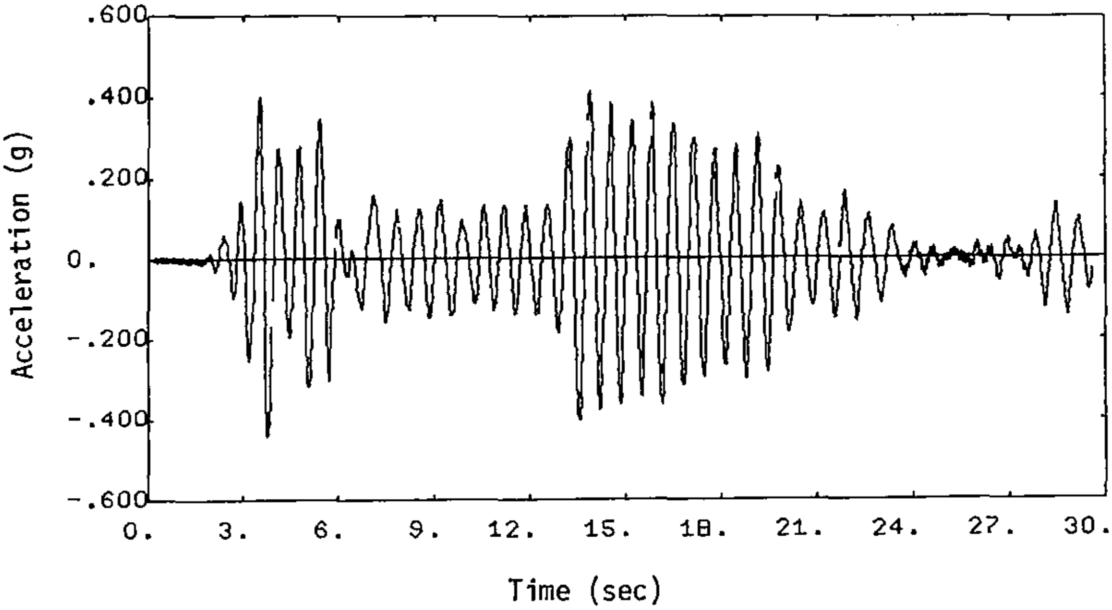

Test A-1-L-5/8 EC

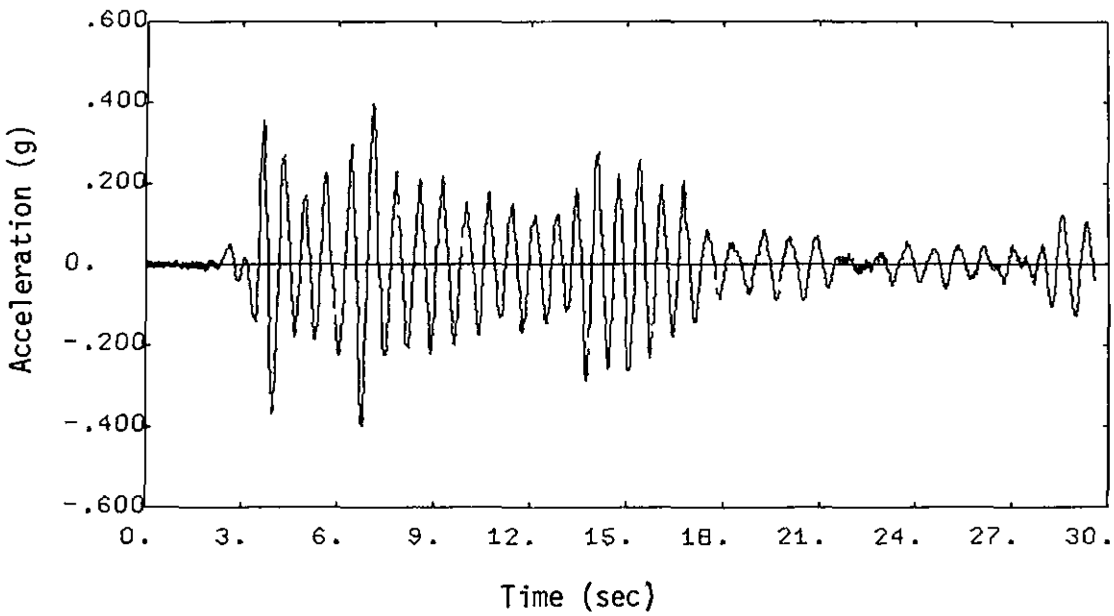

Test A-2-L-5/8 EC

FIGURE 5.8b STORY ACCELERATIONS - LONGITUDINAL TEST, TYPE A

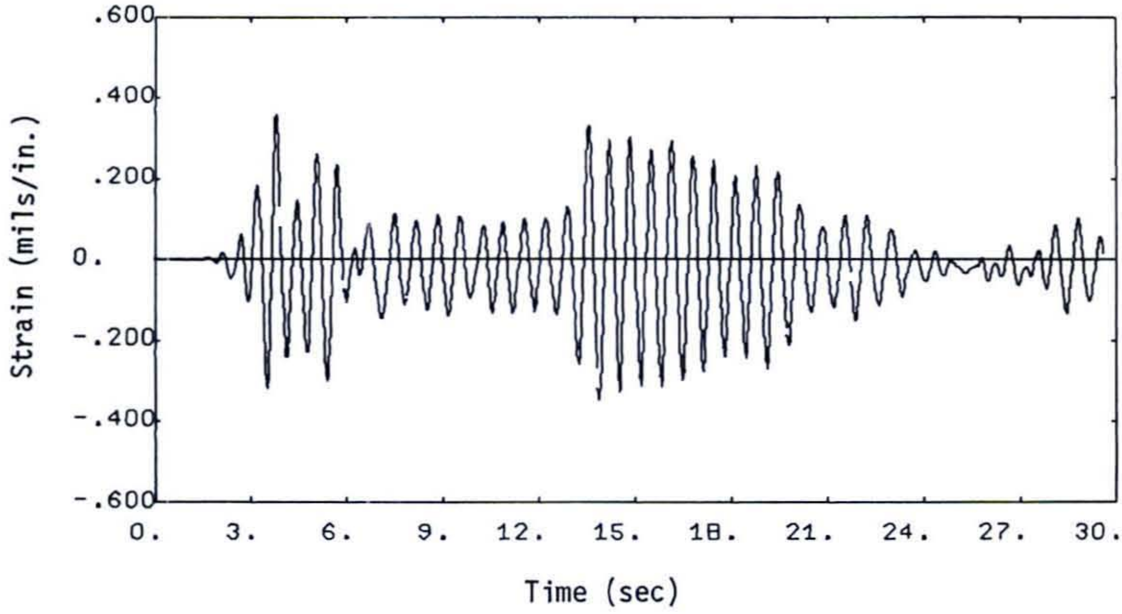

Test A-1-L-5/8 EC

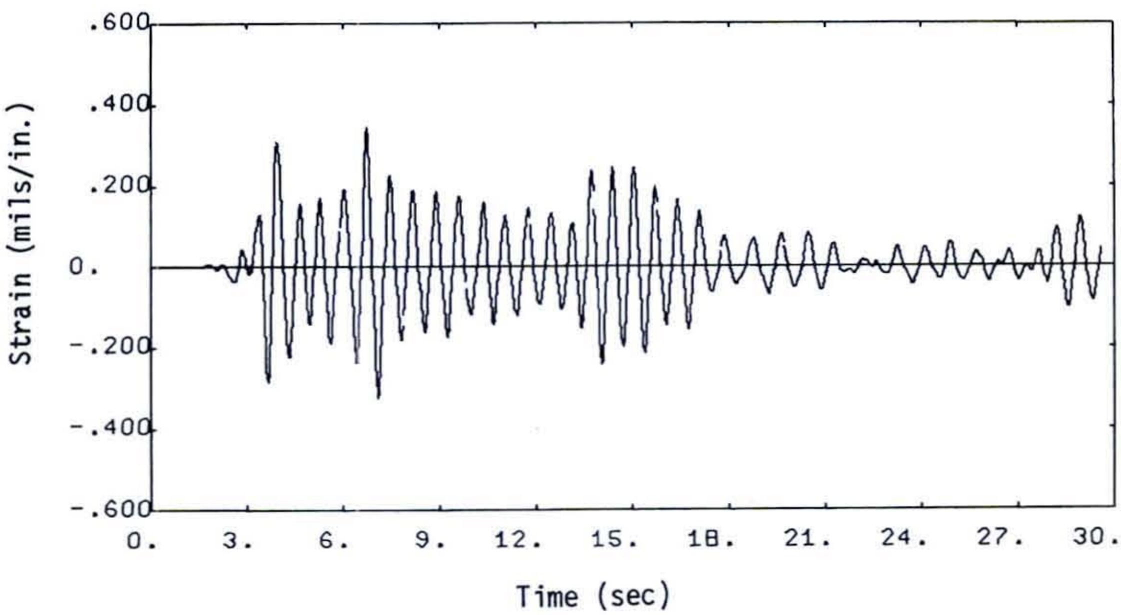

Test A-2-L-5/8 EC

FIGURE 5.8c COLUMN FLEXURAL STRAINS - LONGITUDINAL TEST, TYPE A

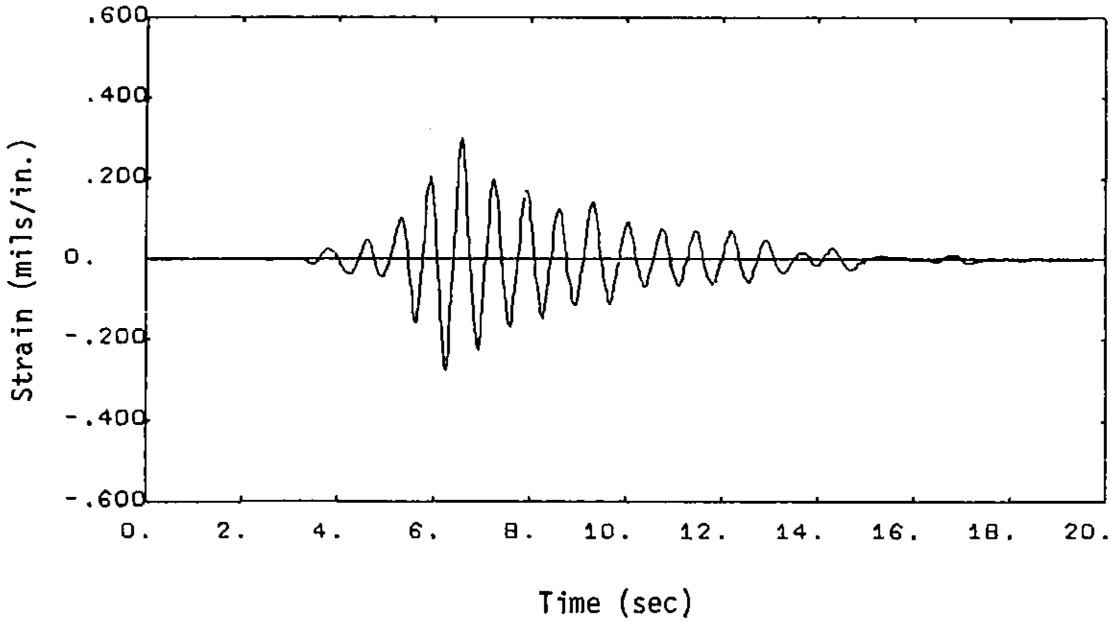

Test A-2-L-5/16 PF

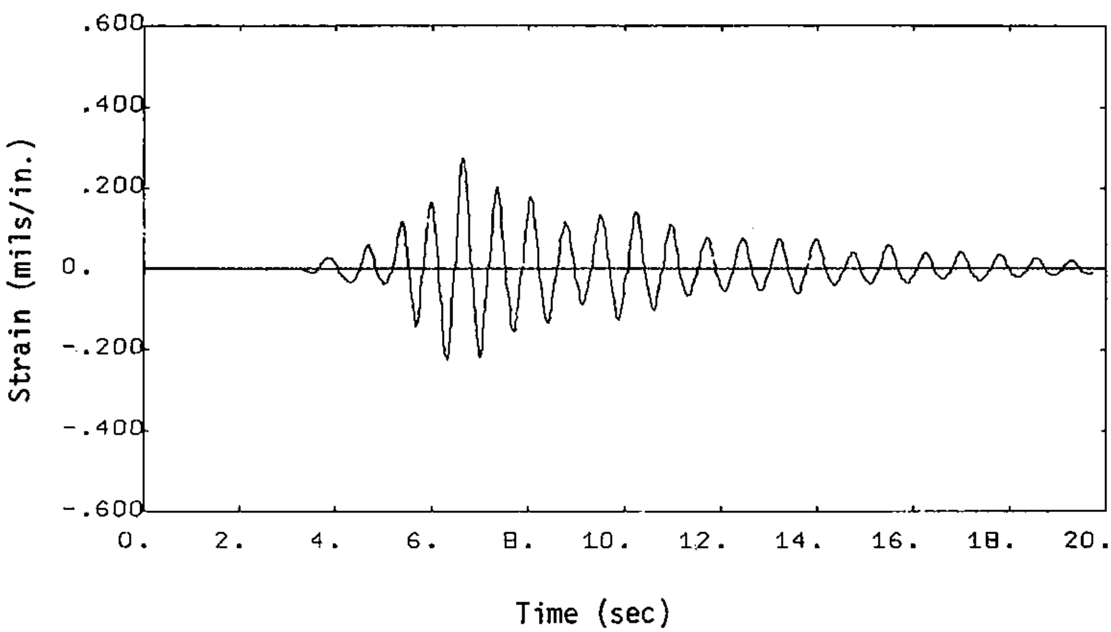

Test A-1-L-5/16 PF

FIGURE 5.9a RELATIVE STORY DISPLACEMENTS - LONGITUDINAL TEST, TYPE A

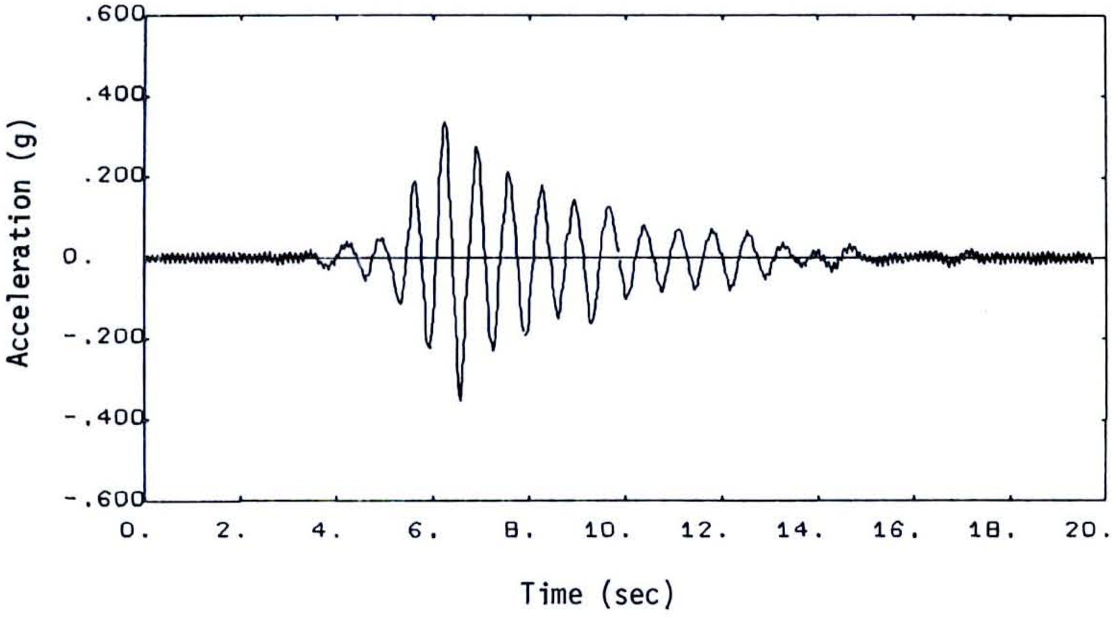

Test A-1-L-5/16 PF

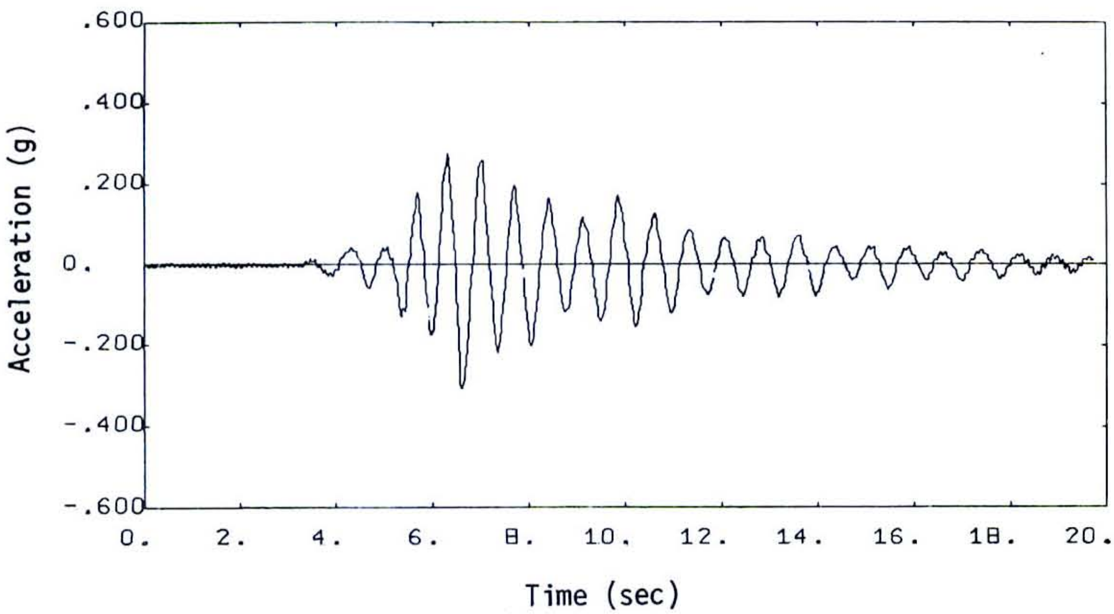

Test A-2-L-5/16 PF

FIGURE 5.9b STORY ACCELERATIONS - LONGITUDINAL TEST, TYPE A

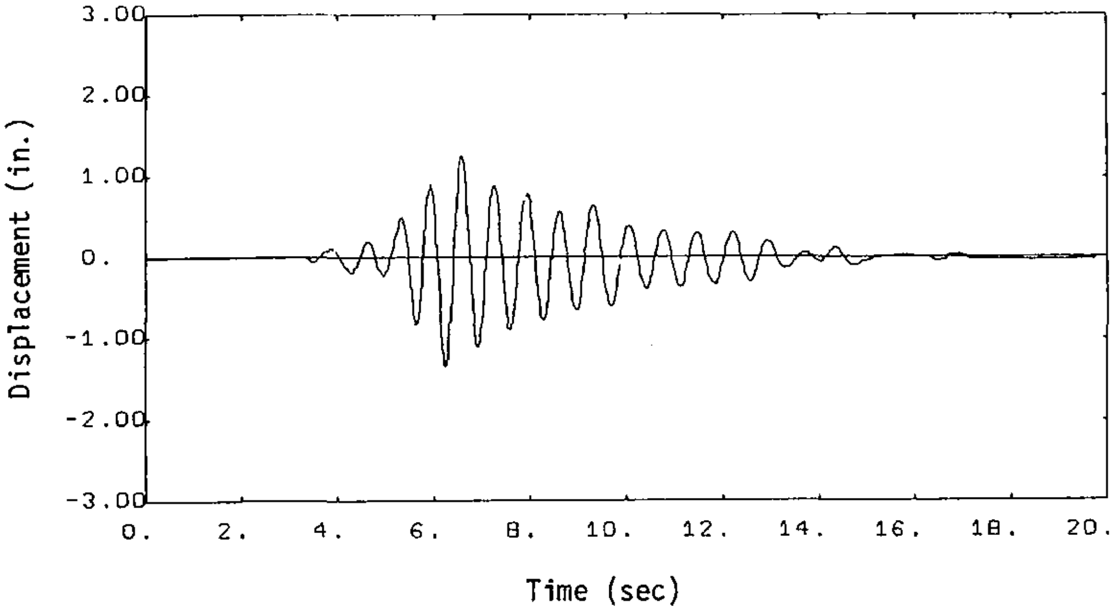

Test A-1-L-5/16 PF

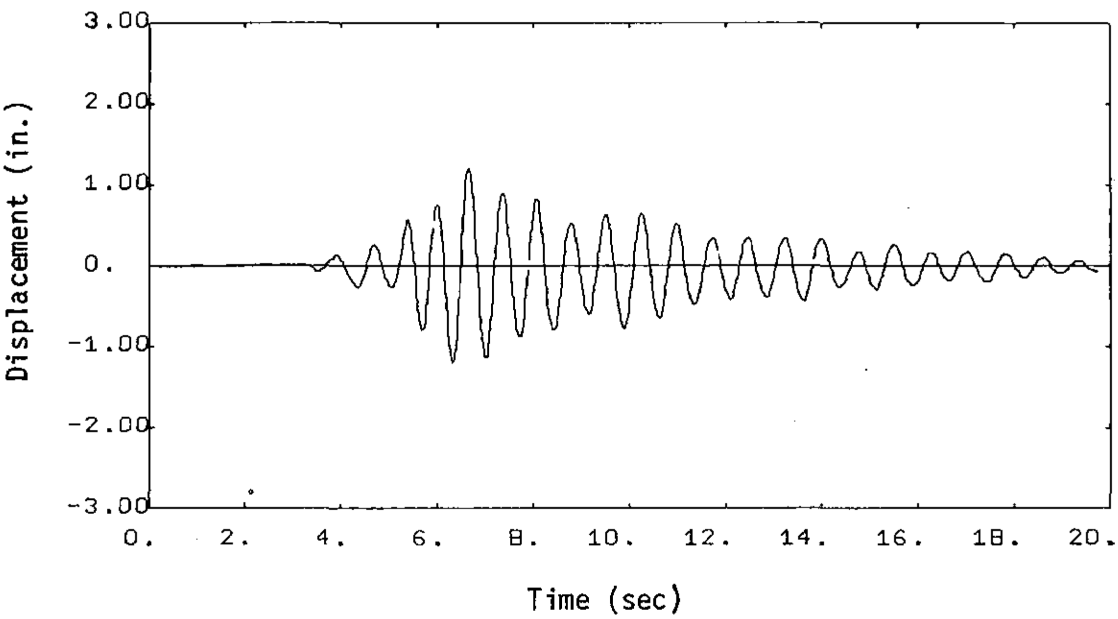

Test A-2-L-5/16 PF

FIGURE 5.9c COLUMN FLEXURAL STRAINS - LONGITUDINAL TEST, TYPE A

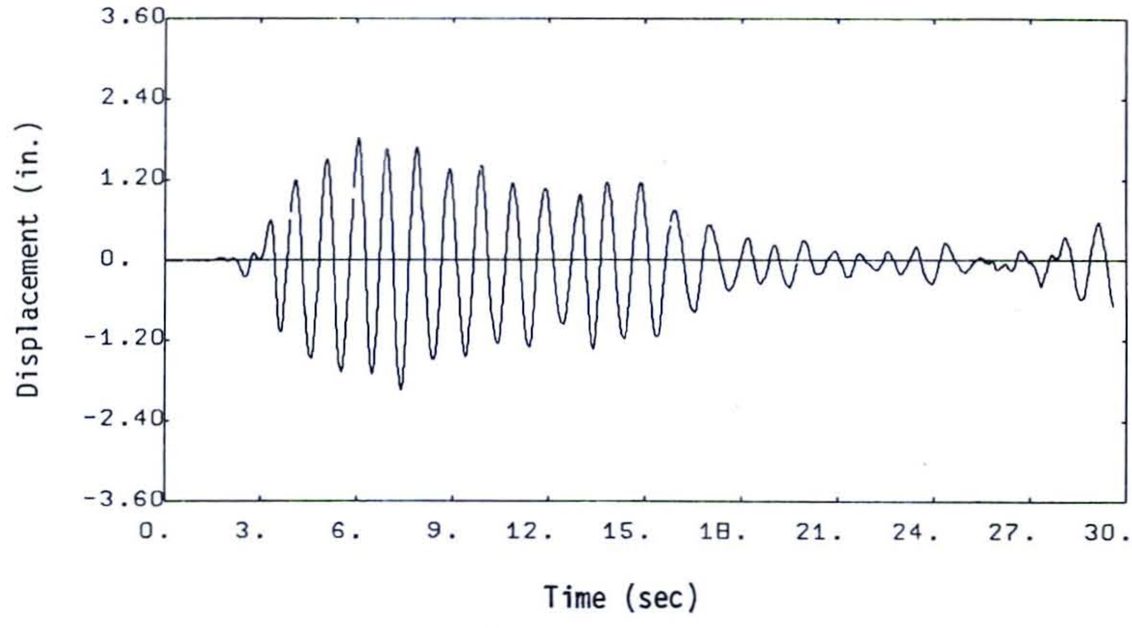

Test B-1-L-1/2 EC

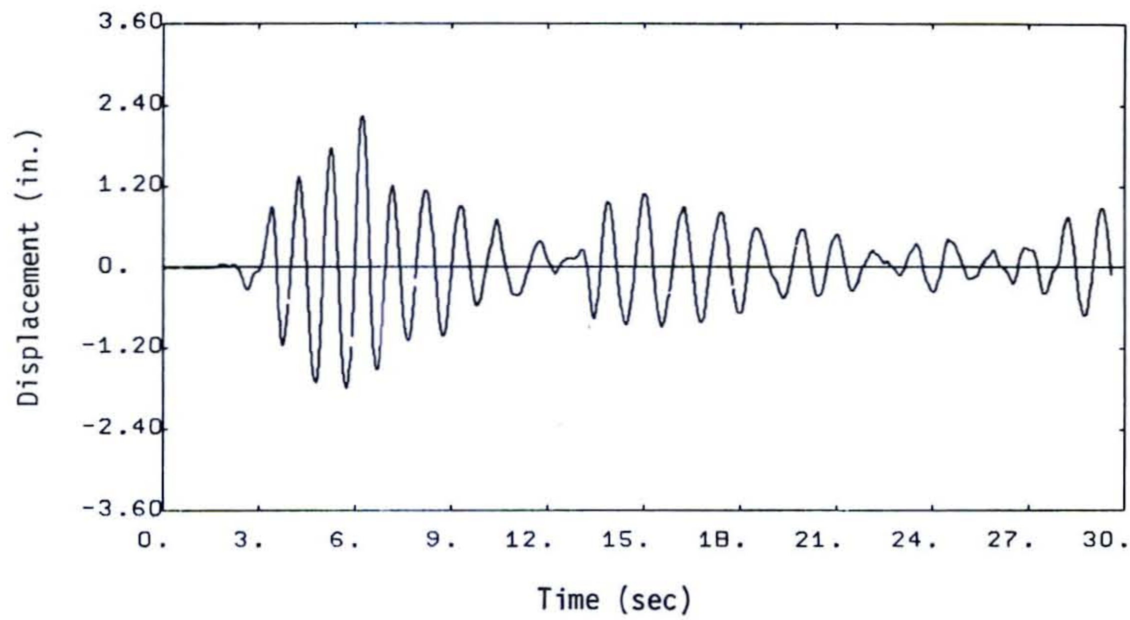

Test B-2-L-1/2 EC

FIGURE 5.10a RELATIVE STORY DISPLACEMENTS - LONGITUDINAL TEST, TYPE B

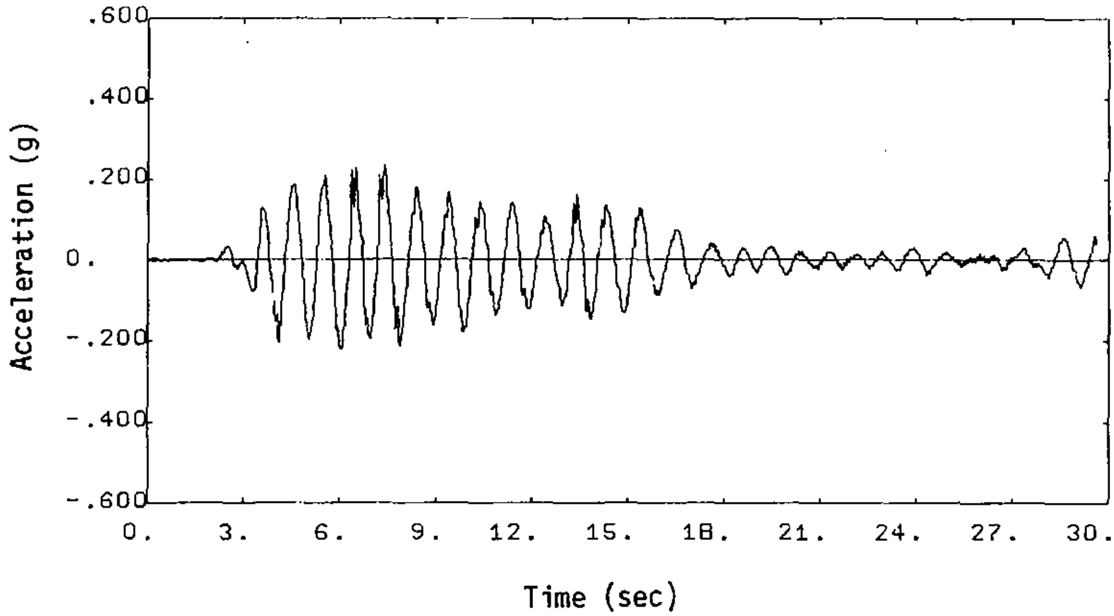

Test B-1-L-1/2 EC

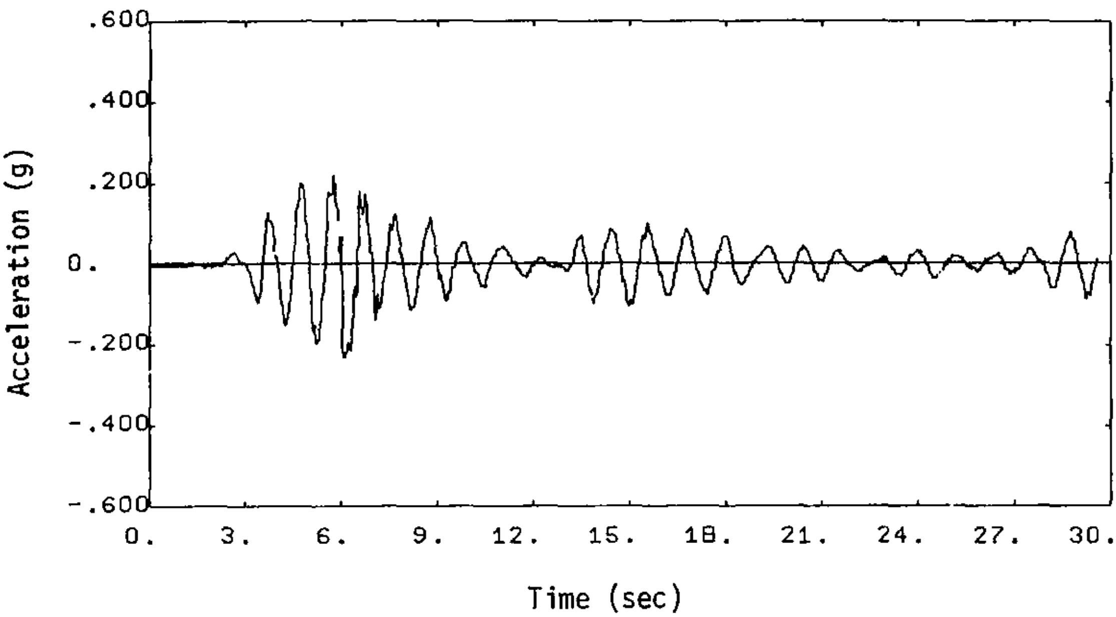

Test B-2-L-1/2 EC

FIGURE 5.10b STORY ACCELERATIONS - LONGITUDINAL TEST, TYPE B

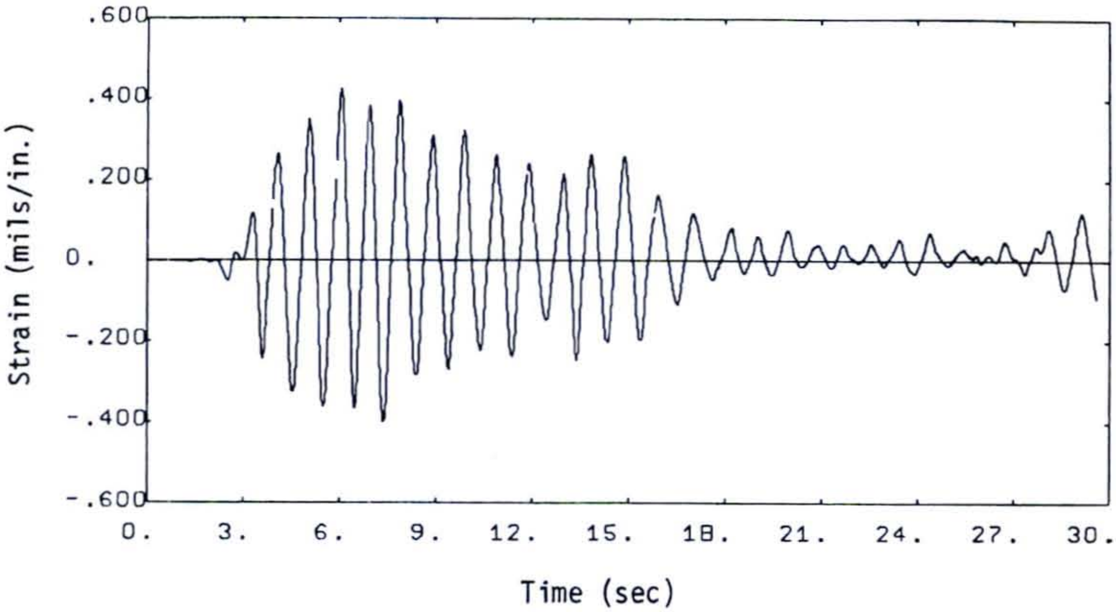

Test B-1-L-1/2 EC

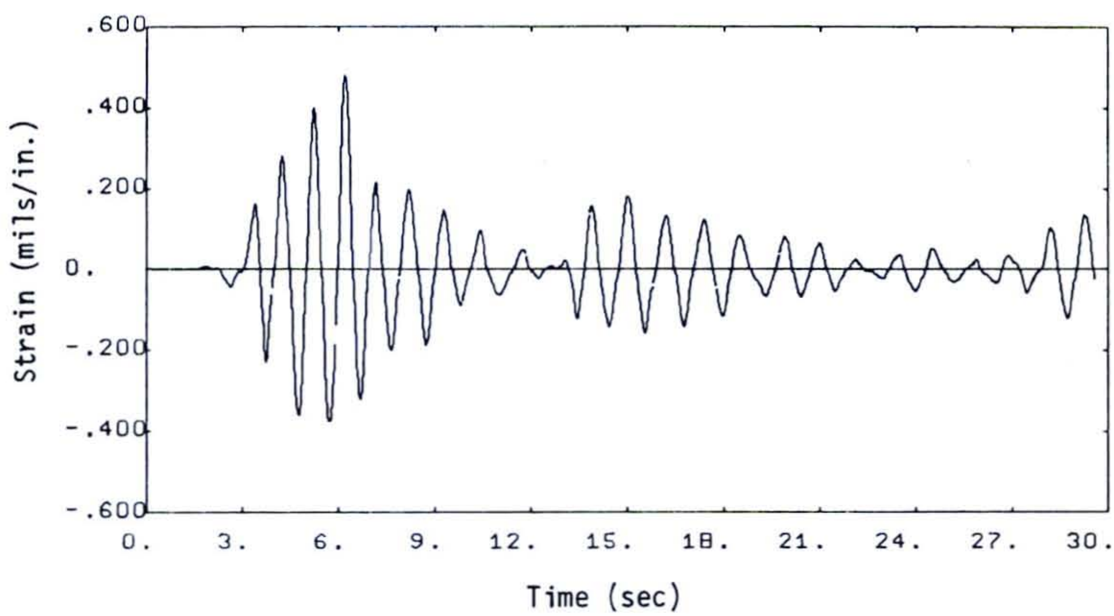

Test B-2-L-1/2 EC

FIGURE 5.10c COLUMN FLEXURAL STRAINS - LONGITUDINAL TEST, TYPE B

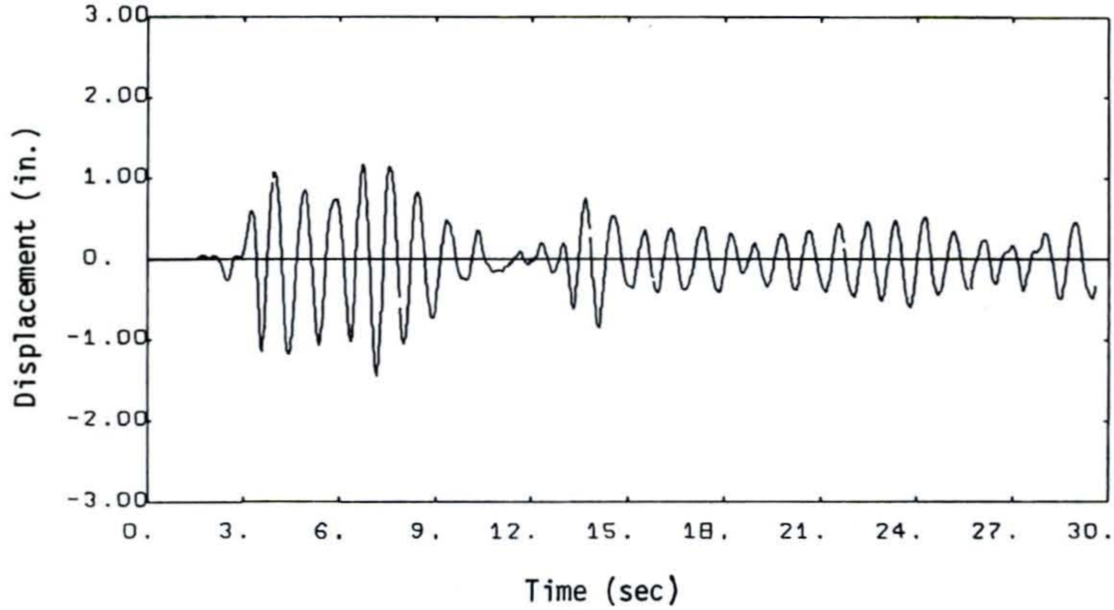

Test C-1-L-1/2 EC

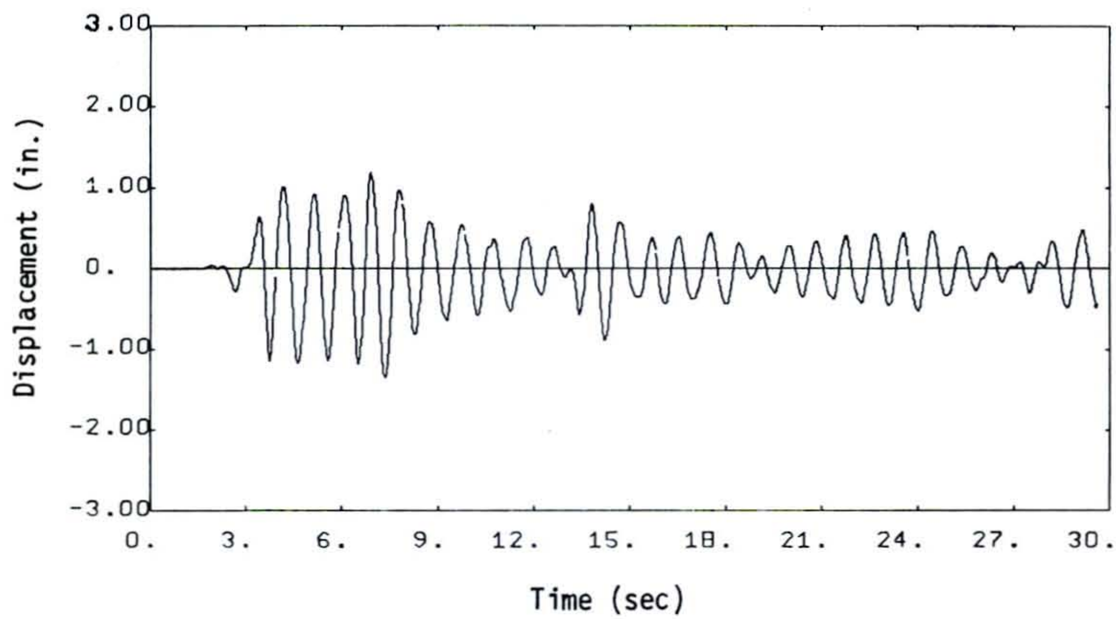

Test C-2-L-1/2 EC

FIGURE 5.11a RELATIVE STORY DISPLACEMENTS - LONGITUDINAL TEST, TYPE C

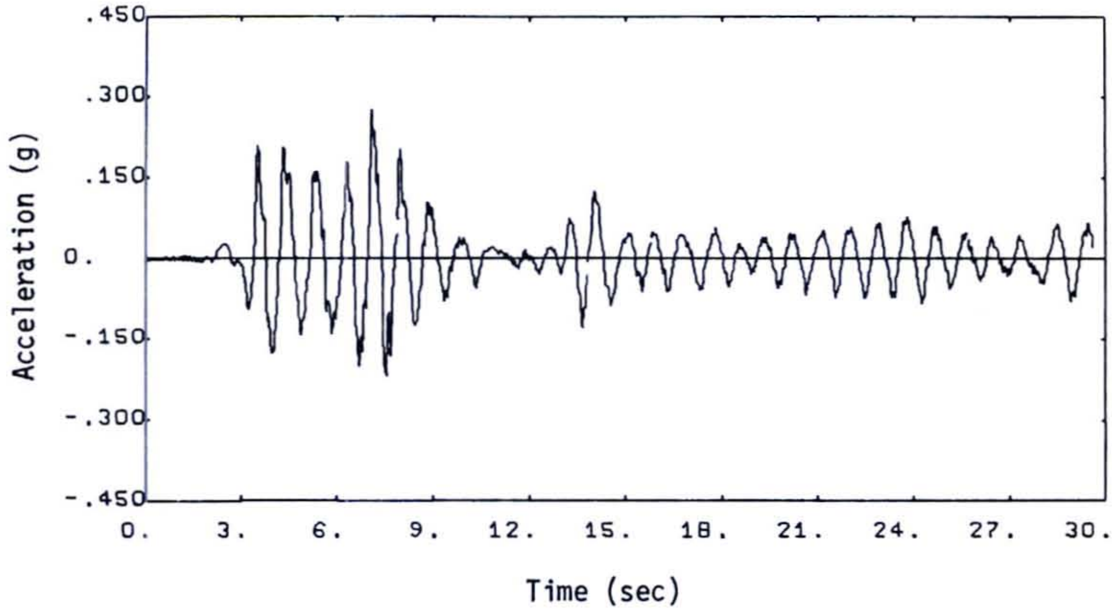

Test C-1-L-1/2 EC

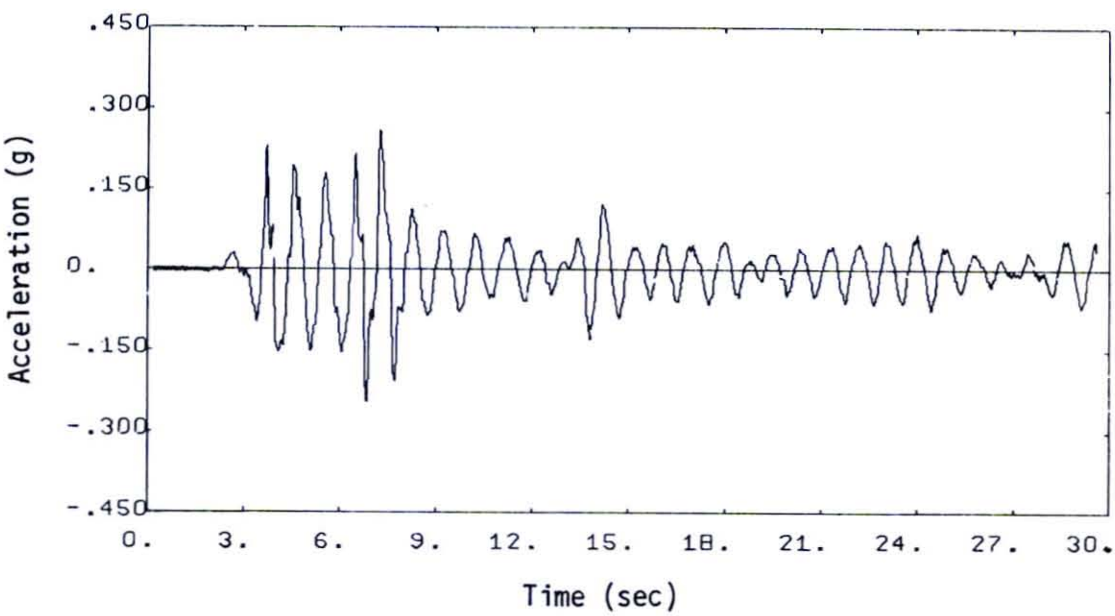

Test C-2-L-1/2 EC

FIGURE 5.11b STORY ACCELERATIONS - LONGITUDINAL TEST, TYPE C

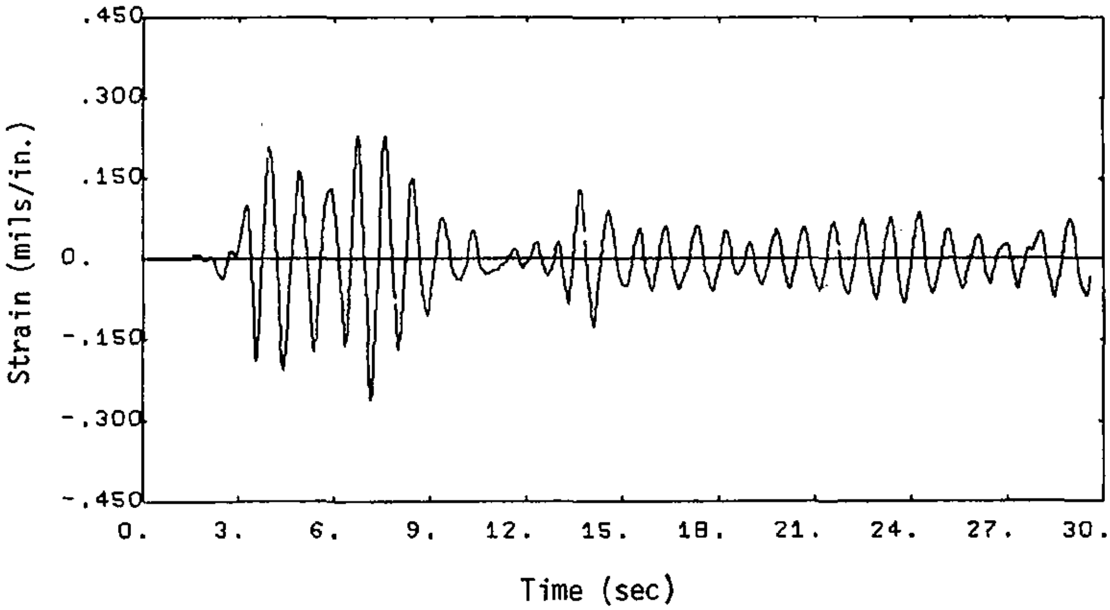

Test C-1-L-1/2 EC

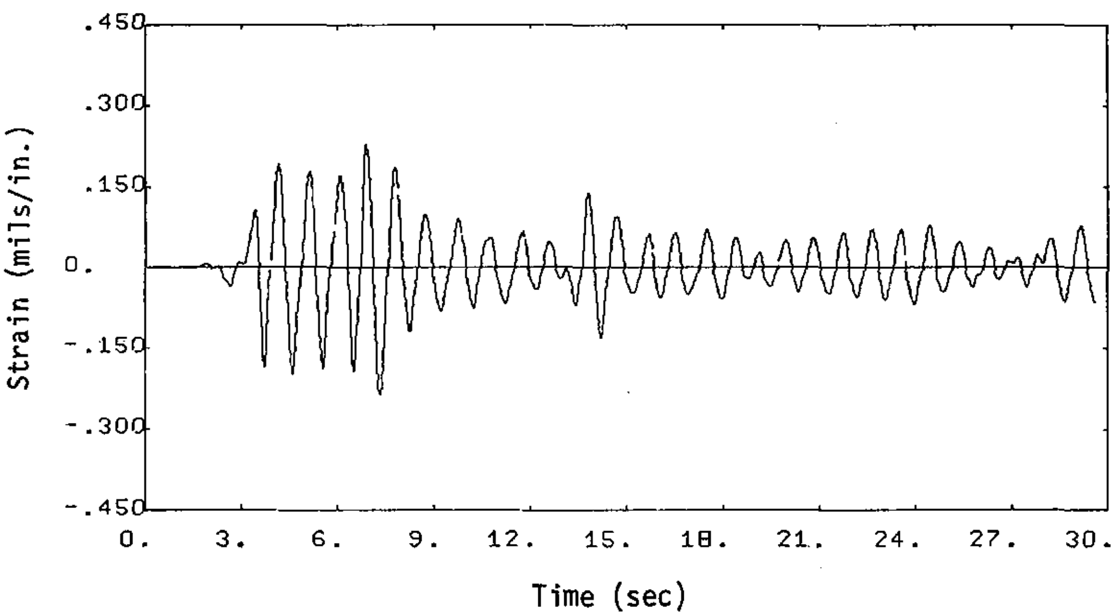

Test C-2-L-1/2 EC

FIGURE 5.11c COLUMN FLEXURAL STRAINS - LONGITUDINAL TEST, TYPE C

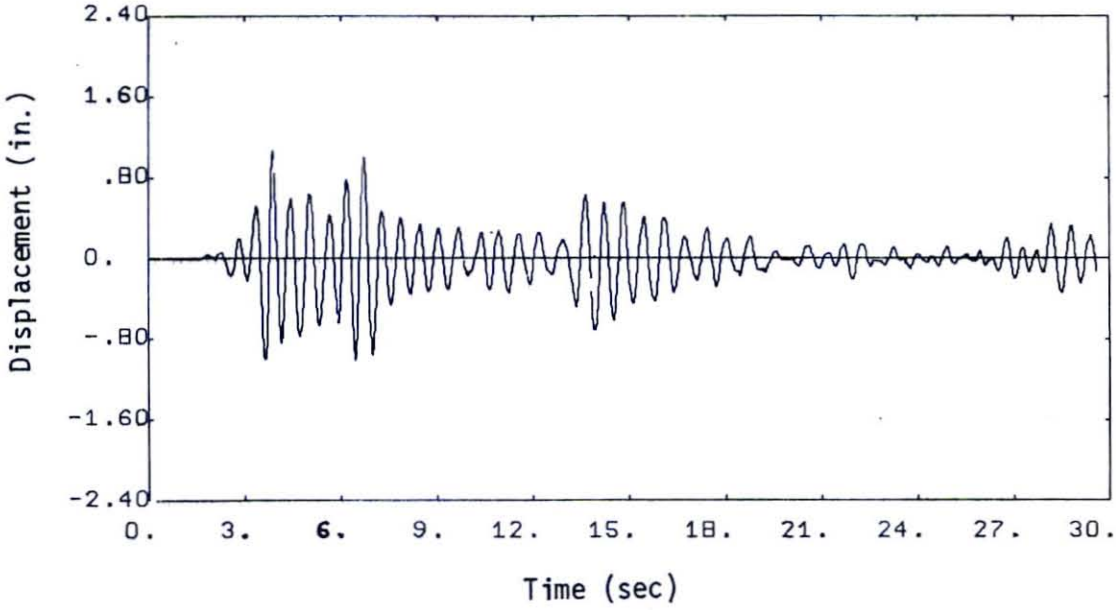

Test D-1-L-1/2 EC

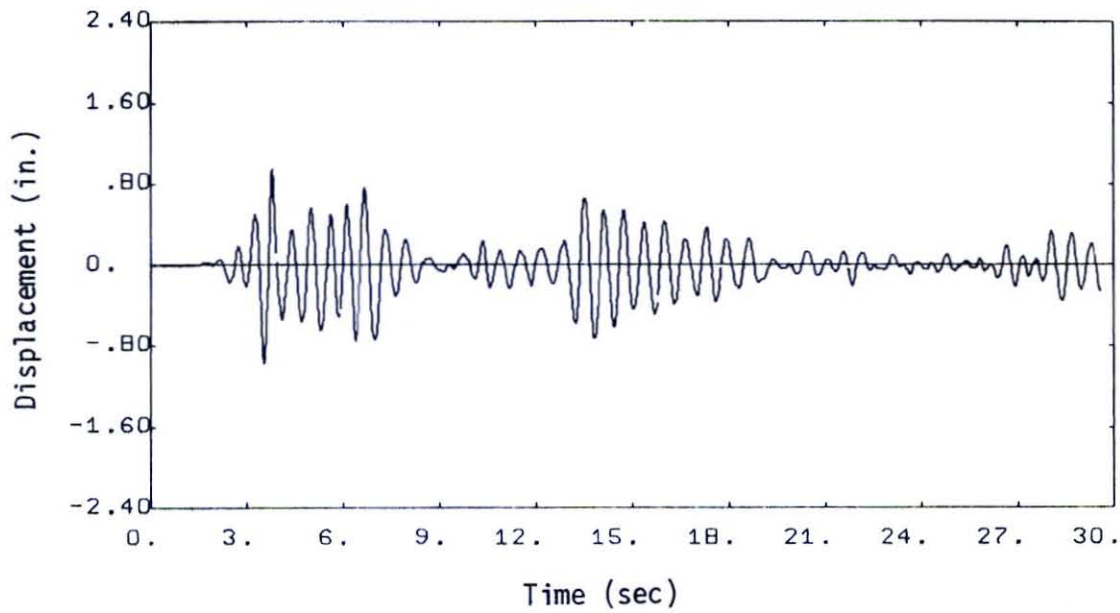

Test D-2-L-1/2 EC

FIGURE 5.12a RELATIVE STORY DISPLACEMENTS - LONGITUDINAL TEST, TYPE D

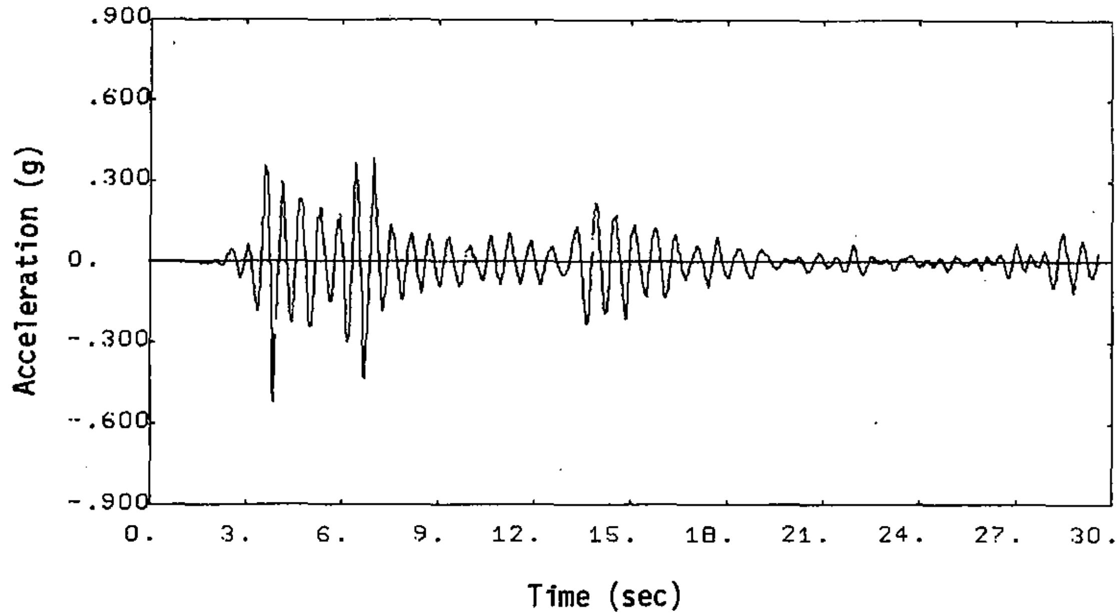

Test D-1-L-1/2 EC

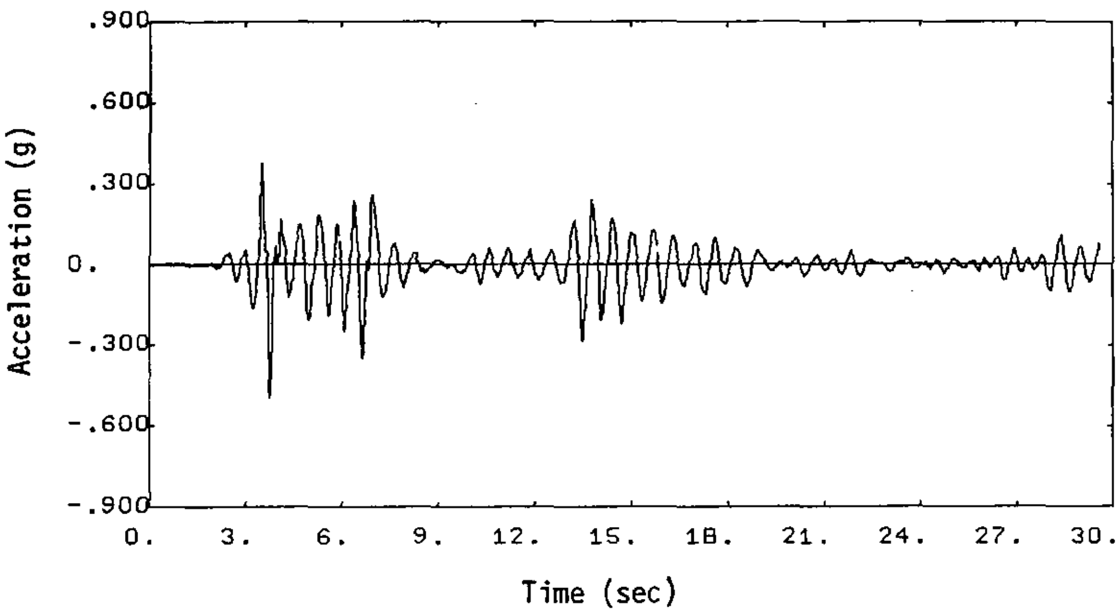

Test D-2-L-1/2 EC

FIGURE 5.12b STORY ACCELERATIONS - LONGITUDINAL TEST, TYPE D

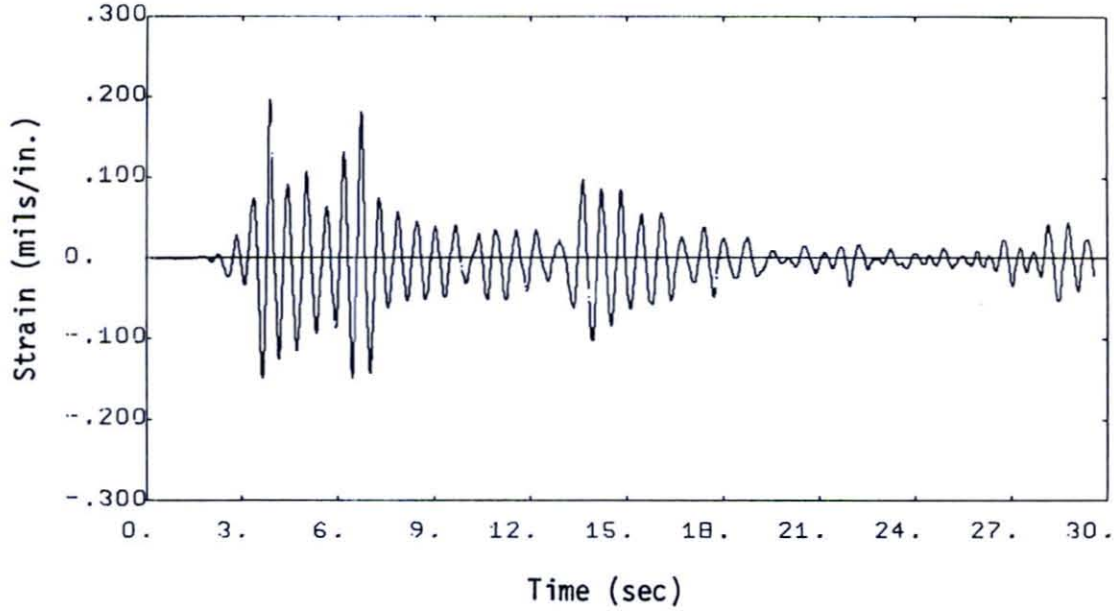

Test D-1-L-1/2 EC

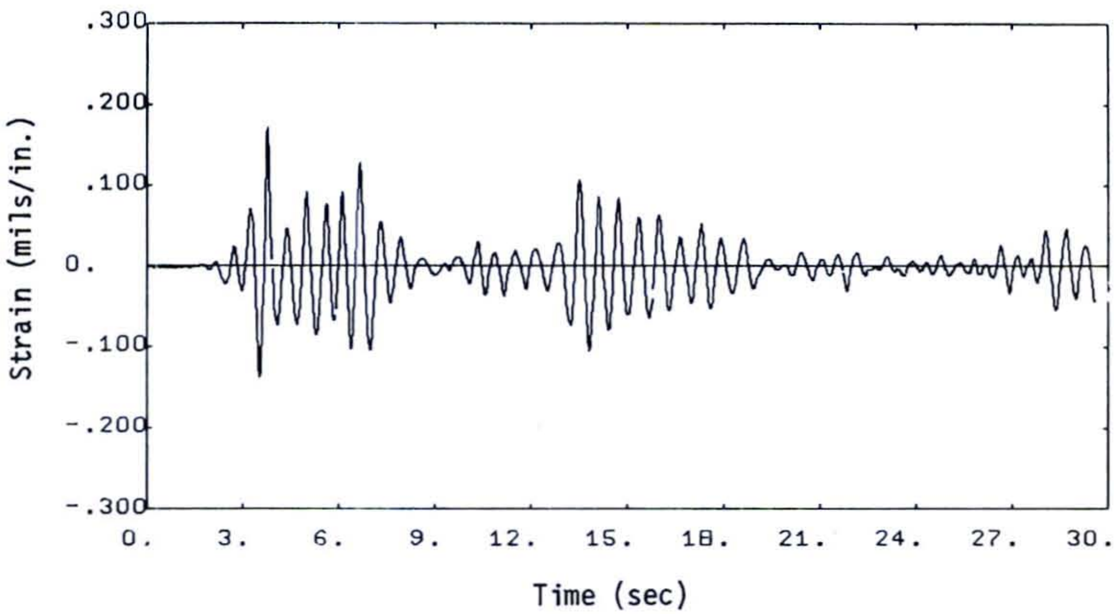

Test D-2-L-1/2 EC

FIGURE 5.12c COLUMN FLEXURAL STRAINS - LONGITUDINAL TEST, TYPE D

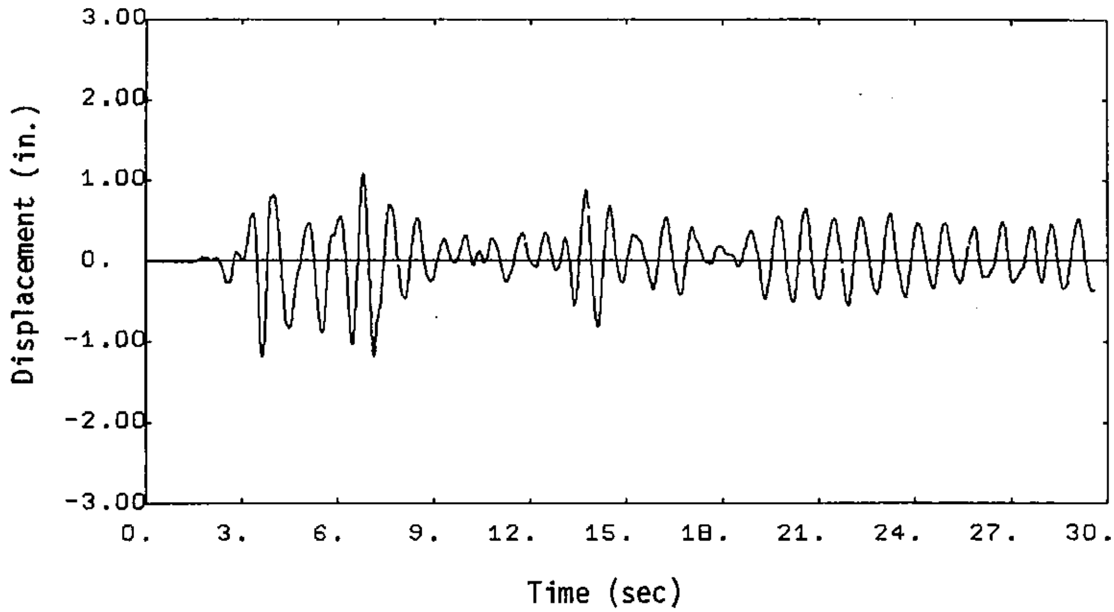

Test E-1-L-5/8 EC

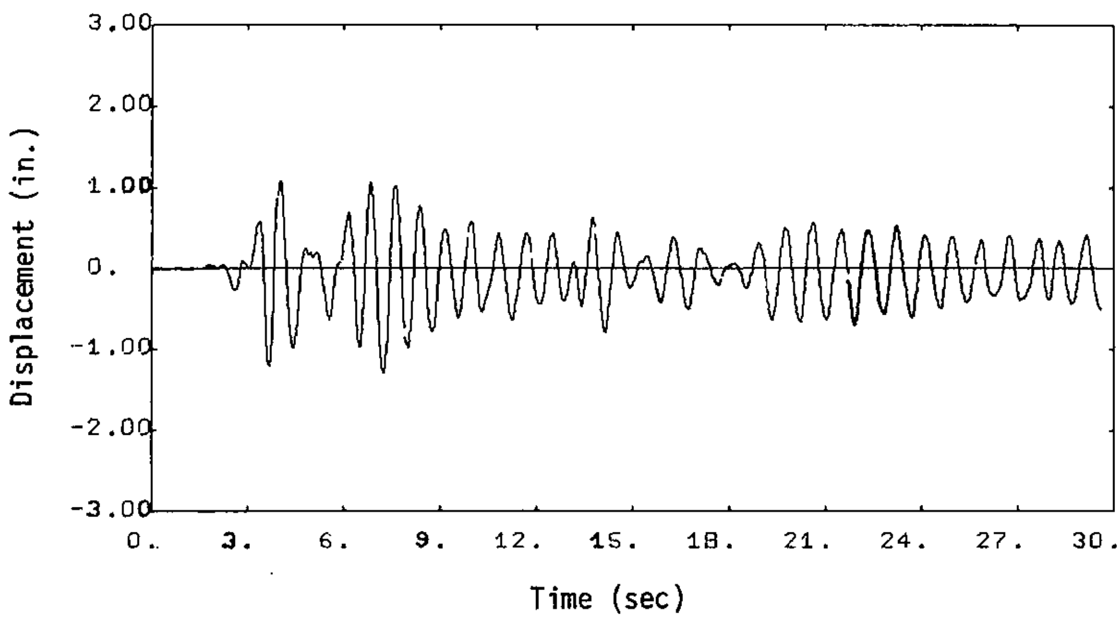

Test E-2-L-5/8 EC

FIGURE 5.13a RELATIVE STORY DISPLACEMENTS - LONGITUDINAL TEST, TYPE E

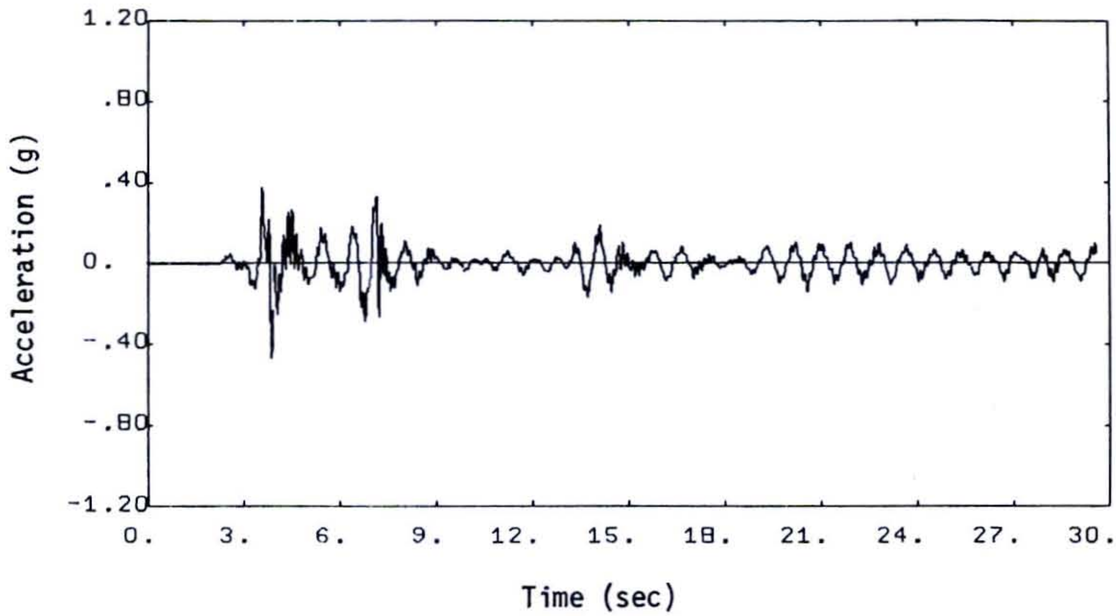

Test E-1-L-5/8 EC

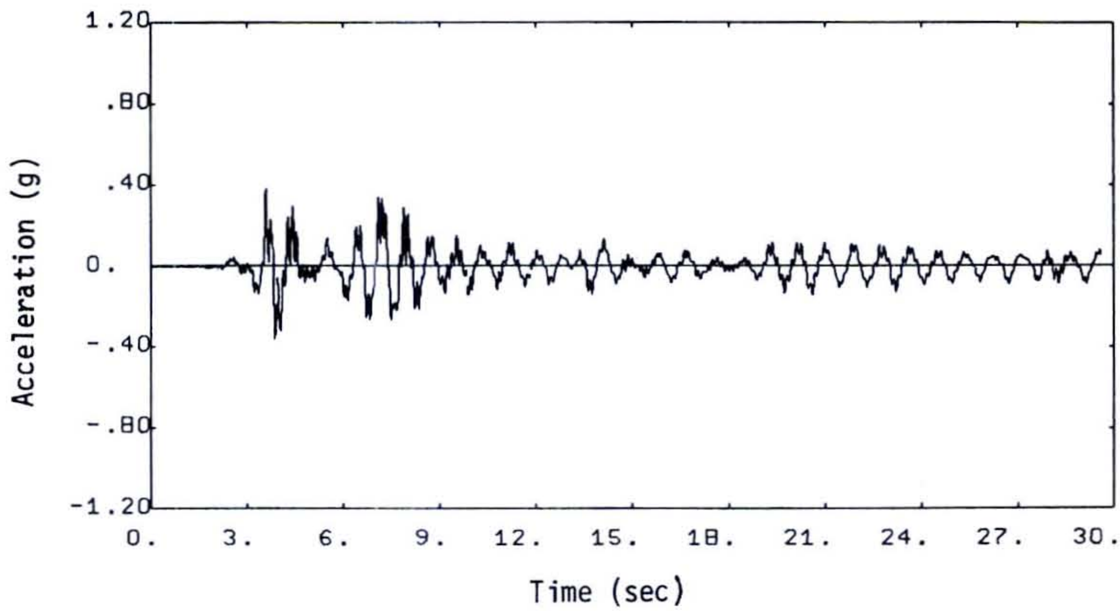

Test E-2-L-5/8 EC

FIGURE 5.13b STORY ACCELERATIONS - LONGITUDINAL TEST, TYPE E

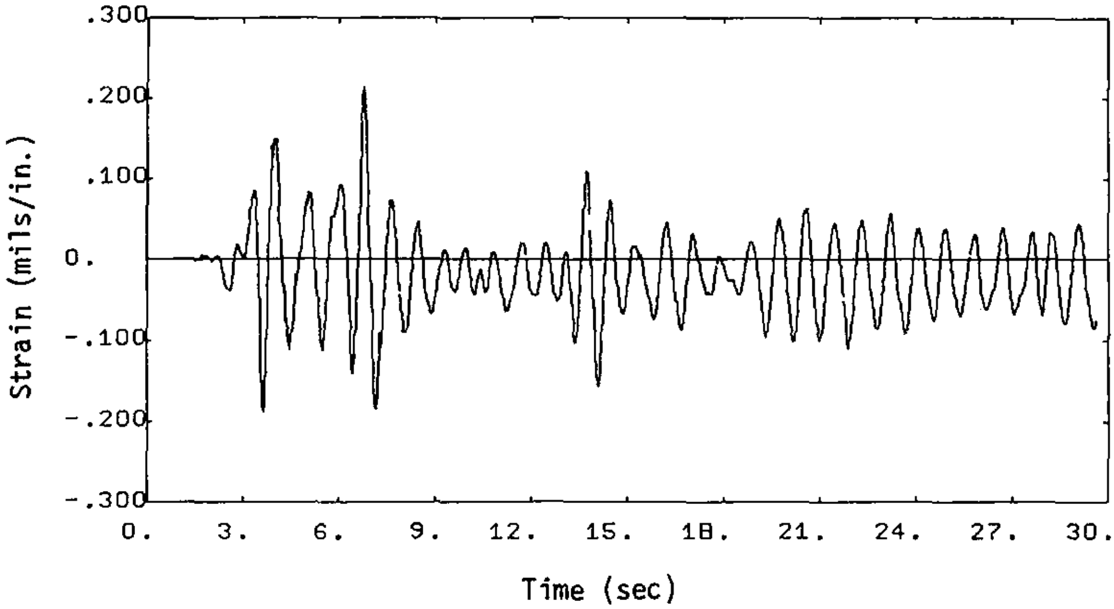

Test E-1-L-5/8 EC

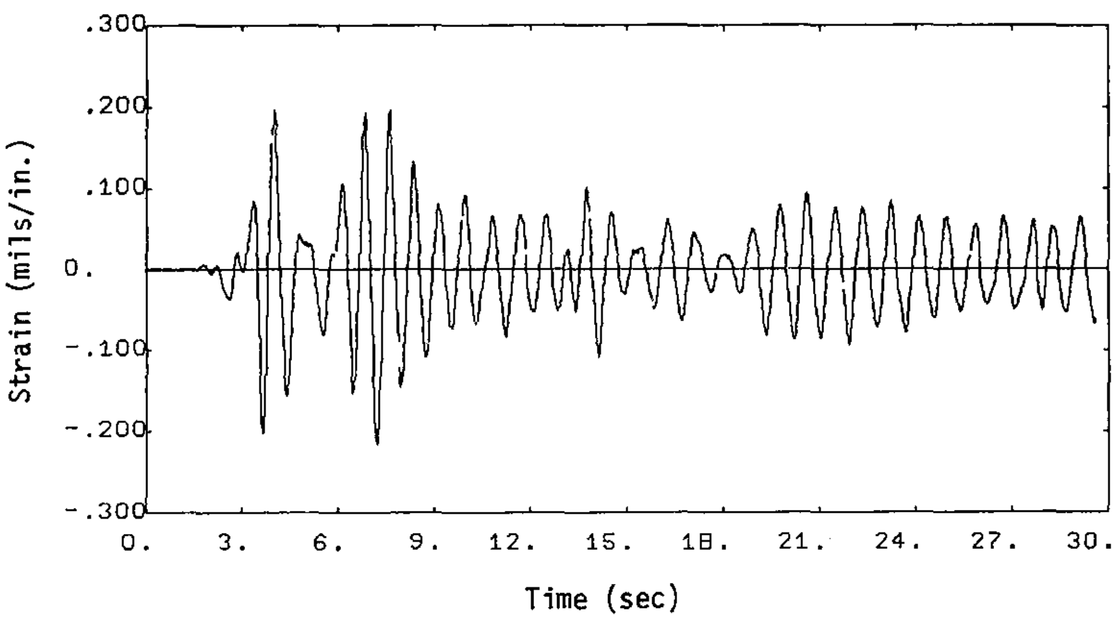

Test E-2-L-5/8 EC

FIGURE 5.13c COLUMN FLEXURAL STRAINS - LONGITUDINAL TEST, TYPE E

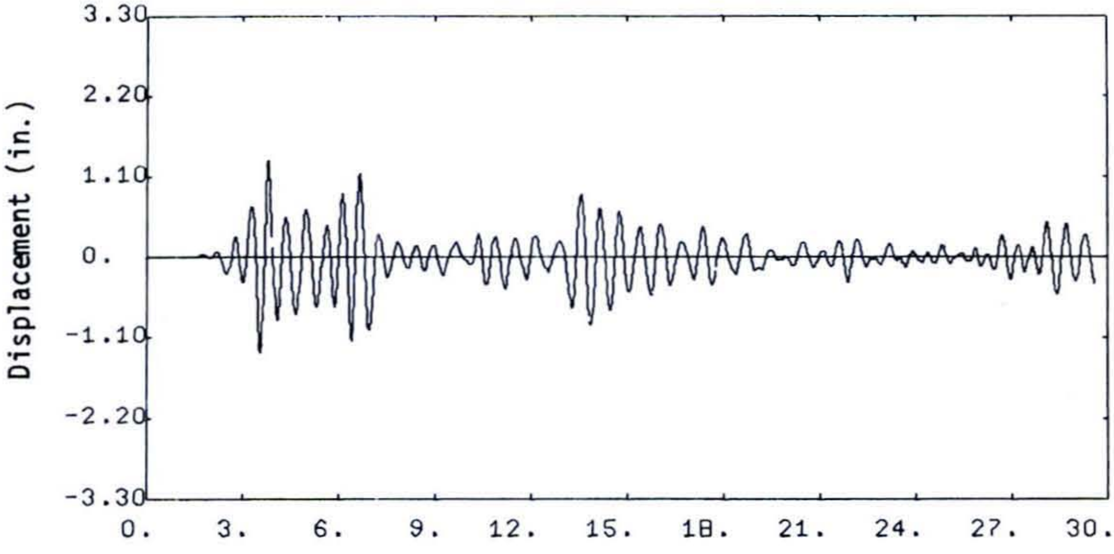

Test F-1-L-3/4 EC

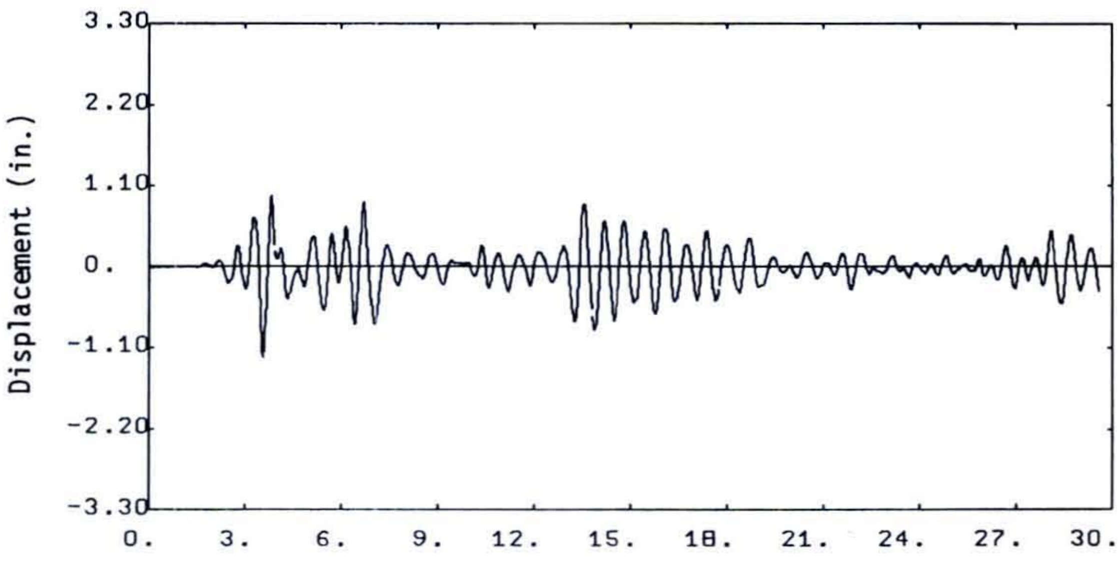

Test F-2-L-3/4 EC

FIGURE 5.14a RELATIVE STORY DISPLACEMENTS - LONGITUDINAL TEST, TYPE F

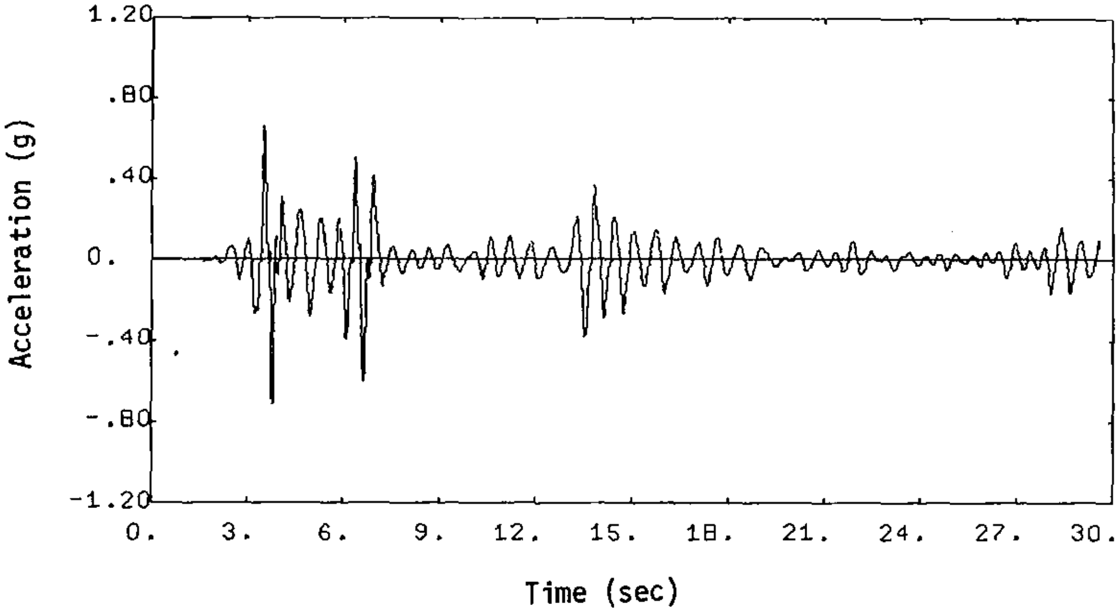

Test F-1-L-3/4 EC

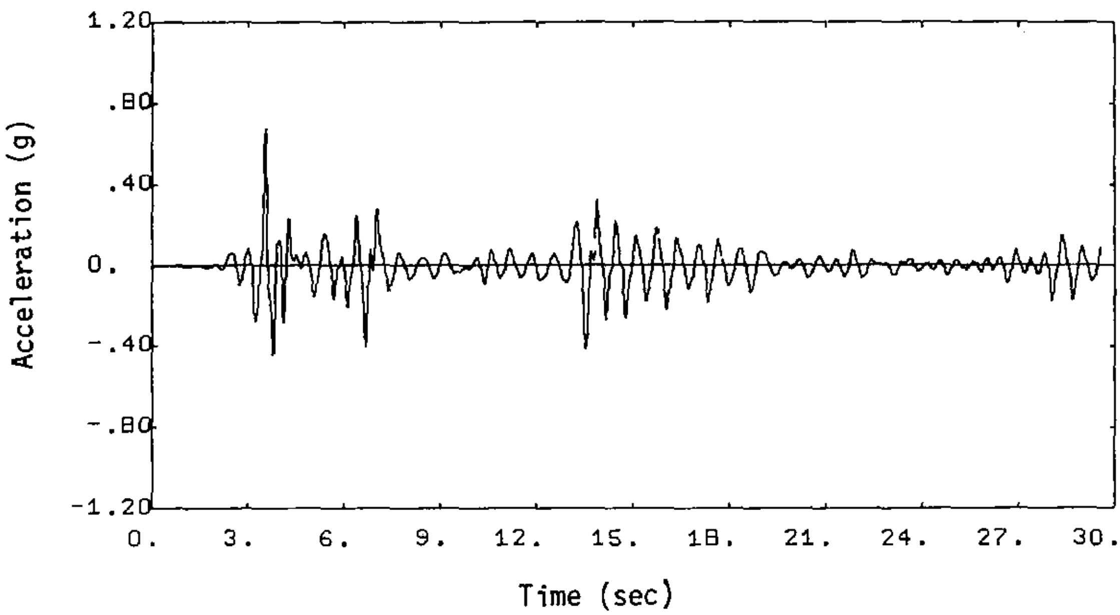

Test F-2-L-3/4 EC

FIGURE 5.14b STORY ACCELERATIONS - LONGITUDINAL TEST, TYPE F

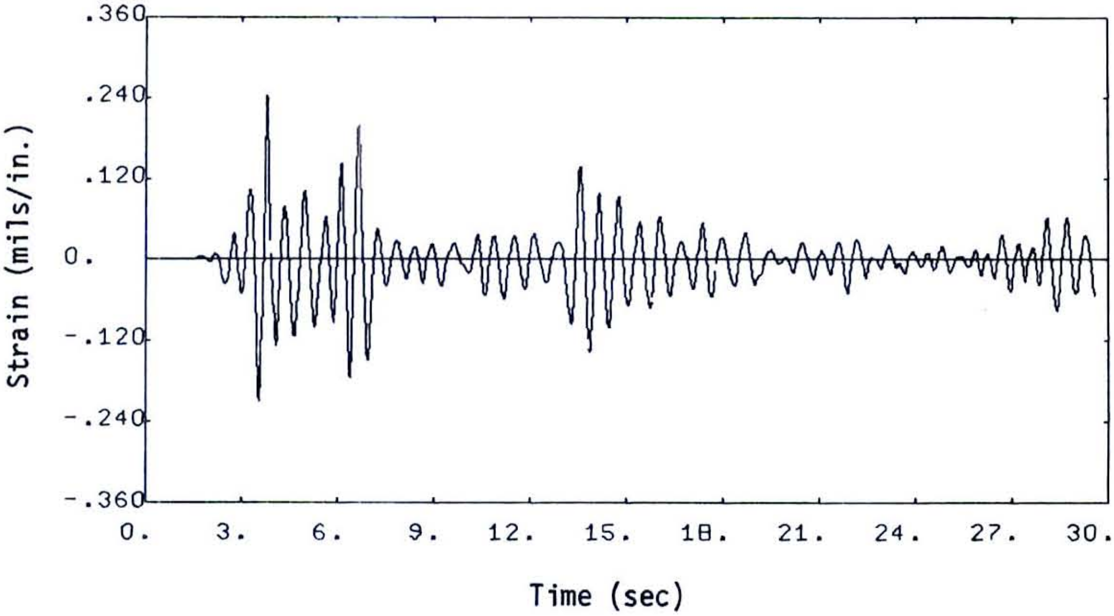

Test F-1-L-3/4 EC

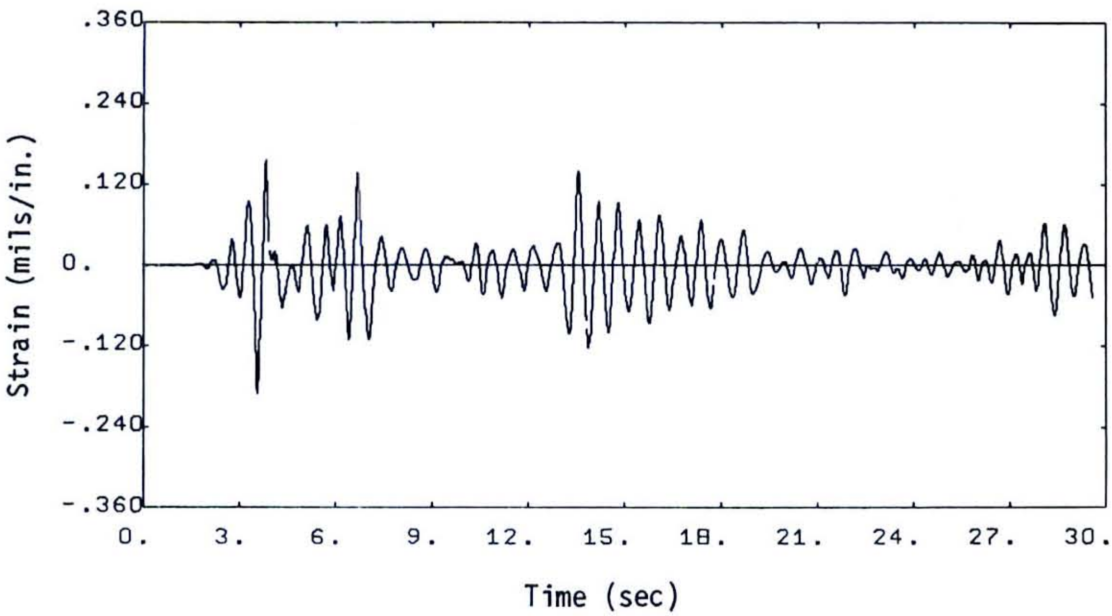

Test F-2-L-3/4 EC

FIGURE 5.14c COLUMN FLEXURAL STRAINS - LONGITUDINAL TEST, TYPE F

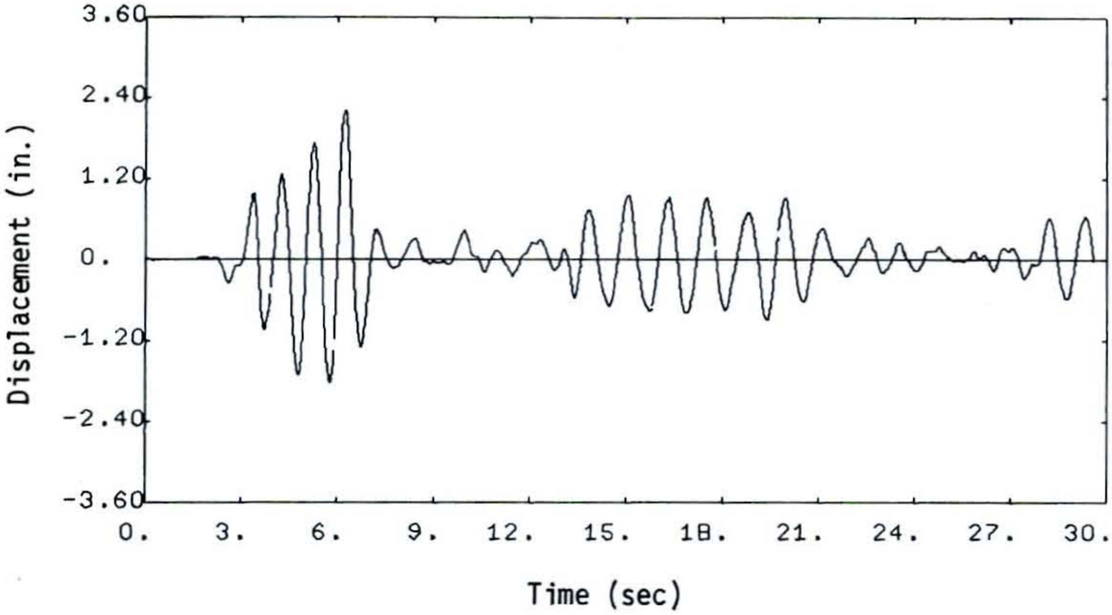

Test G-1-L-1/2 EC

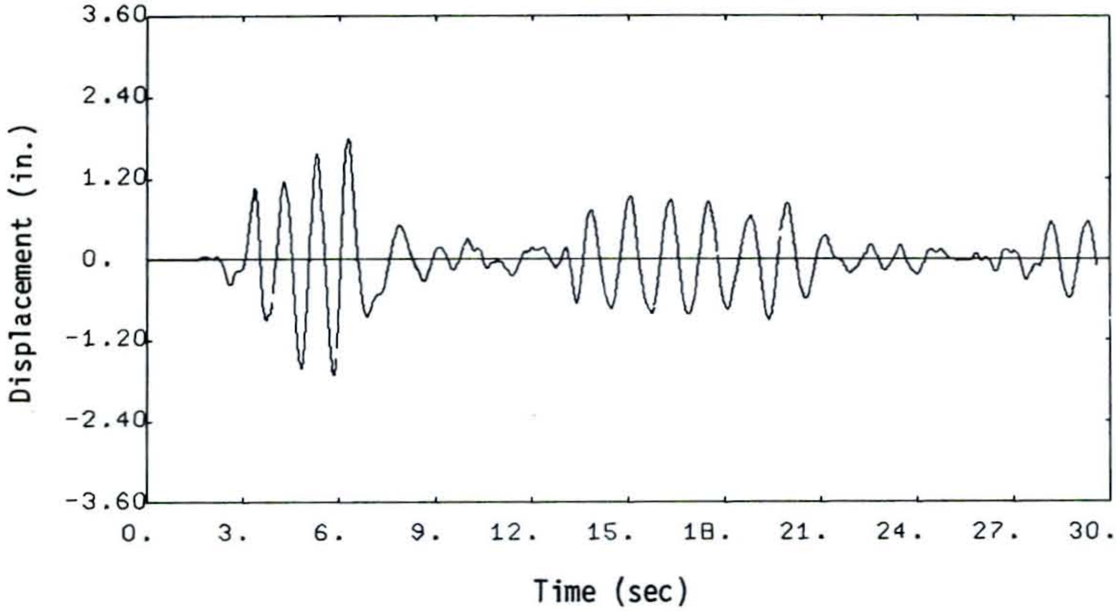

Test G-2-L-1/2 EC

FIGURE 5.15a RELATIVE STORY DISPLACEMENTS - LONGITUDINAL TEST, TYPE G

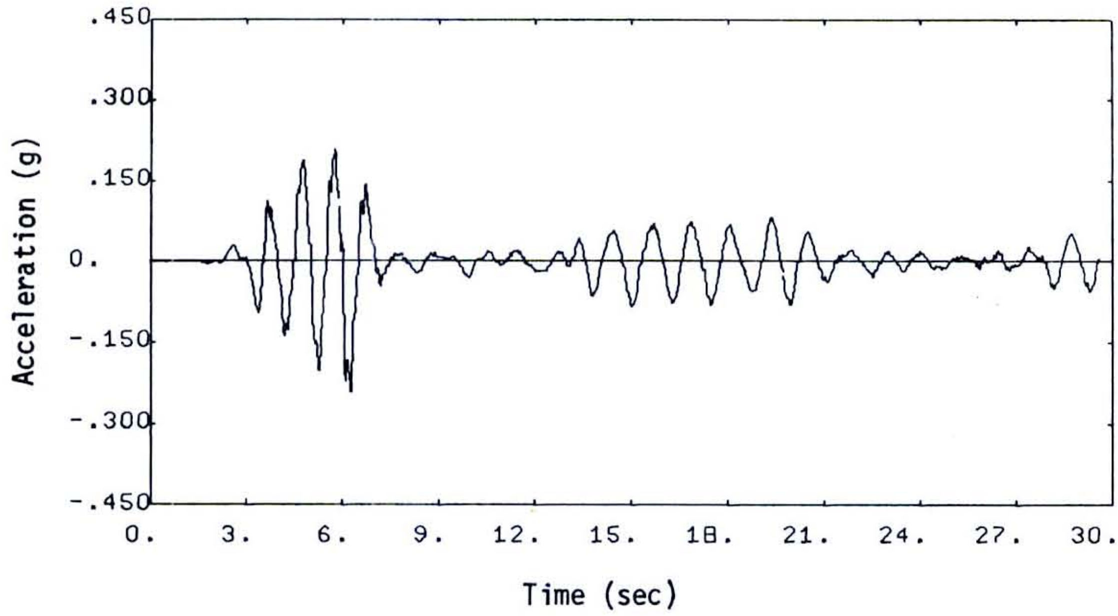

Test G-1-L-1/2 EC

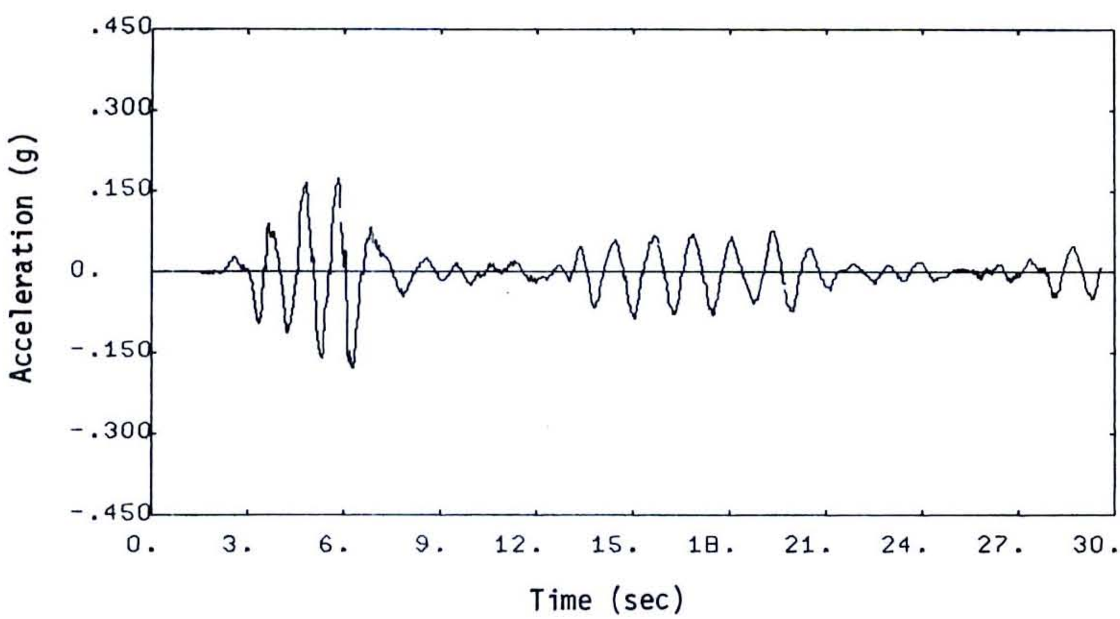

Test G-2-L-1/2 EC

FIGURE 5.15b STORY ACCELERATIONS - LONGITUDINAL TEST, TYPE G

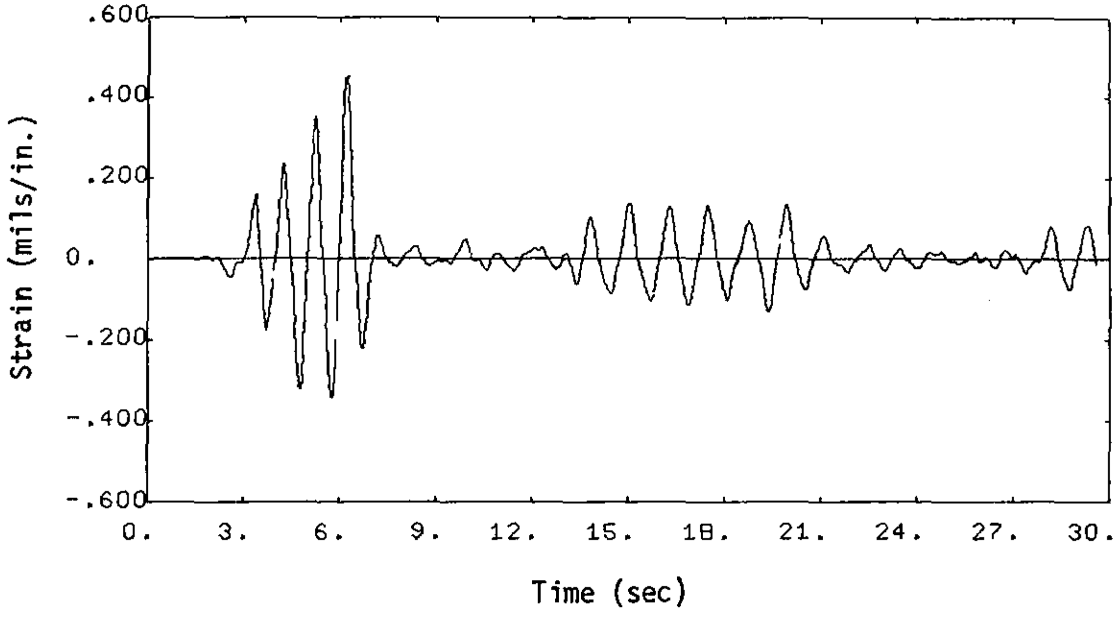

Test G-1-L-1/2 EC

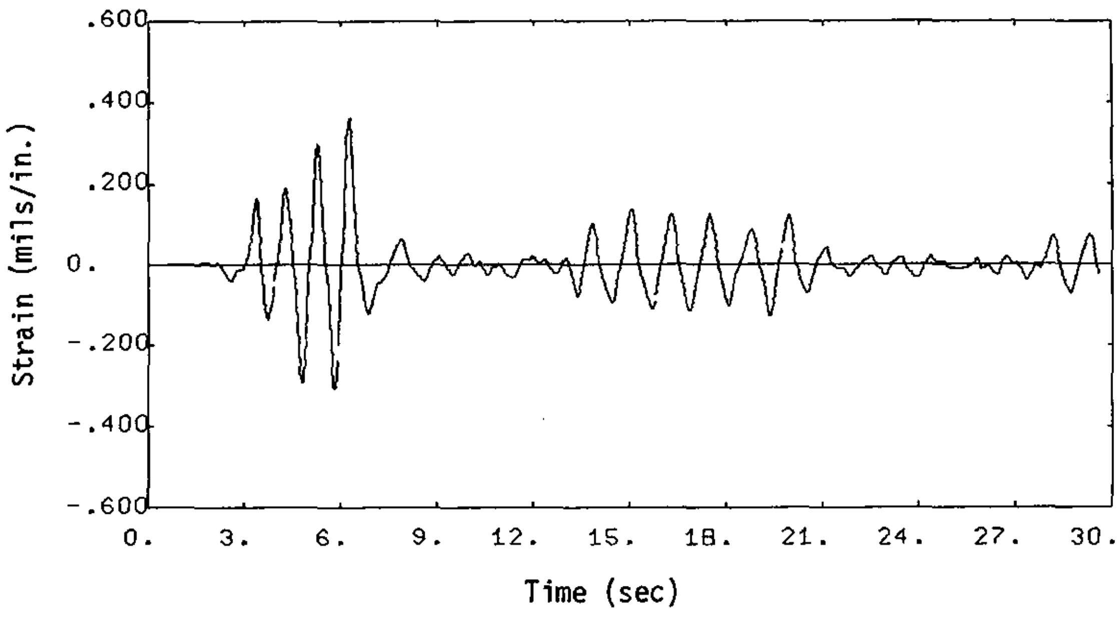

Test G-2-L-1/2 EC

FIGURE 5.15c COLUMN FLEXURAL STRAINS - LONGITUDINAL TEST, TYPE G

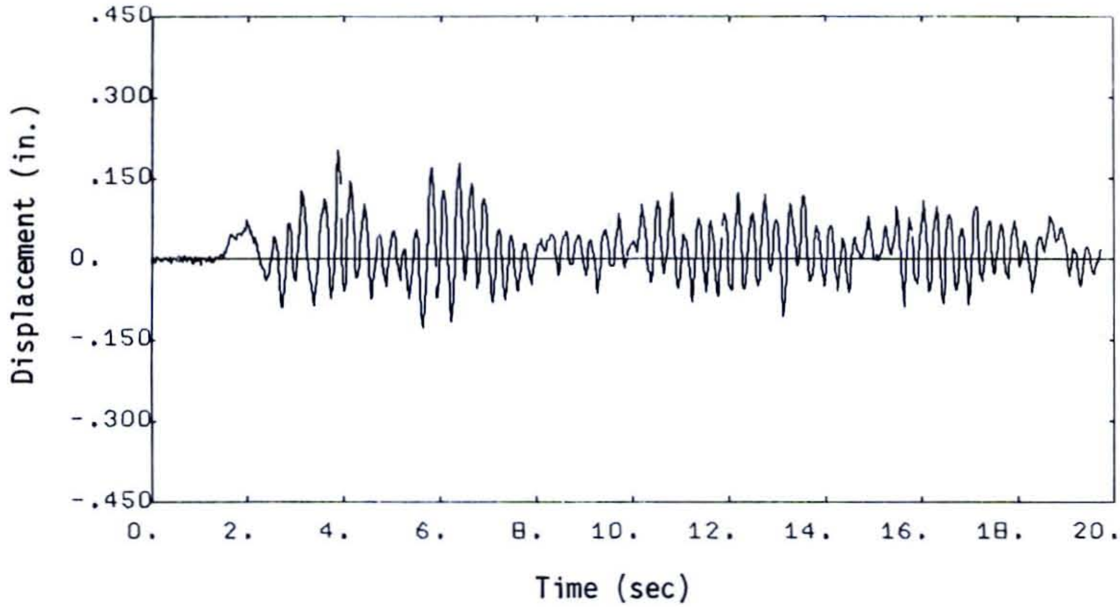

Test A-1-T-1/2 EC

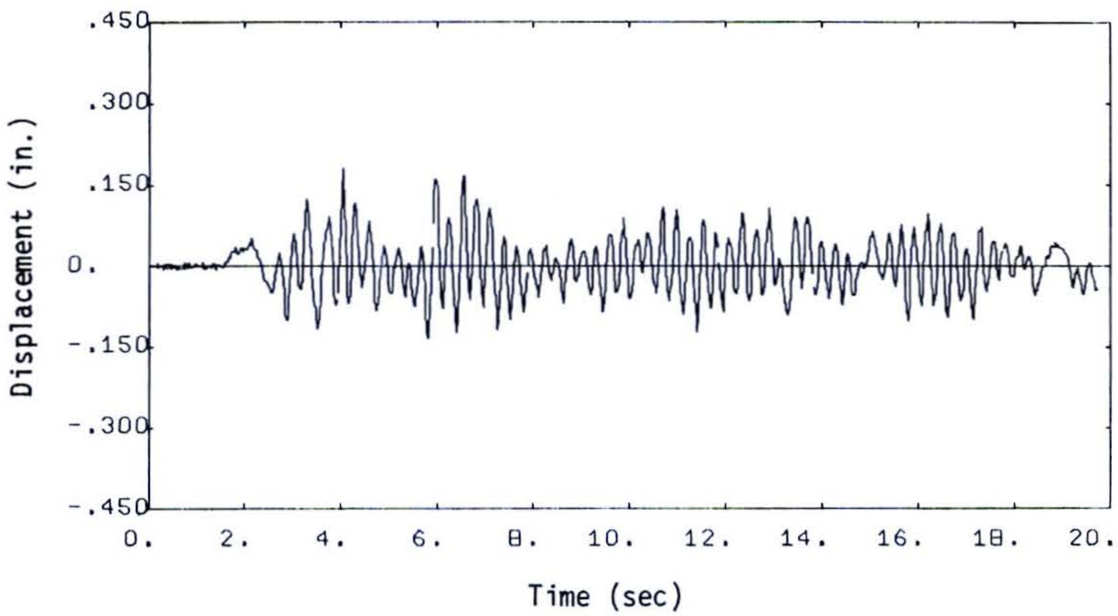

Test A-2-T-1/2 EC

FIGURE 5.16a RELATIVE STORY DISPLACEMENTS - TRANSVERSE TEST, TYPE A

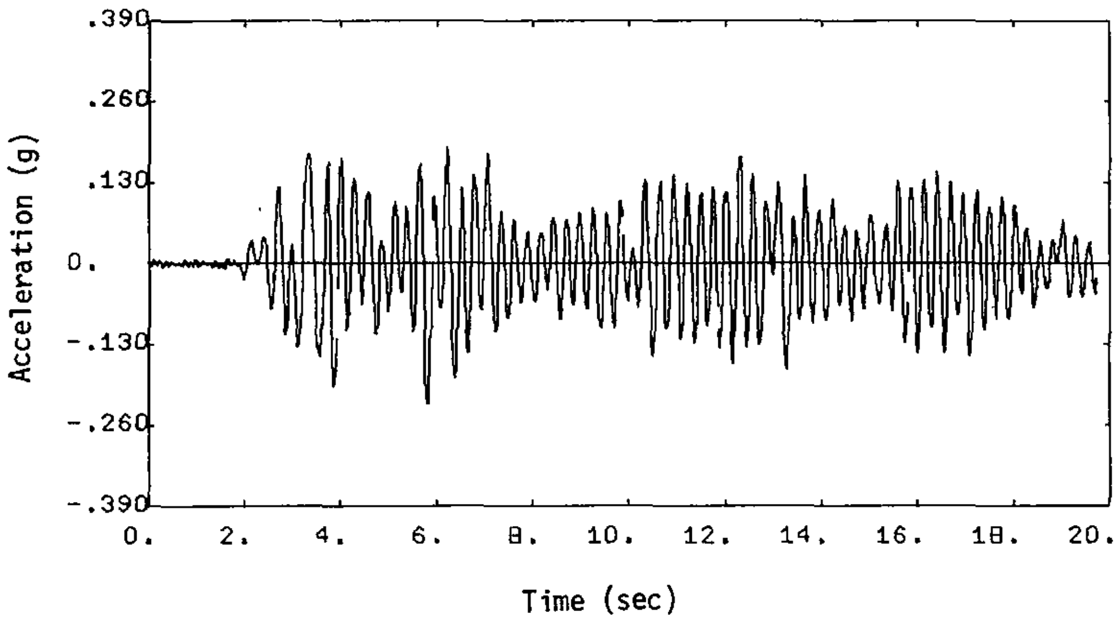

Test A-1-T-1/2 EC

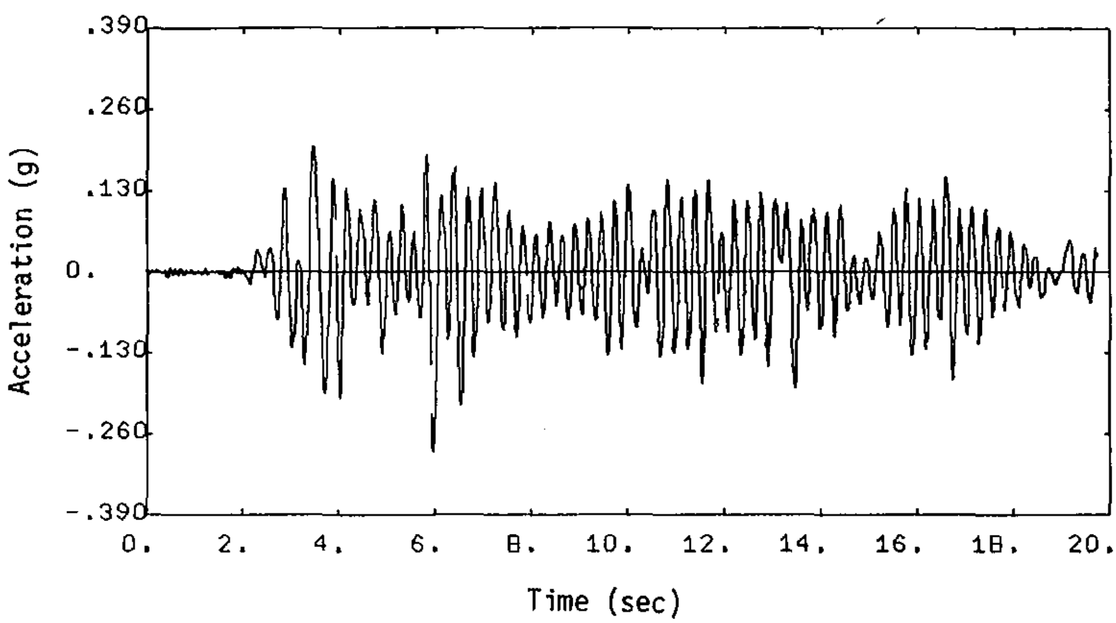

Test A-2-T-1/2 EC

FIGURE 5.16b STORY ACCELERATIONS - TRANSVERSE TEST, TYPE A

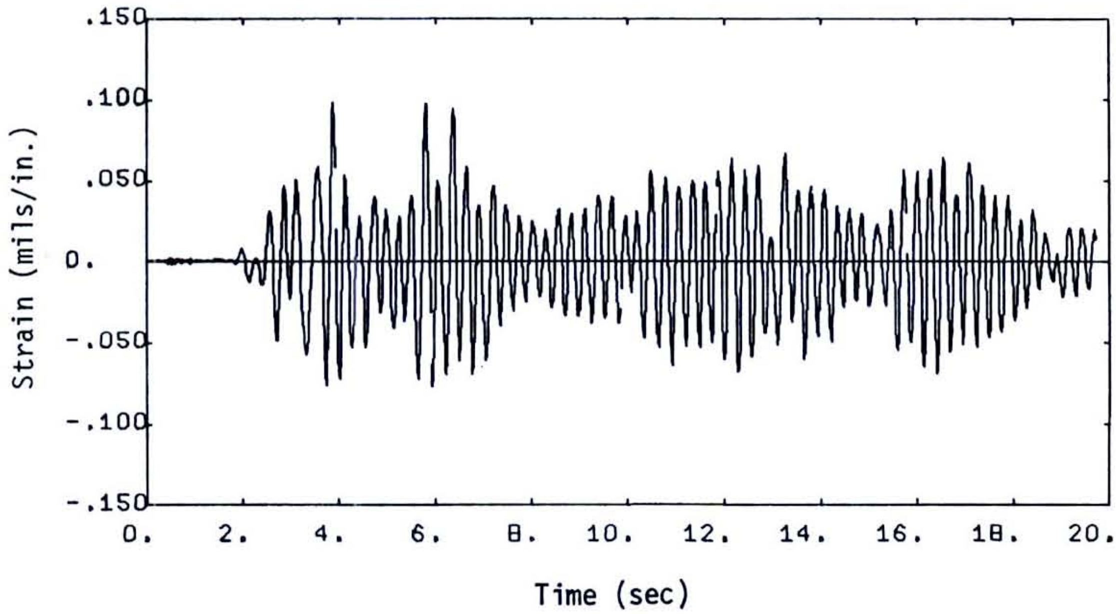

Test A-1-T-1/2 EC

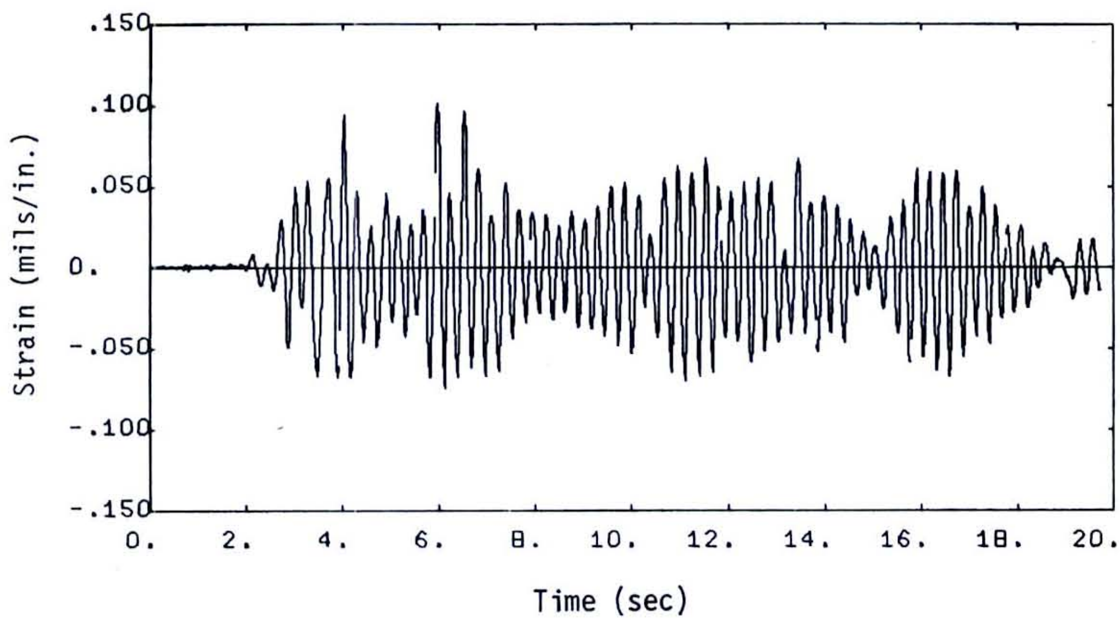

Test A-2-T-1/2 EC

FIGURE 5.16c BRACE AXIAL STRAINS - TRANSVERSE TEST, TYPE A

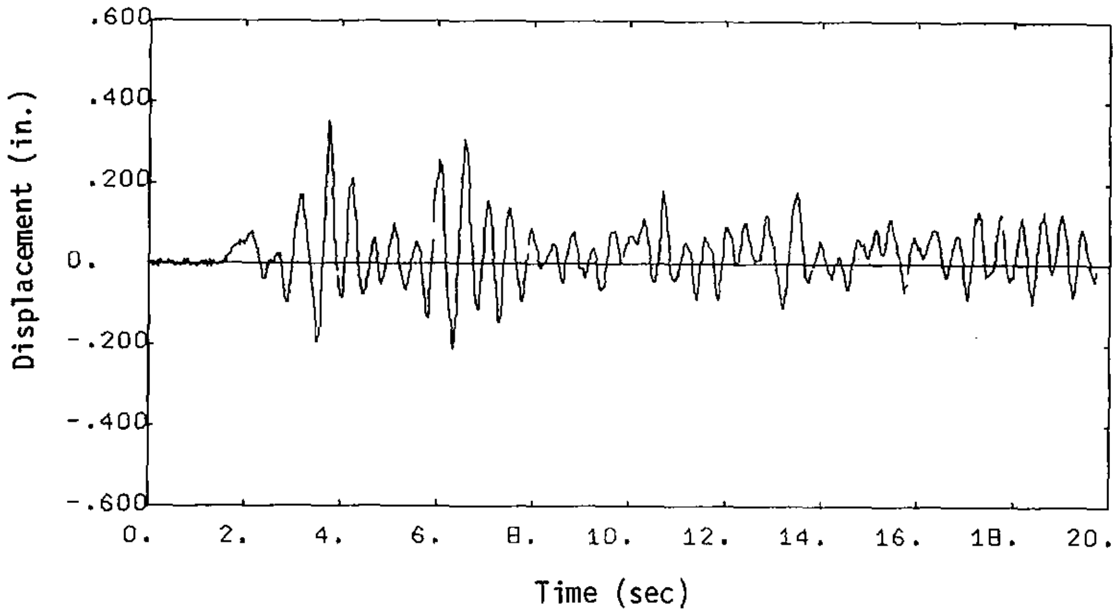

Test B-1-T-1/2 EC

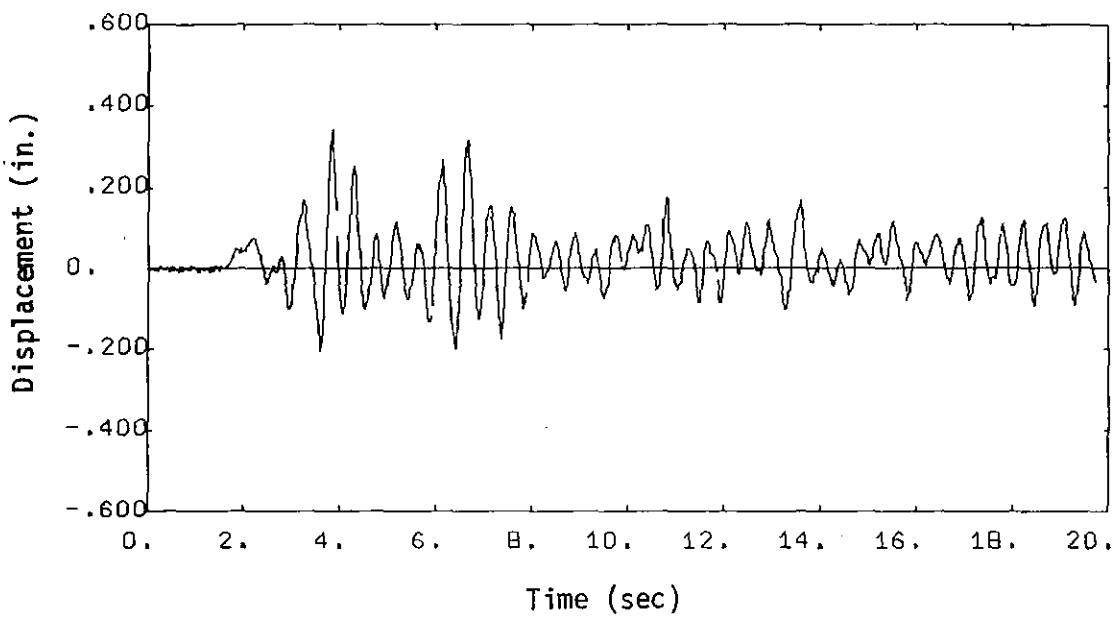

Test B-2-T-1/2 EC

FIGURE 5.17a RELATIVE STORY DISPLACEMENTS - TRANSVERSE TEST, TYPE B

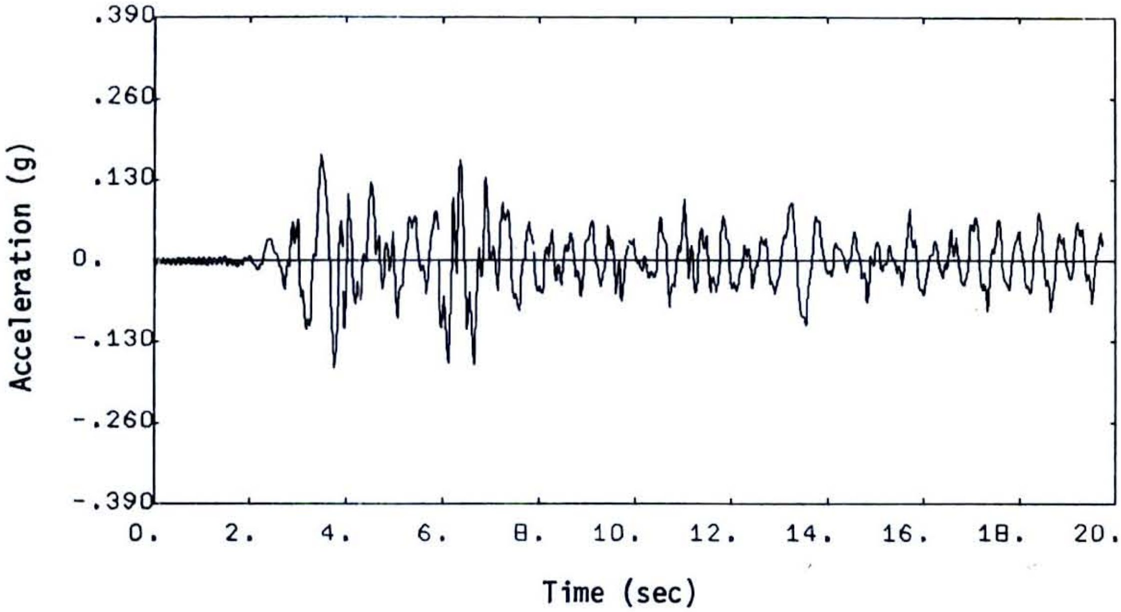

Test B-1-T-1/2 EC

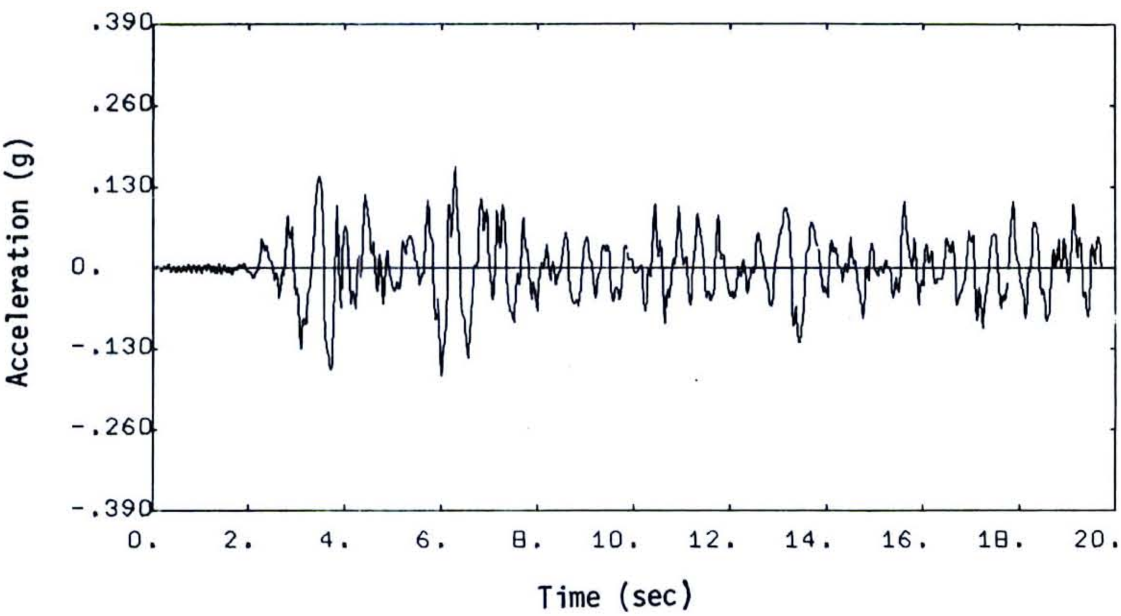

Test B-2-T-1/2 EC

FIGURE 5.17b STORY ACCELERATIONS - TRANSVERSE TEST, TYPE B

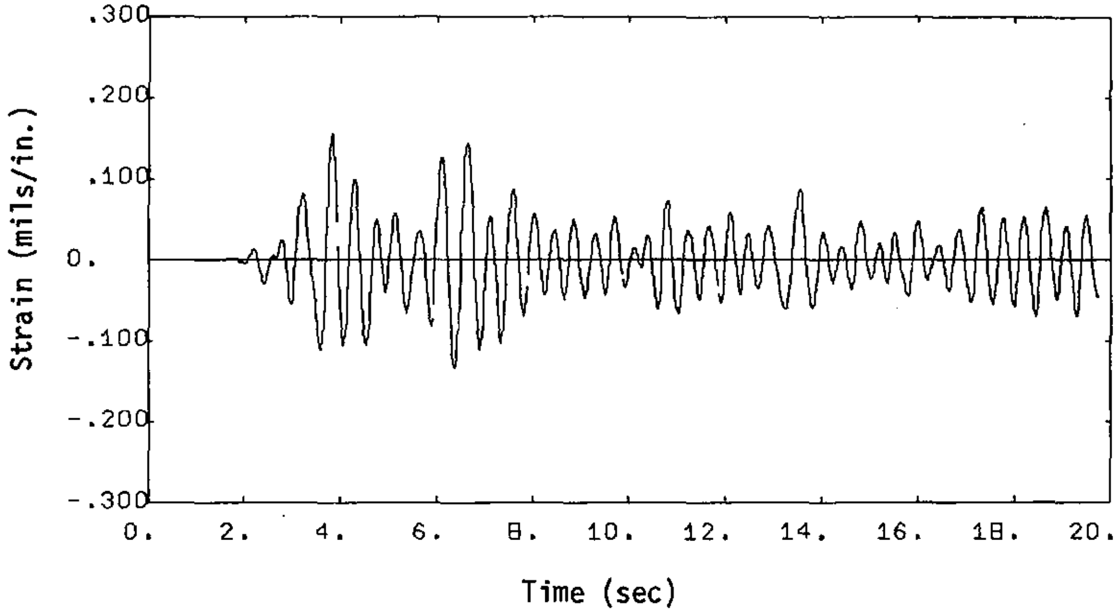

Test B-1-T-1/2 EC

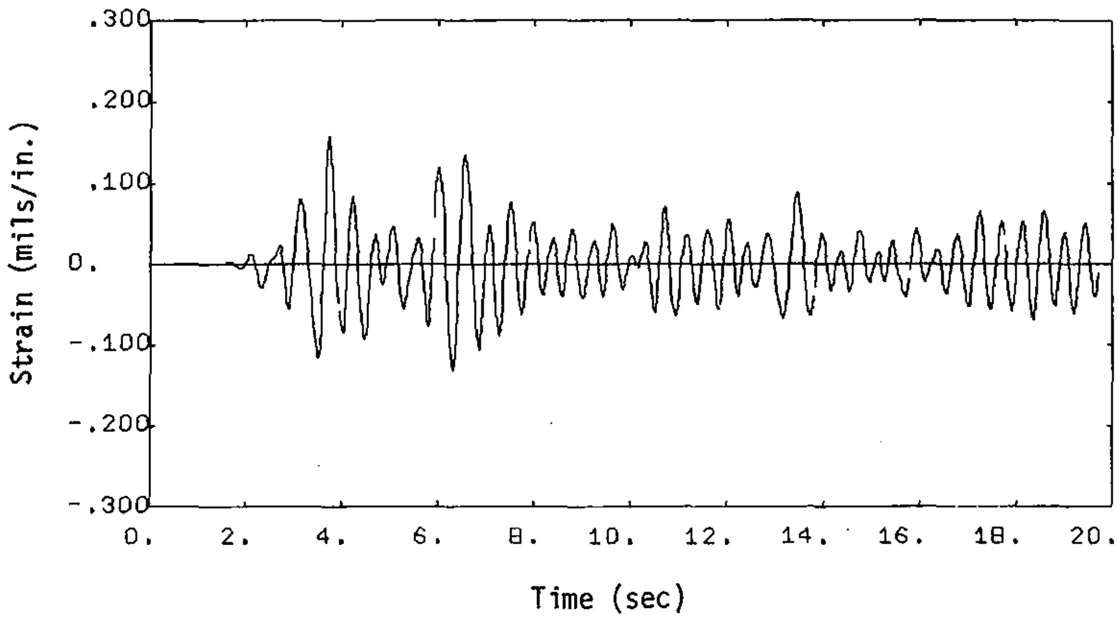

Test B-2-T-1/2 EC

FIGURE 5.17c BRACE AXIAL STRAINS - TRANSVERSE TEST, TYPE B

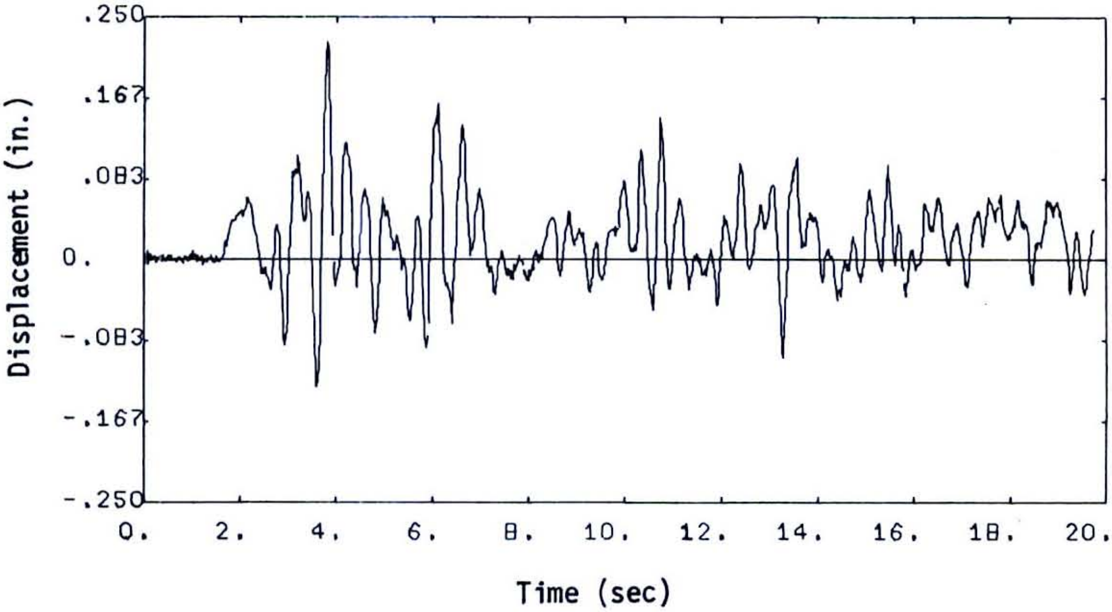

Test C-1-T-1/2 EC

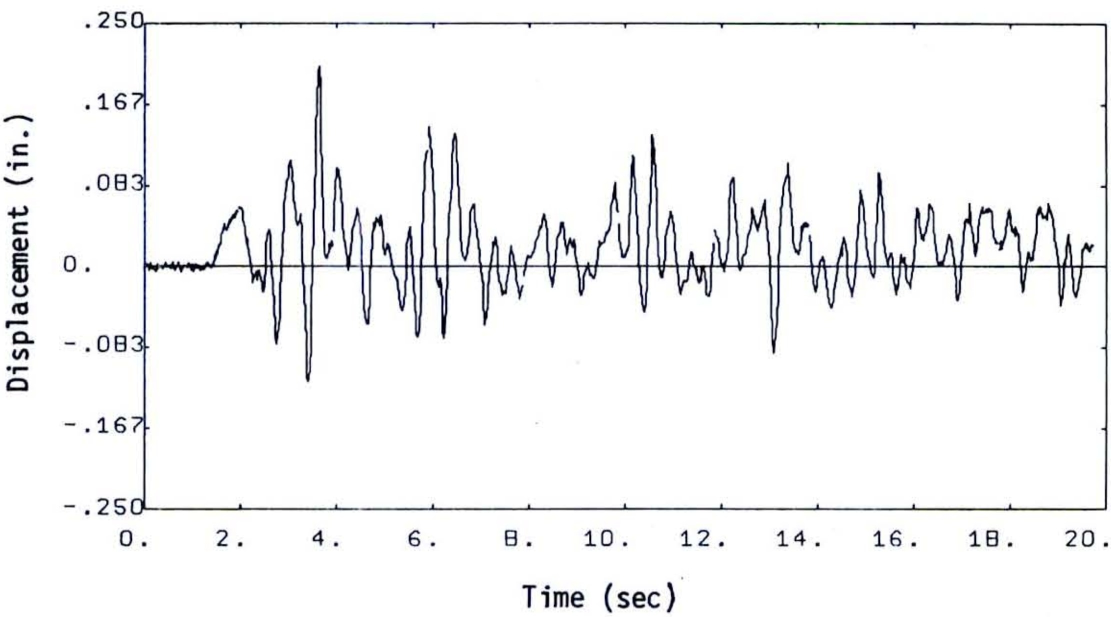

Test C-2-T-1/2 EC

FIGURE 5.18a RELATIVE STORY DISPLACEMENTS - TRANSVERSE TEST, TYPE C

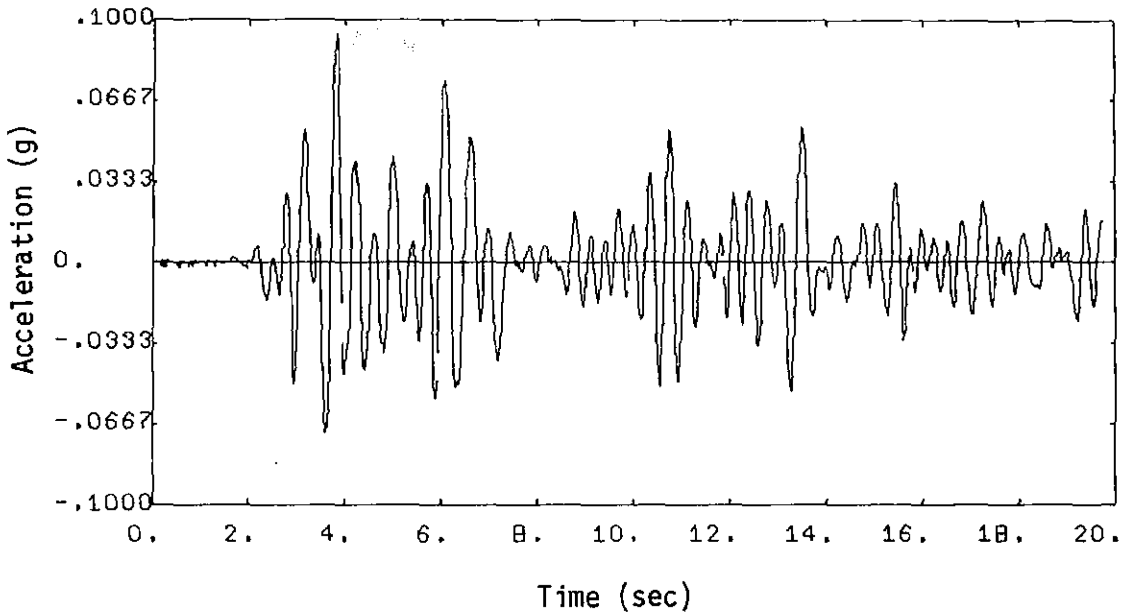

Test C-1-T-1/2 EC

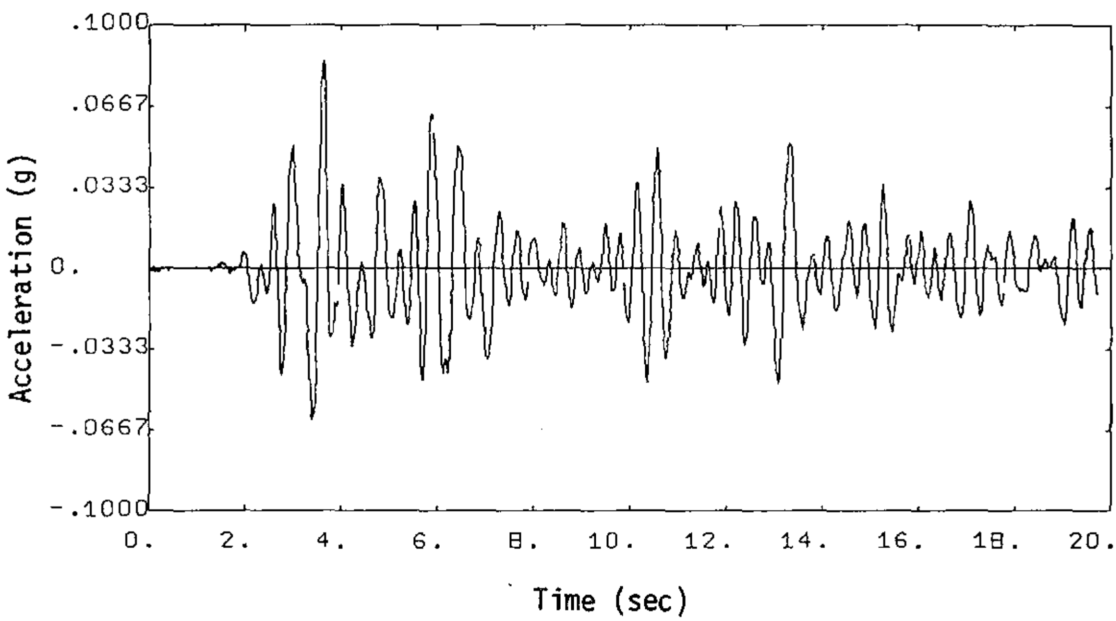

Test C-2-T-1/2 EC

FIGURE 5.18b STORY ACCELERATIONS - TRANSVERSE TEST, TYPE C

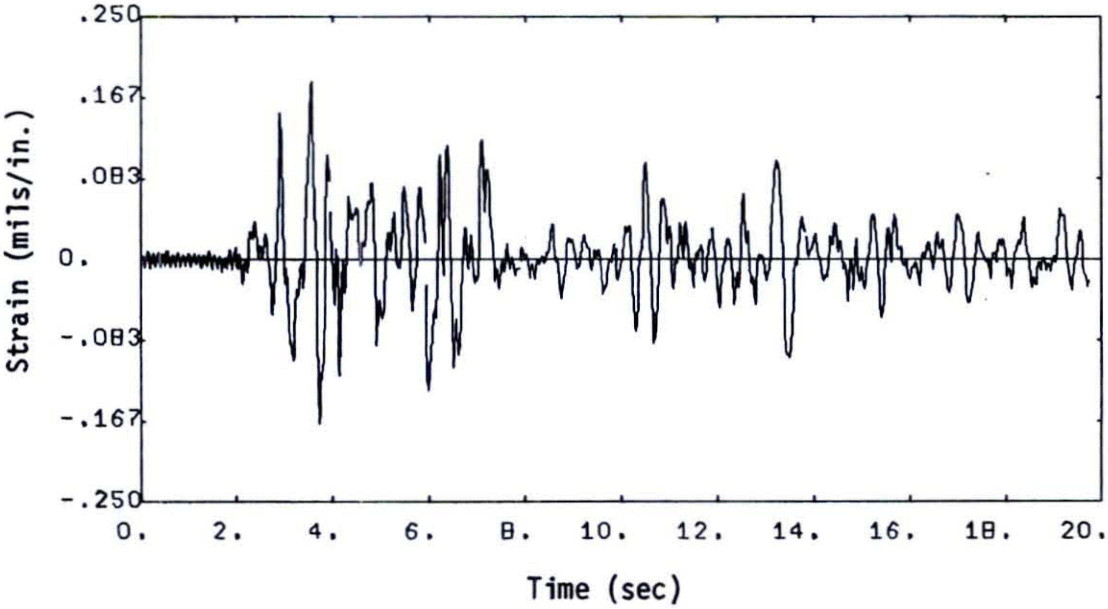

Test C-1-T-1/2 EC

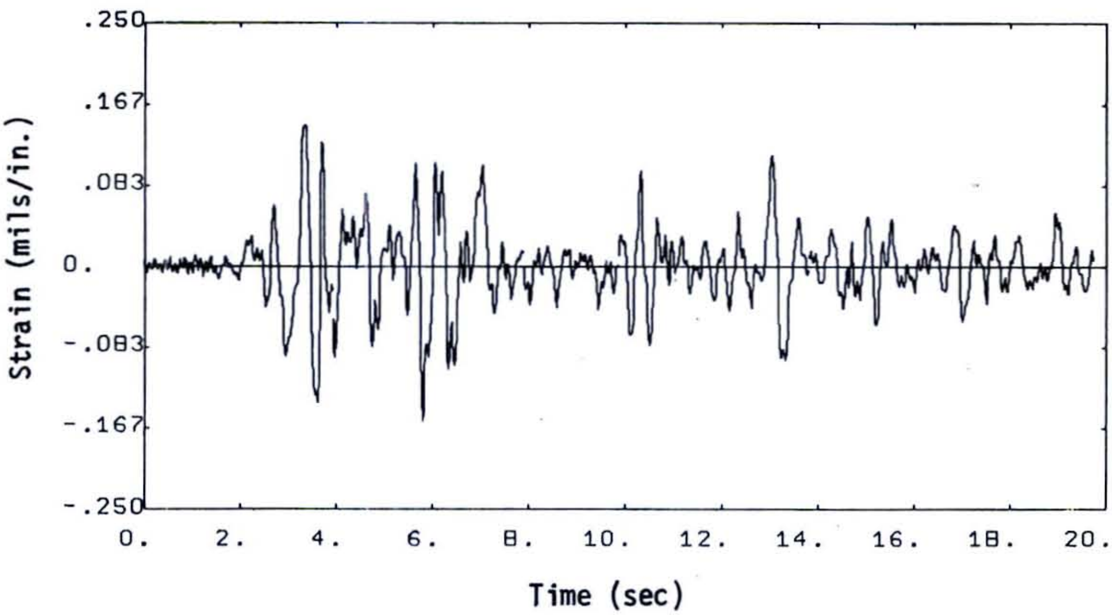

Test C-2-T-1/2 EC

FIGURE 5.18c BRACE AXIAL STRAINS - TRANSVERSE TEST, TYPE C

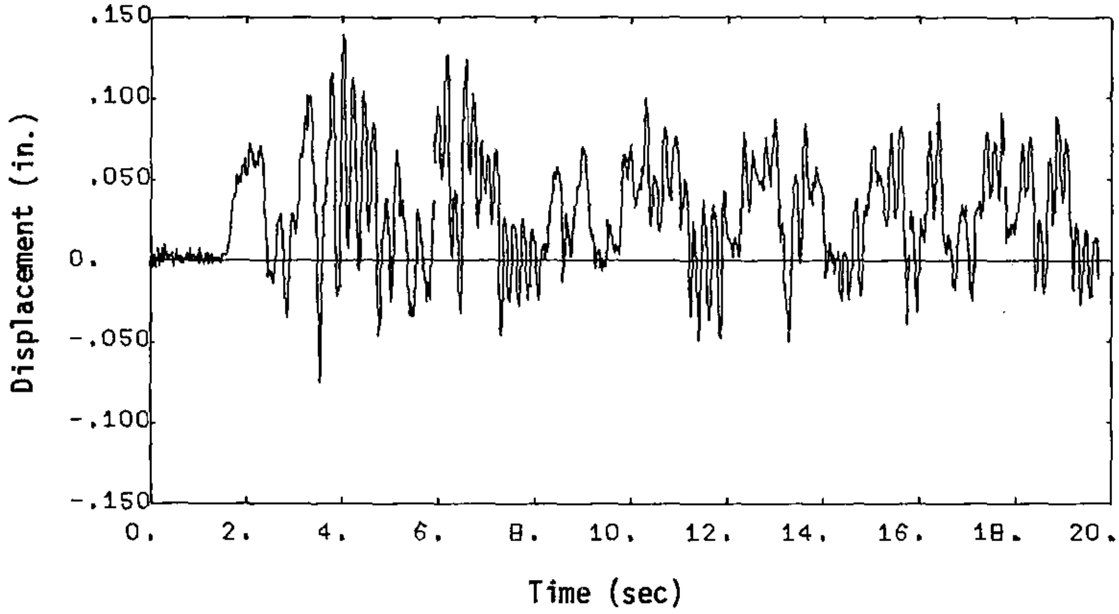

Test D-1-T-3/4 EC

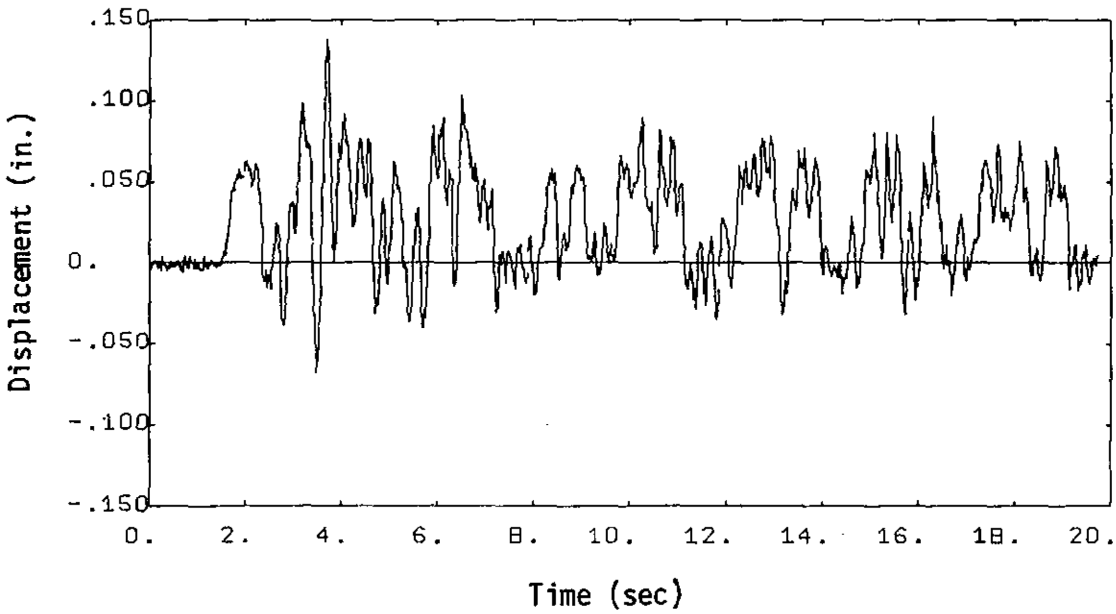

Test D-2-T-3/4 EC

FIGURE 5.19a RELATIVE STORY DISPLACEMENTS - TRANSVERSE TEST, TYPE D

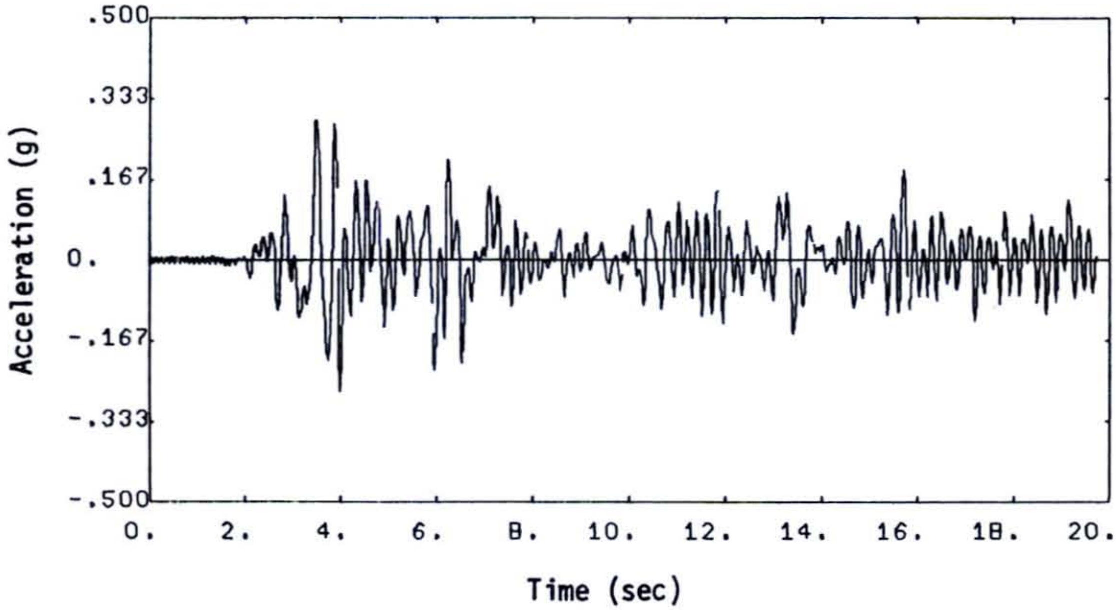

Test D-1-T-3/4 EC

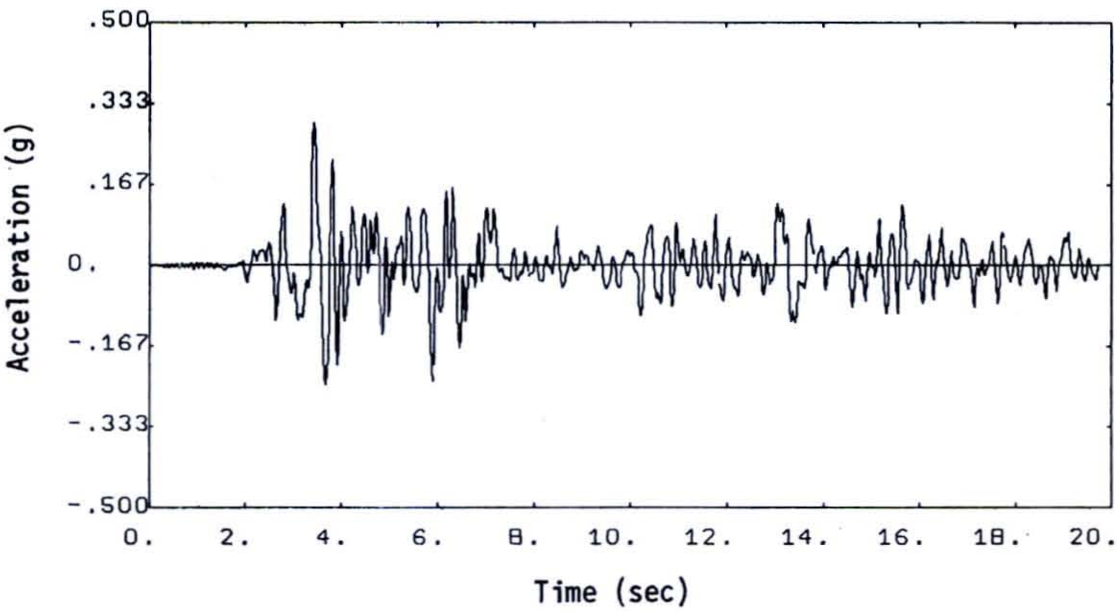

Test D-2-T-3/4 EC

FIGURE 5.19b STORY ACCELERATIONS - TRANSVERSE TEST, TYPE D

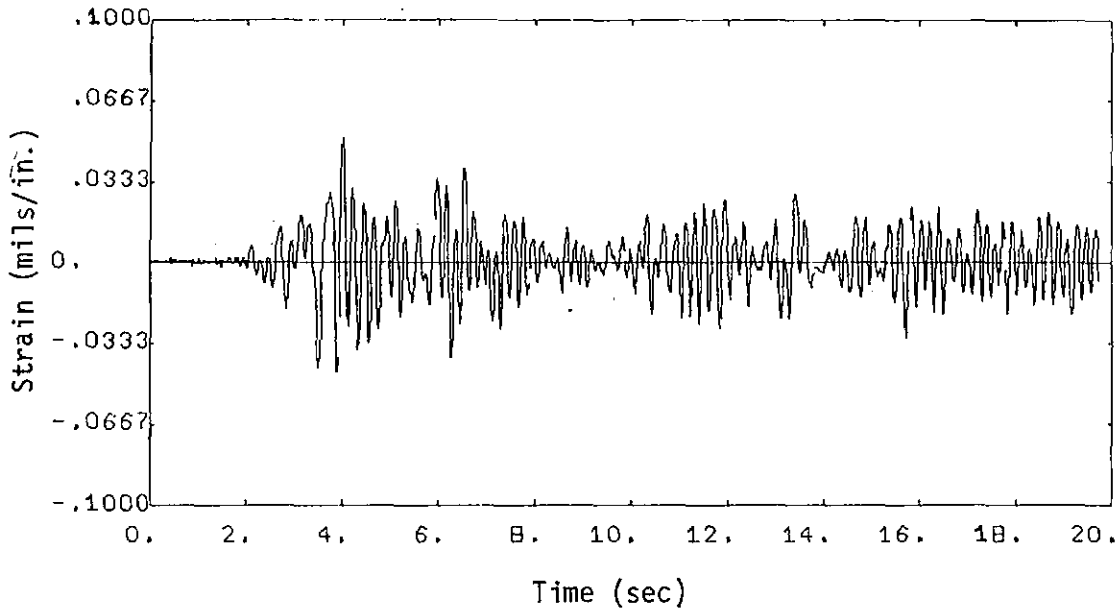

Test D-1-T-3/4 EC

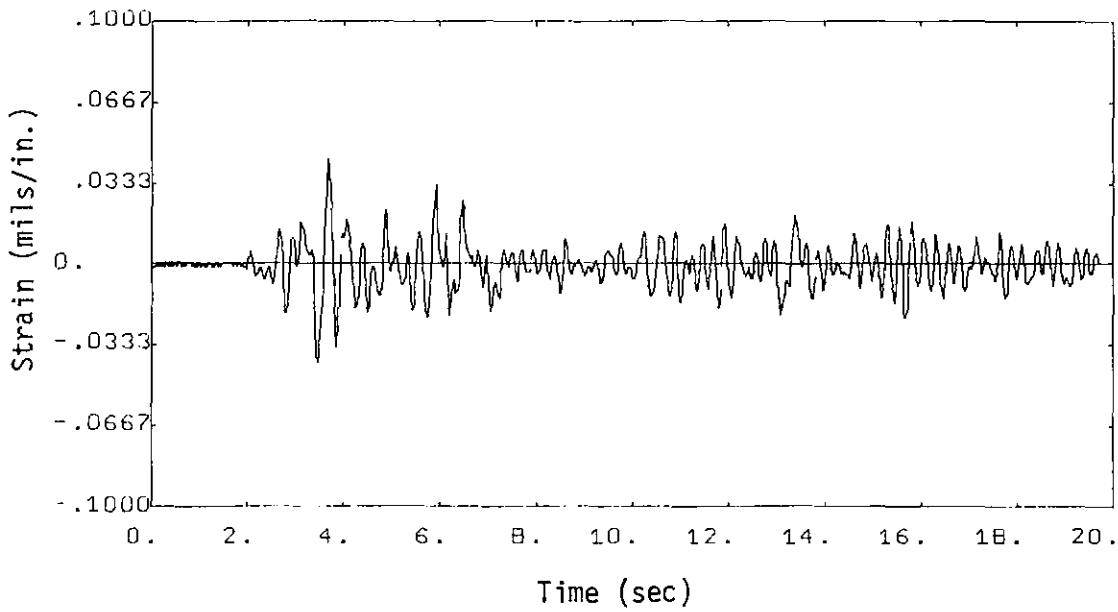

Test D-2-T-3/4 EC

FIGURE 5.19c BRACE AXIAL STRAINS - TRANSVERSE TEST, TYPE D

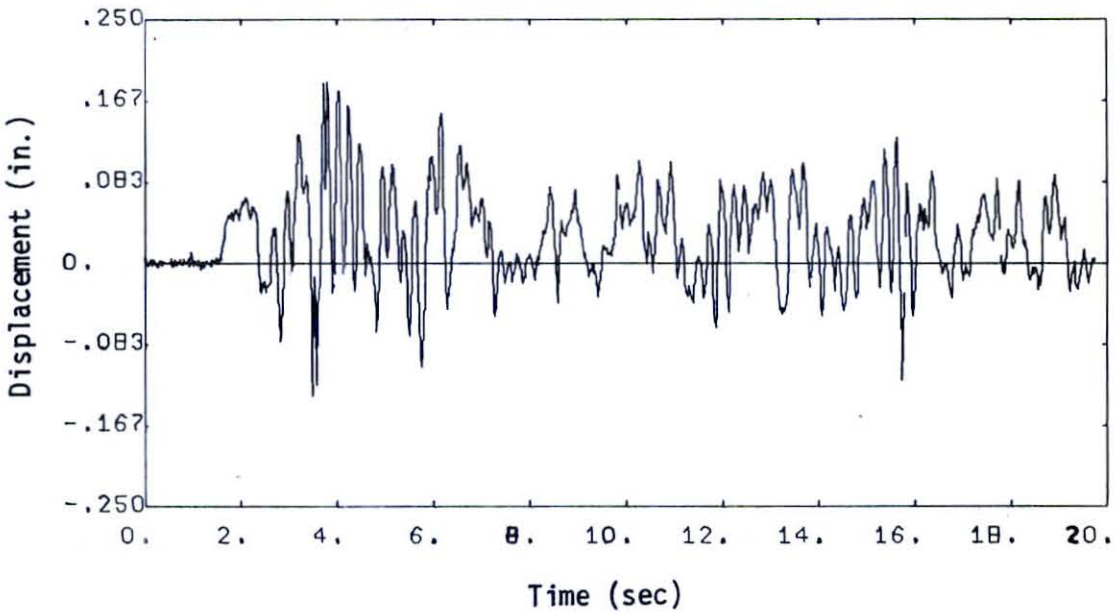

Test E-1-T-1 EC

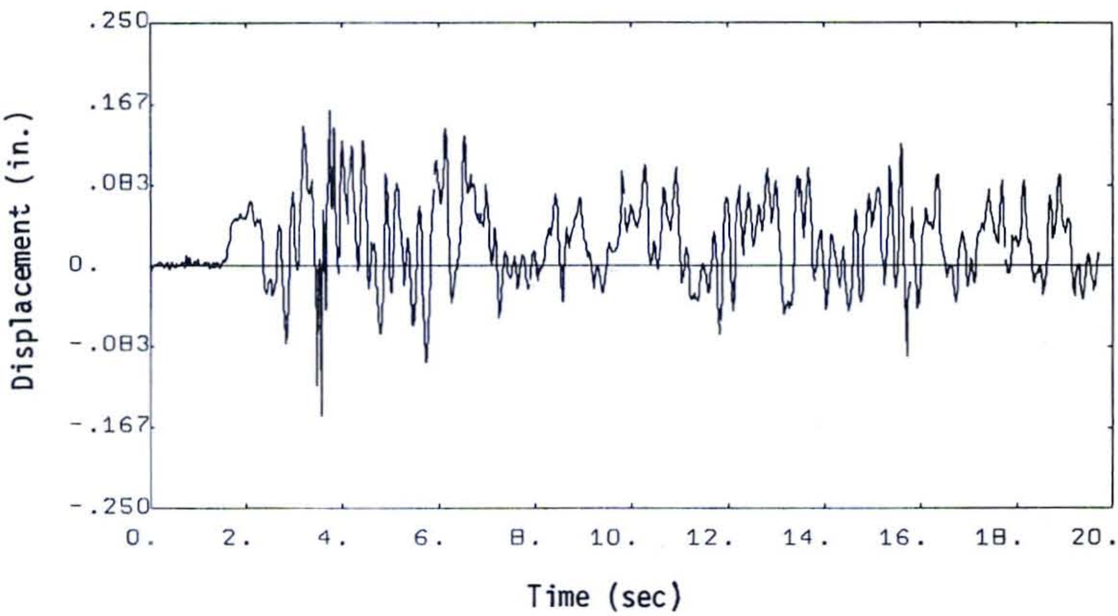

Test E-2-T-1 EC

FIGURE 5.20a RELATIVE STORY DISPLACEMENTS - TRANSVERSE TEST, TYPE E

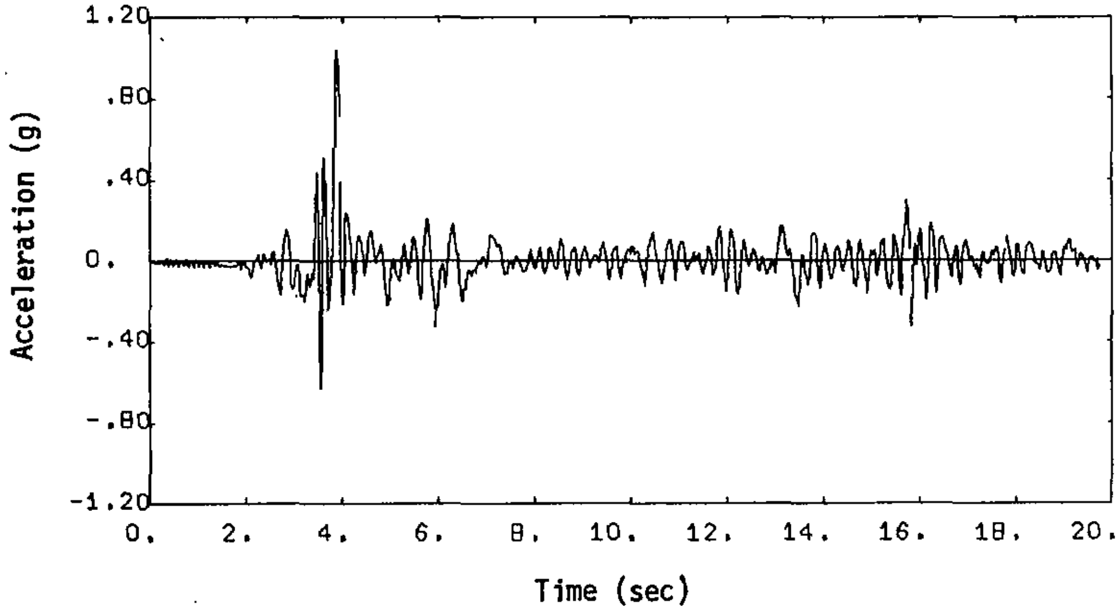

Test E-1-T-1 EC

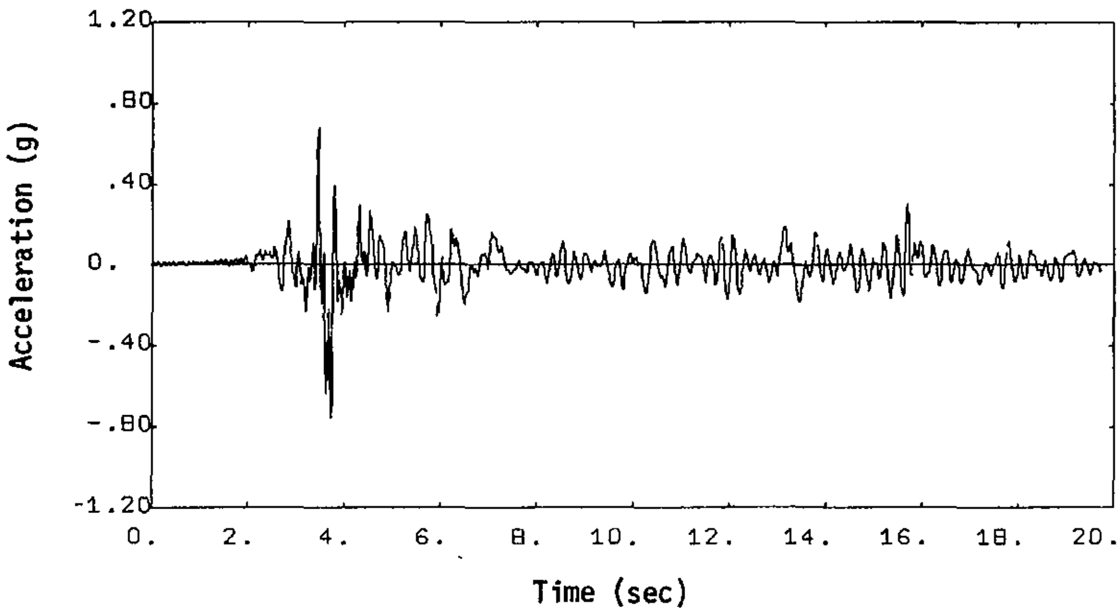

Test E-2-T-1 EC

FIGURE 5.20b STORY ACCELERATIONS - TRANSVERSE TEST, TYPE E

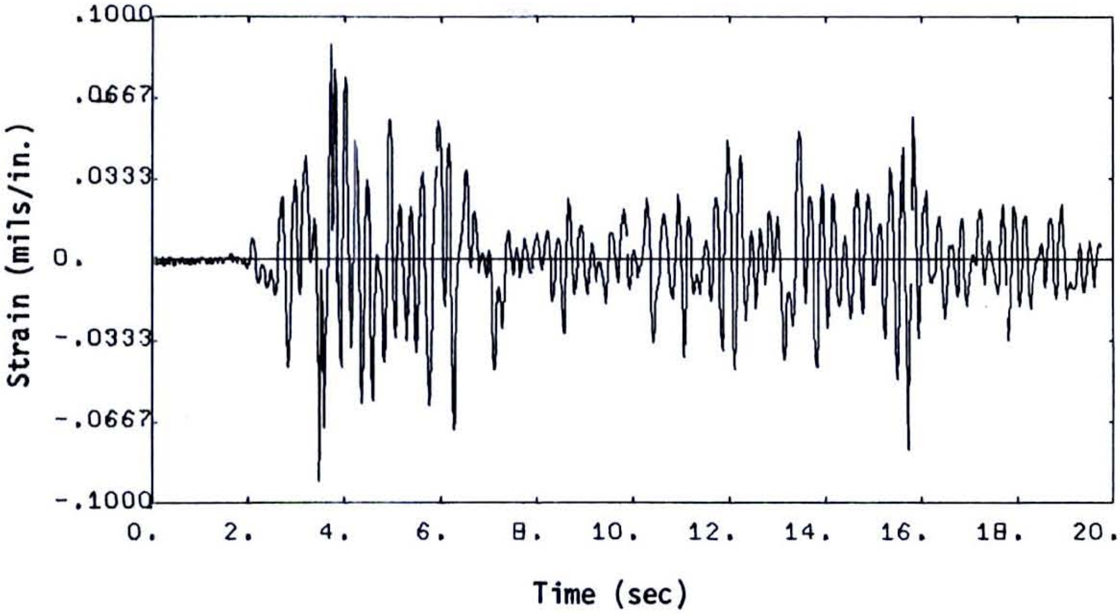

Test E-1-T-1 EC

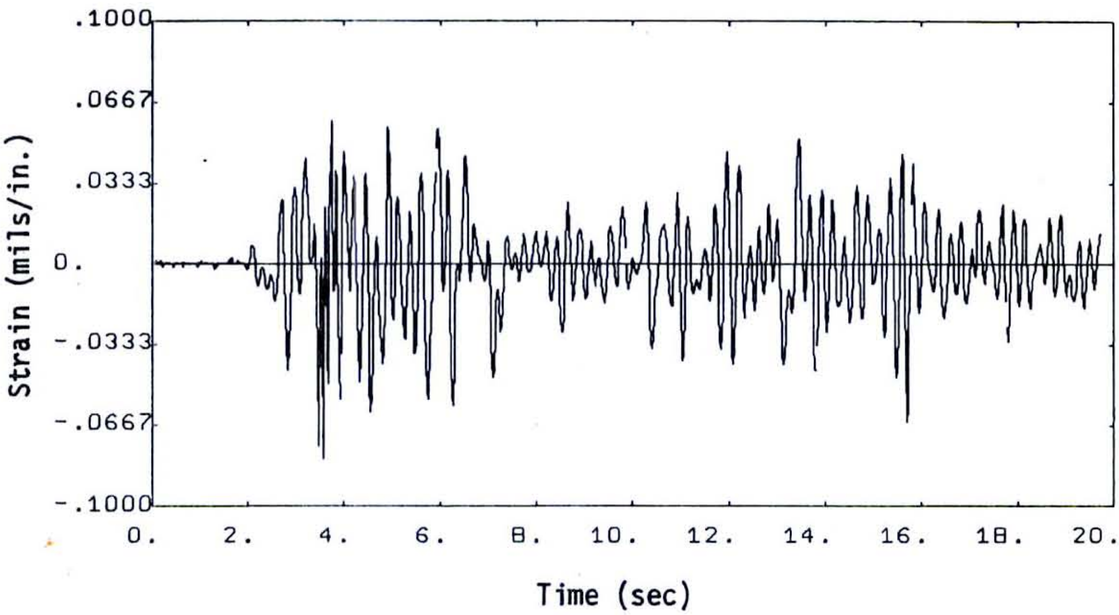

Test E-2-T-1 EC

FIGURE 5.20c BRACE AXIAL STRAINS - TRANSVERSE TEST, TYPE E

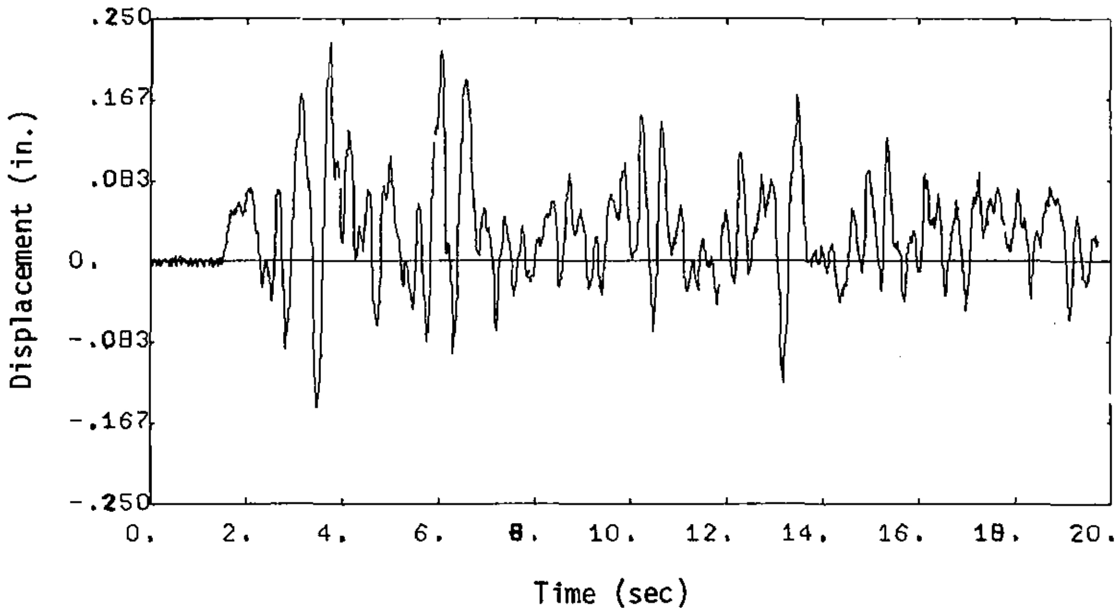

Test H-1-T-1 EC

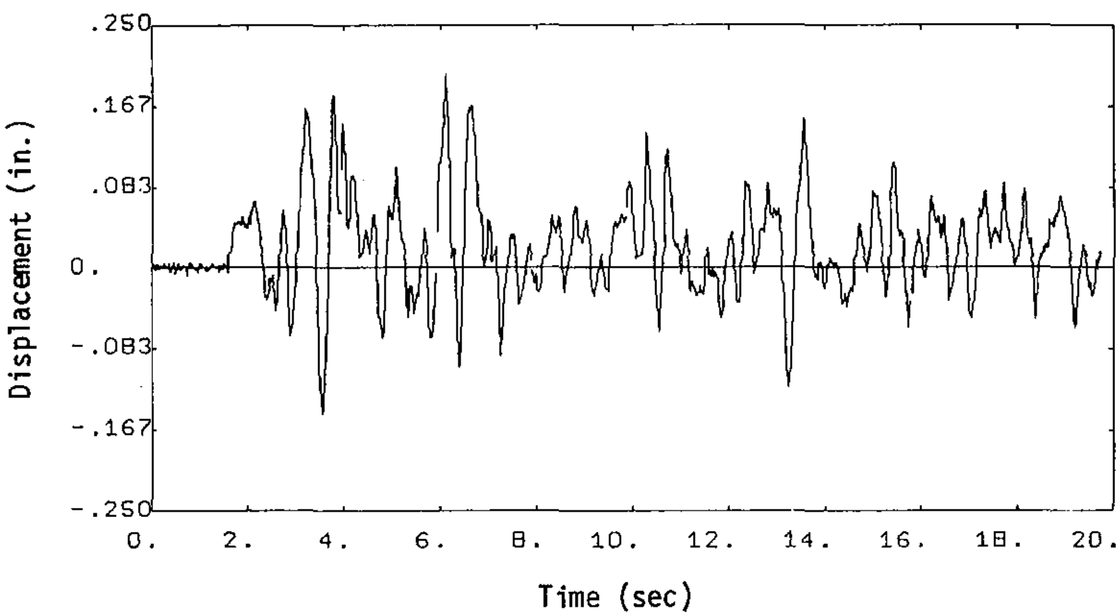

Test H-2-T-1 EC

FIGURE 5.21a RELATIVE STORY DISPLACEMENTS - TRANSVERSE TEST, TYPE H

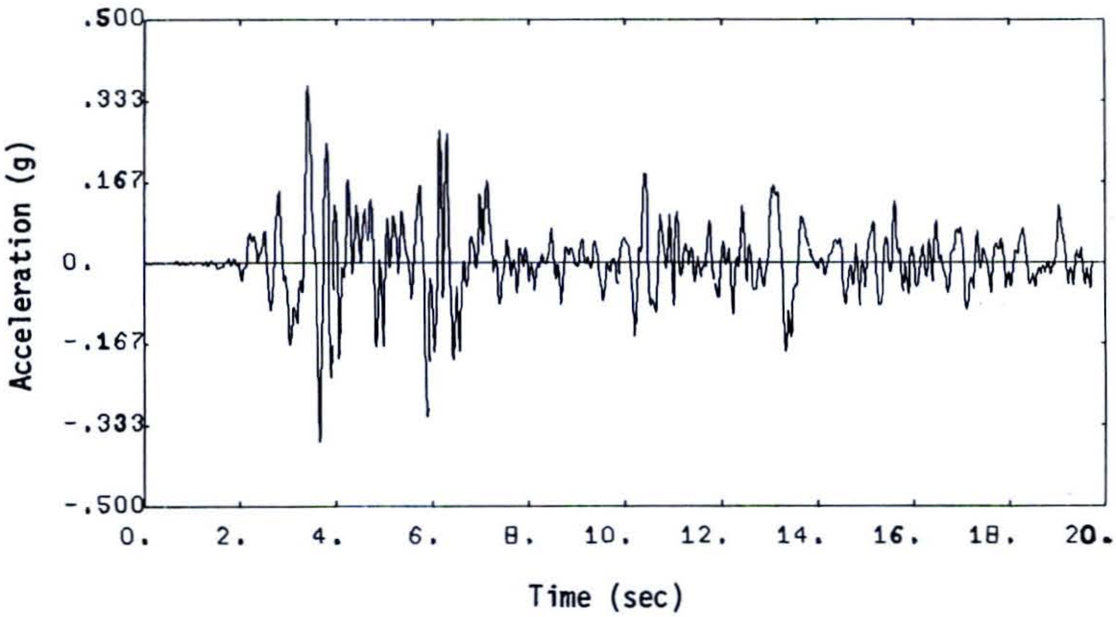

Test H-1-T-1 EC

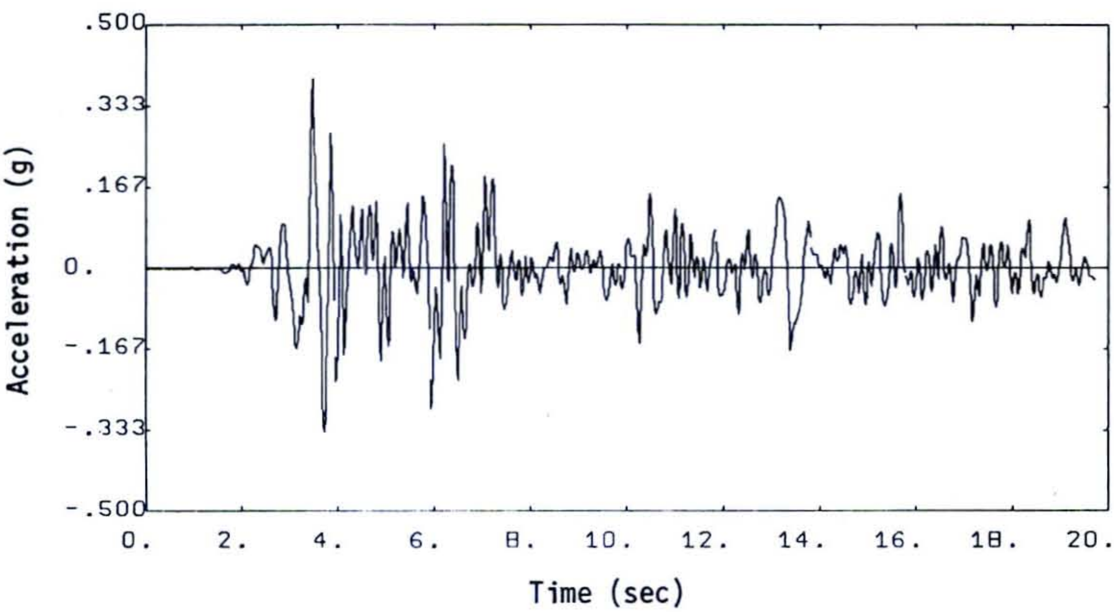

Test H-2-T-1 EC

FIGURE 5.21b STORY ACCELERATIONS - TRANSVERSE TEST, TYPE H

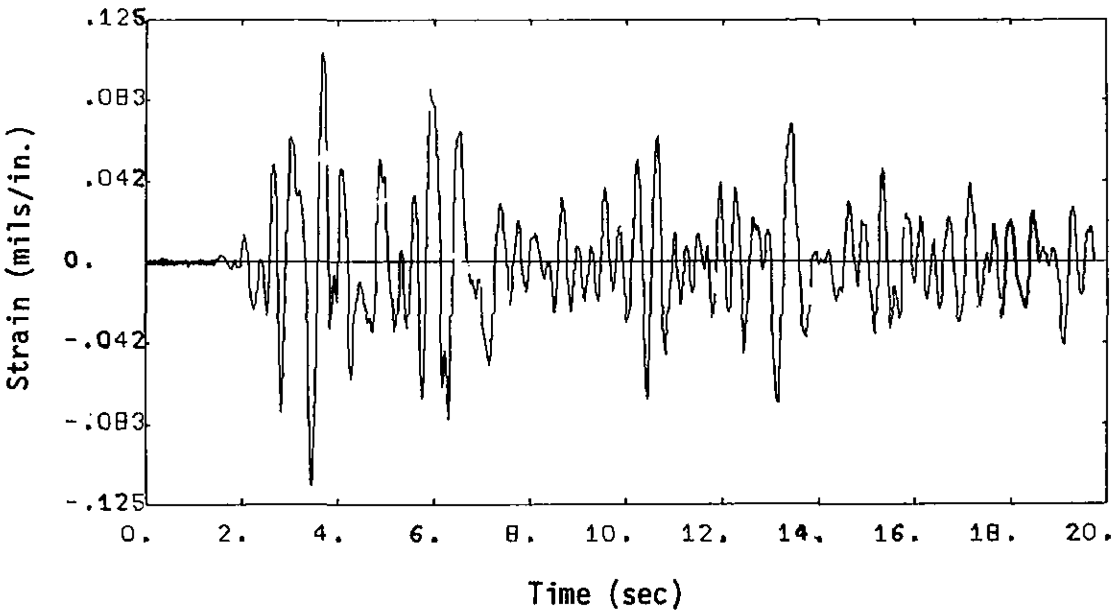

Test H-1-T-1 EC

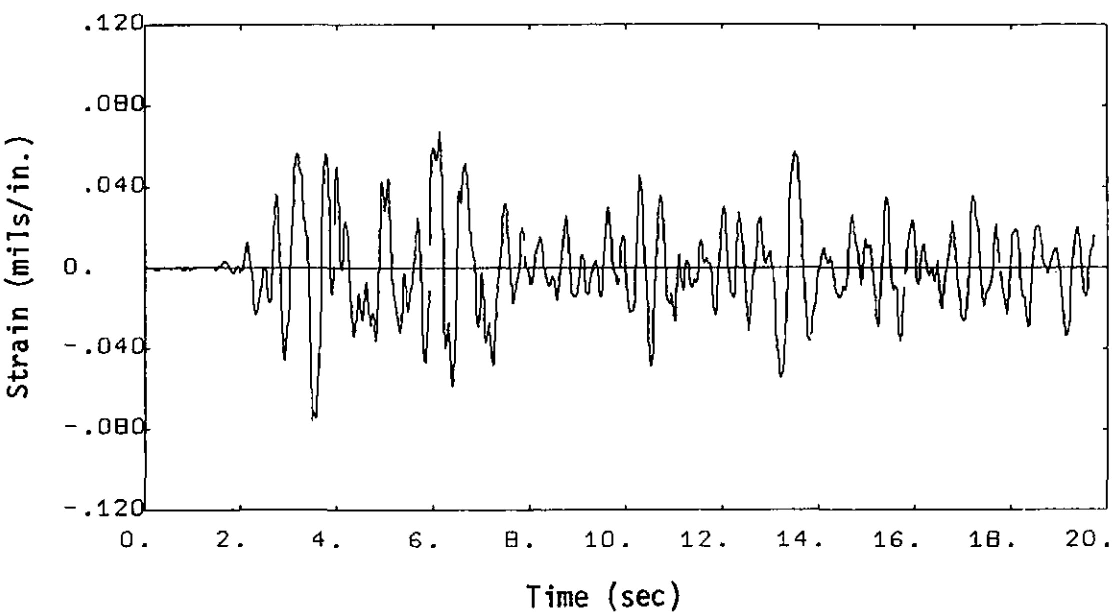

Test H-2-T-1 EC

FIGURE 5.21c BRACE AXIAL STRAINS - TRANSVERSE TEST, TYPE H

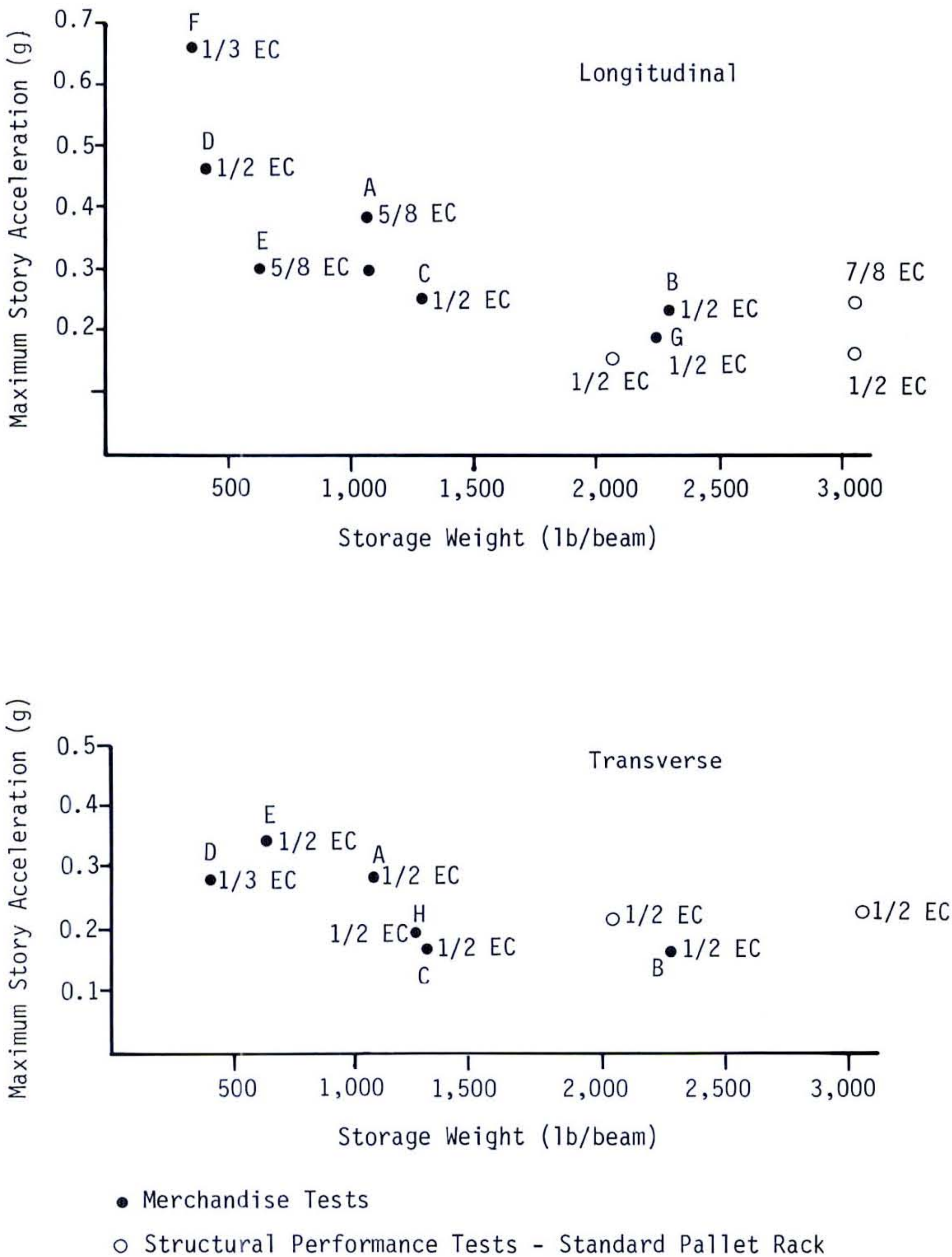

FIGURE 5.22 MAXIMUM STORY ACCELERATIONS VERSUS STORAGE WEIGHTS

INTENTIONALLY LEFT BLANK

6. METHODS OF THEORETICAL RESPONSE ANALYSIS

6.1 Introduction

One of the primary objectives of this test program was to obtain experimental data on the actual performance of various types of full-scale rack structures and subassemblies in order to test the adequacy and effectiveness of the various analytical procedures and assumed mathematical models. Using the same earthquake simulator facility, reconciliations of the experimental and analytical responses have been conducted with great success in several studies of the scale-model steel structures.[17,18,19] In this study, six different rack configurations were modeled analytically, both linearly and nonlinearly. A frequency analysis was performed using linear mathematical models to determine the linear models that fit each rack structure best. A time-history analysis was performed using nonlinear mathematical models to correlate the computed results with those observed during the test.

Time-history analysis requires the use of a rather large digital computer for the treatment of even moderately complex structural systems and therefore is beyond the capabilities of many design offices. Thus, this study also included a simpler method of analysis, the response spectrum method, which takes into account the true dynamic nature of the problem to a greater extent than standard code procedures do. A simplified static design method is found in the widely used *Uniform Building Code*. This study evaluated this method and, for comparison, the comprehensive and nationally applicable design provisions proposed by the Applied Technology Council and known as ATC-3. The periods of vibration and mode shapes used for these methods were obtained from the frequency analysis of the linear mathematical models.

The following sections briefly describe the analytical procedures and computer programs used.

6.2 Frequency Analysis of the Linear Mathematical Models

The frequency analysis of the linear mathematical models was carried out to compare calculated periods of vibration and mode shapes with those observed during the low-amplitude shaking table tests and the pull-release free-vibration tests. The best-fit linear model developed for each rack configuration was used as a basis for developing nonlinear models for time-history analysis, and the calculated periods and mode shapes were used to perform the response spectrum analysis. The calculated fundamental periods of vibration for each structure were used to determine the base shear coefficients for use in the *UBC* and the ATC-3 methods.

Many standard structural dynamics computer programs can do the frequency analysis of two-dimensional linear mathematical models. In this study, the program SAP IV, a multipurpose computer program developed at the University of California, Berkeley, was used to calculate the periods and mode shapes of the rack structures. (See Reference 20 for a complete description of this program.)

6.3 Time-History Analysis of the Nonlinear Mathematical Models

The computer program DRAIN-2D, developed by Kanaan and Powell, was used for all time-history analyses. A detailed description of this program can be found in Reference 21. A brief description follows next.

DRAIN-2D is a general two-dimensional structural program for nonlinear earthquake response analysis. The program uses the direct stiffness method to analyze a structure discretized as an assemblage of elements. Step-by-step integration, assuming constant average nodal accelerations within each integration time step, was used for both elastic and inelastic response analyses. Masses were assumed to be lumped at nodes, each mass having as many as three degrees of freedom.

The equations of motion for a discrete system subjected to rigid base motion are written in the matrix form:

$$\underline{M}\ddot{\underline{v}} + \underline{C}\dot{\underline{v}} + \underline{K}\underline{v} = \underline{M}\underline{I}\ddot{v}_g \qquad (6.1)$$

where $\underline{M}$ is the mass matrix and $\underline{C}$ and $\underline{K}$ are time-dependent tangent damping and stiffness matrices for the structure; $\underline{I}$ is a unit vector, $\ddot{v}_g$ is the base acceleration; and $\underline{v}$, $\dot{\underline{v}}$, and $\ddot{\underline{v}}$ are vectors for relative nodal displacement, velocity, and acceleration, respectively.

Damping capabilities available in the program include arbitrarily linear combination of mass and stiffness matrices. The damping matrix $\underset{\sim}{C}$ is assumed to be:

$$\underset{\sim}{C} = \alpha \underset{\sim}{M} + \beta \underset{\sim}{K} \tag{6.2}$$

where α and β are scalars derived from two sets of modal damping ratios, λ, and periods, T, as follows:

$$\alpha = \frac{4\pi(T_j\lambda_j - T_i\lambda_i)}{T_j^2 - T_i^2} \tag{6.3}$$

$$\beta = \frac{T_iT_j(T_j\lambda_i - T_i\lambda_j)}{\pi(T_j^2 - T_i^2)} \tag{6.4}$$

If only mass-dependent damping is assumed, damping equal to λ_i in a mode with period T_i can be obtained by:

$$\alpha = \frac{4\pi\lambda_i}{T_i} \tag{6.5}$$

Similarly, if only stiffness-dependent damping is assumed:

$$\beta = \frac{\lambda_iT_i}{\pi} \tag{6.6}$$

The main reasons for selecting DRAIN-2D for use in this study are that it can include the semirigid joint as a deformable element body and that various yield mechanisms can be adopted to define bilinear plastic hinge mechanisms. In addition, the geometrical nonlinearity due to the p-δ effect is included in the program.

6.4 Response Spectrum Analysis

This method consists of determining the mode shapes, periods, and participation factors of the modes of the structure by frequency analysis of the mathematical models. A sufficient number of modes were used, and a distribution of lateral forces was determined for each mode. The forces resulting from the response of the individual modes were combined by taking the square root of the sum of the squares (SRSS) of the individual modes.

The portion of the base shear contributed by the nth mode (V_n) is

$$V_n = \frac{[\Sigma m_i \phi_{in}]^2}{[\Sigma m_i \phi_{in}^2]} \cdot S_a \tag{6.7}$$

where:

V_n = base shear for the nth mode, in pounds

ϕ_{in} = the normalized displacement amplitude at the ith level of the structure when vibrating in its nth mode

m_i = mass at ith level

S_a = spectral acceleration in g from the response spectra

Then the forces at the various story levels may be obtained by distributing the base shear force:

$$q_{in} = \frac{m_i \phi_{in}}{\Sigma m_i \phi_{in}} \cdot V_n \tag{6.8}$$

6.5 Standard Code Procedures

The lateral force provisions in modern building codes such as the 1976 *UBC* provide a simplified design method for earthquake resistance in structures of normal dimensions. The minimum lateral force for which a structure has to be designed is given in terms of the design base shear, V, as follows:

$$V = ZIKCSW \tag{6.9}$$

where:

Z = a seismic zoning factor

I = an occupancy importance factor

K = a factor depending on the type of structure or structural system used

$C = \dfrac{1}{15\sqrt{T}}$

S = a factor designed to account for site-structure effects

W = the total dead load plus contents

In this study, the factors of Z and I were assumed to be 1.0; the fundamental periods of vibration, T, for various rack configurations were determined from the frequency analysis of assumed mathematical models.

The value of S can be determined by the following formulas:

For T/T_s = 1.0 or less:

$$S = 1.0 + \frac{T}{T_s} - 0.5\left(\frac{T}{T_s}\right)^2 \geq 1.0 \qquad (6.10)$$

For T/T_s > 1.0:

$$S = 1.2 + 0.6\,\frac{T}{T_s} - 0.3\left(\frac{T}{T_s}\right)^2 \geq 1.0 \qquad (6.10a)$$

where:

T_s = site characteristic period, not to be taken as less than 0.5 sec or more than 2.5 sec

The total base shear, V, is to be divided into two parts: a concentrated load, F_t, is to be applied at the top of the structure, and the balance, $(V - F_t)$, is to be distributed over the entire height of the structure. F_t is given by:

$$F_t = 0.07TV \qquad T \geq 0.7 \text{ sec} \qquad (6.11)$$

$$F_t = 0 \qquad T < 0.7 \text{ sec}$$

The magnitude of the distributed forces, F_x, making up the balance $(V - F_t)$ is:

$$F_x = \frac{(V - F_t)w_x h_x}{\Sigma w_i h_i} \qquad (6.12)$$

where:

w_x, w_i = the story weight assigned to level x or i, respectively

h_x, h_i = the height above the base to level x or i, respectively

For comparison, the lateral forces based on the provisions proposed by ATC-3 were also evaluated. ATC-3 recommends that the structure, considered to be fixed at the base, be designed to resist the lateral seismic base shear V:

$$V = C_s W \tag{6.13}$$

where:

$$C_s = \frac{1.2 A_v S}{R T^{2/3}}$$

A_v = a coefficient representing effective peak velocity-related acceleration

S = a coefficient for the soil-profile characteristics of the site

R = a response modification factor

W = the total dead load plus contents

The values of S are 1.0, 1.2, and 1.5 for site profile types S_1, S_2, and S_3, respectively.

In this study, the value of A_v was assumed to be 0.4 (for Map Area 7 and Seismicity Index 4).

The lateral seismic force, F_x, induced at any level is given by:

$$F_x = C_{vx} V \tag{6.14}$$

where:

$$C_{vx} = \frac{w_x h_x^n}{\Sigma w_i h_i^n}$$

$n = 1 \qquad T \le 0.5$ sec

$n = 2 \qquad T \ge 2.5$ sec

For structures having a period between 0.5 and 2.5 sec, n may be taken as 2 or may be determined by linear interpolation between 1 and 2.

Note that the *UBC* seismic design provisions are to be used for working stress design with a one-third increase in allowable stresses permitted for forces resulting from seismic motion. The ATC-3 provisions are for ultimate strength design using a capacity-reduction factor of 0.9 for cold-formed steel design.

INTENTIONALLY BLANK

7. THEORETICAL PREDICTION OF STRUCTURE RESPONSE-- STANDARD PALLET RACK, LONGITUDINAL DIRECTION

7.1 Frequency Analysis

Basic Model. Figure 7.1 shows the basic mathematical model developed for the standard pallet rack in the longitudinal direction. Because it assumes symmetric response for the two frames, an analytical model for a single frame was considered adequate. The centerline dimensions shown were used, and semirigid beam-column joints and partially fixed bases were assumed in evaluating stiffness. The masses of the dead loads plus concrete blocks and wooden pallets were lumped at the nodes where the pallets were located. The mass per floor was estimated to be about 11.0 and 16.2 $lb\text{-}sec^2/in.$ for the 2/3 and full live load cases, respectively. The minimum net section properties provided by the manufacturer, shown in Table 4.2, are as follows:

	Moment of Inertia ($in.^4$)	Cross-sectional Area ($in.^2$)	Estimated Shear Area ($in.^2$)
Column	1.14	0.69	0.31
Beam	3.27	1.29	1.02

In searching for the best-fit mathematical model, the influences of semirigid connections and column fixity were taken into account. Since standard computer programs such as SAP IV have no capability to handle the semirigid joint problem, some modification to the beam member properties was needed. To deal with the problem of column base fixity, fictitious restraining floor beams were added to simulate the actual column base condition. These two factors are discussed in the following sections.

Influence of Semirigid Joints. General-purpose elastic frame analysis programs usually assume rigid beam-column connections and do not provide for the problem of loose connections. Since the moment connections between columns and beams for this rack configuration are not fully rigid, the beam rigidities must be modified to use the computer program SAP IV for the frequency analysis. The beam rigidities were reduced as follows:

Preceding page blank

$$\left(\frac{I_b}{L_b}\right)_{red} = \left[\frac{1}{1 + \frac{6EI_b}{K_\theta L_b}}\right] \cdot \frac{I_b}{L_b} \tag{7.1}$$

where:

I_b = moment of inertia of beam (in.^{4})

L_b = length of beam (in.)

E = Young's modulus of elasticity (lb/in.^{2})

K_θ = joint rotational spring stiffness (lb-in./rad)

Although this formulation was suggested by Driscoll[22] for determining the effective length of columns with semirigid connections, in this study, it was used to substitute the original unreduced beam rigidity for use in computer analysis.

Influence of Column Base Fixity. The local response measured by the DCDT gages near the column base plates indicated that the column bases provide a considerable restraint against rotation, which in turn reduces the column moments at the first-floor level. Therefore, the bases should not be considered as either fixed or hinged but rather as partially fixed bases. Two alternative methods have usually been employed by structural engineers in connection with the problem of column base fixity. The first method, such as the one suggested by Salmon et al.,[23] uses rotational springs (assumed or experimentally determined) at the column base plates. The other method, such as suggested by Galambos,[24] assumes the bases to be connected to a fictitious restraining beam. The rigidity of such a fictitious floor beam is given by:

$$\frac{I_f}{L_f} = \frac{bd^2}{720} \tag{7.2}$$

where:

I_f = moment of inertia of fictitious beam

L_f = length of fictitious beam

b,d = dimensions of the column perpendicular and parallel to direction of bending, respectively

The rotational spring attached to the column base requires some special routines that may not be readily available for most of the frame-analysis programs. However, because the fictitious restraining beam elements can be easily adopted in the program, the latter approach was used in the development of mathematical models. Thus, Figure 7.1 shows fictitious floor beams connected at the column bases. The floor beams terminate in the middle of two adjacent column bases rather than being continuous in order to prevent any erroneous moments from being carried over to the adjacent column bases.

Comparison of Various Linear Mathematical Models. From the above discussion, the values of K_θ (for semirigid connections) and I_f (column fixity) are the only two adjustable modeling parameters in the development of the best-fit mathematical models. The characteristics of the moment-rotation relation (M-θ) at the beam-column connections were experimentally determined from the subassembly tests reported in Chapter 2 (see Figure 7.2a). From these characteristics, the initial K_θ can be estimated approximately. No experimental data on the column base fixity were available; therefore, Equation (7.2) was used as a basis and adjusted when needed. Seven models were studied by varying the parameters K_θ and I_f as indicated in Table 7.1. In Models 1 through 5, the rack was simulated with 2/3 live load and in Models 6 and 7 with the full live load. The results from Models 1 and 2 clearly show the effects of rigid versus semirigid connections. Model 3 assumed the base to be connected by fictitious floor beams. The value of I_f for these beams was calculated from Equation (7.2) to be 3.7 in.^{4}, assuming b and d to be the dimensions of the column. The calculated periods of vibration and mode shapes from Model 3 do not correlate well with the measured results (shown in footnote of Table 7.1). Models 4 and 5, which assume I_f to be 0.2 in.^{4} and K_θ to range from 10^6 to 1.4×10^6, are in good agreement with the measured results. These parameters were also applied to the rack loaded with the full live load, and good correlation between the calculated and measured results was again obtained. Therefore, it was concluded that valid linear mathematical models should use the parameters $I_f = 0.2$ and $K_\theta = 10^6$ to 1.4×10^6. These modeling parameters were also used in developing nonlinear mathematical models for time-history response analysis.

7.2 Time-History Analysis

Basic Model. The nonlinear mathematical models for the time-history response analysis adopted for this rack configuration (Figure 7.3) are similar to the linear models except that beam-column connections were modeled as deformable elements and the DRAIN-2D computer program was used. As shown in Figure 7.3, each joint element is connected to two nodes and is influenced by only the relative rotational displacement between the nodes. The translation displacement of the nodes should also be made to be identical, in which case these nodes should also have identical coordinates. The bilinear yield mechanism of the moment-rotation relationship for the semirigid connection was idealized as shown in Figure 7.2b. With reference to the experimentally determined M-θ relationship from the subassembly tests (Figure 7.2a), the parameters M_1, M_2, K_θ, and p can be assigned and adjusted as appropriate from the measured beam-column test results. The yield interaction surfaces for columns and beams were estimated as illustrated in Figure 7.4. The calculated yield moments of beams and columns ($M_y = S \times F_y$, where S is the section modulus and F_y is the yield stress) are 65 kip-in. and 34 kip-in., respectively. The average compression force at yield was estimated to be approximately 22 kips in accordance with AISI 3.6.1. The detailed procedures for obtaining the theoretical axial yield force can be seen in Appendix A.

Results. Four case studies were performed. Table 7.2 summarizes the parameters finally used for each case. These parameters yielded the best possible analytical results in comparison with the corresponding experimental data. As can be seen from the table, all member properties, masses per story level, and initial joint rotational springs remained essentially the same as those used in the frequency analysis of the best-fit linear models. The improvement of data correlation was accomplished by varying only the damping and the binlinear yield mechanism of the semirigid connection element. The time-history analysis was carried out with an integration time step of about 0.0196 sec, the same time interval as for digitization of the recorded data. This was considered to be adequate for numerical stability criteria because the periods of vibration were estimated in the ranges of 1.5 to 2.0 sec, 0.4 to 0.5 sec, and 0.2 to 0.3 sec for the first, second, and third modes, respectively (see Table 7.1).

Case 1 (SP-L-2/3-1/4 EC). For this case, the model was simulated with 2/3 live load and subjected to an input signal about 1/4 that of the actual El Centro record. Mass-proportional damping corresponding to about 3% of the first-mode viscous damping was prescribed for the model. An initial joint rotational spring (K_θ) of 1.4×10^6 lb-in./rad and a moment of inertia of the fictitious floor beam (I_f) of 0.2 in.^{4} were assumed. Figure 7.5 shows the predicted and measured story displacements relative to the table, which demonstrate good agreement both in phase and magnitude, although the calculated values are slightly lower than those observed during the test. These slightly low predicted displacements could have been increased by using slightly lower damping in the model. Figure 7.6 shows the computed and measured end rotations of the first-floor center column. Again a good comparison is indicated.

Case 2 (SP-L-1-1/4 PF). In this case study, the model was simulated with the full live load, and an input signal approximately 1/4 that of the actual Parkfield record was used. All the modeling parameters such as K_θ, I_f, and α used in Case 1 remained unchanged except by assigning new floor masses and using the 1/4 Parkfield signal. Figure 7.7 compares the measured data with the predicted results of the story displacements and the column end rotation near the top end of the first-floor center column. There is a good correlation, although the predicted displacements are slightly smaller than those measured. The response for both Case 1 and Case 2 was linear, and no material yielding was detected, either from the analytical or the experimental observations.

Case 3 (SP-L-1-1/2 EC). For this model, the rack remained loaded with the full live load but was subjected to an input signal 1/2 the actual El Centro record. This test run was the first instance in which material yielding at the critical column member was observed from the shaking table tests. The theoretically estimated yield rotation at the center bottom-story column was about 1.73×10^{-3} rad. The detailed procedures for evaluating the yield rotation are illustrated in Appendix A. Unfortunately, because of the failure of the data-acquisition system at about 11 sec, only response records of 10 sec are presented in this study. For the analytical prediction, the values of K_θ and α were assigned slightly different values from those of Case 2. The mass-proportional damping corresponding to about 4.5% first-mode viscous damping was prescribed. The parameter K_θ was assigned a value of 10^6 lb-in./rad compared with the value of 1.4×10^6 lb-in./rad used in Case 2. Figures 7.8 and 7.9 show good agreement between the predicted and measured results. It is apparent that a single mathematical model can be used to predict both linear and nonlinear response of the rack structure by varying only damping (α) and joint rotational spring (K_θ).

Case 4 (SP-L-1-1/2 PF). This case is another example of nonlinear response prediction. The nonlinearity is evident when the periods of vibration showing in the displacement time-history plots are changed. Both predicted and measured column end rotations are also seen to exceed the theoretical column end rotation at the initiation of yielding ($\phi_y = 1.73 \times 10^{-3}$ rad). A comparison of predicted and measured results shown in Figure 7.10 is again excellent. Although some permanent displacement at each story level was detected before conducting the test run, these displacements were not incorporated into the analytical model.

7.3 Response Spectrum Analysis

Seven cases were analyzed by this method. Table 7.3 summarizes the base shears and overturning moments determined along with the input signal and damping used for each case. As can be seen from the table, the effect on base shear of the higher modes is in the range of 10% to 20% of the total. However, the higher mode participation in the case of the base overturning moments is negligible. Three individual cases were selected for presentation in this report. Figure 7.11 shows the calculated periods of vibration and normalized mode shapes obtained from the frequency analysis of the linear mathematical model simulated with the full live load (see Table 7.1). Figures 7.12 to 7.14 show the story forces, story shears, and story overturning moments for various modes of vibration representative of three typical test cases. A comparison of the calculated story forces for the first mode and the SRSS reveals the importance of higher-mode participation. The effects of higher modes should therefore be considered when the story forces are needed in the design.

7.4 *UBC* and ATC-3 Methods

The base shears determined by the *UBC* and ATC methods are shown in Table 7.4. The fundamental periods of vibration used in the base shear calculations were determined from the frequency analysis of the linear mathematical models (see Table 7.1). In the evaluation of base shears by the *UBC* method, K, Z, and I were assumed to be 1.0 and the minimum value of CS was used (i.e., $S = 1.0$ for the best site condition). The response modification factor R in the ATC method was assumed to be 4.5 because the rack could be classified as an ordinary moment steel frame. The value of A_v was assigned to be 0.4, appropriate for an area of Seismicity Index 4. Table 7.5 shows base story forces for ultimate strength design. The base story forces for the *UBC* method were multiplied by a factor of 1.28, as required in ultimate strength design. The base story forces for the ATC method were modified by a capacity-reduction factor of 0.9. The results from the ATC method are slightly higher than those from the *UBC* method.

The lateral forces determined by the *UBC* method are roughly equivalent to those using the response spectrum method with an intensity of about 1/2 to 5/8 that of the actual El Centro record. However, if the maximum value of CS were to be assumed (i.e., $S = 1.5$ for the worst site condition), the *UBC* lateral forces would probably be equivalent to those developed by the full El Centro or Parkfield record.

Figure 7.15 is a comparison of story forces, shears, and overturning moments determined from three seismic design analysis methods. Only the first-mode response spectrum analysis results are presented. The adequacy and limitations of the various approaches to the seismic design of racks is discussed in Chapter 13.

TABLE 7.1
LINEAR MATHEMATICAL MODELS - STANDARD PALLET RACK, LONGITUDINAL DIRECTION

Model	Live Load	Column Base		Beam Element		Period* (sec)			Mode Shape*		
		Case	I_f	K_θ	I'_b	1	2	3	1	2	3
1	2/3	pinned	no	∞	3.27	1.20	0.32	0.17	1.00 0.89 0.66	1.00 -2.77 -1.14	1.00 -2.16 1.40
2	"	"	no	10^6	0.47	1.90	0.43	0.18	1.00 0.82 0.52	1.00 -0.51 -1.13	1.00 -2.49 1.99
3	"	semi-fixed	3.7	10^6	0.47	1.30	0.36	0.18	1.00 0.69 0.28	1.00 -0.97 -1.17	1.00 -2.70 3.10
4	"	"	0.2	10^6	0.47	1.59	0.42	0.19	1.00 0.77 0.42	1.00 -0.66 -1.18	1.00 -2.52 2.25
5	"	"	0.2	1.4×10^6	0.62	1.55	0.40	0.19	1.00 0.78 0.44	1.00 -0.62 -1.18	1.00 -2.45 2.15
6	full	"	0.2	10^6	0.47	1.95	0.51	0.23	1.00 0.77 0.42	1.00 -0.66 -1.18	1.00 -2.52 2.25
7	"	"	0.2	1.4×10^6	0.62	1.92	0.50	0.23	1.00 0.80 0.47	1.00 -0.55 -1.16	1.00 -2.45 2.15

I_f = Moment of inertia of fictitious floor beam (in.^{4})

K_θ = Initial rotational joint spring (lb-in./rad)

I'_b = Reduced moment of inertia of beam due to semirigid connection (in.^{4})

*Experimentally determined periods and mode shapes are:

Period:

2/3 Live Load	Full Live Load
T_1 = 1.50 - 1.66 sec	T_1 = 1.80 - 2.10 sec
T_2 = 0.43 sec	T_2 = 0.53 sec
T_3 = 0.22 sec	T_3 = 0.26 sec

Mode Shape (Average):

1st Mode	2nd Mode	3rd Mode
1.00	1.00	1.00
0.79	-0.62	-2.42
0.44	-1.15	2.08

TABLE 7.2

MODELING PARAMETERS FOR TIME-HISTORY ANALYSIS - STANDARD PALLET RACK, LONGITUDINAL DIRECTION

Case	Designation	Input Signal	Live Load	Beam			Column			Semirigid Joint (See Figure 7.2b)				Column Base	Damping		Remarks
				I_b (in.^{4})	A_b (in.^{2})	A_b' (in.^{2})	I_c (in.^{4})	A_c (in.^{2})	A_c' (in.^{2})	K_θ $\frac{\text{lb-in.}}{\text{rad}}$	P	M_1 (lb-in.)	M_2 (lb-in.)	I_f (in.^{4})	α	λ (%)	
1	SP-L- 2/3-1/4 EC	1/4 EC	2/3	3.27	1.23	1.02	1.15	0.69	0.31	1.4 x 10^6	0.8	12 x 10^3	20 x 10^3	0.2	0.235	3.0	linear response
2	SP-L 1-1/4 PF	1/4 PF	full	"	"	"	"	"	"	"	"	"	"	"	"	3.7	"
3	SP-L 1-1/2 EC	1/2 EC	"	"	"	"	"	"	"	10^6	"	"	"	"	0.285	4.5	nonlinear response
4	SP-L 1-1/2 PF	1/2 PF	"	"	"	"	"	"	"	0.9 x 10^6	0.78	"	"	"	0.285	4.5	"

Notes: 2/3 live load = 11.0 lb-sec^2/in. per story level
Full live load = 16.2 lb-sec^2/in. per story load
A_b', A_c' = Estimated shear areas of beam and column, respectively

TABLE 7.3

SUMMARY OF RESULTS FROM RESPONSE SPECTRUM ANALYSIS - STANDARD PALLET RACK, LONGITUDINAL DIRECTION

Case	Designation	Live Load	Input Signal		Base Shear (lb)		Base Over-turning Moment (kip-in.)	
			Signal	Damping (%)	1st Mode	SRSS	1st Mode	SRSS
1	SP-L-2/3-1/4 EC	2/3	1/4 EC	3	407	445	55	56
2	SP-L-2/3-1/2 EC	"	1/2 EC	5	756	854	89	91
3	SP-L-1-1/4 PF	full	1/4 PF	3	774	815	104	105
4	SP-L-1-1/4 EC	"	1/4 EC	3	567	650	76	76
5	SP-L-1-1/2 EC	"	1/2 EC	5	1,030	1,210	138	140
6	SP-L-1-1/2 PF	"	1/2 PF	5	1,290	1,402	174	175
7	SP-L-1-5/8 EC	"	5/8 EC	5	1,254	1,486	167	169

TABLE 7.4

DETERMINATION OF BASE SHEAR USING THE *UBC* METHOD AND THE ATC METHOD - STANDARD PALLET RACK, LONGITUDINAL DIRECTION

Live Load	T (sec)	W (lb)	1976 *UBC*		ATC-3	
			C	V (lb)	C_s	V (lb)
2/3	1.6	12,750	0.052	662	0.078	994
Full	2.0	18,750	0.047	887	0.067	1,265
			$V = ZIKCSW$ $C = \frac{1}{15\sqrt{T}}$ $K = 1.0$ $I = Z = 1.0$ $S = 1.0$ (minimum)		$V = C_s W$ $C_s = \frac{1.2\ A_v S}{RT^{2/3}}$ $A_v = 0.4$ $S = 1.0$ (minimum) $R = 4.5$	

TABLE 7.5

BASE STORY FORCES FOR ULTIMATE STRENGTH DESIGN - STANDARD PALLET RACK, LONGITUDINAL DIRECTION

Live Load	*UBC* Method*		ATC Method†		Response Spectrum Method			
	Base Shear (lb)	Base Overturning Moment (kip-in.)	Base Shear (lb)	Base Overturning Moment (kip-in.)	1st Mode Base Shear (lb)	1st Mode Base Overturning Moment (kip-in.)	Damping (%)	Signal
2/3	847	123	1,104	160	407	55	3	1/4 EC
"	"	"	"	"	756	89	5	1/2 EC
Full	1,135	165	1,406	209	774	104	3	1/4 PF
"	"	"	"	"	567	76	3	1/4 EC
"	"	"	"	"	1,030	138	5	1/2 EC
"	"	"	"	"	1,290	174	5	1/2 PF
"	"	"	"	"	1,254	167	5	5/8 EC

*The factored code forces required in ultimate strength design (1.7/1.33 = 1.28)

†A capacity-reduction factor of 0.9 is applied.

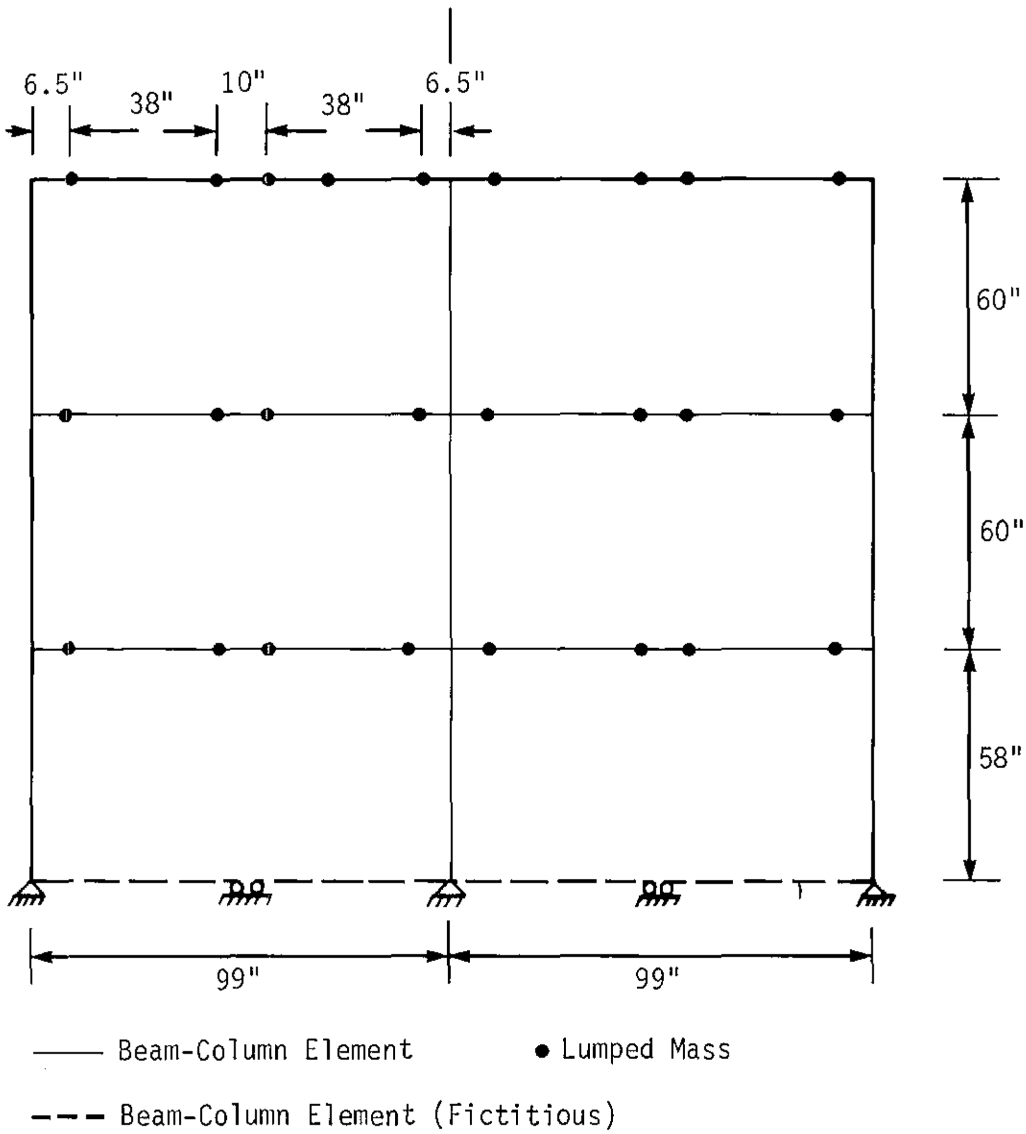

FIGURE 7.1 MATHEMATICAL MODEL (SAP IV) - STANDARD PALLET RACK, LONGITUDINAL DIRECTION

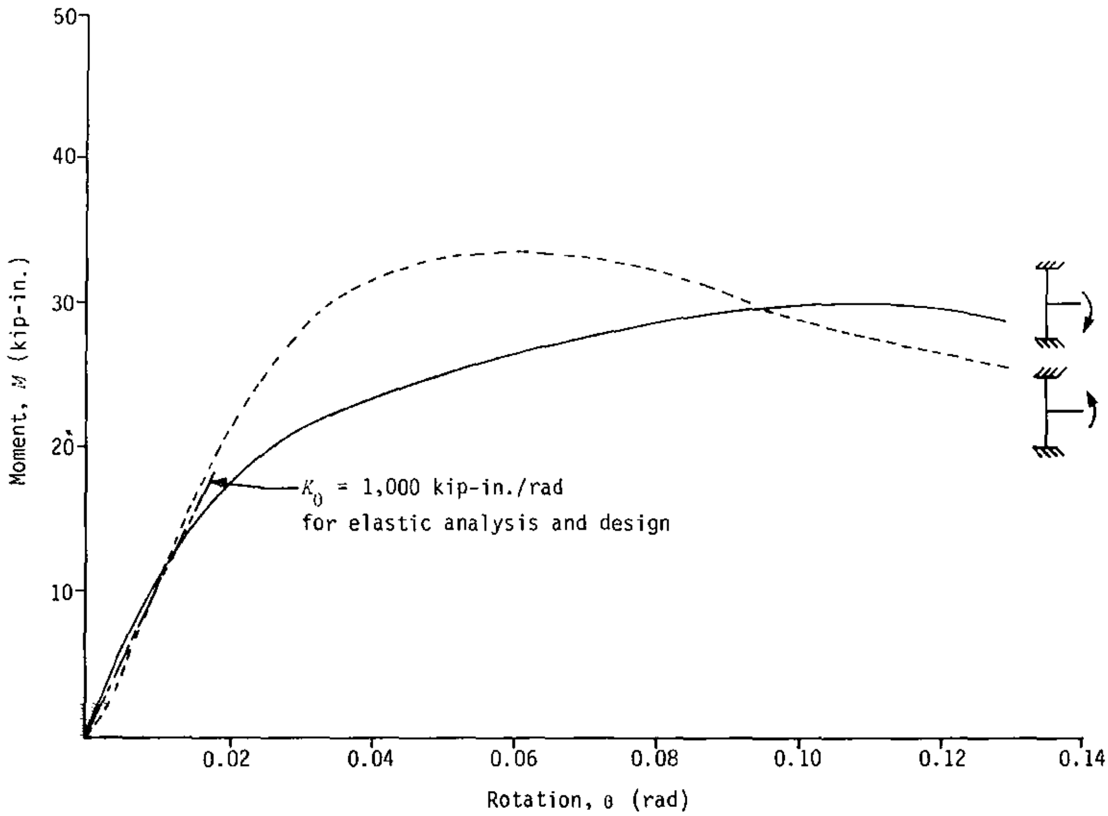

a. Experimentally Obtained M-θ Curves

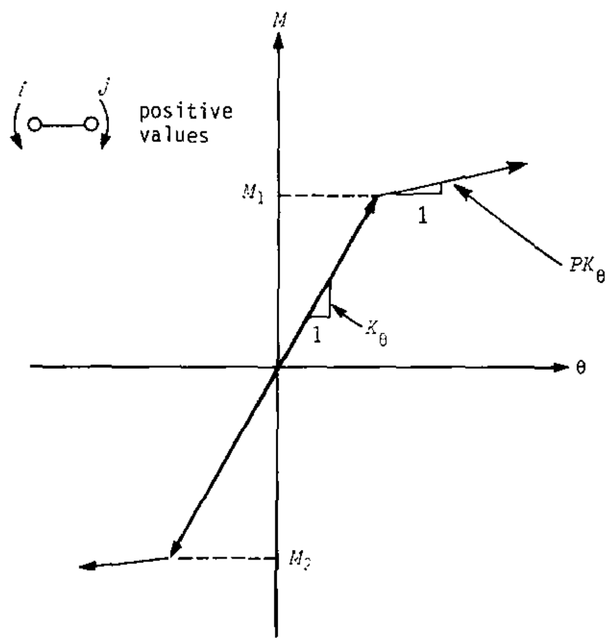

b. Idealized M-θ Curves

FIGURE 7.2 MOMENT-ROTATION RELATIONSHIP FOR SEMIRIGID CONNECTION

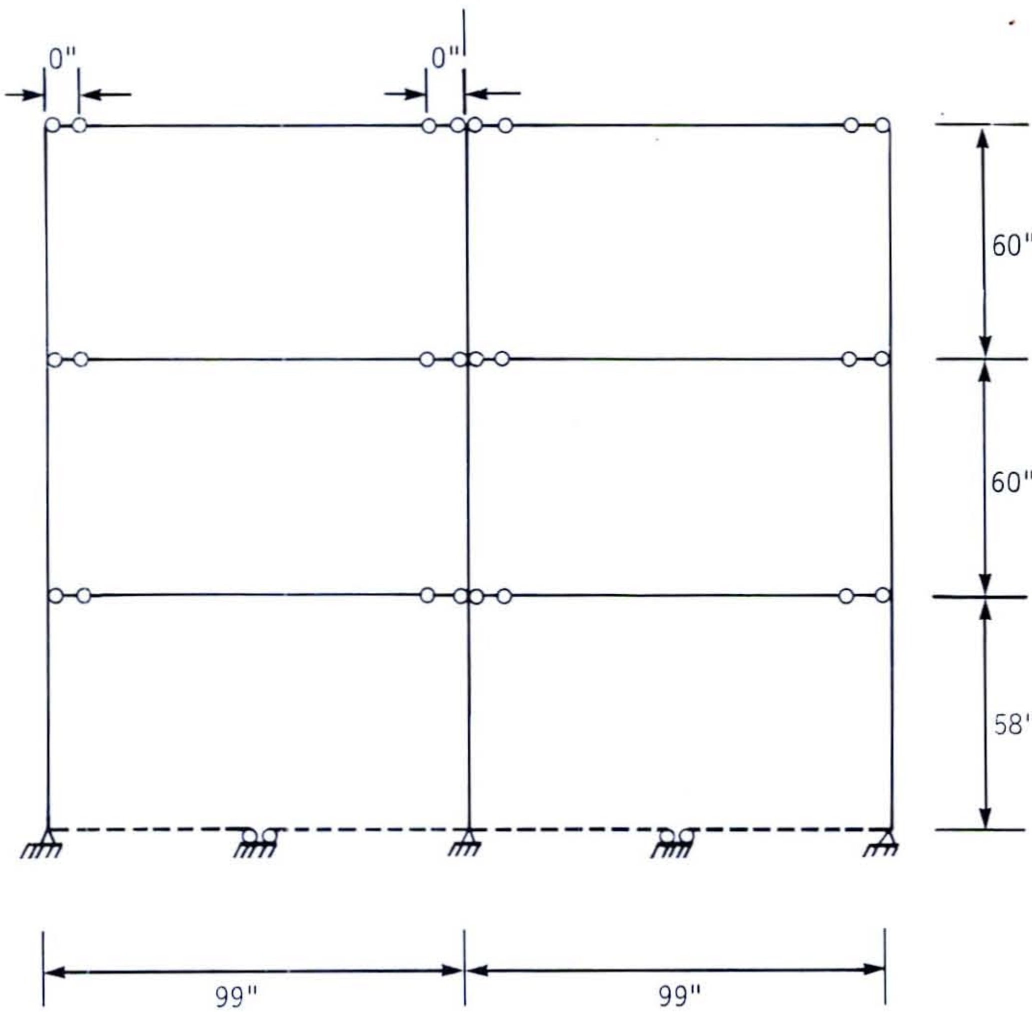

— Beam-Column Element

o—o Semirigid Connection Element

--- Beam-Column Element (Fictitious)

● Lumped Mass (not shown, same as linear model)

FIGURE 7.3 MATHEMATICAL MODEL (DRAIN-2D) - STANDARD PALLET RACK, LONGITUDINAL DIRECTION

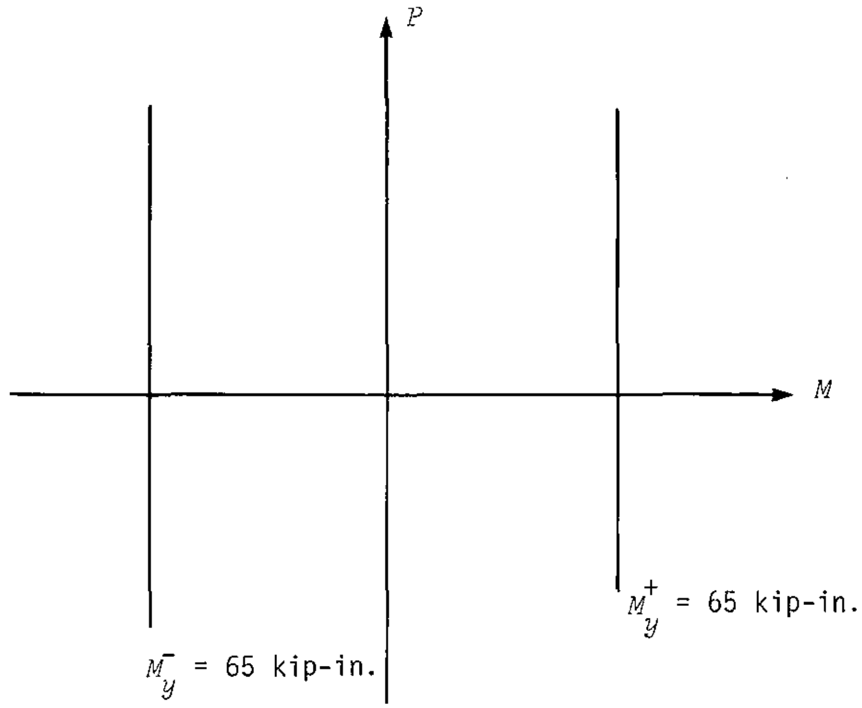

a. Beam

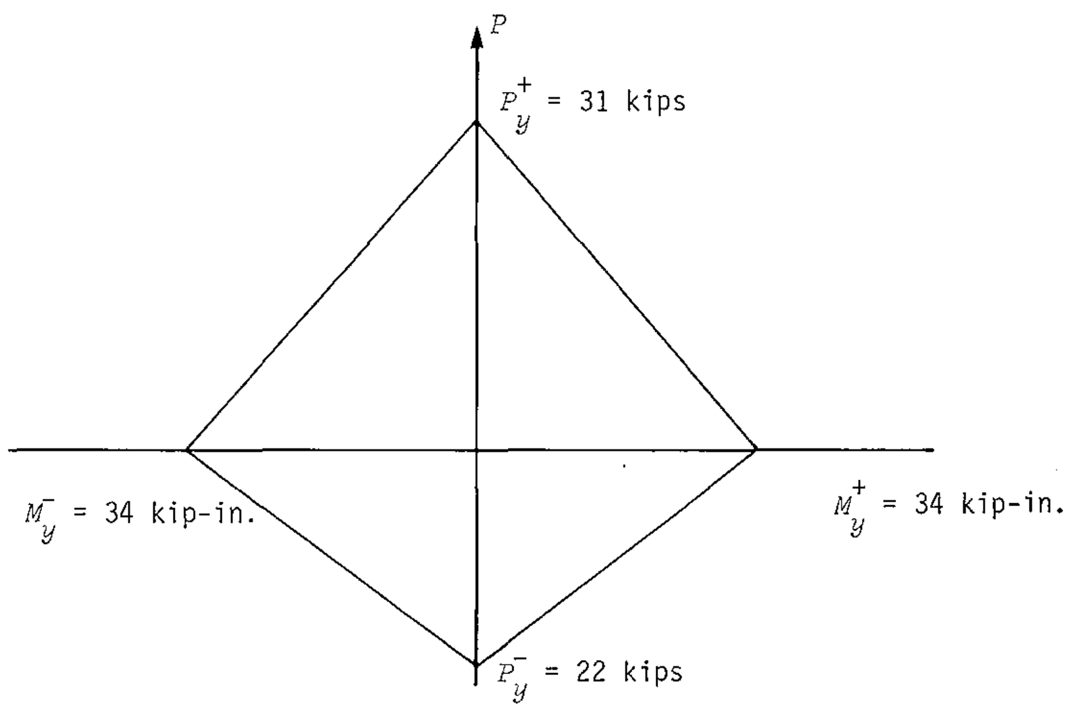

b. Column

FIGURE 7.4 YIELD INTERACTION SURFACES - STANDARD PALLET RACK, LONGITUDINAL DIRECTION

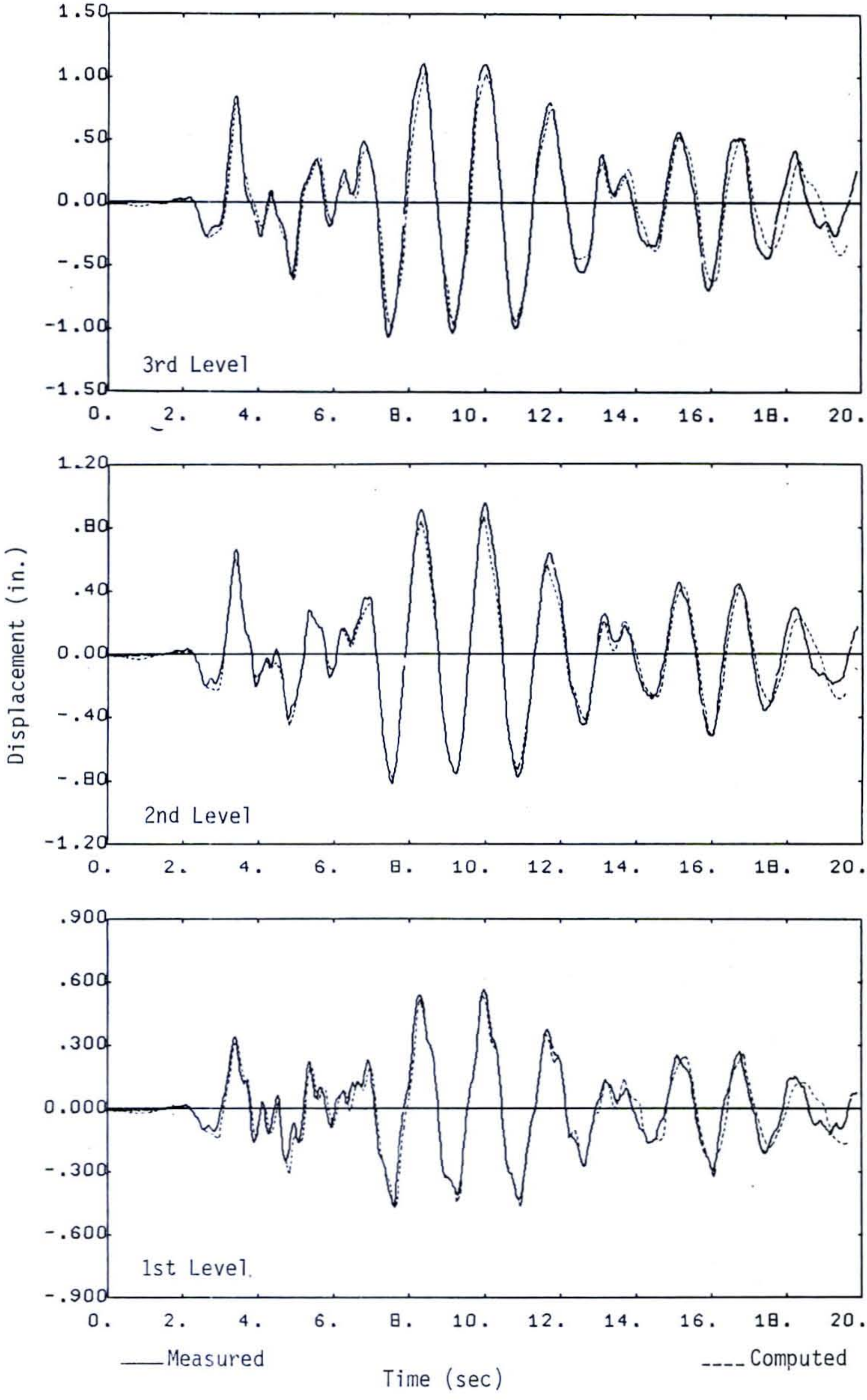

FIGURE 7.5 MEASURED AND COMPUTED STORY DISPLACEMENTS (SP-L-2/3-1/4 EC)

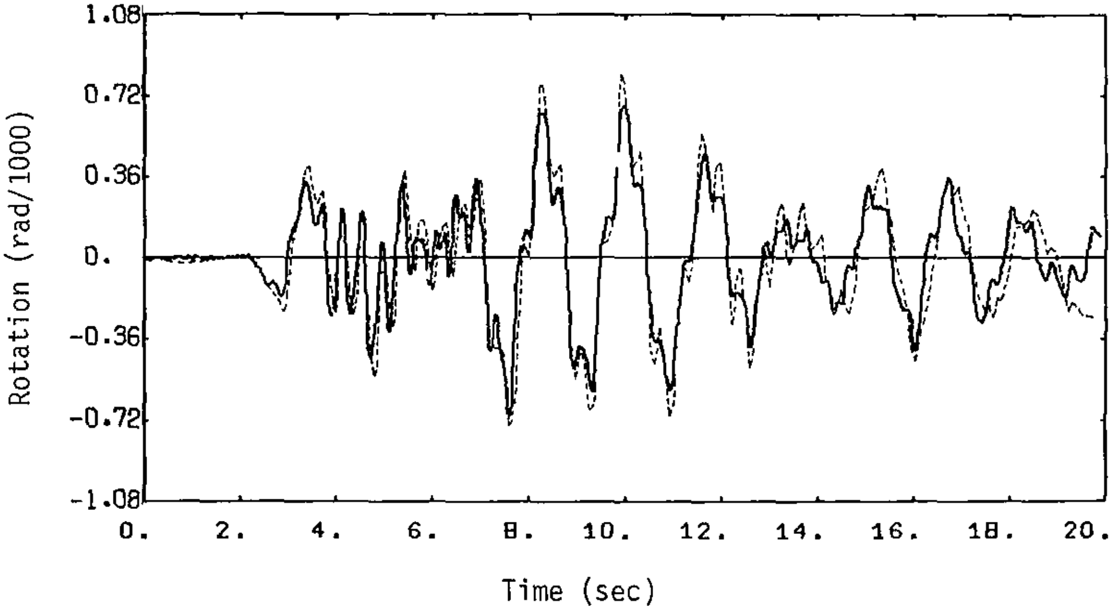

Center Bottom Column Near Top End

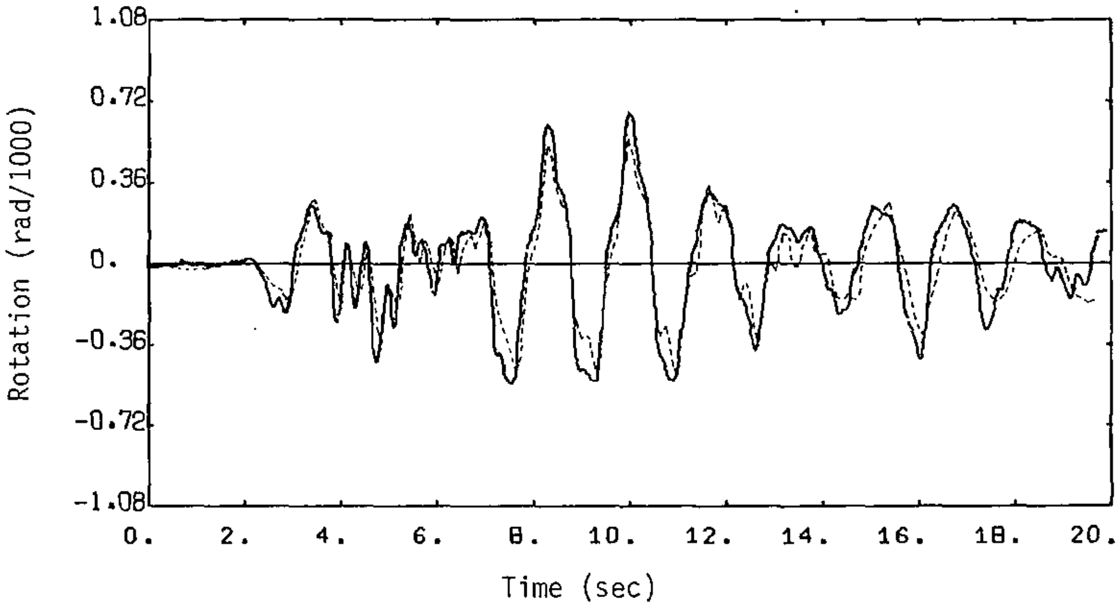

Center Bottom Column Near Base Plate

——— Measured ---- Computed

FIGURE 7.6 MEASURED AND COMPUTED LOCAL RESPONSES
(SP-L-2/3-1/4 EC)

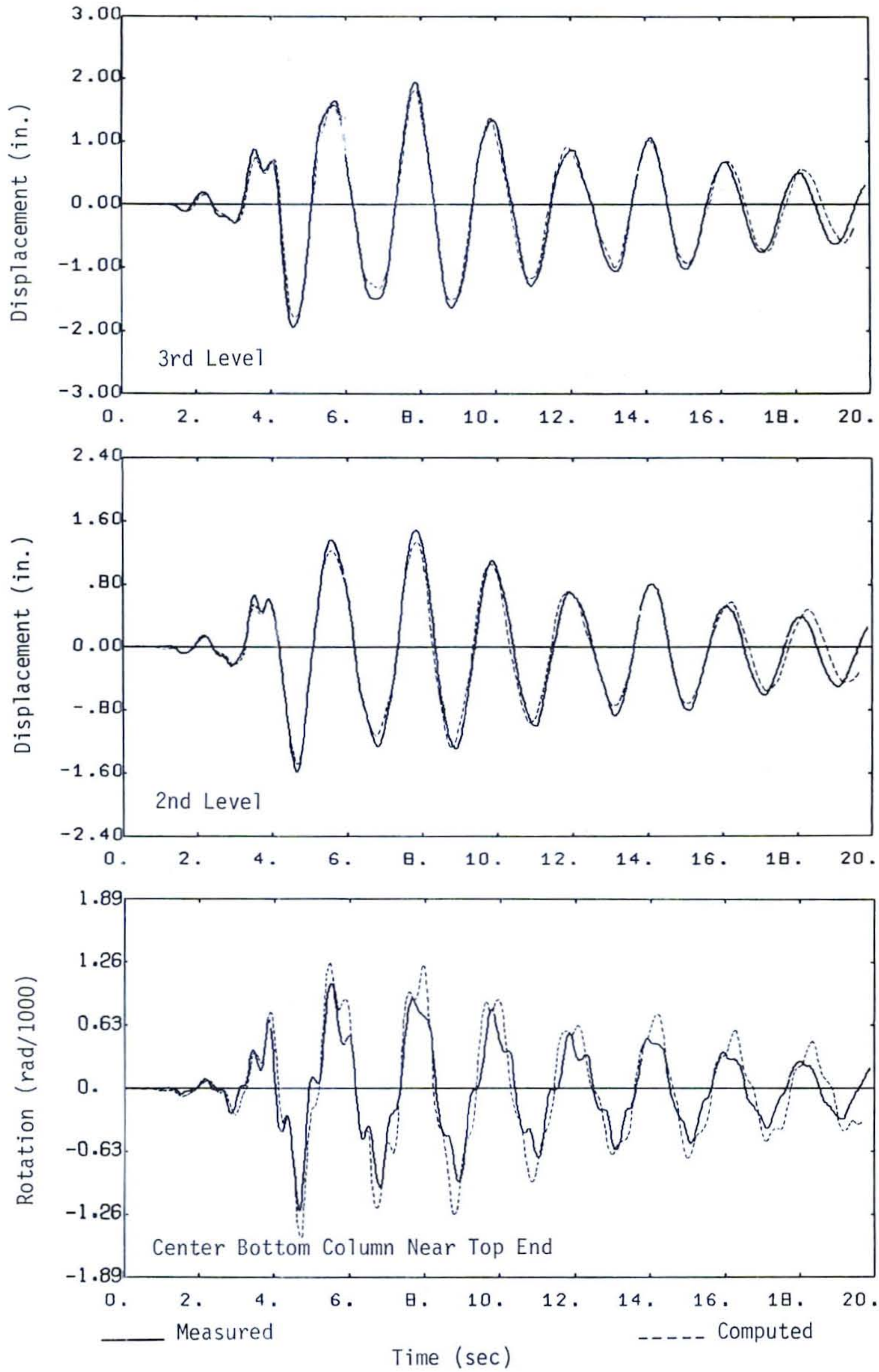

FIGURE 7.7 MEASURED AND COMPUTED RESULTS
(SP-L-1-1/4 PF)

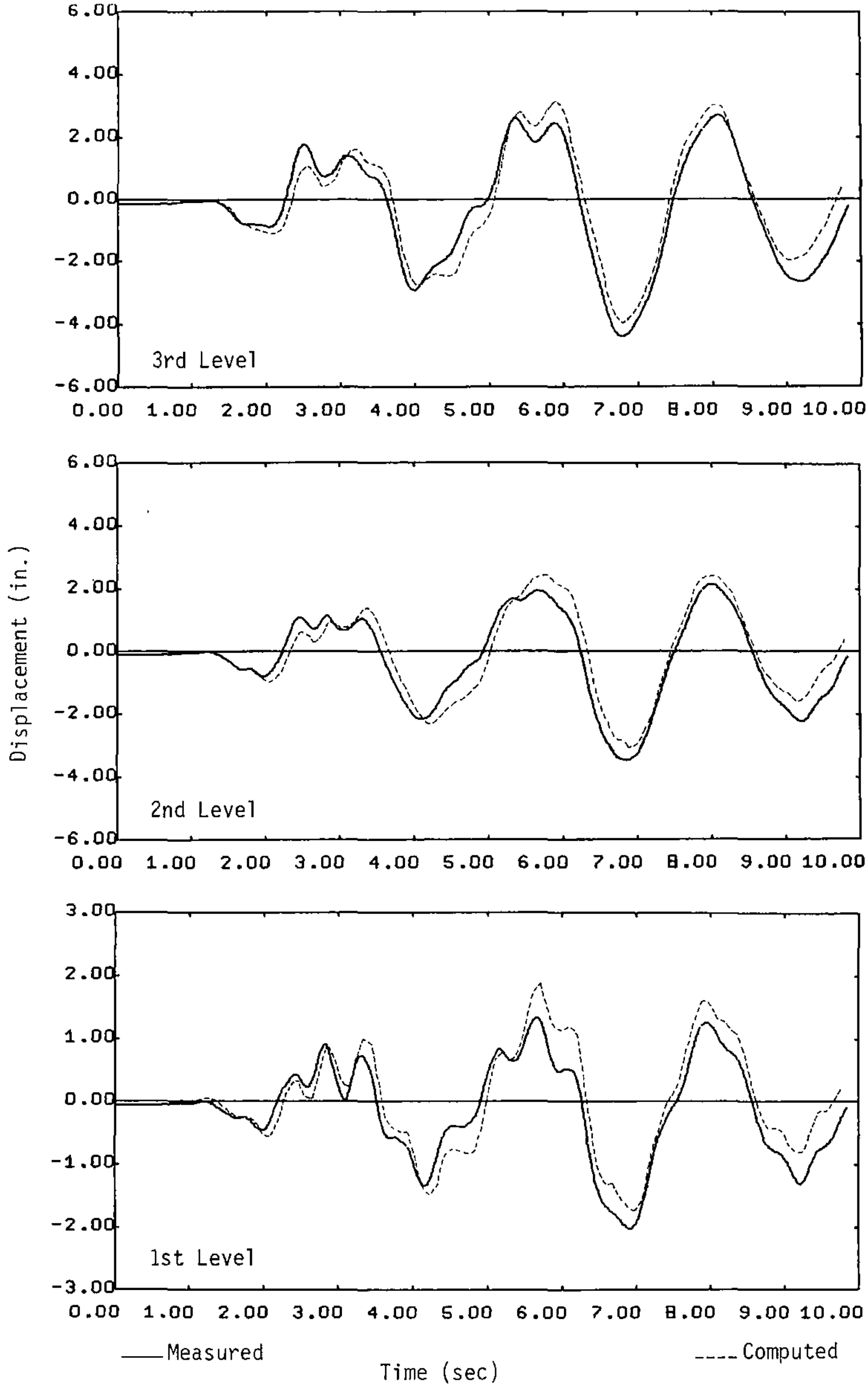

FIGURE 7.8 MEASURED AND COMPUTED STORY DISPLACEMENTS (SP-L-1-1/2 EC)

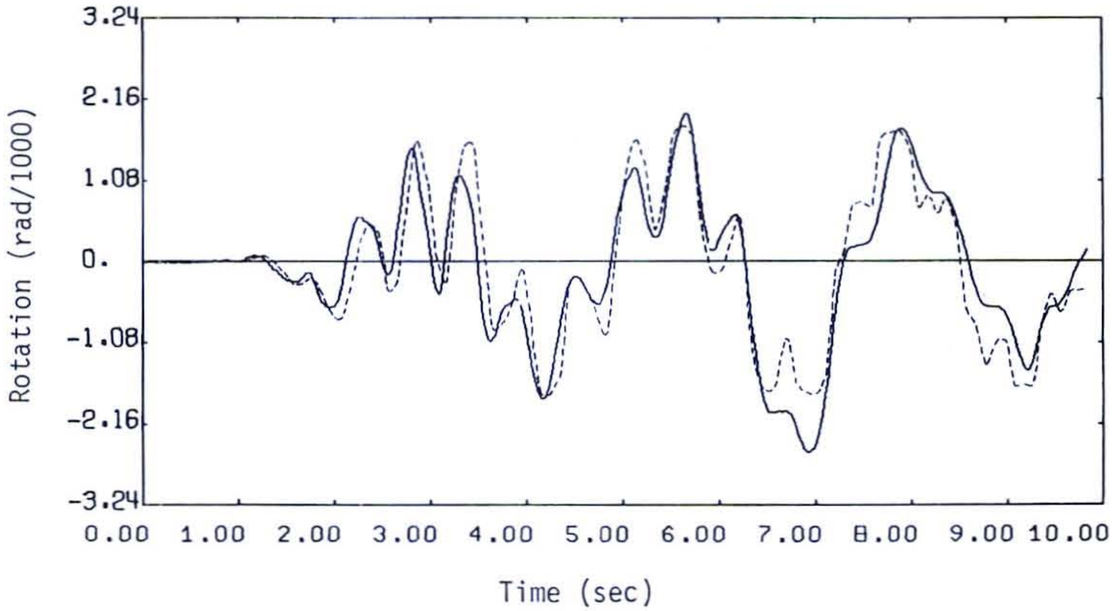

Center Bottom Column Near Top End

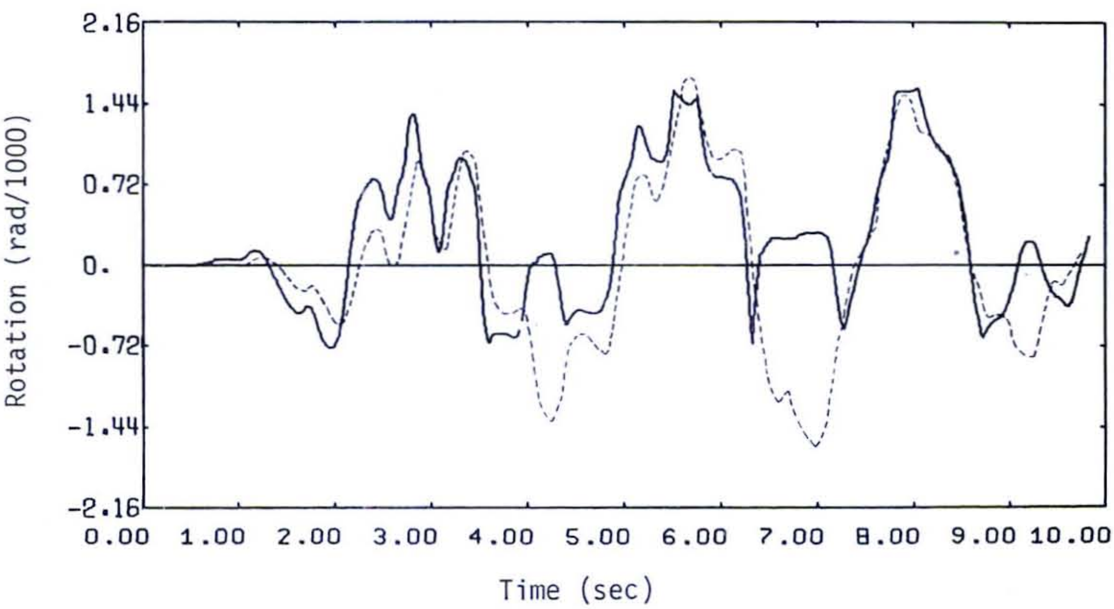

Center Bottom Column Near Base Plate

____ Measured ---- Computed

FIGURE 7.9 MEASURED AND COMPUTED LOCAL RESPONSES (SP-L-1-1/2 EC)

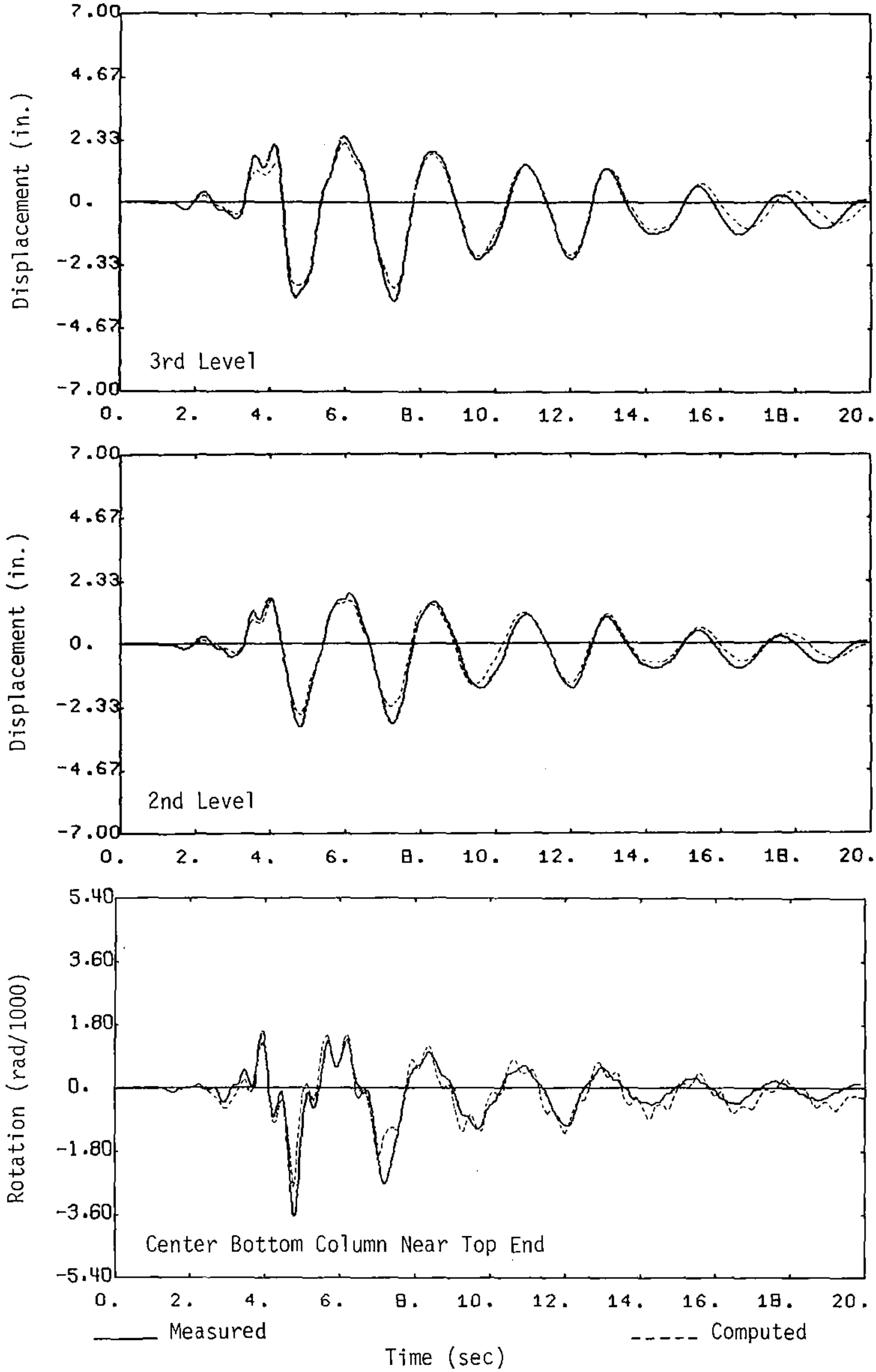

FIGURE 7.10 MEASURED AND COMPUTED RESULTS
(SP-L-1-1/2 PF)

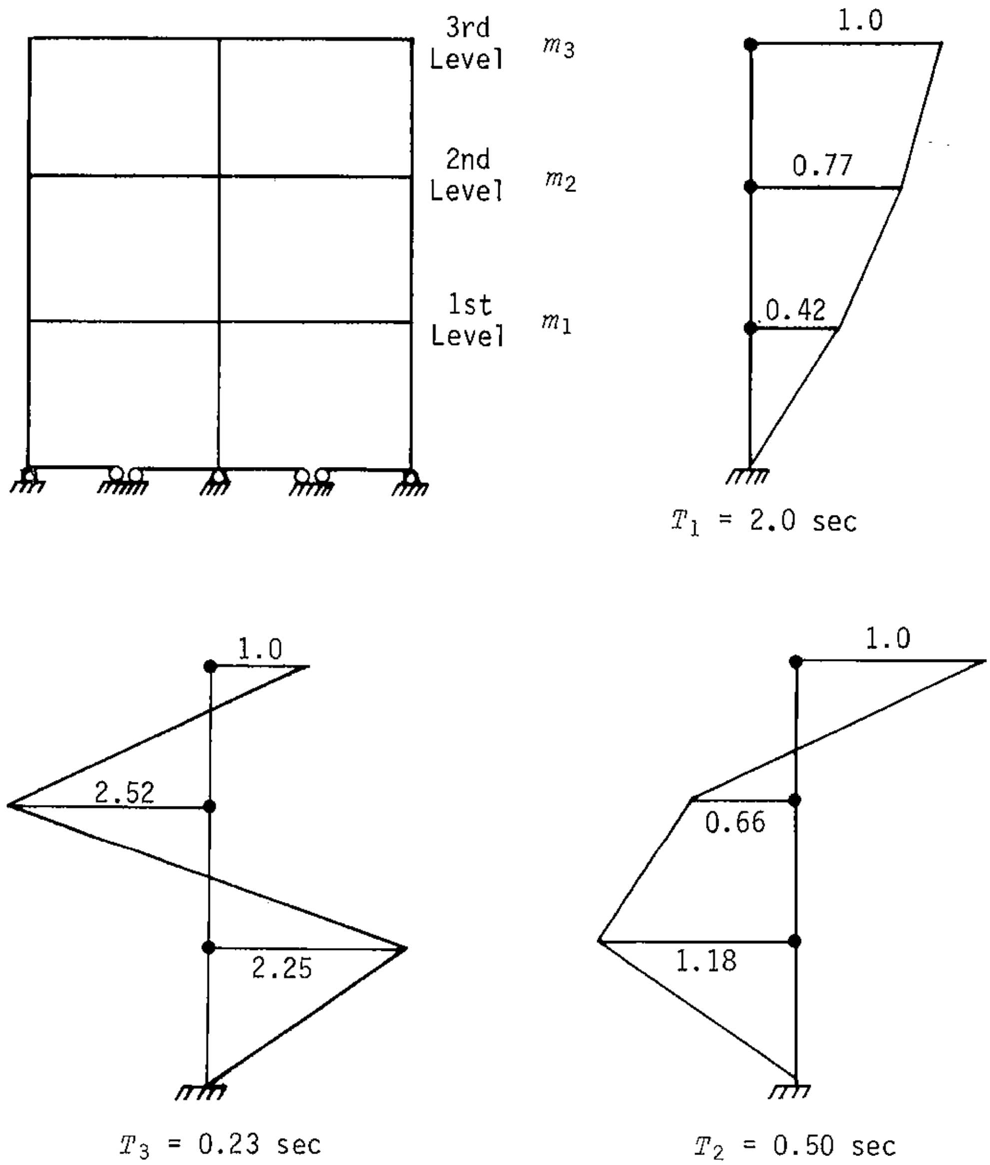

$K_\theta = 10^6$ lb-in./rad

$I_f = 0.2$ in.^{4}

$m_1 = m_2 = m_3$
$= 16.2$ lb-sec^2/in.

FIGURE 7.11 CALCULATED PERIODS OF VIBRATION AND MODE SHAPES - STANDARD PALLET RACK, LONGITUDINAL DIRECTION, FULL LIVE LOAD

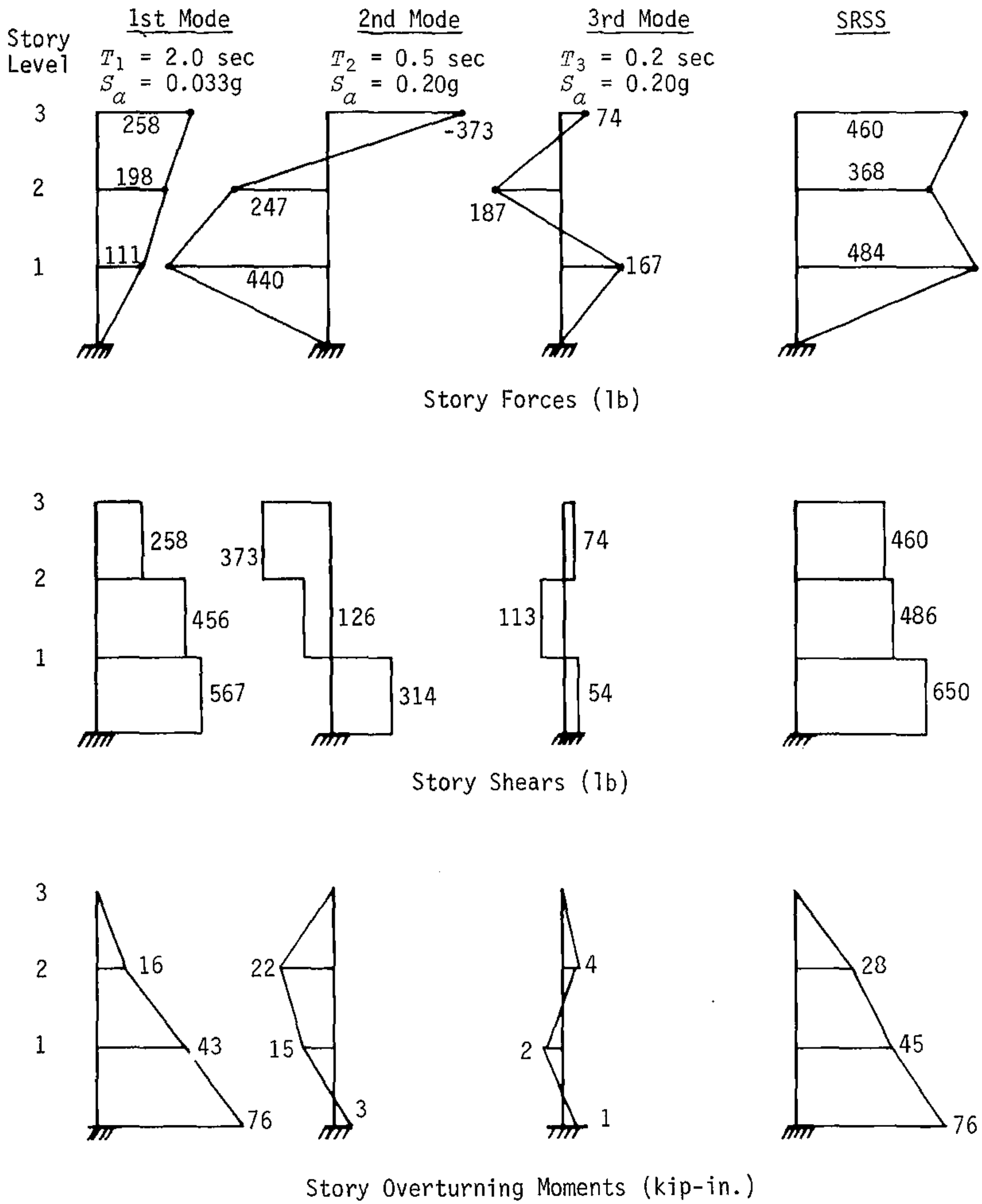

FIGURE 7.12 RESULTS OF RESPONSE SPECTRUM ANALYSIS (SP-L-1-1/4 EC)

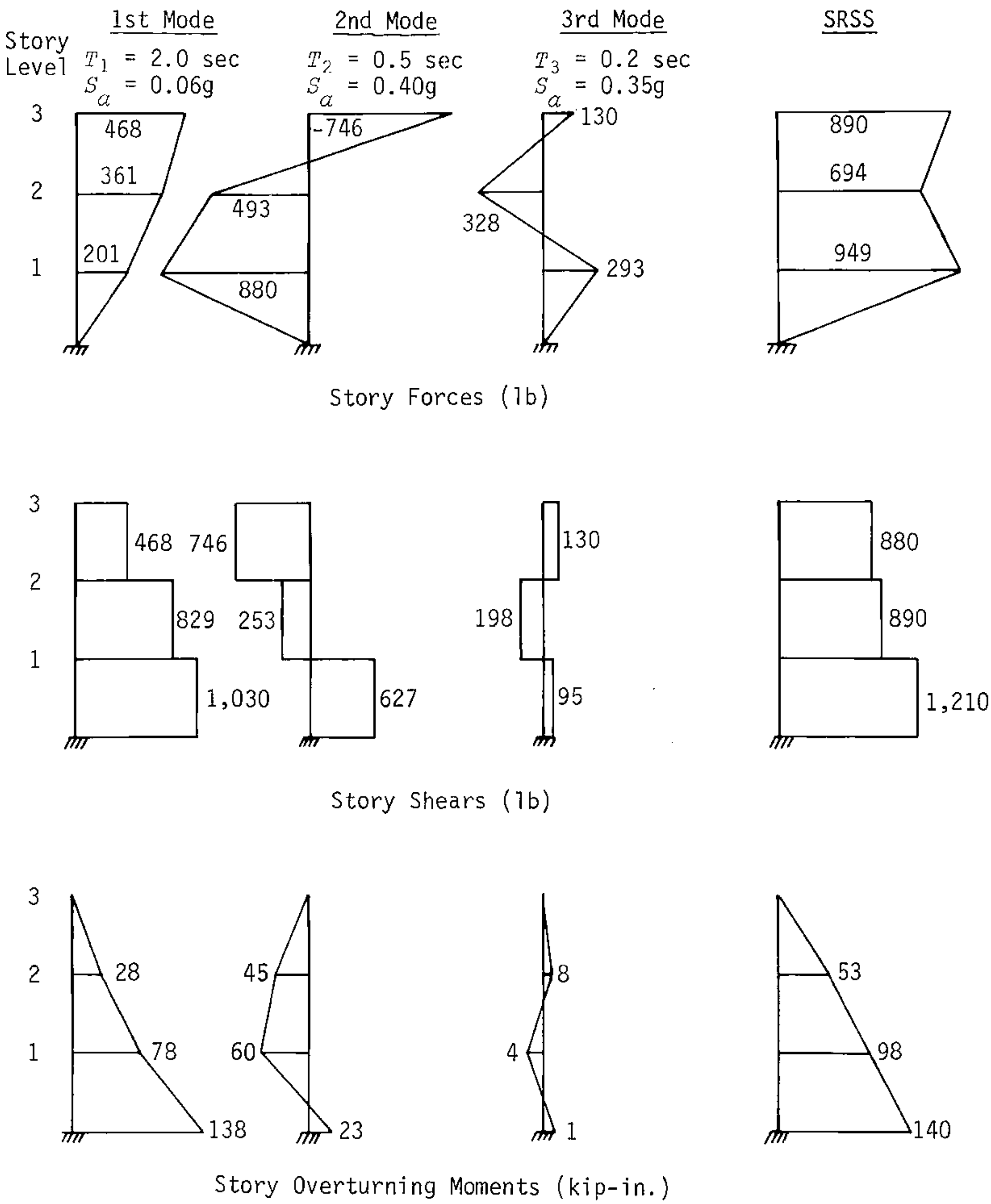

FIGURE 7.13 RESULTS OF RESPONSE SPECTRUM ANALYSIS (SP-L-1-1/2 EC)

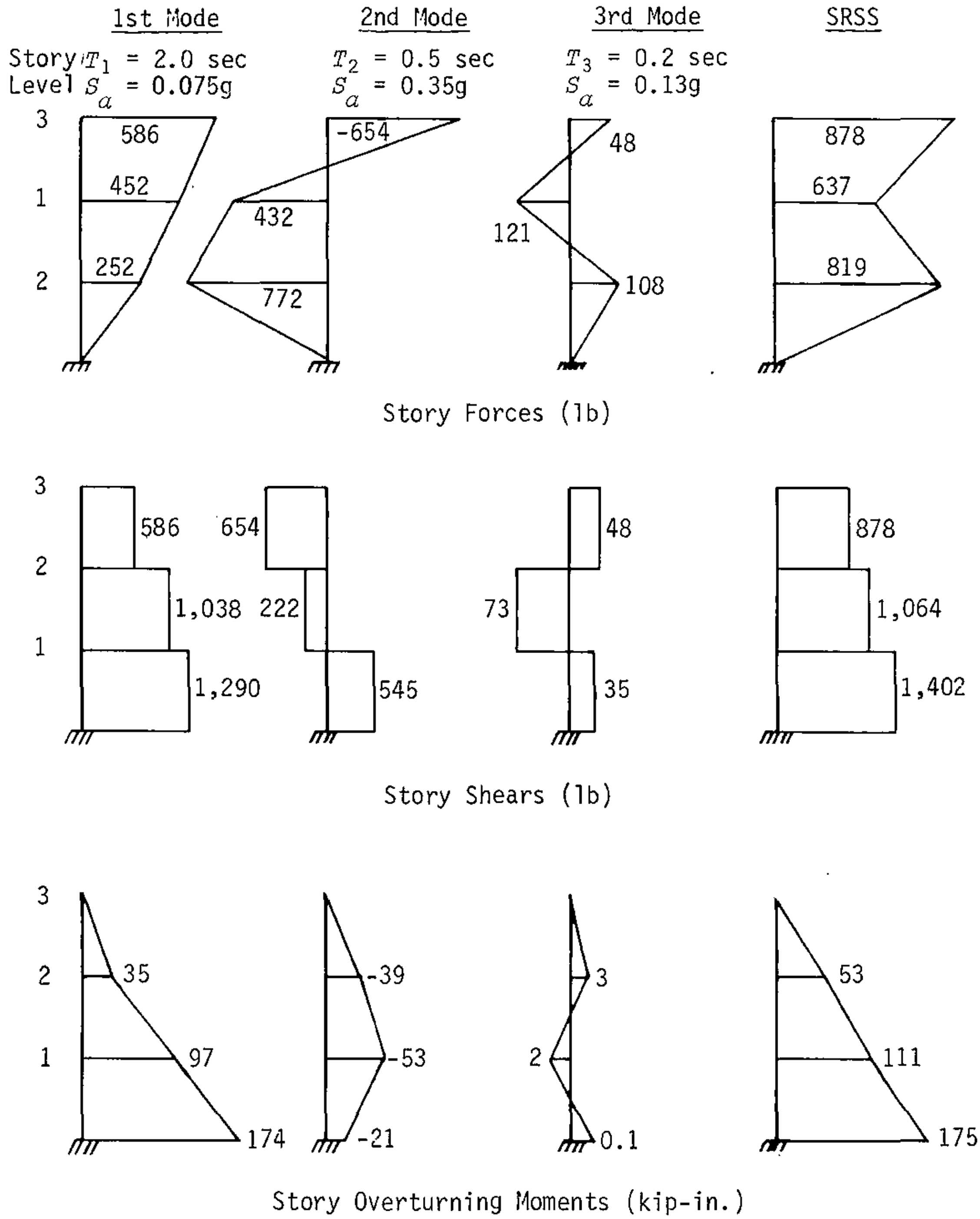

FIGURE 7.14 RESULTS OF RESPONSE SPECTRUM ANALYSIS
(SP-L-1-1/2 PF)

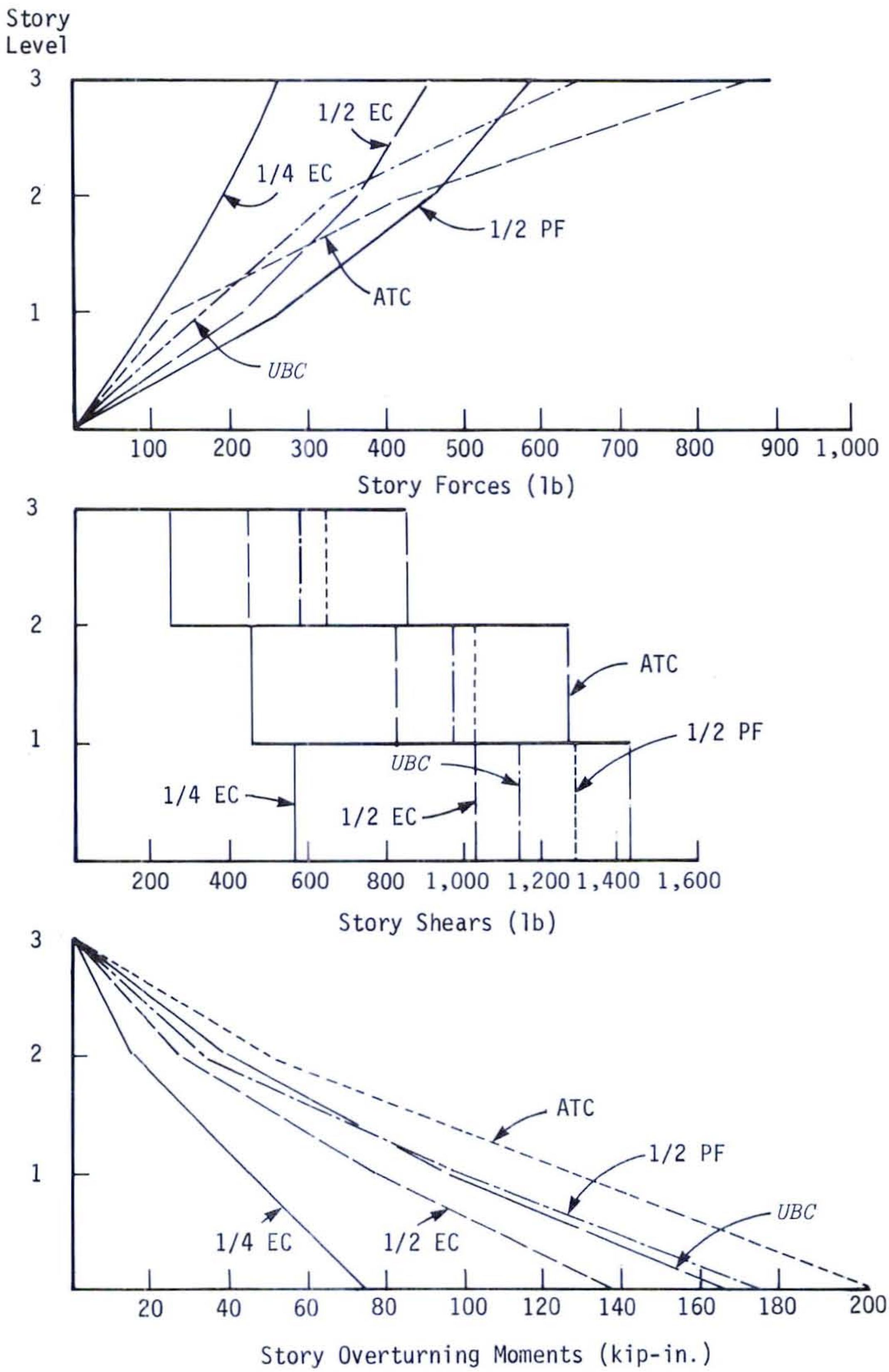

FIGURE 7.15 RESULTS OF THE *UBC* METHOD, THE ATC METHOD, AND THE RESPONSE SPECTRUM METHOD - STANDARD PALLET RACK, FULL LIVE LOAD, LONGITUDINAL DIRECTION

8. THEORETICAL PREDICTION OF STRUCTURE RESPONSE--STANDARD PALLET RACK, TRANSVERSE DIRECTION

8.1 Frequency Analysis

Basic Model. Figure 8.1 shows the basic mathematical model developed for the standard pallet rack in the transverse direction. Because it assumes symmetric response for the three upright frames, an analytical model for a single frame was considered adequate for this rack configuration. Centerline dimensions were used, and fictitious restraining beams were used to account for the semifixed column bases. The localized deformation at the connections between the open-section bracing members and the open-section columns as discussed in Section 4.9 were also considered. Thus, truss members for this braced-frame system were modeled as composite axial force members consisting of two parts: an open-section bracing member and the lips of columns. The entire mass was lumped equally at the six nodal joints, and the mass per story level was estimated to be 7.4 lb-sec^2/in. for 2/3 live load and 10.8 lb-sec^2/in. for the full live load. The minimum net section properties provided by the manufacturer (see Table 4.2) are as follows:

	Moment of Inertia (in.^{4})	Cross-sectional Area (in.^{2})	Estimated Shear Area (in.^{2})
Column	0.88	0.69	0.43
Brace	-	0.32	-

The best-fit mathematical models were established by varying the section properties of the fictitious restraining beams and the composite bracing members. The influence of partially fixed column bases was discussed in Section 7.1. In this section, only the influence of localized deformation at the connections between the open-section bracing members and the open-section columns is discussed.

Influence of Localized Deformation. In modeling this braced-frame system, local deformation at the connections between the braces and column members had to be considered. The total deformation of the bracing members consists of two parts: the deformation due to the bracing member and the localized deformation of the column lip at the connection between the bracing and

Preceding page blank

column members. No quantitative experimental data are available on the influence of local deformation. Because of this, it was assumed that the composite axial bracing member consisted of two parts; its stiffness was reduced as follows:

$$\left(\frac{EA}{l}\right)_{red} = \frac{1}{k} \left(\frac{EA}{l}\right) \tag{8.1}$$

where:

E = Young's modulus of elasticity (lb/in.^{2})

A = cross-sectional area of brace (in.^{2})

l = unbraced length of brace (in.)

k = a factor to account for local deformation at the diagonal-to-column connection

Comparison of Various Linear Mathematical Models. From the above discussion, the values k and I_f are the only adjustable modeling parameters in the development of the best-fit mathematical models. Because no experimental data on the values of k and I_f are available, the trial-and-error procedures of assigning various combinations of k and I_f were used. The results are shown in Table 8.1. A comparison of Models 1 and 2 clearly shows that local deformation at the connections between the open-section bracing members and the open-section columns has a considerable influence on dynamic response properties. Model 1 assumed no local deformation (k = 1), whereas Model 2 has a k value of 10 assigned. The calculated fundamental periods of vibration were 0.38 and 0.68 sec for Models 1 and 2, respectively. The results for Models 3 and 4 demonstrate that the calculated periods and mode shapes varied very little when I_f was varied from 3.7 to 0.2 in^4. The value 3.7 was based on Galambos' formula (Equation [7.2]), and 0.2 was the value finally selected for modeling the standard pallet rack in the longitudinal direction. Model 5, with I_f = 0.2 and k = 12, was found to be the best model for the 2/3 live load. A comparison of the results from Model 5 and the measured data from the low-amplitude shaking table tests and the pull-release free-vibration tests is quite good. The same parameters were used in modeling the full-live-load case, and good correlation was again indicated (Model 6).

8.2 Time-History Analysis

Basic Model. The basic mathematical model used for the time-history response analysis was similar to the linear mathematical model (Figure 8.1) except that DRAIN-2D was used instead of SAP IV. For the time-history analysis, the bracing members were modeled as composite axial force members and assumed as bilinear yielding elements as shown in Figure 8.2a. The yield capacities in tension (P_y^+) and compression (P_y^-) of the bracing members were estimated to be 14.4 kips and 4.6 kips, respectively, in accordance with AISI 3.6.1 ($F_{a_1} > F_{a_2}$, i.e., torsional-flexural buckling is critical). The yield interaction surface of the column elements was assumed to be as indicated in Figure 8.2b. The axial force and bending capacities of the column elements were also based on AISI 3.6.1, as illustrated in Appendix A.

Results. Three case runs were performed. Table 8.2 summarizes the parameters finally used for each case. These parameters yielded reasonably good analytical results in comparison with the corresponding experimental data. All parameters used for the time-history analysis remained essentially the same as those obtained for the best-fit linear mathematical models. The damping and the assumed yield mechanism (Figure 8.2) were the only new parameters in the time-history response analysis. The analysis was carried out with an integration time step of about 0.0196 sec, the same time interval of digitization as for the recorded data. This was considered to be adequate for numerical stability criteria as compared with the calculated periods of vibration from Models 5 to 7, shown in Table 8.1.

Case 1 (SP-T-2/3-1/4 EC). For this case, the model was simulated with the 2/3 live load and subjected to an input signal approximately 1/4 that of the actual El Centro record. Mass-proportional damping corresponding to about 1.5% of the first-mode viscous damping was prescribed. The parameters k and I_f were assumed to be 12 and 0.2, respectively. Figure 8.3 shows the measured and predicted relative story displacements, which correlate well both in phase and magnitude. Good agreement is also found in Figure 8.4 between the predicted and the measured axial strains of the bracing and column members located in the center upright frame.

Case 2 (SP-T-1-1/4 PF). For this case, the model was loaded with the full live load, and an input earthquake signal of 1/4 the actual Parkfield record was applied. All modeling parameters and member properties used in the previous case remained unchanged, with the exception of story mass and input signal. Figures 8.5 and 8.6 show measured and predicted results. The correlation was considered good except during the latter stage of response, which was essentially in a state of free-decay response. The calculated amplitudes were slightly higher than those observed during the test. These higher results could have been reduced by using a higher damping value in the model.

Case 3 (SP-T-1-1/2 EC). As in the shaking table test results, significant torsional response and material yielding were observed for this test case. A rather brittle fracture occurred at the weld connecting the northwest column to the base plate, and noticeable buckling was observed near the base of all except the northeast column. Because of the unsymmetric response, the theoretical prediction using the two-dimensional model became unrealistic.

Figure 8.7 shows measured and computed story displacements. Note that the measured displacements were based on the measurements on the center upright frame, whereas the computed results were based on the DRAIN-2D model. In the DRAIN-2D model, k was assumed to be 14 rather than 12, as was assumed in Cases 1 and 2. The correlation was good during the first few significant cycles until the weld fracture occurred and significant torsional response took place.

8.3 Response Spectrum Analysis

Five cases were analyzed by the response spectrum method. Table 8.3 summarizes the base shears and overturning moments obtained along with the input signal and damping used for each case. The response spectra corresponding to each input signal were previously shown in Figures 4.18 and 4.19. The effects on the base shears and overturning moments of the higher modes were negligible.

Results from three individual cases were selected for presentation. Figure 8.8 shows the calculated periods and mode shapes obtained from the frequency analysis of the linear mathematical models simulated with the full live load (see Table 8.1). Figures 8.9 through 8.11 present the story forces, story shears, and story overturning moments for various modes of vibration. They clearly indicate that the effects of higher mode contributions at various story levels were insignificant, except for the story forces, which show some strong response participation from the second mode.

8.4 *UBC* and ATC-3 Methods

The base shears determined from the *UBC* and ATC-3 methods are shown in Table 8.4. The fundamental periods of vibration used in the base shear calculation were determined from the frequency analysis of the linear mathematical models (see Table 8.1). In the evaluation of base shears by the *UBC* method, K was assumed to be 1.33 for this braced-frame system. The minimum value of CS was used (i.e., S = 1.25 for the best site condition). The response modification factor R in the ATC method was assumed to be 4.0.

Table 8.5 shows the base story forces for ultimate strength design using various analysis methods. The base story forces for the *UBC* method were multiplied by a factor of 1.6, as required in ultimate strength design. The base story forces for the ATC-3 method were modified by a capacity-reduction factor of 0.9. The results from the *UBC* method are approximately 20% higher than those from the ATC method.

Base shears and base overturning moments results from the *UBC* method are less than those from the response spectrum method using the earthquake signal of 1/2 EC, but slightly greater than those using the signal of 1/2 EC if the worst site condition was assumed (i.e., S = 1.5). This is clearly shown in Figure 8.12 and Table 8.5. A general discussion of the adequacy and limitations of the various analysis methods is presented in Chapter 13.

TABLE 8.1
LINEAR MATHEMATICAL MODELS -
STANDARD PALLET RACK, TRANSVERSE DIRECTION

Model	Live Load	Column Base		Brace Element		Period* (sec)			Mode Shape*		
		Case	I_f	k	$(EA)'$	1	2	3	1	2	3
1	2/3	pinned	no	1	9,380	0.38	0.16	0.14	1.00 0.71 0.45	1.00 -0.35 -1.67	1.00 -2.06 1.02
2	"	"	"	10	938	0.68	0.25	0.16	1.00 0.74 0.48	1.00 -0.63 -1.10	1.00 -3.10 2.65
3	"	semi-fixed	3.7	10	938	0.62	0.24	0.16	1.00 0.70 0.37	1.00 -0.88 -1.05	1.00 -3.50 3.87
4	"	"	0.2	10	938	0.65	0.24	0.16	1.00 0.70 0.37	1.00 -0.77 -1.08	1.00 -3.27 3.24
5	"	"	0.2	12	780	0.69	0.26	0.17	1.00 0.72 0.41	1.00 -0.78 -1.08	1.00 -3.28 3.29
6	full	"	0.2	12	780	0.83	0.31	0.20	1.00 0.72 0.41	1.00 -0.78 -1.08	1.00 -3.28 3.29
7	"	"	0.2	14	670	0.89	0.30	0.20	1.00 0.72 0.41	1.00 -0.78 -1.08	1.00 -3.28 3.32

I_f = Moment of inertia of fictitious floor beam (in.^{4})

k = Factor to take into account local deformation at the brace-column connection

$(EA)'$ = Reduced section properties of bracing member (kips)

*Experimentally determined periods and mode shapes are:

Period: 2/3 Live Load — T_1 = 0.68 - 0.71 sec, T_2 = 0.24 sec; Full Live Load — T_1 = 0.83 - 0.85 sec, T_2 = 0.30 sec

Mode Shape (Average): 1st Mode

1.00
0.75
0.43

TABLE 8.2

MODELING PARAMETERS FOR TIME-HISTORY ANALYSIS - STANDARD PALLET RACK, TRANSVERSE DIRECTION

Case	Designation	Live Load	Input Signal	Column			Brace		Column Base	Damping		Remarks
				I_c (in.^{4})	A_c (in.^{2})	A'_c (in.^{2})	k	$(EA)'$ (kip)	I_f (in.^{4})	α	λ (%)	
1	SP-T-2/3-1/4 EC	2/3	1/4 EC	0.88	0.69	0.43	12	780	0.2	0.28	1.5	linear response
2	SP-T-1-1/4 PF	full	1/4 PF	"	"	"	12	780	0.2	0.28	2.0	linear response
3	SP-T-1-1/2 EC	"	1/2 EC	"	"	"	14	670	0.2	0.56	4.0	nonlinear response

Notes: 2/3 live load = 7.4 lb-sec^2/in. per story level

Full live load = 10.8 lb-sec^2/in. per story level

A'_c = Estimated shear area of column

TABLE 8.3

SUMMARY OF RESULTS FROM RESPONSE SPECTRUM ANALYSIS - STANDARD PALLET RACK, TRANSVERSE DIRECTION

Case	Designation	Live Load	Input Signal		Base Shear (lb)		Base Over-turning Moment (kip-in.)	
			Signal	Damping (%)	1st Mode	SRSS	1st Mode	SRSS
1	SP-T-2/3-1/4 EC	2/3	1/4 EC	1.5	1,187	1,198	162	162
2	SP-T-2/3-1/2 EC	"	1/2 EC	3.0	1,822	1,848	249	249
3	SP-T-1-1/4 PF	full	1/4 PF	1.5	1,140	1,152	156	156
4	SP-T-1-1/4 EC	"	1/4 EC	1.5	1,708	1,744	230	230
5	SP-T-1-1/2 EC	"	1/2 EC	3.0	2,799	2,855	377	377

TABLE 8.4

DETERMINATION OF BASE SHEAR USING THE *UBC* METHOD AND THE ATC METHOD - STANDARD PALLET RACK, TRANSVERSE DIRECTION

Live Load	T (sec)	W (lb)	1976 *UBC*		ATC-3	
			C	V (lb)	C_s	V (lb)
2/3	0.69	8,500	0.080	1,130	0.154	1,309
Full	0.83	12,500	0.073	1,518	0.136	1,700
			$V = ZIKCSW$ $C = \frac{1}{15\sqrt{T}}$ $K = 1.33$ $I = Z = 1.0$ $S = 1.25$ (minimum)		$V = C_sW$ $C_s = \frac{1.2\ A_vS}{RT^{2/3}}$ $A_v = 0.4$ $S = 1.0$ (minimum) $R = 4.0$	

TABLE 8.5

BASE STORY FORCES FOR ULTIMATE STRENGTH DESIGN - STANDARD PALLET RACK, TRANSVERSE DIRECTION

Live Load	*UBC* Method*		ATC Method†		Response Spectrum Method			
	Base Shear (lb)	Base Overturning Moment (kip-in.)	Base Shear (lb)	Base Overturning Moment (kip-in.)	1st Mode Base Shear (lb)	1st Mode Base Overturning Moment (kip-in.)	Damping (%)	Signal
2/3	1,808	258	1,454	206	1,187	162	1.5	1/4 EC
"	"	"	"	"	1,822	249	3.0	1/2 EC
Full	2,428	346	1,889	272	1,140	156	1.5	1/4 PF
"	"	"	"	"	1,708	230	1.5	1/4 EC
"	"	"	"	"	2,799	377	3.0	1/2 EC

* The factored code forces required in ultimate strength design ($\frac{1.7}{1.33} \times 1.25 = 1.6$)

† A capacity-reduction factor of 0.9 is applied.

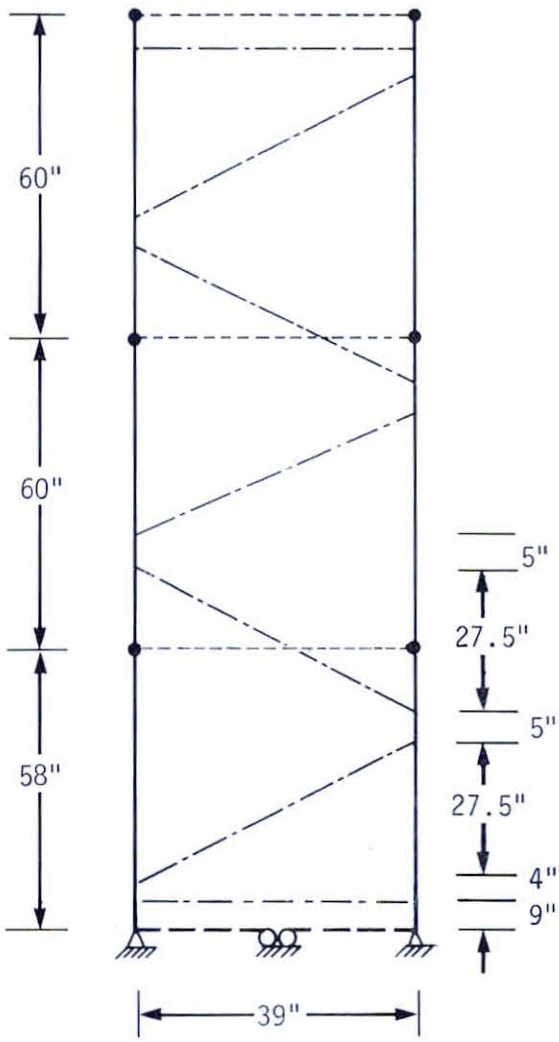

—— Beam-Column Element   —-— Truss Element

— — Beam-Column Element, (Fictitious)   ----- Truss Element (Fictitious)

• Lumped Mass

FIGURE 8.1 MATHEMATICAL MODEL (SAP IV AND DRAIN-2D) - STANDARD PALLET RACK, TRANSVERSE DIRECTION

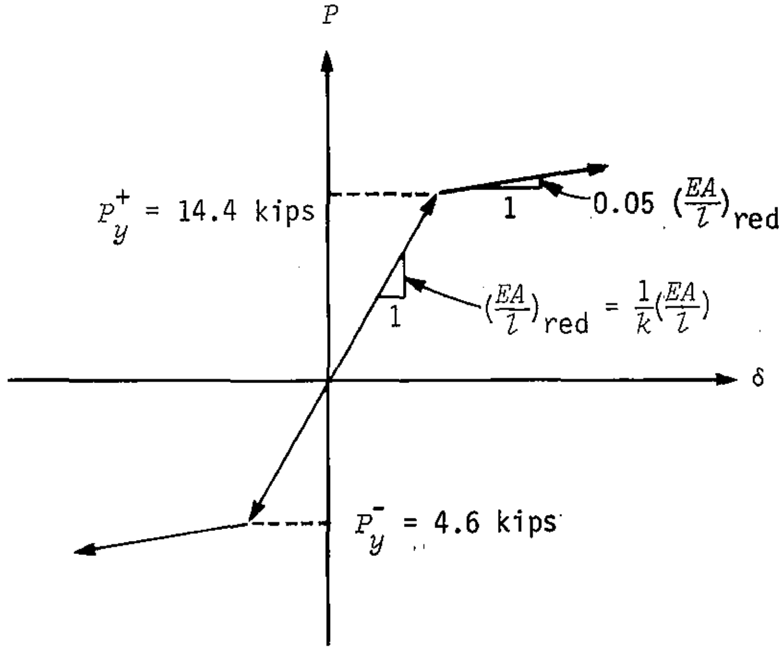

a. Bilinear Yield Mechanism for Braces

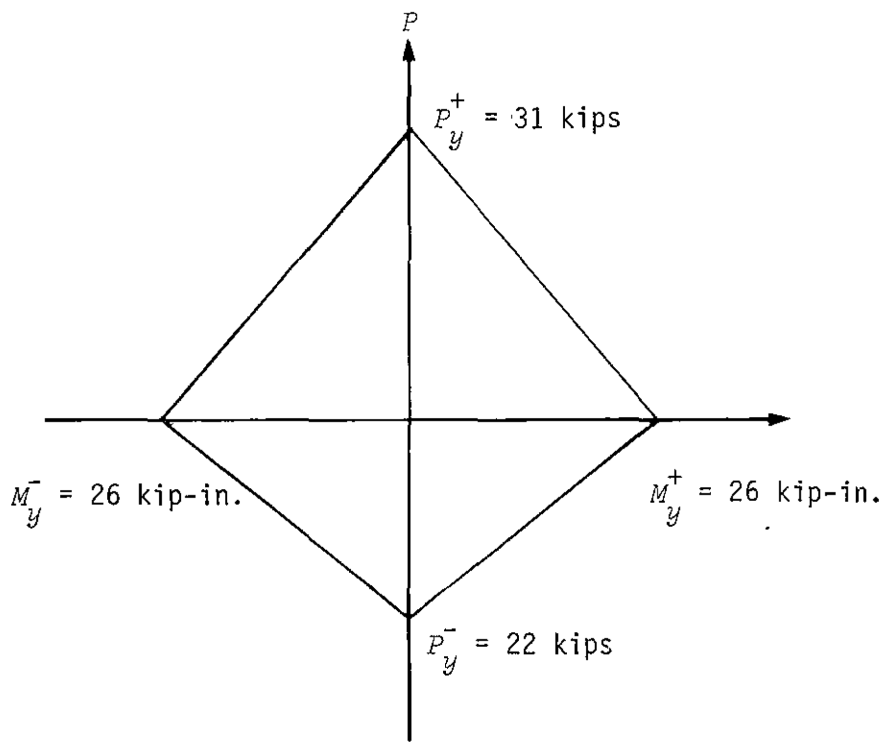

b. Yield Interaction Surface for Columns

FIGURE 8.2 YIELD MECHANISM AND INTERACTION SURFACE - STANDARD PALLET RACK, TRANSVERSE DIRECTION

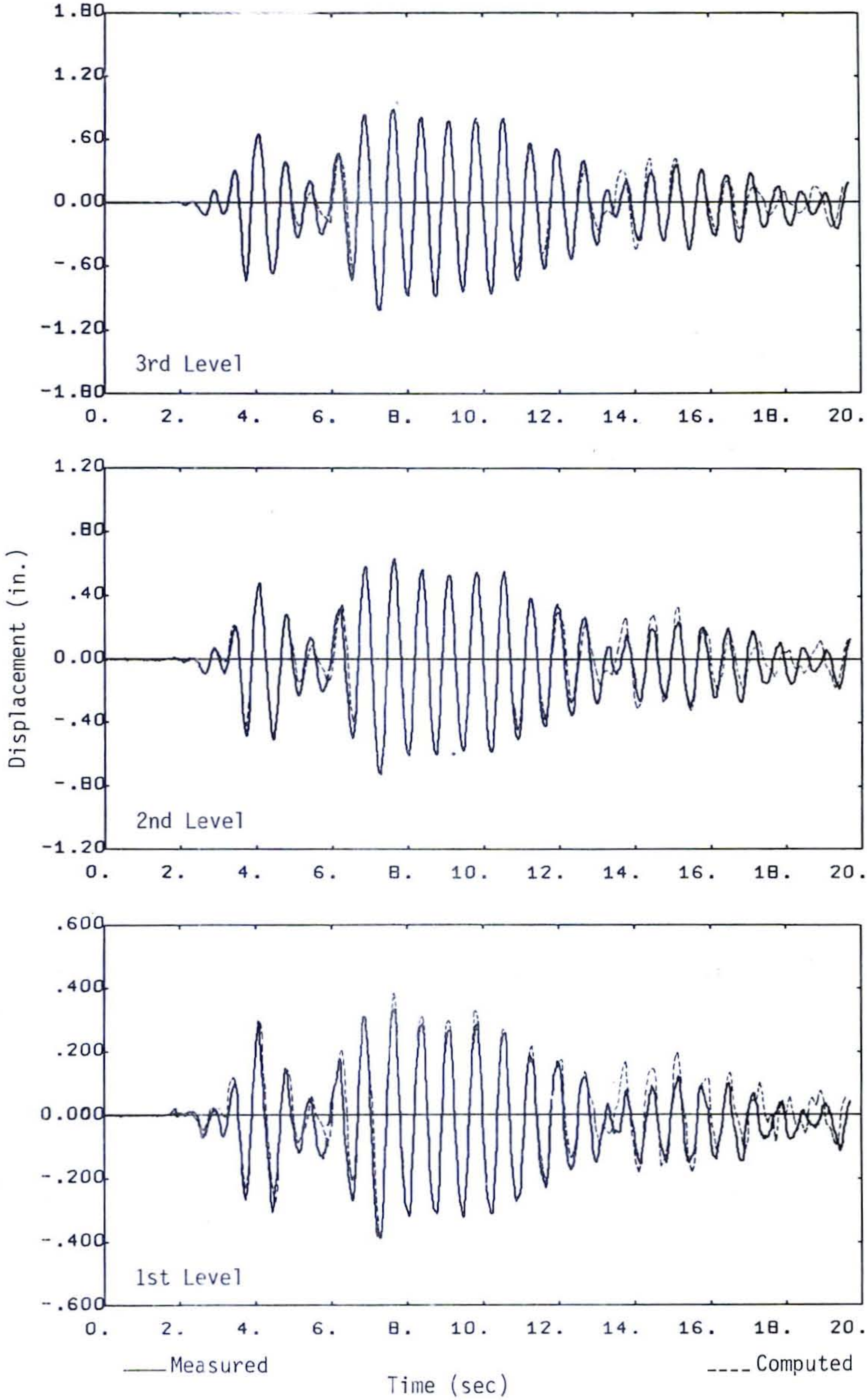

FIGURE 8.3 MEASURED AND COMPUTED STORY DISPLACEMENTS (SP-T-2/3-1/4 EC)

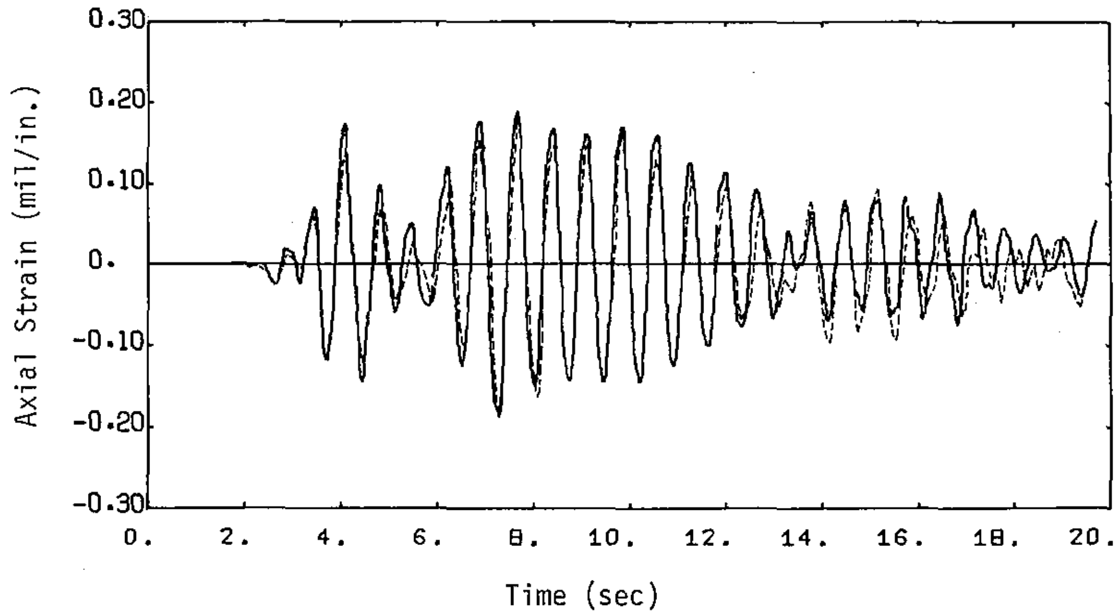

Bottom Diagonal

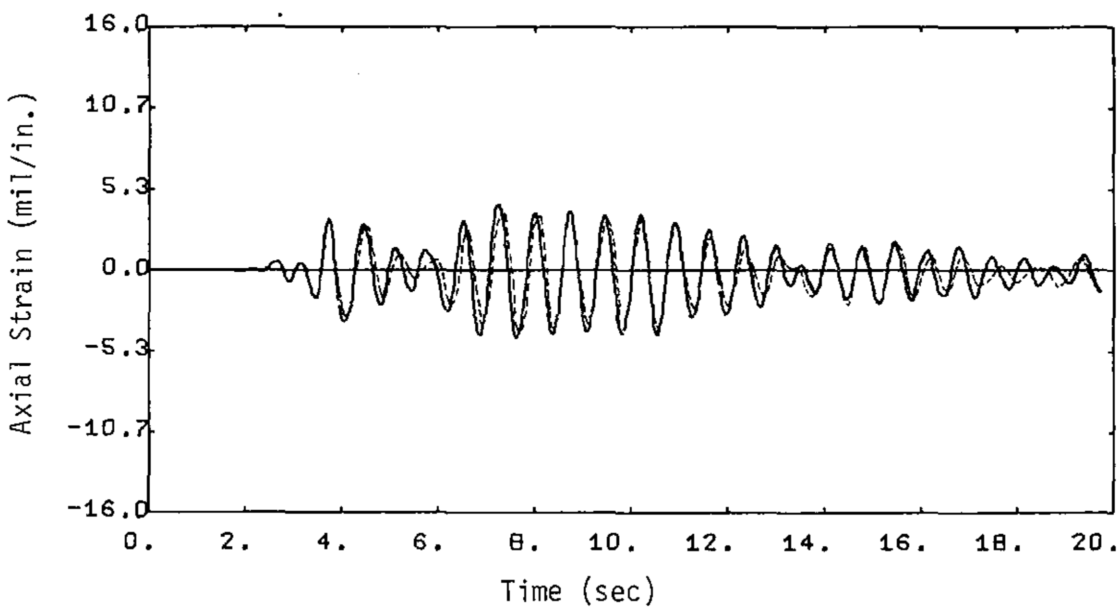

Bottom Column Near Base Plate

——— Measured ---- Computed

FIGURE 8.4 MEASURED AND COMPUTED LOCAL RESPONSES (SP-T-2/3-1/4 EC)

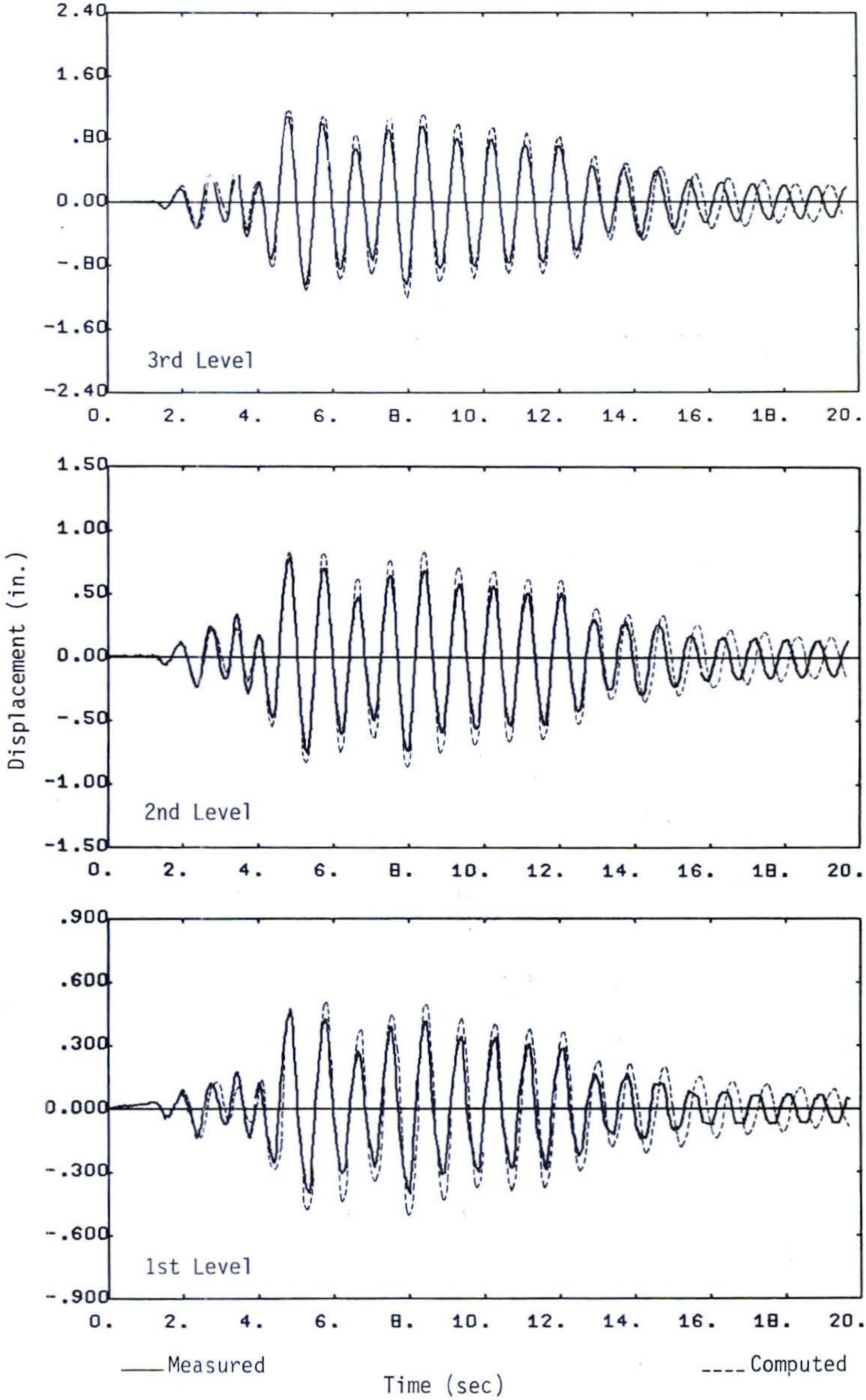

FIGURE 8.5 MEASURED AND COMPUTED STORY DISPLACEMENTS (SP-T-1-1/4 PF)

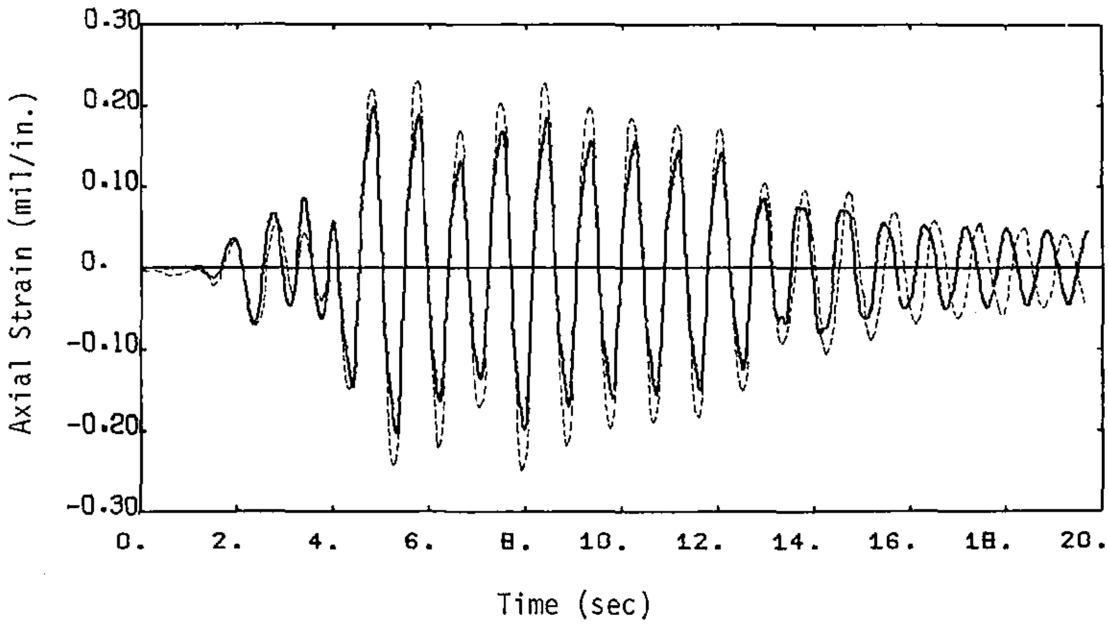

Bottom Diagonal

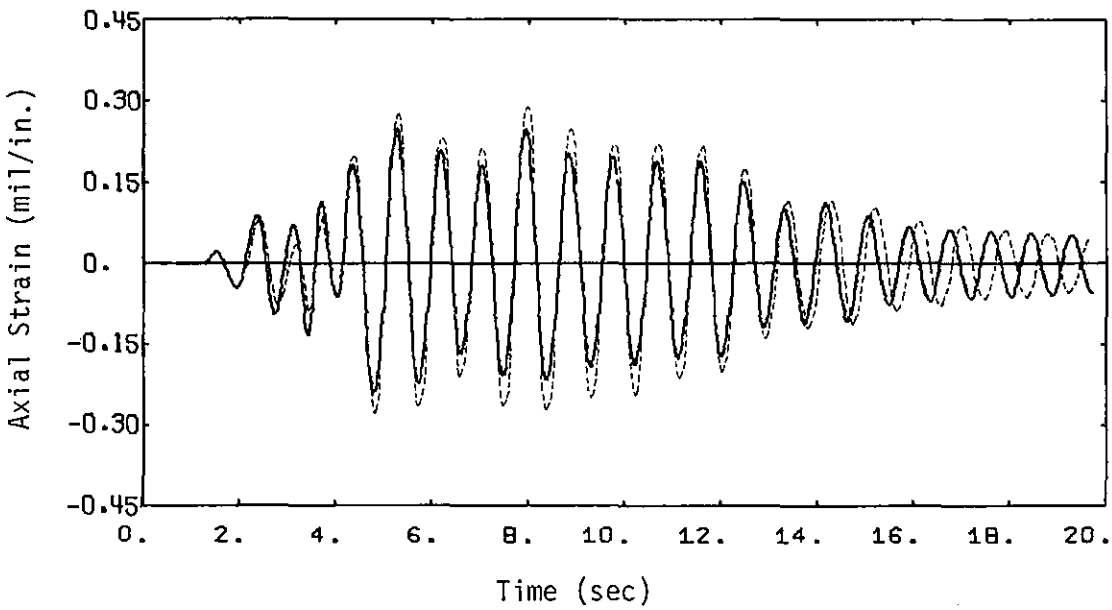

Bottom Column Near Base Plate

——— Measured   - - - - Computed

FIGURE 8.6 MEASURED AND COMPUTED LOCAL RESPONSES (SP-T-1-1/4 PF)

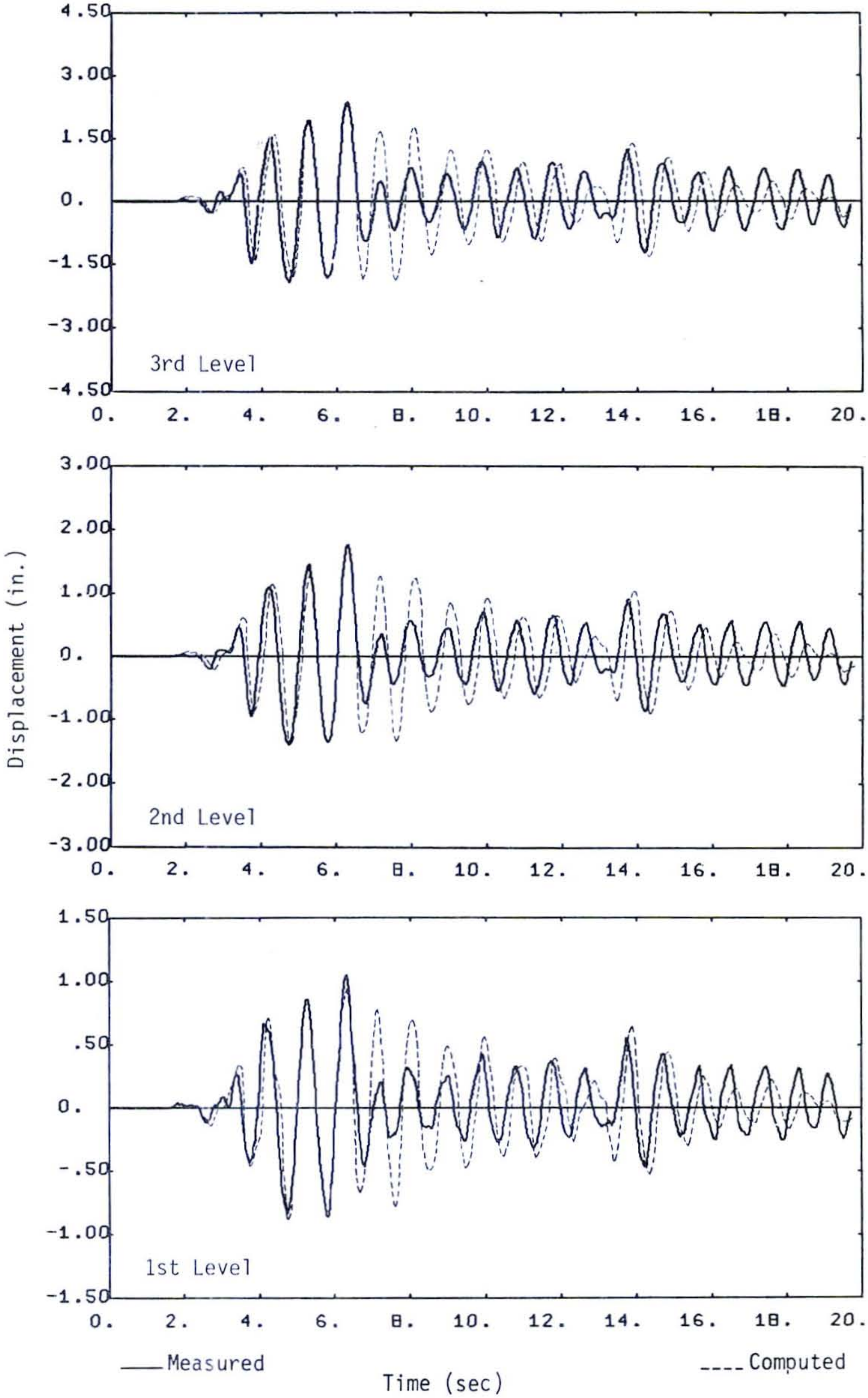

FIGURE 8.7 MEASURED AND COMPUTED STORY DISPLACEMENTS (SP-T-1-1/2 EC)

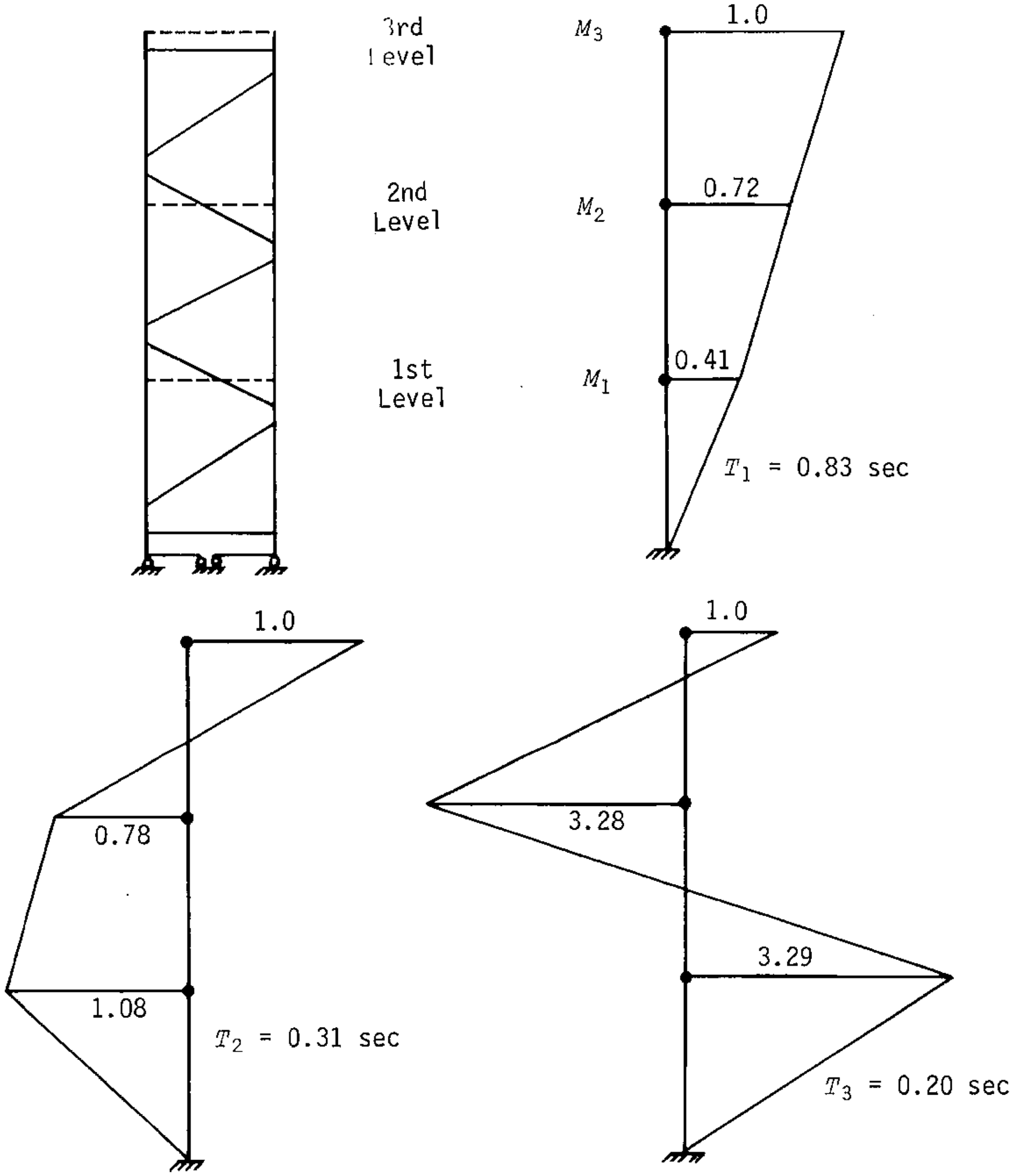

$k = 12$

$I_f = 0.2$ in.^{4}

$m_1 = m_2 = m_3 =$
$= 10.8$ lb-sec^2/in.

FIGURE 8.8 CALCULATED PERIODS OF VIBRATION AND MODE SHAPES - STANDARD PALLET RACK, TRANSVERSE DIRECTION, FULL LIVE LOAD

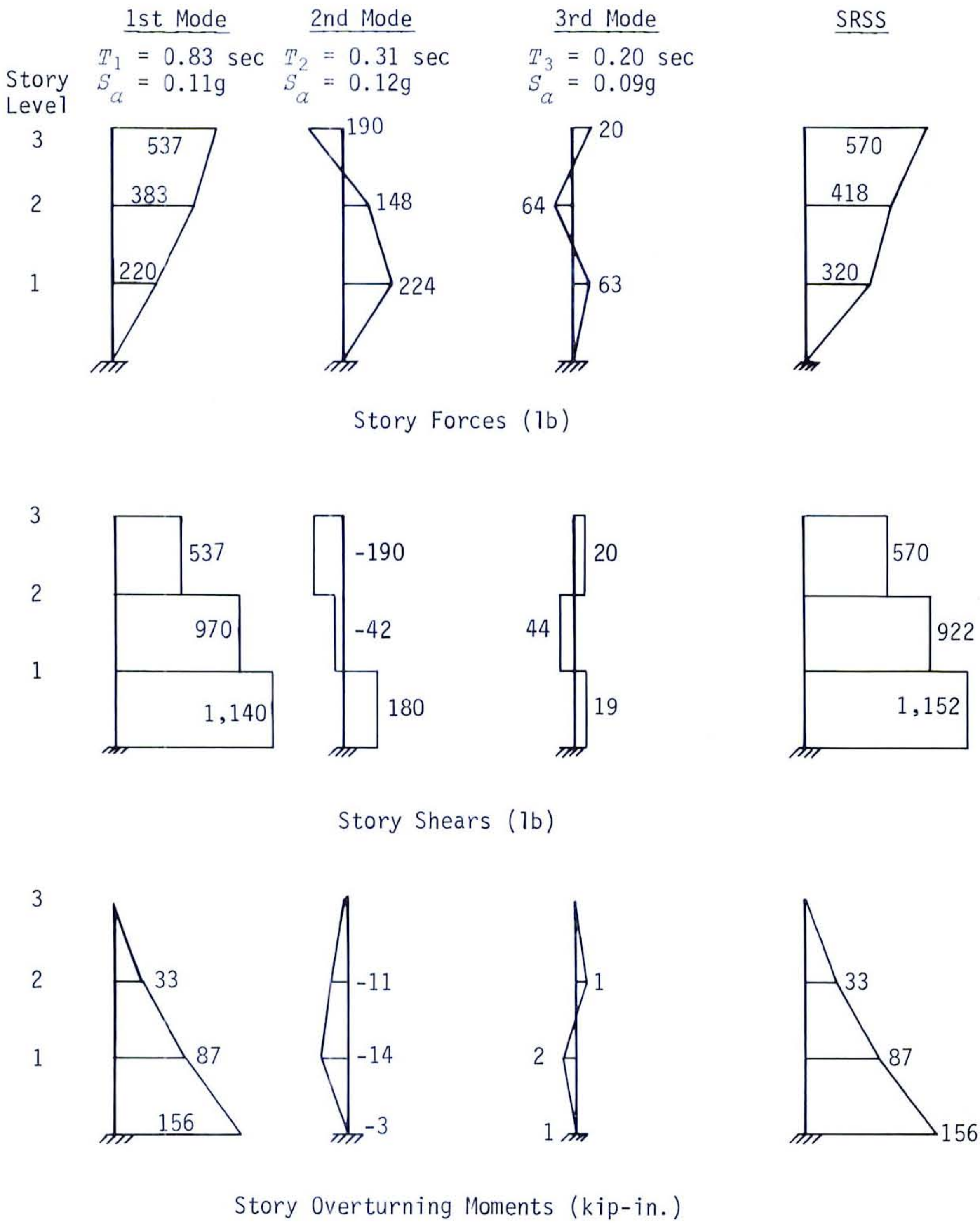

FIGURE 8.9 RESULTS OF RESPONSE SPECTRUM ANALYSIS (SP-T-1-1/4 PF)

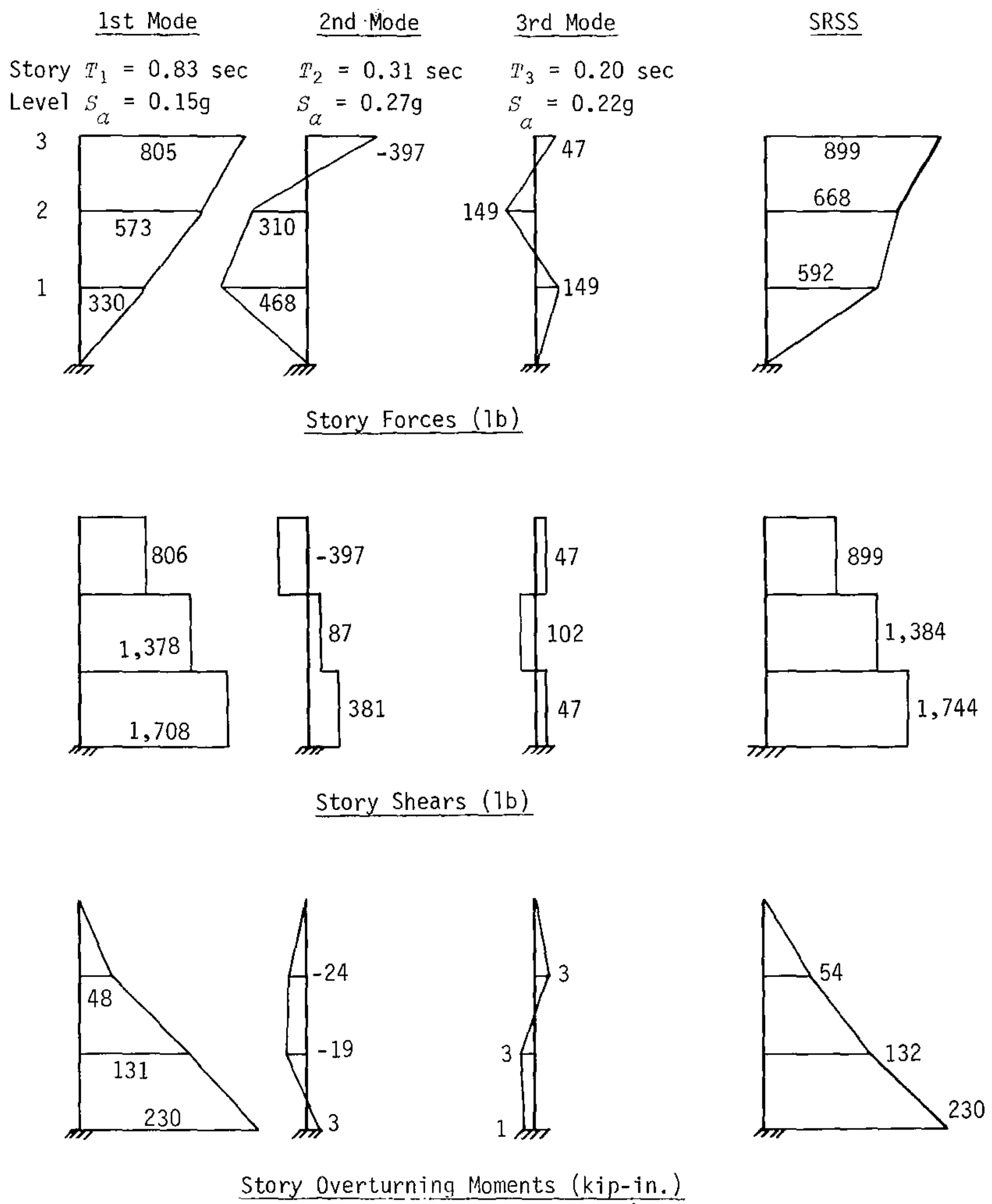

FIGURE 8.10 RESULTS OF RESPONSE SPECTRUM ANALYSIS
(SP-T-1-1/4 EC)

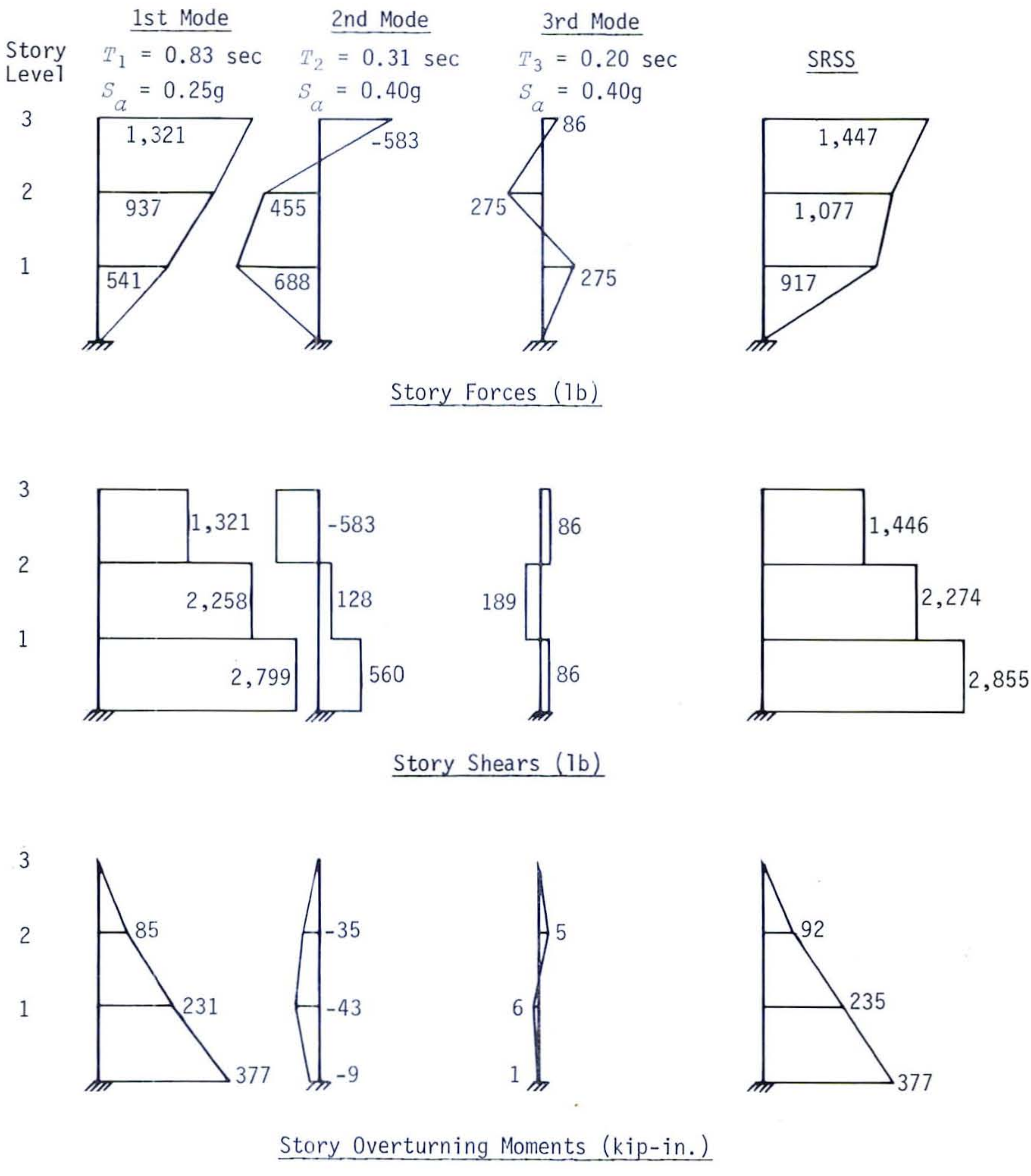

FIGURE 8.11 RESULTS OF RESPONSE SPECTRUM ANALYSIS (SP-T-1-1/2 EC)

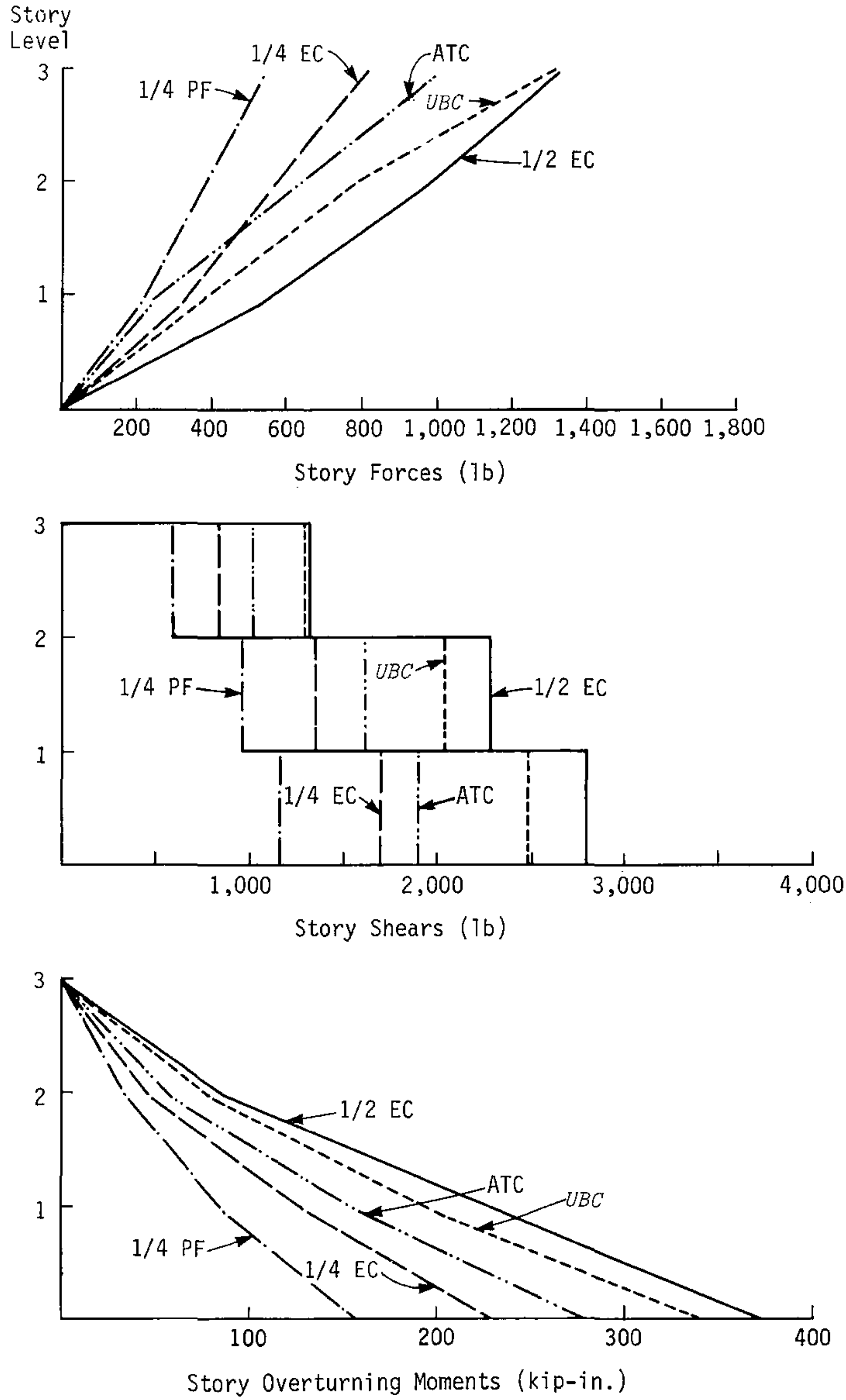

FIGURE 8.12 RESULTS OF THE *UBC* METHOD, THE ATC METHOD, AND THE RESPONSE SPECTRUM METHOD - STANDARD PALLET RACK, FULL LIVE LOAD, TRANSVERSE DIRECTION

9. THEORETICAL PREDICTION OF STRUCTURE RESPONSE-- DRIVE-IN RACK, LONGITUDINAL DIRECTION

9.1 Frequency Analysis

Basic Model. In the longitudinal direction, the drive-in rack assembly consists of two upright and two anchor frames, as shown in Figure 4.5. Although the structural systems and stiffnesses for these two types of frames are quite different, no torsion was detected from the experimentally obtained displacement time-history plots (see Section 4.11). A theoretical calculation also indicated the torsional effect to be insignificant (see Appendix B). This negligible torsional effect makes possible two-dimensional modeling of this structure. Figure 9.1 shows the basic mathematical model developed for this rack assembly. It consists of one upright and one anchor frame connected by three fictitious rigid springs at the floor levels. Half of the total mass was included in the model. The masses at the first, second, and third levels were assumed to be 17.0 lb-sec^2/in. and 24.8 lb-sec^2/in., for the 2/3 and full live load cases, respectively. The mass at the fourth level was very small (0.2 lb-sec^2/in.) and could be neglected. Centerline dimensions were used. Semirigid beam-column connections and partially fixed base conditions were assumed in the model. The minimum net section properties supplied by the manufacturer (see Table 4.2) are as follows:

	Moment of Inertia (in.^{4})	Cross-sectional Area (in.^{2})	Estimated Shear Area (in.^{2})
Column (upright frame)	3.78	1.32	0.63
Column (anchor frame)	2.21	0.75	0.41
Beam (anchor frame)	1.18	1.09	-
Overhead Tie (upright frame)	0.29	0.46	-

The effects of semirigid connections and partially fixed bases were discussed in Section 7.1. The best-fit mathematical models were developed using the basic model and various combinations of the parameters I_f and K_θ.

Comparison of Various Linear Mathematical Models. A trial-and-error procedure of assigning various combinations of K_θ and I_f was used in determining the best-fit mathematical model. The results are shown in Table 9.1. A comparison of the results from Models 1 and 3 indicates a considerable influence of semirigid connections on dynamic response properties. Model 1 assumed rigid beam-column connections, whereas Model 3 considered flexible joints with an assumed K_θ value of 10^6 lb-in./rad. Comparison of Models 2 and 3 demonstrates the influence of the modeling parameter I_f. Model 2 had an assigned I_f value of 2.5 in.^{4} on the basis of Equation (7.2). The value of 0.2 in.^{4} used in Model 3 was based on previous experience in modeling the standard pallet racks. Model 3 is seen to be the best-fit model for the 2/3 live load case. The correlation between the measured and computed periods and mode shapes for the first mode is excellent. The same values of I_f and K_θ were used in modeling the full live load case. Good correlation between the measured and calculated results is again evident.

9.2 Time-History Analysis

Basic Model. The nonlinear mathematical model (Figure 9.2) for the longitudinal time-history analysis of the drive-in rack assembly is similar to the linear model (Figure 9.1) except that DRAIN-2D, including the semirigid connections as deformable elements, was used. As shown in Figure 9.2, each semirigid joint element was connected to two nodes and was influenced only by the relative rotational displacement between the nodes. The translational displacements of the nodes were constrained to be identical.

The yield interaction surfaces for columns and beams were estimated as shown in a and b of Figure 9.3. The calculated column and beam moments at yield ($M_y = S \times F_y$) based on the section modulus and the specified minimum yield stress (see Table 4.2) are indicated in the plots. The average compression column forces at yield were estimated to be 20 kips for the anchor frame and 30 kips for the upright frame. The procedures for determining these theoretical axial yield forces are similar to those shown in Appendix A. The bilinear yield mechanism of moment-rotation relationships for semirigid connections was idealized as shown in Figure 9.3c. The parameters K_θ, M_1, M_2, and P were chosen and approximately adjusted to provide good correlation between the calculated and measured results.

Results. Three model cases were studied. Table 9.2 summarizes the parameters finally used for each case. These parameters resulted in the best possible analytical results compared with the corresponding experimental data. From previous modeling experience, it was learned that a single mathematical model can be used to predict the seismic responses with different gravity load cases (i.e., full live load versus 2/3 live load). Therefore, only the time-history analysis using the full live load was performed and reported in this study.

The same parameters used in the frequency analysis of the best-fit linear mathematical model were used for the time-history analysis. Data correlation was improved by trying various damping values and mechanisms for yielding of the semirigid connections. The assumed yield interaction surfaces of beams and columns remained unchanged for each model case. The time-history analysis was carried out with an integration time step of 0.0197 sec, the same time interval as was used for digitization of the recorded data.

Case 1 (DI-L-1-1/4 EC). For this case, the model was simulated with the full live load and subjected to an input signal of 1/4 the actual El Centro record. Mass-proportional damping corresponding to about 5% of the first-mode viscous damping was assigned to the model. The initial joint rotational spring, K_θ, and the moment of inertia of the fictitious floor beam, I_f, were prescribed to be 10^6 lb-in./rad and 0.2 in.^{4}, respectively. Figure 9.4 shows the computed and measured story displacements relative to the table. The correlation is seen to be very good. The computed and measured column end rotations shown in Figure 9.5 do not correlate as well, however. Fairly good agreement in magnitude is obtained, but poor correlation in phase is evident. Nevertheless, the analytical estimates of local response quantities are considered to be adequate because a two-dimensional analytical model was used to simulate the actual three-dimensional structural system.

Case 2 (DI-L-1-1/2 EC). In this case study, the model was subjected to an input signal of 1/2 the actual El Centro record. All other modeling parameters used in Case 1 remained unchanged except for a slightly smaller value of K_θ. Mass-proportional damping corresponding to about 6% of the first-mode viscous damping was prescribed for Case 2. The computed and measured story displacements relative to the table are presented in Figure 9.6. The correlation is considered to be good. As in the Case 1 model, the agreement between the computed and measured local responses (Figure 9.7) is not as good as that for the floor displacements.

Case 3 (DI-L-1-1/2 PF). For this analytical model study, all model parameters assigned to the Case 2 model remained unchanged except for the input signal, which was 1/2 the actual Parkfield record. The correlation between the measured and computed story displacements relative to the table shown in Figure 9.8 is excellent until after 16 sec, when the motion of the shaking table stopped and the free-decay vibration started.

None of the longitudinal shaking table tests conducted for the drive-in rack assembly showed any evidence of material yielding or structural damage. Because the amplification of story shear due to the p-δ effect was found to be very significant (and for safety purposes), this test series was concluded when the input excitation reached 5/8 of the El Centro record. Consistent with this, the predicted time-history responses for the above three model cases were considered to be linear, and no evidence of material yielding was detected from the analysis.

9.3 Response Spectrum Analysis

Six cases were analyzed by the response spectrum method. Table 9.3 summarizes the base shears and overturning moments obtained along with the input signal and damping value used for each case. The response spectra corresponding to each input signal were shown previously in Figures 4.18 and 4.19. As can be seen from the tabulated results, the effects of the higher modes on the base overturning moments were negligible, but the effects of the higher modes on the base shears were very significant.

Three individual cases were selected for presentation in this report. Figure 9.9 shows the calculated periods of vibration and mode shapes obtained from the frequency analysis of the linear mathematical models loaded with the full live load (see Table 9.1). Figures 9.10 to 9.12 present the story forces, story shears, and story overturning moments for various modes of vibration and input signals. An examination of the calculated story forces and shears shown in Figures 9.10 through 9.12 clearly indicates the importance of the higher-mode contribution. This finding is consistent with the results of the time-history analysis (Figures 9.5 and 9.7), which show a strong second-mode contribution.

9.4 *UBC* and ATC-3 Methods

The base story shears determined by the *UBC* and ATC methods are presented in Table 9.4. The fundamental periods of vibration used in the base shear calculation were obtained from the frequency analysis of the linear mathematical models (see Table 9.1). In the base shear calculation by the *UBC* method, K was assumed to be 1.0 and the minimum value of CS was used (i.e., S = 1.0 for the best site condition). For the ATC method, the value of R was assumed to be 4.5. The other parameters used are also indicated in Table 9.4.

Table 9.5 shows the base story shears and overturning moments for ultimate strength design. The base story forces for the *UBC* method were multiplied by a factor of 1.2?, as required in ultimate strength design. The base story forces for the ATC method were modified by a capacity-reduction factor of 0.9. A comparison of the results from the *UBC* and ATC methods indicates that higher lateral forces were required by the ATC method.

Figure 9.13 shows that the base shears and overturning moments of the *UBC* method were slightly smaller than those from the response spectrum method using 1/2 the El Centro signal but were slightly larger than those using 1/2 the Parkfield signal. However, if the worst site condition were to be assumed (i.e., S = 1.5), the *UBC* lateral forces would greatly exceed those developed by 1/2 the El Centro or Parkfield record. A general discussion of the adequacy and limitations of the various analysis methods is presented in Chapter 13.

TABLE 9.1

LINEAR MATHEMATICAL MODELS - DRIVE-IN RACK, LONGITUDINAL DIRECTION

Model	Live Load	Column Base		Beam Element			Period* (sec)			Mode Shape*		
		Case	I_f	K_θ	I_b'	I_b''	1	2	3	1	2	3
1	2/3	semi-fixed	0.2	∞	1.18	0.29	1.29	0.32	0.14	1.00 0.88 0.68 0.37	1.00 0.43 -0.29 0.51	1.00 0.15 -0.42 0.39
2	"	"	2.5	10^6	0.22	0.14	1.66	0.36	0.15	1.00 0.79 0.52 0.22	1.00 0.33 -0.35 -0.43	1.00 0.11 -0.39 0.41
3	"	"	0.2	10^6	0.22	0.14	2.0	0.39	0.15	1.00 0.82 0.57 0.28	1.00 0.36 -0.32 -0.45	1.00 0.13 -0.39 0.40
4	"	"	0.2	0.5×10^6	0.12	0.10	2.3	0.42	0.15	1.00 0.79 0.54 0.25	1.00 0.34 -0.32 -0.43	1.00 0.11 -0.36 0.37
5	full	"	0.2	10^6	0.22	0.14	2.4	0.47	0.18	1.00 0.82 0.57 0.28	1.00 0.37 -0.32 -0.46	1.00 0.13 -0.39 0.40
6	"	"	0.2	0.5×10^6	0.12	0.10	2.8	0.50	0.18	1.00 0.80 0.54 0.25	1.00 0.35 -0.32 -0.44	1.00 0.12 -0.38 0.39

I_f = Moment of inertia of fictitious floor beam (in.^{4})

K_θ = Initial joint rotational spring (lb-in./rad)

I_b', I_b'' = Reduced moment of inertia of beam in the anchor and upright frames, respectively

*Experimentally determined periods and mode shapes are:

Period: 2/3 Live Load — T_1 = 2.1 sec, T_2 = 0.4 sec; Full Live Load — T_1 = 2.4 - 2.5 sec, T_2 = 0.5 sec

Mode Shape (Average): 1st Mode

1.00
0.80
0.59
0.31

TABLE 9.2

MODELING PARAMETERS FOR TIME-HISTORY ANALYSIS - DRIVE-IN RACK, LONGITUDINAL DIRECTION

Case	Designation	Input Signal	Live Load	Beam			Column			Semirigid Joints (See Figure 9.3)				Column Base	Damping	
				I_b (in.^{4})	A_b (in.^{2})	A'_b (in.^{2})	I_c (in.^{4})	A_c (in.^{2})	A'_c (in.^{2})	K_θ ($\frac{\text{lb-in.}}{\text{rad}}$)	P	M_1 (kip-in.)	M_2 (kip-in.)	I_f (in.^{4})	α	λ (%)
1	DI-L-1-1/4 EC	1/4 EC	full	1.18 (0.29)	1.09 (0.46)		2.21 (3.78)	0.75 (1.32)	0.41 (0.63)	10^6	0.8	12	12	0.2	0.26	5
2	DI-L-1-1/2 EC	1/2 EC	"	"	"		"	"	"	0.7 x 10^6	"	"	"	"	0.27	6
3	DI-L-1-1/2 PF	1/2 PF	"	"	"		"	"	"	"	"	"	"	"	"	6

Notes: The upper and lower figures refer to the section properties of anchor and upright frames, respectively

Full live load = 24.8 lb-sec^2/in. per story level

A'_b, A'_c = estimated shear area of beam and columns, respectively

TABLE 9.3

SUMMARY OF RESULTS FROM RESPONSE SPECTRUM ANALYSIS - DRIVE-IN RACK, LONGITUDINAL DIRECTION

Case	Designation	Live Load	Input Signal		Base Shear (lb)		Base Over-turning Moment (kip-in.)	
			Signal	Damping (%)	1st Mode	SRSS	1st Mode	SRSS
1	DI-L-2/3-1/4 EC	2/3	1/4 EC	4	1,128	1,529	186	186
2	DI-L-2/3-1/2 EC	"	1/2 EC	6	2,051	2,835	338	338
3	DI-L-1-1/4 EC	full	1/4 EC	4	1,892	2,326	312	312
4	DI-L-1-1/4 PF	"	1/4 PF	4	1,494	1,914	246	246
5	DI-L-1-1/2 EC	"	1/2 EC	6	3,485	4,460	574	574
6	DI-L-1-1/2 PF	"	1/2 PF	6	2,880	3,657	476	476

TABLE 9.4

DETERMINATION OF BASE SHEAR USING THE *UBC* METHOD AND THE ATC METHOD - DRIVE-IN RACK, LONGITUDINAL DIRECTION

Live Load	T (sec)	W (lb)	1976 *UBC*		ATC-3	
			C	V (lb)	C_s	V (lb)
2/3	2.0	39,450	0.047	1,854	0.067	2,643
full	2.4	57,450	0.043	2,470	0.060	3,447
			$V = ZIKCSW$ $C = \frac{1}{15\sqrt{T}}$ $K = 1.0$ $I = Z = 1.0$ $S = 1.0$ (minimum)		$V = C_sW$ $C_s = \frac{1.2\ A_vS}{RT^{2/3}}$ $A_v = 0.4$ $S = 1.0$ (minimum) $R = 4.5$	

TABLE 9.5

BASE STORY FORCES FOR ULTIMATE STRENGTH DESIGN - DRIVE-IN RACK, LONGITUDINAL DIRECTION

Live Load	*UBC* Method*		ATC Method†		Response Spectrum Method			
	Base Shear (lb)	Base Overturning Moment (kip-in.)	Base Shear (lb)	Base Overturning Moment (kip-in.)	1st Mode Base Shear (lb)	1st Mode Base Overturning Moment (kip-in.)	Damping (%)	Signal
2/3	2,373	411	2,937	527	1,128	186	4	1/4 EC
"	"	"	"	"	2,057	338	6	1/2 EC
Full	3,162	552	3,829	702	1,892	312	4	1/4 EC
"	"	"	"	"	1,494	246	4	1/4 PF
"	"	"	"	"	3,485	574	6	1/2 EC
"	"	"	"	"	2,888	476	6	1/2 PF

*The factored code forces required in ultimate strength design (1.7/1.33 = 1.28)

†A capacity-reduction factor of 0.9 is applied.

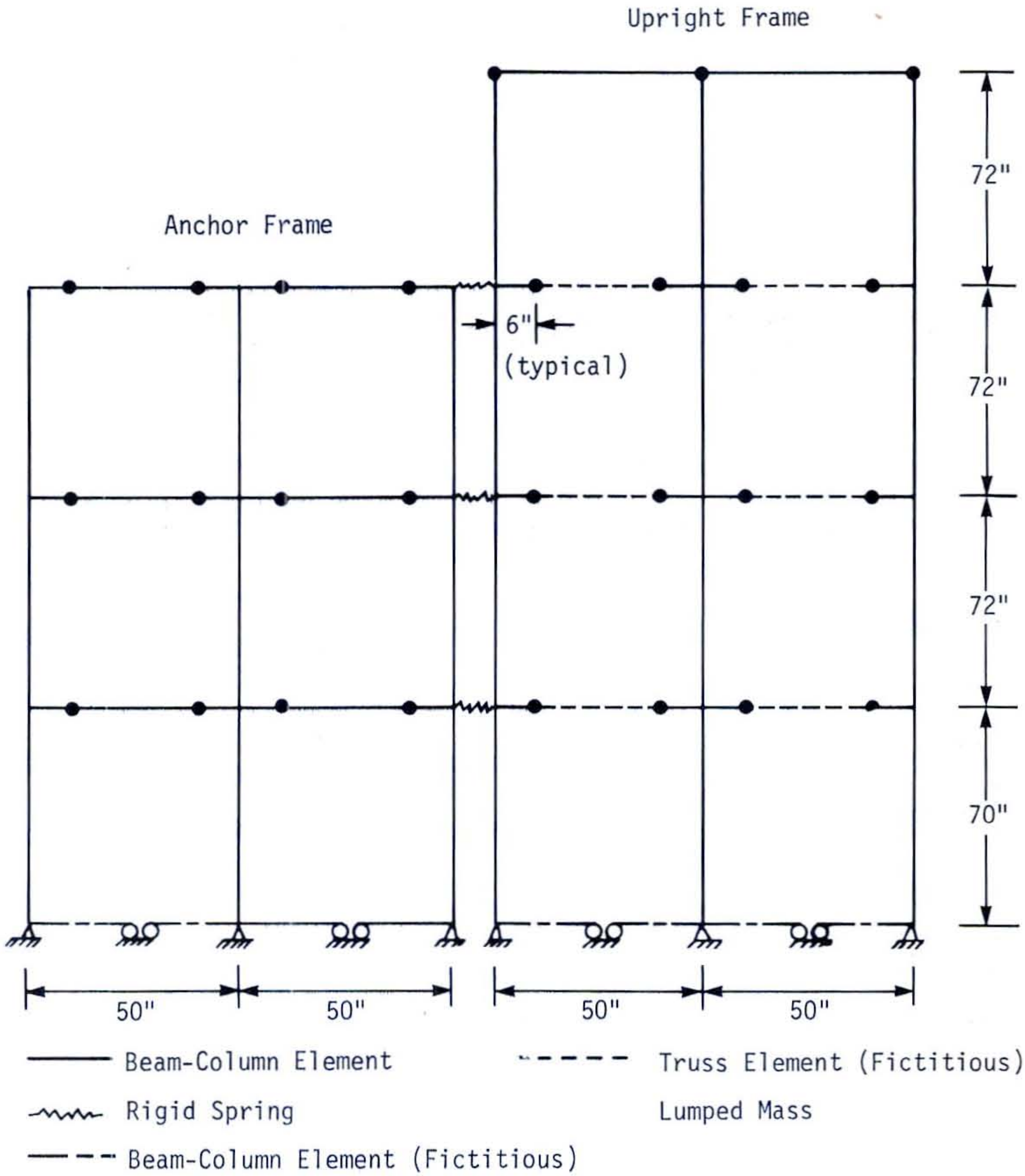

FIGURE 9.1 MATHEMATICAL MODEL (SAP IV) - DRIVE-IN RACK, LONGITUDINAL DIRECTION

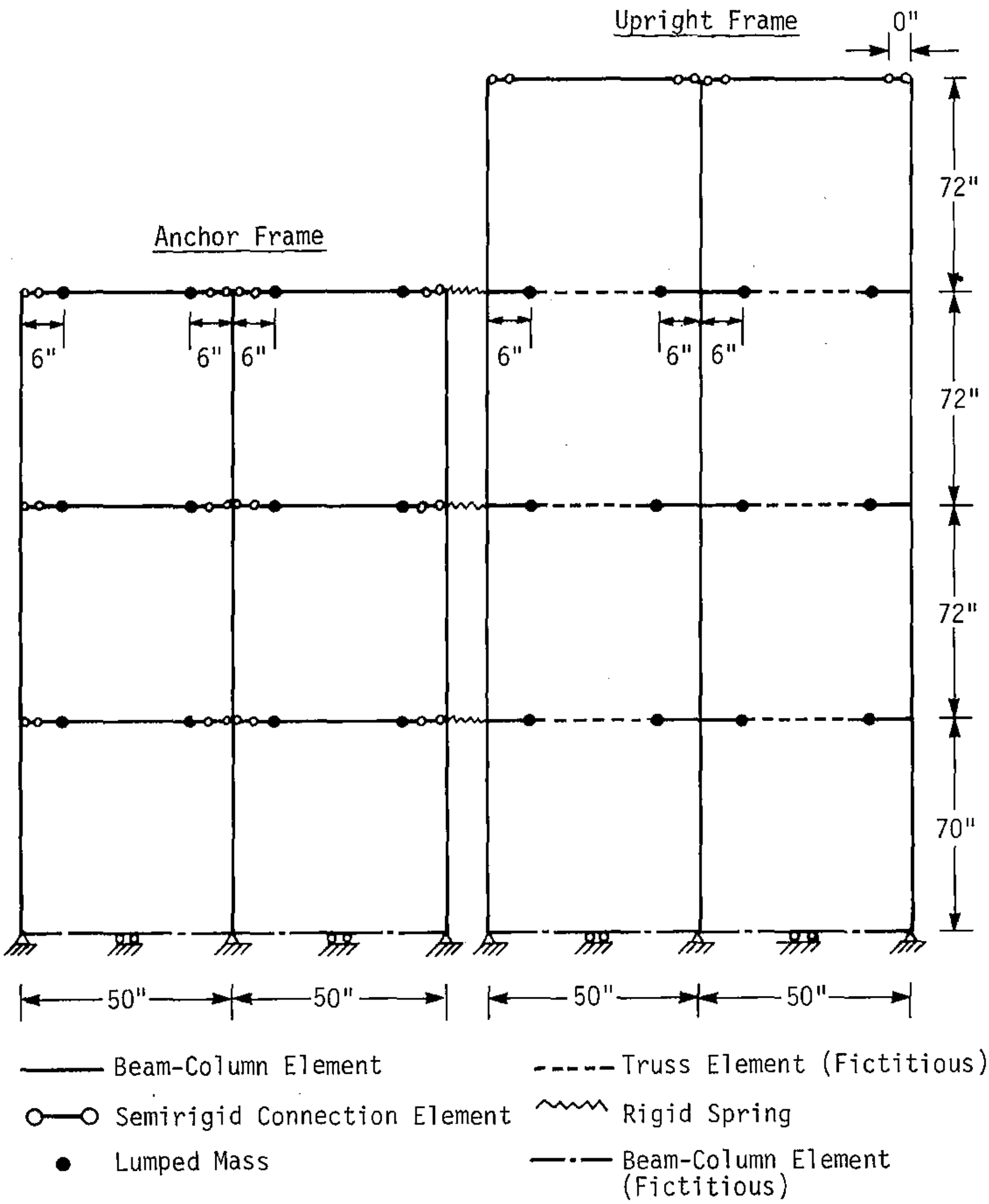

FIGURE 9.2 MATHEMATICAL MODEL (DRAIN-2D) - DRIVE-IN RACK, LONGITUDINAL DIRECTION

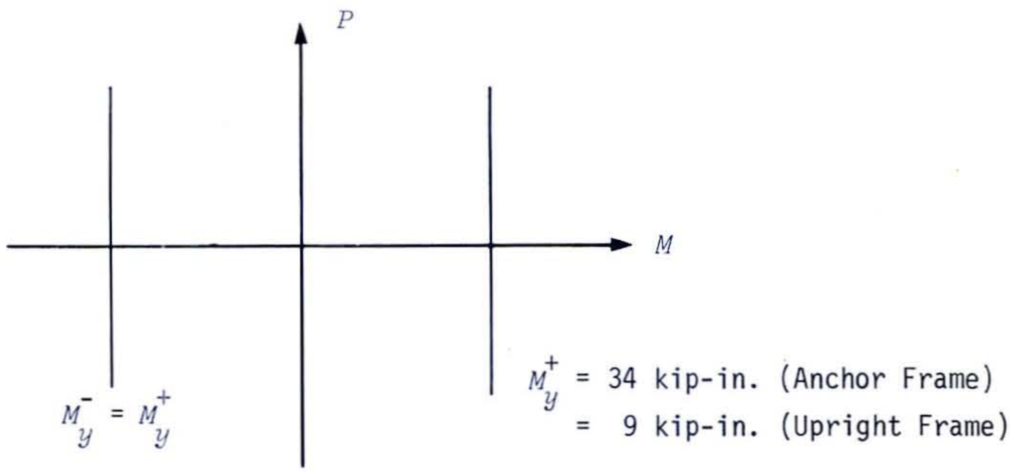

a. Yield Interaction Surface for Beams

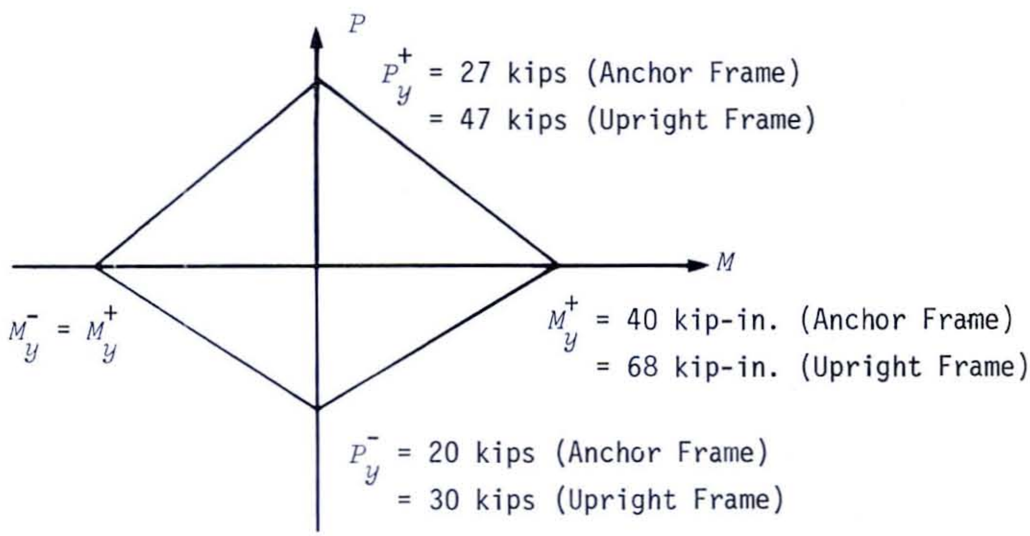

b. Yield Interaction Surface for Columns

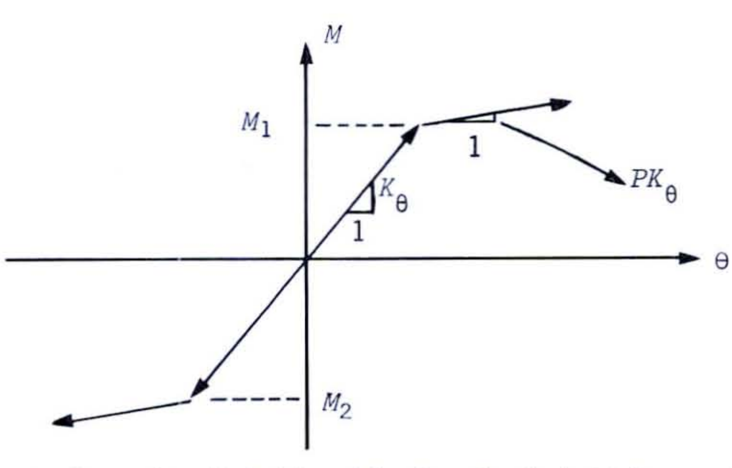

c. Moment-Rotation Relationship for Semirigid Connections

FIGURE 9.3 YIELD MECHANISM AND INTERACTION SURFACES - DRIVE-IN RACK, LONGITUDINAL DIRECTION

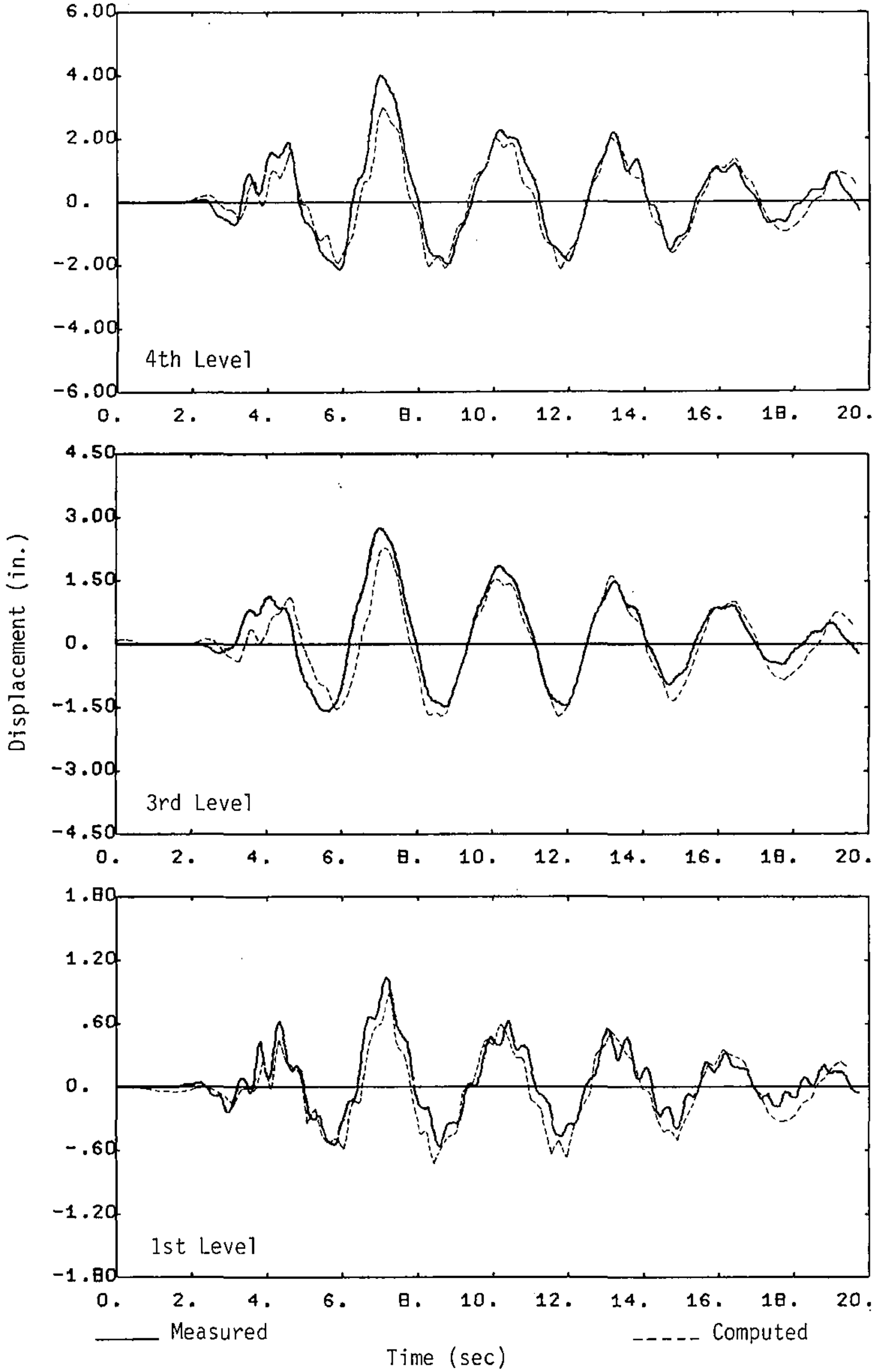

FIGURE 9.4 MEASURED AND COMPUTED STORY DISPLACEMENTS (DI-L-1-1/4 EC)

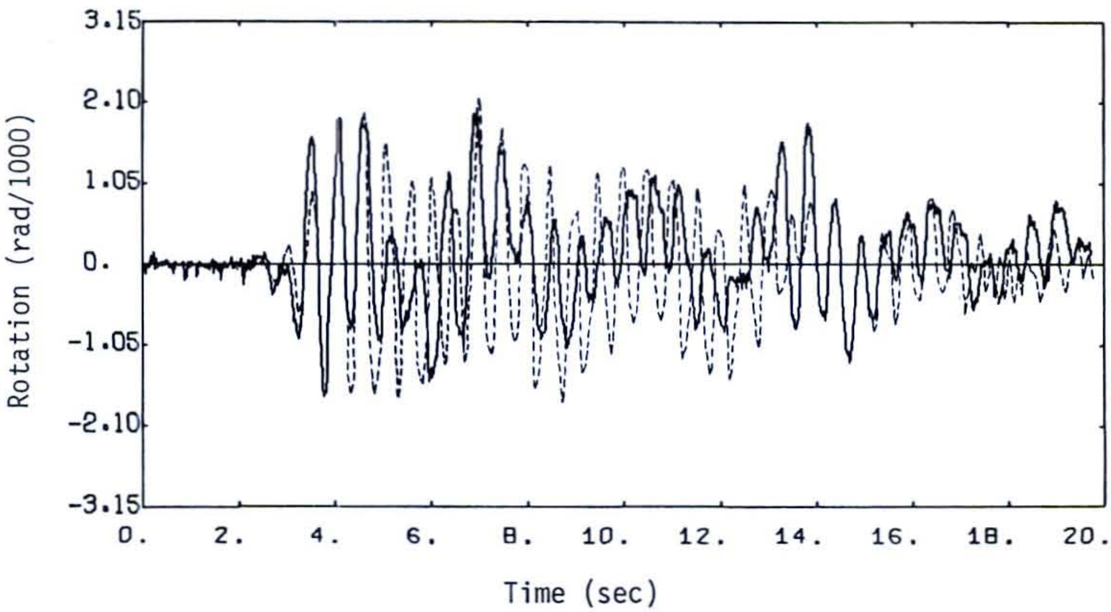

Center Bottom Column Near Top End -- Upright

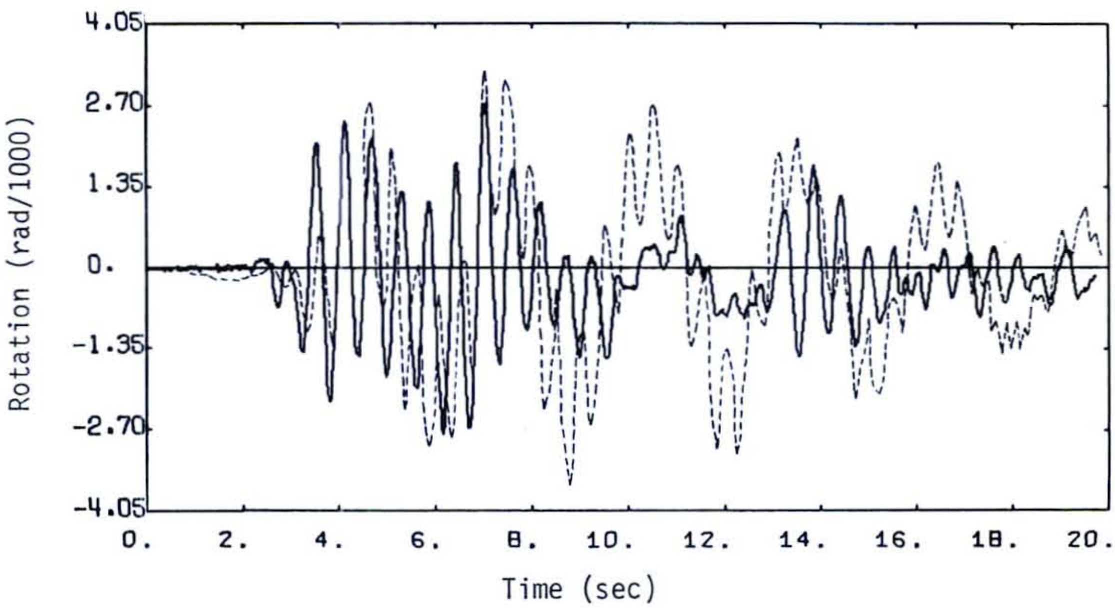

Center Bottom Column Near Top End -- Anchor

——— Measured ---- Computed

FIGURE 9.5 MEASURED AND COMPUTED LOCAL RESPONSES
(DI-L-1-1/4 EC)

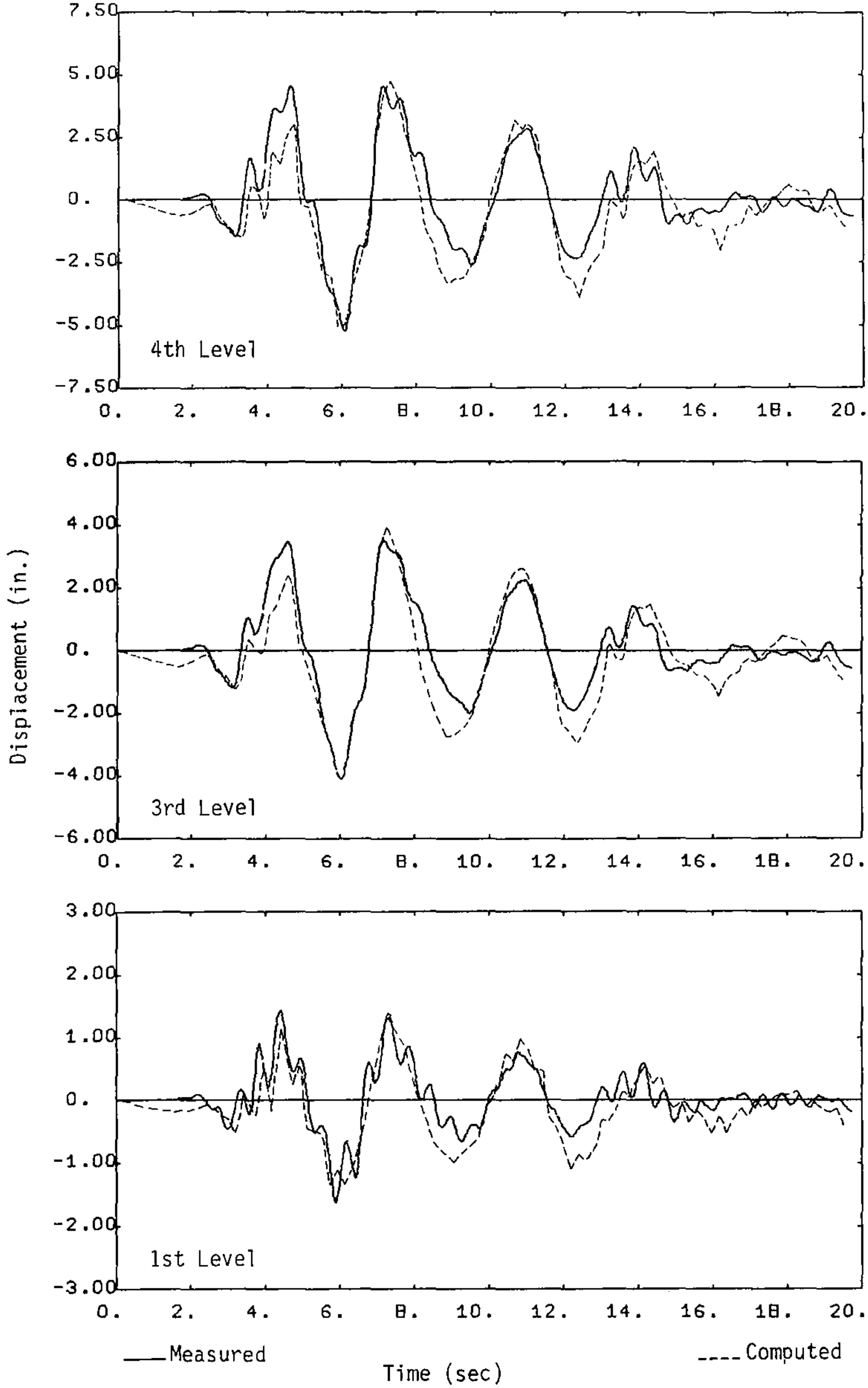

FIGURE 9.6 MEASURED AND COMPUTED STORY DISPLACEMENTS (DI-L-1-1/2 EC)

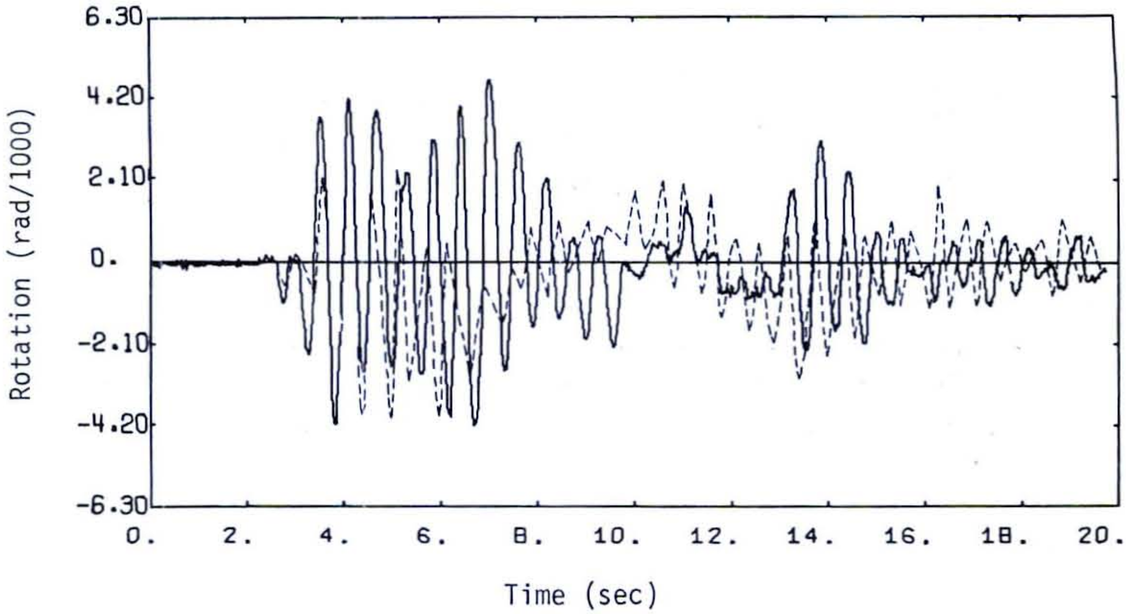

Center Bottom Column Near Top End -- Upright

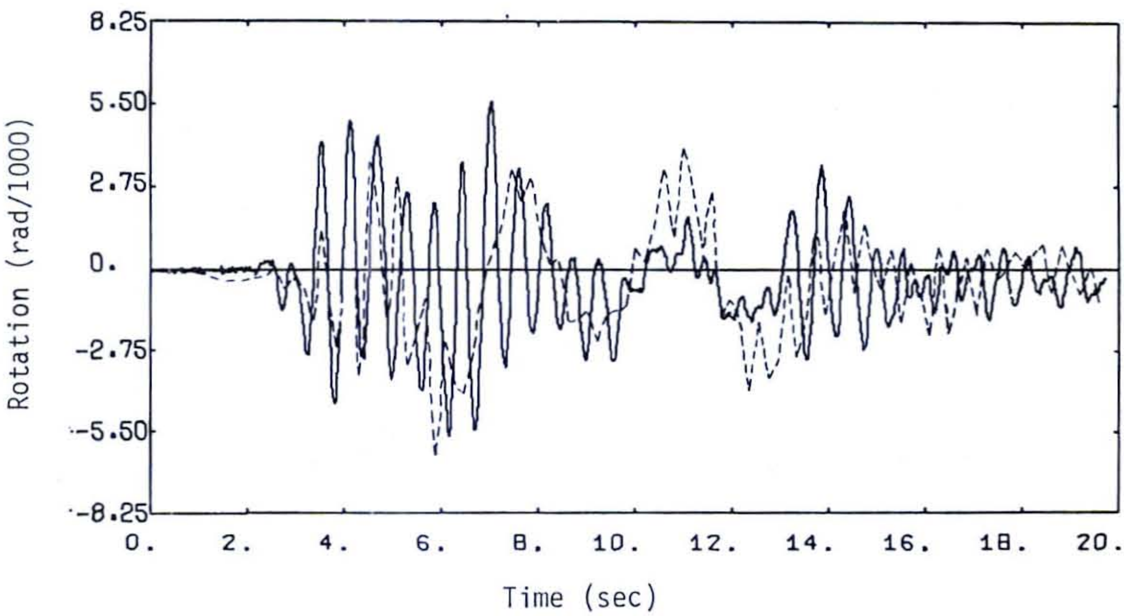

Center Bottom Column Near Top End -- Anchor

_____ Measured ---- Computed

FIGURE 9.7 MEASURED AND COMPUTED LOCAL RESPONSES (DI-L-1-1/2 EC)

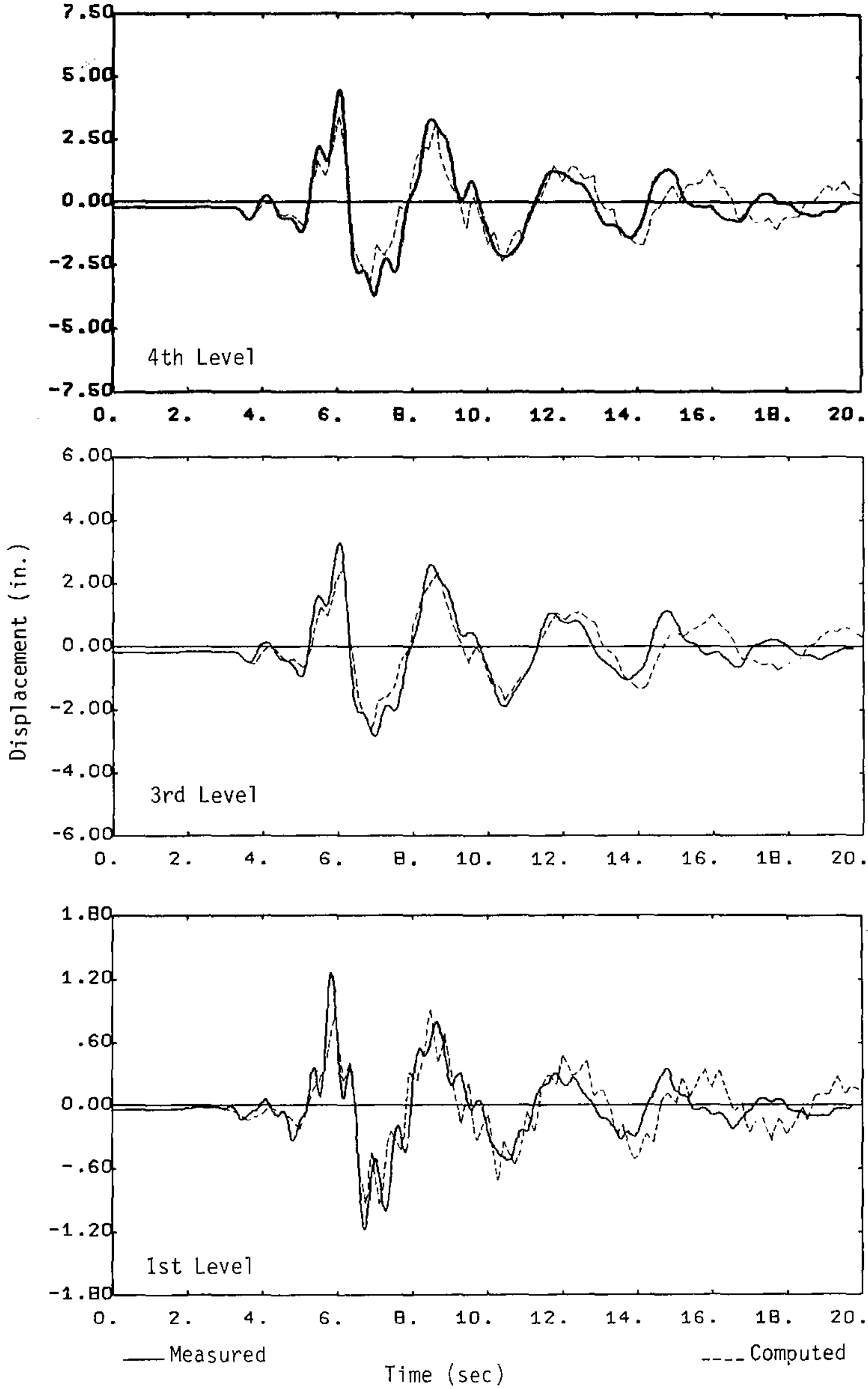

FIGURE 9.8 MEASURED AND COMPUTED STORY DISPLACEMENTS (DI-L-1-1/2 PF)

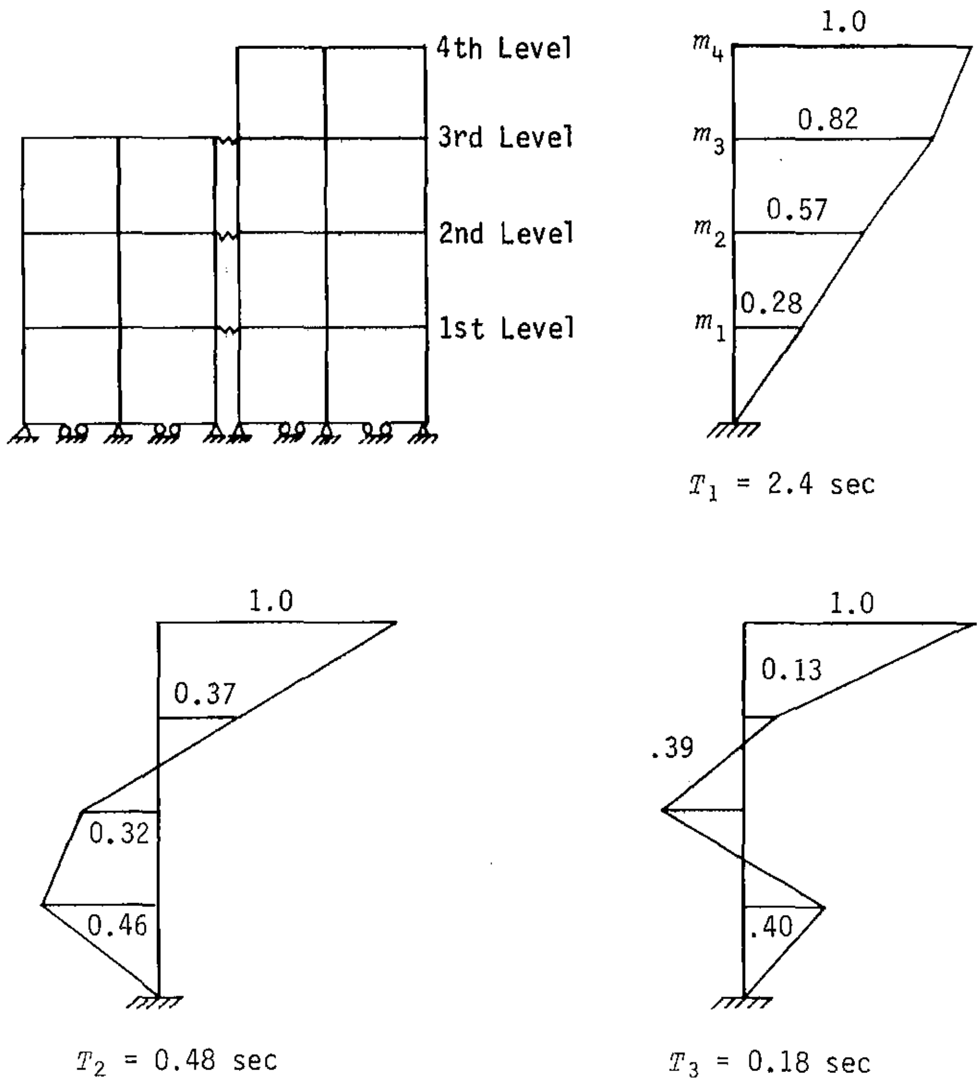

$m_4 = 0.2 \dfrac{\text{lb-sec}^2}{\text{in.}}$ $\qquad K_\theta = 10^6 \dfrac{\text{lb-in.}}{\text{rad}}$

$m_3 = m_2 = m_1$ $\qquad I_f = 0.20 \text{ in.}^4$

$= 24.8 \dfrac{\text{lb-sec}^2}{\text{in.}}$

FIGURE 9.9 CALCULATED PERIOD OF VIBRATION AND MODE SHAPES - DRIVE-IN RACK, LONGITUDINAL DIRECTION, FULL LIVE LOAD

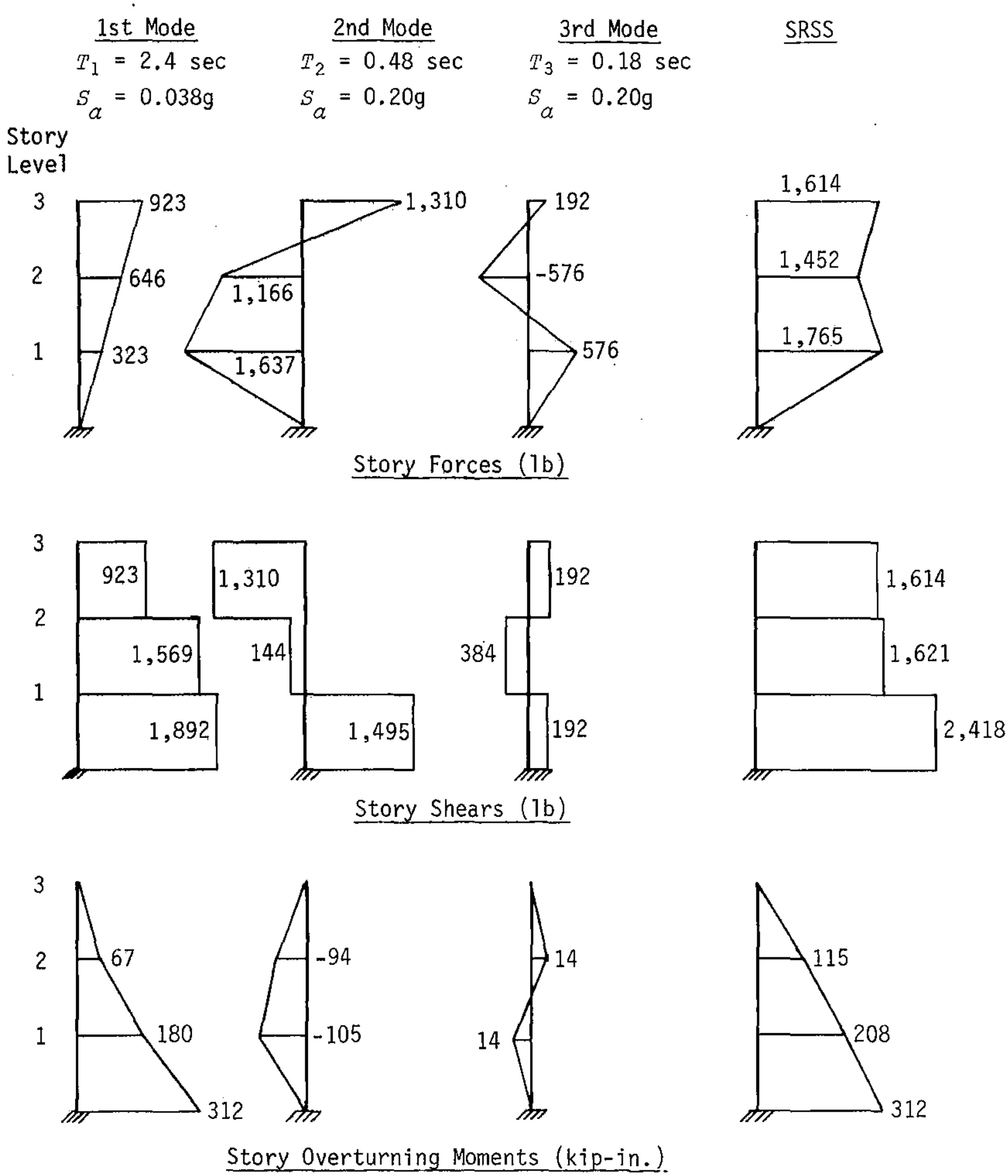

FIGURE 9.10 RESULTS OF RESPONSE SPECTRUM METHOD (DI-L-1-1/4 EC)

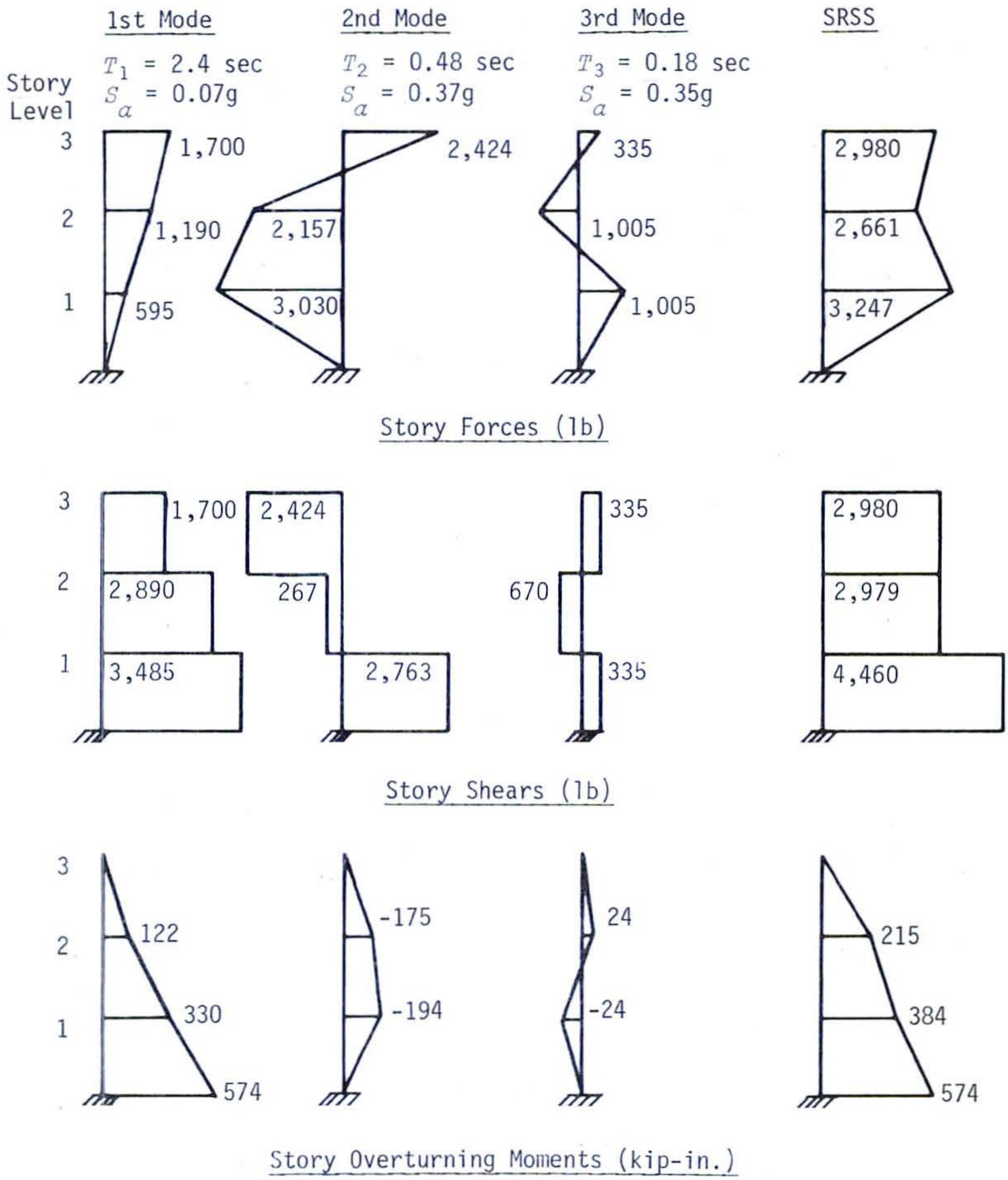

FIGURE 9.11 RESULTS OF RESPONSE SPECTRUM ANALYSIS (DI-L-1-1/2 EC)

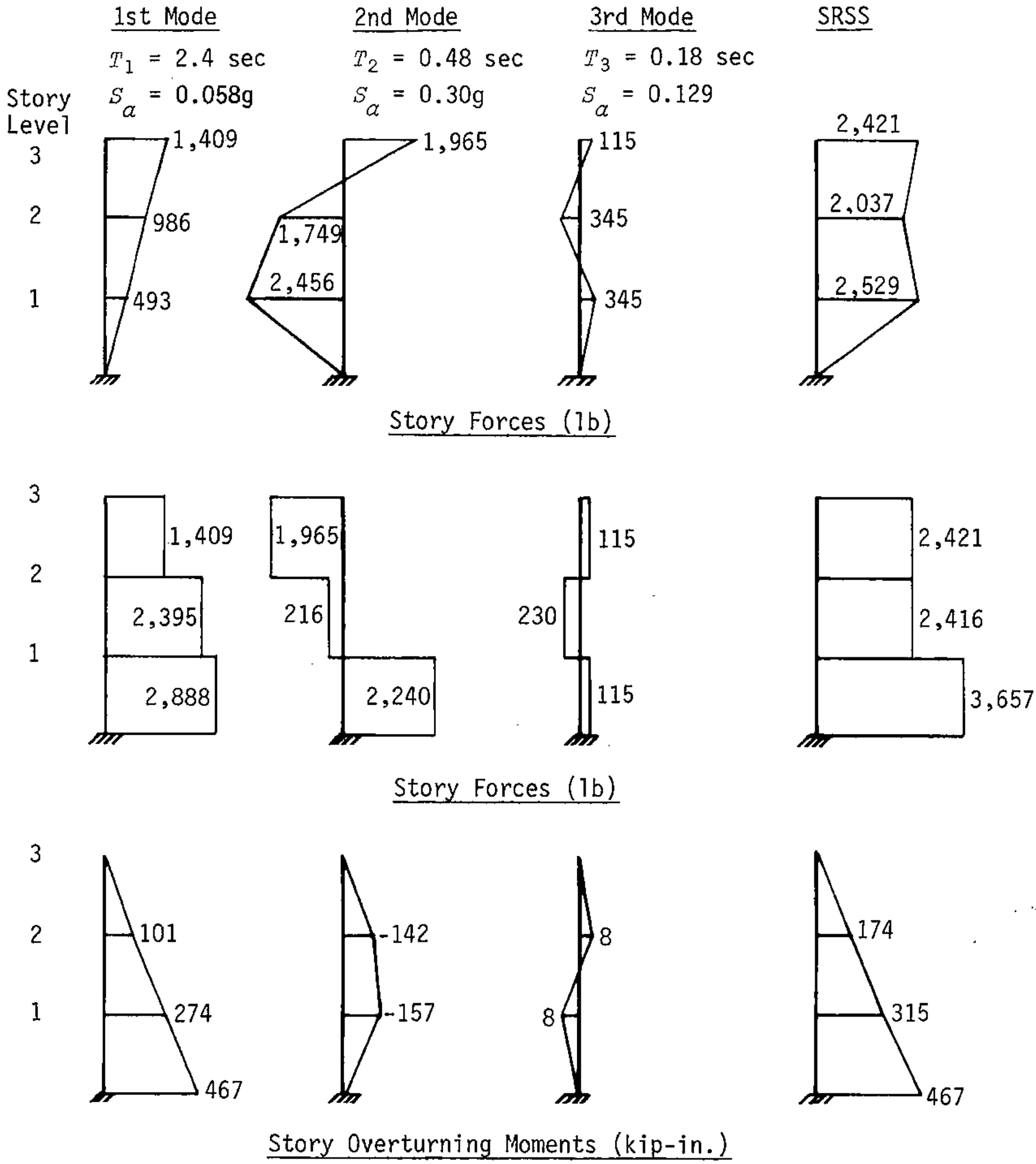

FIGURE 9.12 RESULTS OF RESPONSE SPECTRUM ANALYSIS (DI-L-1-1/2 PF)

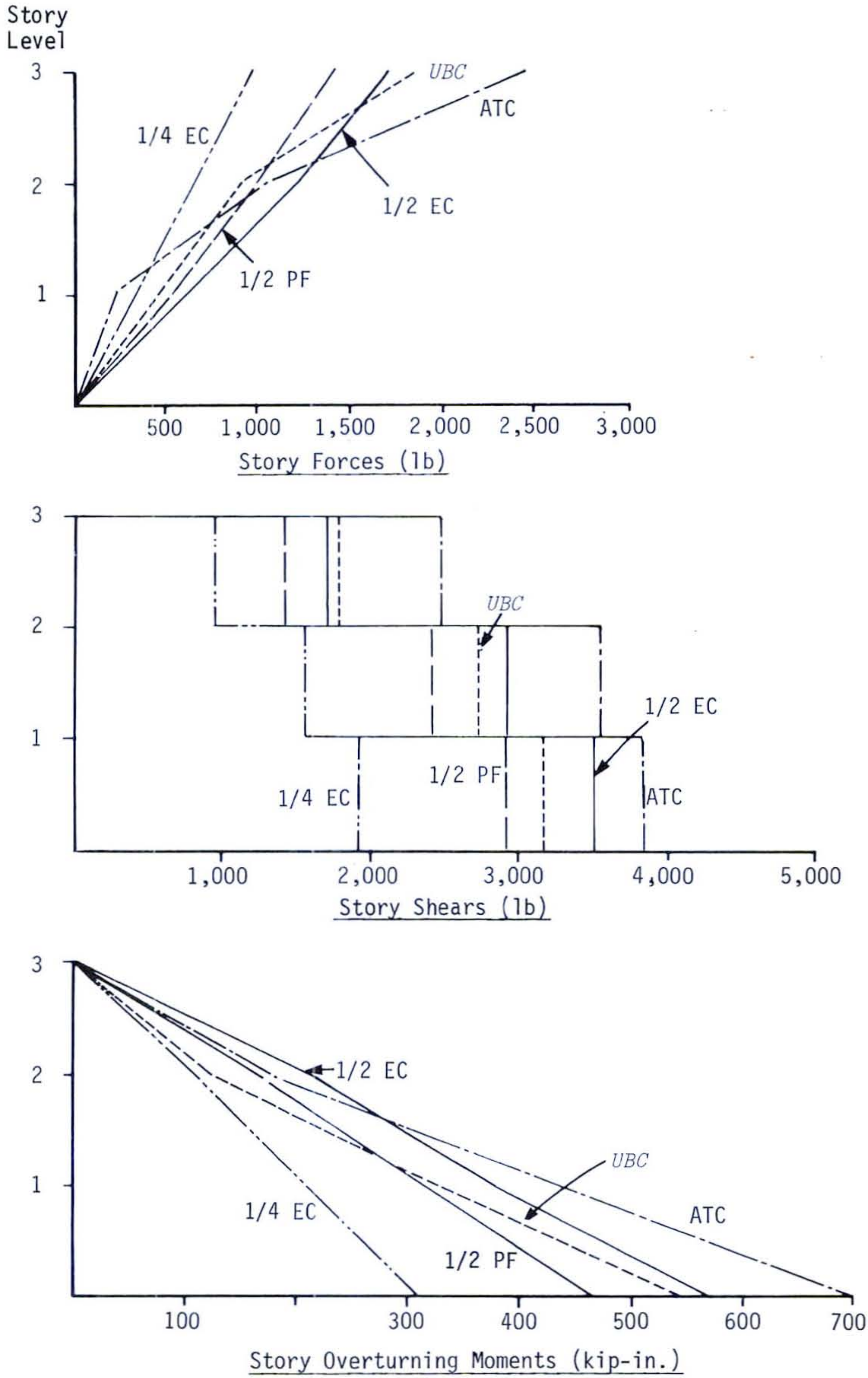

FIGURE 9.13 RESULTS OF THE *UBC* METHOD, THE ATC METHOD, AND RESPONSE SPECTRUM METHOD - DRIVE-IN RACK, FULL LIVE LOAD, LONGITUDINAL DIRECTION

10. THEORETICAL PREDICTION OF STRUCTURE RESPONSE--DRIVE-IN RACK, TRANSVERSE DIRECTION

10.1 Frequency Analysis

Basic Model. Figure 10.1 shows the mathematical models developed for the drive-in rack assembly in the transverse direction. Because symmetric response for three frames was observed during the tests, an analytical model for a single frame was considered to be adequate for analysis of this rack configuration. One-third of the estimated total mass was lumped in this basic model and distributed equally to twelve nodal joints as shown in the figure. The mass per story level was estimated to be approximately 11.4 lb-sec^2/in. for the 2/3 live load case. Centerline dimensions were used, and the fictitious restraining floor beams were used to account for the partially fixed column bases. The localized deformation at the connections between the open-section bracing members and the open-section columns were also considered. The minimum net section properties provided by the manufacturer are as follows:

	Moment of Inertia (in.^{4})	Cross-sectional Area (in.^{2})	Estimated Shear Area (in.^{2})
Column (upright)	1.56	1.32	0.82
Column (anchor)	0.94	0.75	0.45
Brace	-	0.33	-
Row Spacer	-	0.26	-

The influence of partially fixed column bases and localized deformation at the brace-column connections were discussed in Sections 7.1 and 8.1 respectively.

Comparison of Various Linear Mathematical Models. As was done for the standard pallet rack in the transverse direction, trial-and-error procedures were used to obtain the best-fit mathematical model by assuming various combinations of k and I_f. Table 10.1 shows the computed dynamic properties for various mathematical models along with the experimentally determined results. A comparison of Models 1 and 3 clearly shows the influence of local deformation at the brace-column connections on dynamic response. Model 1 assumed no local deformation (k = 1); Model 3 assigned k a value of 10. The calculated fundamental periods

Preceding page blank

of vibration were 0.36 sec for Model 1 and 0.67 sec for Model 3. The results calculated from Models 2 and 3 demonstrate that the periods and mode shapes varied very little with the change of I_f from 3.0 in.^{4} to 0.2 in.^{4}.

A comparison of the results from Models 3 and 4 also shows the influence of the local deformation parameter, k. The best-fit mathematical model is seen to be Model 4, which assumed k equal to 7 and I_f equal to 0.2. The Model 4 results show good agreement with the experimentally obtained results. No analytical study of the full-live-load case was performed because no experimental data were available for comparison.

10.2 Time-History Analysis

Basic Model. The basic mathematical model used for the time-history analysis was similar to that used for the frequency analysis (Figure 10.1) except for the use of DRAIN-2D instead of SAP IV. In modeling the bracing members for the time-history analysis, the approach used successfully for the standard pallet rack assembly in the transverse direction was again adopted. The members were treated as composite axial force members (see Figure 10.2). The figure also shows estimated capabilities of tension and compression at initiation of yield in accordance with AISI 3.6.1 ($F_{a2} > F_{a1}$, i.e., flexural buckling is critical). The lower plot of Figure 10.2 shows the assumed yield interaction surfaces of the columns. The procedures for calculating the axial forces and bending capacities are similar to those shown in Appendix A.

Results. Because considerable buckling of the bottom diagonal braces in the upright frames was observed when the table was shaken by 1/4 the Parkfield signal, only two cases were analyzed, and all were in the range of nonlinear response. Table 10.2 summarizes the parameters finally used for each case. These parameters resulted in the best possible analytical results in comparison with the corresponding experimental data. It can be seen that all parameters used for the time-history analysis remained essentially the same as those obtained for the best-fit linear mathematical model. The damping and yield mechanism (Figure 10.2) were the only new parameters introduced. The time-history analysis was carried out with an integration time step of 0.0196 sec, the same time interval as for digitization of the recorded data. This was considered to be adequate because the response was primarily in the first mode of vibration.

Case 1 (DI-T-2/3-1/4 EC). For this case, the model was simulated with the 2/3 live load and subjected to an input signal 1/4 that of the actual El Centro record. Mass-proportional damping corresponding to about 2% of the first-mode viscous damping was assigned. The parameters k and I_f were assumed to be 7 and 0.2, respectively. The correlation between the measured and computed story displacements relative to the table shown in Figure 10.3, is seen to be very good; similarly good correlation was obtained for the bottom diagonal axial strains shown in Figure 10.4.

Case 2 (DI-T-2/3-1/4 PF). For this model, the 2/3 live load was simulated, and an input signal of 1/4 the actual Parkfield record was applied. All modeling parameters used in Case 1 remained unchanged except k, which was assigned a value of 7.5. Figure 10.5 shows the measured and computed story displacements relative to the table. The correlation between them was considered to be good, considering the buckling of the bottom diagonal members in the upright frames during the shaking table testing. The poorly correlated results in the later part of the response were essentially in the state of free-decay vibration, after the table was stopped at about 16 sec.

10.3 Response Spectrum Analysis

Three cases were analyzed by the response spectrum method. Table 10.3 summarizes the results. The response spectra corresponding to each input signal were previously shown in Figures 4.18 and 4.19. It can be seen from Table 10.3 that the effect of higher-mode participation on the base shears and overturning moments was negligible.

Figure 10.6 shows the calculated periods of vibration and mode shapes determined from the frequency analysis of the linear mathematical models (Table 10.1). Figures 10.7 and 10.8 present the story forces, story shears, and story overturning moments for various modes of vibration and for the input signals of 1/4 the El Centro record and 1/4 the Parkfield record, respectively. The results also show clearly the insignificance of higher-mode participation.

10.4 *UBC* and ATC-3 Methods

The base shears determined from the *UBC* and ATC methods are presented in Table 10.4. The fundamental period of vibration used in the base shear calculation was analytically estimated from the frequency analysis of the linear mathematical models (Table 10.1). The best site condition was assumed in the evaluation of base shears by the *UBC* and ATC methods.

Table 10.5 shows the base shears and overturning moments for ultimate strength design, as determined by the *UBC*, ATC, and response spectrum methods. The base story forces from the *UBC* method were multiplied by a factor of 1.6, as required in ultimate strength design. A capacity-reduction factor of 0.9 was applied in the case of the ATC method. The calculated base shears required for ultimate strength design for the *UBC* method are approximately 15% larger than those by the ATC method. The base shears and overturning moments from the *UBC* method were greater than those from the response spectrum method using 1/4 PF and 1/4 EC but slightly less than those using the signal of 1/2 EC even when the worst site condition was assumed (i.e., S = 1.5). This is clearly demonstrated in Figure 10.9 and Table 10.5.

A general discussion of the adequacy and limitations of the various analysis methods is addressed in Chapter 13.

TABLE 10.1

LINEAR MATHEMATICAL MODELS - DRIVE-IN RACK, TRANSVERSE DIRECTION

Model	Live Load	Column Base		Brace Element		Period* (sec)			Mode Shape*		
		Case	I_f	k	$(EA)'$	1	2	3	1	2	3
1	2/3	semi-fixed	0.2	1	9,617	0.36	0.12	0.08	1.10 1.00 0.78 0.51	1.46 1.00 -0.48 -1.29	1.37 1.00 -2.42 1.70
2	"	"	3.0	10	962	0.63	0.21	0.13	1.05 1.00 0.78 0.41	1.37 1.00 -0.48 -1.25	1.90 1.00 -2.40 2.07
3	"	"	0.2	10	962	0.67	0.22	0.13	1.05 1.00 0.76 0.44	1.35 1.00 -0.40 -1.27	1.87 1.00 -2.31 1.77
4	"	"	0.2	7	1,374	0.58	0.19	0.12	1.05 1.00 0.80 0.47	1.32 1.00 -0.53 -1.23	1.67 1.00 -2.33 1.77

I_f = Moment of inertia of fictitious floor beam (in.^{4})

k = Factor to take into account local deformation at the brace-column connection

$(EA)'$ = Reduced section properties of bracing member (kips)

*Experimentally determined fundamental period and mode shape are:

Period: T_1 = 0.56 - 0.59 sec

Mode Shape: 1st Mode

1.05
1.00
0.79
0.52

TABLE 10.2

MODELING PARAMETERS FOR TIME-HISTORY ANALYSIS - DRIVE-IN RACK, TRANSVERSE DIRECTION

Case	Designation	Live Load	Input Signal	Column			Brace		Column Base	Damping		Remarks
				I_c (in.^{4})	A_c (in.^{2})	A_c' (in.^{2})	k	$(EA)'$ (kips)	I_f (in.^{4})	α	λ (%)	
1	DI-T-2/3-1/4 EC	2/3	1/4 EC	0.94 (1.56)	0.75 (1.32)	0.45 (0.82)	7	1,374	0.2	0.42	2	nonlinear response
2	DI-T-2/3-1/4 PF	"	1/4 PF	"	"	"	7.5	1,282	0.2	0.42	2	"

Notes: 2/3 live load = 11.4 lb-sec^2/in.

The upper and lower figures refer to the column properties of anchor and upright frames, respectively.

A_c' = estimated shear area of column.

TABLE 10.3

SUMMARY OF RESULTS FROM RESPONSE SPECTRUM ANALYSIS - DRIVE-IN RACK, TRANSVERSE DIRECTION

Case	Designation	Live Load	Input Signal		Base Shear (lb)		Base Overturning Moment (kip-in.)	
			Signal	Damping (%)	1st Mode	SRSS	1st Mode	SRSS
1	DI-T-2/3-1/4 EC	2/3	1/4 EC	2	2,316	2,332	368	368
2	DI-T-2/3-1/4 PF	"	1/4 PF	2	2,560	2,561	406	406
3	DI-T-2/3-1/2 EC	"	1/2 EC	3	4,266	4,300	680	680

TABLE 10.4

DETERMINATION OF BASE SHEAR USING THE *UBC* METHOD AND THE ATC METHOD - DRIVE-IN RACK, TRANSVERSE DIRECTION

Live Load	T (sec)	W (lb)	1976 *UBC*		ATC-3	
			C	V (lb)	C_s	V (lb)
2/3	0.58	13,200	0.088	1,853	0.173	2,284
			$V = ZIKCSW$ $C = \frac{1}{15\sqrt{T}}$ $K = 1.33$ $I = Z = 1.0$ $S = 1.2$ (minimum)		$V = C_s W$ $C_s = \frac{1.2\ A_v S}{RT^{2/3}}$ $A_v = 0.4$ $S = 1.0$ (minimum) $R = 4.0$	

TABLE 10.5

BASE STORY FORCES FOR ULTIMATE STRENGTH DESIGN -
DRIVE-IN RACK, TRANSVERSE DIRECTION

Live Load	*UBC* Method*		ATC Method†		Response Spectrum Method			
	Base Shear (lb)	Base Overturning Moment (kip-in.)	Base Shear (lb)	Base Overturning Moment (kip-in.)	1st Mode Base Shear (lb)	1st Mode Base Overturning Moment (kip-in.)	Damping (%)	Signal
2/3	2,964	493	2,538	422	2,316	368	2.0	1/4 EC
"	"	"	"	"	2,560	406	2.0	1/4 PF
"	"	"	"	"	4,266	680	3.0	1/2 EC

* The factored code forces required in ultimate strength design $(\frac{1.7}{1.33} \times 1.25 = 1.6)$

† A capacity reduction factor of 0.9 is applied.

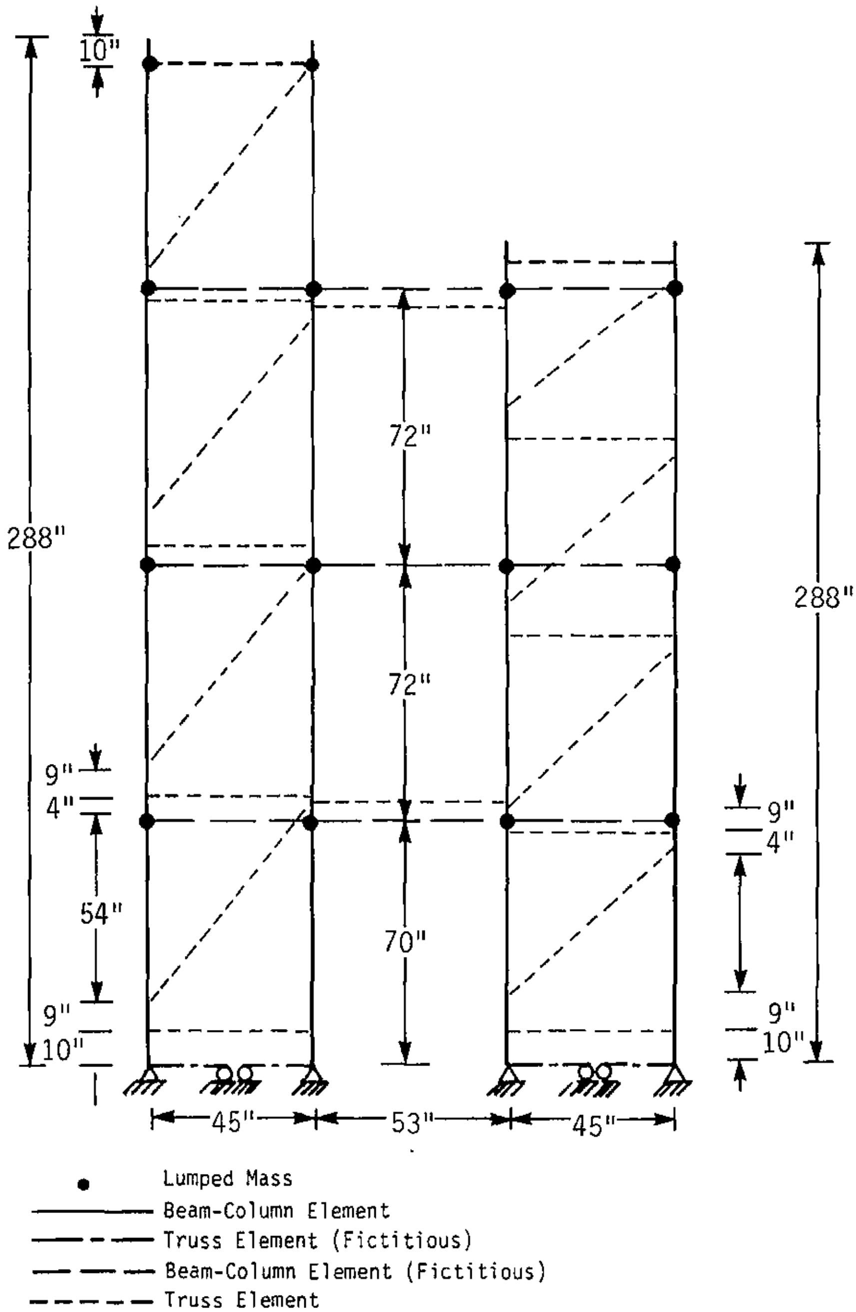

FIGURE 10.1 MATHEMATICAL MODEL (SAP IV AND DRAIN-2D) - DRIVE-IN RACK, TRANSVERSE DIRECTION

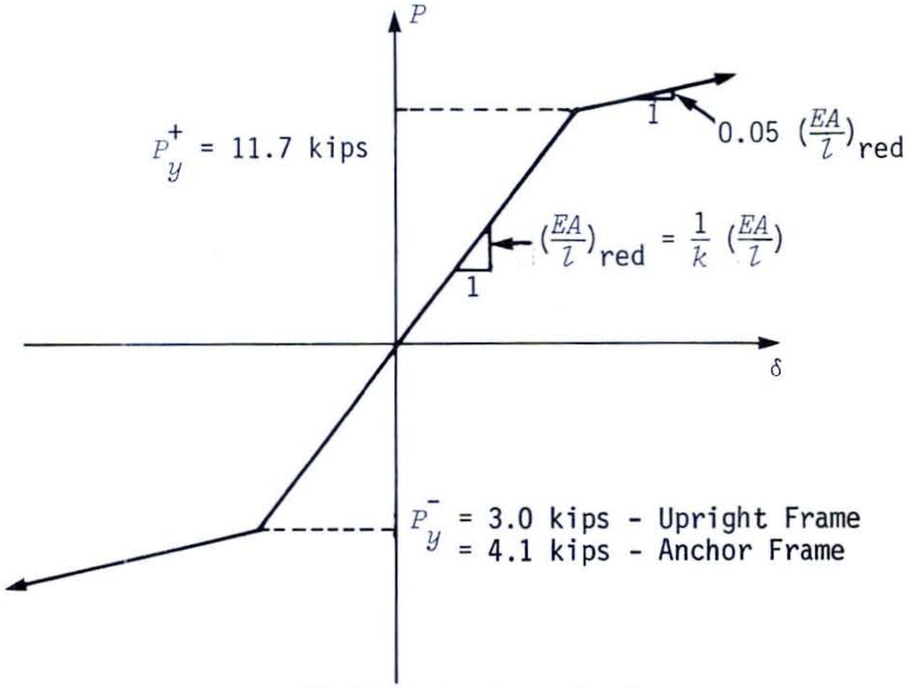

a. Bilinear Yield Mechanisms for Braces

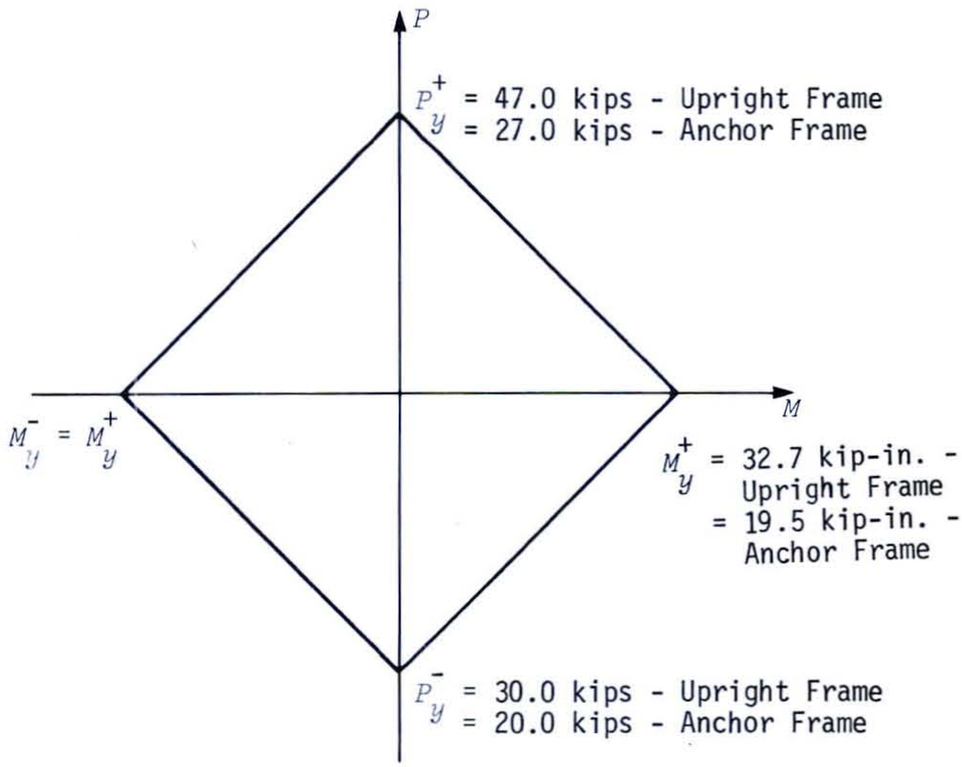

b. Interaction Surfaces for Columns

FIGURE 10.2 YIELD MECHANISM AND INTERACTION SURFACE - DRIVE-IN RACK, TRANSVERSE DIRECTION

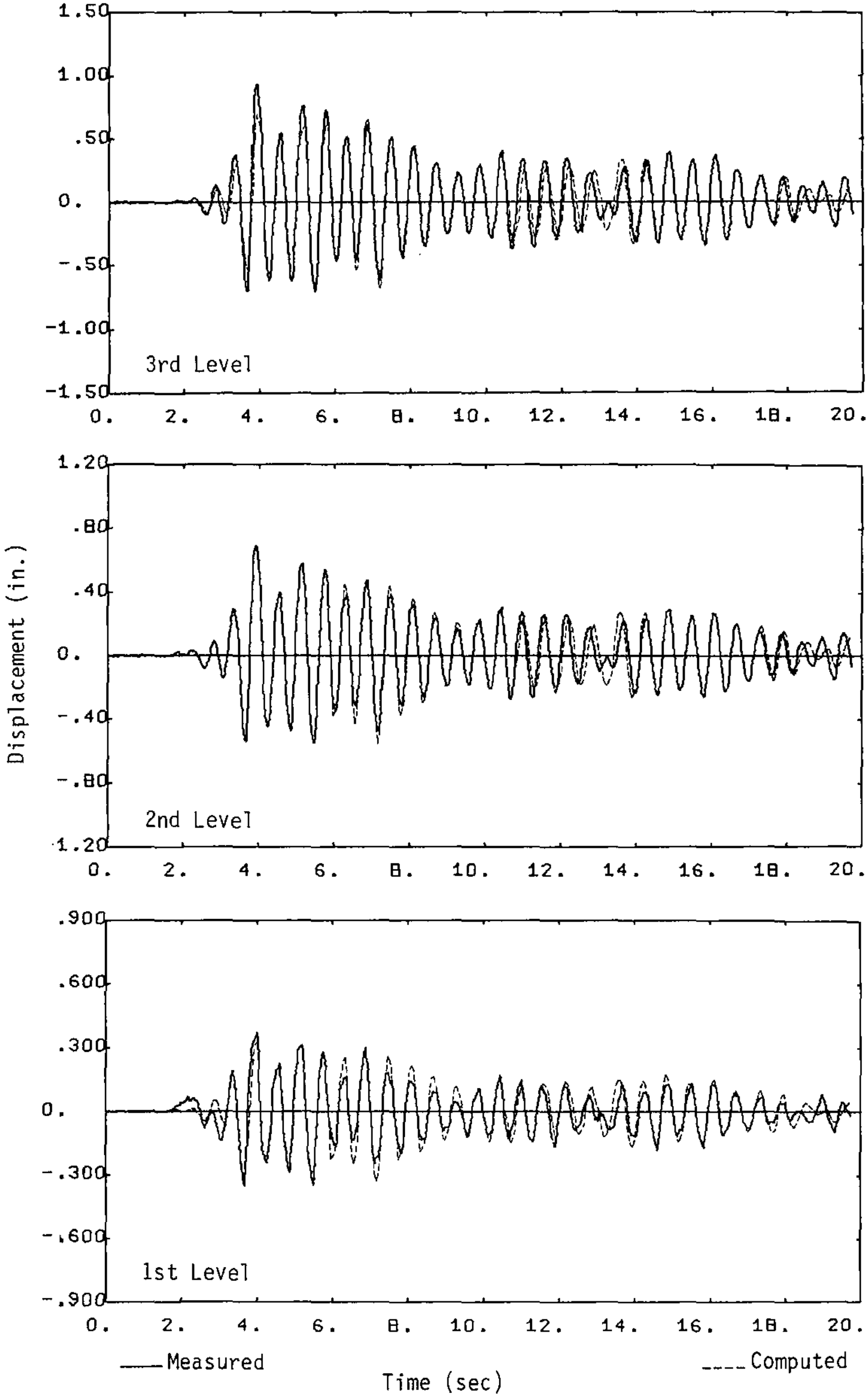

FIGURE 10.3 MEASURED AND COMPUTED STORY DISPLACEMENTS (DI-T-2/3-1/4 EC)

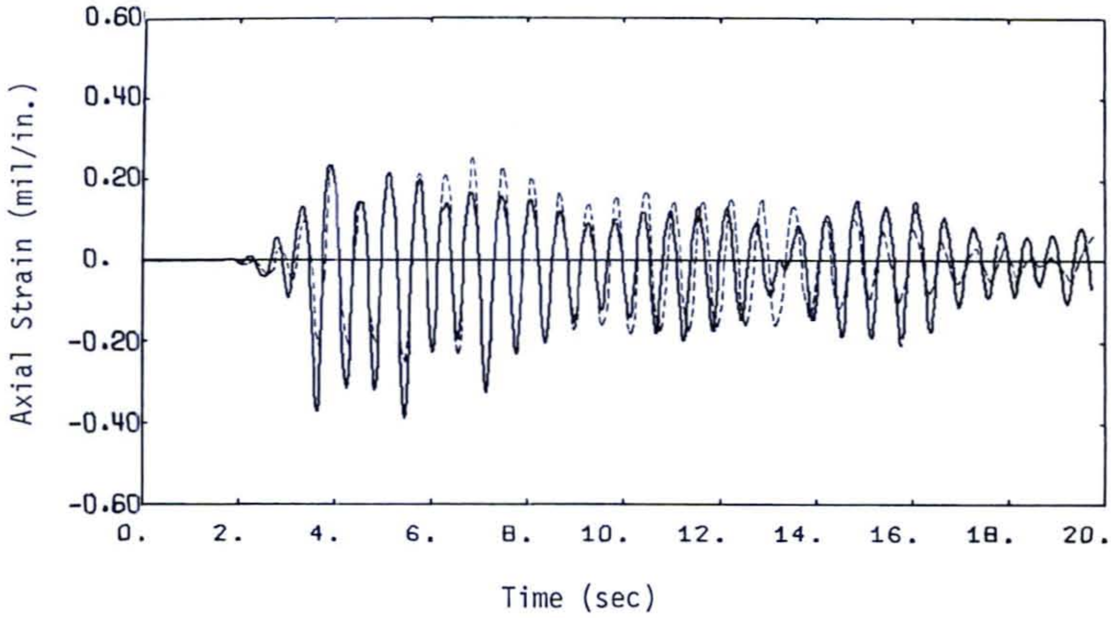

Bottom Diagonal -- Upright

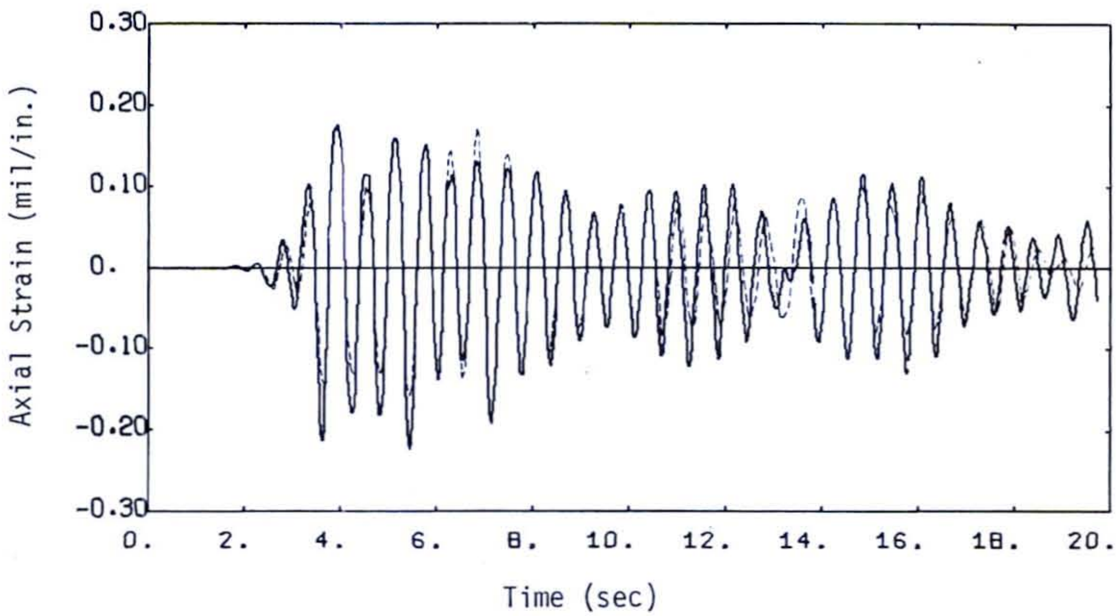

Bottom Diagonal -- Anchor

_____ Measured ---- Computed

FIGURE 10.4 MEASURED AND COMPUTED LOCAL RESPONSES (DI-T-2/3-1/4 EC)

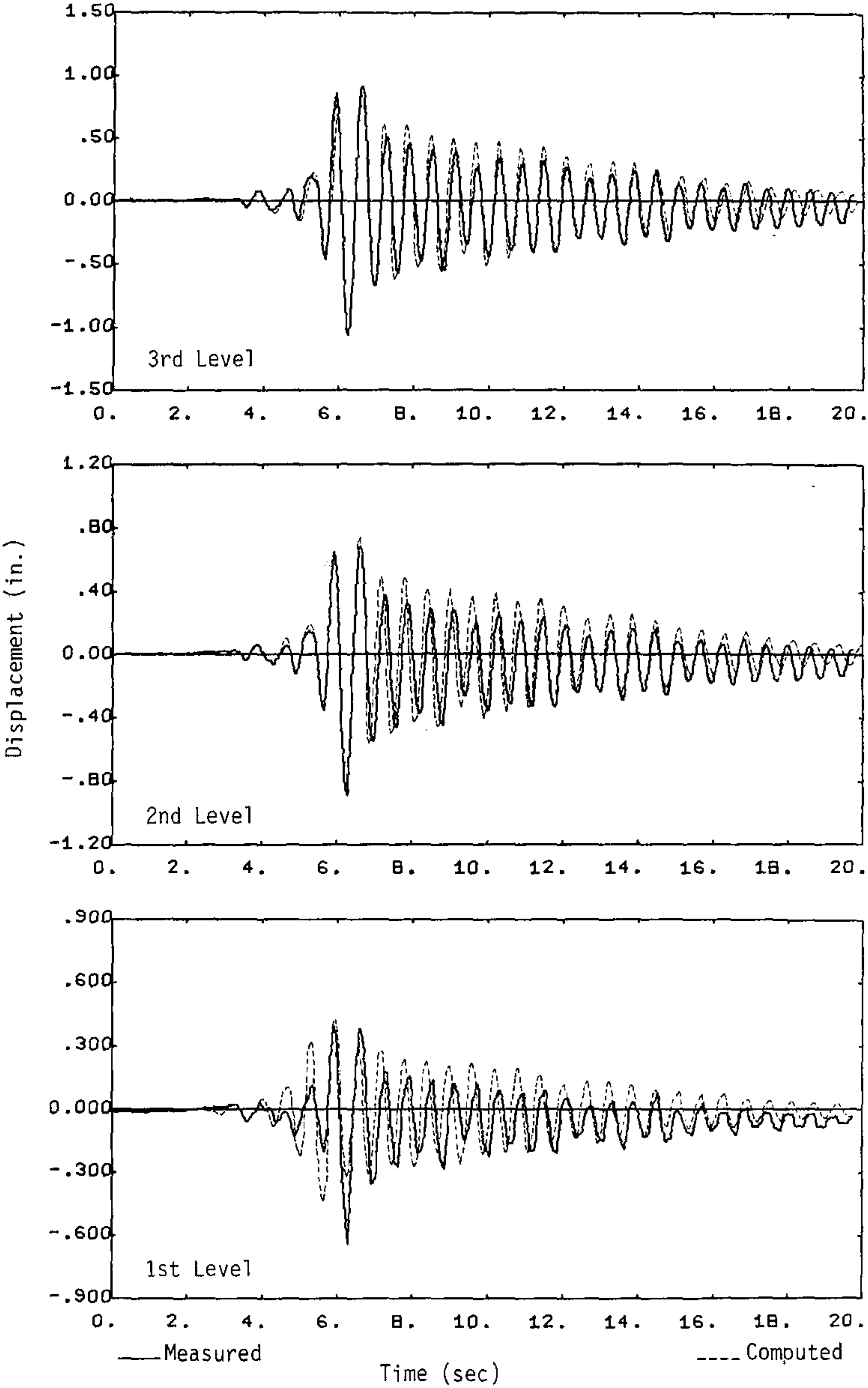

FIGURE 10.5 MEASURED AND COMPUTED STORY DISPLACEMENTS (DI-T-2/3-1/4 PF)

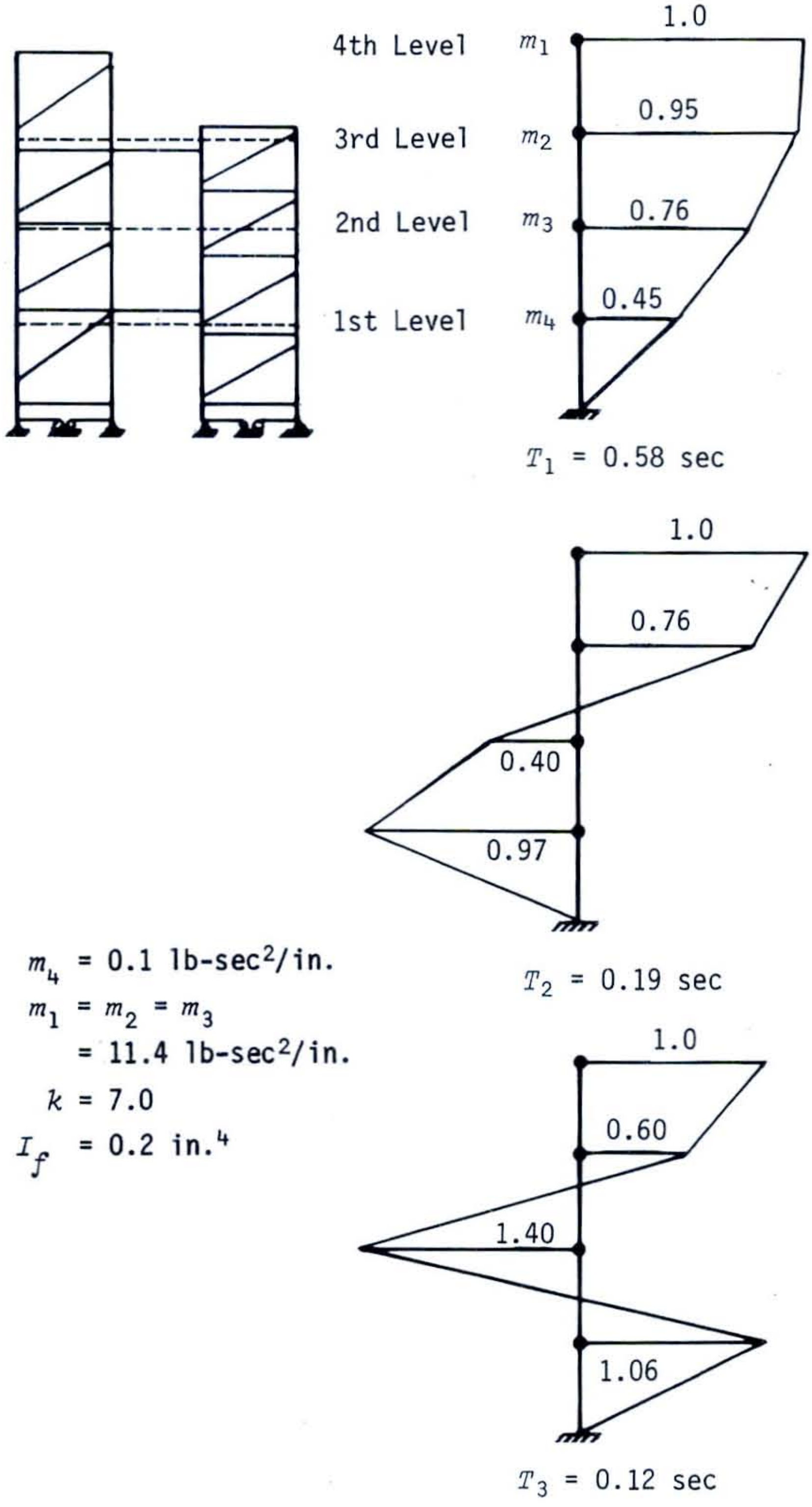

FIGURE 10.6 CALCULATED PERIODS OF VIBRATION AND MODE SHAPES - DRIVE-IN RACK, TRANSVERSE DIRECTION, 2/3 LIVE LOAD

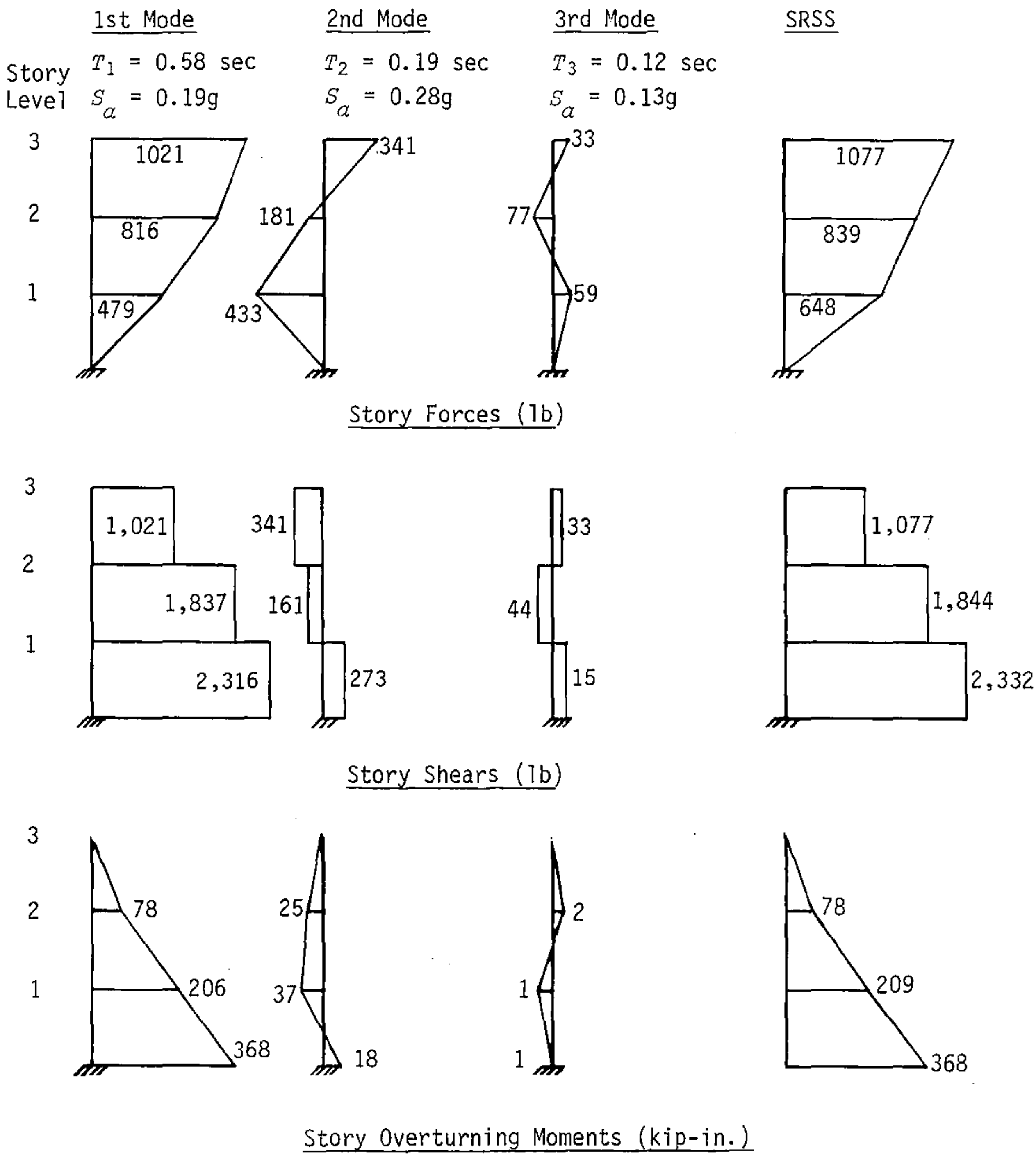

FIGURE 10.7 RESULTS OF RESPONSE SPECTRUM METHOD (DI-T-2/3-1/4 EC)

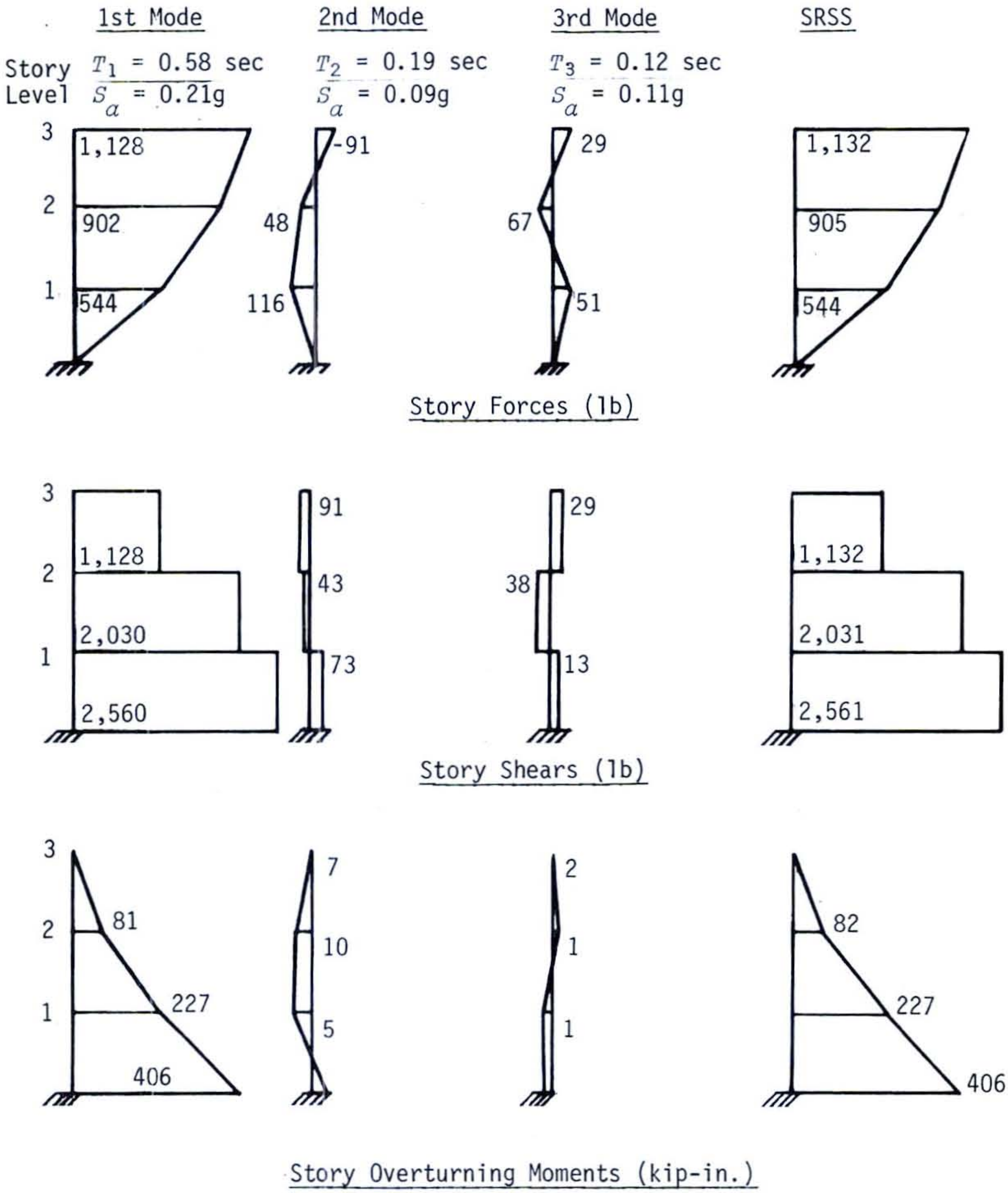

FIGURE 10.8 RESULTS OF RESPONSE SPECTRUM METHOD (DI-T-2/3-1/4 PF)

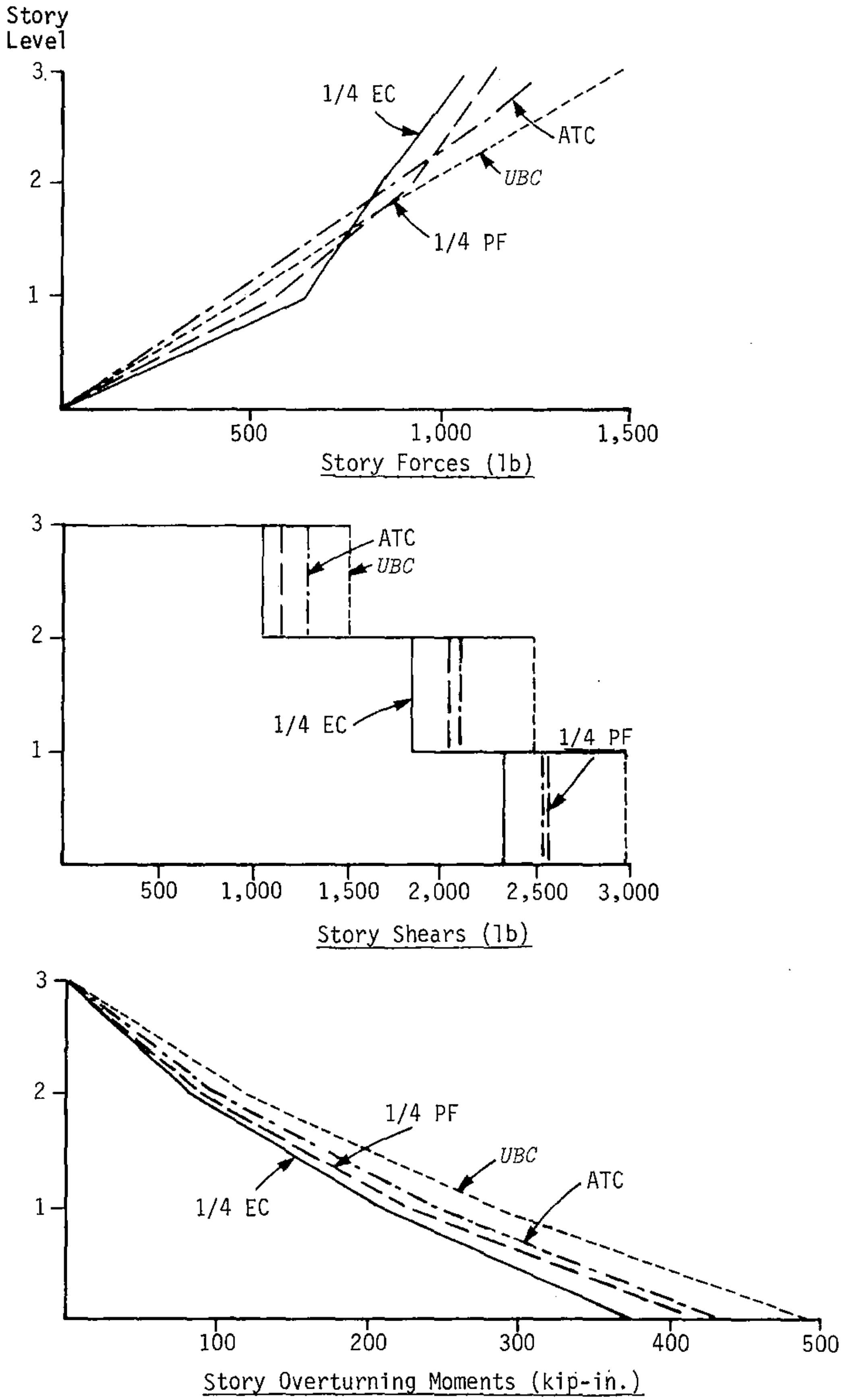

FIGURE 10.9 RESULTS OF THE *UBC* METHOD, THE ATC METHOD, AND THE RESPONSE SPECTRUM METHOD - DRIVE-IN RACK, TRANSVERSE DIRECTION

11. THEORETICAL PREDICTION OF STRUCTURE RESPONSE--STACKER RACK, LONGITUDINAL DIRECTION

11.1 Frequency Analysis

Basic Model. In the longitudinal direction, the stacker rack assembly consists of four identical parallel frames with two pairs of diagonal rods between the two interior frames (see Figure 4.8). Although these two pairs (upper and lower) of diagonal rods are not vertically aligned, the experimentally obtained displacement records show that the response was nearly symmetric, and no torsion was observed. This negligible asymmetry makes possible a two-dimensional analytical study.

Figure 11.1 shows the basic mathematical model developed for this rack assembly. In this model, the four resisting frames were represented as a single frame, and the diagonal rods were assumed to be connected directly to the column members. In modeling, the 1-in. diagonal rods were treated as composites consisting of three parts: solid section, threaded portion, and rod support. Because of the local deformation at the rod support in addition to the deformation due to the rod member, the stiffness of the composite members was reduced according to Equation (8.1). The parameter k was again applied to this model.

During seismic excitation, these diagonal rods behave nonlinearly because of their very low compression capacity and because of the deformation of the rod supports. Figure 10.2a generally illustrates the nonlinear response behavior of the rods. This bilinear yield mechanism is intended to model tensile yielding and compression buckling and will be discussed in Section 11.2. However, to model this structure linearly, it was assumed that the diagonal members would yield in tension and compression and would have an appropriately assumed value of k.

Fictitious floor beams were again introduced to account for the column fixity, and the entire story mass was lumped equally at the nodal points connecting the columns and the fictitious truss elements. The mass per story was estimated to be 45.5 lb-sec^2/in. for the full live load (2,000 lb/pallet). The mass at the sixth (top) story was so small as to be considered negligible.

The minimum net section properties provided by the manufacturer are:

	Moment of Inertia ($in.^4$)	Cross-sectional Area ($in.^2$)	Estimated Shear Area ($in.^2$)
Column	4 x 1.15	4 x 0.69	4 x 0.31
Horizontal Tie	4 x 0.67	4 x 0.54	4 x 0.27
Diagonal Rod	-	0.785	-

Comparison of Various Linear Mathematical Models. The trial-and-error procedure of assigning various combinations of k and I_f was used. The results are shown in Table 11.1. A comparison of the results of Models 1 and 3 indicates that k has a considerable influence on the dynamic response properties. Model 1 assumed no local deformation (i.e., the rod support was perfectly rigid), and Model 3 considered local deformation with an assumed k of 14. The results from Models 2, 3, and 4 demonstrate that the effects of the column fixity (I_f) on the dynamic response were not significant: the calculated periods and mode shapes of vibration were almost identical. A further comparison of Models 3 and 5 also shows the importance of the parameter k. The fundamental periods of vibration increased about 10% with an increase in k from 14 to 20. The periods obtained from free-decay data during the low-amplitude shaking table tests ranged from 0.88 sec to 0.95 sec. Experimentally obtained mode shapes (first mode) are also shown in Table 11.1 for comparison with the calculated results. Since the parameter I_f had no significant influence on the calculated response properties, Model 3, with $I_f = 0.2$ in.^{4} and $k = 14$, was selected as the best-fit model. (Note that the parameter $I_f = 0.2$ had been used successfully to model the standard pallet and drive-in rack structures.)

11.2 Time-History Analysis

Basic Model. The nonlinear mathematical model for the longitudinal time-history analysis of the stacker rack assembly is similar to the linear model shown in Figure 11.1 except that DRAIN-2D was used instead of SAP IV. The composite axial force members were treated as bilinear yielding elements with very low compression capacity. Figure 11.2a shows the assumed bilinear yield mechanism of the diagonal rods intended to model tensile yielding and compression buckling. Figure 11.2b shows the yield interaction surface for columns. The calculated column yield moment ($M_y = F_y \times S$) was approximately 34 kip-in.

The average tensile and compression forces were estimated to be 31 kips and 18 kips, respectively. The detailed procedures for obtaining the theoretical compression force at the initiation of yield are similar to those illustrated in Appendix A.

Results. Only two cases were studied. These were believed to be the only cases in which no diagonal rod was loose during the shaking table tests. In addition, a certain amount of pretension was applied (by tightening the bolts at the ends of rods) before testing. Table 11.2 summarizes the parameters finally used for each case. These parameters resulted in the best possible analytical results in comparison with the corresponding experimental results. All member properties, mass per story level, and the parameter I_f remained unchanged from those used in the frequency analysis. However, the parameter k was reduced to 7 because it was assumed that the diagonals took tension only and had very little compression capacity (in contrast to the assumption in the linear model that both cross diagonals were in action). The time-history analysis was again carried out with an integration time step of about 0.0196 sec, the same time interval as for digitization of recorded data.

Case 1 (ST-L-1-1/4 EC). For this case, the model was simulated with the full live load and subjected to an input signal of 1/4 the El Centro record. Mass-proportional damping corresponding to about 3.6% of the first-mode viscous damping was prescribed. The computed and measured story displacements relative to the table are presented in Figure 11.3. The model successfully predicted the two major stages of response as indicated. The latter stage of response (after about 15 sec) was not included in the analytical prediction because the response was insignificant. The computed and measured axial strains of both bottom diagonal rods are shown in Figure 11.4. Agreement between analysis and experiment is again considered very good.

Case 2 (ST-L-1-1/4 PF). For this model study, all model parameters assigned to the Case 1 model remained unchanged with the exception of the input signal, which was 1/4 the Parkfield record. A comparison of the computed and measured story displacements relative to the table as shown in Figure 11.5 shows excellent agreement. The latter stage of response was not included in the analytical prediction because the shaking table stopped at about 15 sec.

Correlations between the predicted and measured local responses, shown in Figure 11.6, are again considered to be excellent.

11.3 Response Spectrum Analysis

Four cases were analyzed by the response spectrum method. Table 11.3 summarizes the base shears and overturning moments obtained along with the input signal and damping used for each case. The response spectra corresponding to each input signal were previously shown in Figures 4.18 and 4.19. As shown in Table 11.3, higher-mode participation had a negligible effect on base shears and overturning moments for every case under consideration. It is interesting to note that the base shears and overturning moments calculated from the 1/2 El Centro signal and the 1/2 Parkfield signal were identical.

Two individual cases, with input signals of 1/4 the El Centro record and 1/2 the Parkfield record, were selected for presentation in this report. Figure 11.7 shows the periods of vibration and mode shapes determined from the frequency analysis of the linear mathematical models (see Table 11.1). Figures 11.8 and 11.9 present the story forces, story shears, and story overturning moments for various modes of vibration and for the input signals of 1/4 the El Centro record and 1/2 the Parkfield record. With the exception of story forces, these two figures show that the effects of higher modes on the story shears and overturning moments were insignificant.

11.4 *UBC* and ATC-3 Methods

The base story shears obtained from the *UBC* method and the ATC method are presented in Table 11.4. The fundamental period of vibration was determined from the frequency analysis of the best-fit linear model with assigned parameters of $k = 14$ and $I_f = 0.2$ in.^{4} (See Table 11.1.) K was assumed to be 1.33 in the *UBC* method, and R was assumed to be 4.0 in the ATC method. The other parameters involved in the base shear calculation are also indicated in Table 11.4. The best site condition was assumed in the calculation.

Table 11.5 presents the base story forces required for ultimate strength design for the response spectrum method, the *UBC* method, and the ATC method. Figure 11.10 shows that the lateral forces for the *UBC* method were substantially greater than those for the response spectrum method using 1/2 the El Centro signal or 1/2 the Parkfield signal.

A general discussion of the adequacy and limitations of various analysis methods is presented in Chapter 13.

TABLE 11.1
LINEAR MATHEMATICAL MODELS - STACKER RACK, LONGITUDINAL DIRECTION

Model	Live Load	Column Base		Brace Element		Period* (sec)			Mode Shape*		
		Case	I_f	k	$(EA)'$	1	2	3	1	2	3
1	full	semi-fixed	0.2	2	11,580	0.53	0.23	0.16	1.0 1.42 1.28 0.58 0.34 0.09	1.0 -1.58 -1.21 2.48 6.43 1.37	1.0 0.96 -0.95 -0.44 0.22 0.01
2	"	pinned	0	14	1,649	0.91	0.33	0.20	1.0 1.02 0.84 0.54 0.30 0.04	1.0 0.88 -0.12 -0.99 -0.97 -0.16	1.0 0.42 -0.68 -0.19 0.68 0.14
3	"	semi-fixed	0.2	14	1,649	0.91	0.33	0.20	1.0 1.02 0.84 0.54 0.29 0.04	1.0 0.88 -0.13 -0.99 -0.96 -0.15	1.0 0.42 -0.68 -0.19 0.68 0.13
4	"	"	3.7	14	1,649	0.91	0.33	0.19	1.0 1.02 0.83 0.54 0.28 0.03	1.0 0.88 -0.14 -1.0 -0.94 -0.13	1.0 0.42 -0.68 -0.17 0.68 0.12
5	"	"	0.2	20	1,158	1.01	0.36	0.20	1.0 0.99 0.80 0.53 0.28 0.04	1.0 0.80 -0.14 -0.89 -0.79 -0.11	1.0 0.39 -0.67 -0.16 0.71 0.14

I_f = Moment of inertia of fictitious floor beam (in.^{4})

k = Factor to take into account local deformation at the brace-column connection

$(EA)'$ = Reduced section properties of bracing member (kips)

*Experimentally determined fundamental period T_1 = 0.88-0.95 sec.

TABLE 11.2

MODELING PARAMETERS FOR TIME-HISTORY ANALYSIS

STACKER RACK, LONGITUDINAL DIRECTION

Case	Designation	Live Load	Input Signal	Horizontal Tie			Column			Diagonal		Column Base	Damping		Remarks
				I_b (in.^{4})	A_b (in.^{2})	A_b' (in.^{2})	I_c (in.^{4})	A_c (in.^{2})	A_c' (in.^{2})	k	$(EA)'$ (kips)	I_f (in.^{4})	α	λ (%)	
1	ST-L-1-1/4 EC	full	1/4 EC	4 x 0.67	4 x 0.54	4 x 0.27	4 x 1.15	4 x 0.69	4 x 0.31	7	3,298	0.2	0.5	3.6	nonlinear response
2	ST-L-1-1/4 PF	"	1/4 PF	"	"	"	"	"	"	7	"	"	0.5	3.6	"

Notes: Full live load = 45.4 lb-sec^2/in. per story level (1st to 5th levels)

A_b', A_c' = estimated shear area of horizontal tie and column, respectively

TABLE 11.3

SUMMARY OF RESULTS FROM RESPONSE SPECTRUM ANALYSIS - STACKER RACK, LONGITUDINAL DIRECTION

Case	Designation	Live Load	Input Signal		Base Shear (lb)		Base Over-turning Moment (kip-in.)	
			Signal	Damping (%)	1st Mode	SRSS	1st Mode	SRSS
1	ST-L-1-1/4 EC	full	1/4 EC	3	7,969	8,430	1,483	1,483
2	ST-L-1-1/4 PF	"	1/4 PF	3	6,743	7,039	1,255	1,255
3	ST-L-1-1/2 EC	"	1/2 EC	5	12,260	13,158	2,282	2,282
4	ST-L-1-1/2 PF	"	1/2 PF	5	12,260	12,766	2,282	2,282

TABLE 11.4

DETERMINATION OF BASE SHEAR USING THE *UBC* METHOD AND THE ATC METHOD - STACKER RACK, LONGITUDINAL DIRECTION

Live Load	T (sec)	W (lb)	1976 *UBC*		ATC-3	
			C	V (lb)	C_s	V (lb)
full	0.91	88,000	0.070	10,650	0.128	11,264
			$V = ZIKCSW$ $C = \frac{1}{15\sqrt{T}}$ $K = 1.33$ $I = Z = 1.0$ $S = 1.3$ (minimum)		$V = C_s W$ $C_s = \frac{1.2\ A_v S}{RT^{2/3}}$ $A_v = 0.4$ $S = 1.0$ (minimum) $R = 4.0$	

TABLE 11.5

BASE STORY FORCES FOR ULTIMATE STRENGTH DESIGN - STACKER RACK, LONGITUDINAL DIRECTION

Live Load	UBC Method		ATC Method†		Response Spectrum Method			
	Base Shear (lb)	Base Overturning Moment (kip-in.)	Base Shear (lb)	Base Overturning Moment (kip-in.)	1st Mode Base Shear (lb)	1st Mode Base Overturning Moement (kip-in.)	Damping (%)	Signal
Full	17,040	3,263	12,516	2,354	7,969	1,483	3	1/4 EC
"	"	"	"	"	6,743	1,255	3	1/4 PF
"	"	"	"	"	12,260	2,282	5	1/2 EC
"	"	"	"	"	12,260	2,282	5	1/2 PF

* Factor code forces required in ultimate strength design ($\frac{1.7}{1.33}$ x 1.25 = 1.6)

† A capacity-reduction factor of 0.9 is applied.

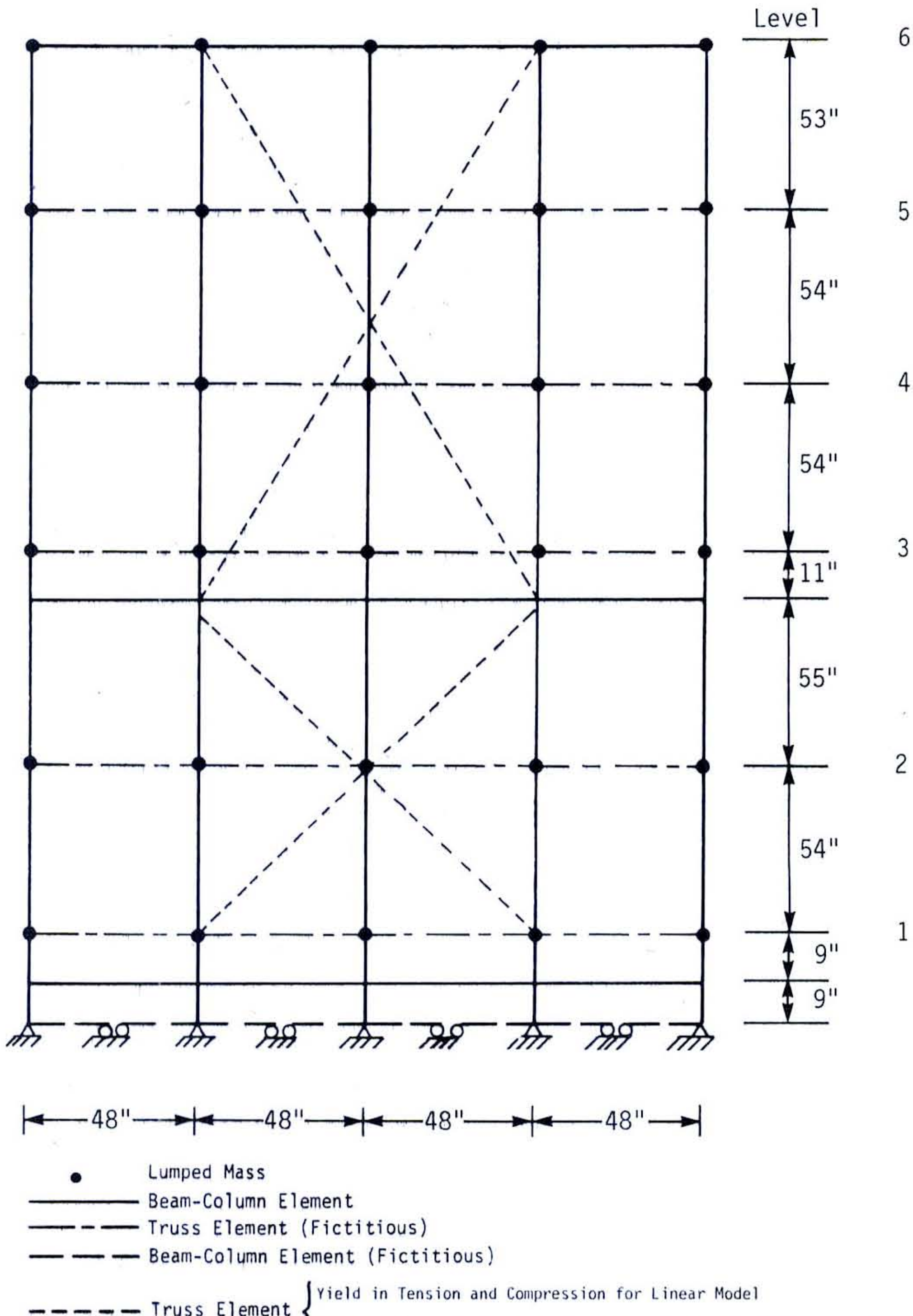

FIGURE 11.1 MATHEMATICAL MODEL (SAP IV AND DRAIN-2D) - STACKER RACK, LONGITUDINAL DIRECTION

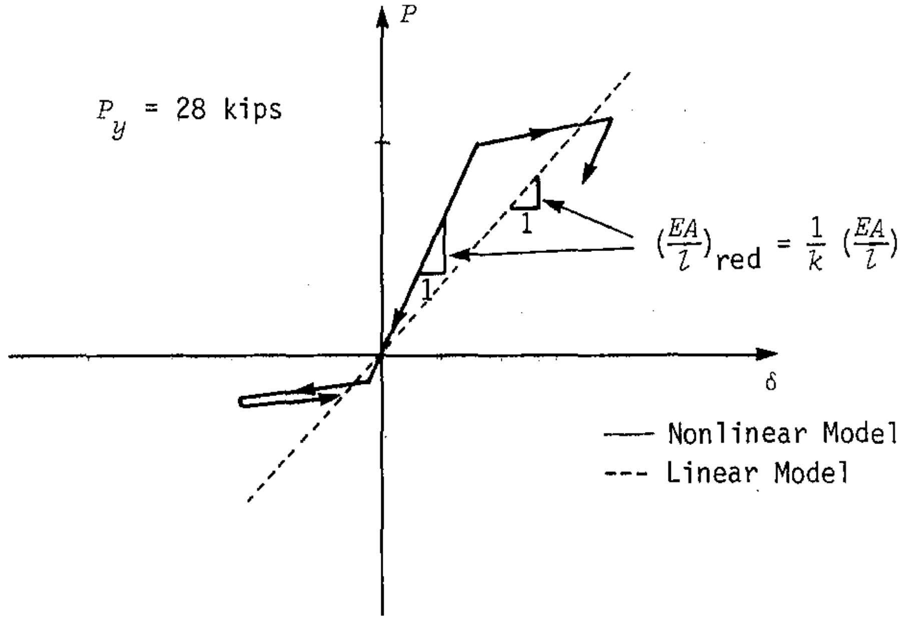

a. Bilinear Yield Mechanism for Diagonal Rods

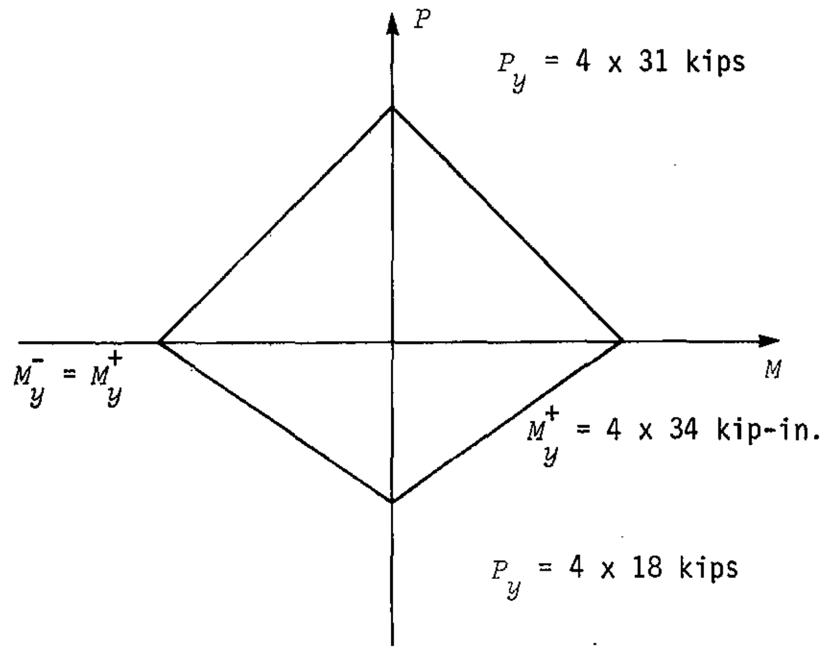

b. Yield Interaction Surface for Columns

FIGURE 11.2 YIELD MECHANISM AND INTERACTION SURFACE - STACKER RACK, LONGITUDINAL DIRECTION

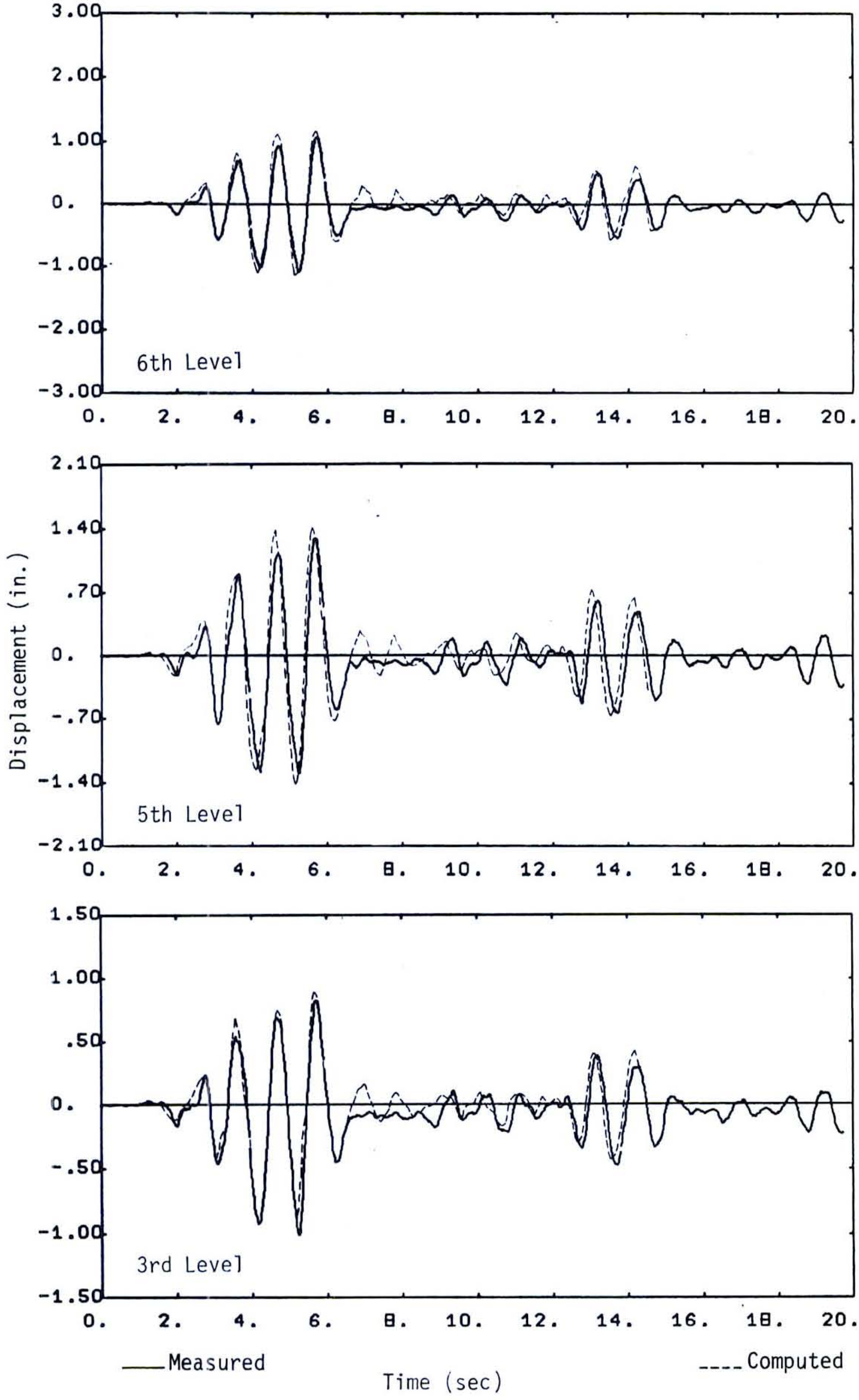

FIGURE 11.3 MEASURED AND COMPUTED STORY DISPLACEMENTS (ST-L-1-1/4 EC)

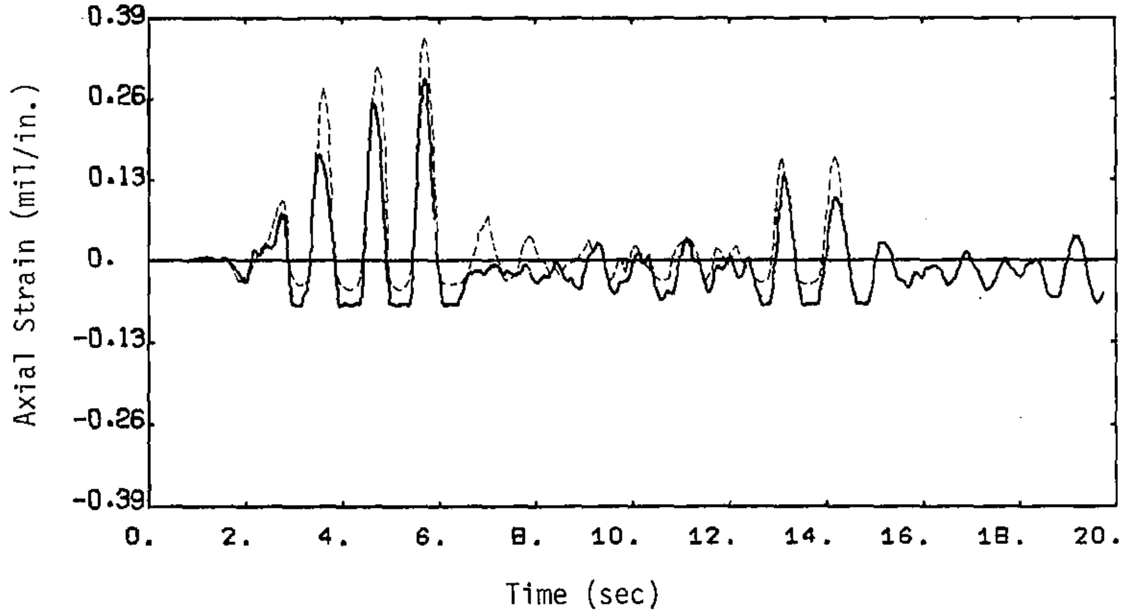

Bottom Diagonal Rod 1

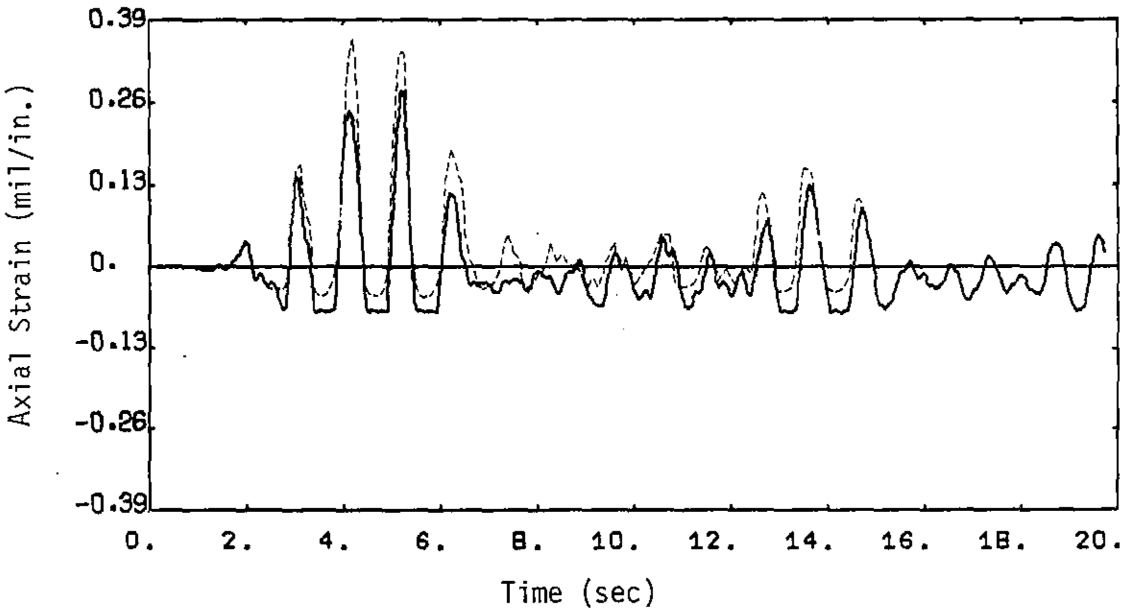

Bottom Diagonal Rod 2

——— Measured   - - - - Computed

FIGURE 11.4 MEASURED AND COMPUTED LOCAL RESPONSES (ST-L-1-1/4 EC)

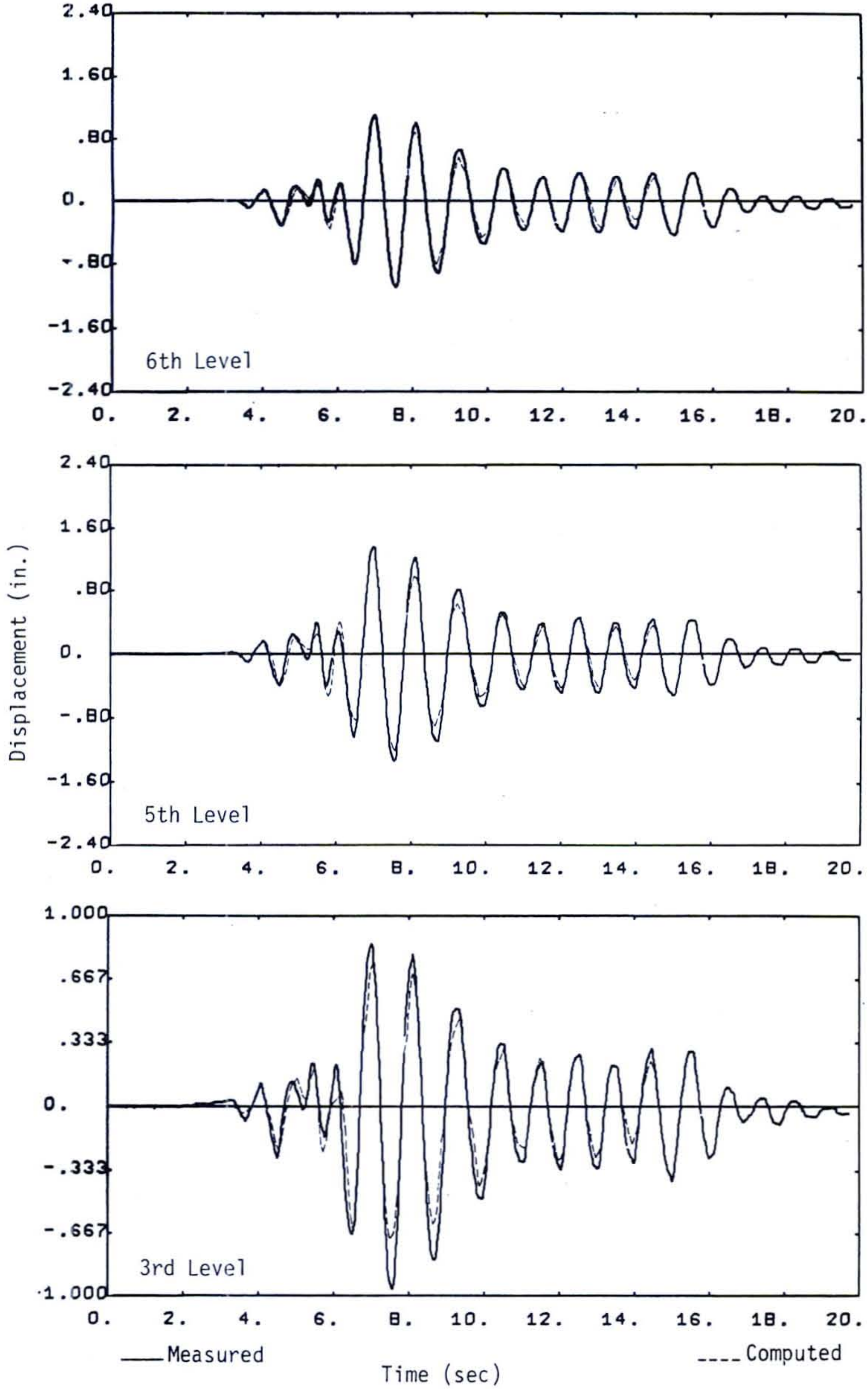

FIGURE 11.5 MEASURED AND COMPUTED STORY DISPLACEMENTS (ST-L-1-1/4 PF)

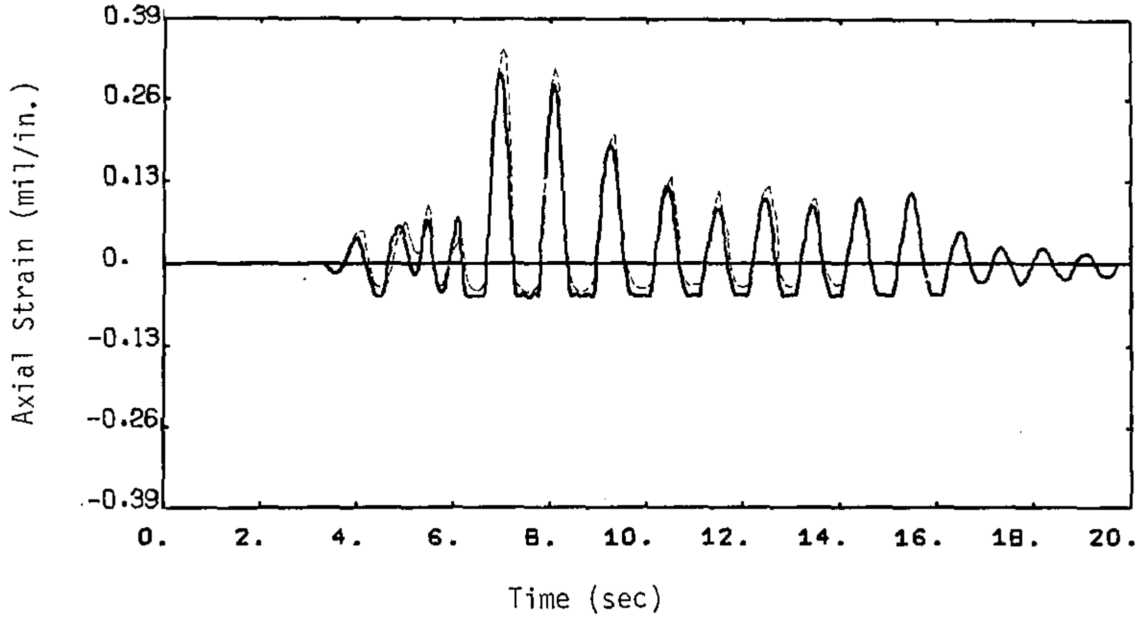

Bottom Diagonal Rod 1

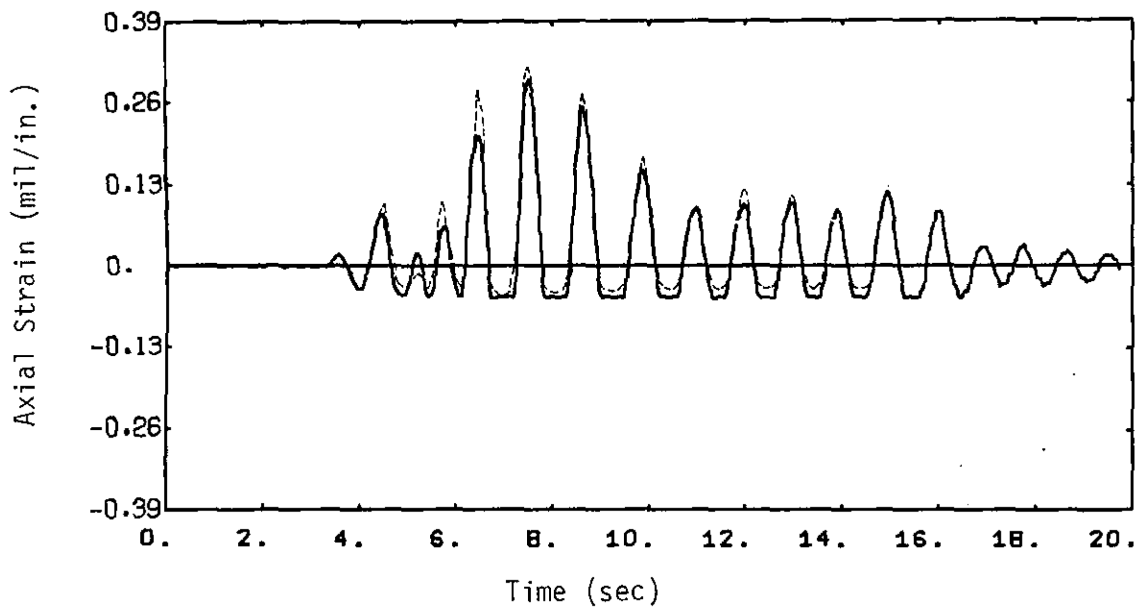

Bottom Diagonal Rod 2

——— Measured ---- Computed

FIGURE 11.6 MEASURED AND COMPUTED LOCAL RESPONSES (ST-L-1-1/4 PF)

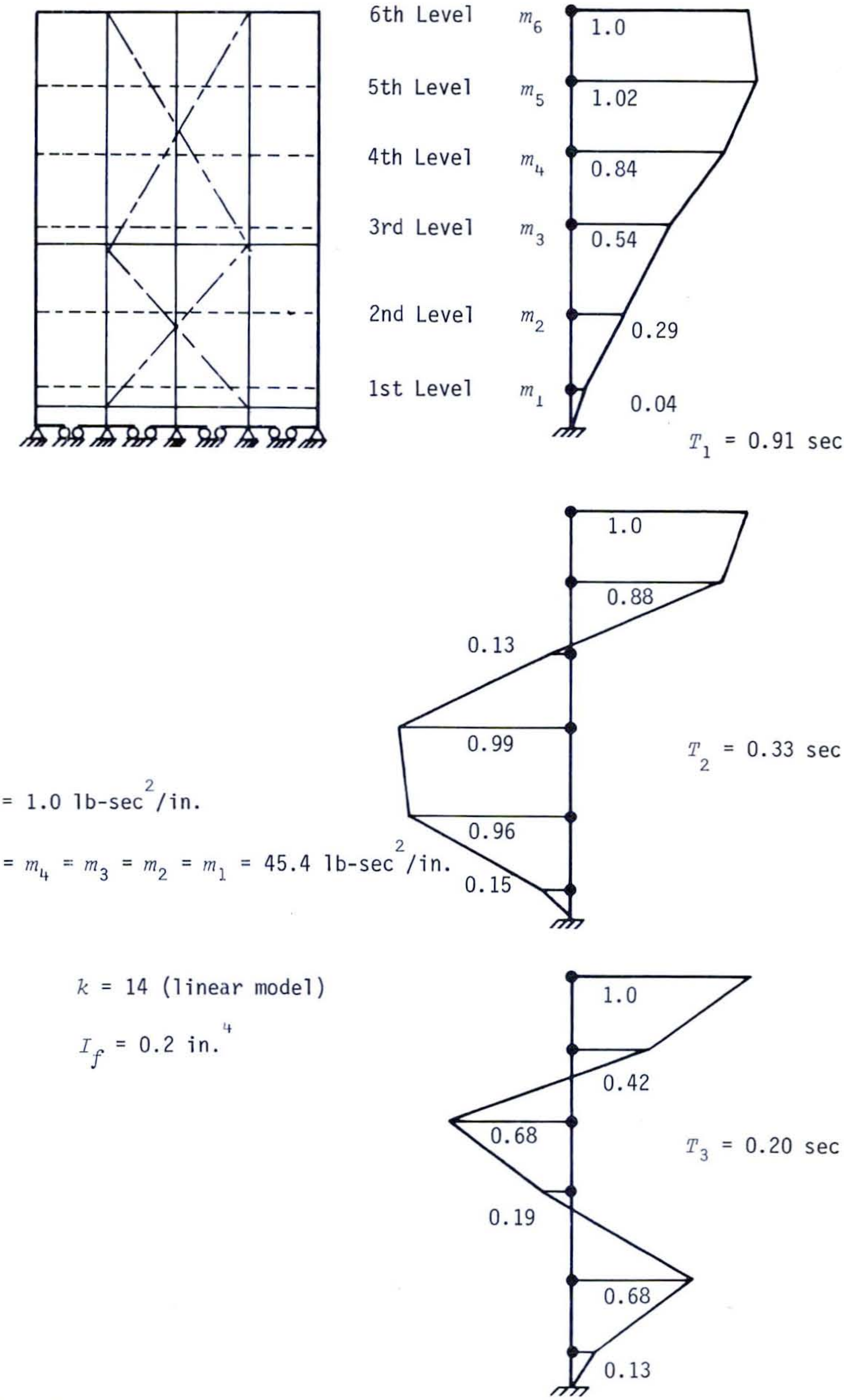

FIGURE 11.7 CALCULATED PERIODS OF VIBRATION AND MODE SHAPES - STACKER RACK, LONGITUDINAL DIRECTION

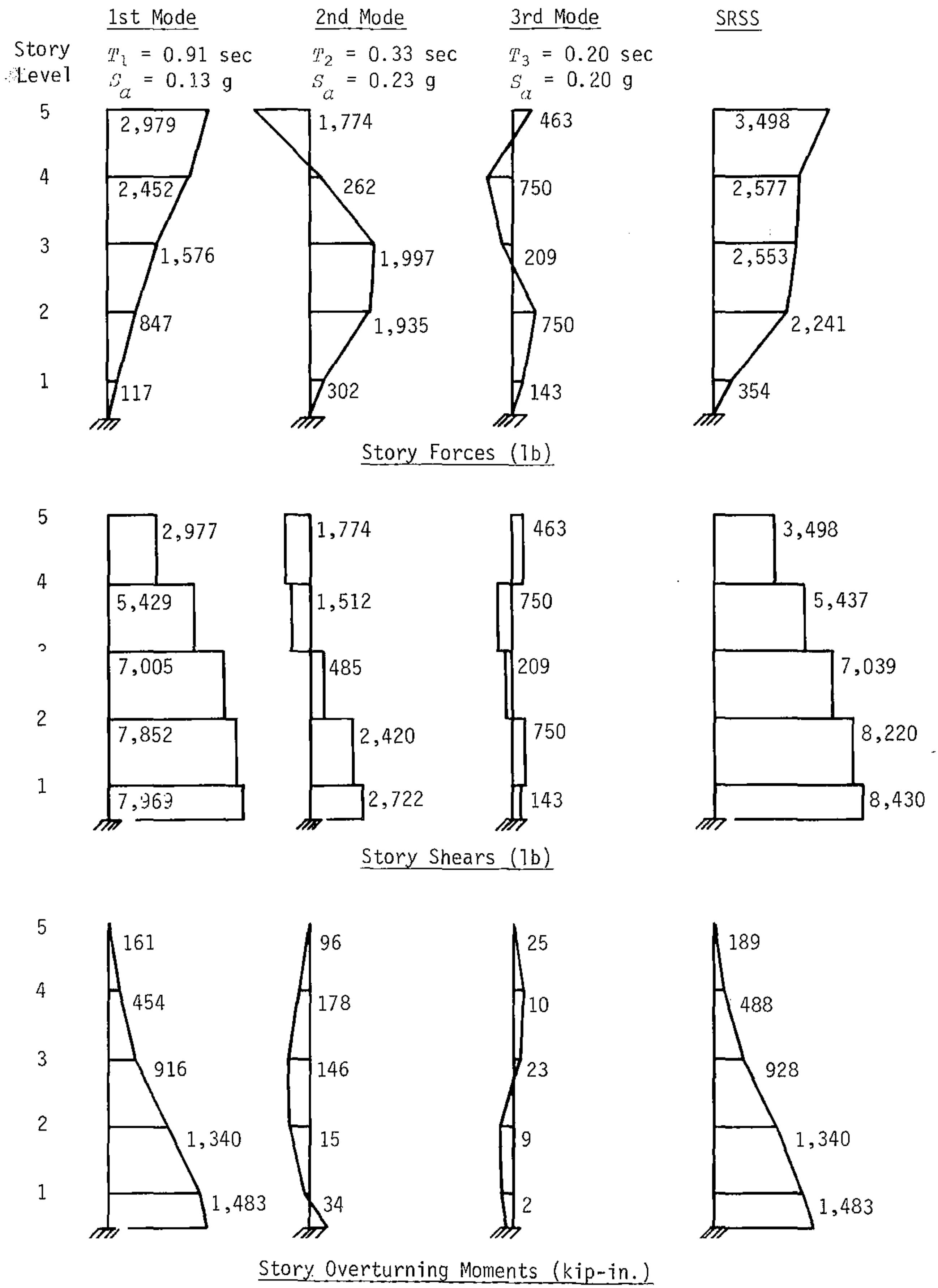

FIGURE 11.8 RESULTS OF RESPONSE SPECTRUM ANALYSIS (ST-L-1-1/4 EC)

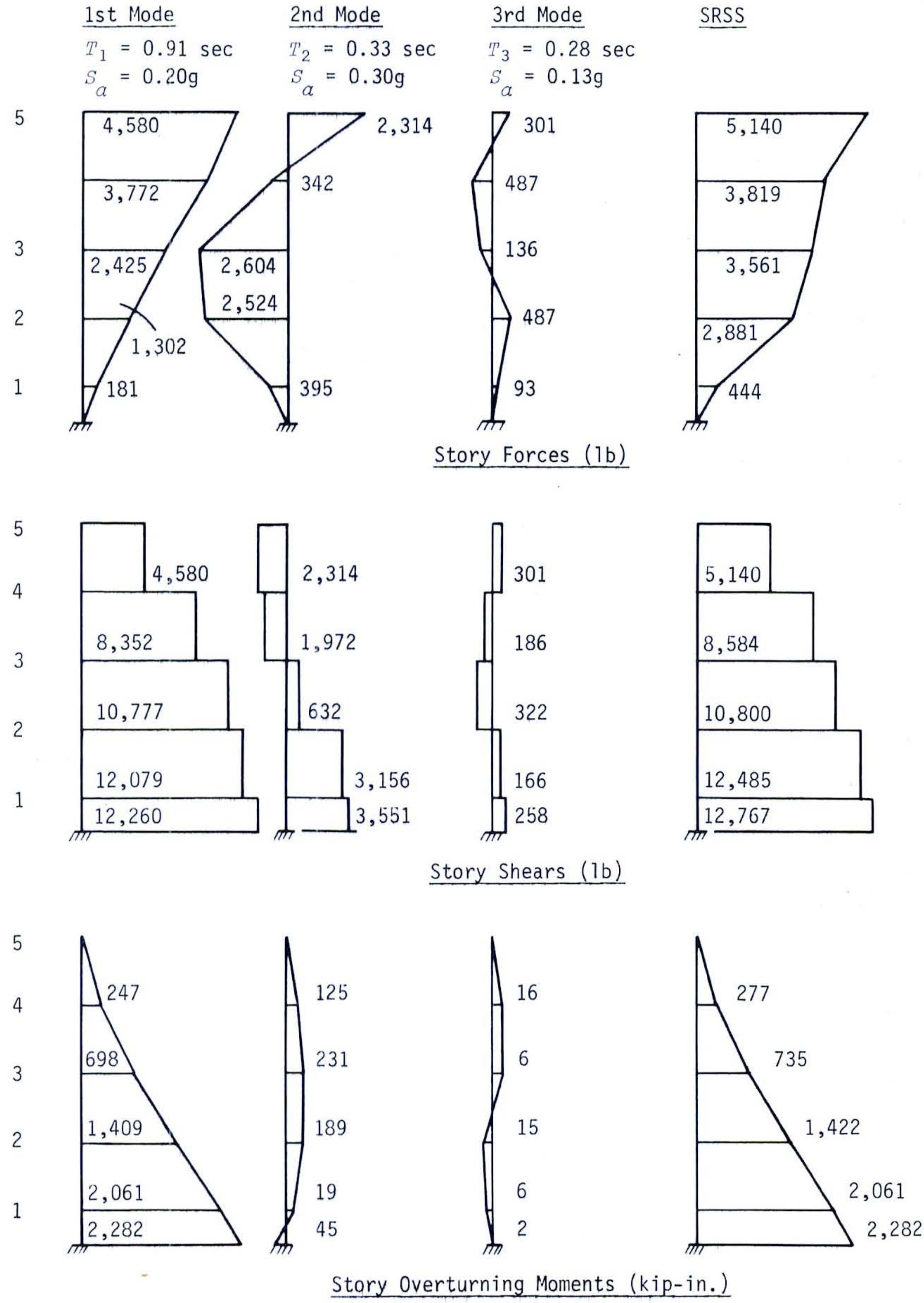

FIGURE 11.9 RESULTS OF RESPONSE SPECTRUM ANALYSIS (ST-L-1-1/2 PF)

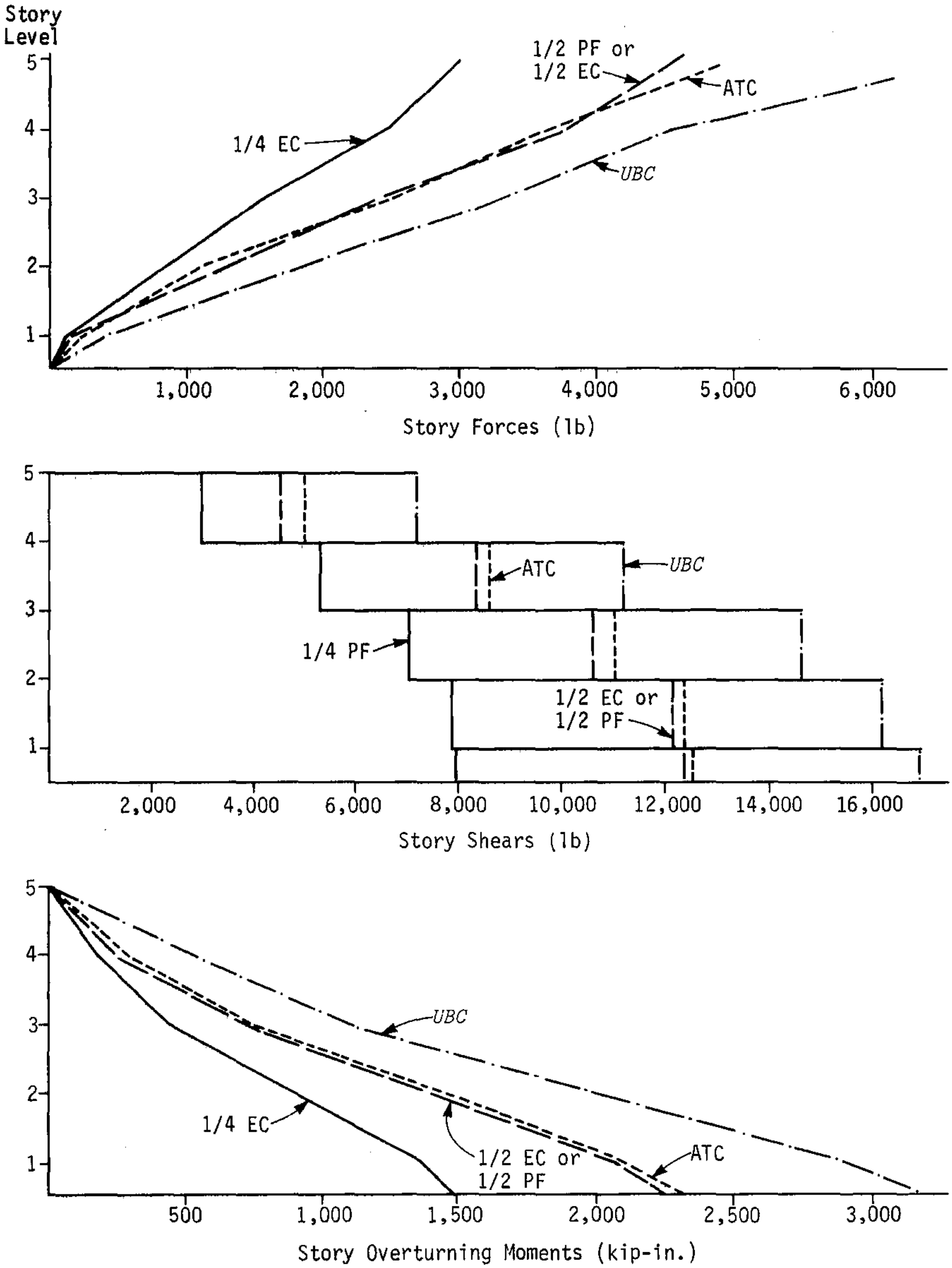

FIGURE 11.10 RESULTS OF THE *UBC* METHOD, THE ATC METHOD, AND THE RESPONSE SPECTRUM METHOD - STACKER RACK, LONGITUDINAL DIRECTION, FULL LIVE LOAD

12. THEORETICAL PREDICTION OF STRUCTURE RESPONSE--STACKER RACK, TRANSVERSE DIRECTION

12.1 Frequency Analysis

Basic Model. In the transverse direction, the stacker rack assembly consists of ten identical upright frames, which, in turn, form five double upright frames parallel to the direction of shaking table motion. Examination of the local response measurements of the column axial strains near the base plates showed antisymmetric response in phase, each upright frame responding independently. Because of this antisymmetry, an analytical model for a single upright frame, shown in Figure 12.1, was considered adequate for this rack configuration. The centerline dimensions were used, and fictitious floor beams were added to account for the semifixed column base condition. The localized deformation at the connections between the open-section columns and the open-section braces was also considered, as discussed in Section 8.1. Ten percent of the entire mass was lumped equally at the ten nodal points. Thus, the mass per story level was estimated to be about 2.47 lb-sec^2/in. for the 1/2 live load and 4.54 lb-sec^2/in. for the full live load. The mass at the sixth (top) level was very small, and, for practical purposes, it could be ignored. The minimum net section properties supplied by the manufacturer are as follows:

	Moment of Inertia (in.^{4})	Cross-sectional Area (in.^{2})	Estimated Shear Area (in.^{2})
Column	0.88	0.69	0.43
Brace	-	0.32	-

The best-fit mathematical models were established by varying the parameters I_f and k, as was done for the standard pallet rack and the drive-in rack in the transverse direction.

Comparison of Various Linear Mathematical Models. The values of k and I_f were the only parameters adjusted in the development of the best-fit mathematical model. Because no experimental data on the values of I_f and k were available, a trial-and-error procedure of assigning various combinations of

k and I_f was applied. The results are shown in Table 12.1. The first four cases used 1/2 live load, and the last two cases used full live load.

A comparison of the results from Models 1 and 2 clearly demonstrates the influence on the dynamic response properties of the localized deformation at the connections between the columns and bracing members. Model 1 assumed no local deformation (k = 1); Model 2 assigned k a value of 5.

The results from Models 3 and 4 show that the calculated dynamic properties varied very little with the changes of I_f from 0.2 in.^{4} to 3.7 in.^{4}, which is consistent with the findings for the standard pallet rack and the drive-in rack in the transverse direction.

It can be seen that Model 2 was the best-fit mathematical model when compared with the low-amplitude shaking table test results. However, the results from Model 3 compared quite well with the high-amplitude shaking table test data (with the input signal of 1/2 the El Centro record; see Table 4.21). For the full-live-load case, the results from Model 5 are seen to be in good agreement with the experimentally obtained data from the low-amplitude shaking table tests.

12.2 Time-History Analysis

Basic Model. The mathematical model used for the time-history analysis was similar to the model used for the frequency analysis except that DRAIN-2D took the place of SAP IV. The bracing members were treated as composite axial force members, and the bilinear yield mechanism shown in the upper plot of Figure 12.2 was assumed. The yielding capacities of the bracing members were estimated to be 14.4 kips and 3.1 kips, in accordance with AISI 3.6.1 ($F_{a1} > F_{a2}$, i.e., torsional-flexural buckling is critical). The yield interaction surface of the columns was assumed to be as shown in the lower plot of Figure 12.2. The detailed procedures for estimating the average compression yield capacity P_y and the bending capacity M_y of the columns were as described in Appendix A.

Results. Three cases simulated with the full live load were subjected to time-history analysis. Table 12.2 summarizes the parameters finally adopted for each case. These parameters yielded the best possible analytical results in comparison with the corresponding experimental data. It can be seen from the table that all parameters for the time-history analysis remained essentially the same as those used in the frequency analysis of the best-fit linear models. The damping, the yield mechanism, and the interaction surface of members were the only new parameters used in the time-history response analysis. The analysis was carried out with an integration time step of about 0.0196 sec, the same time interval as for digitization of recorded data. Because the time-history response was primarily in the first mode (0.63 sec to 0.76 sec), this was considered to be adequate for numerical stability.

Case 1 (ST-T-1-1/4 EC). For this case, the model was subjected to an input signal of approximately 1/4 that of the actual El Centro record. Mass-proportional damping corresponding to about 3% of the first-mode viscous damping was assigned. The parameters k and I_f were assumed to be 7 and 0.2, respectively. Correlations between the story displacements relative to the table predicted with this model and the results obtained experimentally are presented in Figure 12.3. The model successfully predicted the two significant stages of response. The correlation during the early stage is considered excellent; the predicted amplitudes in the late stage are slightly higher than the measured data. Figure 12.4 shows good correlation in local responses between the predicted results and the measured results.

Case 2 (ST-T-1-1/4 PF). For this model, all model parameters and member properties used in Case 1 remained unchanged except that the input signal was changed to 1/4 the Parkfield record. A comparison of the measured and computed story displacements relative to the table as shown in Figure 12.5 is considered excellent. Figure 12.6 presents the measured and computed local responses. It can be seen from the upper plot of this figure that the correlation between the measured and predicted axial strains of the bottom story diagonal brace is excellent, whereas the agreement between the measured and computed axial strains of the bottom floor column is good in phase but poor in magnitude. Some permanent set that was not predicted by the analysis was shown from the measurements of the column axial strain.

Case 3 (ST-T-1-1/2 PF). In the shaking table tests with the input signal of 1/2 the Parkfield record, all interior bottom diagonal braces failed in torsional-flexural buckling and some minor distress was observed for all interior columns near the base plates. For the analytical study, a value of 12 was used for the model parameter k rather than 7 as was used in the two previous cases, which had lower-amplitude input excitation. Mass-proportional damping corresponding to about 5% of the first-mode viscous damping was assigned to the model.

Figure 12.7 shows the results obtained from this model and from the experiments. The upper two plots show the measured and predicted story displacements, and the bottom plot shows the diagonal axial strains. The agreement between computed and measured story displacements is considered excellent. The correlation of diagonal axial strains was not as good; however, the analytical estimates of strain magnitude are considered adequate. The permanent set as shown in the experimental plot during the latter stage of response is due to structural damage caused by torsional-flexural buckling of the bottom diagonal.

12.3 Response Spectrum Analysis

The four cases analyzed by the response spectrum method are summarized in Table 12.3. The response spectra corresponding to each case were shown previously in Figures 4.18 and 4.19. It can be seen from the table that the effects on the base shears and overturning moments of higher-mode participation were negligible. The results from two individual cases were selected for presentation in this report. Figure 12.8 shows the calculated periods of vibration and mode shapes from the frequency analysis. Figures 12.9 and 12.10 present the story forces, story shears, and story overturning moments for various modes of vibration when the model was subjected to input signals of 1/4 the Parkfield record and 1/2 the El Centro record. These figures clearly demonstrate that the higher-mode contribution to the response was negligible.

12.4 *UBC* and ATC-3 Methods

The base shears determined from the *UBC* and ATC methods are presented in Table 12.4. The fundamental period of vibration used in the base shear calculations was determined from the frequency analysis of the best-fit mathematical model. The parameter K was set at 1.33 for the *UBC* method, and R was set at 4.0 for the ATC method. Table 12.4 also shows the other parameters relating to the use of these two code methods. Note that the best site condition was assumed in the base shear calculation.

Table 12.5 shows the base shears and overturning moments for ultimate strength design as determined by the *UBC* method, the ATC method, and the response spectrum method. As required in ultimate strength design, a factor of 1.6 was applied to the results from the *UBC* method, and a reduction factor of 0.9 was applied to the results from the ATC method.

The base story forces for ultimate strength design from the *UBC* are approximately equivalent to those from the response spectrum method using 1/2 the El Centro signal but smaller than those using 1/2 the Parkfield signal. This is clearly shown in Figure 12.11 and in Table 12.5. However, if the worst site condition were assumed (i.e., $S = 1.5$), the results from the *UBC* method would be about equivalent to those using 1/2 the Parkfield signal.

A general discussion of the adequacy and limitations of the various analysis methods is presented in Chapter 13.

TABLE 12.1

LINEAR MATHEMATICAL MODELS -

STACKER RACK, TRANSVERSE DIRECTION

Model	Live Load	Column Base		Brace Element		Period* (sec)			Mode Shape*		
		Case	I_f	k	$(EA)'$	1	2	3	1	2	3
1	1/2	semi-fixed	0.2	1	9,440	0.30	0.10	0.07	1.00 0.86 0.69 0.50 0.27 0.15	1.00 0.62 0.05 -0.61 -0.77 -0.72	1.00 0.66 -0.21 -1.69 0.62 1.40
2	"	"	0.2	5	1,888	0.42	0.14	0.08	1.00 0.91 0.77 0.59 0.33 0.11	1.00 0.71 0.04 -0.70 -0.85 -0.43	1.00 0.68 -0.62 -1.07 1.02 0.94
3	"	"	0.2	7	1,349	0.47	0.15	0.09	1.00 0.93 0.79 0.61 0.34 0.10	1.00 0.73 0.04 -0.71 -0.87 -0.37	1.00 0.66 -0.66 -0.94 1.04 0.78
4	"	"	3.7	7	1,349	0.46	0.14	0.09	1.00 0.92 0.78 0.59 0.30 0.07	1.00 0.73 0.08 -0.77 -0.81 -0.25	1.00 0.65 -0.75 -0.84 1.26 0.60
5	full	"	0.2	7	1,349	0.63	0.20	0.13	1.00 0.93 0.80 0.61 0.34 0.10	1.00 0.75 0.06 -0.71 -0.87 -0.37	1.00 0.70 -0.65 -0.98 1.06 0.79
6	"	"	0.2	12	787	0.76	0.24	0.15	1.00 0.94 0.82 0.64 0.35 0.09	1.00 0.77 0.52 -0.73 -0.88 -0.31	1.00 0.66 -0.67 -0.81 1.03 0.60

I_f = Moment of inertia of fictitious floor beam (in.^{4})

k = Factor to take into account local deformation at the brace-column connection

$(EA)'$ = Reduced section properties of bracing member (kips)

*Experimentally determined fundamental period and mode shapes are:

Period: 1/2 Live Load: T_1 = 0.41 - 0.43 sec; Full Live Load: T_1 = 0.56 - 0.65 sec

Mode Shape (Average): 1st Mode

1.00
0.84
0.72
0.55
0.30
0.09

TABLE 12.2

MODELING PARAMETERS FOR TIME-HISTORY ANALYSIS - STACKER RACK, TRANSVERSE DIRECTION

Case	Designation	Live Load	Input Signal	Column			Brace		Column Base	Damping		Remarks
				I_c (in.^{4})	A_c (in.^{2})	A'_c (in.^{2})	k	$(EA)'$ (kips)	I_f (in.^{4})	α	λ (%)	
1	ST-T-1-1/4 EC	full	1/4 EC	0.88	0.69	0.43	7	1,349	0.2	0.63	3	linear response
2	ST-T-1-1/4 PF	"	1/4 PF	"	"	"	7	1,349	"	0.63	3	nonlinear response
3	ST-T-1-1/2 PF	"	1/2 PF	"	"	"	12	787	"	0.84	5	"

Notes: Full live load = 4.54 lb-sec^2/in. per story level (per frame)

A'_c = estimated shear area for column

TABLE 12.3

SUMMARY OF RESULTS FROM RESPONSE SPECTRUM ANALYSIS - STACKER RACK, TRANSVERSE DIRECTION

Case	Designation	Live Load	Input Signal		Base Shear (lb)		Base Over-turning Moment (kip-in.)	
			Signal	Damping (%)	1st Mode	SRSS	1st Mode	SRSS
1	ST-T-1-1/4 EC	full	1/4 EC	3	1,235	1,258	219	219
2	ST-T-1-1/4 PF	"	1/4 PF	3	1,372	1,376	243	243
3	ST-T-1-1/2 EC	"	1/2 EC	5	1,921	1,959	335	335
4	ST-T-1-1/2 PF	"	1/2 PF	5	2,401	2,406	426	426

TABLE 12.4
DETERMINATION OF BASE SHEAR USING THE *UBC* METHOD AND THE ATC METHOD - STACKER RACK, TRANSVERSE DIRECTION

Live Load	T (sec)	W (lb)	1976 *UBC*		ATC-3	
			C	V (lb)	C_s	V (lb)
Full	0.63	8,800	0.084	1,162	0.164	1,443
			$V = ZIKCSW$ $C = \dfrac{1}{15\sqrt{T}}$ $K = 1.33$ $I = Z = 1.0$ $S = 1.2$ (minimum)		$V = C_s W$ $C_s = \dfrac{1.2\ A_v S}{RT^{2/3}}$ $A_v = 0.4$ $S = 1.0$ (minimum) $R = 4.0$	

TABLE 12.5

BASE STORY FORCES FOR ULTIMATE STRENGTH DESIGN - STACKER RACK, TRANSVERSE DIRECTION

Live Load	*UBC* Method*		ATC Method†		Response Spectrum Method			
	Base Shear (lb)	Base Overturning Moment (kip-in.)	Base Shear (lb)	Base Overturning Moment (kip-in.)	1st Mode Base Shear (lb)	1st Mode Base Overturning Moment (kip-in.)	Damping (%)	Signal
Full	1,859	340	1,603	298	1,235	219	3	1/4 EC
"	"	"	"	"	1,372	243	3	1/4 PF
"	"	"	"	"	1,921	335	5	1/2 EC
"	"	"	"	"	2,401	426	5	1/2 PF

* Factor code forces required in ultimate strength design ($\frac{1.7}{1.33}$ x 1.25 = 1.6)

† A capacity-reduction factor of 0.9 is applied.

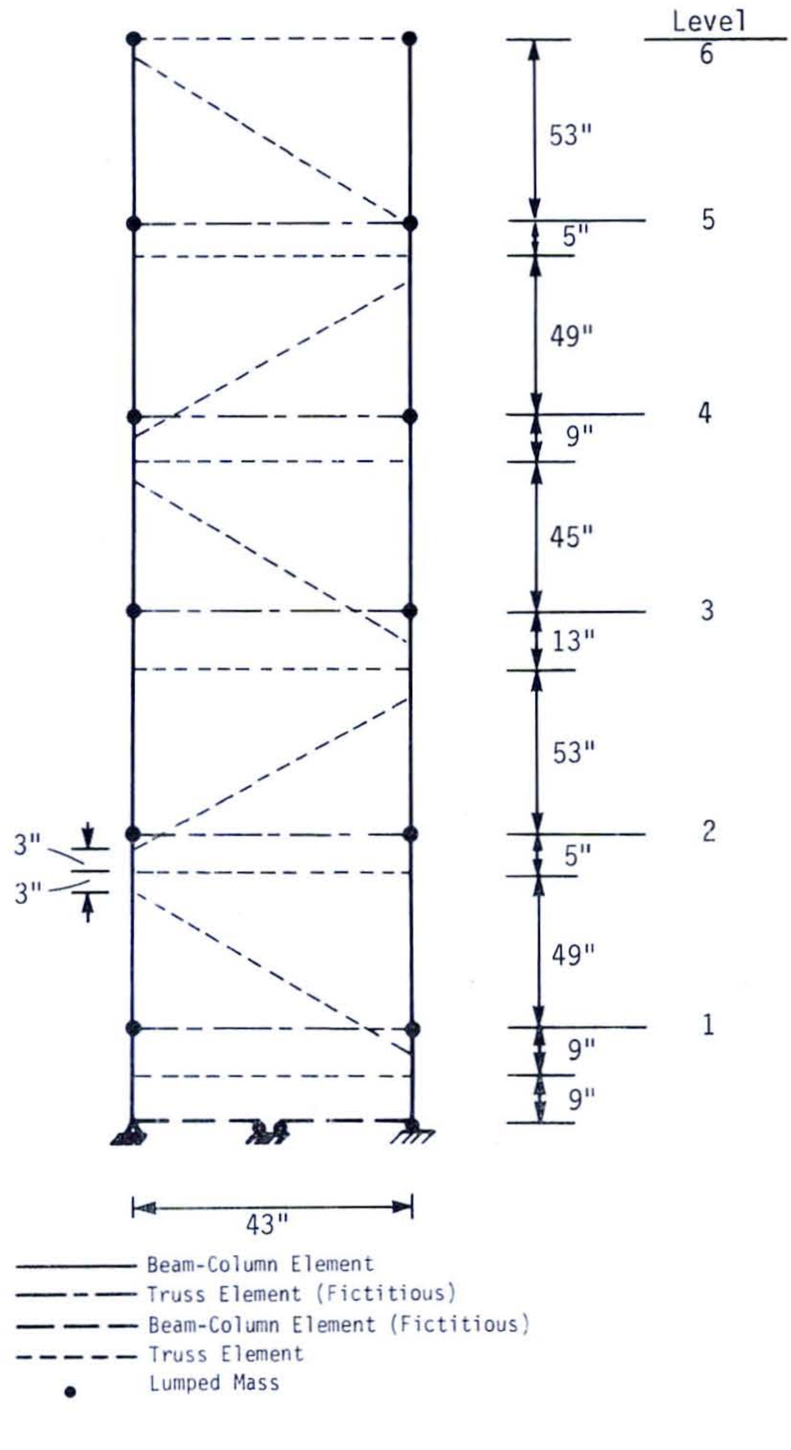

FIGURE 12.1 MATHEMATICAL MODEL (SAP IV AND DRAIN-2D) - STACKER RACK, TRANSVERSE DIRECTION

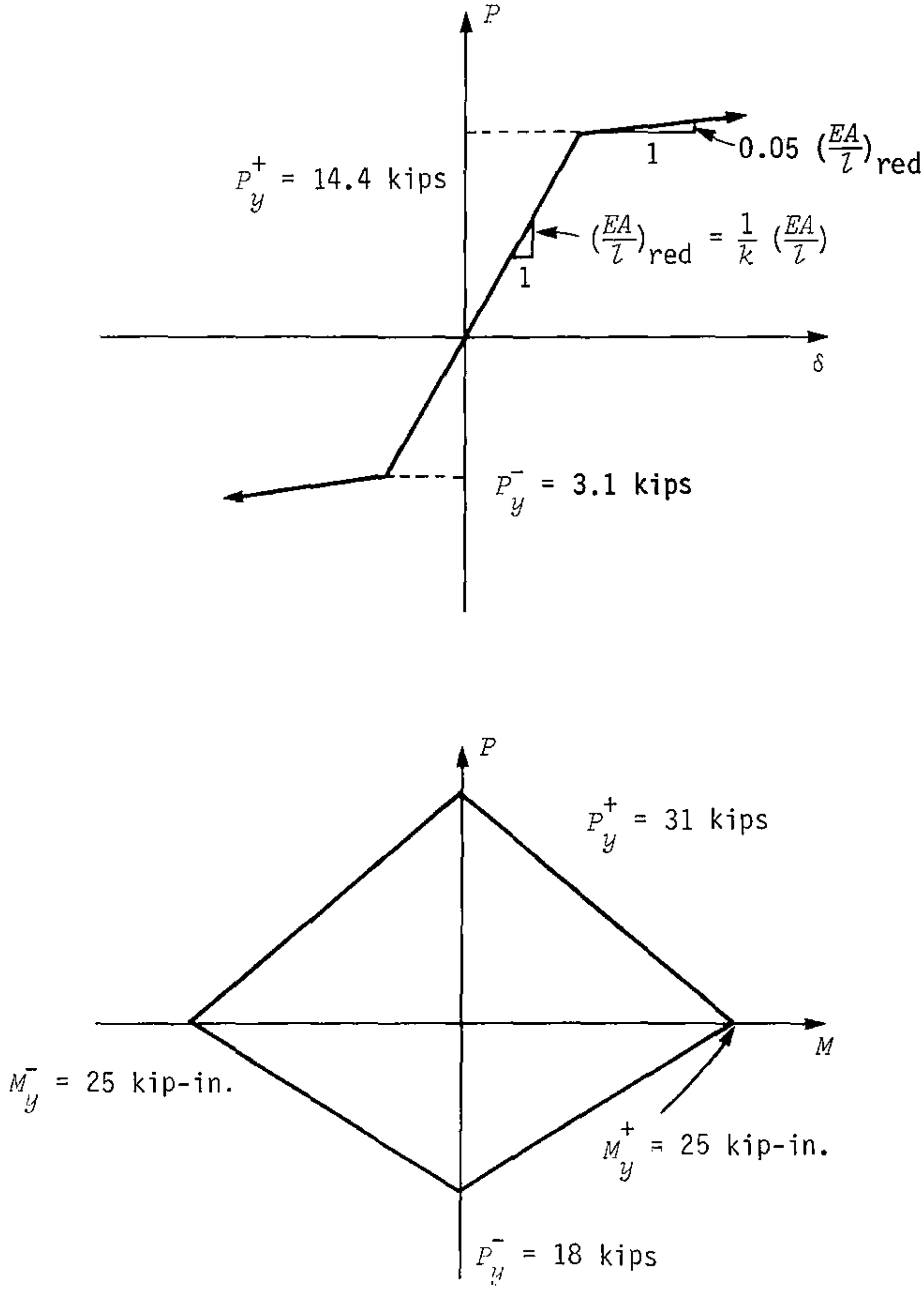

FIGURE 12.2 YIELD MECHANISM AND INTERACTION SURFACE - STACKER RACK, TRANSVERSE DIRECTION

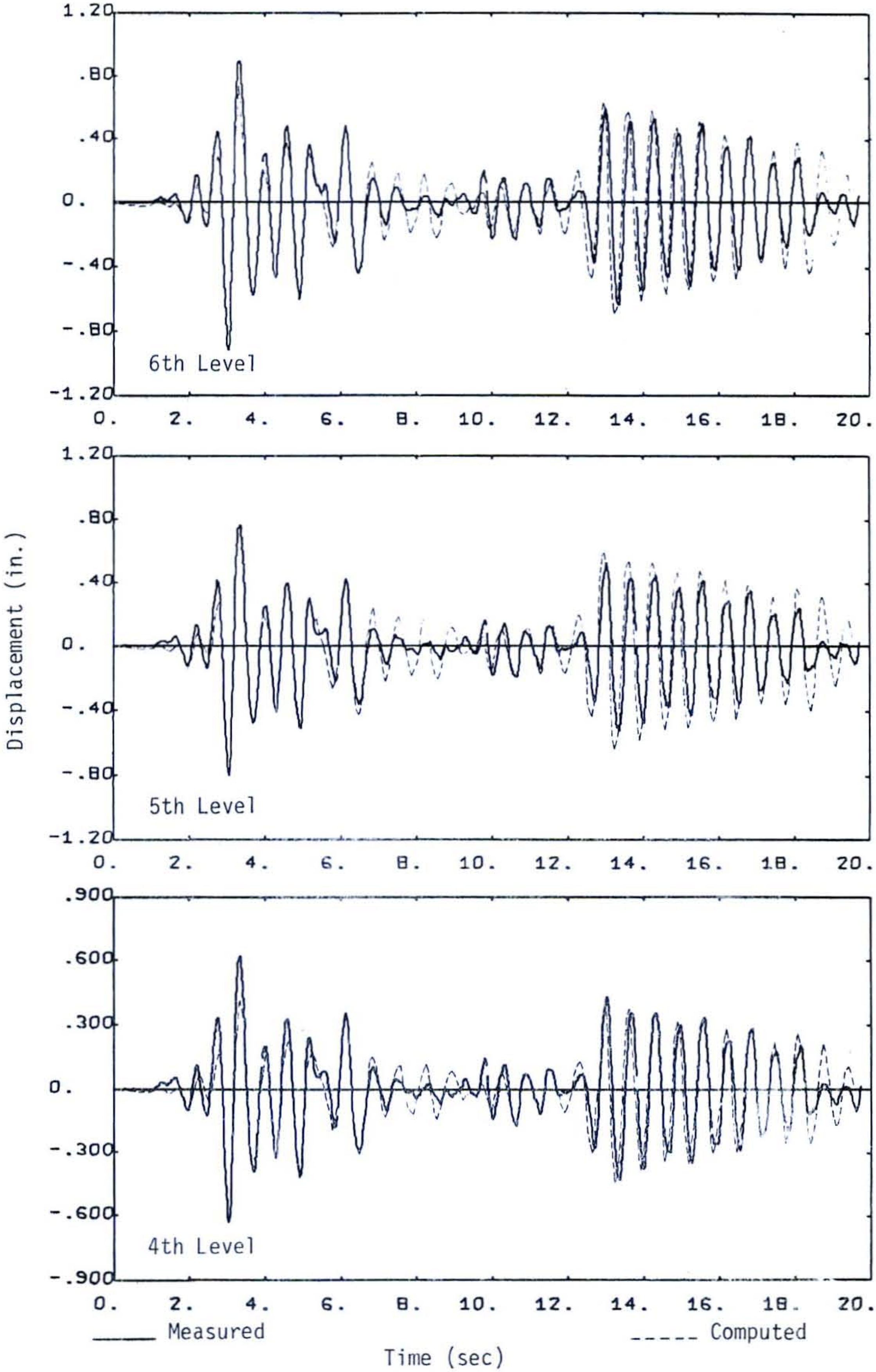

FIGURE 12.3 MEASURED AND COMPUTED STORY DISPLACEMENTS (ST-T-1-1/4 EC)

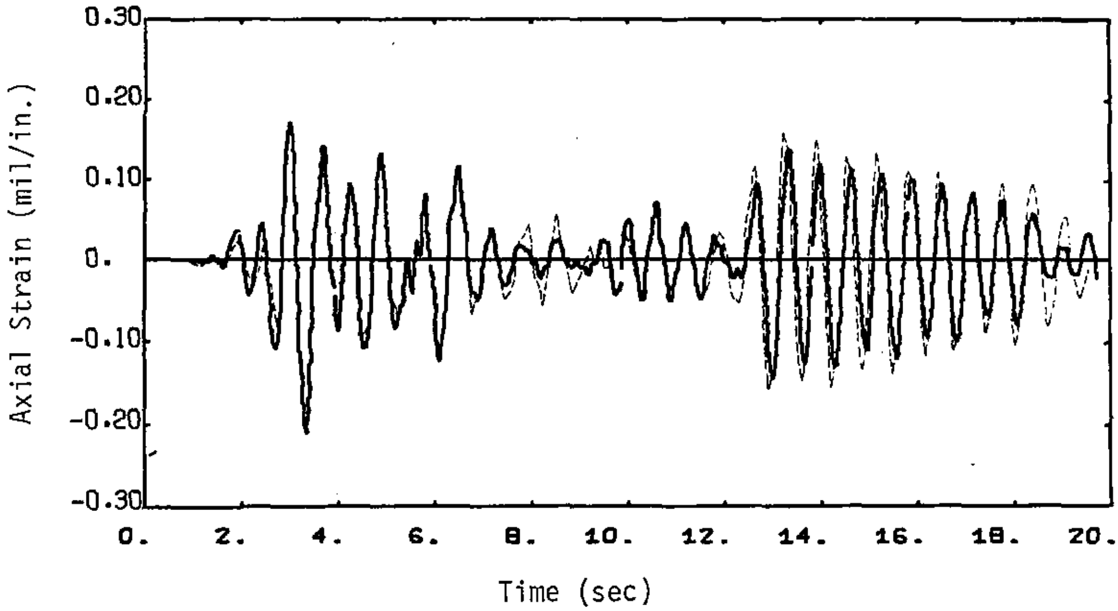

Bottom Floor Diagonal

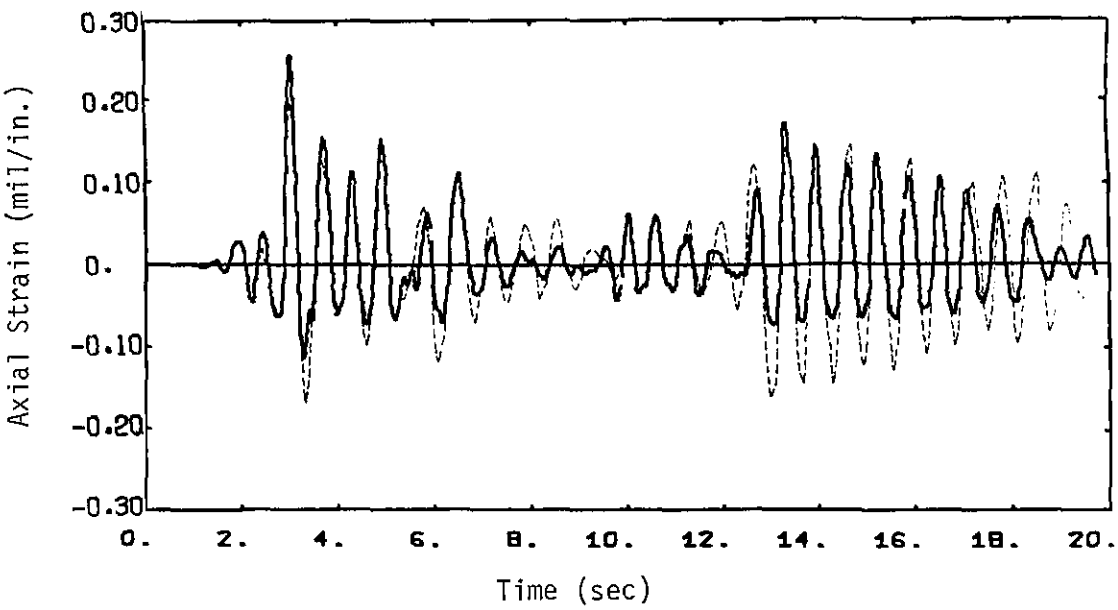

Bottom Floor Column

——— Measured

– – – – Computed

FIGURE 12.4 MEASURED AND COMPUTED LOCAL RESPONSES (ST-T-1-1/4 EC)

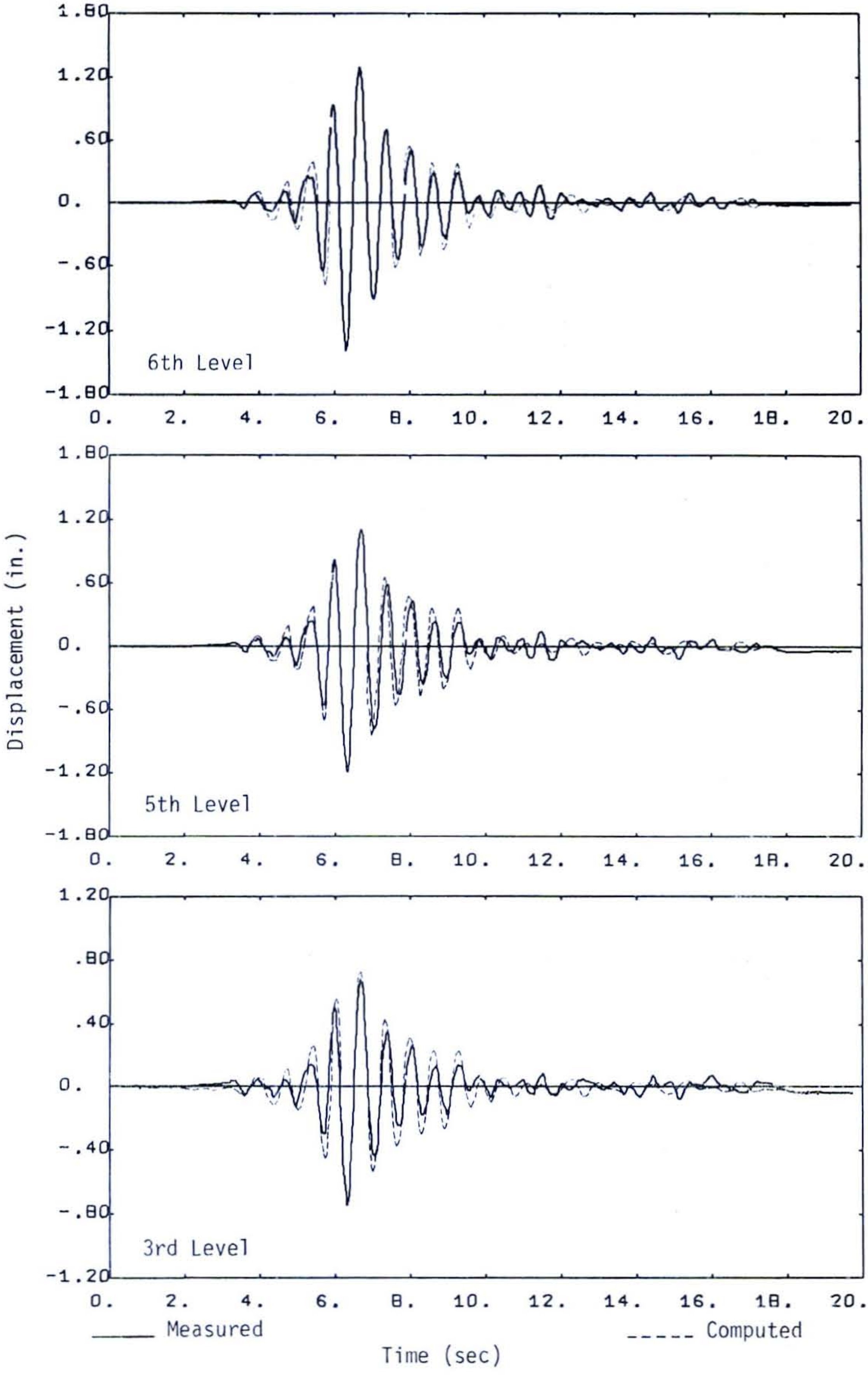

FIGURE 12.5 MEASURED AND COMPUTED STORY DISPLACEMENTS (ST-T-1-1/4 PF)

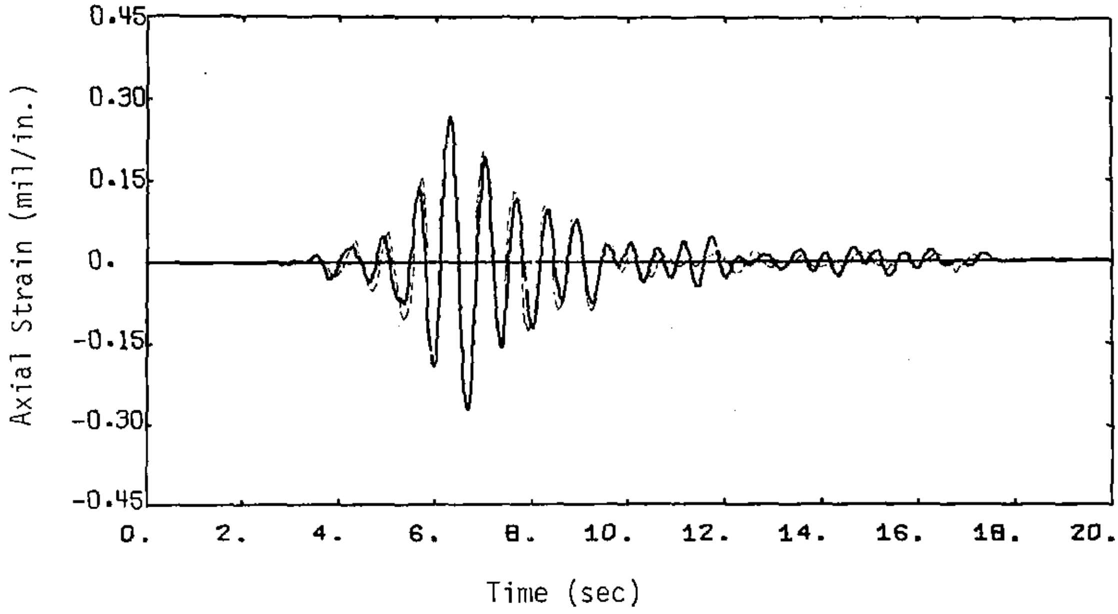

Bottom Floor Diagonal

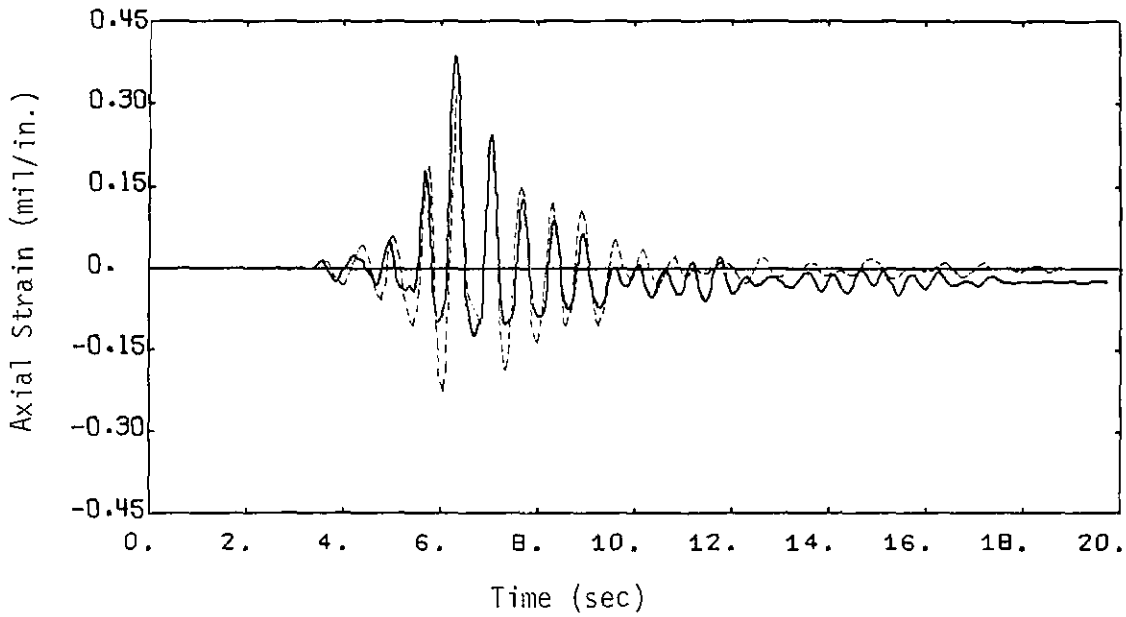

Bottom Floor Column

——— Measured —— —— Computed

FIGURE 12.6 MEASURED AND COMPUTED LOCAL RESPONSES (ST-T-1-1/4 PF)

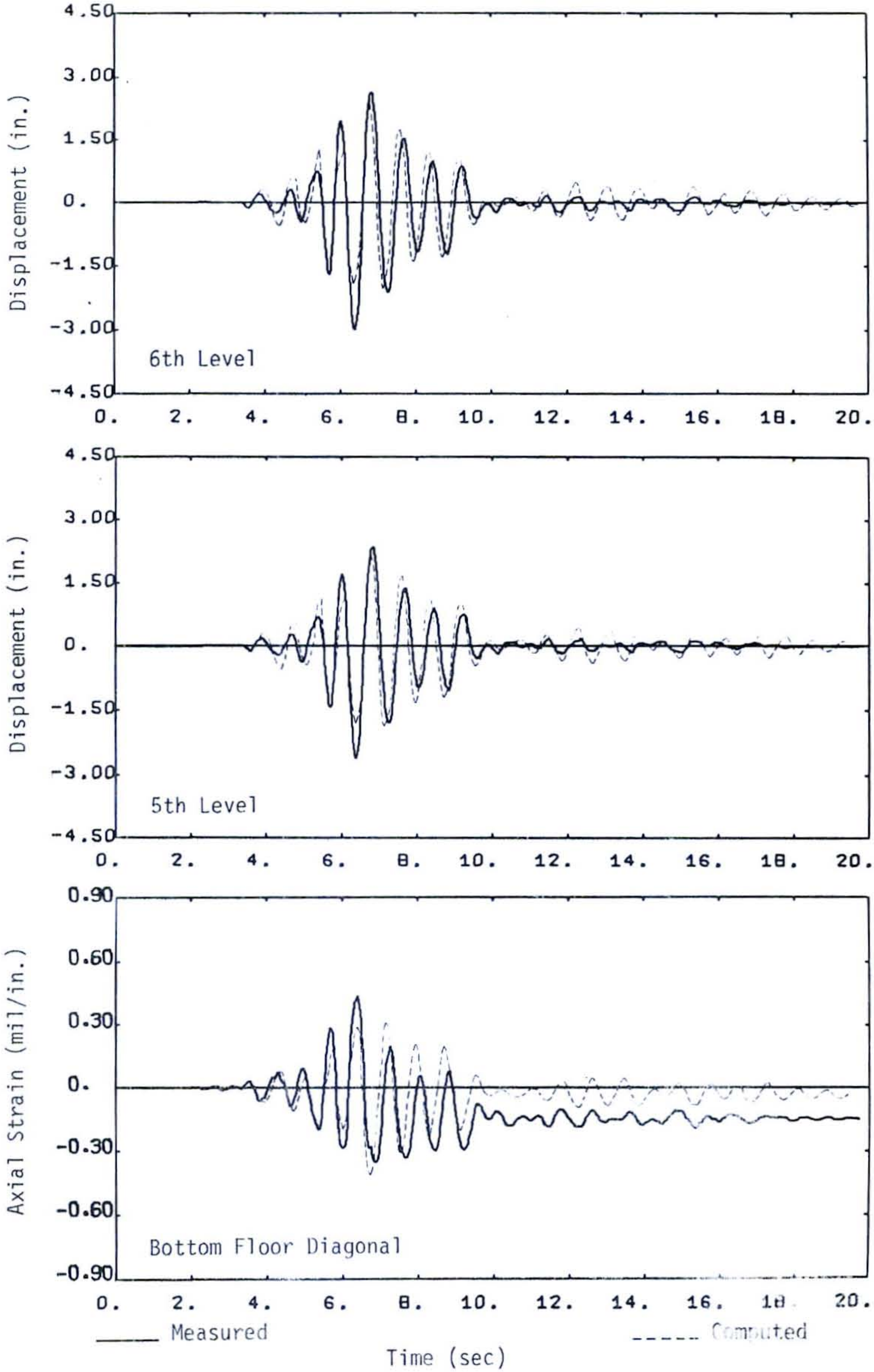

FIGURE 12.7 MEASURED AND COMPUTED RESULTS
(ST-T-1-1/2 PF)

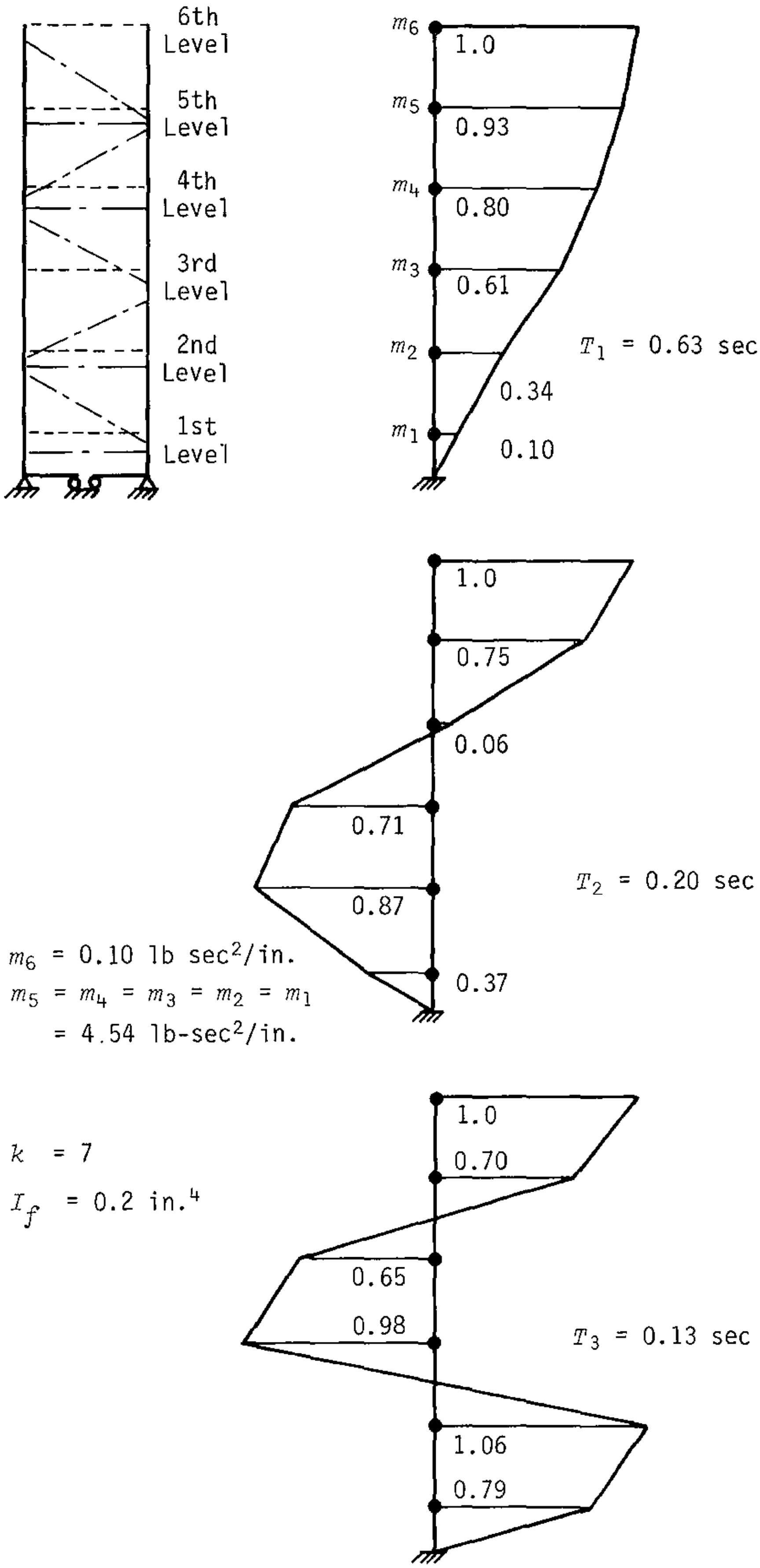

FIGURE 12.8 CALCULATED PERIODS OF VIBRATION AND MODE SHAPES - STACKER RACK, TRANSVERSE DIRECTION, FULL LIVE LOAD

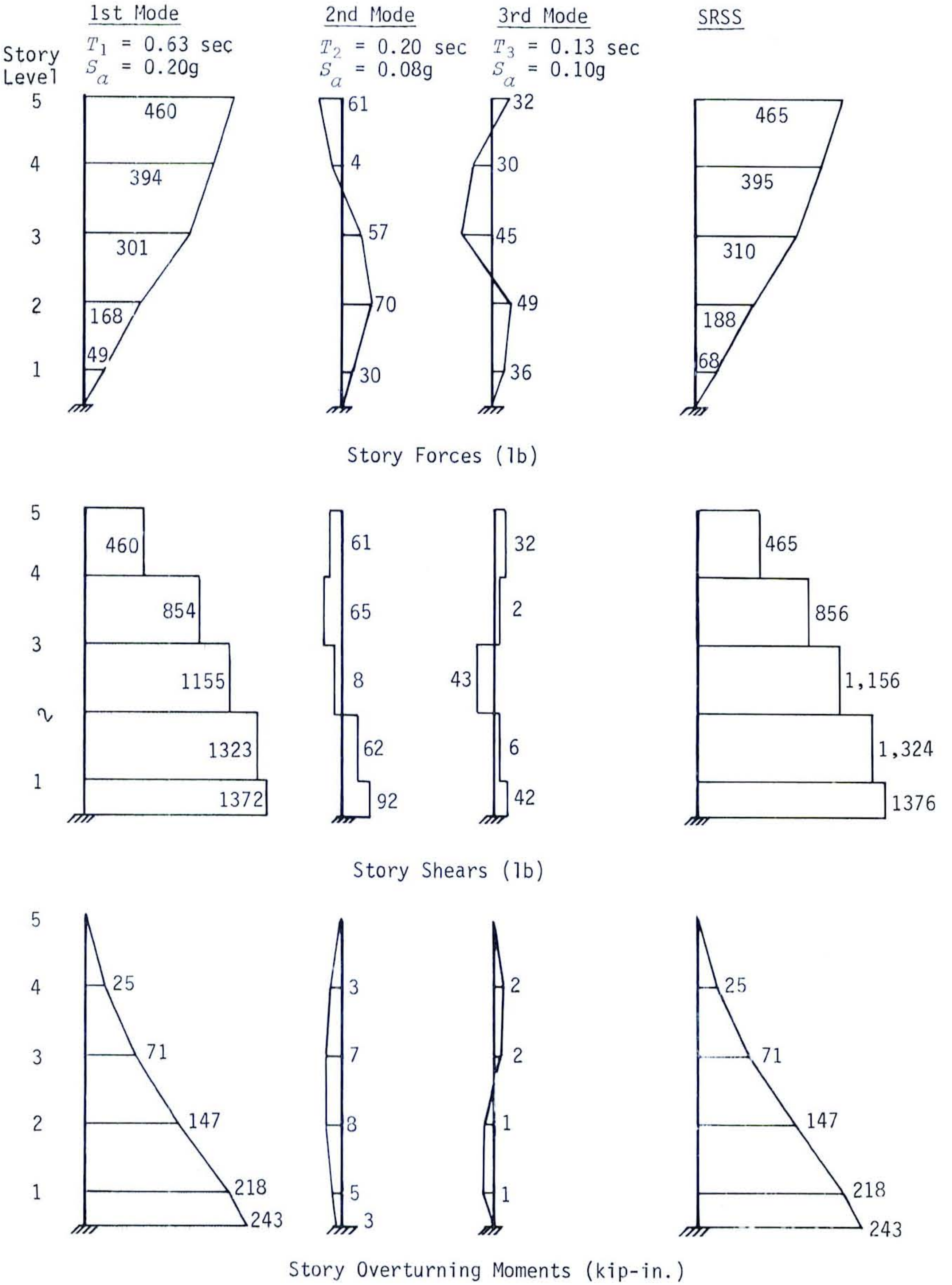

FIGURE 12.9 RESULTS OF RESPONSE SPECTRUM ANALYSIS (ST-T-1-1/4 PF)

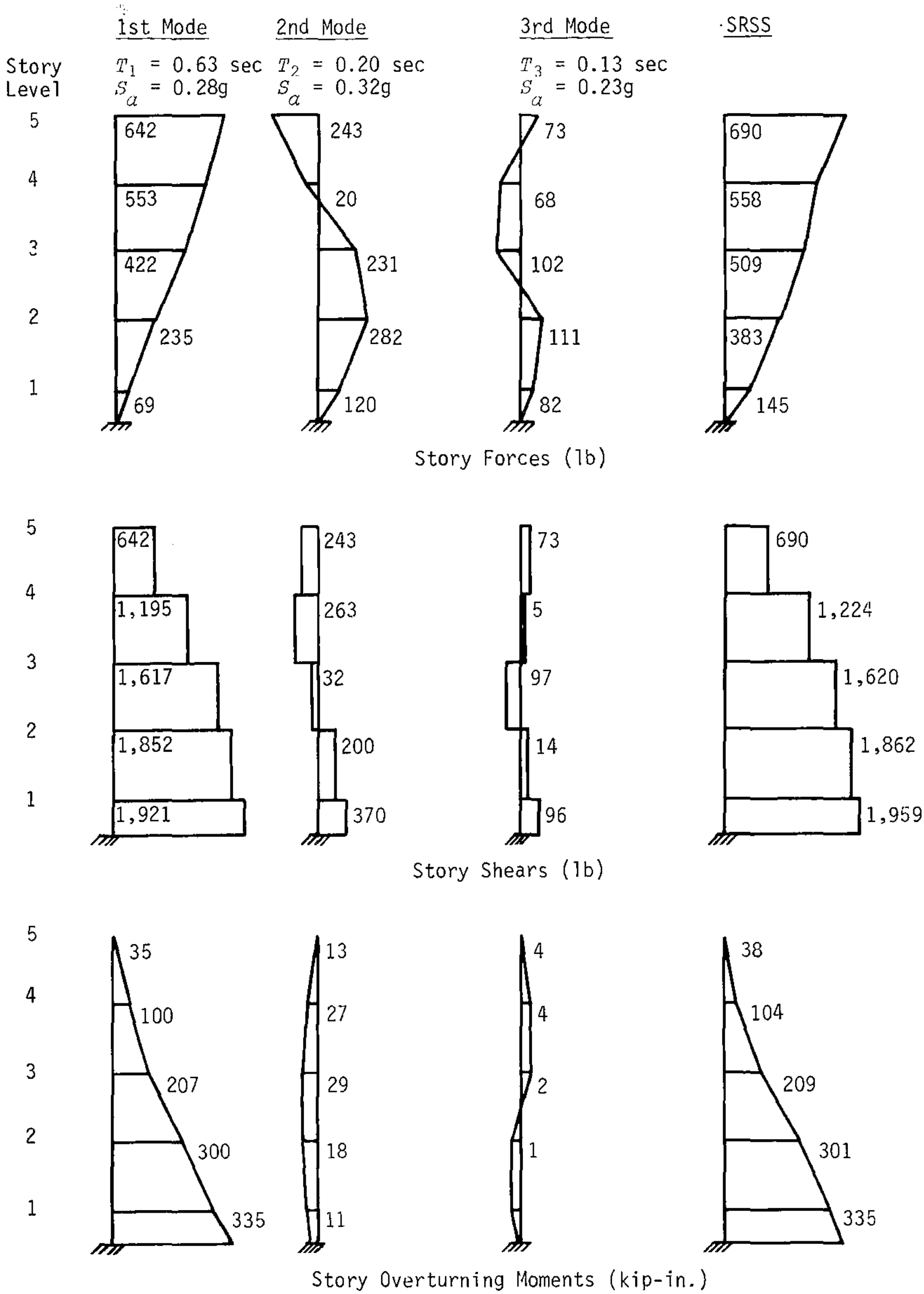

FIGURE 12.10 RESULTS OF RESPONSE SPECTRUM ANALYSIS
(ST-T-1-1/2 EC)

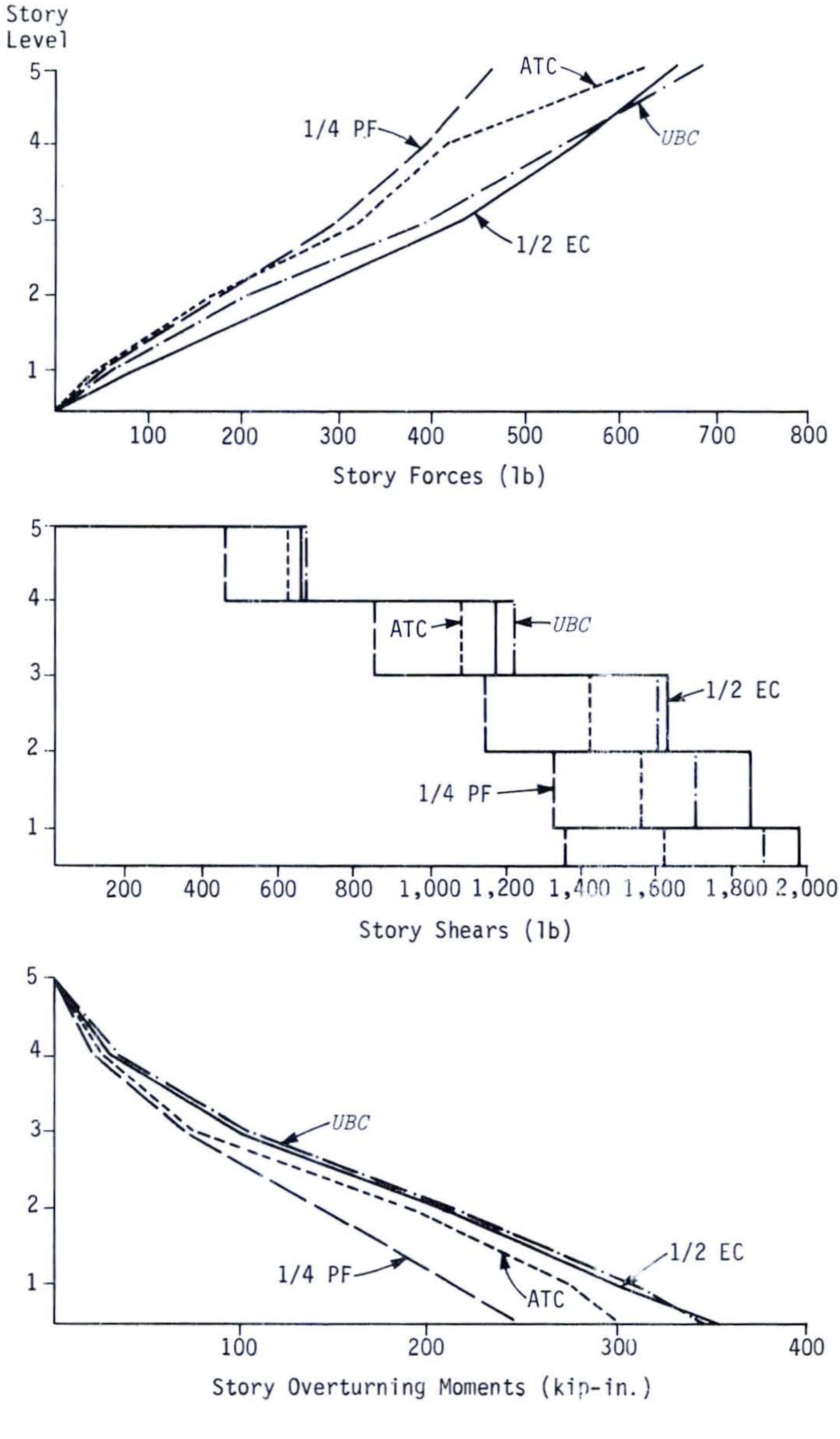

FIGURE 12.11 RESULTS OF THE *UBC* METHOD, THE ATC METHOD, AND THE RESPONSE SPECTRUM METHOD - STACKER RACK, TRANSVERSE DIRECTION, FULL LIVE LOAD

13. EVALUATION OF SEISMIC DESIGN CRITERIA AND PROCEDURES

13.1 Introduction

Two types of seismic design criteria and appropriate analysis are in general use. The simpler of the two approaches, the method used by the *UBC* and by RMI, provides equivalent static lateral force criteria for the design of rack structures. The second approach employs a dynamic response analysis of the structure, which results in a more realistic distribution of lateral forces in the structures. The dynamic analysis is a comprehensive structual analysis (usually a computer analysis) based on site-specific earthquake design criteria established on the basis of a geotechnical investigation. This type of analysis is essential to unusual or more important rack structures (1) when a better understanding of structural response to earthquake loading is needed or (2) when an accurate distribution of lateral force in the structure is desired.

Two methods of dynamic analysis are the time-history method and the response spectrum method. The time-history method is more detailed than the response spectrum method, and it facilitates direct combination of the effects of various modes of vibration. It is also useful for inelastic and nonlinear analysis. However, the time-history approach requires the use of a rather large computer for the treatment of even moderately complex systems and therefore is often beyond the capabilities of many design offices. Also, the time-history approach requires the use of several time-history records in order to obtain useful results.

In the response spectrum method, a design response spectrum is used to obtain equivalent maximum lateral story forces on a structure for several modes of vibration to simulate the effects of the earthquake. The several modes must then be combined by some statistical means, such as the square-root-of-the-sum-of-the-squares method.

13.2 Comparison of Various Equivalent Static Lateral Force Criteria

The seismic design base shear coefficients for moment-resisting frames and braced frames from the *UBC* requirements and the RMI specifications are plot-

Preceding page blank

ted in Figures 13.1 and 13.2, respectively. (In 1976 and 1979,[25] the *UBC* offered a choice of three alternative coefficients.) The importance of considering the dynamic response characteristics of storage racks (i.e., the variation of base shear coefficients with respect to the period of vibration) is readily apparent in the figures. The parameters used in the *UBC* method are also indicated in the figures.

Figure 13.3 shows base shear coefficients for moment-resisting frame systems in accordance with the requirements of the 1976 *UBC* Zone 4 (Z = 1.0) and the ATC-3 map area 7 (Seismicity Index 4, A_v = 0.4). The base shear coefficient from the *UBC* method was multiplied by a factor of 1.28 (1.7/1.33) to equate working stress design to ultimate strength design, and the base shear coefficient from the ATC method was modified by a capacity-reduction factor of 0.9. The response modification factor R in the ATC method was assumed to be 4.5 because the rack could be classified as an ordinary moment steel frame. The factor of K in the *UBC* method was assigned a value of 1.0. It is clearly shown in Figure 13.3 that the lateral seismic forces of the ATC method will be higher than those of the *UBC* method.

However, the base shear coefficients shown in Figure 13.4 for the braced-frame system indicate that the lateral forces from the *UBC* method are higher than those of the ATC method. The factor of K in the *UBC* method was assigned a value of 1.33, and the base shear was multiplied by 1.6 (1.7/1.33 x 1.25) to equate working stress design to ultimate strength design. The response modification factor R in the ATC method was assumed to be 4.0, and the base shear coefficient was modified by a capacity-reduction factor of 0.9.

13.3 Applicability of the *UBC* Method

Since the 1976 (or 1979) *UBC* method is widely used for seismic design, it is used in this section to discuss the adequacy and validity of equivalent static lateral force criteria in rack design.

Table 13.1 summarizes the building code demand (requirement) versus rack capacity of all rack configurations considered in this report along with the actual performance from the shaking table tests. The lateral forces were determined using the 1976 *UBC* Zone 4 seismic requirements assuming the best site conditions (i.e., minimum S) and both the AISI 3.6.1 and 1979 RMI[26] were used for calculating rack capacity. Torsional-flexural behavior was ignored in calculating the M-P stress ratio. Table 13.2 summarizes the base shears for all racks considered, using the *UBC* method and the response spectrum method.

In the remainder of this section, the applicability of the *UBC* method is discussed for each test configuration with the help of Tables 13.1 and 13.2.

Standard Pallet Rack. In the longitudinal direction, the lateral force capacity of this rack configuration was less than that prescribed by the *UBC* Zone 4 lateral force provisions (see Table 13.1). The analytical studies reported in Section 7.4 show that the lateral forces in accordance with the *UBC* method were approximately equivalent to those by the response spectrum method using an input signal of about 1/2 to 5/8 the actual El Centro record (see Table 13.2 or Table 7.5). In addition, the response spectrum analysis showed that higher mode contribution had a significant effect on the base shears. However, because of the structure's high damping capacity (from 3% to 9% of critical) and the early nonlinear behavior at the beam-column connections, the forces developed in the structure by a strong earthquake are greatly reduced by inelastic action.

This behavior was observed in the experiments reported in Section 4.8 (or see Table 13.1). During the shaking table tests, the amplitude of the table motion was increased progressively to cause member yielding. With the El Centro earthquake, normalized to peak of 0.43g in the horizontal direction (about 1-1/3 EC) and a peak of 0.21g in the vertical direction, the rotational ductility ratio reached 2.6 at the top end of the first-floor center column before observable minor local distress occurred. This clearly indicates that the *UBC* method provides substantial earthquake resistance for this rack configuration.

In the transverse direction, the lateral force capacity of the standard pallet rack was also less than that of the seismic provisions of *UBC* Zone 4 (see Table 13.1). The lateral forces by the *UBC* method were less than those from the response spectrum method using an input signal of 1/2 the El Centro record but greater than those using 1/2 the Parkfield record (Table 13.2). The effects of higher mode contribution on the base shears were found to be negligible. However, because of the low damping capacity observed (0.5% to 1.6% of critical) and the rigidity of the rack in this test direction, the rack can only undergo small amounts of inelastic deformation in the transverse direction. During the shaking table tests, the structure suffered no visible damage until the test run using the input signal of about 5/8 the actual El Centro record. For this test run, all column members buckled noticeably near the base plates, and welds fractured at a column base and a column-brace connection. All diagonal braces were found to be within the yield limit.

The *UBC* seismic provisions seem adequate for the standard pallet rack in the transverse direction. However, some early damage would be expected in moderate earthquakes. A larger load factor than the 1.25 prescribed by the *UBC* requirements for all members in braced frames would be desirable to preclude early damage during strong earthquake shaking. This will be discussed later in this section.

Drive-in Rack. As discussed in the analytical studies of the drive-in rack in the longitudinal direction (Section 9.4), the lateral forces prescribed by the *UBC* method were slightly lower than those by the response spectrum method using the input signal of 1/2 the El Centro record but were slightly higher than those from the input signal of 1/2 the Parkfield record (Table 13.2). As in the case of the standard pallet rack in the longitudinal direction, higher mode participation had a significant effect on the base shear.

The seismic resistance capacity of this rack was found to be less than that prescribed by the *UBC* Zone 4 seismic provisions (Table 13.1). However, no material yielding or structural damage was observed during the shaking table tests. The input signal for the last test run was scaled to a maximum horizontal acceleration of 5/8 that of the actual El Centro record with the addition of appropriately scaled vertical accelerations. The tests could have been continued with increasing amplitude of motion, but, from the experience of the collapse of the double pallet rack, and for safety, it was decided to stop the test. As in the case of the standard pallet rack in the longitudinal direction, the damping values for this test configuration were very high (4% to 9% of critical). From these observations, it appears that the seismic provisions of the *UBC* provide adequate earthquake resistance for the drive-in rack in the longitudinal direction.

In the transverse direction, the seismic resistance capacity of the drive-in rack was found to be slightly less than the requirements of the seismic provisions of the *UBC* Zone 4 (Table 13.1). The estimated lateral forces were approximately equivalent to those by the response spectrum method using the input signal of 1/4 to 1/2 the Parkfield or El Centro records (Table 13.2).

The considerable buckling that was observed in the bottom diagonal members of the upright frame when the structure was excited by 1/4 the Parkfield signal appeared because the predominant period of excitation (0.59 sec) coincided with the response spectrum peaks shown in Figure 4.19. The resulting high-amplitude structural response caused unexpected buckling at a table excitation of such low intensity. In addition, the rack configuration was poorly arranged, using the same size diagonal bracing members for both the upright and anchor frames. As a result, the diagonal members in the upright frame were very weak compared to those in the anchor frame (the slenderness ratios were 177 for the diagonal members in the upright frame and 150 in the anchor frame). If the diagonal members had been carefully designed and arranged, this rack configuration could have resisted lateral forces developed from a stronger earthquake without major damage.

Stacker Rack. The seismic resistance capacity of the stacker rack in the longitudinal direction was found to be slightly greater than the minimum design requirements of the *UBC* Zone 4 (Table 13.1). The calculated lateral forces for the *UBC* method were substantially greater than those by the response spectrum method using the input signal of 1/2 the El Centro or the Parkfield records (Table 13.2). In addition, the response spectrum analysis (Section 11.3) showed the effects of higher-mode contribution on the base story shears to be negligible for this high-rise rack configuration.

No material yielding or structural damage was observed when the input table motion was increased to 3/4 the El Centro record. This test run was conducted when the diagonal rods were loose. When the test was carried out using the same input signal of 3/4 EC and the diagonal rods were tightened with some pretension, noticeable buckling of interior columns between the bottom and middle rod supports was observed. Thus, if the diagonal rods are loosely connected, this rack configuration could likely resist seismic forces developed from a stronger earthquake without structural damage.

A better alternative for improving the seismic performance of stacker racks in the longitudinal direction would be to make the diagonal connections at, and with, horizontal framing members. Another way would be to design the rack assembly so that it would qualify as a dual bracing system, consisting of a braced frame and moment-resisting frames. Such designs will take 100% of the total lateral force in the braced frame and, as a backup, take 25% in the moment-resisting frames (note that for a dual bracing system a value of K smaller than 1.33 may be assigned).

In the transverse direction, the seismic resistance capacity of the stacker rack was found to be less than the minimum requirements of the *UBC* Zone 4 (Table 13.1). The lateral forces estimated from the *UBC* method were approximately equivalent to those by the response spectrum method using the input signal of 1/2 the El Centro period, but smaller than those using 1/2 the Parkfield record.

Considerable buckling occurred unexpectedly at the bottom diagonal members during the test run using the input signal of 1/2 the Parkfield record because the predominant period of vibration during this test run (0.78 sec) coincided with the range of higher-amplitude spectral values (see Figure 4.19), which developed large lateral forces in the structure. In addition, all interior bottom columns buckled near the base plates.

The *UBC* seismic provisions with a load factor of 1.25 for braced frames may not provide adequate earthquake resistance for this high-rise rack.

Summary. The following conclusions can be drawn from the above discussion:

- As in the case of building structures, the ductility and energy-dissipation capacity of racks is much larger in the longitudinal direction (moment-resisting frame) than in the transverse direction (braced frame).

Thus the racks can undergo sizable amounts of inelastic deformation in the longitudinal direction without suffering major damage but can only undergo minor amounts of inelastic deformation in the transverse direction. However, in the longitudinal direction, the racks have the potential for instability due to large displacement during severe earthquake shaking (i.e., due to amplification from the p-δ effect). In the transverse direction, the racks can be expected to undergo some early damage during moderate earthquake shaking, but they are less likely to collapse. The results of the shaking table tests justify the use of a load factor for all members in braced frames.

- The lateral force provisions recommended in the *UBC* (Standard No. 27-11) appear generally to provide adequate seismic resistance in racks similar to those studied in this report except that the load factor (or modifier) of 1.25 recommended in the 1976 *UBC* for all members in braced frames may be inadequate. A larger load factor or modifications to the rack installation are needed to preclude early nonductile damage during strong earthquake shaking.

- The weight W in the *UBC* method should be the weight of the racks plus contents. Values of K of 1.0 and 1.33 are recommended for the moment-resisting frame system and the braced frame system. However, in the longitudinal direction of the stacker rack, a value of K smaller than 1.33 may be assigned if the rack assembly can qualify as a dual bracing system consisting of a braced frame and moment-resisting frames.

- The *UBC* formulas for determining the fundamental periods of vibration, such as $T = 0.05\ h_n/\sqrt{D}$ and $T = 0.1N$, are not applicable for rack structures. The Rayleigh method (Equation 12-3 in the *UBC*) or a frequency analysis using an appropriate mathematical model (computer-analysis method) are more desirable.

- In the absence of the values of T and T_s (characteristic site period), the base shear coefficients of 0.1 and 0.2 can be used for the moment-resisting frame system and the braced-frame system, respectively (see Figures 13.1 and 13.2).

- The use of more detailed dynamic analysis procedures should not be ruled out, particularly in the design of an unusual rack structure. The response spectrum approach is a simple method of dynamic analysis that takes into account the true dynamic nature of the problem to a greater extent than does the *UBC* procedure.

- In the longitudinal direction (moment-resisting frame), the maximum interstory drift observed exceeded the

UBC drift limit ($0.005H \times 3/K$). The maximum drifts observed from the shaking table tests were $0.07H$ and $0.03H$ for the standard pallet and the drive-in racks, respectively. This illustrates that the racks in the moment-resisting frame direction can tolerate much greater drift than the *UBC* drift limit. However, during a very severe earthquake (or the maximum credible earthquake), there is a potential for collapse due to excessive drift or the p-δ effect.

13.4 Seismic Analysis Procedures

Design Examples. Examples of seismic analysis procedures in accordance with the Zone 4 lateral force provisions of the 1976 *UBC* are presented in Appendices D through H of this report. These examples cover all racks studied in the report except for the stacker rack in the transverse direction, the configuration of which is essentially the same as that of the standard pallet in the transverse direction. The following paragraphs discuss the mathematical modeling assumptions and the modeling parameters used in the examples.

Mathematical Models. The first step in either linear or nonlinear seismic design analysis is to develop appropriate mathematical models. The techniques used to develop mathematical models for the rack configurations considered in this report were presented in Chapters 7 to 12. Good correlation between the measured and predicted response properties (periods and mode shapes) was obtained for each rack assembly considered. In the design examples, as for all mathematical models developed in this study, rack storage levels are assumed to be sufficiently rigid, and two-dimensional frame models are considered adequate for practical purposes. Minimum net section properties supplied by manufacturers and centerline dimensions are used. A general-purpose elastic analysis program (SAP IV) is used for analysis.

Modeling Parameters. A brief discussion of the modeling parameters -- K_θ (semirigid joints), I_f (semifixed column bases), and k (localized deformation at connections between the open-section column and open-section bracing members) -- that are required in theoretical prediction of rack response is presented in the following.

The influence of semirigid joints in the longitudinal direction of the standard pallet and drive-in racks was already discussed in Sections 7.1 and

9.1. To predict the seismic response and capacity of racks analytically, the behavior of beam-to-column connections can be modeled by joint rotational springs obtained experimentally (Chapter 2). A summary of the joint springs (K_θ) determined in this program and which can be used for elastic analysis and design is shown in Table 2.2. The table indicates that the values of K_θ are in the range of 300 to 1,000 lb-in./rad except for a very high K_θ value for one type of rack made of hot-rolled steel. The experimentally determined values of K_θ shown in the table can be used as a reference for the proper selection of K_θ if no experimental data for specific rack components under consideration are available. With an appropriately assumed K_θ, the beam rigidities can be modified for elastic analysis according to Equation (7.1).

Because the local responses measured by the DCDT gages indicated a considerable restraint against rotation near the column base plates, the bases should not be considered as either fixed or hinged but rather as partially fixed. Fictitious floor beams are introduced to account for this effect (Chapters 7 to 12). For all rack assemblies considered in this study, it was found that a value of I_f of 0.2 in.^{4} provided the best results in comparison with measured responses. It was also found that the parameter I_f was more sensitive in the rack's longitudinal direction than in its transverse direction. No quantitative experimental data are available, however, and it is therefore recommended that the value for I_f of 0.2 in.^{4} be used in response analysis to account for semifixed column bases.

In modeling the braced-frame system for the racks tested on the shaking table (the standard pallet, drive-in, and stacker racks in the transverse direction), localized deformation at the connections between the open-section columns and the open-section bracing members has to be considered. The bracing member can be treated as a composite and its stiffness reduced as shown in Equation (8.1), using the reduction factor k. Although no quantitative experimental data are available, in Sections 8.1, 10.1, and 12.1, the values of k were found to be in the range of 7 to 12. Experimental investigations are needed to define the parameter k for braced-frame systems as subassembly tests are needed to define K_θ for semirigid-frame systems. However, the factor k in the range studied in this report could be used until the experimentally determined data become available.

For linear mathematical modeling of the diagonal rods in the longitudinal direction of the stacker rack, the truss element with an assumed reduction factor k can be applied. A value for k of 14 for the rack configuration tested was found to provide the best-fit model in comparison with the experimentally obtained periods and mode shapes (Section 11.1).

TABLE 13.1

SUMMARY OF SEISMIC PERFORMANCE OF RACK STRUCTURES

Rack	Direction	*UBC* Demand Versus Rack Capacity			Behavior During Shaking-Table Tests		
		Critical Element	Stress Ratio*		Input Signal	Mode of Damage	Reference
			$\frac{P}{P_a}$	$\frac{P}{P_a} + \frac{M}{M_a}$			
Standard Pallet	longi-tudinal	1st floor center column	--	1.32 (1.41)	1-1/3 EC plus vertical	Minor local distress at top of both 1st-floor columns near connectors	Table 4.4
Standard Pallet	trans-verse	column near base plates	--	1.32 (1.48)	5/8 EC plus vertical	Noticeable buckling of all columns near bases. Welds of a column base broke.	Table 4.5
Drive-In	longi-tudinal	1st floor center column - anchor frame	--	1.37 (1.47)	5/8 EC plus vertical	No visible damage	Table 4.8
Drive-In	trans-verse	bottom diagonal braces - upright frame	1.20 (1.20)	--	1/4 PF	All bottom diagonal braces of the upright frames buckled.	Table 4.9
Stacker	longi-tudinal	first interior columns near bases	--	0.83 (0.92)	3/4 EC	Buckling of interior columns between the bottom and middle rod supports	Table 4.10
Stacker	trans-verse	bottom diagonal braces	1.26 (1.26)	--	1/2 PF	All interior bottom diagonals buckled. All interior bottom columns buckled near the base plates.	Table 4.11

*The upper figures are based on AISI 3.6.1, and the lower figures are based on the 1979 RMI specification. The one-third increase permitted for allowable stresses resulting from earthquake forces was included. Procedures for analysis are similar to those in Appendices D through H, except that the minimum *CS* was assumed in this table.

TABLE 13.2

SUMMARY OF BASE SHEARS FOR ULTIMATE STRENGTH DESIGN: *UBC* METHOD AND RESPONSE SPECTRUM METHOD

Rack	Direction	Base Shear (lb)					
		UBC Method*	Response Spectrum Method†				Reference
			1/4 EC	1/4 PF	1/2 EC	1/2 PF	
Standard Pallet	longitudinal	1,135	564 (3%)	774 (3%)	1,030 (5%)	1,290 (5%)	Table 7.5
Standard Pallet	transverse	2,428	1,708 (1.5%)	1,140 (1.5%)	2,799 (3%)	--	Table 8.5
Drive-In	longitudinal	3,162	1,892 (4%)	1,494 (4%)	3,485 (6%)	2,888 (6%)	Table 9.5
Drive-In	transverse	2,964	2,316 (2%)	2,560 (2%)	4,266 (3%)	--	Table 10.5
Stacker	longitudinal	17,040	7,969 (3%)	6,743 (3%)	12,260 (5%)	12,260 (5%)	Table 11.5
Stacker	transverse	1,859	1,235 (3%)	1,372 (3%)	1,921 (5%)	2,401 (5%)	Table 12.5

*The minimum value of S, for the best site condition, is used.

†Damping values assumed are shown in parentheses.

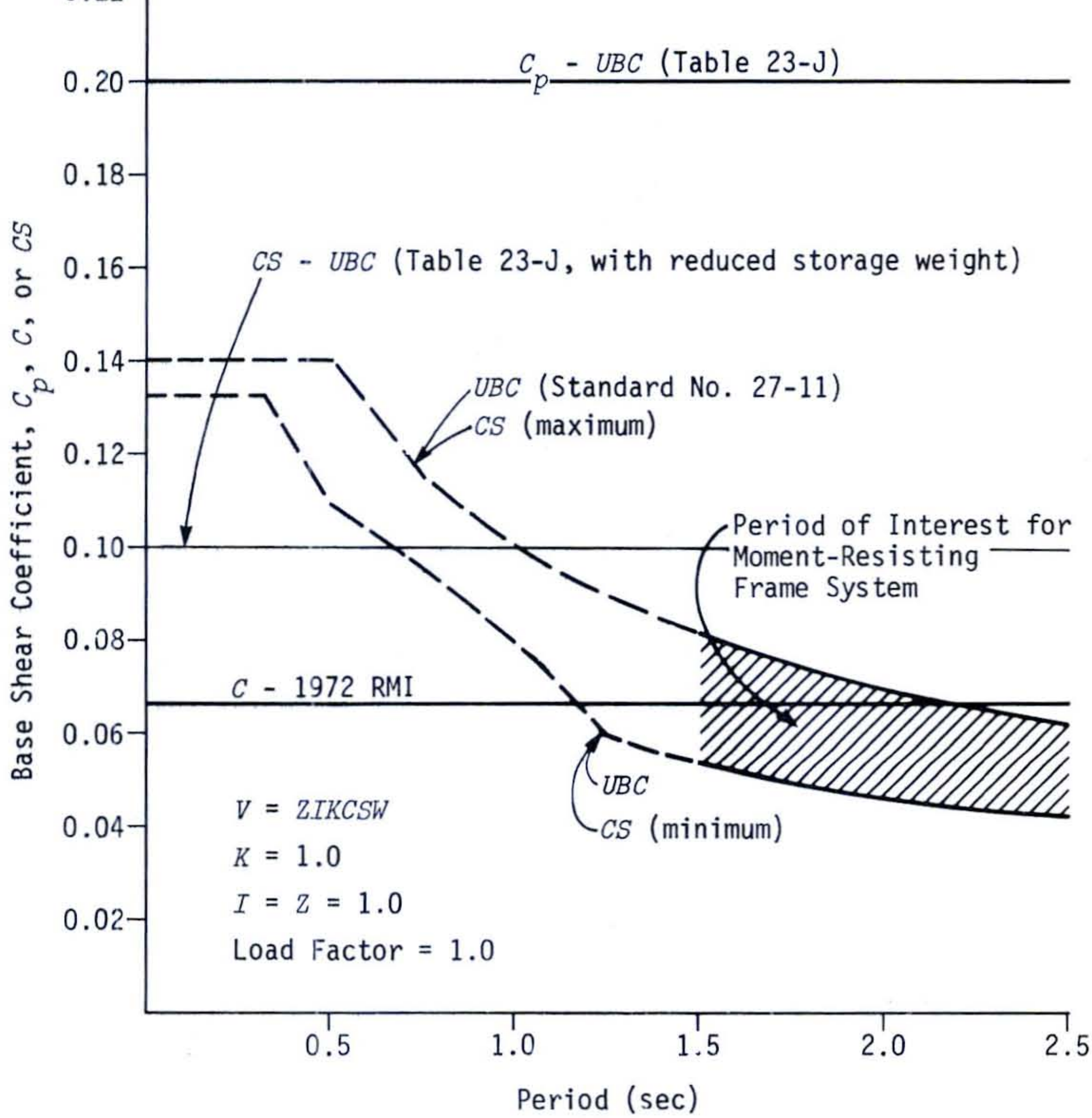

FIGURE 13.1 *UBC* AND RMI BASE SHEAR COEFFICIENTS - MOMENT-RESISTING FRAME SYSTEM

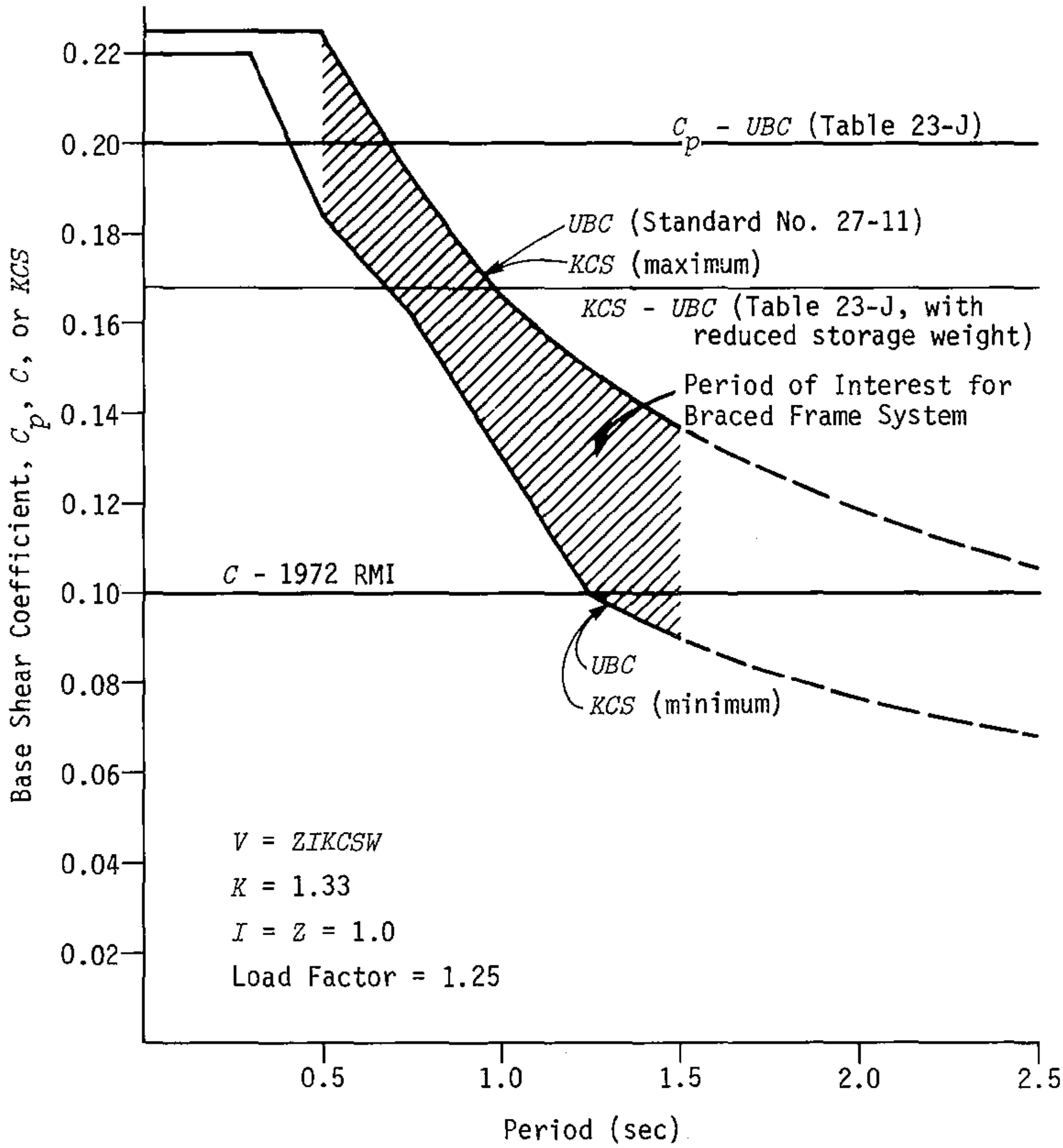

FIGURE 13.2 *UBC* AND RMI BASE SHEAR COEFFICIENTS - BRACED FRAME SYSTEM

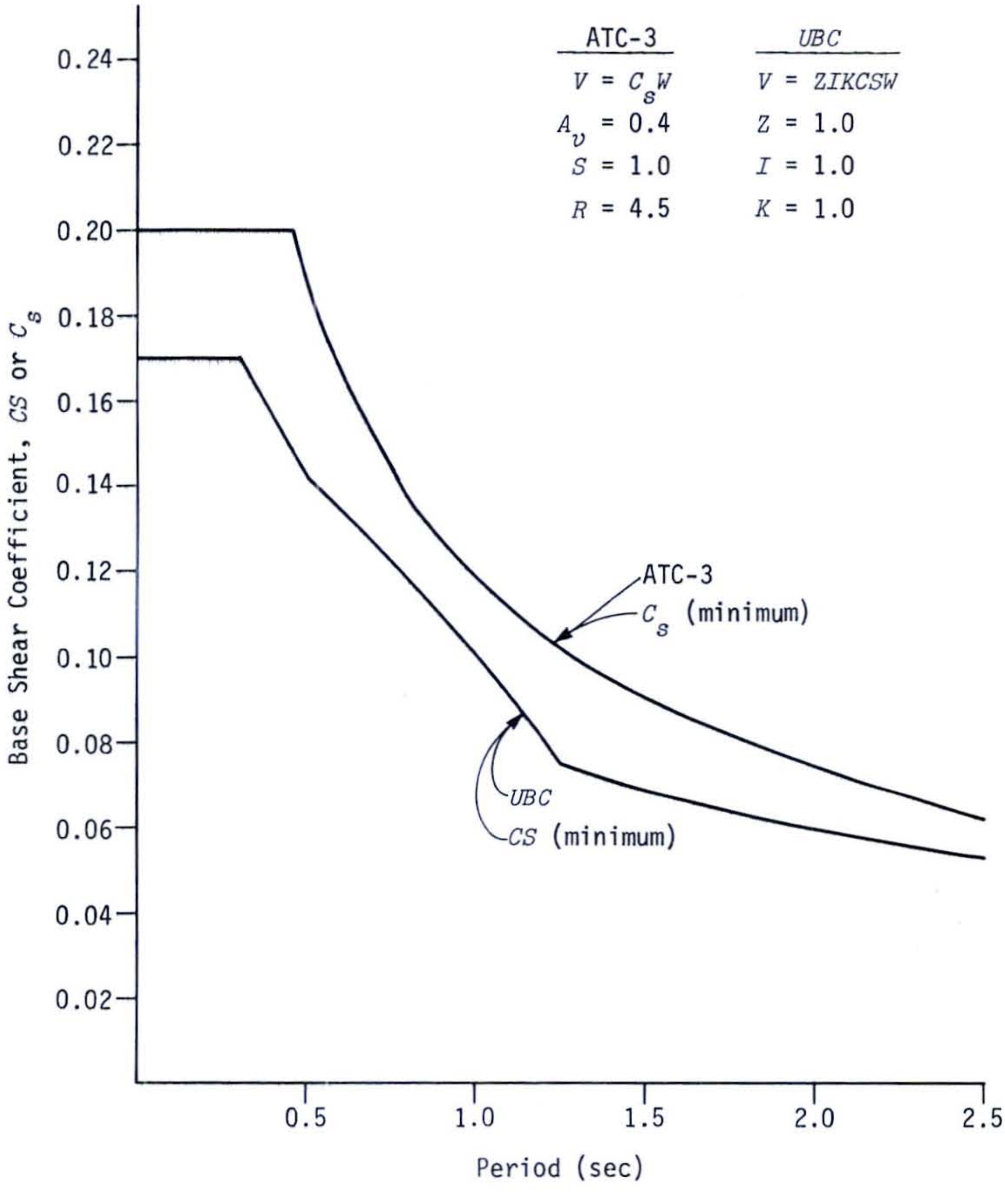

FIGURE 13.3 *UBC* AND ATC-3 BASE SHEAR COEFFICIENTS ADJUSTED FOR ULTIMATE STRENGTH DESIGN - MOMENT-RESISTING FRAME SYSTEM

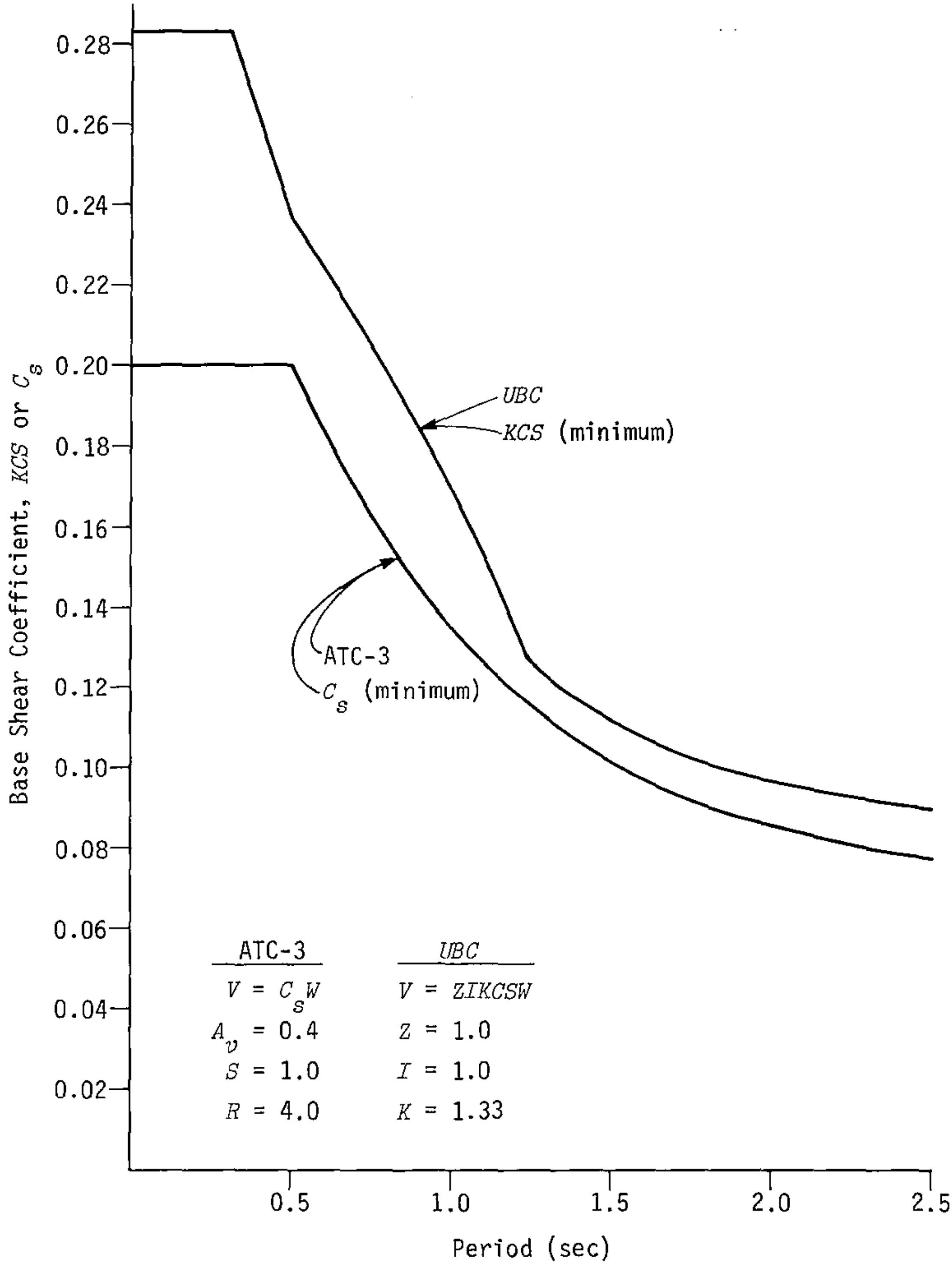

FIGURE 13.4 *UBC* AND ATC-3 BASE SHEAR COEFFICIENTS ADJUSTED FOR ULTIMATE STRENGTH DESIGN - BRACED FRAME SYSTEM

14. CONCLUSIONS AND RECOMMENDATIONS

14.1 Subassembly Tests

Results from the cantilever and portal tests conducted at Stanford University and Cornell University and by several manufacturers were reported in this study. In all, tests of 24 types of rack components from 7 different manufacturers were correlated and compared. The following conclusions can be drawn.

- In all tests, the strength of the rack assembly was governed by the connection rather than by the beam itself. Deformation in the connectors, tearing of the column perforations, and fracturing of the beam-connector weld were commonly observed as the mode of failure.
- In most test cases, the moment-rotation (M-θ) relationships are very nonlinear. It is sometimes difficult to define a suitable linear range for elastic design and analysis.
- In general, the M-θ relationships for both test methods (portal and cantilever) are similar in shape and moment capacity. However, the stiffness from the cantilever tests is lower than that from the portal tests. The difference in K_θ values estimated for elastic analysis and design is on the order of 2.
- The values of K_θ from the cantilever tests are in the range of 300 to 1,000 kip in./rad from various combinations of rack components, with the exception of very high K_θ values for one type of rack made of hot-rolled structural steel.
- The study of the influence of different values of K_θ (500 versus 1,000 kip-in./rad) used in accordance with the 1976 *UBC* seismic design requirements, shows that the member forces are approximately 5% to 6% larger when K_θ = 500 kip-in./rad. The standard pallet rack used in the shaking table tests was used for this analysis.
- The cantilever test is sufficient for practical engineering purposes. The test is simple and requires only lateral load and displacement measurements, which are easy to carry out. However the test should be conducted for loading in both the positive and the negative directions
- To predict the seismic response and capacity of the full-scale rack structures analytically, the behavior

of beam-to-column connections can be modeled by linear or nonlinear rotational springs obtained experimentally for positive and negative moments.

14.2 Merchandise Tests

Both shaking table and pull-release free-vibration tests were conducted to study the seismic response characteristics of the various types of merchandise, both tied to the rack with metal straps and not tied to the rack. Single-degree-of-freedom tests were performed: the rack was anchored to the shaking table, loaded with merchandise, and tested in both the longitudinal and transverse directions. The conclusions that can be drawn from this study, for the specific types of merchandise tested and for horizontal excitation only, are as follows:

- Substantial horizontal diaphragm action can be developed through the combination of stored material and pallets or metal decking, regardless of the type of material or whether it is tied to the rack.
- For all tests, little difference in global and local responses was found between the cases in which merchandise was tied to the rack and those in which merchandise was not tied to the rack. This finding justifies the use of tied live loads for the analytical response predictions.
- The damping values determined from the pull tests for merchandise that was not tied are slightly higher than those for tied merchandise. However, the pull tests show no difference in periods of vibration between the two test cases.
- In all tests of merchandise that was not tied, all merchandise tested was very stable, and no movement of stored material was observed except for some of the uppermost cartons of paper products. The maximum floor (pallet accelerations measured in the longitudinal test direction ranged from approximately 0.2g for the cases of canned goods (2,300 lb/beam) to 0.7g for lightweight paper products (500 lb/beam).

Because the merchandise tests were not conducted for vertical acceleration, Appendix C, which surveys merchandise and rack damage during two recent earthquakes, was included in this report.

14.3 Full-Scale Rack Tests

Four types of typical full-scale storage racks were subjected to simulated earthquake motions using the 20-ft-square shaking table facility at the Richmond field station of the University of California, Berkeley. The types of storage racks tested were: single standard pallet rack, back-to-back pallet rack, drive-in rack, and stacker rack. Three racks were anchored to the table and tested under live loads simulated by concrete blocks (1,000 lb/block) in each of the two principal directions. One rack (the back-to-back pallet rack) was tested without anchors to the table. In addition, at Stanford University, two types of full-scale standard pallet rack, provided by two different manufacturers, were subjected to static cyclic tests in each of the two principal directions. The findings from these two testing programs are summarized as follows:

- In general, the racks performed well during the shaking table tests, with the exception of the drive-in and stacker racks in the transverse direction. Considerable buckling was observed in first-story diagonal members of these two rack configurations when the racks were excited at very low levels (1/4 PF and 1/2 PF, respectively).
- The global and local response amplitudes measured from the shaking table tests for the pallet rack that was not anchored to the table are higher than those for the anchored rack under the same input signal.
- The base plates for all racks that were anchored to the table (or the floor for the static cyclic tests) provide a significant fixity against rotation, which, in turn, reduces the moment at the first-level columns.
- The fundamental periods of vibration range from 2 sec to 3 sec for the standard pallet and drive-in racks in the longitudinal direction and 0.5 sec to 1.0 sec for the standard pallet, drive-in, and stacker racks in the transverse direction.
- The first-mode damping values are much larger in the longitudinal direction (ranging from 3% to 9% of critical) than in the transverse direction (ranging from 0.5% to 3% of critical).
- The contribution to story shear of the p-δ effect is very significant in the moment-resisting-frame direction and should be considered in response prediction and design.

- During the shaking table tests, the maximum drifts observed for the standard pallet and the drive-in racks in the longitudinal direction were 0.07 and 0.03 times the story height (H), respectively. This indicates that the racks can tolerate much greater drift than that allowed in the *UBC* method ($0.005H \times 3/K$) or the ATC method ($0.015H$).

- For the racks tested on the shaking table, strong localized deformations were observed at the connections between the open-section bracing members and the open-section columns. In general, this type of deformation should be considered in making detailed response predictions in the braced-frame rack configuration.

- The higher-mode contribution to global and local responses is insignificant for all racks except for the standard pallet and drive-in racks in the longitudinal direction. The response spectrum analyses for these two rack configurations show the effects on the base shear of the higher mode contribution in the range of 10% to 20%.

- In the longitudinal direction, the drive-in rack assembly consists of two upright and two anchor frames. Although the structural systems and stiffnesses for these two types of frames are quite different, no torsion was detected from the experimentally obtained displacement time-history plots. A theoretical calculation also indicated the torsional effect to be insignificant. This negligible torsional effect makes possible two-dimensional modeling of this structure. However, this finding may be valid only for this specific rack configuration. In industry practice, drive-in racks often contain more than four frames, and the torsional effect during earthquake excitation may thus be significant. It is therefore recommended that the torsional effect be evaluated by the procedures described in Appendix B.

- In the transverse direction, the connections of the columns to the braces and the columns to the base plates with only a few button welds are not sufficient to develop the full capacities of the members. This undesirable design practice can be easily improved by fully welding around these connections.

- In the transverse direction of the drive-in rack, considerable buckling was observed in the bottom diagonal members of the upright frame when the structure was excited at very low levels. This is mainly because the rack was poorly designed, using the same size diagonal bracing members for both the upright and anchor frames. As a result, the diagonal members in the upright frame were very weak in comparison with those in the anchor frame (the slenderness ratios were 177 for the diagonal members in the upright frame and 150 in the anchor frame). If the diagonal members had been carefully designed and arranged, this rack configuration could have resisted lateral forces developed from a stronger earthquake without major damage.

- A better alternative for improving the seismic performance of stacker racks in the longitudinal direction would be to make the diagonal connections at, and with, horizontal framing members. Another alternative would be to design the stacker rack in the longitudinal direction so that it would qualify as a dual bracing system consisting of a braced frame and moment-resisting frames.

14.4 Theoretical Prediction of the Response of Rack Structures

One of the primary objectives of the structural performance shaking table tests was to obtain experimental data on the actual performance of various types of full-scale rack structures in order to test the adequacy and effectiveness of the various analytical procedures and assumed mathematical models. The frequency analysis of the linear mathematical models was carried out to compare the calculated periods of vibration and mode shapes with those observed during the low-amplitude shaking table tests and the pull-release free-vibration tests. The best-fit linear model developed for each rack configuration was used as a basis for developing nonlinear models for time-history analysis, and the calculated periods and mode shapes were used to perform the response spectrum analysis. The calculated fundamental periods of vibration for each structure were used to determine the base shear coefficients for use in the *UBC* and the ATC-3 methods. The conclusions that can be drawn from this study are as follows:

- In general, the responses predicted theoretically for all racks studied in this report were in good agreement with the experimental results.
- A good linear mathematical model is essential for the response prediction for each rack assembly. So long as the best-fit linear model is established, this single mathematical model with appropriate modification can be used to predict both linear and nonlinear time-history responses of the rack structure by varying only damping and yield mechanisms.
- To develop appropriate mathematical models, rack storage levels are assumed to be sufficiently rigid, and two-dimensional models are considered to be adequate for practical purposes. Fictitious restrain-

ing floor beams can be added to simulate the actual column base condition. Minimum net section properties and centerline dimensions are used.

- Modeling parameters such as K_θ (semirigid joints) I_f (semifixed column bases), and k (localized deformation at connections between the open-section column and open-section bracing members) should be considered in theoretical prediction of rack response.

- To predict the seismic response and capacity of racks analytically, the behavior of beam-to-column connections can be modeled by joint rotational springs obtained experimentally from subassembly tests. With an appropriately assigned K_θ, the beam rigidities can be modified for elastic analysis according to Equation (7.1).

- Fictitious floor beams are introduced to account for actual column base condition. For all rack assemblies considered in this study, it was found that a value of I_f of 0.2 in.^{4} provided the best results in comparison with measured responses. It was also found that the parameter I_f was more sensitive in the rack's longitudinal direction than in its transverse direction. No quantitative experimental data are available, however, and it is therefore recommended that the value for I_f of 0.2 in.^{4} be used in response analysis to account for semifixed column bases for racks similar to those considered here.

- In modeling the braced-frame system for the racks tested on the shaking table (the standard pallet, drive-in, and stacker racks in the transverse direction), localized deformation at the connections between the open-section columns and the open-section bracing members had to be considered.

  The bracing member can be treated as a composite and its stiffness reduced as shown in Equation (8.1), using the reduction factor k. Although no quantitative experimental data are available, the values of k were found to be in the range of 7 to 12. Experimental investigations are needed to define the parameter k for braced-frame systems as subassembly tests are needed to define K_θ for semirigid-frame systems. However, the factor k in the range studied in this report could be used until the experimentally determined data become available.

- For linear mathematical modeling of the diagonal rods in the longitudinal direction of the stacker rack, the truss element with an assumed reduction factor k can be applied. A value of k of 14 was found to provide the best-fit model in comparison with the experimentally obtained periods and mode shapes.

- In the longitudinal direction, the lateral forces determined by the *UBC* method are roughly equivalent to those using the response spectrum method with intensity levels of slightly more than 1/2 the El Centro or Parkfield record. However, in the transverse direction, the *UBC* lateral forces are approximately equivalent to 1/4 to 1/2 the El Centro and Parkfield records.

- For the braced-frame systems, the lateral forces determined from the *UBC* are higher than those of the ATC method. For this comparison, the base shears for the *UBC* method were multiplied by a factor of 1.6 to equate working stress design to ultimate strength design; the base shears from the ATC method were modified by a capacity-reduction factor of 0.9, and a response modification factor *R* of 4.0 was used.

- For the moment-resisting frame system, the results from the ATC method are slightly higher than those from the *UBC* method. The base shears from the *UBC* method were multiplied by a factor of 1.28, to equate working stress design to ultimate strength design. A reduction factor of 0.9 was applied to the ATC method, and a factor *R* of 4.5 was used.

- The torsional-flexural behavior in racks is very complex. At present, no satisfactory way of handling this problem is available.[10] During the shaking table tests, the torsional-flexural buckling was observed in the diagonal members of the drive-in and stacker racks tested in the transverse direction. Therefore, the formulas in AISI 3.6.1 or in the 1979 RMI specification for determining the allowable stress for torsional-flexural buckling should be used with caution. In this study, the torsional-flexural behavior was considered only in calculating axial forces in bracing members but was ignored in determining column capacities subjected to the combined bending and axial forces (i.e., the *M-P* interaction equation).

14.5 Seismic Design Criteria and Procedures

The following conclusions and recommendations can be drawn from this study:

- The lateral force provisions recommended in the 1976 *UBC* (Standard No. 27-11) appear generally to provide adequate seismic resistance in racks similar to those studied in this report except that the load factor (modifier) of 1.25 recommended in the *UBC* for all members in braced frames may not be adequate. A larger load factor or modifications to the rack fabrication are needed to preclude early nonductile damage during strong earthquake shaking. A better alternative for improving the seismic performance of braced frames would be to make the diagonal connections at horizontal members[27] (see Appendix I for a brief discussion of eccentric braced frames to resist seismic forces).

- Values of K of 1.0 and 1.33 are recommended for the moment-resisting-frame system and the braced-frame system, respectively. However, in the longitudinal direction of the stacker rack, a value of K smaller than 1.33 may be assigned if the rack assembly can qualify as a dual bracing system consisting of a braced frame and moment-resisting frames.
- The *UBC* formulas for determining the fundamental periods of vibration, such as $T = 0.05\, h_n/\sqrt{D}$ and $T = 0.1N$, are not applicable to rack structures. The Rayleigh method (Equation 12-3 in the *UBC*) or a frequency analysis using an appropriate mathematical model (computer-analysis method) are more desirable.
- The use of more detailed dynamic analysis procedures should not be ruled out, particularly in the design of an unusual rack structure. The response spectrum approach is a simple method of dynamic analysis that takes into account the true dynamic nature of the problem to a greater extent than does the *UBC* procedure.

Seismic design procedures according to the 1976 *UBC* and 1979 RMI specifications are illustrated in Appendices D through H of this report.

14.6 Further Studies

The following further studies (in order of importance) are recommended:

- This study shows that the *UBC* method generally provides adequate earthquake resistance except that a larger load factor or some design modifications to braced-frame systems are needed to preclude early nonductile damage during a strong earthquake. If eccentric bracing is proposed as a means of improving the seismic performance of braced frames as described in Appendix I, dynamic analyses and static-cyclic tests similar to those conducted at the University of California, Berkeley, in connection with the development of eccentrically braced frames for buildings are needed to justify the applicability of this system to rack structures. Experiments on a shaking table are also very desirable.

- Although it was deemed necessary for this study to conduct the full-scale rack tests independently in each of the two principal directions, this test method does not realistically represent actual earthquake shaking. Shaking table tests should therefore be conducted to investigate the response characteristics of storage racks at different orientations.

- Although this study recommends the Rayleigh method (Equation 12-3 in the *UBC*) or a frequency analysis using an appropriate mathematical model for determining periods of vibration, it will be beneficial to the rack industry to develop empirical period formulas for static code use and a limit value on the design period, such as are used in the ATC-3 method.

- Although this study recommends seismic design criteria consistent with the philosophy of the *UBC* for rack design, the ATC method could be widely used in the near future. Because of this, it will be beneficial to determine appropriate values for the response modification factor, R.

- Results from the shaking table and static-cyclic tests revealed that the column bases should not be considered either fixed or hinged but rather as partially fixed. Quantitative experimental data are needed to appropriately incorporate this parameter into mathematical models to account for actual column base conditions. In addition, experimental investigations are needed to define the parameter K for braced-frame systems as subassembly tests are needed to define K_θ for semirigid-frame systems.

15. REFERENCES

1. Rack Manufacturers Institute, *Interim Specification for the Design, Testing, and Utilization of Industrial Storage Racks*, Pittsburgh, Pennsylvania, 1972.

2. International Conference of Building Officials, *Uniform Building Code*, Whittier, California, 1973.

3. *Seismic Investigation of Steel Industrial Storage Racks*, prepared for the Rack Manufacturers Institute, Pittsburgh, Pennsylvania, by URS/John A. Blume & Associates, Engineers, San Francisco, California, November 1973.

4. *Commentary on Seismic Investigation of Steel Industrial Storage Racks*, prepared for the Rack Manufacturers Institute, Pittsburgh, Pennsylvania, by URS/John A. Blume & Associates, Engineers, San Francisco, California, December 1973.

5. *Seismic Design Examples of Steel Industrial Storage Racks*, prepared for the Rack Manufacturers Institute, Pittsburgh, Pennsylvania, by URS/John A. Blume & Associates, Engineers, San Francisco, California, March 1974.

6. *Supplement to the Seismic Design Examples of Steel Industrial Storage Racks*, prepared for the Rack Manufacturers Institute, Pittsburgh, Pennsylvania, by URS/John A. Blume & Associates, Engineers, San Francisco, California, July 1975.

7. International Conference of Building Officials, *Uniform Building Code*, Whittier, California, 1976.

8. Applied Technology Council, *Tentative Provisions for the Development of Seismic Regulations for Buildings*, Palo Alto, California, 1978.

9. Krawinkler, H., N. G. Cofie, and C. A. Kircher, *Experimental Study on the Seismic Behavior of Industrial Storage Racks*, The John A. Blume Earthquake Engineering Center, Stanford University, November 1979.

Preceding page blank

10. *Interpretation of Pallet Rack Test Results*, prepared for the Rack Manufacturers Institute, Pittsburgh, Pennsylvania, by T. Peköz, Cornell University, Ithaca, New York, February 1978.

11. Rack Manufacturers Institute, *Specification for the Design, Testing, and Utilization of Industrial Steel Storage Racks*, Pittsburgh, Pennsylvania, 1976 Edition (approved March 1, 1977).

12. *Pallet Rack Design Criteria*, prepared for the Rack Manufacturers Institute, Pittsburgh, Pennsylvania, by T. Peköz, Cornell University, Ithaca, New York, February 1978.

13. "Don't Make Racks an Afterthought," *Handling & Shipping*, November 1976.

14. Rea. D., and J. Penzien, "Structural Research Using an Earthquake Simulator," *Proceedings*, Structural Engineers Association of California Conference, Monterey, California, 1972.

15. Wilson, E. L., *SMIS: Symbolic Matrix Interpretative System*, U.C. SESM 73-3, Department of Civil Engineering, University of California, Berkeley, January 1973.

16. American Iron and Steel Institute, *Specification for the Design of Cold-Formed Steel Structural Members*, New York, 1968.

17. Tang, D. T., and R. W. Clough, "Shaking-Table Earthquake Response of Steel Frame," *Journal of the Structural Division*, American Society of Civil Engineers, Vol. 105, No. ST1, January 1979.

18. Clough, R. W., and A. A. Huckelbridge, *Preliminary Experimental Study of Seismic Uplift of a Steel Frame*, UCB/EERC-72/22, Earthquake Engineering Research Center, University of California, Berkeley, August 1977.

19. Clough, R. W., and Y. Ghanaat, "Seismic Behavior of Diagonal Steel Wind Bracing," *Proceedings of the Second U. S. National Conference on Earthquake Engineering*, Stanford University, August 1979.

20. Bathe, K.-J., E. L. Wilson, and F. E. Peterson, *SAP IV: A Structural Analysis Program for Static and Dynamic Response to Linear Systems*, EERC 73-11, Earthquake Engineering Research Center, University of California, Berkeley, June 1973 (revised April 19, 1974).

21. Kanaan, A., and G.H. Powell, *General Purpose Computer Program for Inelastic Dynamic Response of Plane Structures*, EERC 73-5, Earthquake Engineering Research Center, University of California, Berkeley, April 1973 (revised September 1973 and August 1975).

22. Driscoll, G. C., "Effective Length of Columns with Semi-rigid Connections," *Engineering Journal*, American Institute of Steel Construction, Vol. 13, No. 4, 1976.

23. Salmon, C. G., L. Schenker, and B. G. Johnston, "Moment-Rotation Characteristics of Column Anchorages," *Transactions*, American Society of Civil Engineers, Vol. 122, 1957.

24. Galambos, T. V., "Influence of Partial Base Fixity on Frame Stability," *Journal of the Structural Division*, American Society of Civil Engineers, Vol. 86, No. ST5, May 1960.

25. International Conference of Building Officials, *Uniform Building Code*, Whittier, California, 1979.

26. Rack Manufacturers Institute, *Specification for the Design, Testing, and Utilization of Industrial Steel Storage Racks*, Pittsburgh, Pennsylvania, 1979 Edition.

27. Roeder, C. W., and E. P. Popov, *Inelastic Behavior of Eccentrically Braced Steel Frames under Cyclic Loading*, EERC 77-18, Earthquake Engineering Research Center, University of California, Berkeley, August 1977.

APPENDIX A

Evaluation of Theoretical Column Moments (Rotations) at Yield: Standard Pallet Rack

1. Parameters*

- Columns (minimum):

$$I_{cx} = 1.144 \text{ in.}^4, \quad r_x = 1.288 \text{ in.}$$
$$I_{cy} = 0.879 \text{ in.}^4, \quad r_y = 1.130 \text{ in.}$$
$$A = 0.688 \text{ in.}^2$$

$$L_{cx} = \text{unbraced length} = 52 \text{ in.}$$
$$L_{cy} = \text{unbraced length} = 53 \text{ in.}$$

- Beams:

$$I_b = 3.265 \text{ in.}^4$$
$$L_b = 96 \text{ in.}$$

- Joint Springs:

K_θ = 1.0×10^6 lb-in./rad (experimentally obtained, see Figure 7.2a)

- Fictitious Floor Beams:

I_f = 0.2 in.^{4} (see Section 7.1)

L_f = L_b

2. Determination of Effective Lengths in a Frame with Semirigid Beam Connections and a Partially Fixed Base

To account for semirigid joints, the beam rigidities are reduced as follows:

$$\left(\frac{I_b}{L_b}\right)_{red} = \frac{1}{1 + \dfrac{6EI_b}{K_\theta L_b}} \times \frac{I_b}{L_b}$$

For $K_\theta = 1.0 \times 10^6$,

$$\left(\frac{I_b}{L_b}\right)_{red} = \frac{1}{1 + \dfrac{6 \times 30 \times 10^6}{10^6 \times 96} \times 3.265} \times \frac{3.265}{96} = 0.0048 \text{ in.}^3$$

The value of K is determined from the alignment chart in the seventh edition of the American Institute of Steel Construction's *Manual of Steel Construction*. G_T and G_B are determined as follows:

*See Figure D for the mathematical model for this rack configuration.

$$G_T = \frac{\Sigma\, I_c/L_c}{\Sigma\, I_b/L_b}$$

$$= \frac{2 \times 1.144/52}{2 \times 0.0048} = \frac{0.022}{0.0048}$$

$$= 4.58$$

$$G_B = \frac{0.022}{2 \times \frac{0.2}{96}}$$

$$= 5.28$$

From the alignment chart:

$$K = 2.2$$

If K_θ is assigned a value of 1.4×10^6, the values obtained are:

$$\left(\frac{I_b}{L_b}\right)_{\text{red}} = 0.0063 \text{ in.}^3$$

$$K = 2.05$$

A value of $K = 2.1$ is therefore assigned to the center, bottom-story column.

3. Determination of Ultimate Axial Load P_{ult} Using AISI 3.6.1

$$\frac{K_x L_x}{r_x} = \frac{2.1 \times 52}{1.288} = 84.8$$

$$\frac{K_y L_y}{r_y} = \frac{1.0 \times 53}{1.130} = 46.9 \quad \text{(The larger value, 84.8, governs.)}$$

$$Q = 0.94$$

$$F_y = 45 \text{ kip/in.}^2$$

$$\frac{C_c}{\sqrt{Q}} = \frac{\sqrt{2\pi^2(E/F_y)}}{\sqrt{Q}} = 117 > 84.8$$

Because $C_c/\sqrt{Q}$ is greater than KL/r, the following equation is used:

$$F_{a1} = 0.522QF_y - \left(\frac{QF_y(KL/r)}{1{,}494}\right)^2$$

$$= 22.08 - 5.76$$

$$= 16.32 \text{ kip/in.}^2$$

The following equation uses the factor of safety of 1.92 prescribed by the AISI.

$$P_{ult} = F_{al} \times A \times 1.92$$

$$= 16.32 \times 0.688 \times 1.92$$

$$= 21.6 \text{ kips}$$

4. Application of the Interaction Equation

The theoretical bending moment at yield, M_y, may be predicted by the following interaction equation:

$$\frac{M_y}{M_{ult}} + \frac{P}{P_{ult}} = 1$$

where:

M_{ult} = ultimate bending moment when no axial load is present = SFy = 0.756 x 45

= 34.0 kip-in.

P_{ult} = ultimate axial load when no bending moment is present

= 21.6 kips

P = actual axial load as measured

For the longitudinal test using full live load:

$$P = P_D + P_S$$

where:

P_D = axial load due to dead weight and contents

= 9.4 kips

P_S = axial load due to seismic excitation

$\simeq$ 0 (center bottom story column)

Thus:

$$P = 9.4 \text{ kips}$$

Therefore:

$$M_y = (1 - \frac{9.4}{21.6}) \times 34.0$$

$$= 19.2 \text{ kip-in.}$$

Using the relationship between M and ϕ discussed in Section 4. ϕ_y can be determined to be 1.73×10^{-3} rad.

For the longitudinal test using 2/3 live load:

$$P = 6.4 \text{ kips}$$

and therefore:

$$M_y = (1 - \frac{6.4}{21.6}) \times 34.0$$
$$= 23.8 \text{ kip-in.}$$

and:

$$\phi_y = 2.14 \times 10^{-3} \text{ rad}$$

M_y and ϕ_y can be determined similarly for the transverse tests, with the following differences:

$$M_{ult} = SF_y = 0.596 \times 45$$
$$= 26.8 \text{ kip-in.}$$

P_S = axial load due to overturning moments determined by inertia forces

APPENDIX B

Evaluation of Torsional Effect: Drive-In Rack, Longitudinal Direction

1. First-Floor Plan of Drive-In Rack

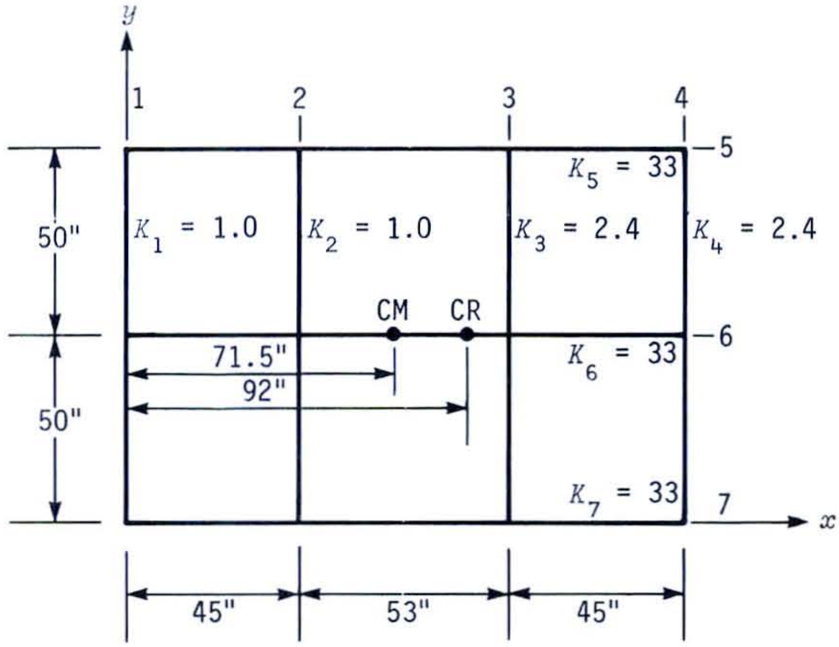

K_i = in-plane relative lateral stiffness (calculation of K_i has not been shown)

2. Centers of Rigidity and Mass

The coordinates of the center of rigidity (CR) are given by:

$$\overline{X}_1 = \frac{\Sigma\ k_i x}{\Sigma\ k_i}$$

$$= \frac{(2.4 \times 143) + (2.4 \times 98) + (1 \times 45)}{2.4 + 2.4 + 1 + 1}$$

$$= 92 \text{ in.}$$

$$\overline{Y}_1 = 50 \text{ in.}$$

The coordinates of the center of mass (CM) are given by:

$$\overline{X} = 71.5 \text{ in.}$$

$$\overline{Y} = 50 \text{ in.}$$

3. Distribution of Story Shear (P_y)

The horizontal shear, V_y, registered by a particular frame with its axis parallel to the y-direction, can be expressed as:

$$V_y = \left(\frac{k_y}{\Sigma k_y}\right) P_y \pm \left(\frac{k_y \bar{y}}{J_r}\right) P_y e$$

where:

k_y = lateral relative stiffness of the frame along the y-axis

k_x = lateral relative stiffness of the frame along the x-axis

$\bar{x}$ or $\bar{y}$ = perpendicular distance from CR to the axis of a particular frame

J_r = rotational stiffness of all frames

$= \Sigma\ (k_x \bar{y}^2 + k_y \bar{x}^2)$

$= (33 \times 50^2) + (33 \times 50^2) + (1 \times 92^2) + (1 \times 47^2) + (2.4 \times 6^2) + (2.4 \times 51^2)$

$= 182{,}000$

e = distance between CR and CM

= 20.5 in.

For the exterior upright frame (Frame 1)

$$V_y = \frac{1}{6.8} P_y + \frac{1 \times 92}{182{,}000} P_y \times 20.5$$

$$= \underbrace{0.147 P_y}_{\text{translation}} + \underbrace{0.01 P_y}_{\text{rotation}}$$

For the exterior anchor frame (Frame 4),

$$V_y = \frac{2.4}{6.8} P_y - \frac{2.4 \times 51}{182{,}000} P_y \times 20.5$$

$$= \underbrace{0.35 P_y}_{\text{translation}} - \underbrace{0.014 P_y}_{\text{rotation}}$$

APPENDIX C

Merchandise and Rack Performance During
Two Recent Earthquakes

This appendix presents information on rack damage and merchandise behavior collected after two recent strong earthquakes. No attempt has been made to reach conclusions or to find reasons for what happened; to do so would require an extensive engineering evaluation and more detailed information.

1. Miyagi-Ken-Oki, Japan, Earthquake

On June 12, 1978, an earthquake of Richter magnitude 7.4 caused considerable damage in the city of Sendai and the surrounding area. The epicentral distance to Sendai was approximately 100 km; peak horizontal ground accelerations ranged from 0.20g to 0.33g.

Figures C-1 through C-4 are photographs taken in Miyagi Prefecture about two weeks after the earthquake. By this time, some of the damaged merchandise had been cleaned up and some of the damaged racks had been removed from their original locations. Examination of the photographs shows that the modes of failure were consistent with what was observed during the shaking table tests. Buckling in the diagonal braces of braced-frame systems and damage at the top ends of first-level columns of pallet racks are apparent in the photographs.

Fukuda Tokuzo, in a paper (in Japanese) presented to the Japan National Conference on Merchandise Distribution held in Tokyo in October of 1979, detailed his field observations of merchandise damage following the earthquake and offered recommendations for safety measures to be taken in anticipation of future earthquake shaking. A brief summary of his observations and recommendations is translated as follows:

Field Observations:

- Total merchandise damage in the Miyagi Prefecture was estimated at $25 million.
- Of all glass containers filled with liquids (beer, juice, etc.), 30%-50% suffered damage; however, bottles of wine or soy sauce stored in wooden cases suffered little damage.
- Vegetable oil that had been stored in glass bottles covered the floor of every warehouse observed. The bottles broke when they struck each other during the shaking.

- Merchandise stored on pallets suffered more damage than merchandise that was not stored on pallets.
- Less damage occurred to merchandise stored in the middle levels of racks than to merchandise on the top and bottom levels.
- Merchandise on the lower levels of racks was often damaged by liquid that spilled from the upper levels.
- Barrels of tobacco were stable whether stored on their sides or on their ends.
- Large sheets of paper used for printing were disarranged to such an extent as to make them unusable.
- Soft drink bottles wrapped in heavy paper as a protection against light suffered little damage.
- Fire extinguishers hit by falling objects tended to discharge their contents.
- Often, overhead doors could not be opened because of the weight of large sacks of rice, which had fallen against them.

Recommendations:

- Store liquid-filled glass containers on the bottom level of racks.
- Store liquids and dry materials separately.
- Tie merchandise to the racks if it is stored on the upper levels.
- Roughen the surface of pallets so that merchandise will slide less.
- Store bottles of vegetable oil or dye in wooden boxes.
- Store forklifts outside warehouses when the lifts are not in use.

2. Imperial County, California, Earthquake

On October 15, 1979, an earthquake of Richter magnitude 6.6 occurred in the Imperial Valley of California. The epicenter of the main shock was on the Imperial fault just south of the California-Mexico border (about 16 km east of Calexico). Numerous aftershocks were felt the first two days, the largest of which was 5.5. Thirty-three accelerographs located 6 to 196 km from the epicenter recorded accelerations ranging from 1.74g to 0.06g. The instrument at El Centro Station 9, the same station that recorded the 1940 accelerogram that became the classic record of strong-motion shaking (the EC signal used in this project), recorded 0.4g with a 7.4-sec bracketed duration (time span between the first and last peaks greater than 0.1g).

In general, this shaking did not result in extensive building damage, but there was widespread spilling of library books, stored merchandise, and other shelved items. The 6-story Imperial County Service Building, however, was seriously damaged (see *Reconnaissance Report on Imperial County, California Earthquake, October 15, 1979*, which was published by the Earthquake Engineering Research Institute, Berkeley, California, in February 1980).

Two days after the earthquake, Michael Wilms, of Unarco Materials Storage, visited the Imperial Valley to survey rack damage and merchandise performance during the earthquake. In an unpublished report (made available for this study by Advisory Committee Member H. H. Klein, Chief Engineer of Unarco), Mr. Wilms said that he had seen every place in the Imperial Valley that used pallet racks. The following is a summary of his observations.

- No pallet racks were reported to be damaged.
- Packages that weighed from 20 to 40 lb and had a corresponding volume of 1/2 to 3/4 ft^3 were most prone to earthquake-induced movement.
- Bulk stacking was less earthquake-resistant than pallet stacking.
- Items with a height-to-depth ratio of 4 or larger were most prone to overturning.

(a) Buckling at Top End of First-Story Column

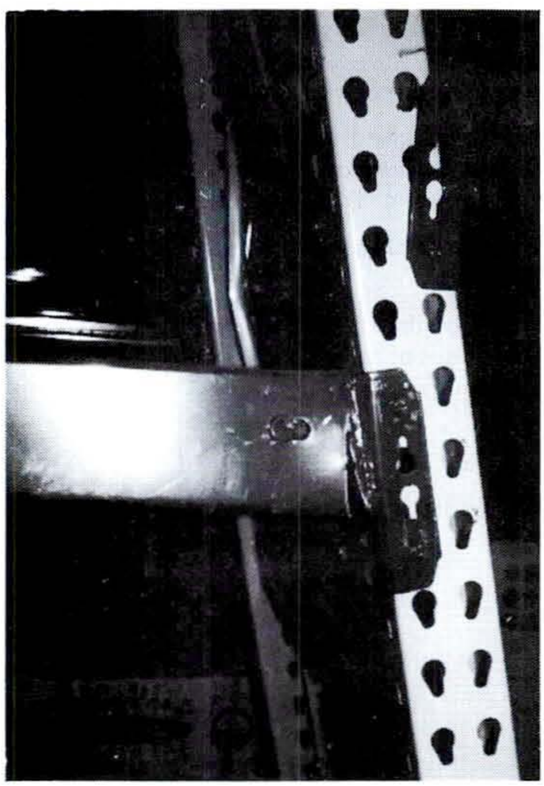

(b) Failure of Beam-Column Connection

FIGURE C.1 DAMAGED STANDARD PALLET RACK

FIGURE C.2 PERMANENT DEFORMATION OF RACKS

FIGURE C.3 STANDARD PALLET RACK - BUCKLING AT TOP END OF FIRST-STORY COLUMN

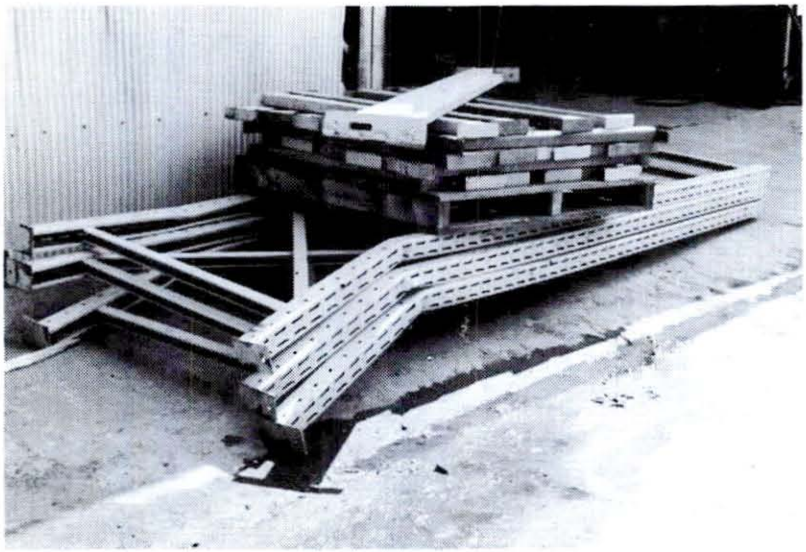

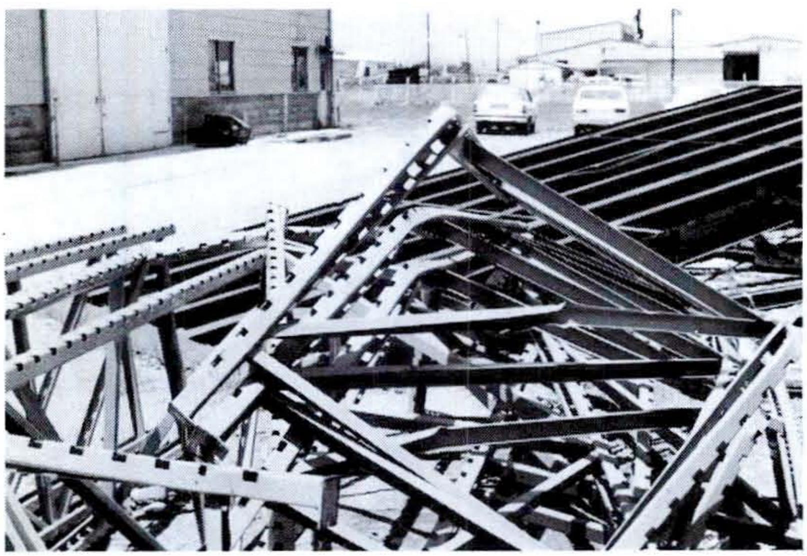

FIGURE C.4 DAMAGED STANDARD PALLET RACKS AFTER REMOVAL FROM WAREHOUSE

APPENDIX D

Seismic Design Example - Standard Pallet Rack, Longitudinal Direction

D

1. Given

- Rack configuration as shown in Figure 4.2
- Live load of 3,000 lb/pallet
- Minimum net section properties supplied by the manufacturer as follows:

	Moment of Inertia, I (in.^{4})	Cross-sectional Area, A (in.^{2})	Section Modulus, S (in.^{3})	Radii of Gyration, r_x, r_y (in.^{2})
Column	1.15	0.69	0.76	1.29/1.13
Beam	3.27	1.23	1.50	--

- Values assigned to parameters as follows:

  Semirigid joints: $K_\theta = 10^6$ lb-in./rad

  Column bases: $I_f = 0.2$ in.^{4}

- Characteristic site period: $T_s = 1.0$ sec (assumed)

2. Required

- To determine lateral forces in accordance with the 1976 *UBC* seismic design criteria
- To determine member capacities in accordance with the RMI specification

3. Mathematical Model

The mathematical model for this rack configuration is shown in Figure D. The moment of inertia of the beam was modified in accordance with Equation (7.1). The fundamental period of vibration, T, determined using SAP IV was 2.0 sec.

4. Base Shear

The base shear V is expressed as:

$$V = ZIKCSW$$

where:

Z = 1.0 for Zone 4

I = 1.0

S = 1.2 from Equation (6.10)

K = 1.0 for a moment-resisting frame

$$C = \frac{1}{15\sqrt{T}} = \frac{1}{15\sqrt{2.0}} = 0.047$$

$$W = 3 \times 6,250 = 18,750 \text{ lb/frame}$$

Thus:

$$V = 1,064 \text{ lb}$$

5. Lateral Force Distribution

The base shear V is distributed over the height of the rack, as Figure D shows, in accordance with Equations (6.11) and (6.12):

$$F_t = 0.07TV = 149 \text{ lb}$$

$$F_x = \frac{(V - F_t)w_x h_x}{\Sigma w_i h_i}$$

$$= \frac{915\ h_x}{\Sigma h_i}$$

$$F_3 = 149 + \frac{915 \times 178}{354}$$

$$= 609 \text{ lb}$$

$$F_2 = \frac{915 \times 118}{354}$$

$$= 305 \text{ lb}$$

$$F_1 = \frac{915 \times 58}{354}$$

$$= 150 \text{ lb}$$

6. Member Forces and Capacities

Member Forces: When the calculated lateral forces, F_x, are applied at each level, the member forces can be determined either from the computer analysis or by hand calculation. The most critical element is found at the top end of the center bottom column. The following results were obtained using computer analysis:

$$M = 16,284 \text{ lb-in.}$$
$$P = 9,380 \text{ lb}$$

p-δ Effect: The amplification ratio due to the p-δ effect recommended in ATC-3 is used in lieu of the arbitrary moment amplification term in Section 3.4 of the RMI specifications.

amplification ratio $= 1 + \theta + \theta^2 + \theta^3 + \ldots$

where:

θ = initial increment $= \dfrac{P_x \Delta}{V_x h_{sx}}$

$V_x = V$ = base shear = 1,064 lb

$P_x = W$ = the summation of all weights supported above
= 18,750 lb

$h_{sx} = h_1$ = story height
= 58 in.

$\Delta = \delta_1$ = first-floor displacement due to lateral forces F_i applied at each floor level
= 1.2 in. (from computer analysis)

Thus:

$$\theta = \frac{18,750 \times 1.2}{1,064 \times 58} = 0.36$$

amplification ratio = 1.0 + 0.36 + 0.13 + 0.05 + ...
= 1.56

M' = modified moment
= $1.56M$
= 1.56 x 16,284
= 25,403 lb-in.

P = 9,380 lb (unchanged)

Member Capacities: The interaction (M-P) equation is used to evaluate member capacities. The one-third increase in allowable forces permitted for forces resulting from seismic motion is applied. Torsional-flexural behavior is ignored in the calculation. The interaction equation is:

$$\frac{P}{P_a} + \frac{M'}{M_a} \leq 1.0$$

where:

P_a = allowable average compression force (see Appendix A)

$$= F_{a1} \times A \times 1.33/j$$

$$= 16{,}320 \times 0.69 \times 1.33/1.15$$

$$= 14{,}980/1.15 \text{ lb}$$

$$= 13{,}026 \text{ lb}$$

M_a = allowable bending moment

= $S \times F_y \times 0.6 \times 1.33$ (approximate; see Section 3.4 of the RMI specification for a more sophisticated evaluation)

$$= 0.76 \times 45{,}000 \times 0.6 \times 1.33$$

$$= 27{,}300 \text{ lb-in.}$$

Thus:

$$\frac{P}{P_a} + \frac{M'}{M_a} = \frac{9{,}380}{13{,}026} + \frac{25{,}403}{27{,}300}$$

$$= 0.72 + 0.93$$

$$= 1.65 > 1.0$$

The results show that the column members are undersized according to the 1976 *UBC* Zone 4 seismic design criteria. The above procedures should be repeated using the next larger member size.

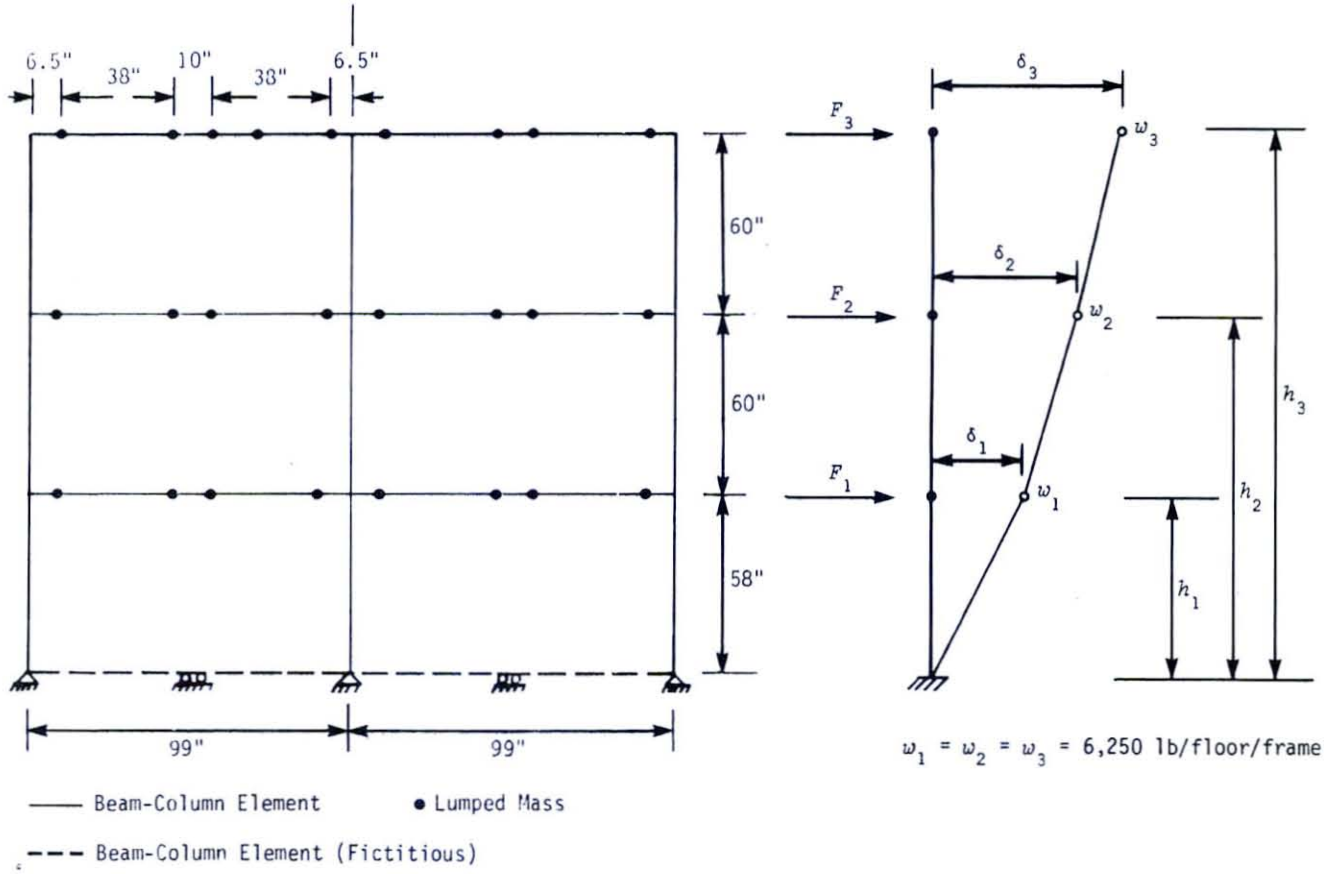

FIGURE D MATHEMATICAL MODEL - STANDARD PALLET RACK, LONGITUDINAL DIRECTION

APPENDIX E

Seismic Design Example - Standard Pallet Rack, Transverse Direction

1. Given

- Rack configuration as shown in Figure 4.2
- Live load of 3,000 lb/pallet
- Minimum net section properties supplied by the manufacturer as follows:

	Moment of Inertia, I (in.^{4})	Cross-sectional Area, A (in.^{2})	Section Modulus, S (in.^{3})	Radii of Gyration, r_x, r_y (in.^{2})
Column	0.88	0.69	0.586	1.288/1.130
Brace	-	0.32	--	0.628/0.409

- Values assigned to parameters as follows:

  Localized deformation: $k = 12$

  Column bases: $I_f = 0.2$ in.^{4}

- Characteristic site period: $T_s = 1.0$ sec (assumed)

2. Required

- To determine lateral forces in accordance with the 1976 *UBC* seismic design criteria
- To determine member capacities in accordance with the RMI specification

3. Mathematical Model

The mathematical model for the standard pallet rack in the transverse direction using the center upright frame is shown in Figure E. One-third of the total estimated mass is lumped in the model for frequency analysis. The value of EA of the brace was modified in accordance with Equation (8.1). The fundamental period of vibration, T, determined using SAP IV was found to be 0.83 sec.

4. Base Shear

The base shear V is expressed as follows:

$$V = ZIKCSW$$

where:

Z = 1.0 for Zone 4

I = 1.0

S = 1.49 from Equation (6.10)

K = 1.33 for a braced-frame system

$$C = \frac{1}{15\sqrt{T}} = \frac{1}{15\sqrt{0.83}} = 0.073$$

$$W = 3 \times 4{,}167 = 12{,}500 \text{ lb/frame}$$

Thus:

$$V = 1{,}809 \text{ lb}$$

5. Lateral Force Distribution

The base shear V is distributed over the height of the rack, as shown in Figure E, in accordance with Equations (6.11) and (6.12):

$$F_t = 0.07TV = 106 \text{ lb}$$

$$F_x = \frac{(V - F_t)w_x h_x}{\Sigma w_i h_i}$$

$$= \frac{1{,}703\ h_x}{\Sigma h_i}$$

$$F_3 = 106 + \frac{1{,}703 \times 178}{354}$$

$$= 962 \text{ lb}$$

$$F_2 = \frac{1{,}703 \times 118}{354}$$

$$= 568 \text{ lb}$$

$$F_1 = \frac{1{,}703 \times 58}{354}$$

$$= 279 \text{ lb}$$

6. Member Forces and Capacities

Member Forces: A load factor of 1.25 is required by 1976 *UBC* seismic design provisions for all members in braced frames. Computer analysis using the calculated lateral forces applied at each level shows the critical member force to be as follows.

For the column near the base plate:

$$M = M_s = 5{,}200 \times 1.25 = 6{,}500 \text{ lb}$$

$$P = P_s + P_d$$

$$= 6{,}258 \times 1.25 + 9{,}380$$

$$= 17{,}202 \text{ lb-in.}$$

For the bottom diagonal:

$$P = P_s = 2{,}578 \times 1.25 = 3{,}222 \text{ lb}$$

The subscripts s and d shown above denote moment or force due to seismic and gravity loads, respectively.

Member Capacities: The amplification of story shear due to the p-δ effect is insignificant for braced frames and need not be considered.

For the column near the base plate:

$$\frac{P}{P_a} + \frac{M}{M_a} \leqq 1.0$$

where:

P_a = 13,026 lb (same as for Appendix D)

M_a = $S \times F \times 0.6 \times 1.33$ (approximate; see Section 3.4 of the RMI specification for a more sophisticated evaluation)

$= 0.586 \times 45{,}000 \times 0.6 \times 1.33$

$= 21{,}040$ lb-in.

Thus:

$$\frac{P}{P_a} + \frac{M}{M_a} = \frac{17{,}202}{13{,}026} + \frac{6{,}500}{21{,}040}$$

$$= 1.32 + 0.31 = 1.63 > 1.0$$

For the bottom diagonal:

$$\frac{P}{P_a} = \frac{3{,}222}{3{,}190} = 1.01$$

where:

P_a = allowable average compression force from RMI specification (note: $F_{a2} < F_{a1}$)

$= F_{a2} \times A \times 1.33$

$= 7{,}500 \times 0.32 \times 1.33$

$= 3{,}190$ lb

The above analysis indicates that the columns in this rack direction are undersized and must be redesigned; however, the bracing members are adequate for this rack.

The connections between the columns and bracing members and columns near the base plates should be designed to develop the full capacity of the members, or they should be based on the member forces calculated above without the one-third increase usually permitted (and required by the 1976 *UBC*) for stresses resulting from seismic forces.

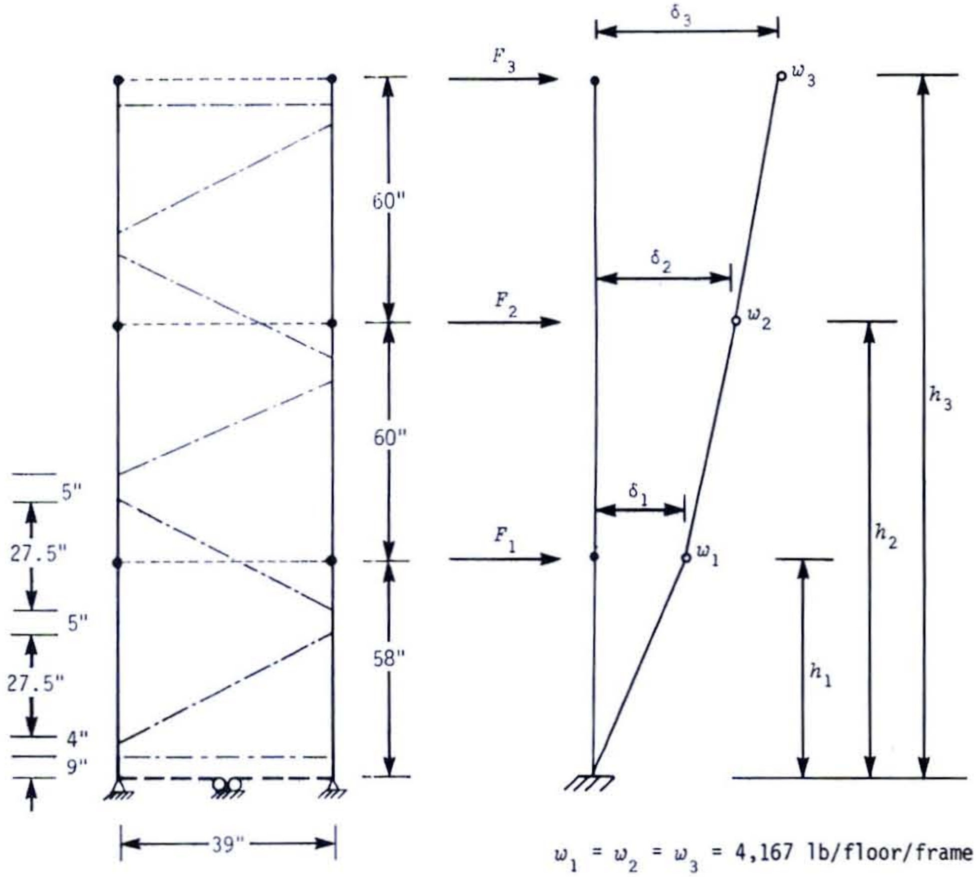

—— Beam-Column Element

- - - Beam-Column Element, (Fictitious)

• Lumped Mass

–·– Truss Element

----- Truss Element (Fictitious)

FIGURE E MATHEMATICAL MODEL - STANDARD PALLET RACK, TRANSVERSE DIRECTION

APPENDIX F

Seismic Design Example - Drive-In Rack, Longitudinal Direction

F

1. Given

- Rack configuration as shown in Figure 4.5
- Live load of 3,000 lb/pallet
- Minimum net section properties supplied by the manufacturer as follows:

	Moment of Inertia, I (in.^{4})	Cross-sectional Area, A (in.^{2})	Section Modulus, S (in.^{3})	Radii of Gyration, r_x, r_y (in.^{2})
Column (upright frame)	3.78	1.32	1.89	1.69/1.09
Column (anchor frame)	2.21	0.75	1.10	1.71/1.12
Beam (anchor frame)	1.18	1.09	0.94	--
Overhead Tie (upright frame)	0.32	0.46	0.27	--

- Values assigned to parameters as follows:

  Semirigid joints: $K_\theta = 10^6$ lb-in/rad

  Column bases: $I_f = 0.2$ in.^{4}

- Characteristic site period: $T_s = 1.0$ sec (assumed)

2. Required

- To determine lateral forces in accordance with the 1976 *UBC* seismic design criteria
- To determine member capacities in accordance with the RMI specification

3. Mathematical Model

A two-dimensional frame system is assumed. It consists of one upright frame and one anchor frame connected by three fictitious rigid springs at the floor levels (see Figure F). Half of the total weight (or mass) is lumped in the model. The mass at the top floor is very small and can be considered negligible. The moments of inertia of beams and overhead ties were modified in accordance with Equation (7.1). The fundamental period of vibration, T, determined from the frequency analysis of the mathematical model using SAP IV is 2.4 sec.

4. Base Shear

The base shear V is determined as follows:

$$V = ZIKCSW$$

where:

$$Z = 1.0 \text{ for Zone 4}$$

$$I = 1.0$$

$$S = 1.0 \text{ from Equation (6.10)}$$

$$K = 1.0 \text{ for a moment-resisting frame}$$

$$C = \frac{1}{15\sqrt{T}} = \frac{1}{15\sqrt{2.4}} = 0.043$$

$$W = 3 \times 9{,}575 = 28{,}725 \text{ lb}$$

Thus:

$$V = 1{,}235 \text{ lb}$$

5. Lateral Force Distribution

The base shear V is distributed over the height of the rack, as shown in Figure F, in accordance with Equations (6.11) and (6.12):

$$F_t = 0.07TV$$

$$= 0.07 \times 2.4 \times 1{,}235$$

$$= 207 \text{ lb}$$

$$F_x = \frac{(V - F_t)\ w_x h_x}{\Sigma w_i h_i}$$

$$= \frac{1{,}028\ h_x}{\Sigma h_i}$$

$$F_3 = 207 + 1{,}028 \times \frac{214}{426}$$

$$= 723 \text{ lb}$$

$$F_2 = \frac{1{,}028 \times 142}{426}$$

$$= 343 \text{ lb}$$

$$F_1 = \frac{1{,}028 \times 70}{426}$$

$$= 169 \text{ lb}$$

6. Member Forces and Capacities

Member Forces: The member forces can be determined using the lateral forces F_x prescribed above. The most critical members are found to be at the top ends of the center first-floor columns of both anchor and upright frames, according to the computer analysis.

$$P = 9{,}560 \text{ lb}$$
$$M = 15{,}600 \text{ lb-in.}$$

Anchor Frame

$$P = 9{,}560 \text{ lb}$$
$$M = 15{,}700 \text{ lb-in.}$$

Upright Frame

p-δ Effect: The amplification ratio due to the p-δ effect recommended in ATC-3 is used in lieu of the arbitrary moment amplification term in Section 3.4 of the RMI specification.

$$\text{amplification ratio} = 1 + \theta + \theta^2 + \ldots$$

where:

$$\theta = \text{initial increment} = \frac{P_x \Delta}{V_x h_{sx}}$$

$$V_x = V = 1{,}235 \text{ lb}$$

$$P_x = W = 28{,}725 \text{ lb}$$

$$h_{sx} = h_1 = 70 \text{ in.}$$

$$\Delta = \delta_1 = 1.2 \text{ (from computer analysis)}$$

Thus:

$$\theta = \frac{28{,}725 \times 1.2}{1{,}235 \times 70} = 0.40$$

$$\text{amplification ratio} = 1 + 0.40 + 0.16 + 0.06 + \ldots$$
$$= 1.62$$

For the anchor frame:

$$M' = 1.62 \times 15{,}600$$
$$= 25{,}272$$

$$P = 9{,}560 \text{ lb}$$

For the upright frame:

$$M' = 1.62 \times 15{,}700$$
$$= 25{,}434 \text{ lb-in.}$$

$$P = 9{,}560 \text{ lb}$$

Member Capacities: The interaction equation is used to evaluate member capacities. Torsional-flexural behavior is ignored in the calculation. The one-third increase in allowable forces permitted for forces resulting from seismic motion is considered.

$$\frac{P}{P_a} + \frac{M'}{M_a} \leq 1.0$$

where:

$$P_a = F_{a1} \times A \times 1.33/j$$
$$= 14{,}000 \times 0.75 \times 1.33/1.15$$
$$= 12{,}190 \text{ lb -- anchor frame}$$
$$= 11{,}730 \times 1.32 \times 1.33/1.15$$
$$= 17{,}900 \text{ lb -- upright frame}$$

$M_a = S \times F_y \times 0.6 \times 1.33$ (approximate; see Section 3.4 of the RMI specification for a more sophisticated evaluation)

$$= 1.10 \times 36{,}000 \times 0.6 \times 1.33$$
$$= 31{,}600 \text{ lb-in. -- anchor frame}$$
$$= 1.89 \times 36{,}000 \times 0.6 \times 1.33$$
$$= 54{,}270 \text{ lb-in. -- upright frame}$$

For the anchor frame:

$$\frac{P}{P_a} + \frac{M'}{M_a} = \frac{9{,}560}{12{,}190} + \frac{25{,}272}{31{,}600}$$
$$= 0.78 + 0.80$$
$$= 1.58 > 1.0$$

For the upright frame:

$$\frac{P}{P_a} + \frac{M'}{M_a} = \frac{9{,}560}{17{,}900} + \frac{25{,}430}{54{,}270}$$

$$= 0.54 + 0.47$$
$$= 1.01$$

The above analysis shows that the anchor frame columns are undersized and must be redesigned; the upright frame columns are adequate according to the 1976 *UBC* Zone 4 seismic provisions.

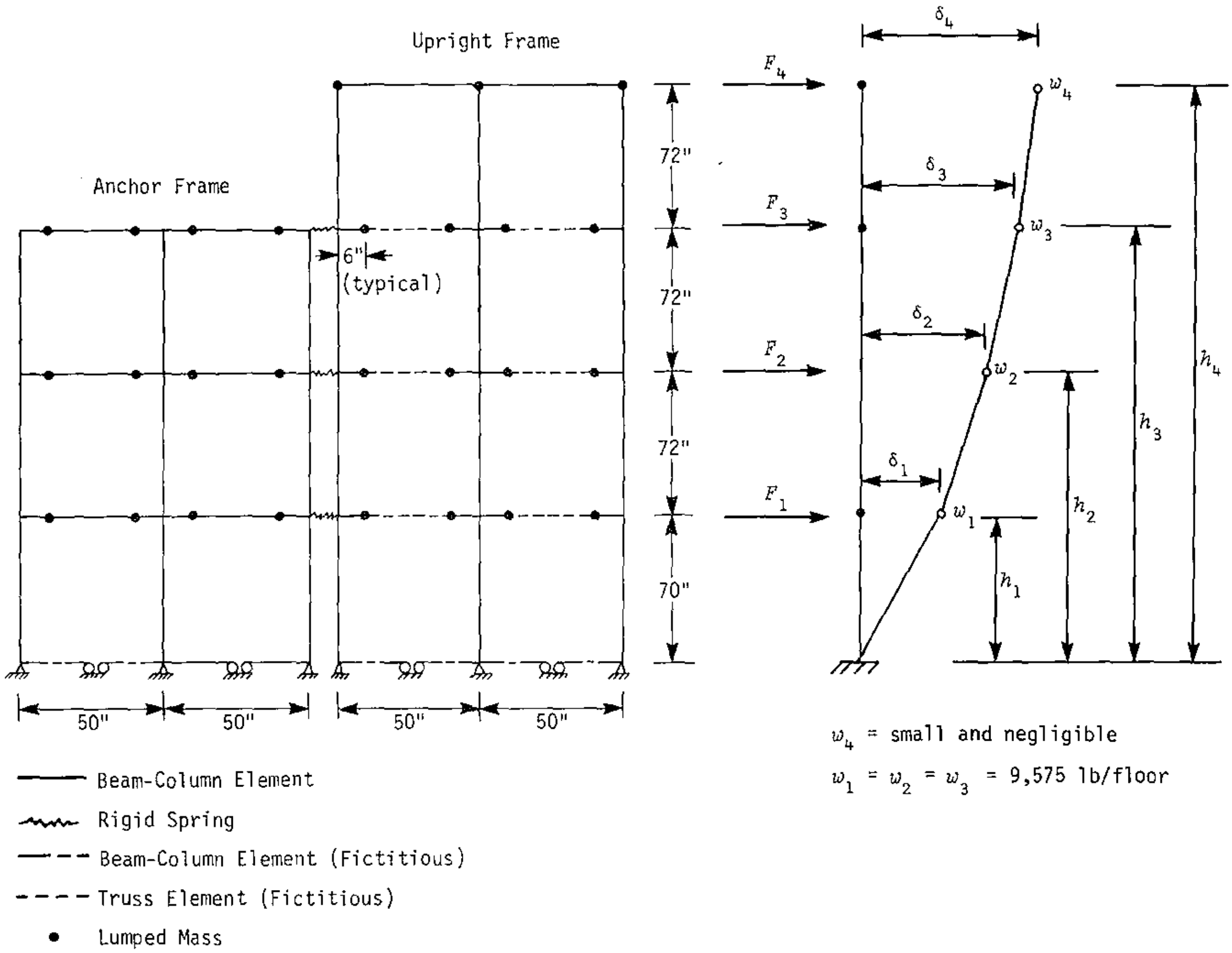

FIGURE F MATHEMATICAL MODEL - DRIVE-IN RACK, LONGITUDINAL DIRECTION

APPENDIX G

Seismic Design Example - Drive-In Rack,
Transverse Direction

1. Given

- Rack configuration as shown in Figure 4.5
- Live load of 2,000 lb/pallet
- Minimum net section properties supplied by the manufacturer as follows:

	Moment of Inertia, I (in.^{4})	Cross-sectional Area, A (in.^{2})	Section Modulus, S (in.^{3})	Radii of Gyration, r_x, r_y (in.^{2})
Column (upright)	1.56	1.32	0.90	1.69/1.09
Column (anchor)	0.94	0.75	0.54	1.71/1.12
Brace	-	0.33	-	0.92/0.39
Row Spacer	-	0.26	-	--

- Values assigned to parameters as follows:

  Localized deformation: $k = 7$

  Column bases: $I_f = 0.2$ in.^{4}

- Characteristic site period: $T_s = 1.0$ sec (assumed)

2. Required

- To determine lateral forces in accordance with the 1976 *UBC* seismic design criteria
- To determine member capacities in accordance with the RMI specification

3. Mathematic Model

Figure G shows the mathematical model developed for the drive-in rack assembly in the transverse direction. A single frame (center) is selected for analysis and one-third of the estimated total mass is lumped in the model. The mass at the top (4th) level is very small and can be neglected. The value of EA of the braces was modified in accordance with Equation (8.1). The fundamental period of vibration, T, determined using SAP IV was found to be 0.58 sec.

4. Base Shear

The base shear V is expressed as follows:

$$V = ZIKCSW$$

where:

Z = 1.0 for Zone 4

I = 1.0

S = 1.4 from Equation (6.10)

K = 1.33 for a braced-frame system

$$C = \frac{1}{15\sqrt{T}} = \frac{1}{15\sqrt{0.58}} = 0.088$$

W = 3 x 4,400 = 13,200 lb/frame

Thus:

V = 2,162 lb

5. Lateral Force Distribution

The base shear V is distributed over the height of the rack as shown in Figure G, in accordance with Equations (6.11) and (6.12).

$$F_t = 0$$

$$F_x = \frac{(V - F_t)w_x h_x}{\Sigma w_i h_i}$$

$$= \frac{2{,}162\ h_x}{\Sigma h_i}$$

$$F_3 = \frac{2{,}162 \times 214}{426}$$

$$= 1{,}086 \text{ lb}$$

$$F_2 = \frac{2{,}162 \times 142}{426}$$

$$= 721 \text{ lb}$$

$$F_1 = \frac{2{,}162 \times 70}{426}$$

$$= 355 \text{ lb}$$

6. Member Forces and Capacities

Member Forces: A load factor of 1.25 is applied for all members in this braced-frame system. The computer analysis, applying the calculated lateral forces at each story level, shows the following axial compression forces in the first-level diagonal braces:

$$P = 1.25 \times 2{,}398 = 2{,}998 \text{ lb -- upright}$$
$$= 1.25 \times 1{,}848 = 2{,}310 \text{ lb -- anchor}$$

Member Capacities: The allowable average compression loads with the permitted one-third increase in allowable forces are as follows:

$$P_a = F_{a1} \times A \times 1.33 \text{ (note: } F_{a2} > F_{a1}\text{)}$$
$$= 6{,}600 \times 0.33 \times 1.33$$
$$= 2{,}897 \text{ lb -- anchor frame}$$
$$= 4{,}850 \times 0.33 \times 1.33$$
$$= 2{,}129 \text{ lb -- upright frame}$$

$$\frac{P}{P_a} = \frac{2{,}310}{2{,}897} = 0.80 < 1.0 \text{ -- anchor frame}$$

$$= \frac{2{,}998}{2{,}129} = 1.41 > 1.0 \text{ -- upright frame}$$

This indicates that the diagonal members in the upright frame ($l/r = 177$) are undersized but the diagonal members in the anchor frame ($l/r = 151$) are adequate. Note that the column capacities are all within the allowable limits; the calculations are not shown here.

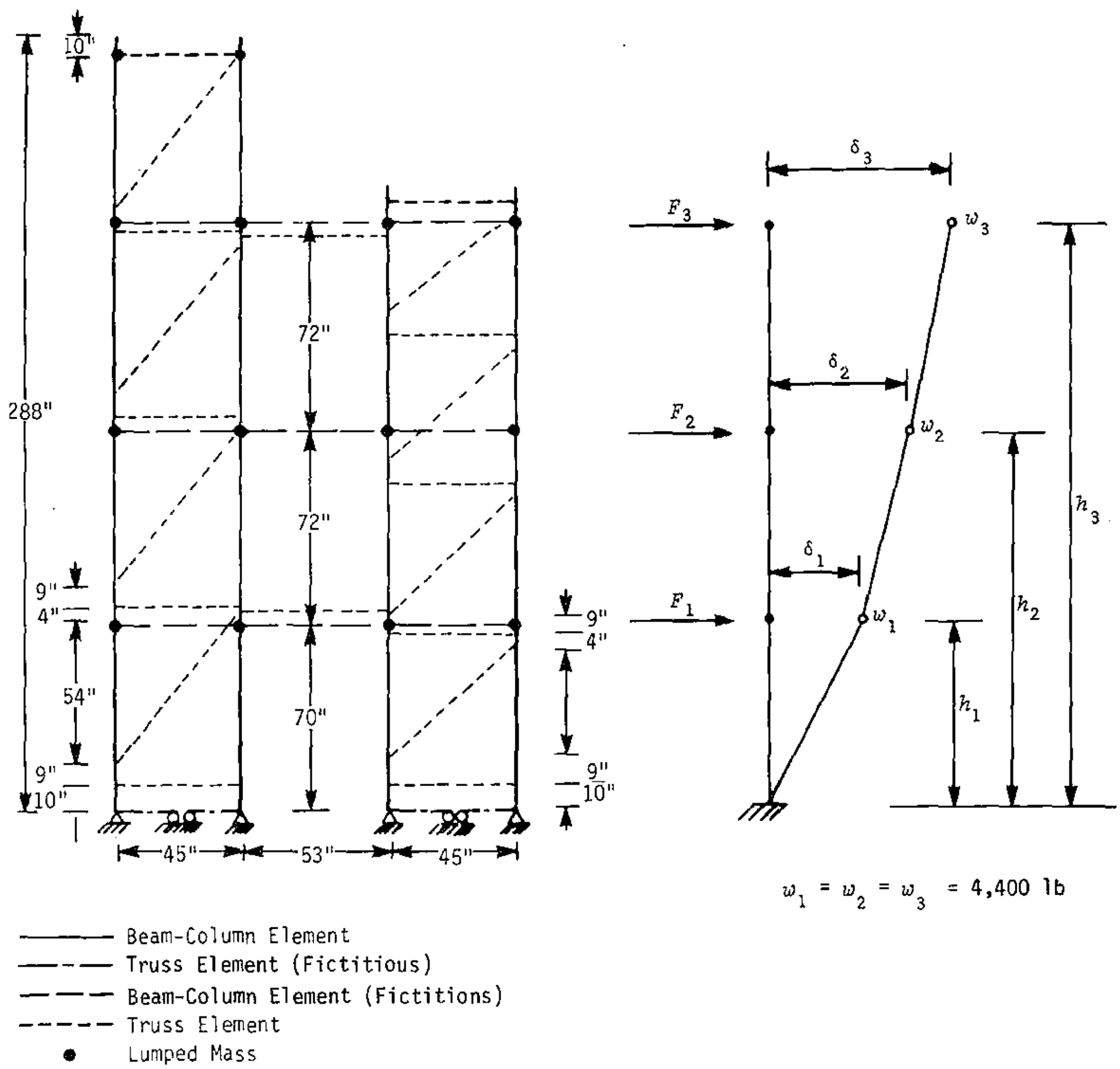

FIGURE G MATHEMATICAL MODEL - DRIVE-IN RACK, TRANSVERSE DIRECTION

APPENDIX H

Seismic Design Example - Stacker
Rack, Longitudinal Direction

H

1. Given

- Rack configuration as shown in Figure 4.8
- Live load of 2,000 lb/pallet
- Minimum net section properties supplied by the manufacturer as follows:

	Moment of Inertia, I (in.^{4})	Cross-sectional Area, A (in.^{2})	Section Modulus, S (in.^{3})	Radii of Gyration, r_x, r_y (in.^{2})
Column	4 x 1.15	4 x 0.69	0.76	1.29/1.13
Horizontal Tie	4 x 0.67	4 x 0.54	--	--
Diagonal Rod	--	0.785	--	--

- Values assigned to parameters as follows:

  Localized deformation: $k = 14$

  Column bases: $I_f = 0.2$ in.^{4}

- Characteristic site period: $T_s = 1.0$ (assumed)

2. Required

- To determine lateral forces in accordance with the 1976 *UBC* seismic design criteria
- To determine member capacities in accordance with the RMI specification

3. Mathematical Model

The four resisting frames are represented as a single frame, and the diagonal rods are assumed to be connected directly to the column members. The 1-in. diagonal rods are treated as composites consisting of a solid section, a threaded portion, and a rod support. During the seismic excitation, these diagonal rods will behave nonlinearly, because of their very low compression capacity. However, to model this structure linearly, it is assumed that the diagonal members will yield in tension and compression (i.e., they are treated as truss elements), and they are thus assigned an appropriately assumed value of k. The value of EA of the diagonal rods was modified in accordance with Equation (8.1).

The fundamental period of vibration, T, determined from the frequency analysis of the mathematical model using SAP IV is 0.91 sec.

4. Base Shear

The base shear V is determined as follows:

$$V = ZIKCSW$$

where:

$$Z = 1.0 \text{ for Zone 4}$$

$$I = 1.0$$

$$S = 1.49 \text{ from Equation (6.10)}$$

$$K = 1.33 \text{ for a braced-frame system}$$

$$C = \frac{1}{15\sqrt{T}} = \frac{1}{15\sqrt{0.91}} = 0.070$$

$$W = 88{,}000 \text{ lb (total)}$$

Thus:

$$V = 12{,}208 \text{ lb}$$

5. Lateral Force Distribution

The base shear V is distributed over the height of the rack, as shown in Figure H, in accordance with Equations (6.11) and (6.12).

$$F_t = 0.07TV$$
$$= 778 \text{ lb}$$

$$F_x = \frac{(V - F_t)w_x h_x}{\Sigma w_i h_i}$$

$$F_6 = 11{,}430 \times 0.01 + 778 = 892 \text{ lb}$$

$$F_5 = 11{,}430 \times 0.366 = 4{,}183 \text{ lb}$$

$$F_4 = 11{,}430 \times 0.285 = 3{,}258 \text{ lb}$$

$$F_3 = 11{,}430 \times 0.205 = 2{,}343 \text{ lb}$$

$$F_2 = 11{,}430 \times 0.107 = 1{,}223 \text{ lb}$$

$$F_1 = 11{,}430 \times 0.027 = 309 \text{ lb}$$

6. Member Forces and Capacities

Member Forces: To determine the diagonal forces due to the *UBC* lateral forces, it is assumed that the diagonals will take mostly tension and only very little compression. It is further assumed that the second-level story shear will be totally carried by one of the bottom diagonal rods. The diagonal tension with a load factor of 1.25 is determined as follows:

$$P = (V - F_1) \times \frac{145}{96} \times 1.25$$

$$= (12,208 - 309) \times \frac{145}{96} \times 1.25$$

$$= 22,465 \text{ lb}$$

The most critical column member is the first interior column near the base plate.

$$P = P_s + P_d$$

where:

$$P_s = \frac{23,438}{4}$$

$$= 5,860 \text{ lb/column}$$

$$P_d = 5,400 \text{ lb/column}$$

$$P = 5,860 \times 1.25 + 5,400$$

$$= 7,325 + 5,400$$

$$= 12,725 \text{ lb}$$

$$M = \frac{21,635}{4} \times 1.25$$

$$= 6,761 \text{ lb-in./column}$$

The p-δ effect is not significant in this rack configuration.

Member Capacities:

P_a = allowable diagonal tension

$$= F_y \times A \times 0.6 \times 1.33$$

$$= 36,000 \times 0.78 \times 0.6 \times 1.33$$

$$= 22,408 \text{ lb}$$

P_a = allowable average compression force of column (torsional-flexural behavior is ignored)

$$= F_{a1} \times A \times 1.33/j$$

$$= 20,530 \times 0.69 \times 1.33/1.15$$

$$= 16,330$$

M_a = allowable bending capacity of column (approximate; see Section 3.4 of the RMI specification for a more sophisticated evaluation)

$$= F_y \times S \times 0.60 \times 1.33$$

$$= 45{,}000 \times 0.76 \times 0.6 \times 1.33$$

$$= 27{,}130 \text{ lb-in.}$$

For diagonal rods:

$$\frac{P}{P_a} = \frac{22{,}465}{22{,}408} = 1.0$$

For columns:

$$\frac{P}{P_a} + \frac{M}{M_a} = \frac{12{,}725}{16{,}330} + \frac{6{,}761}{27{,}130}$$

$$= 0.78 + 0.25$$

$$= 1.03$$

These results show that the diagonal and column members meet the requirements of the 1976 *UBC* Zone 4 seismic design criteria.

7. Remarks

The mathematical model developed for this example is adequate in determining the fundamental period of vibration and diagonal forces. However, the column member forces estimated from this two-dimensional model can only be considered approximate because a single composite frame, representing four identical frames and the diagonal rods assumed to be connected directly to the column members, may not truly represent an actual three-dimensional configuration.

The example shown above uses a braced-frame system designed with a value of K of 1.33. However, for this rack configuration, a value of K smaller than 1.33 may be used if the system can qualify as a dual bracing system consisting of a braced frame and moment-resisting frames. Such designs will take 100% of the total lateral force in the braced frame and, as a backup, take 25% in the moment-resisting frames.

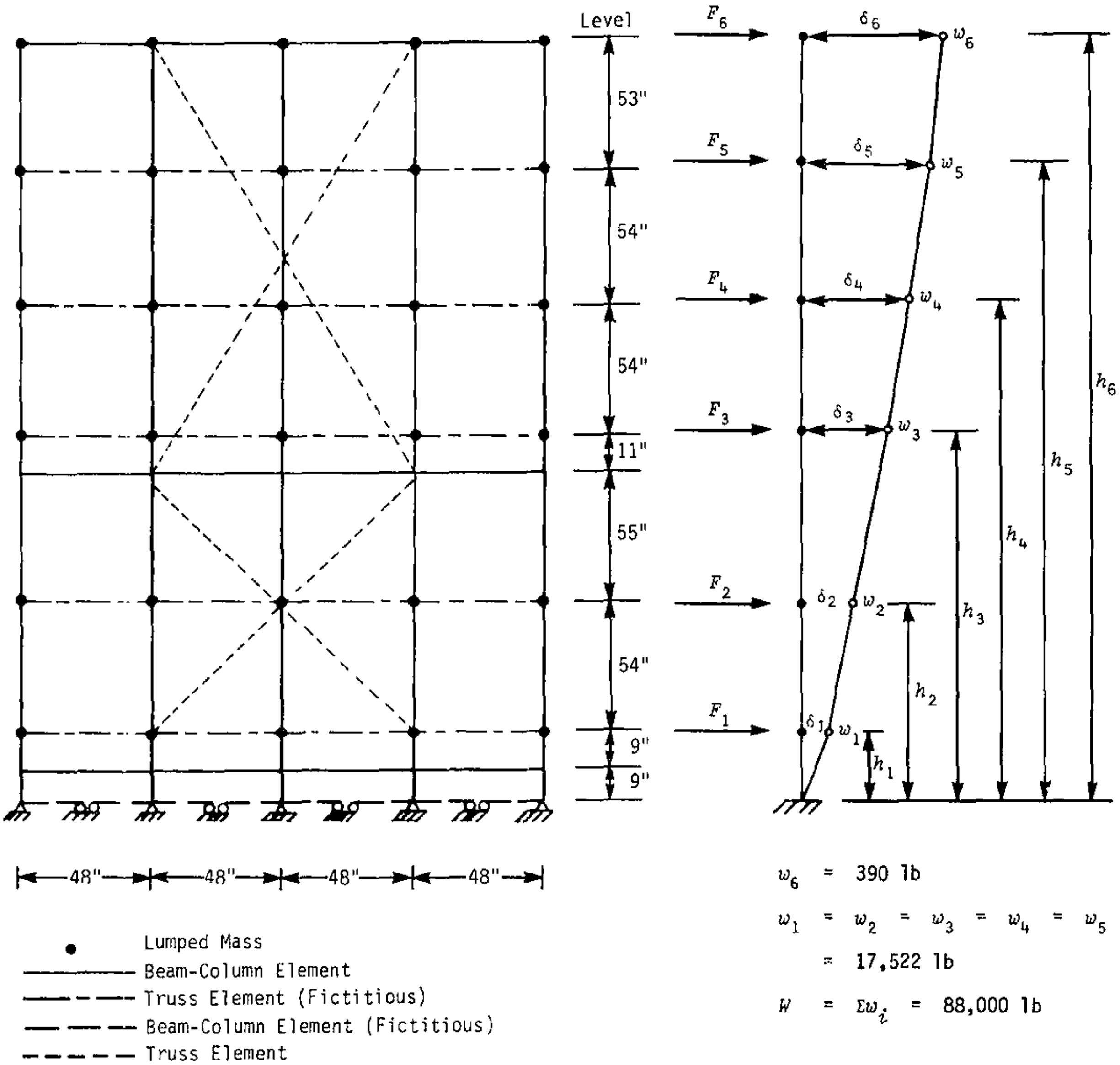

FIGURE H MATHEMATICAL MODEL - STACKER RACK, LONGITUDINAL DIRECTION

APPENDIX I

Eccentrically Braced Systems

In the shaking table tests, braced frames did not perform well when the diagonal braces were connected conventionally into the columns. Considerable buckling was observed in the first-level diagonal members of the drive-in and stacker racks when the racks were excited at very low intensity levels, i.e., 1/4 PF and 1/2 PF, respectively. Thus, a larger load factor than the 1.25 recommended in the *UBC* or some design modification is needed to preclude early nonductile damage during strong earthquake shaking.

In a new system proposed for improving seismic performance, diagonal bracing is connected into beams some distance from the beam-column connections so that any inelastic deformation from the seismic loading of a strong earthquake will occur in the section between the brace and the beam-column connection and not in the columns or braces. This system was developed for building structures by C. W. Roeder and E. P. Popov in their paper presented at the 1977 convention of the American Society of Civil Engineers held in San Francisco (or see Reference 27). Since then, it has been used in four California buildings designed with moment-resisting frames to improve seismic performance and reduce material and erection costs (see *Engineering News-Record*, October 25, 1979).

Although the system was developed for buildings, it can also be applied to rack structures. Figure I shows three possible eccentric bracing schemes. The first scheme, which uses rigid beam-column connections, is the best, but it is probably not feasible for racks because of the difficulty of achieving rigid connections between members of the size used in racks. The second scheme, using pinned beam-column connections, is unsatisfactory for racks because the beam moment will be high enough that the beams could buckle. The most feasible scheme for racks is the third one, which uses semirigid connections such as are actually found in many racks.

Dynamic analyses and static-cyclic tests similar to those conducted at the University of California, Berkeley, for typical building construction members will be needed to justify the applicability of this system to racks. Experiments on a shaking table are also desirable.

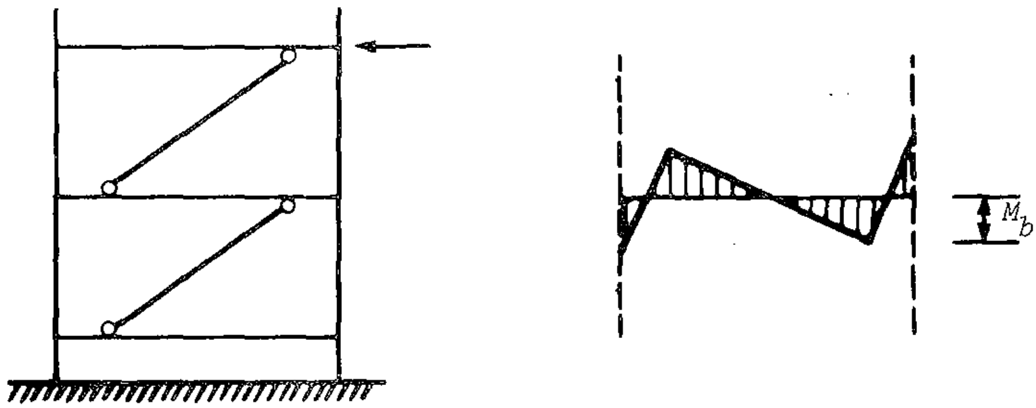

1. Rigid Beam-Column Connections

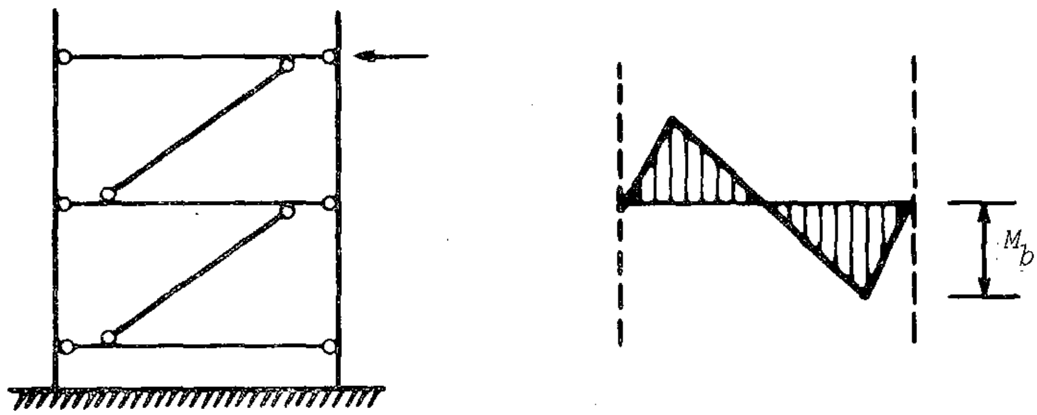

2. Pinned Beam-Column Connections

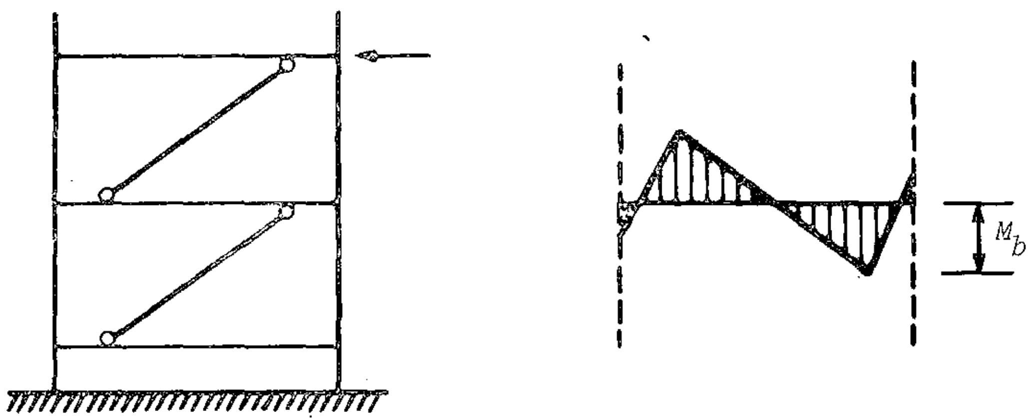

3. Semirigid Beam-Column Connections

M_b = beam moment

FIGURE I ECCENTRICALLY BRACED SYSTEMS